Advances in Astronomy

Dwarf-Galaxy Cosmology

Guest Editors: Regina Schulte-Ladbeck, Ulrich Hopp,
Elias Brinks, and Andrey Kravtsov

Dwarf-Galaxy Cosmology

Advances in Astronomy

Dwarf-Galaxy Cosmology

Guest Editors: Regina Schulte-Ladbeck, Ulrich Hopp, Elias Brinks, and Andrey Kravtsov

Editorial Board

Contents

Hindawi Publishing Corporation
Advances in Astronomy
Volume 2010, Article ID 930426, 2 pages
doi:10.1155/2010/930426

Editorial
Dwarf-Galaxy Cosmology

Regina Schulte-Ladbeck,[1] Ulrich Hopp,[2,3] Elias Brinks,[4] and Andrey Kravtsov[5]

[1] *Department of Physics and Astronomy, University of Pittsburgh, Pittsburgh, PA 15260, USA*
[2] *Universitäts-Sternwarte, Ludwig-Maximilians-Universität München, 81679 München, Germany*
[3] *Max-Planck Institut für Extraterrestrische Physik, 85748 Garching, Germany*
[4] *Centre for Astrophysics Research, University of Hertfordshire, Hatfield AL10 9AB, UK*
[5] *Kavli Institute for Cosmological Physics, The Department of Astronomy and Astrophysics, The University of Chicago, Chicago, IL 60637, USA*

Correspondence should be addressed to Regina Schulte-Ladbeck, rsl@pitt.edu

Received 3 February 2010; Accepted 3 February 2010

Dwarf galaxies provide opportunities for drawing inferences about the processes in the early universe by observing our "cosmological backyard"—the Local Group and its vicinity. This special issue of the open-access journal Advances in Astronomy is a snapshot of the current state of the art of dwarf-galaxy cosmology. The issue contains fourteen review papers, and one original research article. All papers were peer-reviewed by a minimum of two referees.

Dwarf galaxies continue to challenge our cosmological models and models of galaxy formation. Two well-known problems are the "missing satellites problem" and the "cores versus cusps problem."

The dilemma posed by the fact that observations seem to indicate an approximately constant dark matter density in the inner parts of galaxies, while cosmological simulations prefer a steep, power-law-like behavior that is assessed by W. J. G. de Blok in the paper "*The core-cusp problem*." A. Kravtsov reviews the quandary that predicted subhalos outnumber observed dwarf galaxies of the Local Group. In his paper "*Dark matter substructure and dwarf galactic satellites*," he emphasizes insights that have been gained from cosmological simulations and their tension with observational data.

The observer's viewpoint of the missing satellites problem is provided by B. Willman in the review "*In pursuit of the least luminous galaxies*." Her paper focuses on the progress made with the help of the Sloan Digital Sky Survey data and gives perspectives on the potential for contributions to this research by future surveys and new telescopes. Her paper is complemented by H. Jerjen's review "*Dwarf cosmology with the Stromlo missing satellites survey*." He makes the case that the southern hemisphere has been largely unexplored to faint magnitude levels with modern digital imaging data and discusses the prospects for a complete census of the Milky Way satellite population. An approach to finding missing dwarf galaxies that is independent of their luminous stellar content is through detecting their gravitational lensing signal. E. Zackrisson and T. Riehm examine the many ways through which lensing by subhalos can manifest itself in their paper titled "*Gravitational lensing as a probe of cold dark matter subhalos*."

Early cosmological simulations also predict large numbers of dwarf galaxies in voids, which, since this is not confirmed by observations either, is another face of the missing dwarfs issue. It is currently hoped that a better understanding of the physics that controls star formation might resolve the discrepancies between the simulated and observed dwarf galaxies in both environments. Work has therefore focused on how gas is accreted and retained in dwarf-galaxy-sized halos to form stars. In "*The first galaxies and the likely discovery of their fossils in the local group*," M. Ricotti reviews simulations of the formation and fate of preionization dwarfs. M. Hoeft and S. Gottlöber describe what progress has been made with high-resolution simulations to tackle the issue of "*Dwarf galaxies in voids: dark matter halos and gas cooling*." K. Nagamine adds his views

on how to include star formation processes in cosmological simulations in "*Star formation history of dwarf galaxies in cosmological hydrodynamic simulations*."

These papers are accompanied by a review of the current knowledge of the star-formation histories of dwarf galaxies that has been gained from observations. M. Cignoni and M. Tosi describe experimental approaches and results in "*Star formation histories of dwarf galaxies from the colour-magnitude diagrams of their resolved stellar populations*."

Several papers address how dynamical interactions influence the evolution of dwarf galaxies. In "*Environmental mechanisms shaping the nature of dwarf galaxies: the view of computer simulations*," L. Mayer describes a mechanism for transforming disky dwarfs into dwarf spheroidals, and discusses implications for the substructure problem. L. V. Sales et al. consider "*The effect of tidal stripping on composite stellar populations in dwarf spheroidal galaxies*." Their dwarf galaxy model follows the evolution of two kinematically and spatially segregated stellar components. They ask how these can be distinguished after having interacted with the potential of a massive galaxy. F. Bournaud, in "*Tidal dwarf galaxies and missing baryons*," discusses a tension that exists between model predictions that tidal dwarfs should not contain a significant mass fraction from the dark matter halos of their progenitor spiral galaxies, and existing observations which do suggest the presence of an unseen component.

Dwarf spheroidal galaxies are considered to provide good astronomical sites for the study of the nature of dark matter. In "*Kinematics of Milky Way satellites: mass estimates, rotation limits, and proper motions*," L. Strigari reviews the evidence for the presence of dark matter in dwarf spheroidal companions of the Milky Way. M. Kuhlen portrays prospects for the detection of the hypothetical dark matter particle. His paper is titled "*The dark matter annihilation signal from dwarf galaxies and subhalos*." A. Kosowsky makes the case that dwarf spheroidals are not only important for testing the dark matter hypothesis, but also the competing, modified Newtonian gravity hypothesis. His paper critically analyzes "*Dwarf galaxies, MOND, and relativistic gravitation*."

A. Kosowsky aptly summarizes what we consider the spirit of this special issue: "Until the predominant picture of dark matter cosmology can explain all of the observations, other competing ideas should be pursued, either as a way of sharpening the case for dark matter cosmology, or, perhaps, uncovering an eventual replacement. . . . We should not allow the successes of our leading theories to blind us to other possibilities."

There is much opportunity for theoretical and observational innovation in the area of dwarf-galaxy cosmology. We asked the authors of our review papers to write them in the style of a tutorial and at a level suitable for beginning graduate students. We hope our special issue will reach a wide audience of graduate students and beginning researchers, in particular since all of the papers, under the open-access model, are accessible free of charge to anyone with a computer and an internet connection.

We would like to thank the members of the editorial board of Advances in Astronomy, the authors and referees of articles submitted to the special issue, and the staff of Hindawi publisher. Without their support and hard work, this special issue would not have come into being.

We hope you will enjoy reading "*Dwarf-galaxy cosmology*."

Regina Schulte-Ladbeck
Ulrich Hopp
Elias Brinks
Andrey Kravtsov

Hindawi Publishing Corporation
Advances in Astronomy
Volume 2010, Article ID 789293, 14 pages
doi:10.1155/2010/789293

Review Article

The Core-Cusp Problem

W. J. G. de Blok

Department of Astronomy, University of Cape Town, Rondebosch 7700, South Africa

Correspondence should be addressed to W. J. G. de Blok, edeblok@ast.uct.ac.za

Received 4 May 2009; Revised 18 August 2009; Accepted 12 October 2009

Academic Editor: Elias Brinks

This paper gives an overview of the attempts to determine the distribution of dark matter in low surface brightness disk and gas-rich dwarf galaxies, both through observations and computer simulations. Observations seem to indicate an approximately constant dark matter density in the inner parts of galaxies, while cosmological computer simulations indicate a steep power-law-like behaviour. This difference has become known as the "core/cusp problem," and it remains one of the unsolved problems in small-scale cosmology.

1. Introduction

Dark matter is one of the main ingredients of the universe. Early optical measurements of the rotation of spiral galaxies indicated the possible presence of large amounts of dark matter in their outer parts (e.g., [1]), though in many cases the rotation curve could also be explained by the stars alone (e.g., [2, 3]). Observations at even larger distances from the galaxy centers, using the 21 cm line of neutral hydrogen, definitively confirmed the mass discrepancy [4–6]. For an extensive review, see Sofue and Rubin [7]. Most of these early observations concentrated on late-type disk galaxies, which all share the property of having an almost constant rotation velocity in their outer parts (the so-called "flat rotation curve"). As the dynamical contribution of the stars and the gas is insufficient to explain the high rotation velocities in the outer parts, this implies that most of the observed rotation there must be due to some other material, the "dark matter." The observed constant velocity suggests that the dark matter in the outer parts of galaxies has a mass density profile closely resembling that of an isothermal sphere, that is, $\rho \sim r^{-2}$.

In the inner parts of galaxies stars are obviously present and they must be the cause of a (possibly large) fraction of the observed rotation velocity. This therefore leads to a transition from the inner parts, where the stars contribute to (and in many cases dominate) the dynamics, to the outer parts where the dark matter is important (e.g., [2, 3, 8, 9]).

The rotation velocity associated with dark matter in the inner parts of disk galaxies is found to rise approximately linearly with radius. This solid-body behaviour can be interpreted as indicating the presence of a central core in the dark matter distribution, spanning a significant fraction of the optical disk. Some authors adopt a nonsingular isothermal sphere to describe this kind of dark matter mass distribution (e.g., [10]), while others prefer a pseudoisothermal sphere (e.g., [11, 12]). Both models describe the data well (see [13]), and by the late 1980s they had become the de facto description of the distribution of dark matter in (gas-rich, late-type) dwarfs and disk galaxies.

In this paper we use the *pseudoisothermal* (PI) sphere to represent the cored models, though this particular choice does not affect any of the discussion in this paper. The mass density distribution of the PI sphere is given by

$$\rho_{\mathrm{PI}}(r) = \frac{\rho_0}{1 + (r/R_C\ )^2}, \tag{1}$$

where ρ_0 is the central density, and R_C is the core radius of the halo. This density distribution leads to an asymptotic flat velocity V_∞ given by $V_\infty = (4\pi G \rho_0 R_C^2)^{1/2}$, where G is the gravitational constant.

In the early 1990s, the first results of numerical N-body simulations of dark matter halos based on the collisionless cold dark matter (CDM) prescription became available. These did not show the observed core-like behaviour in

their inner parts, but were better described by a steep power law mass-density distribution, the so-called *cusp*. Fits to the mass-distributions as derived from these early simulations [14–16] indicated an inner distribution $\rho \sim r^{\alpha}$ with $\alpha = -1$. (In the following we will use α to indicate the inner mass density power law slope.)

The results from these and later simulations are based on the (Λ)CDM paradigm, where most of the mass energy of our universe consists of collisionless CDM in combination with a cosmological constant Λ. This ΛCDM paradigm provides a comprehensive description of the universe at large-scales (as shown most recently by the Wilkinson Microwave Anisotropy Probe (WMAP) results; see [17]). However, despite these great successes, it should be kept in mind that the cusp and the central dark matter distribution are not predicted from first principles by ΛCDM. Rather, these properties are derived from analytical fits made to dark-matter-only numerical simulations. While the quality and quantity of these simulations has improved by orders of magnitude over the years, there is as yet no "cosmological theory" that explains and correctly predicts the distribution of dark matter in galaxies from first principles.

The value $\alpha = -1$ found in the early CDM simulations is very different from that expected in the PI model, where the constant density core ($\rho \sim r^0$) implies $\alpha = 0$. These two cases thus lead to two very different descriptions of the dark matter distribution in galaxies. The "cusp" ($\alpha = -1$) models gives rise to a rapidly increasing "spiky" dark matter density towards the center, while the "core" model ($\alpha = 0$) has an approximately constant dark matter density. The cusp model therefore has a rotation curve that will rise as the square root of the radius, while the core model rotation curve rises in a linear fashion. The difference in shapes between the rotation curves of both models is quite pronounced, and, in principle, it should therefore be possible to identify CDM haloes in real galaxies by measuring their rotation curves.

Over the last 15 years or so, much effort has been put into determining the central mass distribution in galaxies using their rotation curves, and comparing them with the outcomes of ever more sophisticated numerical simulations. To first order, one can summarize this work as observational determinations yielding slopes $\alpha \sim 0$, while simulations produce $\alpha \sim -1$ slopes. This persistent difference is known as the "core/cusp controversy," sometimes also described as "the small-scale crisis in cosmology". The attempts to reconcile the observations and simulations, either by trying to improve them, or by trying to quantify systematic effects or missing physics, are the subjects of this paper. I give a brief overview of past and present work dealing with the determination of the central dark matter density distribution in galaxies, with an emphasis on the observational efforts. An overview like this, touching on many different topics in galaxy evolution, cosmology and computational astrophysics, is never complete, and only a small (but hopefully somewhat representative) fraction of the many papers relevant to this topic can be referred to in the limited space available. The rest of this paper is organised as follows. Section 2 gives a description of the results that numerical simulations have produced over the years. Section 3 deals with the observational determinations of the dark matter density distribution. Section 4 discusses physical scenarios that have been proposed to reconcile the core and cusp distributions. Section 5 briefly summarizes the work discussed.

2. Cold Dark Matter Cusps

The presence of a cusp in the centers of CDM halos is one of the earliest and strongest results derived from cosmological N-body simulations. Dubinski and Carlberg [14] were among the first to investigate the density profiles of CDM halos and found that the inner parts of these simulated halos could be characterized by a power law slope $\alpha = -1$. They did not rule out the existence of central cores but noted that these would have to be smaller than the resolution of their simulations ($\sim$1.4 kpc). Subsequent simulations, at higher and higher resolutions, made the presence of cores in simulated CDM haloes increasingly unlikely.

A systematic study by Navarro et al. [15, 16] of simulated CDM halos, derived assuming many different sets of cosmological parameters, found that the innermost dark matter mass density distribution could be well described by a characteristic $\alpha = -1$ inner slope for all simulated halos, independent of mass, size, or cosmology. A similar general result was found for the outer mass profile, with a steeper slope of $\alpha = -3$. Navarro et al. [16] called this the "universal density profile" and it is described by

$$\rho_{\mathrm{NFW}}(r) = \frac{\rho_i}{(r/R_s)(1 + r/R_s)^2}, \tag{2}$$

where ρ_i is related to the density of the universe at the time of the time of halo collapse and R_s is the characteristic radius of the halo. This kind of profile is also known as the "NFW profile."

The corresponding rotation curve is given by

$$V(r) = \sqrt{\frac{\ln(1+cx) - cx/(1+cx)}{x[\ln(1+c) - c/(1+c)]}}, \tag{3}$$

with $x = r/R_{200}$. This curve is parameterized by a radius R_{200} and a concentration parameter $c = R_{200}/R_s$. Here R_{200} is the radius at which the density contrast with respect to the critical density of the universe exceeds 200, roughly the virial radius; V_{200} is the circular velocity at R_{200} [15]. The parameters c and V_{200} are tightly related through the assumed cosmology. Indeed, one can be expressed as a function of the other, with only a small scatter [18]. That is, the range of (c, V_{200}) combinations that describes "real" CDM rotation curves is tightly constrained by the ΛCDM cosmology.

Simulations by Moore et al. [19] indicated an even steeper inner slope. They found that their simulated halos could be best described by a function

$$\rho_{\mathrm{M99}}(r) = \frac{\rho_i}{(r/R_s)^{1.5}(1 + r/R_s)^{1.5}}, \tag{4}$$

that is, with an inner slope $\alpha = -1.5$ and an outer slope $\alpha = -3$.

The difference between these two results indicated that issues such as numerical convergence, initial conditions, analysis or interpretation could still play a role in defining the inner slope. As ever more powerful computers and increasingly higher resolution simulations became available, the value and behavior of the inner slope of CDM halos has therefore been extensively discussed in the literature. For example, to give but an incomplete listing of the many papers that have appeared on this topic, Klypin et al. [20] derived slopes $\alpha = -1.5$ for their simulated halos. From phase-space density arguments, Taylor and Navarro [21] argue that the density profile should resemble an NFW profile, but converging to an inner slope $\alpha = -0.75$, instead of the $\alpha = -1$ value. Colín et al. [22] investigated low-mass haloes and found that they were best described using NFW profiles (i.e., $\alpha = -1$). Diemand et al. [23] found that CDM halos have cusps with a slope $\alpha \simeq -1.2$.

Many studies assumed that the central cusp consisted of a region, where the mass density behaved as a power law with a constant slope. Navarro et al. [24] and Hayashi et al. [25] suggested that this did not have to be the case. They did not find evidence for an asymptotic power law slope, but instead noted that the slope kept getting shallower towards smaller radii without converging to a single asymptotic value. At the smallest resolved radii they derive slopes of ~ -1.2 for "galaxy-sized" halos (as measured at $\sim$1.3 kpc), and ~ -1.35 for "dwarf galaxy" halos (as measured at $\sim$0.4 kpc). These values are significantly steeper than the original NFW slope, but not as steep as the Moore et al. [19] value. Navarro et al. [24] introduce a new fitting formula to quantify their results. For reasonable choices of its input parameters, this formula yields an extrapolated slope of $\alpha \sim -0.7$ at $r \sim 0.01$ kpc.

Stoehr [26] also finds a gradual turnover in slope towards smaller radii. Though his simulations formally resolve only radii $\sim$1 kpc (where a slope of $\alpha \sim -1$ is measured), an extrapolation of his favoured fitting function towards smaller radii results in a decreasing slope ending up as a flat slope ($\alpha = 0$) around $r \sim 0.01$ kpc.

Merritt et al. [27] and Graham et al. [28] showed that the density distribution presented in Navarro et al. [24] could be equally well described by a Sérsic function. In the context of CDM halos they refer to this function as an Einasto model. For completeness, this profile is given by

$$\rho_{\mathrm{Ein}}(r) = \rho_e \exp\left(-d_n\left[\left(\frac{r}{r_e}\right)^{1/n} - 1\right]\right), \quad (5)$$

where n determines the shape of the profile, and d_n is a function of n which enables the use of the density ρ_e measured at the effective radius r_e. The latter is defined as the radius of the volume containing half of the total mass. In terms of observationally more accessible quantities this can be written as

$$\rho_{\mathrm{Ein}}(r) = \rho_{-2,\mathrm{Ein}} \exp\left(-2n\left[\left(\frac{r}{r_{-2,\mathrm{Ein}}}\right)^{1/n} - 1\right]\right), \quad (6)$$

where $r_{-2,\mathrm{Ein}}$ is the radius at which the logarithmic derivative of the density profile equals -2, and $\rho_{-2,\mathrm{Ein}}$ is the density at that radius. The two versions of radius and density are related by $\rho_{-2,\mathrm{Ein}} = \rho_e \exp(d_n - 2n)$ and $r_{-2,\mathrm{Ein}} = (2n/d_n)^n r_e$.

A further discussion of this model is beyond the scope of this paper, except to note that for typical parameterisations of CDM galaxy halos one derives a slope of $\alpha \sim -1.3 \pm 0.2$ at a radius of 1 kpc and of $\alpha \simeq -0.9 \pm 0.2$ at a radius of 0.1 kpc. The precise values depend on the exact values of n and r_{-2}; the values just listed assume $4 < n < 8$ and $r_{-2} = 10$ kpc, as shown in Graham et al. [28]. (Less steep slope values listed in the same paper are derived assuming $r_{-2} = 100$ kpc and are thus more appropriate for giant or group-sized CDM halos.)

Amongst the highest resolution measurements of the inner slope of CDM halos so far are those by Navarro et al. [29] and Stadel et al. [30]. The former were done as part of the Acquarius project [31]. Navarro et al. [29] found no convergence to a single asymptotic slope. Rather, as before, the slope keeps decreasing with decreasing radius. At $r = 0.1$ kpc, which is approximately the smallest reliably resolved radius, the slope has a value $\alpha \simeq -0.85$. At $r = 1$ kpc the value is $\alpha \simeq -1.4$. An Einasto profile with $n = 5.9$ provides a good fit to the change in slope with radius.

In an independent, but equally detailed simulation, Stadel et al. [30] find a similar behavior, as well as comparable slope values. They quote a slope $\alpha = -0.8$ at 120 pc, and $\alpha = -1.4$ at 2 kpc.

Even though the details of the simulations, the analytical fits and the interpretation and analysis differ, we can still draw some conclusions from the previous discussion. All simulations and fitting functions considered here produce slopes $\alpha \lesssim -1$ at a radius of 1 kpc. At radii less than 1 kpc the most recent simulations tend to produce slightly more shallow slopes where a typical value seems to be $\alpha \simeq -0.8$ at 0.1 kpc. From an observer's perspective, all models described here produce slopes $\alpha \sim -0.8$ or steeper at the smallest observationally accessible radii, and will thus all produce results very similar to those derived using a "standard" NFW profile. In the simulations, radii less than 0.1 kpc cannot yet be reliably resolved, and the values of the slope derived there depend on the validity of the assumed analytical fitting function.

3. Observations

3.1. Early Measurements. The first comparisons of the HI rotation curves of gas-rich dwarf galaxies with those predicted by CDM profiles were presented in Moore [32] and Flores and Primack [33]. The dynamics of these galaxies are dominated by dark matter, and they are therefore thought to be good probes of its distribution. Both studies note a large discrepancy between the observed rotation velocities and those predicted, especially in the inner parts. They show that the PI model gives a superior description, implying that the halos of these late-type dwarf galaxies are best characterized by an approximately constant-density core. Moore [32] briefly addresses some of the observational uncertainties that might affect the data, such as resolution, projection effects due to inclination, and the effects of pressure support, and concludes that they are not significant enough to affect

the results. He also notes that it is conceivable that, during the galaxy formation process, gas settling in the halo will have affected the dark matter distribution. Usually this is thought to take place in the form of a process called "adiabatic contraction" [34], which has the effect of contracting the inner dark matter distribution (increasing the density). If currently derived halo properties are the result of this process, then the initial halos must have been of even lower density, exacerbating the discrepancy.

Navarro et al. [35] argue that baryonic processes might be the cause of the observed core distribution. They use N-body simulations to model the effect of star formation on the baryons and the dark matter, and find that a central dark matter core can be created if a large fraction of the baryons is suddenly expelled into the halo. They estimate that star formation rates of up to 10 $M_\odot$ yr^{-1} are needed over a dynamical time scale of a galaxy for the process to have the desired impact.

After analysing the same four dwarf galaxies that Moore [32] investigated, Burkert [36] comes to the conclusion that their rotation curves, after appropriate scaling, are self-similar (see also [37]). He notes that it is unlikely that baryonic blow-outs and mass-flows can cause this kind of behaviour, unless fine-tuned, and attributes the slow rise of the rotation curve to the intrinsic properties of the dark matter (i.e., a dark matter core). He also finds tentative evidence that the mass density in the outer parts of these dwarfs drops off as r^{-3} (consistent with CDM), and not with r^{-2} (as suggested by the asymptotically flat rotation curves of spiral galaxies). Based on this, he introduces what has since become known as the "Burkert-profile":

$$\rho_{\mathrm{Bur}} = \frac{\rho_0 r_0^3}{(r + r_0)(r^2 + r_0^2)}, \tag{7}$$

with ρ_0 the central density, and r_0 the scale radius, similar to the core radius R_C of the PI model. This model is thus characterised by $\alpha = 0$ in the inner parts, and $\alpha = -3$ in the outer parts.

A paper by Gelato and Sommer-Larsen [38] presents a more detailed analysis of the baryonic blow-out process and its impact on the halo structure. They attempt to reproduce the observed rotation curve of DDO 154 by simulating NFW halos, and subjecting them to the effect of violent gas outflows, which are simulated by suddenly changing the disk potential in the simulations. In order for the final rotation curve to resemble the observed curve, they need to suddenly blow out 33 to 75 percent of the initial disk material. They note that they can reproduce the rotation curve of DDO 154 for a rather wide range of blow-out scenarios, and suggest that the fine-tuning argument put forward by Burkert [36] may not be applicable.

The blow-out process immediately gives rise to a number of observational consequences. Firstly, a period of star formation intense enough to blow out the majority of the baryons should leave behind a substantial (by now) old stellar population. In practice, however, these dwarfs are seen to be dominated by a young stellar population. Is there a discrepancy here? Secondly, what happens to the baryons that are blown out? Do they stay in the halo? Presumably they will be in the form of hot gas. Is this hot gas detectable? Or, if the gas cools down, can we see it raining back on the disk? Discussing these questions in detail is beyond the scope of this paper, but note that there are a number of starbursting dwarf galaxies in our local universe where one can attempt to study these phenomena directly. As an example, Ott et al. [39] analyse the properties of the hot and cold gas in 8 dwarf galaxies that are in a starburst phase. They show that outflows of hot gas are possible, but also that the presence of (tidal) cold gas can again confine the hot gas. In the galaxies in their sample, approximately 1 percent of the total ISM is in the form of hot, coronal gas. The outflows are found to be efficient in removing hot, metal-rich gas. Whether these processes can, in the early universe, also remove the bulk of the ISM is still an open question. It is clear that with this kind of analysis we are no longer in the realm of cosmology, but are dealing with "messy" astrophysics.

Fortunately, there is an alternative way to study the dark matter distribution. Navarro et al. [35] already note that the blow-out process can only be effective in dwarf galaxies. In more massive galaxies, such as spiral galaxies, the potential well is too deep to efficiently remove the gas. Finding and investigating more massive dark-matter dominated galaxies may therefore be a more effective way to explore the core/cusp issue. These galaxies, fortunately, do exist, and are called Low Surface Brightness (LSB) galaxies.

3.2. LSB Galaxies. The term LSB galaxies is used here to indicate late-type, gas-rich, dark-matter-dominated disk galaxies. Their optical component is well described by an exponential disk with an (extrapolated) inclination-corrected central surface brightness fainter than $\mu_{0,B} \sim 23$ mag arcsec^{-2} [40–42]. Despite their low surface brightness, their integrated luminosity is a few magnitudes brighter than that of late-type dwarf galaxies ($M_B \sim -18$ to ~ -20 for LSB galaxies, as opposed to $M_B \gtrsim -16$ for the dwarf galaxies). As noted, they are gas-rich ($M_{\mathrm{HI}}/L_B \gtrsim 1$; see [43–45]), and their interstellar medium has a low metallicity [46, 47]. Their optical appearance is dominated by an exponential disk with a young, blue population, with little evidence for a dominant old population. Additionally, these galaxies do not have large dominant bulges, and seem to have had a star formation history with only sporadic star formation [48–50]. Central light concentrations, if present at all, tend to be only fractionally brighter than that of the extrapolated exponential disk. In terms of their spatial distribution, they are found on the outskirts of the large-scale structure filaments [51, 52]. In short, most observational evidence indicates that these galaxies have had a quiescent evolution, with little evidence for major merging episodes, interactions, or other processes that might have stirred up the baryonic and dark matter (see also [53, 54]).

As for the term "LSB galaxies," there is some confusion in the literature about what type of galaxies it applies to. The type of LSB galaxies most commonly studied, in particular with regards to the core/cusp controversy, are the late-type LSB galaxies whose properties are described previously.

The other type of LSB galaxies often discussed in the literature is the massive, early-type, bulge-dominated LSB galaxies. These galaxies have properties entirely different from the late-type LSB galaxies [55, 56]. The massive LSB galaxies are a lot more luminous and their optical appearance is dominated by a bright central bulge with a clearly detectable old population [57]. Many of them have low-level AGN activity [58]. All indications are that the evolution of these galaxies has been entirely different from that of late-type LSB galaxies; if anything, they resemble S0 galaxies with extended disks, rather than late-type galaxies. The presence of the dominant bulge also indicates that their central dynamics are likely to be dominated by the stars, rather than dark matter. In the following, the term "LSB galaxies" therefore refers to late-type LSB galaxies only.

3.3. Early HI Observations of LSB Galaxies. The first detailed studies of large samples of LSB galaxies soon led to the picture of them being unevolved, gas-rich disk galaxies, as described previously. The observation that they followed the same Tully-Fisher relation as normal galaxies [59] was intriguing, as this implied they had to be dark-matter dominated. Follow-up radio synthesis observations in HI [60] soon confirmed this. Though the resolution of these early observations was limited, the derived rotation curves clearly resembled those of late-type dwarf and "normal" disk galaxies: a slow rise, followed by a gradual flattening. When expressed in terms of scale lengths, the rotation curves of LSB and HSB galaxies of equal luminosity turned out to be very similar, indicating that LSB galaxies are in general low density objects [61].

Mass models derived using the rotation curves clearly showed that for reasonable assumptions for the stellar mass-to-light ratio, $\Upsilon_\star$, the dynamics of LSB galaxies had to be dominated by dark matter [62]. Assuming that the stars had to dominate the dynamics in the inner parts (the so-called maximum disk solution) led to unrealistically high $\Upsilon_\star$ values, and, even when taken at face value, still showed a need for a moderate amount of dark matter at small radii (see also [63]).

The distribution of the dark matter at first sight seemed similar to that in gas-rich dwarf galaxies [62]. Because of the limited resolution of the data, de Blok and McGaugh [62] did not attempt fits with the NFW model, but noted that the halos had to be extended, diffuse and low density.

A first attempt at comparing the HI data with CDM predictions was made by McGaugh and de Blok [63]. Rather than making fits to the rotation curve, they simply assumed that the typical velocity V_{200} of the halo had to equal the outer (maximum) rotation velocity of the galaxy. The strict cosmological relation between c and V_{200} then automatically yields a value of c compatible with ΛCDM. Adopting these values, the resulting halo rotation curve turned out to be very different from the observed curve, in a similar way as the Moore [32] analysis; the NFW curve is too steep and rises too quickly in the inner parts. The only way the halo curve could be made to resemble the observed curve, was by abandoning the cosmological (c, V_{200}) relation.

Similar conclusions were derived by Côté et al. [64]. They presented high-resolution HI observations of dwarfs in the nearby Centaurus and Sculptor groups, and noted that the derived rotation curves did not agree with the NFW model.

A possible explanation that was soon put forward was that there were still unrecognized systematic effects in the data, that would give the false impression of a core-like behaviour. Initially, attention was focussed on the resolution of the de Blok et al. [60] HI observations. These had beam sizes of $\sim 15''$, resulting in the HI disks of the LSB galaxies investigated having a diameter of between 3 and 18 independent beams. This limited resolution can potentially affect the shapes of the rotation curves through a process called "beam smearing," as also mentioned in de Blok et al. [60]. In observations with limited resolution, the beam smearing process decreases the observed velocities (compared to the true velocities), and in extreme cases can turn any steeply rising rotation curve into a slowly rising solid-body one. This would therefore give the impression of a core being present in the data, while the true distribution could still be cuspy. In their paper, de Blok and McGaugh [62] argued, through modelling of these beam smearing effects, as well as the direct detections of steeply rising rotation curves in the data, that while some beam smearing was indeed present, the effect was not strong enough to completely "hide" the dynamical signature of a cusp, and concluded that the data were consistent with the existence of dark matter cores.

An alternative interpretation was given in van den Bosch et al. [65] who used the de Blok and McGaugh [62] data, along with high-resolution literature rotation curves of a number of late-type "normal" and dwarf galaxies, such as DDO154 and NGC 247. They derived and applied explicit analytical corrections for beam smearing and concluded that the LSB galaxy HI data were consistent with both cored and cuspy halos. In their analysis of the other gas-rich dwarf and late-type galaxies, they found evidence for cores in the dwarf galaxies, but detected a steep mass-density slope—consistent with a cusp—in NGC 247, the one late-type disk galaxy that met their sample selection criteria.

In a related paper, van den Bosch and Swaters [66] derive similar conclusions for a different, larger sample of dwarf galaxies observed in HI as part of the Westerbork HI Survey of Irregular and Spiral Galaxies (WHISP) [67]. They attempt to correct for adiabatic contraction and resolution and conclude that, while in a majority of the galaxies they investigate a core is somewhat preferred in terms of fit quality, they cannot exclude halo models that have a steep inner mass-density slope.

Clearly, with this wide range of (sometimes contradictory) conclusions, obtaining higher resolution data is the only way to put stronger constraints on the exact distribution of dark matter in galaxies.

3.4. Hα Observations. After the initial HI observations, the most efficient way to improve the resolution was by obtaining observations in the Hα line. These usually took the form of long-slit spectra taken along the major axes of the galaxies,

and resulted in an order of magnitude improvement in resolution. Typical observations now had resolutions of a few arcseconds, instead of a few tens of arcseconds.

Some of the first Hα long-slit rotation curves of LSB galaxies were presented by Swaters et al. [68]. They found that the Hα curves indeed did rise somewhat more steeply in the inner parts than the HI curves, and for one or two galaxies very much so, but they noted that on the whole the HI and Hα curves were consistent when the beam smearing effects were taken into account. The Hα curves and corresponding mass models did still indicate that LSB galaxies had to be dominated by dark matter. The curves also still rose less steeply than those of higher surface brightness late-type galaxies of a similar luminosity, as indicated by the agreement between the curves when they were radially scaled using their exponential disk-scale lengths.

A large set of high-resolution, Hα long-slit rotation curves was published and analysed by McGaugh et al. [69], de Blok et al. [70, 71], and de Blok and Bosma [72]. Many of these galaxies had been part of the de Blok and McGaugh [62] sample, and a direct comparison between the Hα and HI rotation curves showed that in the majority of cases, beam smearing effects were present, but not significant enough to alter the previous conclusions regarding the dark matter distribution. In the few cases where there were large differences this could be explained by inclination effects or elliptical beam shapes in the HI observations.

The Hα curves thus showed that the inner, slowly rising slopes could not be caused by resolution effects. This meant that for reasonable (stellar population synthesis inspired) $\Upsilon_\star$ values, LSB galaxies were still dark matter dominated throughout their disk, even though the Hα curves formally allowed maximum disk fits with even higher $\Upsilon_\star$ values than the HI observations did. These high values are, however, completely at odds with the observed colours and star formation histories, and still imply a significant dark matter fraction.

Comparison of mass models assuming PI and NFW models showed that the data were better described by the PI models. In many cases, NFW models did yield reasonable fits, but usually with very low concentrations and high V_{200} values, inconsistent with the cosmological (c, V_{200}) relation. Taken at face-value these results would imply that the halos of LSB galaxies have barely collapsed, and have typical velocities many times higher than those of the galaxies that inhabit them. The low c-values are, however, due to the intrinsically different shape of the NFW rotation curves compared to the solid-body observed curves. An NFW curve has an inner velocity slope $v \propto r^{1/2}$, and the only way this kind of curve can fit the observed solid-body $v \propto r$ curve is by stretching, resulting in the low c and high V_{200} values.

The observational inner mass density slopes were derived by de Blok et al. [70] and plotted against the resolution (physical radius of the innermost point) of the rotation curve. A comparison with the expected slopes from various halo models showed that the majority of the data scattered towards the predicted slopes of the PI model. They also showed that for resolutions of $\sim$1 kpc the PI and NFW models yielded identical slopes. This would go some way towards explaining why some of the lower resolution HI observations were unable to distinguish between models. The behaviour of the change in slope when going from the lower resolution HI observation to higher resolution Hα observations is consistent with that expected from the PI model, as shown in de Blok and Bosma [72]. Clearly, for unambiguous determinations of the inner mass density slope, resolutions of better than a kpc are needed.

Independent observations and analyses came to similar conclusions. Marchesini et al. [73] obtained long-slit Hα observations of some of the de Blok and McGaugh [62] galaxies, and also found little evidence for strong beam smearing, as well as strong evidence for the existance of dark matter cores. Zackrisson et al. [74] obtained long-slit observations of the rotation curves of six extremely blue and bulge-less LSB galaxies and also finds strong evidence for the presence of cores in the dark matter distribution of these galaxies. Salucci [75] analysed the rotation curves of over a hundred rotation curves of disk galaxies, and found clear signatures for the existence of dark matter cores in these galaxies. This analysis is complementary to the work on LSB galaxies, as it also analyses less dark-matter-dominated galaxies. Borriello and Salucci [76] analysed Hα rotation curves of a number of dark matter dominated galaxies, and also found strong evidence for core-like dark matter distributions. They also fit Burkert haloes to their data and find that these also provide good fits. Analysis for a sample of $\sim$25 spiral galaxies is presented in Donato et al. [77], and leads to similar conclusions. They also find that the core radius of the dark matter distribution is related to the disk-scale length.

Hayashi et al. [25] find that the Hα rotation curves are consistent with steep slopes. de Blok [78] suggests that these conclusions are based on artificial constraints imposed on the fitting functions. Once these constraints are removed, 17 of the 20 galaxies with the highest-quality data are best fitted with cored models. Three are possibly consistent with cuspy models; two of these are high-surface brightness dwarf galaxies that are likely dominated by stars.

3.5. Possible Systematic Effects. At first glance, the observational data seems to provide good evidence for the presence of cores in LSB galaxies. This does of course not exclude the possibility that systematic effects might be present in the data that could give the (false) impression of cores. A number of studies have therefore focused on these effects and asked whether the detected cores could still be consistent with cuspy halo models.

The systematic effects that were investigated fall into two categories.

(1) *Pointing Problems*. If small offsets exist between the central slit position and the true, dynamical center, this will cause the spectrograph slit to miss the cusp. This could be due to inaccurate telescope pointings or, alternatively, if large physical offsets between the dynamical and photometric centers of galaxies exist, the measured slopes will also be biased downwards.

(2) *Noncircular Motions.* The fundamental assumption in the observational analyses discussed so far is that the gas moves on circular orbits. If for some reason the orbits are elliptical, or of the gas motions are disturbed, this will also lead to an underestimate of the slope.

These effects are difficult to recognize in long-slit, one-dimensional Hα data without additional information. Many authors therefore, apart from modeling these effects, also emphasized the need for high-resolution, two-dimensional velocity fields. These make pointing problems irrelevant, while noncircular motions can be directly measured. Fortunately, these velocity fields are now available (see Section 3.6), largely superseding the results derived from the Hα rotation curves. Nevertheless, for completeness, the further analysis of the Hα curves is briefly discussed here.

In de Blok et al. [79] a first attempt was made at modeling the observational systematic effects. Their main conclusion was that NFW halos can be made to resemble dark matter cores only if, either systematic noncircular motions with an amplitude of $\sim$20 km s^{-1} exist in all disks, or systematic telescope pointing offsets of $\sim$3-4$''$ exist for all observations, or if the dynamical and photometric centers are systematically offset in all galaxies by $\sim$0.5–1 kpc.

Marchesini et al. [73] and de Blok and Bosma [72] compare independent sets of observations of the same galaxies, obtained at different telescopes, by independent groups, using independent data sets, and find no evidence for telescope pointing errors. In general, galaxies can be acquired and positioned on the slit with a repeatability accuracy of 0.3$''$ or so.

Using further modeling, de Blok et al. [79] find that a halo model with a mildly cuspy slope $\alpha = -0.2 \pm 0.2$ gives the best description of the data in the presence of realistic observational effects. It is interesting to note that this best-fitting slope had already been derived by Kravtsov et al. [80] on the basis of the de Blok et al. [60] data.

An analysis by Spekkens et al. [81] of long-slit Hα rotation curves of 165 low-mass galaxies comes to the same conclusion. Depending on how they select their sample, they find best-fitting slopes of $\alpha = -0.22 \pm 0.08$ to $\alpha = -0.28 \pm 0.06$. They also model pointing and slit offsets, but come to the conclusion that, after correction, their data are consistent with cuspy haloes. Swaters et al. [82] also present extensive modeling of high-resolution long-slit Hα rotation curves, and show that while their data are consistent with $\alpha = 0$ cores, steeper slopes cannot be ruled out.

Given the difference in interpretation of otherwise similar samples, a double-blind analysis of the modeling performed by the various groups would have been interesting. However, with the availability of high-resolution velocity fields, this is now a moot issue.

Rhee et al. [83] attempt to model many of the observational effects using numerical simulations. Most of their conclusions apply to long-slit observations. The systematic effects they investigate (dealing with inclination effects, noncircular motions and profile shapes) have now been directly tested on high-resolution velocity fields and do not critically affect the data (e.g., [74, 84–89]).

3.6. High-Resolution Velocity Fields. As noted, high-resolution two-dimensional velocity fields provide the context which long-slit observations are missing. With these velocity fields the pointing problem becomes irrelevant, offsets between kinematical and dynamical centers can be directly measured, as can noncircular motions. Following is a brief overview of the various observational studies that have presented and analysed these velocity fields within the context of the core/cusp debate.

Some of the first high-resolution optical velocity fields of late-type dwarf and LSB galaxies were presented by Blais-Ouellette et al. [90]. They analyse Hα Fabry-Perot data of IC 2574 and NGC 3109, two nearby dwarf galaxies, and derive slowly rising rotation curves, consistent with a core. This work was later expanded in Blais-Ouellette et al. [91], and led to the work presented in Spano et al. [92], where optical velocity fields of 36 galaxies of different morphological types are presented. All three studies find that the PI model generally provided better fits than NFW models. If NFW models give fits of comparable quality, then this is usually at the cost of an unrealistically low $\Upsilon_\star$ value and noncosmological (c, V_{200}) values. A similarly large collection of Hα velocity fields is presented in Dicaire et al. [93]. They do not explicitly address the core/cusp issue, but show that when bars are present, their influence on the velocity fields is very noticable.

Kuzio de Naray et al. [88, 89] present DensePak velocity fields of LSB galaxies, many of them taken from the de Blok and McGaugh [62] sample. Their conclusions are that NFW models provide a worse fit than PI models, for all values of $\Upsilon_\star$. Where an NFW model could be fit, the c-values generally again do not match the cosmological CDM (c, V_{200}) relation. They introduce a "cusp mass excess." When the predicted (c, V_{200}) relation is assumed, and the V_{200} velocities are matched with those in the outermost observed velocities, the inner parts require about $\sim$2 times more dark matter mass than is implied by the observed rotation curves.

Kuzio de Naray et al. [88, 89] also explore noncircular motions. They find that random velocities with an amplitude of $\sim$20 km s^{-1} are needed to bring the observed curves in agreement with the CDM predictions. A comparison of simulated long-slit observations (extracted from the velocity fields) with the original long-slit data from McGaugh et al. [69] and de Blok and Bosma [72] shows good agreement.

Swaters et al. [94] present a DensePak velocity field of the late-type dwarf galaxy DDO 39. They derive a rotation curve, and show that its slope is steeper than implied by lower resolution HI data, and also different from earlier long-slit data from de Blok and Bosma [72]. They indicate that measurable noncircular motions are present, but do not explicitly quantify them. They show fit results for NFW halos, but do not show the corresponding results for a core model, so further comparisons are difficult to make.

Weldrake et al. [95] present the HI velocity field of NGC 6822, a nearby Local Group dwarf galaxy. Their data have a linear resolution of about 20 pc, so beam smearing is definitely not a problem. The rotation curve shows a strong preference for a core-like model, but they do not quantify possible noncircular motions. Salucci et al. [96] present

similarly high-resolution HI data (including VLA B array) of the dwarf galaxy DDO 47. Their analysis shows the dynamics are not consistent with a cusp. Similar results are derived in Gentile et al. [97] for a number of spiral galaxies.

Simon et al. [98] present results from CO and Hα velocity fields of 5 low-mass dark-matter-dominated galaxies (see also [99, 100]). They derive a range of slopes, from core-like ($\alpha = -0.01$ for NGC 2976) to cuspy ($\alpha = -1.20$ for NGC 5963). Note that NGC 5963 has an inner bright disk, and it may therefore not be dark-matter-dominated all the way to the center, making the value of its mass-density slope uncertain (see also [101]). The average slope they derive is $\alpha = -0.73 \pm 0.44$. Their analysis method differs in a few aspects from the other studies referenced in this paper. Firstly, their inner slope values are derived from a single power law fit to the entire rotation curve. Most of their models do not take into account the gas component due to a lack of HI observations. In low-mass galaxies the gas can dynamically be more important than the stars (especially in the outer parts), and correcting for this component could potentially change the derived slopes.

More importantly, the mass models in Simon et al. [98] are derived under the explicit assumption of a constant inclination and position angle for each galaxy. Most velocity fields of nearby galaxies show radial inclination and position angle trends, especially in the outer parts (e.g., [87]). Simon et al. [98] attribute these to radial velocities that give the impression of changes in inclination and position angle. Nevertheless, the noncircular velocities derived in this way are typically less than $\sim 20\,\mathrm{km\,s^{-1}}$, and in a few galaxies less than $\sim 5\,\mathrm{km\,s^{-1}}$. Whether these velocities are real or whether inclination and position angle changes are preferred would be an interesting topic of further study. Simon et al. [98] also derive harmonic decompositions of the velocity fields to study noncircular motions, but they do not list the values of the harmonic coefficients. It would be similarly interesting to compare these with results derived for other disk and LSB galaxies.

Direct measurements of noncircular motions are presented in Gentile et al. [84]. Using high-resolution HI observations, they make a harmonic decomposition of the velocity field, and show that noncircular motions are only present at the level of a few km $\mathrm{s^{-1}}$. This is a factor of ~ 10 lower than what is needed for the noncircular motions to wipe out the kinematical signature of a cusp and to give the impression of a core.

An analysis by Gentile et al. [102] of another gas-rich dwarf galaxy, NGC 3741, based on the entire 3D HI data cube, showed noncircular motions around $5-10\,\mathrm{km\ s^{-1}}$, and a strong preference for a core model. NFW models could be accommodated, but with the usual caveat of the fit parameters not being consistent with the cosmological (c, V_{200}) relation.

Trachternach et al. [85] present harmonic decompositions of the velocity fields of galaxies from The HI Nearby Galaxy Survey (THINGS; [103]). The THINGS survey covers a large range in galaxy properties, from luminous early-type disk galaxies to late-type dwarfs. Trachternach et al. [85] find a relation between the median strength of the noncircular motions and the luminosity of the galaxies, indicating that the noncircular motions are associated with the baryons. Luminous disk galaxies have noncircular motions up to $\sim 30\,\mathrm{km\,s^{-1}}$, mostly associated with bars and spiral arms. These then decrease rapidly to a level of only a few km $\mathrm{s^{-1}}$ for dwarf galaxies like DDO 154. They also found that offsets between photometric and kinematic centers were typically ~ 200 pc or less.

This low level of noncircular motions seems inconsistent with observations by Pizzella et al. [104], who find significant noncircular motions in a sample of 4 LSB galaxies. However, their galaxies all contain bright bulges and are therefore probably more representative of the class of giant LSB galaxies, rather than the late-type ones discussed in this paper (in this regard see also [105]).

Finally, McGaugh et al. [106] and Gentile et al. [107] show that the core/cusp issue is not limited to the very inner parts of galaxies. As mentioned before, the shape of the NFW curve is fundamentally different from that of observed curves. One can try and work out the implications in two ways. McGaugh et al. [106] match the observed outer rotation velocities with those of corresponding cosmological NFW halos (effectively identifying NFW halos that have a similar dark matter density at these outer radii as real galaxies), and find that these halos are too massive. Due to the cusp mass excess their average density is then also a factor of 2-3 too high (see also [87]). Gentile et al. [107] take a different approach and identify halos that have the same enclosed mass as observed galaxies. Again, due to the cusp mass excess, this results in halos that, compared to what can be derived for real galaxies, are more dense in the center and less dense in the outer parts. Due to the fundamentally different shapes of the mass distributions, the core/cusp issue is therefore not limited to the inner parts, but is relevant at all radii.

4. Effects of Baryons and Triaxiality

The high-resolution velocity fields thus seem to indicate mass distributions that are cored. As many observational effects such as pointing, center offsets, and even noncircular motions seem to be too small to be the cause of the observed cores, many studies have attempted to explain the apparent presence of cores as the result of processes such as interactions between and merging of dark matter halos, or the effect of baryons on the dark matter distribution. Following is a brief discussion of some of these effects.

4.1. Feedback and Merging. It was already noted that violent, large-scale star formation might be able to explain the cores in gas-rich dwarf galaxies, but not in more massive galaxies [15]. The implied large bursts of star formation are also not consistent with the quiescent evolution of LSB galaxies. An alternative way to achieve the removal of the cusp was proposed by Weinberg and Katz [108]. They model a rotating rigid bar in a disk which is embedded in a CDM halo and show that this bar creates a wake in the dark matter. This trailing wake slows down the bar, transferring some of the bar

angular momentum to the dark matter. This "puffs up" the dark matter distribution thus forming a core. Recent numerical simulation work by Dubinski et al. [109] does, however, suggest that the bar does not destroy the central cusp, and may even increase the halo density slightly.

A very detailed case study of the effects of bars and feedback is presented in Valenzuela et al. [110]. They attempt to reproduce the observed rotation curves of NGC 6822 and NGC 3109 using NFW halos and a variety of feedback effects and noncircular motions. They present numerical models including gas dynamics, and tune them to resemble the two target galaxies. Whilst they succeed in matching the rotation curves, it is not clear whether these results can be generalized, due to, for example, the different assumptions that are made in determining inclinations and position angles of the models, compared to the data. Although the authors present simulated velocity fields, they do not make a direct comparison between observed and simulated velocity fields, which would provide much additional information on the bar and feedback effects.

Dekel et al. [111, 112] argue that merging of cuspy halos inevitably leads to a cusp. The only way to prevent this from happening is to puff up the dark matter distribution of the infalling halos before they merge. This way the halos get disrupted more easily and a core-like distribution can be gradually built up. The authors describe the scenario as speculative, however, and note that it is unlikely that supernovae will be able to cause the puffing up for any galaxy with $V > 100\,\mathrm{km\ s^{-1}}$. Boylan-Kolchin and Ma [113] show that for this process to work, none of the merging halos can be cuspy to start with, as only mergers between cored halos give a cored merger product. Any merger involving a cusp inevitably leads to a cuspy end-product. Dehnen [114] also shows that the final slope always equals that of the steepest component. Setting up cored halos and ensuring that they remain cored is apparently not trivial.

4.2. Dynamical Friction. El-Zant et al. [115] propose a different way to make halos cored; they note that merging gas clouds of $\sim 10^5\ M_\odot$ (for dwarfs) to $\sim 10^8\ M_\odot$ (for spirals) can disrupt cusps through dynamical friction. If this happens early enough in the universe (when halos were smaller), this process could be very efficient. Similar scenarios are presented in Tonini et al. [116]. Romano-Díaz et al. [117] in their study also argue that the effect of the baryons on the halo structure must be significant. They suggest that in the presence of baryons, initially a very steep cusp is formed (with $\alpha \sim -2$), which is then heated by subhalos through dynamical friction, and, subsequently, from the inside out becomes shallower. According to their analysis, the end result is a density profile that is less steep than $\alpha = -1$ in the inner few kpc, and may even be cored in the very center.

Jardel and Sellwood [118] take the opposite view. They model the dynamical friction process, but argue that it is difficult to find "free-floating" baryon clumps massive enough to make this process happen, as these clumps must not be associated with dark matter (due to the cusp that will then be formed; see what is mentioned before). They note that work by Kaufmann et al. [119] implies clump masses that are two orders of magnitude too small.

The processes just described are similar to those proposed by Mashchenko et al. [120, 121]; see also Ricotti and Wilkinson [122]. They make it all happen in the early universe, when mass scales and the required amount of baryons were both smaller. Their numerical simulations suggest that cusps can be erased in the very early universe ($z \lesssim 10$) when (proto-) galaxies had approximately the size of the HI holes and shells observed in the disks of present-day, gas-rich spiral and dwarf galaxies. In objects that small, a random motion of only $\sim 7\,\mathrm{km\ s^{-1}}$ (i.e., equal to the HI velocity dispersion observed in local disk galaxies) is sufficient to disrupt the cusp and keep the halos cored until the present day. Note though that in a recent analysis, Ceverino and Klypin [123] perform similar calculations, but find that halos remain cuspy, and suggest that differences in the simulation approach might be responsible for this.

Chen and McGaugh [124] also argue against the idea of creating cores at high redshift. Their argument is that cuspy halos cannot explain gravitational lensing results, but demand halos with an even steeper mass distribution (a singular isothermal sphere with slope $\alpha = -2$). This means that if the halos of the elliptical galaxies that do the lensing indeed form with NFW-like profiles, these need to steepen over the course of their evolution, using some process for which the quiescent adiabatic contraction is the most likely candidate. LSB galaxies, on the other hand, need to experience vigorous bursts of early star formation that drive feedback to erase the initial cusp. These scenarios are at odds with what we know about the evolution of these galaxies; ellipticals typically undergo a large amount of merging, with the associated vigorous star formation, as evidenced by their extensive old stellar populations. LSB galaxies show no evidence at all for any kind of violent interactions, nor intense star formation. Dynamical friction and adiabatic contraction thus seem to place demands on the evolution of elliptical and LSB galaxies contrary to what can be derived from their star formation histories.

4.3. Triaxiality. Hayashi and Navarro [125] and Hayashi et al. [126] show that introducing an elliptical disturbance in an NFW potential can lead to systematic (noncircular) motions that, when unrecognized, could be interpreted as evidence for a core. Their arguments particularly apply to long-slit Hα observations, where indeed the context of a velocity field is not available to gauge the validity of the circular motion assumption. As described earlier, work on high-resolution velocity fields by Gentile et al. [84], Trachternach et al. [85], and Kuzio de Naray et al. [89] has put significant observational constraints on the strength of noncircular motions and the ellipticity of the (equatorial) potential. For a large sample of disk and dwarf galaxies, this potential is consistent with being round and the noncircular motions are too small to give the illusion of cores in long-slit observations.

The results from Hayashi and Navarro [125], and Hayashi et al. [126] assume massless disks. Bailin et al. [127]

present results from simulations of self-consistent massive disks in triaxial halos and find that the baryons circularize the potential rapidly, even for low-mass disks, thus wiping out a large part of the triaxiality signal. Widrow [128] also presents models of "live" disks in triaxial halos, and can approximate an observed LSB rotation curve by introducing triaxiality in the halo.

In all these studies it would be interesting to compare simulated velocity fields with the observed ones. As has become clear from the preceding discussion, modeling the long-slit rotation curves leaves too many ambiguities which only studies of the velocity fields can address. In an observational study, Kuzio de Naray et al. [89] subject model NFW velocity fields to the DensePak observing procedure, and show that even in the presence of observational uncertainties the signature of an NFW velocity field can be observed.

They show that axisymmetric NFW velocity fields are unable to reproduce the observed velocity fields for any combination of inclination and viewing angle. They derive NFW velocity fields in an elliptical potential, and show that the only way these can be made to resemble the observations is by having the observer's line of sight along the minor axis of the potential for 6 out of the 7 galaxies investigated, inconsistent with a random distribution of the line of sight.

Kuzio de Naray et al. [89] also note that the kind of rapidly varying ellipticity of the potential as proposed by Hayashi et al. [126] might help in better describing the data, but that the problem of a preferred viewing angle will remain. For an elliptical potential with a random viewing angle, one also expects, once in a while, to observe a rotation curve that is steeper than the corresponding axisymmetric NFW profile. Rotation curves like that are, however, exceedingly rare, if not absent, in the available observations.

5. Summary

Rotation curves of LSB and late-type, gas-rich dwarf galaxies indicate the presence of constant-density or mildy cuspy ($\alpha \sim -0.2$) dark matter cores, contradicting the predictions of cosmological simulations. The most recent simulations still indicate resolved mass density slopes that are too steep to be easily reconciled with the observations (typically $\alpha \sim -0.8$ at a radius ~ 0.1 kpc). Claims of shallow slopes at even smaller radii depend on the validity of the analytical description chosen for the mass-density profile.

Whereas early HI observations and long-slit Hα rotation curves still left some room for observational (pointing, resolution) or physical (noncircular motions, triaxiality) systematic effects to create the illusion of cores in the presence of a cuspy mass distribution, the high-resolution optical and HI velocity fields that have since become available significantly reduce the potential impact of these effects. Measured noncircular motions and potential ellipticities are too small to create the illusion of a core in an intrinsically cuspy halo.

This indicates either that halos did not have cusps to begin with, or that an as yet not understood subtle interplay between dark matter and baryons wipes out the cusp, where the quiescent evolution of LSB galaxies severely limits the form this interplay can take. Adiabatic contraction and dynamical friction yield contradictory results, while models of massless disks in triaxial halos result in preferred viewing directions. LSB galaxy disks, despite their low $\Upsilon_\star$ values, are not entirely massless, and observations and simulations will need to take this into account. Similarly, the difficulties in reconciling a possible underlying triaxial potential with the circularizing effects of the baryons also needs to be investigated. In short, studies which, constrained and informed by the high-quality observations now available, self-consistently describe and model the interactions between the dark matter and the baryons in a cosmological context are likely the way forward in resolving the core/cusp problem.

Acknowledgments

The author thank the anonymous referees for the constructive comments. His work is based upon research supported by the South African Research Chairs Initiative of the Department of Science and Technology and National Research Foundation.

References

[1] V. C. Rubin, N. Thonnard, and W. K. Ford, "Extended rotation curves of high-luminosity spiral galaxies. iv - systematic dynamical properties, sa through sc," *The Astrophysical Journal*, vol. 225, p. L107, 1978.

[2] A. Kalnajs, "Mass distribution and dark halos," in *Internal Kinematics and Dynamics of Galaxies*, Proceedings of the Symposium no. 100, p. 87, 1983.

[3] S. M. Kent, "Dark matter in spiral galaxies—I: galaxies with optical rotation curves," *Astronomical Journal*, vol. 91, pp. 1301–1327, 1986.

[4] A. Bosma, *The distribution and kinematics of neutral hydrogen in spiral galaxies of various morphological types*, Ph.D. thesis, University of Groningen, Groningen, The Netherlands, 1978.

[5] A. Bosma, "21-cm line studies of spiral galaxies—I: observations of the galaxies NGC 5033, 3198, 5055, 2841, and 7331," *Astronomical Journal*, vol. 86, pp. 1791–1846, 1981.

[6] A. Bosma, "21-cm line studies of spiral galaxies—II: the distribution and kinematics of neutral hydrogen in spiral galaxies of various morphological types," *Astronomical Journal*, vol. 86, pp. 1825–1846, 1981.

[7] Y. Sofue and V. Rubin, "Rotation curves of spiral galaxies," *Annual Review of Astronomy and Astrophysics*, vol. 39, no. 1, pp. 137–174, 2001.

[8] S. M. Kent, "Dark matter in spiral galaxies—II: galaxies with H I rotation curves," *Astronomical Journal*, vol. 93, pp. 816–832, 1987.

[9] T. S. van Albada and R. Sancisi, "Dark matter in spiral galaxies [and discussion]," *Philosophical Transactions of the Royal Society A*, vol. 320, no. 1556, pp. 447–464, 1986.

[10] E. Athanassoula, A. Bosma, and S. Papaioannou, "Halo parameters of spiral galaxies," *Astronomy & Astrophysics*, vol. 179, no. 1-2, pp. 23–40, 1987.

[11] K. G. Begeman, A. H. Broeils, and R. H. Sanders, "Extended rotation curves of spiral galaxies—dark haloes and modified dynamics," *Monthly Notices of the Royal Astronomical Society*, vol. 249, p. 523, 1991.

[12] A. H. Broeils, *Dark and Visible Matter in Spiral Galaxies*, Ph.D. thesis, University of Groningen, Groningen, The Netherlands, 1992.

[13] J. Kormendy and K. C. Freeman, "Scaling laws for dark matter halos in late-type and dwarf spheroidal galaxies," in *Dark Matter in Galaxies*, International Astronomical Union Symposium no. 220, pp. 377–397, 2004.

[14] J. Dubinski and R. G. Carlberg, "The structure of cold dark matter halos," *The Astrophysical Journal*, vol. 378, no. 2, pp. 496–503, 1991.

[15] J. F. Navarro, C. S. Frenk, and S. D. M. White, "The structure of cold dark matter halos," *The Astrophysical Journal*, vol. 462, no. 2, pp. 563–575, 1996.

[16] J. F. Navarro, C. S. Frenk, and S. D. M. White, "A universal density profile from hierarchical clustering," *The Astrophysical Journal*, vol. 490, no. 2, pp. 493–508, 1997.

[17] D. N. Spergel, R. Bean, O. Doré, et al., "Three-year Wilkinson Microwave Anisotropy Probe (WMAP) observations: implications for cosmology," *Astrophysical Journal, Supplement Series*, vol. 170, no. 2, pp. 377–408, 2007.

[18] J. S. Bullock, T. S. Kolatt, Y. Sigad, et al., "Profiles of dark haloes: evolution, scatter and environment," *Monthly Notices of the Royal Astronomical Society*, vol. 321, no. 3, pp. 559–575, 2001.

[19] B. Moore, T. Quinn, F. Governato, J. Stadel, and G. Lake, "Cold collapse and the core catastrophe," *Monthly Notices of the Royal Astronomical Society*, vol. 310, no. 4, pp. 1147–1152, 1999.

[20] A. Klypin, A. V. Kravtsov, J. S. Bullock, and J. R. Primack, "Resolving the structure of cold dark matter halos," *The Astrophysical Journal*, vol. 554, no. 2, pp. 903–915, 2001.

[21] J. E. Taylor and J. F. Navarro, "The phase-space density profiles of cold dark matter halos," *The Astrophysical Journal*, vol. 563, no. 2, pp. 483–488, 2001.

[22] P. Colín, A. Klypin, O. Valenzuela, and S. Gottlöber, "Dwarf dark matter halos," *The Astrophysical Journal*, vol. 612, no. 1, pp. 50–57, 2004.

[23] J. Diemand, M. Zemp, B. Moore, J. Stadel, and M. Carollo, "Cusps in cold dark matter haloes," *Monthly Notices of the Royal Astronomical Society*, vol. 364, no. 2, pp. 665–673, 2005.

[24] J. F. Navarro, E. Hayashi, C. Power, et al., "The inner structure of ΛCDM haloes—III. Universality and asymptotic slopes," *Monthly Notices of the Royal Astronomical Society*, vol. 349, no. 3, pp. 1039–1051, 2004.

[25] E. Hayashi, J. F. Navarro, C. Power, et al., "The inner structure of ΛCDM haloes—II: halo mass profiles and low surface brightness galaxy rotation curves," *Monthly Notices of the Royal Astronomical Society*, vol. 355, no. 3, pp. 794–812, 2004.

[26] F. Stoehr, "Circular velocity profiles of dark matter haloes," *Monthly Notices of the Royal Astronomical Society*, vol. 365, no. 1, pp. 147–152, 2006.

[27] D. Merritt, J. F. Navarro, A. Ludlow, and A. Jenkins, "A universal density profile for dark and luminous matter?" *The Astrophysical Journal*, vol. 624, no. 2, pp. L85–L88, 2005.

[28] A. W. Graham, D. Merritt, B. Moore, J. Diemand, and B. Terzić, "Empirical models for dark matter halos. II. Inner profile slopes, dynamical profiles, and ρ/σ^3," *Astronomical Journal*, vol. 132, no. 6, pp. 2701–2710, 2006.

[29] J. F. Navarro, A. Ludlow, V. Springel, et al., "The diversity and similarity of cold dark matter halos," arXiv, astro-ph, 2008.

[30] J. Stadel, D. Potter, B. Moore, et al., "Quantifying the heart of darkness with GHALO—a multi-billion particle simulation of our galactic halo," *Monthly Notices of the Royal Astronomical Society*, vol. 398, no. 1, pp. L21–L25.

[31] V. Springel, J. Wang, M. Vogelsberger, et al., "The Aquarius Project: the subhaloes of galactic haloes," *Monthly Notices of the Royal Astronomical Society*, vol. 391, no. 4, pp. 1685–1711, 2008.

[32] B. Moore, "Evidence against dissipation-less dark matter from observations of galaxy haloes," *Nature*, vol. 370, no. 6491, pp. 629–631, 1994.

[33] R. A. Flores and J. R. Primack, "Observational and theoretical constraints on singular dark matter halos," *The Astrophysical Journal*, vol. 427, no. 1, pp. L1–L4, 1994.

[34] G. R. Blumenthal, S. M. Faber, R. Flores, and J. R. Primack, "Contraction of dark matter galactic halos due to baryonic infall," *The Astrophysical Journal*, vol. 301, pp. 27–34, 1986.

[35] J. F. Navarro, V. R. Eke, and C. S. Frenk, "The cores of dwarf galaxy haloes," *Monthly Notices of the Royal Astronomical Society*, vol. 283, no. 3, pp. L72–L78, 1996.

[36] A. Burkert, "The structure of dark matter halos in dwarf galaxies," *The Astrophysical Journal*, vol. 447, no. 1, pp. L25–L28, 1995.

[37] P. Salucci and A. Burkert, "Dark matter scaling relations," *The Astrophysical Journal*, vol. 537, no. 1, pp. L9–L12, 2000.

[38] S. Gelato and J. Sommer-Larsen, "On DDO 154 and cold dark matter halo profiles," *Monthly Notices of the Royal Astronomical Society*, vol. 303, no. 2, pp. 321–328, 1999.

[39] J. Ott, F. Walter, and E. Brinks, "A chandra X-ray survey of nearby dwarf starburst galaxies—II. Starburst properties and outflows," *Monthly Notices of the Royal Astronomical Society*, vol. 358, no. 4, pp. 1453–1471, 2005.

[40] S. S. Mcgaugh and G. D. Bothun, "Structural characteristics and stellar composition of low surface brightness disk galaxies," *Astronomical Journal*, vol. 107, no. 2, pp. 530–542, 1994.

[41] S. S. Mcgaugh, J. M. Schombert, and G. D. Bothun, "The morphology of low surface brightness disk galaxies," *Astronomical Journal*, vol. 109, no. 5, pp. 2019–2033, 1995.

[42] W. J. G. de Blok, J. M. van der Hulst, and G. D. Bothun, "Surface photometry of low surface brightness galaxies," *Monthly Notices of the Royal Astronomical Society*, vol. 274, p. 235, 1995.

[43] J. M. Schombert, G. D. Bothun, S. E. Schneider, and S. S. Mcgaugh, "A catalog of low surface brightness galaxies. List II," *Astronomical Journal*, vol. 103, no. 4, pp. 1107–1133, 1992.

[44] S. S. McGaugh and W. J. G. de Blok, "Gas mass fractions and the evolution of spiral galaxies," *The Astrophysical Journal*, vol. 481, no. 2, pp. 689–702, 1997.

[45] J. M. Schombert, S. S. Mcgaugh, and J. A. Eder, "Gas mass fractions and the evolution of low surface brightness dwarf galaxies," *Astronomical Journal*, vol. 121, no. 5, pp. 2420–2430, 2001.

[46] S. S. Mcgaugh, "Oxygen abundances in low surface brightness disk galaxies," *The Astrophysical Journal*, vol. 426, no. 1, pp. 135–149, 1994.

[47] W. J. G. de Blok and J. M. van der Hulst, "Star formation and the interstellar medium in low surface brightness galaxies: I. Oxygen abundances and abundance gradients in low surface brightness disk galaxies," *Astronomy & Astrophysics*, vol. 335, no. 2, pp. 421–430, 1998.

[48] J. M. van der Hulst, E. D. Skillman, T. R. Smith, G. D. Bothun, S. S. Mcgaugh, and W. J. G. de Blok, "Star formation thresholds in low surface brightness galaxies," *Astronomical Journal*, vol. 106, no. 2, pp. 548–559, 1993.

[49] L. B. van den Hoek, W. J. G. de Blok, J. M. van der Hulst, and T. de Jong, "The evolution of the stellar populations in low surface brightness galaxies," *Astronomy & Astrophysics*, vol. 357, no. 2, pp. 397–413, 2000.

[50] J. P. E. Gerritsen and W. J. G. de Blok, "Star formation and the interstellar medium in low surface brightness galaxies—III: why they are blue, thin and poor in molecular gas," *Astronomy & Astrophysics*, vol. 342, no. 3, pp. 655–664, 1999.

[51] G. D. Bothun, J. M. Schombert, C. D. Impey, D. Sprayberry, and S. S. McGaugh, "The small scale environment of low surface brightness disk galaxies," *Astronomical Journal*, vol. 106, no. 2, pp. 530–547, 1993.

[52] H. J. Mo, S. S. McGaugh, and G. D. Bothun, "Spatial distribution of low surface brightness galaxies," *Monthly Notices of the Royal Astronomical Society*, vol. 267, no. 1, pp. 129–140, 1994.

[53] G. Bothun, C. Impey, and S. McGaugh, "Low-surface-brightness galaxies: hidden galaxies revealed," *Publications of the Astronomical Society of the Pacific*, vol. 109, no. 737, pp. 745–758, 1997.

[54] C. Impey and G. Bothun, "Low surface brightness galaxies," *Annual Review of Astronomy and Astrophysics*, vol. 35, no. 1, pp. 267–307, 1997.

[55] D. Sprayberry, C. D. Impey, G. D. Bothun, and M. J. Irwin, "Properties of the class of giant low surface brightness spiral galaxies," *Astronomical Journal*, vol. 109, no. 2, pp. 558–571, 1995.

[56] T. E. Pickering, C. D. Impey, J. H. van Gorkom, and G. D. Bothun, "Neutral hydrogen distributions and kinematics of giant low surface brightness disk galaxies," *Astronomical Journal*, vol. 114, no. 5, pp. 1858–1882, 1997.

[57] M. Beijersbergen, W. J. G. de Blok, and J. M. van der Hulst, "Surface photometry of bulge dominated low surface brightness galaxies," *Astronomy & Astrophysics*, vol. 351, no. 3, pp. 903–919, 1999.

[58] J. Schombert, "Active galactic nucleus activity in giant, low surface brightness galaxies," *Astronomical Journal*, vol. 116, no. 4, pp. 1650–1656, 1998.

[59] M. A. Zwaan, J. M. van der Hulst, W. J. G. de Blok, and S. S. McGaugh, "The Tully-Fisher relation for low surface brightness galaxies: implications for galaxy evolution," *Monthly Notices of the Royal Astronomical Society*, vol. 273, pp. L35–L38, 1995.

[60] W. J. G. de Blok, S. S. McGaugh, and J. M. van der Hulst, "HI observations of low surface brightness galaxies: probing low-density galaxies," *Monthly Notices of the Royal Astronomical Society*, vol. 283, no. 1, pp. 18–54, 1996.

[61] W. J. G. de Blok and S. S. McGaugh, "Does low surface brightness mean low density?" *The Astrophysical Journal*, vol. 469, pp. L89–L92, 1996.

[62] W. J. G. de Blok and S. S. McGaugh, "The dark and visible matter content of low surface brightness disc galaxies," *Monthly Notices of the Royal Astronomical Society*, vol. 290, no. 3, pp. 533–552, 1997.

[63] S. S. McGaugh and W. J. G. de Blok, "Testing the dark matter hypothesis with low surface brightness galaxies and other evidence," *The Astrophysical Journal*, vol. 499, no. 1, pp. 41–65, 1998.

[64] S. Côté, C. Carignan, and K. C. Freeman, "The various kinematics of dwarf irregular galaxies in nearby groups and their dark matter distributions," *Astronomical Journal*, vol. 120, no. 6, pp. 3027–3059, 2000.

[65] F. C. van den Bosch, B. E. Robertson, J. J. Dalcanton, and W. J. G. de Blok, "Constraints on the structure of dark matter halos from the rotation curves of low surface brightness galaxies," *Astronomical Journal*, vol. 119, no. 4, pp. 1579–1591, 2000.

[66] F. C. van den Bosch and R. A. Swaters, "Dwarf galaxy rotation curves and the core problem of dark matter haloes," *Monthly Notices of the Royal Astronomical Society*, vol. 325, no. 3, pp. 1017–1038, 2001.

[67] J. M. van der Hulst, T. S. van Albada, and R. Sancisi, "The Westerbork HI survey of irregular and spiral galaxies, WHISP," in *Gas and Galaxy Evolution*, vol. 240, p. 451, 2001.

[68] R. A. Swaters, B. F. Madore, and M. Trewhella, "High-resolution rotation curves of low surface brightness galaxies," *The Astrophysical Journal*, vol. 531, no. 2, pp. L107–L110, 2000.

[69] S. S. McGaugh, V. C. Rubin, and W. J. G. de Blok, "High-resolution rotation curves of low surface brightness galaxies. I. Data," *Astronomical Journal*, vol. 122, no. 5, pp. 2381–2395, 2001.

[70] W. J. G. de Blok, S. S. McGaugh, A. Bosma, and V. C. Rubin, "Mass density profiles of low surface brightness galaxies," *The Astrophysical Journal*, vol. 552, no. 1, pp. L23–L26, 2001.

[71] W. J. G. de Blok, S. S. McGaugh, and V. C. Rubin, "High-resolution rotation curves of low surface brightness galaxies. II. Mass models," *Astronomical Journal*, vol. 122, no. 5, pp. 2396–2427, 2001.

[72] W. J. G. de Blok and A. Bosma, "High-resolution rotation curves of low surface brightness galaxies," *Astronomy & Astrophysics*, vol. 385, no. 3, pp. 816–846, 2002.

[73] D. Marchesini, E. D'Onghia, G. Chincarini, et al., "Hα rotation curves: the soft core question," *The Astrophysical Journal*, vol. 575, no. 2, pp. 801–813, 2002.

[74] E. Zackrisson, N. Bergvall, T. Marquart, and G. Östlin, "The dark matter halos of the bluest low surface brightness galaxies," *Astronomy & Astrophysics*, vol. 452, no. 3, pp. 857–868, 2006.

[75] P. Salucci, "The constant-density region of the dark haloes of spiral galaxies," *Monthly Notices of the Royal Astronomical Society*, vol. 320, no. 1, pp. L1–L5, 2001.

[76] A. Borriello and P. Salucci, "The dark matter distribution in disc galaxies," *Monthly Notices of the Royal Astronomical Society*, vol. 323, no. 2, pp. 285–292, 2001.

[77] F. Donato, G. Gentile, and P. Salucci, "Cores of dark matter haloes correlate with stellar scalelengths," *Monthly Notices of the Royal Astronomical Society*, vol. 353, no. 2, pp. L17–L22, 2004.

[78] W. J. G. de Blok, "Halo mass profiles and low surface brightness galaxy rotation curves," *The Astrophysical Journal*, vol. 634, no. 1, pp. 227–238, 2005.

[79] W. J. G. de Blok, A. Bosma, and S. McGaugh, "Simulating observations of dark matter dominated galaxies: towards the optimal halo profile," *Monthly Notices of the Royal Astronomical Society*, vol. 340, no. 2, pp. 657–678, 2003.

[80] A. V. Kravtsov, A. A. Klypin, J. S. Bullock, and J. R. Primack, "The cores of dark matter-dominated galaxies: theory versus observations," *The Astrophysical Journal*, vol. 502, no. 1, pp. 48–58, 1998.

[81] K. Spekkens, R. Giovanelli, and M. P. Haynes, "The CUSP/core problem in galactic halos: long-slit spectra for a large dwarf galaxy sample," *Astronomical Journal*, vol. 129, no. 5, pp. 2119–2137, 2005.

[82] R. A. Swaters, B. F. Madore, F. C. van den Bosch, and M. Balcells, "The central mass distribution in dwarf and low surface brightness galaxies," *The Astrophysical Journal*, vol. 583, no. 2, pp. 732–751, 2003.

[83] G. Rhee, O. Valenzuela, A. Klypin, J. Holtzman, and B. Moorthy, "The rotation curves of dwarf galaxies: a problem for cold dark matter?" *The Astrophysical Journal*, vol. 617, no. 2, pp. 1059–1076, 2004.

[84] G. Gentile, A. Burkert, P. Salucci, U. Klein, and F. Walter, "The dwarf galaxy DDO 47 as a dark matter laboratory: testing cusps hiding in triaxial halos," *The Astrophysical Journal*, vol. 634, no. 2, pp. L145–L148, 2005.

[85] C. Trachternach, W. J. G. de Blok, F. Walter, E. Brinks, and R. C. Kennicutt, "Dynamical centers and noncircular motions in things galaxies: implications for dark matter halos," *Astronomical Journal*, vol. 136, no. 6, pp. 2720–2760, 2008.

[86] S.-H. Oh, W. J. G. de Blok, F. Walter, E. Brinks, and R. C. Kennicutt, "High-resolution dark matter density profiles of things dwarf galaxies: correcting for noncircular motions," *Astronomical Journal*, vol. 136, no. 6, pp. 2761–2781, 2008.

[87] W. J. G. de Blok, F. Walter, E. Brinks, C. Trachternach, S.-H. Oh, and R. C. Kennicutt, "High-resolution rotation curves and galaxy mass models from things," *Astronomical Journal*, vol. 136, no. 6, pp. 2648–2719, 2008.

[88] R. K. de Naray, S. S. McGaugh, and W. J. G. de Blok, "Mass models for low surface brightness galaxies with high-resolution optical velocity fields," *The Astrophysical Journal*, vol. 676, no. 2, pp. 920–943, 2008.

[89] R. Kuzio de Naray, S. S. McGaugh, and J. C. Mihos, "Constraining the NFW potential with observations and modeling of low surface brightness galaxy velocity fields," *The Astrophysical Journal*, vol. 692, pp. 1321–1332, 2009.

[90] S. Blais-Ouellette, P. Amram, and C. Carignan, "Accurate determination of the mass distribution in spiral galaxies. II. Testing the shape of dark halos," *Astronomical Journal*, vol. 121, no. 4, pp. 1952–1964, 2001.

[91] S. Blais-Ouellette, P. Amram, C. Carignan, and R. Swaters, "Accurate determination of the mass distribution in spiral galaxies III. Fabry-Perot imaging spectroscopy of 6 spiral galaxies," *Astronomy & Astrophysics*, vol. 420, no. 1, pp. 147–161, 2004.

[92] M. Spano, M. Marcelin, P. Amram, C. Carignan, B. Epinat, and O. Hernandez, "GHASP: an Hα kinematic survey of spiral and irregular galaxies—V. Dark matter distribution in 36 nearby spiral galaxies," *Monthly Notices of the Royal Astronomical Society*, vol. 383, no. 1, pp. 297–316, 2008.

[93] I. Dicaire, C. Carignan, P. Amram, et al., "Hα kinematics of the spitzer infrared nearby galaxies survey—II," *Monthly Notices of the Royal Astronomical Society*, vol. 385, no. 2, pp. 553–605, 2008.

[94] R. A. Swaters, M. A. W. Verheijen, M. A. Bershady, and D. R. Andersen, "The kinematics in the core of the low surface brightness galaxy DDO 39," *The Astrophysical Journal*, vol. 587, no. 1, pp. L19–L22, 2003.

[95] D. T. F. Weldrake, W. J. G. de Blok, and F. Walter, "A high-resolution rotation curve of NGC 6822: a test-case for cold dark matter," *Monthly Notices of the Royal Astronomical Society*, vol. 340, no. 1, pp. 12–28, 2003.

[96] P. Salucci, F. Walter, and A. Borriello, "ΛCDM and the distribution of dark matter in galaxies: a constant-density halo around DDO 47," *Astronomy & Astrophysics*, vol. 409, no. 1, pp. 53–56, 2003.

[97] G. Gentile, P. Salucci, U. Klein, D. Vergani, and P. Kalberla, "The cored distribution of dark matter in spiral galaxies," *Monthly Notices of the Royal Astronomical Society*, vol. 351, no. 3, pp. 903–922, 2004.

[98] J. D. Simon, A. D. Bolatto, A. Leroy, L. Blitz, and E. L. Gates, "High-resolution measurements of the halos of four dark matter-dominated galaxies: deviations from a universal density profile," *The Astrophysical Journal*, vol. 621, no. 2, pp. 757–776, 2005.

[99] J. D. Simon, A. D. Bolatto, A. Leroy, and L. Blitz, "High-resolution measurements of the dark matter halo of NGC 2976: evidence for a shallow density profile," *The Astrophysical Journal*, vol. 596, no. 2, pp. 957–981, 2003.

[100] A. D. Bolatto, J. D. Simon, A. Leroy, and L. Blitz, "The density profile of the dark matter halo of NGC 4605," *The Astrophysical Journal*, vol. 565, no. 1, pp. 238–243, 2002.

[101] A. Bosma, E. Athanassoula, and J. M. van der Hulst, "A 21-cm line study of ngc 5963, an sc galaxy with a low-surface brightness disk," *Astronomy & Astrophysics*, vol. 198, p. 100, 1988.

[102] G. Gentile, P. Salucci, U. Klein, and G. L. Granato, "NGC 3741: the dark halo profile from the most extended rotation curve," *Monthly Notices of the Royal Astronomical Society*, vol. 375, no. 1, pp. 199–212, 2007.

[103] F. Walter, E. Brinks, W. J. G. de Blok, et al., "Things: the Hi nearby galaxy survay," *Astronomical Journal*, vol. 136, no. 6, pp. 2563–2647, 2008.

[104] A. Pizzella, D. Tamburro, M. Corsini, and F. Bertola, "Detection of non-ordered central gas motions in a sample of four low surface brightness galaxies," *Astronomy & Astrophysics*, vol. 482, no. 1, pp. 53–58, 2008.

[105] L. Coccato, R. A. Swaters, V. C. Rubin, S. D'Odorico, and S. S. McGaugh, "VIMOS-VLT integral field kinematics of the giant low surface brightness galaxy ESO 323-G064," *Astronomy & Astrophysics*, vol. 490, no. 2, pp. 589–600, 2008.

[106] S. S. McGaugh, W. J. G. de Blok, J. M. Schombert, R. Kuzio de Naray, and J. H. Kim, "The rotation velocity attributable to dark matter at intermediate radii in disk galaxies," *The Astrophysical Journal*, vol. 659, no. 1, pp. 149–161, 2007.

[107] G. Gentile, C. Tonini, and P. Salucci, "ΛCDM halo density profiles: where do actual halos converge to NFW ones?" *Astronomy & Astrophysics*, vol. 467, no. 3, pp. 925–931, 2007.

[108] M. D. Weinberg and N. Katz, "Bar-driven dark halo evolution: a resolution of the cusp-core controversy," *The Astrophysical Journal*, vol. 580, no. 2, pp. 627–633, 2002.

[109] J. Dubinski, I. Berentzen, and I. Shlosman, "Anatomy of the bar instability in cuspy dark matter halos," *The Astrophysical Journal*, vol. 697, no. 1, pp. 293–310, 2009.

[110] O. Valenzuela, G. Rhee, A. Klypin, et al., "Is there evidence for flat cores in the halos of dwarf galaxies? The case of NGC 3109 and NGC 6822," *The Astrophysical Journal*, vol. 657, no. 2, pp. 773–789, 2007.

[111] A. Dekel, I. Arad, J. Devor, and Y. Birnboim, "Dark halo cusp: asymptotic convergence," *The Astrophysical Journal*, vol. 588, no. 2, pp. 680–695, 2003.

[112] A. Dekel, J. Devor, and G. Hetzroni, "Galactic halo cusp-core: tidal compression in mergers," *Monthly Notices of the Royal Astronomical Society*, vol. 341, no. 1, pp. 326–342, 2003.

[113] M. Boylan-Kolchin and C.-P. Ma, "Major mergers of galaxy haloes: cuspy or cored inner density profile?" *Monthly Notices of the Royal Astronomical Society*, vol. 349, no. 3, pp. 1117–1129, 2004.

[114] W. Dehnen, "Phase-space mixing and the merging of cusps," *Monthly Notices of the Royal Astronomical Society*, vol. 360, no. 3, pp. 892–900, 2005.

[115] A. El-Zant, I. Shlosman, and Y. Hoffman, "Dark halos: the flattening of the density cusp by dynamical friction," *The Astrophysical Journal*, vol. 560, no. 2, pp. 636–643, 2001.

[116] C. Tonini, A. Lapi, and P. Salucci, "Angular momentum transfer in dark matter halos: erasing the CUSP," *The Astrophysical Journal*, vol. 649, no. 2, pp. 591–598, 2006.

[117] E. Romano-Díaz, I. Shlosman, Y. Hoffman, and C. Heller, "Erasing dark matter cusps in cosmological galactic halos with baryons," *The Astrophysical Journal*, vol. 685, no. 2, pp. L105–L108, 2008.

[118] J. R. Jardel and J. A. Sellwood, "Halo density reduction by baryonic settling?" *The Astrophysical Journal*, vol. 691, pp. 1300–1306, 2009.

[119] T. Kaufmann, L. Mayer, J. Wadsley, J. Stadel, and B. Moore, "Cooling flows within galactic haloes: the kinematics and properties of infalling multiphase gas," *Monthly Notices of the Royal Astronomical Society*, vol. 370, no. 4, pp. 1612–1622, 2006.

[120] S. Mashchenko, H. M. P. Couchman, and J. Wadsley, "The removal of cusps from galaxy centres by stellar feedback in the early Universe," *Nature*, vol. 442, no. 7102, pp. 539–542, 2006.

[121] S. Mashchenko, J. Wadsley, and H. M. P. Couchman, "Stellar feedback in dwarf galaxy formation," *Science*, vol. 319, no. 5860, pp. 174–177, 2008.

[122] M. Ricotti and M. I. Wilkinson, "On the origin of dark matter cores in dwarf galaxies," *Monthly Notices of the Royal Astronomical Society*, vol. 353, no. 3, pp. 867–873, 2004.

[123] D. Ceverino and A. Klypin, "The role of stellar feedback in the formation of galaxies," *The Astrophysical Journal*, vol. 695, pp. 292–309, 2009.

[124] D.-M. Chen and S. S. McGaugh, "Contradiction between strong lensing statistics and a feedback solution to the cusp/core problem," http://arxiv.org/abs/0808.0225.

[125] E. Hayashi and J. F. Navarro, "Hiding cusps in cores: kinematics of disc galaxies in triaxial dark matter haloes," *Monthly Notices of the Royal Astronomical Society*, vol. 373, no. 3, pp. 1117–1124, 2006.

[126] E. Hayashi, J. F. Navarro, and V. Springel, "The shape of the gravitational potential in cold dark matter haloes," *Monthly Notices of the Royal Astronomical Society*, vol. 377, no. 1, pp. 50–62, 2007.

[127] J. Bailin, J. D. Simon, A. D. Bolatto, B. K. Gibson, and C. Power, "Self-consistent massive disks in triaxial dark matter halos," *The Astrophysical Journal*, vol. 667, no. 1, pp. 191–201, 2007.

[128] L. M. Widrow, "Dynamical models for disk galaxies with triaxial halos," *The Astrophysical Journal*, vol. 679, no. 2, pp. 1232–1238, 2008.

Hindawi Publishing Corporation
Advances in Astronomy
Volume 2010, Article ID 281913, 21 pages
doi:10.1155/2010/281913

Review Article

Dark Matter Substructure and Dwarf Galactic Satellites

Andrey Kravtsov

Department of Astronomy & Astrophysics, Kavli Institute for Cosmological Physics, The University of Chicago, Chicago, IL 60637, USA

Correspondence should be addressed to Andrey Kravtsov, andrey@oddjob.uchicago.edu

Received 8 June 2009; Accepted 31 August 2009

Academic Editor: Ulrich Hopp

A decade ago cosmological simulations of increasingly higher resolution were used to demonstrate that virialized regions of Cold Dark Matter (CDM) halos are filled with a multitude of dense, gravitationally bound clumps. These dark matter *subhalos* are central regions of halos that survived strong gravitational tidal forces and dynamical friction during the hierarchical sequence of merging and accretion via which the CDM halos form. Comparisons with observations revealed that there is a glaring discrepancy between abundance of subhalos and luminous satellites of the Milky Way and Andromeda as a function of their circular velocity or bound mass within a fixed aperture. This large discrepancy, which became known as the "substructure" or the "missing satellites" problem, begs for an explanation. In this paper, the author reviews the progress made during the last several years both in quantifying the problem and in exploring possible scenarios in which it could be accommodated and explained in the context of galaxy formation in the framework of the CDM paradigm of structure formation. In particular, he shows that the observed luminosity function, radial distribution, and the remarkable similarity of the inner density profiles of luminous satellites can be understood within hierarchical CDM framework using a simple model in which efficiency of star formation monotonically decreases with decreasing virial mass satellites had before their accretion *without any actual sharp galaxy formation threshold*.

1. Introduction

In the hierarchical scenario of galaxy formation [1], theoretically rooted in the Cold Dark Matter (CDM) structure formation model [2], galaxies form via cooling and condensation of gas in dark matter halos, which grow via an hierarchical sequence of mergers and accretion. The density perturbations in these models have amplitude that increases with decreasing scale down to ~ 1 comoving parsec or below [3], with the smallest fluctuation scale defined by the specific properties of the particles assumed to constitute the majority of the CDM. Smaller perturbations thus collapse first and then grow and merge to form larger and larger objects, with details of the evolution determined by expansion history of the universe (i.e., by parameters describing the background cosmological model) and by the shape of the density fluctuation power spectrum [4].

An example of such evolution in the flat ΛCDM model is illustrated in Figure 1, which shows collapse of a $\approx 10^{12} M_{\odot}$ object. The figure shows that during the early stages of evolution the matter that is incorporated into the final halo collapses into a large number of relatively small clumps with a filamentary, web-like spatial distribution. Further evolution, mediated by the competition between gravity and expansion of space, is a sequence of accretion and mergers that builds objects of progressively larger mass until the single system is formed during the last several billion years of evolution. The figure also shows that cores of some of the small clumps that merge with and are incorporated into larger objects survive until later epochs and are present in the form of *halo substructure* or *subhalos*: small dense clumps within virialized regions of larger halos. (Survival of subhalos is not a trivial result and is due to a relatively compact distribution of mass in CDM halos. Ensuring their survival requires a rather large dynamic range in spatial and mass resolution, which had not been achieved until the late 1990s [5–9].)

The CDM model of structure formation is remarkably successful in explaining a wide range of observations from temperature fluctuations of the cosmic microwave background [10] to galaxy clustering and its evolution [11] both qualitatively and, in many cases, quantitatively. Nevertheless,

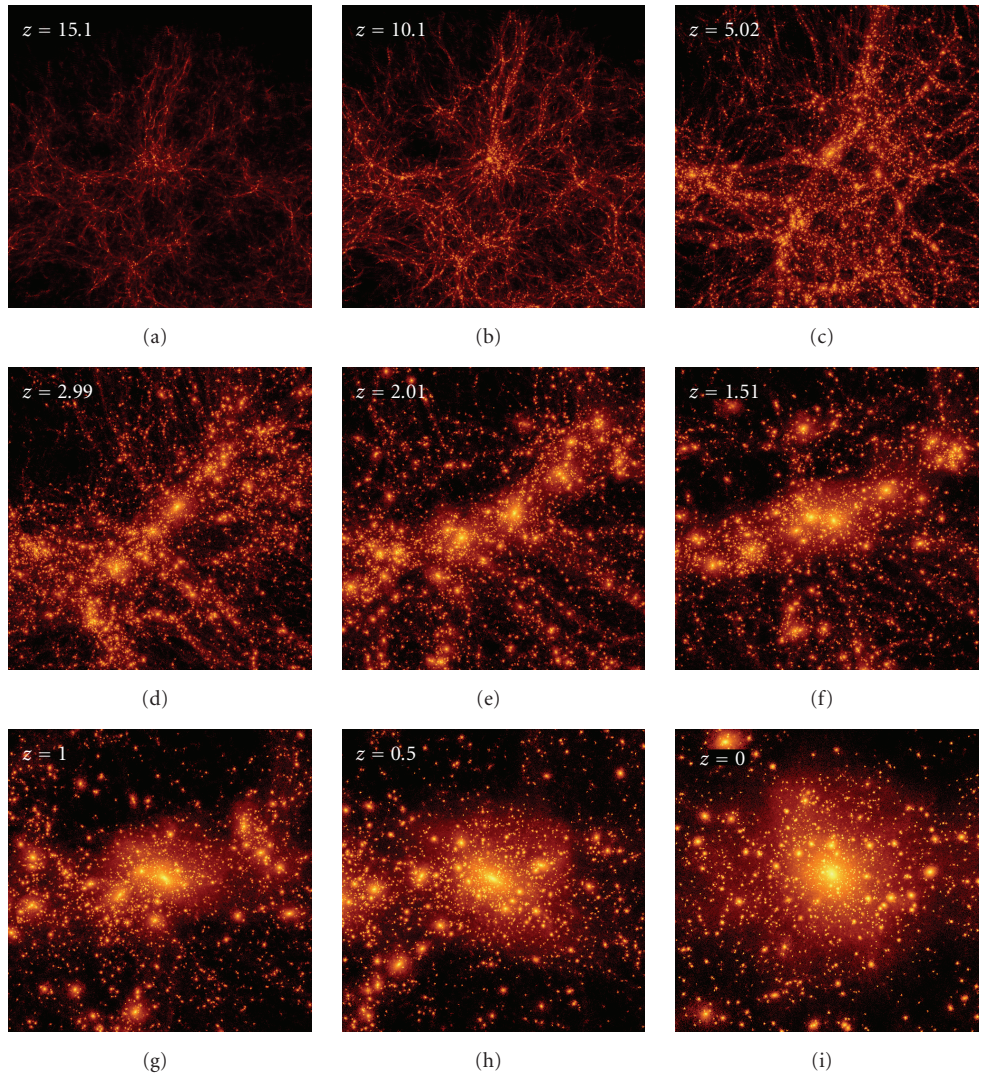

FIGURE 1: Formation of a Milky Way-sized dark matter halo in a cosmological simulation of flat ΛCDM cosmology ($\Omega_m = 1 - \Omega_\Lambda = 0.3$, $h = 0.7$, $\sigma_8 = 0.9$). The panels show an evolutionary sequence at nine redshifts (from left to right and from top to bottom) focusing on the most massive progenitor of the main halo at each epoch (redshift of each epoch is shown in the left upper corner). The rendering shows the dark matter particles with intensity indicating the local matter density on a logarithmic stretch. The build-up of the halo proceeds through a series of spectacular mergers, particularly frequent in the early stages of evolution. Many of the merging clumps survive until the present epoch ($z = 0$) in the form of "substructure." The size of the region shown is about 3 comoving Mpc at $z = 15$, monotonically zooming in to a scale of ≈1 comoving Mpc across at $z = 0$.

many key details of the model are still being developed [12, 13] and its testing is by no means complete.

One area of active investigation is testing predictions of the CDM models at scales from a few kpc to tens of pc (i.e., the smallest scales probed by observations of galaxies). In particular, there is still tension between predictions of the central mass distribution in galaxies [14, 15] and sizes and angular momenta of galactic disks and observational results [16, 17]. Notably, this tension has not gone away during the past 10–15 years, even though both theoretical models and observations have improved dramatically.

Another example of tension between CDM predictions and observations that has been actively explored during the last decade is the fact that satellite systems around galaxies of different luminosity are qualitatively different, even though their dark matter halos are expected to be approximately scaled down versions of each other [18], with their total mass as the scaling parameter. Faint dwarf galaxies usually have no luminous satellites at all, Milky Way and Andromeda have a few dozen, but clusters of galaxies often have thousands of satellites around the brightest cluster galaxy.

The number of gravitationally bound satellite subhalos at a fixed mass relative to the mass of their host CDM halo, on the other hand, is expected to be approximately the same [8, 19, 20]. This is illustrated in Figure 2, which shows distribution of dark matter out to approximately two virial radii around the centers of two CDM halos of masses different by two orders of magnitude. It is clear that it is

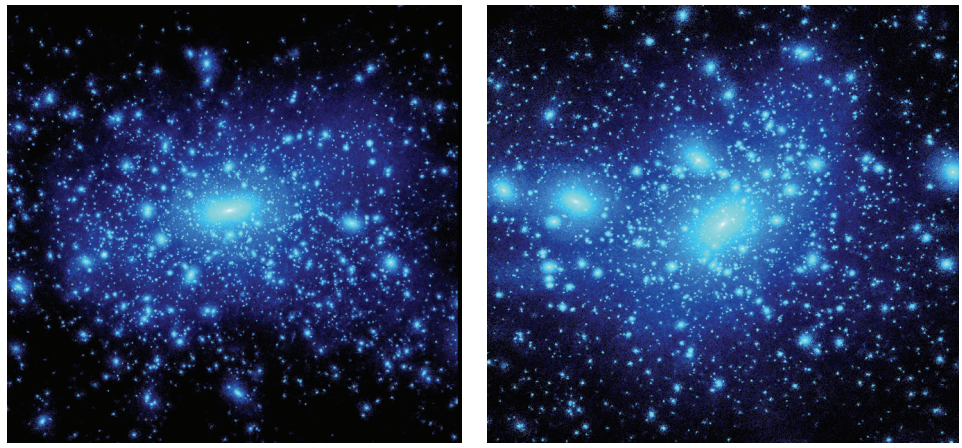

(a) (b)

Figure 2: Comparison of two $z = 0$ halos of masses $3 \times 10^{14} M_\odot$ and $3 \times 10^{12} M_\odot$ formed in flat ΛCDM cosmology ($\Omega_m = 1 - \Omega_\Lambda = 0.3$, $h = 0.7$, $\sigma_8 = 0.9$). In each case the mass distribution around the center of the halo is shown to approximately two virial radii from the center of each halo. Both objects were resolved with similar number of particles and similar spatial resolution relative to the virial radius of the halo in their respective simulations. I leave it as an exercise to the reader to guess the mass of the halo shown in each panel.

not easy to tell the mass of the halo by simply examining the overall mass distribution or by counting the number of subhalos. This is a visual manifestation of approximate (but not exact, see, e.g., [21, 22]) self-similarity of CDM halos of different mass. If we would compare similar images of distribution of luminous matter around galaxies and clusters, the difference would be striking.

The manifestly different observed satellite populations around galaxies of different luminosities and expected approximately self-similar populations of satellite subhalos around halos of different mass is known as the *substructure problem* [8, 23, 24]. In the case of the best studied satellite systems of the Milky Way and Andromeda galaxies, the discrepancy between the predicted abundance of small-mass dark matter clumps and the number of observed luminous satellites as a function of circular velocity (see Section 2) has been also referred to as the "*missing satellites problem.*" (The name derived from the title "Where are the missing galactic satellites?" of one of the papers originally pointing out the discrepancy [24].) The main goal of this paper is to review theoretical and observational progress in quantifying and understanding the problem over the last decade.

2. Quantifying the Substructure and Luminous Satellite Populations

In order to connect theoretical predictions and observations on a quantitative level, we need descriptive statistics to characterize population of theoretical dark matter subhalos and observed luminous satellites. Ideally, one would like theoretical models to be able to predict properties of stellar populations hosted by dark matter halos and subhalos and make comparisons using statistics involving directly observable quantities, such as galaxy luminosities. In practice, however, this is difficult as such predictions require modeling of still rather uncertain processes shaping properties of galaxies during their formation. In addition, the simulations can reach the highest resolution in the regime when complicated and computationally costly galaxy formation processes are not included and all of the matter in the universe is modeled as a uniform collisionless and dissipationless component (i.e., the component that cannot dissipate the kinetic energy it acquires during gravitational collapse and accompanying gravitational interaction and relaxation processes). Such simulations thus give the most accurate knowledge of the dark matter subhalo populations, but can only predict dynamical subhalo properties such as the depth of their potential well or the total mass of gravitationally bound material. Therefore, in comparisons between theoretical predictions and observations so far, the most common strategy was to find a compromise quantity that can be estimated both in dissipationless simulations and in observations.

2.1. Quantifying the Subhalo Populations. Starting with the first studies that made such comparisons using results of numerical simulations [8, 24] the quantity of choice was the *maximum circular velocity*, defined as

$$V_{\max} = \max\left(\frac{Gm(<r)}{r}\right)^{1/2}, \quad (1)$$

where $m(<r) = 4\pi \int \rho(r) r^2 dr$ is the spherically averaged total mass profile about the center of the object. $V_{\max}$ is a measure of the depth of the potential (the potential energy of a self-gravitating system is $W \propto V_{\max}^2$) and can be fairly easily computed in a cosmological simulation once the center of a subhalo is determined. (The detailed description of the procedure of identifying the centers of subhalos is beyond the scope of this paper, but is nevertheless pertinent. While many different algorithms are used in the literature [6, 9, 25–29], all algorithms boil down to the automated search for density peaks (most often in configuration space, but sometimes

in the phase space) field smoothed at a scale comparable to or smaller than the size of the smallest subhalos in the simulations. Once the peaks are identified, the gravitationally bound material around them is usually found by iteratively removing the unbound particles.) The attractive feature of $V_{\max}$ is that it is well defined and does not require estimate of a physical boundary of subhalos, which is often hard to determine. The price is that resolution required to get the $V_{\max}$ correctly for a subhalo is higher, compared, for example, to the total bound mass of subhalo, because $V_{\max}$ is probing the mass distribution in the inner regions of halos.

The total gravitationally bound mass of a subhalo, $m_{\rm sub}$, is less sensitive to the resolution, but requires careful separation between real subhalo particles and unbound particles from the diffuse halo of the host dark matter halo. This can be quite difficult in the inner regions of the host system where density of the background diffuse halo is comparable to the internal density of subhalo or when two subhalos overlap substantially.

An alternative option is to define mass of a subhalo within a fixed physical radius. For suitably chosen radius value, the mass can be measured unambiguously both in simulations and in observations. We will discuss the measurement of the enclosed mass and comparisons between simulations and observations below in Sections 3 and 4.3 (see Figures 8 and 12).

Figure 3 shows the cumulative circular velocity and mass functions (CVF and CMF) of subhalos within the virial radius (defined as $R_\Delta = (3M_\Delta/4\pi\Delta\overline{\rho})^{1/3}$, where $\overline{\rho}$ is the mean matter density in the universe and $\Delta = 337$, corresponding to the $z = 0$ virial overdensity suggested by the spherical collapse model in the ΛCDM cosmology [30]) of a simulated Milky Way sized halo, formation of which was illustrated in Figure 1. Both cumulative functions can be approximated by power laws over the ranges of circular velocity and in units of $V_{\max}$ and virial mass of the host: $\nu \equiv V_{\max}/V_{\max}^{\rm host} \lesssim 0.1$ and $\mu \equiv m_{\rm sub}/M_{\rm vir}^{\rm host} \lesssim 0.001$ with the slopes of $-2.7 \div -3$ and $\approx -0.8 \div -0.9$, respectively. At large circular velocities deviations from the power law can be significant due to small numbers of subhalos.

The highest-resolution simulations (to date) of the individual MW-sized DM halos formed in the concordance ΛCDM cosmology [31–33] show that the power laws with the slopes in the range indicated above describe the CVF and CMF down to $\mu \approx 10^{-7}$ and $\nu \approx 10^{-2}$. Note, however, that over a wider range of subhalo masses the power law can be expected to change slowly reflecting the changing slope of the rms fluctuations as a function of scale, which controls the abundance of halos as a function of mass [34, 35].

The amplitude of the mass and velocity functions is sensitive to the normalization of the power spectrum on small scales [31, 36, 37] and is thus sensitive to the cosmological parameters that control the normalization (such as tilt and normalization σ_8).

For a given cosmology, the normalization of the CVF and CMF scales approximately linearly with the host halo mass [19]: $N(m_{\rm sub} \mid M_{\rm h}) \propto M_{\rm h}$. The halo-to-halo scatter in the normalization of CVF and MCF for a fixed host halo virial mass is described by the Poisson distribution [19]: $\sigma_{N(>\mu)} = \sqrt{N(>\mu)}$. The fractional scatter is, therefore, quite small for small μ and ν (large N).

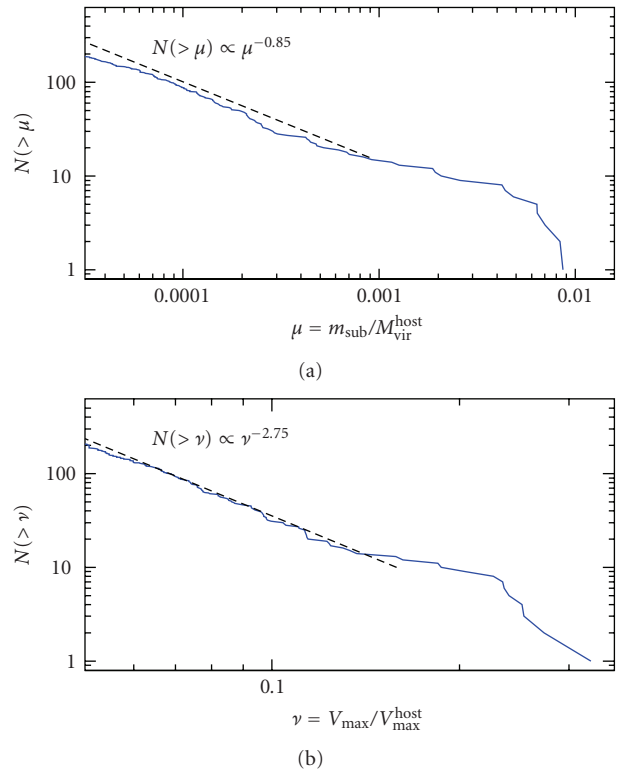

Figure 3: Cumulative circular velocity and mass function of subhalos within the virial radius $R_{337} = 328$ kpc of a halo of virial mass $M_{337} = 2 \times 10^{12} M_\odot$ at $z = 0$. The dashed lines show power laws with the slopes indicated in the legend of each panel.

The mass and circular velocity functions within a given radius describe the overall abundance of subhalos of different mass, but not their radial distribution. The latter depends rather sensitively on how the subhalo samples are selected [38]. This is because subhalos at different distances from their host halo center on average experience different tidal mass loss, which affects different subhalo properties by different amount. Subhalo mass is the most affected quantity as large fraction of halo mass when it accretes is relatively loosely bound and is usually lost quickly. Although circular velocity is determined by the inner mass distribution in the inner mass of subhalos, it is still affected by tidal stripping (albeit to a less degree and slower than the total mass [39]).

The average mass loss experienced by subhalos increases with decreasing distance to the center of the host halo [38]. Therefore, selecting subhalos based on their current bound mass or circular velocity biases the sample against subhalos at smaller radii and results in the radial distribution much less concentrated than the overall mass distribution of the host halo [6, 26, 38–42]. Conversely, one can expect that if the selection of subhalos is made using a quantity not affected by stripping, the bias should be smaller or even disappear altogether.

Figure 4(a) shows the radial distribution of subhalos (the same population as in Figure 3) selected using their current bound mass or circular velocity and density profile of dark matter within an MW-sized host halo. The figure shows that the subhalo distribution is less radially concentrated compared to the overall density profile because selection using current subhalo properties affected by tidal evolution biases the sample against the inner regions. Figure 4(b) shows the radial distribution of subhalos in the same host halo but now selected using circular velocity and mass the subhalos had *before accretion* (which are of course not affected by the tides). In this case, the radial profile is very close to that of the dark matter distribution. This dependence of the radial profile on the property used for subhalo selection should be kept in mind when the observed and predicted radial distributions are compared. The latter are selected based on their luminosity (i.e., the stellar mass), which may be affected by tides much less than either the total bound mass or circular velocity [38, 43].

Finally, the spatial distribution of satellites is not completely spherically symmetric, but is triaxial, which reflects their accretion along filaments and subsequent evolution in the triaxial potential of their host halos [44–46].

2.2. Quantifying Populations of Luminous Galactic Satellites. Although we currently know only a few dozens of nearby satellite galaxies around the Milky Way and Andromeda, these galaxies span a tremendous range of the stellar densities and luminosities. The two brightest satellites of the Milky Way, the Large and Small Magellanic Clouds (LMC and SMC), are easily visible by the naked eye in the southern hemisphere and have, therefore, been known for many hundreds of years, while the faintest satellites have been discovered only very recently using sophisticated search algorithms and the vast data sets of stellar photometry in the Sloan Digital Sky Survey and contain only a few hundred stars [47, 48]. Up until the late 1990s, only a dozen dwarf galaxies were known to exist within 300 kpc of the Milky Way, with a similar number around the Andromeda [49]. These galaxies have luminosities $L \gtrsim 10^5 L_\odot$ and morphologies of the three types: (1) dwarf irregular galaxies (dIrrs, e.g., LMC and SMC)—low surface brightness galaxies of irregular appearance which have substantial amount of gas and thus exhibit continuing star formation, (2) dwarf spheroidal galaxies (dSphs, e.g., Draco or Fornax)—low surface brightness galaxies with spheroidal distribution of stars and no (or very little) ongoing star formation, and (3) dwarf elliptical galaxies (dEs, e.g., M32)—high-surface brightness, low-luminosity ellipticals with no gas and no current star formation. dSph and dE galaxies tend to be located within 200 kpc of their host galaxies, while dIrr galaxies are distributed more uniformly. This tendency is called the "morphological segregation" [49] and appears to exist in other nearby groups of galaxies [50]. The properties of these "classical" dwarf galaxies are reviewed extensively by [49] (see also recent study of scaling relations of dwarf galaxies by [51]).

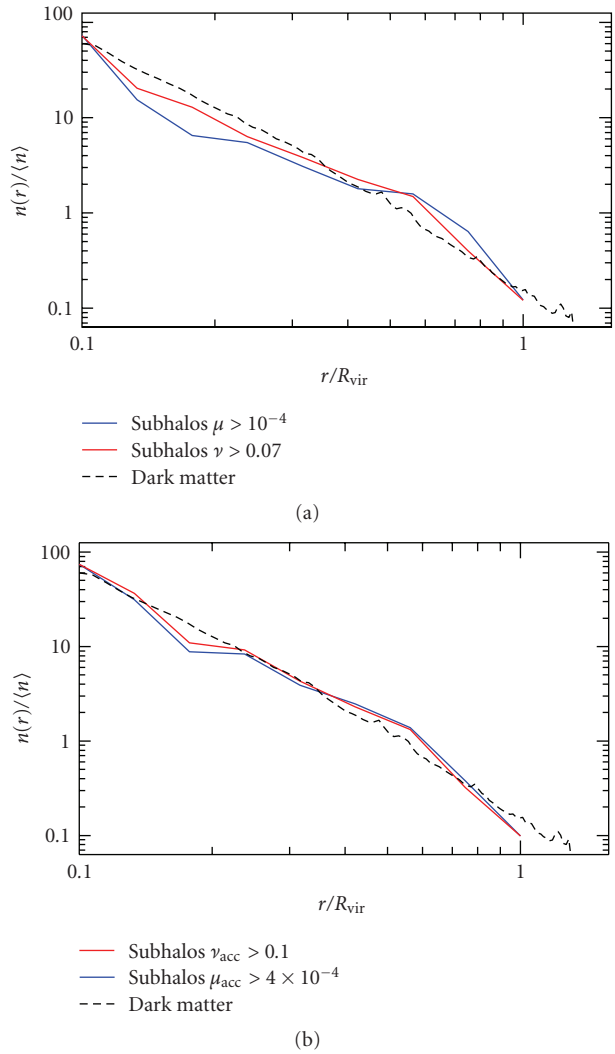

FIGURE 4: Radial distribution of subhalos (solid lines) selected using their different properties ($V_{\rm max}$ and total mass—solid red and blue lines, resp.) compared to the matter density profile in their host halo (dashed lines). (a) shows the profiles for subhalos selected using circular velocity and bound mass a the current epoch, while the lower shows radial distribution of subhalos selected using the corresponding quantities *before* subhalo was accreted unaffected by the subsequent tidal mass loss. Note that minimum threshold values for subhalo selection, $\mu_{\rm min}$ and $\nu_{\rm min}$, are different in (b) because for a typical mass loss many subhalos with smaller circular velocities and masses at the time of accretion fall below the completeness limit of the simulation by $z = 0$.

Despite the wide range of observed properties, all of the nearby dwarfs share some common features in their star formation histories (SFHs). The SFHs of all classical dwarfs are characterized by a rather chaotically varying star formation rates. Most bright dwarfs form stars throughout their evolution, although the majority of stars may be formed in several main episodes spread over ten or more billion years [52–55], and have at least some fraction of stars that formed in the first two billion years of the evolution of the universe. In terms of their SFHs, the main difference between the dwarf

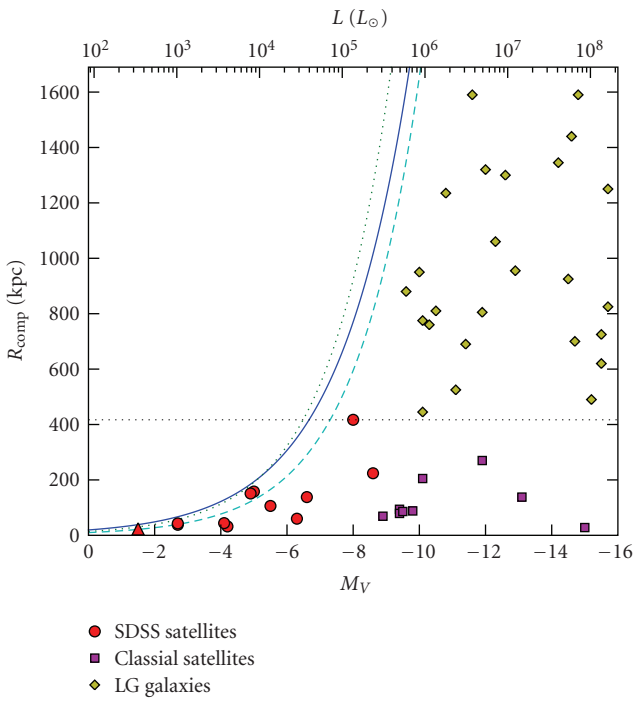

Figure 5: The distance to which the current samples of dwarf satellite galaxies around the Milky Way are complete (dotted, solid and dashed lines correspond to somewhat different assumptions about detection limits of dwarf galaxies, see [56] for details) as a function of galaxy luminosity (absolute V-band magnitude on the bottom scale and physical luminosity in units of solar luminosity at the top scale). The points show different types of observed satellites around the Milky Way and in the Local Group. The horizonthal dotted line indicates the outer radius for satellites counts shown in the Figure 6. Note that the completeness distance of the faintest recently discovered satellites is $\lesssim$50 kpc. Adopted from [56].

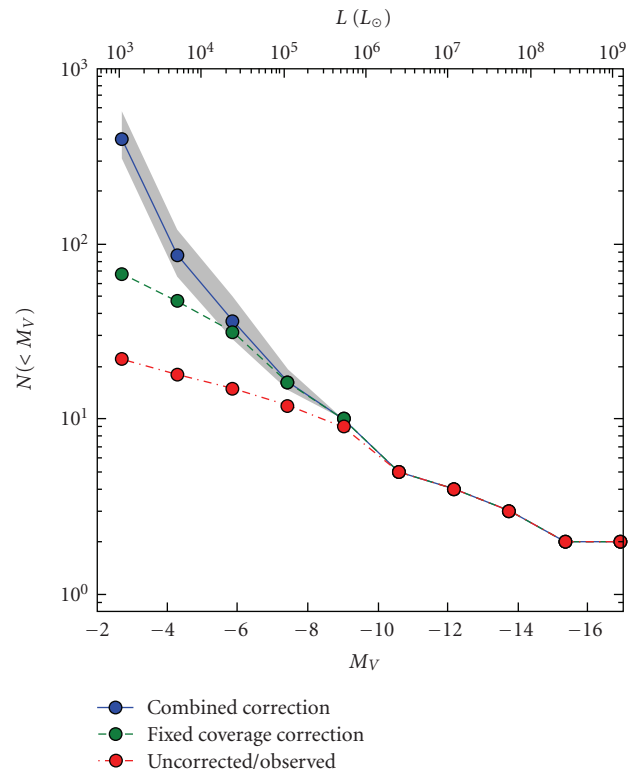

Figure 6: The luminosity function of dwarf galaxies around the Milky Way. The function includes all observed galaxies within 417 kpc of the Milky Way. The red circles connected by the dotted line show the luminosity function as observed, without any corrections for incompleteness. The green circles connected by the dashed line show the observed luminosity function corrected for limited area coverage of surveys on the sky. The blue circles connected by the solid line show luminosity function corrected for the radial bias using radial distribution of subhalos from the Via Lactea I simulation. Adopted from [56].

irregular and dwarf spheroidal galaxies is in the presence or absence of star formation in the last two billion years [54].

The radial distribution of the classical satellites around the Milky Way is rather compact. For the dwarf galaxies within 250 kpc of the Milky Way, the median distance to the center of the Galaxy is ≈70 kpc [39, 57], while the predicted median distance for subhalos is ≈120–140 kpc [39] (see Figure 13). The distribution of the satellites around the Andromeda galaxies is consistent with that of the Milky Way satellites, but is less accurately determined due to larger errors in distances. The spatial distribution of satellites about the Milky Way and Andromeda is also manifestly nonisotropic with the majority of the satellites found in a flattened structure nearly perpendicular to the disk [58–62].

In 1994, a new faint galaxy was discovered in the direction toward the center of the Galaxy (in the Sagittarius constellation [63]). The galaxy is similar to other nearby dwarf spheroidal galaxies in its properties but is remarkably close to the solar system (the distance of only ≈28 kpc) and is in the process of being torn apart by the tidal interactions with the Milky Way. This interaction has produced a spectacular tidal tail, which has wrapped several times along the orbit of the Sagittarius dwarf [64].

The discovery of this new satellite has alerted researchers in the field to the possibility that other satellites may be lurking undiscovered in our cosmic neighborhood. The advent of wide field photometric surveys, such as the Sloan Digital Sky Survey and the targeted surveys of regions around the Andromeda galaxy, and new search techniques has resulted in dozens of new satellite galaxies discovered during the last decade [47, 48, 65–71] with many more discoveries expected in the near future [56, 72]. The majority of the newly discovered galaxies are fainter than the "classical dwarfs" known prior to 1998. Due to their extremely low luminosities (as low as $\sim$1000 $L_\odot$ in the case of the Segue 1 [48]), they have collectively been referred to as the "ultra-faint" dwarfs. Such low luminosities (and implied stellar masses) indicate an extreme mode of galaxy formation, in which the total population of stars produced during galaxy evolution is smaller than a star cluster formed in a single star formation event in more luminous galaxies. (Alternatively, extremely low luminosities of the ultra-faint dwarfs can also be explained as a highly stripped remnants of more luminous dwarfs [43]. While this possibility is not excluded, it is

disfavored by the fact that ultra-faint dwarfs appear to lie on the continuation of the luminosity-metallicity relation of more luminous dwarf galaxies [73].)

More practically, the extreme faintness of the majority of dwarf satellites implies that we have a more or less complete census of them only within the volume of ~30–50 kpc of the Milky Way [56, 74]. Figure 5 shows the distance to which the dwarfs of a given luminosity are complete in the SDSS survey, in which the faintest new dwarfs have been discovered. The figure shows that we have a good census of the volume of the Local Group only for the relatively bright luminosities of the "classical" satellites. At the fainter luminosities of the ultra-faint dwarfs, on the other hand, we can expect to find many more systems at larger radii in the future deep wide area surveys. The exact number we can expect to be discovered depends on their uncertain radial distribution, but given the numbers of already discovered dwarfs and our current knowledge of the radial distribution of brighter satellites (and expected radial distribution of subhalos), we can reasonably expect that at least a hundred faint satellites exist within 400 kpc of the Milky Way. This is illustrated in Figure 6, which shows the luminosity function of the Milky Way satellites corrected for the volume not yet surveyed under different assumptions about radial distribution of the satellites [56].

The basis for considering these extremely faint stellar systems as bona fide galaxies is the fact that unlike star clusters, they are dark matter dominated: that is, the total mass within their stellar extent is much larger than the stellar mass expected for old stellar populations [48]. The total dynamical masses of these galaxies are derived using kinematics of stars. (These faint dwarf spheroidal galaxies do not have cold gas and therefore their mass profiles cannot be measured using the gas rotation curve, as is commonly done for more massive dIrr galaxies.) High-resolution spectroscopy of the red giant stars in the vicinity of each galaxy provides the radial velocities of these stars. The radial velocities can then be modeled using using the Jeans equilibrium equations to derive the total mass profile [75–80]. This modeling requires certain assumptions about the unknown shape of the stellar distribution and velocity distribution of stars, as well as assumptions about the shape and radial profile of the dark matter distribution. The resulting mass profile, therefore, has some uncertainty associated with these assumptions [75, 78, 80].

Additionally, the ultra-faint dwarfs follow scaling relations of the brighter classical satellites such as the luminosity-metallicity relation [73] and, therefore, seem to be the low luminosity brethren within the family of dSph galaxies.

3. Defining the Substructure Problem

As I noted above, comparison of theory and observations in terms of the directly observable quantities such as luminosities is possible only using a galaxy formation model. These models, although actively explored [39, 81–87] (see also Section 4.3) are considerably more uncertain than the predictions of dissipationless simulations on the properties

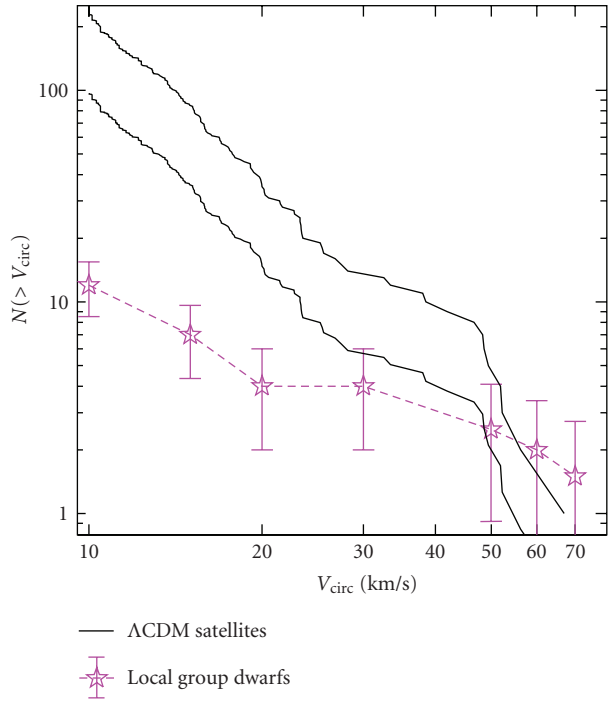

Figure 7: Comparison of the cumulative circular velocity functions, $N(> V_{\rm max})$, of subhalos and dwarf satellites of the Milky Way within the radius of 286 kpc (this radius is chosen to match the maximum distance to observed satellites in the sample and is smaller than the virial radius of the simulated halo, $R_{337} = 326$ kpc). The subhalo VFs are plotted for the host halos with maximum circular velocities of 160 km/s and 208 km/s that should bracket the $V_{\rm max}$ of the actual Milky Way halo. The VF for the observed satellites was constructed using circular velocities estimated from the line-of-sight velocity dispersions as $V_{\rm max} = \sqrt{3}\sigma_r$ (see the discussion in the text for the uncertainties of this conversion).

of dark matter subhalos. Given that observed dwarf satellites are very dark matter dominated, the dissipative processes leading to formation of their stellar component are expected to have a limited effect on the distribution of the dynamically dominant dark matter. Fruitful comparison between simulation predictions and observations is, therefore, possible if a quantity related to the total mass profile can be measured in the latter.

The first attempts at such comparisons [8, 9] assumed isotropy of the stellar orbits and converted the line-of-sight velocity dispersion of stars in dSph satellites, σ_r, to estimate their maximum circular velocities as $V_{\rm max} = \sqrt{3}\sigma_r$. The admittedly oversimplistic conversion was adopted simply due to a lack of well-measured velocity profiles and corresponding constraints on the mass distribution at the time. Figure 7 shows such a comparison for the classical satellites of the Milky Way and subhalo populations in Milky Way-sized halos formed in the concordance ΛCDM cosmology.(I did not include the new ultra-faint satellites in the comparison both because their $V_{\rm max}$ values are much more uncertain and because their total number within the virial radius requires uncertain corrections from the

currently observed number that probes only the nearest few dozen kpc. The velocity dispersions of the ultra-faint dwarfs are very similar to each other ($\sim$5 km/s) and they, therefore, formally have similar $V_{\rm max}$ values according to this simple conversion method (hence, they would all be "bunched up" at about the same $V_{\rm max} \sim 9$ km/s value). The maximum circular velocity of the halos of these galaxies is expected to be reached at radii well beyond the stellar extent and its estimate from the observed velocity dispersions requires substantial extrapolation and assumptions about the density profile outside the radii probed by stars. The errors of the derived values of $V_{\rm max}$ can, therefore, be quite substantial [75, 88]. I will compare the predicted luminosity function of the luminous satellites using a simple galaxy formation model in Section 4.3 (see Figure 11).)

The observed velocity function is compared to the predicted VF of dark matter subhalos within a 286 kpc radius of Milky Way-sized host halos. In literature, the term "Milky Way-sized" is often used to imply a total virial mass of $M_{\rm vir} \approx 10^{12} M_\odot$ and maximum circular velocity of $V_{\rm max} \approx 200$ km/s. However, there is some uncertainty in these numbers. Therefore, the figure shows the VFs for the host halos with $V_{\rm max} = 208$ km/s and 160 km/s. The former is measured directly in a simulation of the halo of that circular velocity, while the latter VF was rescaled as $N(>V_{\rm max}) \propto M_{\rm vir,1}/M_{\rm vir,2} = (V_{\rm max,1}/V_{\rm max,2})^{3.3}$, using scaling measured statistically in the simulations [19].

The simple conversion of σ_r to $V_{\rm max}$ has justly been criticized as too simplistic [89]. Indeed, the conversion factor $\eta \equiv V_{\rm max}/\sigma_r$ requires a good knowledge of mass profile from small radii to the radius $r_{\rm max}$. The mass profile derived from the Jeans equation has errors associated with uncertainties in the anisotropy of stellar orbits, as well as with uncertainties of spatial distribution of stellar system and/or its dynamical state [76, 90]. Most importantly, the mass profile is only directly constrained within the radius where stellar velocities are measured, r_*. If this radius is smaller than $r_{\rm max}$, conversion factor η depends on the form of the density profile assumed for extrapolation. The uncertainties of the derived mass profile within the stellar extent will of course also be magnified increasingly with increasing $r_{\rm max}/r_*$ ratio [90].

Thus, for example, Stoehr et al. [89] have argued that the conversion factor can be quite large ($\eta \gtrsim$ 2–4) if the density profile is shallow in the inner regions probed by the stars. Such large conversion factor would shift the low $V_{\rm max}$ points in Figure 7 to the right closer to the subhalo VF [78, 89, 91] and would imply that there is a sharp drop in the luminosity function of satellites below a certain threshold circular velocity ($V_{\rm max} \approx 30$ km/s). High-resolution simulations of individual satellites, on the other hand, have demonstrated that the CDM satellites retain their *cuspy* inner density profiles, even as they undergo significant tidal stripping [92]. (The profiles can be even steeper than predicted by dissipationless simulations due to the effects of adiabatic contraction during gas condensation towards the center of the dwarf progenitors [93]. Although the effect of baryon condensation in dwarfs are uncertain at present, one can argue that they can reasonably be expected to be modest, given large mass-to-light ratios of faint dwarfs [48].) This implies that η is likely not as large as advocated by Stoehr et al. The main uncertainty in its actual value for a specific satellite is then due to the uncertainty in the density profile and ratio $r_{\rm max}/r_*$.

Recently, Peñarrubia et al. [78] combined the measurements of stellar surface density and $\sigma_r(R)$ profiles to estimate $V_{\rm max}$ values for individual observed MW satellites under the assumption that their stellar systems are embedded into NFW dark matter potentials. Such procedure by itself does not produce a reliable estimate of $V_{\rm max}$, because NFW potentials with a wide range of $V_{\rm max}$ can fit the observed stellar profiles. To break the degeneracy, Peñarrubia et al. have used the relation between $V_{\rm max}$ and $r_{\rm max}$ expected in the concordance ΛCDM cosmology. They showed that this results in estimates of $V_{\rm max}$ which imply $\eta \approx$ 2-3 [43, Figure 4]. This estimate does not take into account effects of tidal stripping on the evolution of the $r_{\rm max}$-$V_{\rm max}$ relation. Typically, subhalos located in the inner regions of the halo are expected to have lost $\sim$60%–90% of their initial mass by $z = 0$ due to tidal stripping [22, 38, 39]. For such mass loss $V_{\rm max}$ changes only by $\approx$20%–30% [39, 78] but $r_{\rm max}$ should change by a factor of $\approx$2-3 [43, 92].

In a subsequent study, Peñarrubia et al. [43] used controlled simulations of subhalo evolution to argue that tidal stripping does not significantly affect their inferred conversion factor η [43, Figure 9]. This conclusion, however, was drawn based on the systems in which both stellar system and DM halo were significantly stripped. In such system, $r_{\rm max}$ is close to the stellar radius and σ_0 and $V_{\rm max}$ evolve in sync. For systems with more realistic mass loss and with stars deeply embedded within $r_{\rm max}$, however, stellar system (and σ_0) may not be affected, while $V_{\rm max}$ can evolve significantly. For such systems, the method of [78] will lead to a significant overestimate of η. Indeed, the systems in [43, Figure 9] for which the method overestimates η (by a factor of $\approx$1.4) the most are the systems with moderate total mass loss and least affected stellar systems. Note that even these systems have likely experienced more tidal loss than most of the real dSph satellites.

Another factor in estimates of $V_{\rm max}$ is anisotropy of stellar velocities in dSph (e.g., [92]). For example, recent analysis of observed velocity dispersion profiles of "classical" dSph by [79], in which the anisotropy of stellar orbits was treated as free parameters, results in estimates of $V_{\rm max}$ of their host subhalos in the range $\sim$10–25 km/s, smaller than would be suggested if correction factor was $\eta \approx$ 2-3.

Regardless of the actual conversion factor value, however, it is clear that it cannot change the main difference between the observed and predicted VFs—the large difference in their slope—unless η strongly depends on $V_{\rm max}$ (there is no observational evidence for this so far).

Another promising approach is to abandon attempts to derive $V_{\rm max}$ altogether and to measure instead the observed mass within the radius where the uncertainty of the measured mass profile is minimal. Such radius is close to the stellar extent of observed galaxies [78, 80, 88, 90]. Figure 8, adopted from [90], shows comparison of the mass functions of subhalos in the Via Lactea I simulation [94]

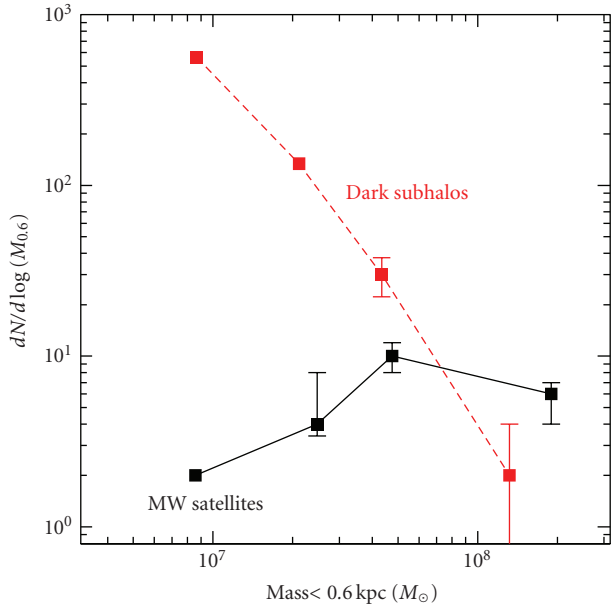

FIGURE 8: The mass function of dwarf satellites of the Milky Way, where masses of subhalos and observed satellites are measured within a fixed physical radius of 0.6 kpc. Adopted from [90].

and observed satellites of the Milky Way, where masses are measured within a fixed physical radius of 600 pc (see also the discussion in Section 4.3 and Figure 12). The figure shows that the simulated and observed mass functions are different, the conclusion similar to that derived from the comparison of the circular velocity functions.

Thus, the discrepancy that is clearly seen in the comparison of circular velocity functions, measured with more uncertainty in observations, persists if the comparison is done using a much better measured quantity. Unfortunately, the stellar distribution in most of the newly discovered ultra-faint dwarf galaxies does not extend out to 600 pc radius and $m(r < 0.6\,\text{kpc}) \equiv m_{0.6}$, therefore, cannot be measured as reliably for these faint systems as for the classical dwarfs. Similar comparisons have to be carried out using masses within smaller radii. This puts stringent requirements on the resolution of the simulations, as they need to reliably predict mass distribution of subhalos within a few hundred parsec radius. Such high-resolution simulations are now available [31–33].

We can draw two main conclusions from the comparisons of the circular velocity functions and the more reliable $m_{0.6}$ mass functions of subhalos and observed satellites presented in the previous sections, even taking into account existing uncertainties in deriving circular velocities and the total dynamical masses for the observed satellites. First, the predicted abundance of the most luminous satellites is in reasonable agreement with the data, even though the statistics are small. Most MW-sized halos simulated in the concordance ΛCDM cosmology have ∼1 SMC/LMC sized ($V_{\max} \approx 50$–70 km/s) subhalos within their virial radius.

This is not a trivial fact because the abundance of the most massive satellites is determined by a subtle interplay between the accretion rate of systems of corresponding circular velocity and their disruption by the combined effects of the dynamical friction and tidal stripping [95]. Dynamical friction causes satellites to sink to the center at a rate which depends on the mass and orbital parameters of satellite orbit. Orbital parameters, in turn, depend on the cosmological environment of the accreting host halo and are mediated by the tidal stripping which reduces satellite mass as it sinks, thereby rendering dynamical friction less efficient [96–99]. The fact that the concordance ΛCDM model makes an ab initio prediction that the number of massive satellites that can host luminous dwarfs is comparable to observations can therefore be viewed as a success of the model.

Second, the *slopes* of both the circular velocity function and the $m_{0.6}$ mass function are different in simulations and observations. This implies that we cannot simply match all of the luminous satellites to the subhalos with the largest $V_{\max}$ and $m_{0.6}$, as was sometimes advocated [89, 91]. The $m_{0.6}$ mass function comparison, in particular, indicates that there should be some subhalos with the $m_{0.6} \sim 10^7 M_\odot$ that do not host the luminous galaxies, and some that do. As I discuss in Section 4.2, this has a strong implication for the physical interpretation of the difference in terms of galaxy formation scenarios.

In summary, *the substructure problem can be stated as the discrepancy in the slopes of the circular velocity and $m_{0.6}$ mass functions inferred for observed satellites of the Milky Way and the slopes of these functions predicted for dark matter subhalos in the* MW*-sized host halos formed in the concordance* ΛCDM *cosmology.*

I believe that stated this way the problem is well defined. Defining the problem in terms of the difference in the actual number of satellites and subhalos is confusing at best, as both numbers are fairly strong functions of subhalo mass or stellar luminosity. Thus, for example, even though the discovery of the ultra-faint dwarfs implies the possible existence of hundreds of them in the halo of the Milky Way [49, 75] (this fact has been used to argue that the substructure problem has been "alleviated"), the most recent simulations show that more than 100 000 subhalos of mass $m_{\text{sub}} > 10^5 M_\odot$ should exist in the Milky Way [31, 32]. (Indeed, it is not obvious a priori that subhalos of mass 10^5-$10^6 M_\odot$ are too small to host luminous stellar systems of stellar mass $M_* \sim 10^3$-$10^4 M_\odot$ [100]—the stellar masses corresponding to the luminosities of the faintest recently discovered dwarfs. After all, the halos of this mass are expected to be hosting formation of the very first stars [101].) The substructure problem stated in the actual *numbers* of satellites is therefore alive and well and has not been alleviated in the least.

I would like to close this section by a brief discussion of the comparison of spatial distribution of observed satellites and subhalos. As I noted above, the radial distribution of the observed satellites of the Milky Way is more compact than the radial distribution of subhalos selected using their present day mass or circular velocity [39, 57, 102]. In addition, the observed satellites are distributed in a quite flattened

structure with its plane almost perpendicular to the disk of the Milky Way [58–62]. Although the spatial distribution of *all* subhalos is expected to be anisotropic, reflecting the anisotropy of their accretion directions along filaments [44, 45] and, possibly, the fact that some of the satellites could have been accreted as part of the same group of galaxies [103], the expected anisotropy is not as strong as that of the observed Milky Way satellites.

Thus, both the radial distribution and anisotropy of the observed satellites do not match the overall distribution of subhalos in CDM halos. This may be yet another side of the same substructure problem coin and the overall spatial distribution of observed satellites needs to be explained together with the differences in the circular velocity function. (Although distribution of satellites around other galaxies is not mapped as accurately as around the Milky Way, there is evidence for similar planar anisotropy around M31 [60]. The evidence for such anisotropy in other disk galaxies is weak at best [104], although measurements for distant galaxies are more difficult as they require very careful handling of projection effects [105].) I will review a few possible explanations for the substructure problem and differences in the spatial distribution in the following section.

4. Possible Solutions

4.1. Modifications to the CDM Model. One possible way to account for the differences of the predicted and observed circular velocity and $m_{0.6}$ mass functions is to assume that ΛCDM model is incorrect on the small scales probed by the dwarf galactic satellites. Indeed, the abundance of satellites is sensitive to the amplitude of the power spectrum on the scales corresponding to the total mass of their host halos. For a halo of mass M the comoving scale of fluctuations that seed their formation is

$$d = 2R = 2\left(\frac{3M}{4\pi\Omega_{\rm m0}\rho_{\rm crit0}}\right)^{1/3} = 360.4\,{\rm kpc}\left(\frac{M}{10^9 M_\odot}\frac{0.3}{\Omega_{\rm m}}\right)^{1/3}\left(\frac{H_0}{70}\right)^{-2/3}, \quad (2)$$

where $\Omega_{\rm m}$ is the present-day total matter density in units of the present-day critical density, $\rho_{\rm crit0} \equiv 3H_0^2/8\pi G$, and H_0 is the current Hubble constant in units of km/s/Mpc.

If the amplitude of density fluctuations on such scales is considerably suppressed compared to the concordance ΛCDM model used in most simulations, the abundance of subhalos can then also be suppressed. Such suppression can be achieved either by suitably varying parameters controlling the amplitude of the small-scale power spectrum within the ΛCDM model itself [36], such as the overall normalization of the power spectrum or its large-scale tilt, or by switching to models in which the amplitude at small scales is suppressed, such as the warm dark matter (WDM) structure formation scenarios [36, 106–109]. In these models the abundance of satellites is suppressed both because fewer halos of dwarf mass form in the first place (due to smaller initial amplitude of fluctuations) and because halos that do form have a less-concentrated internal mass distribution, which makes them more susceptible to tidal disruption after they accrete onto their host halo. Models in which dark matter was assumed to be self-interacting, a property that can lead to DM evaporation, have also been proposed and discussed [110, 111], but these models both run into a contradiction with other observational properties of galaxies and clusters [112–115] and are now strongly disfavored by observational evidence indicating that dark matter self-interaction is weak [116].

The problem, however, is more subtle than simply suppressing the number of satellites. As discussed above, differences exist between observed and predicted slopes of the circular velocity and mass. The slope is controlled by the slope of the primordial fluctuation spectrum around the scale corresponding to the masses of satellite halos and structural properties of the forming halos. It has not yet been demonstrated convincingly whether *both* the circular velocity and the $m_{0.6}$ mass functions can be reproduced in any of the models alternative to CDM. In fact, recent measurements of mass distribution in the central regions of observed satellites put stringent constraints on the phase space density and "warmness" of dark matter [75]. At the same time, measurements of the small-scale density power spectrum of the Lyman α forest indicate that fluctuations with the amplitude expected in the ΛCDM model at the scales that control the abundance of dwarf mass halos are indeed present in the primordial spectrum [117, 118].

While the inner density distribution in observed satellites may still be affected by dark matter warmness in the allowed range of parameter space [77] (see, however, [79]), the models with such parameters would not suppress the overall abundance of satellites considerably. In fact, observations of flux ratios in the multiple image radio lenses appear to *require* an amount of substructure which is even larger than what is typically found in the CDM halos [119–121], disfavoring models with strongly suppressed abundance of small mass subhalos.

There is thus no compelling reason yet to think that the observed properties of galactic satellite populations are more naturally reproduced in these models. In the subsequent discussion, I will therefore use Occam's razor and focus on the possible explanations of the differences between observed satellites and subhalos in simulations within the ΛCDM model. The prime suspect in producing the discrepancy is the still quite uncertain physics of galaxy formation. After all, a similar problem exists for objects of larger masses and luminosities if we compare the slope of the luminosity function and the halo mass function [122–125] or the predicted and observed abundance of galaxies in the nearby low density "field" regions [126].

4.2. Physics of Galaxy Formation. Several plausible physical processes can suppress gas accretion and star formation in dwarf dark matter halos. The cosmological UV background, which reionized the universe at $z \gtrsim 6$, heats the intergalactic gas and establishes a characteristic time-dependent minimum mass for halos that can accrete gas [127–134].

The gas in the low-mass halos may be photoevaporated after reionization [135–137] or blown away by the first generation of supernovae [138–141] (see [142]). At the same time, the ionizing radiation may quickly dissociate molecular hydrogen, the only efficient coolant for low-metallicity gas in such halos, and prevent star formation even before the gas is completely removed [143]. Even if the molecular hydrogen is not dissociated, cooling rate in halos with virial temperature $T_{\rm vir} \lesssim 10^4$ K is considerably lower than in more massive halos [144] and we can therefore expect the formation of dense gaseous disks and star formation to be suppressed in such halos. (The virial virial temperature $T_{\rm vir}$ is related to the virial mass by $kT_{\rm vir} = (1/2)\mu m_p GM_{\rm vir}/R_{\rm vir}$, where isothermal temperature profile is assumed for simplicity. The virial mass and radius are related by definition as $M_{\rm vir} = 4\pi/3 \times \Delta_{\rm vir}\bar{\rho}R_{\rm vir}^3$. Assuming $\Delta_{\rm vir} = 178$ appropriate for $z \gtrsim 1$ regardless of Ω_0, this gives $M_{\rm vir} \approx 5.63 \times 10^7 h^{-1} M_\odot (\Omega_0/0.3)^{-1/2}((1+z)/11)^{-3/2}(T_{\rm vir}/10^4\,{\rm K})^{3/2}$.) Another potential galaxy formation suppression mechanism is the gas stripping effect of shocks from galactic outflows and cosmic accretion [145, 146]. Finally, even if the gas is accreted and cools in small-mass halos, it is not guaranteed that it will form stars if gas does not reach metallicities and surface densities sufficient for efficient formation of molecular gas and subsequent star formation [39, 147–150].

The combined effect of these processes is likely to leave most of dark matter halos with masses $\lesssim$ few $\times 10^9 M_\odot$ dark, and could have imprinted a distinct signature on the properties of the dwarf galaxies that did manage to form stars before reionization. In fact, if all these suppressing effects are as efficient as is usually thought, it is quite remarkable that galaxies such as the recently discovered ultra-faint dwarfs exist at all. One possibility extensively discussed in literature is that they managed to accrete a certain amount of gas and form stars before the universe was reionized [81–84, 87, 151–153]. Direct cosmological simulations do show that dwarf galaxies forming at $z > 6$ bear striking resemblance to the faint dwarf spheroidal galaxies orbiting the Milky Way [154–156] and their predicted abundance around the Milky Way is consistent with estimates of the abundance of the faintest satellites [151]. Alternatively, some authors argued [78, 89, 91, 157] that observed dwarf satellite galaxies could be in much more massive subhalos than was indicated by simple estimates of dynamical masses and circular velocities using stellar velocity dispersions. In this case, the relatively large halo mass could allow an object to resist the suppressing effects of the UV background.

Cosmological simulations also clearly show that the subhalos found within virial radii of larger halos at $z = 0$ have on average lost significant amount of mass and have been considerably more massive in the past [22, 38, 39]. The dramatic loss of mass occurs due to the tidal forces that subhalos experience as they orbit in the potential of the host. A significant fraction of the luminous dwarf satellites therefore can be associated with those subhalos that have been substantially more massive in the past and hence more resilient against galaxy formation suppressing processes. Such subhalos could have had a window of opportunity to form their stellar systems even if the subhalos they are embedded in today have relatively small mass [39].

4.3. Models for Luminous Satellite Population. Given the galaxy formation suppression mechanisms and evolutionary scenarios listed above, the models aiming to explain the substructure problem can be split into the following broad classes: (1) the "*threshold galaxy formation models*" in which luminous satellites are embedded in the most massive subhalos of CDM halos and their relatively small number indicates the suppression of galaxy formation in subhalos of circular velocity smaller than some threshold value [78, 89, 157] and (2) "*selective galaxy formation models*" in which only a fraction of small subhalos of a given *current* $V_{\rm max}$ and mass host luminous satellites while the rest remain dark.

In the second class of models the processes determining whether a subhalo hosts a luminous galaxy can be the reionization epoch [81, 87, 152–154, 158]: subhalos that assemble before the intergalactic medium was heated by ionized radiation become luminous. The observed faint dwarfs can then be the "fossils" of the pre-reionization epoch [154, 155]. Subhalo may also form a stellar system if its mass assembly history was favorable for galaxy formation [39]: namely, luminous subhalos are those that have had sufficiently large mass during a period of their evolution to allow them to overcome the star formation suppression processes.

Several models using a combination of the processes and scenarios outlined above have been shown to reproduce the gross properties of observed population of satellites reasonably well [39, 84, 85, 87]. How can we test different classes of models and differentiate between specific ones?

First, I think the fact the $m_{0.6}$ mass function for observed satellites has a different slope compared to simulation predictions (Figure 8) favors the second class of the selective galaxy formation models, at least for the brighter "classical" satellites. Indeed, given what we know about the average mass loss of subhalos, it is more natural to associate the observed systems with the halos of the largest mass *prior to accretion* [39] rather than with the subhalos with the largest current masses. Second, the predicted number of the weakly evolving pre-reionization objects [84, 151, 153], the extended star formation histories of most of the observed dwarf satellites [53–55, 159] (in fact, in terms of star formation the main difference between the dIrr and dSph galaxies appears to be presence or lack of star formation in the last 2 billion years before $z = 0$ [54]) , and the significant spread in metallicities and certain isotope ratios [160] indicate that majority of "classical" dwarfs have not formed most of their stars before reionization but have formed their stars over rather extended period of time ($\sim$10 Gyr). It is still possible, however, that a sizable fraction of the ultra-faint dwarfs are the "pre-reionization fossils" [151, 155, 161, 162], if star formation efficiency in these objects is greatly suppressed [84] compared to that of brighter dwarfs.

Interesting additional clues and constraints on the galaxy formation models available for the dwarf satellites of the Milky Way are the measurements of the total dynamical mass within their stellar extent. Observations show that the total masses within a fixed aperture of the observed satellites are remarkably similar despite a several order of magnitude span in dwarf satellite luminosities [49, 78, 88, 163, 164]. For example, the range of masses within 0.6 kpc shown in Figure 8 is only an order of magnitude. Furthermore, existence of the tight correlation between total dynamical mass within the half-light radius, $M(r_{\rm half})$, and the corresponding radius $r_{\rm half}$ [79] for bright dSph galaxies implies a very similar inner dark matter density profile of their host halos. Recently, Strigari et al. [88] have shown that the mass estimated within the central 300 pc, $m(< 0.3\,{\rm kpc}) \equiv m_{0.3}$, for all of the dwarfs with kinematic data varies by at most a factor of four, while the luminosity of the galaxies varies by more than four orders of magnitude.

These observational measurements put constraints on the range of masses of CDM subhalos that can host observed satellites. To estimate this range, we should first note that for the CDM halos described by the NFW profile [18] with concentration $c \equiv R_{\rm vir}/r_s$ (where r_s is the scale radius—the radius at which the density profile has logarithmic slope of -2) the dependence of the mass within a fixed small radius $x \equiv r/R_{\rm vir}$ on the total virial mass is

$$m(< x) = M_{\rm vir}\frac{f(cx)}{f(c)}, \quad \text{where } f(x) \equiv \ln(1+x) - \frac{x}{1+x}, \tag{3}$$

and is quite weak for $r = 300\,{\rm pc}$: $m_{0.3} \propto M_{\rm vir}^{0.3\text{–}0.35}$, as shown in Figure 9. Indeed, even for a halo with the Milky Way mass at $z = 0$ we expect $m_{0.3} \approx 4 \times 10^7 M_\odot$, a value not too different from those measured for the nearby dwarf spheroidals. Physically, the weak dependence of the central mass on the total mass of the halo reflects the fact that central regions of halos form very early by mergers of small-mass halos. Given that the rms amplitude of density perturbations on small scales is a weak function of scale, the central regions of halos of different mass form at a similar range of redshifts and thus have similar central densities reflecting the density of the universe when the inner region was assembled. At earlier epochs the dependence is stronger because 300 pc represents a larger fraction of the virial radius of halos.

Note that the relation plotted in Figure 9 is for isolated halos unaffected by tidal stripping. Taking into account effects of tidal stripping results in even flatter relation [86]: $m_{0.3} \propto M_{\rm vir}^{0.25}$, which also has a lower normalization (smaller $m_{0.3}$ for a given $M_{\rm vir}$. This is likely due to a combination of two effects: (1) the halos of larger mass have lower concentrations and thus can be stripped more efficiently and (2) the halos of larger mass can sink to smaller radii after they accrete and experience relatively more tidal stripping. Overall, the effect of tidal stripping and heating on $m_{0.3}$ appears to be substantial and cannot be neglected.

Finally, Figure 9 shows that the virial mass range corresponding to a given range of $m_{0.3}$ is quite different for halos that form at $z > 2$ compared to those that form at later epochs due to the rapidly evolving NFW concentration concentration for a fixed halo mass [165]. The mass $m_{0.3}$ can therefore be only interpreted in the context of a model for subhalo evolutionary histories.

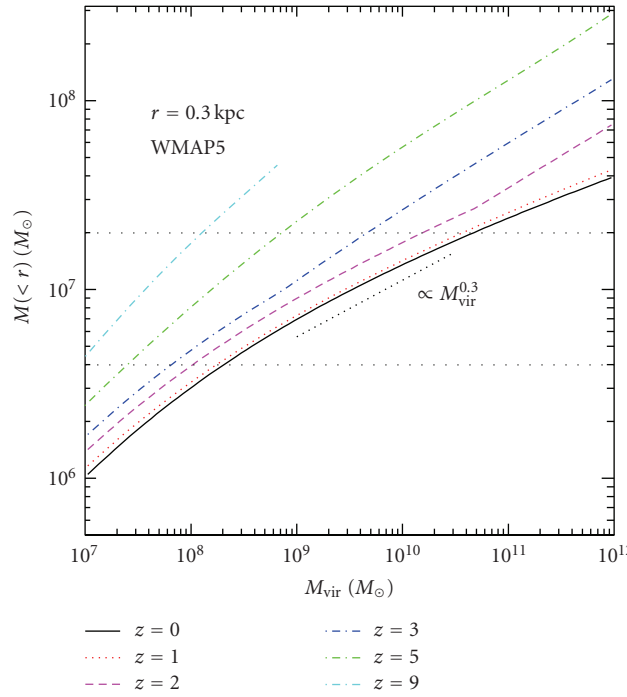

Figure 9: The mass within central 300 pc versus the total virial mass of an NFW halo predicted using the concentration mass relation $c(M_{\rm vir})$ at different redshifts in the concordance WMAP 5-year best fit cosmology. The horizontal dotted lines indicate the range of $m_{0.3}$ masses measured for the Milky Way dwarf satellites.

Several recent studies have used such models to show that the nearly constant central mass of the satellite halos is their natural outcome [84–86]. This outcome can be understood as a combination of the weakness of the $m_{0.3} - M_{\rm vir}$ correlation and the fact that in the galaxy formation models galaxy luminosity L *must* be a nonlinear function of $M_{\rm vir}$ in order to produce a faint-end slope of the galaxy luminosity function much shallower than the slope of the small-mass tail of the halo mass function.

For example, if the faint-end slope of the luminosity function is ξ (i.e., $dn(L)/dL \propto L^\xi$) and the slope of the halo mass function at small mass end is ζ ($dn(M)/dM \propto M^\zeta$) and we assume for simplicity a one-to-one monotonic matching between galaxies and halos $n(> L) = n(> M)$ (see [166–168] for the detailed justification for such assumption), the implied slope of the $L - M_{\rm vir}$ relation is $\beta = (1+\zeta)/(1+\xi)$, which for the fiducial values of $\zeta \approx -2$ and $\xi \approx -1.2$ gives $\beta \approx 5$. In semianalytic models, such a steep nonlinear $L - M_{\rm vir}$ relation is usually assumed to be set by either suppression of gas accretion due to UV heating or by gas blowout due to SN feedback, e.g., [83]). If I instead assume the faint-end slope of $\xi \approx 1.5$-1.6 as suggested by recent measurement of [125], the relation is shallower but is still nonlinear: $\beta \approx 2$.

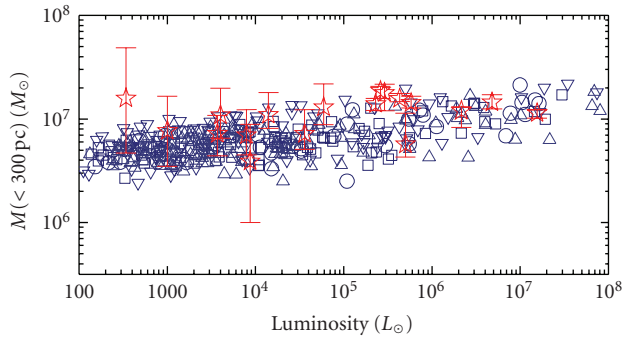

FIGURE 10: The mass within the central 300 pc versus luminosity for the dwarf satellites of the Milky Way (stars with error bars, see [88]). The open symbols of different types show the expected relation for subhalos in three different Milky Way-sized halos formed in the simulations of the concordance ΛCDM cosmology if the luminosity of the subhalos is related to their virial mass at accretion epoch as $L = 5 \times 10^3 L_\odot (M_{\mathrm{vir,acc}}/10^9 M_\odot)^{2.5}$ (see text for discussion).

Regardless of the specific processes producing the non-linear luminosity-mass relation, for a relation of the form $L \propto M_{\mathrm{vir}}^{\beta}$, we have $L \propto m_{0.3}^{\gamma}$, where $\gamma \approx \beta/0.25$, using the $m_{0.3} - M_{\mathrm{vir}}$ relation above taking into account effects of tidal stripping. To account for a smaller than a factor of four spread in central masses for approximately four orders of magnitude spread in luminosity one needs $\gamma \approx 6$–8 or $\beta \approx 2$–4, the values not too different from the estimate above. Thus, *the weak correlation of the $m_{0.3}$ and luminosity will be the natural outcome of any* CDM*-based galaxy formation model which reproduces the slope of the faint end of the galaxy luminosity function.*

Within the framework I just described, the slope of the $m_{0.3} - L$ correlation depends on the slope of the $L - M_{\mathrm{vir,acc}}$ correlation β. The models published so far [84–86], as well as the simple model above with the slope $\beta \approx$ 2-3, predict that the slope of the $L - m_{0.3}$ relation is shallow but is nevertheless not zero. Constraining this slope with future observations will tighten constraints on the galaxy formation models and will tell us more about the $L - M_{\mathrm{vir}}$ correlation if such exists.

To illustrate the points just made, Figure 10 shows the $m_{0.3} - L$ relation for the observed nearby dwarfs [88] and subhalos found within $300h^{-1}$ kpc around three different MW-sized halos formed in the concordance cosmological model (see [39, 151] for simulation details).(The simulations used here do not reliably resolve the mass within 300 pc. Therefore, in order to calculate the mass I have used the mass and concentration of each subhalo at the epoch when it was accreted and computed evolution of their density profile given the mass loss they experienced by the present epoch, as measured in cosmological simulations, and using results of controlled high-resolution simulations of tidal evolution [43], which predict the evolution of the NFW concentration of halos as a function of tidal mass loss. The mass $m_{0.3}$ was then computed from the evolved density profile.) To assign luminosity to a given subhalo I follow the logic of the model presented in [39], which posits that the brightest observed satellites should correspond to the subhalos which have the largest mass before they were accreted. In this model the luminosity of stellar systems should positively correlate with the mass of its host subhalo *before it was accreted* onto the MW progenitor, $M_{\mathrm{vir,acc}}$:

$$L_V = 5 \times 10^3 L_\odot \left(\frac{M_{\mathrm{vir,acc}}}{10^9 M_\odot}\right)^{2.5}. \quad (4)$$

The power law form of the relation is motivated by the approximately power law form of the galaxy luminosity and halo mass functions at faint luminosities and small masses. The actual parameters were chosen such that luminosities of the most massive subhalos roughly match the luminosities of the most massive satellites, such as the SMC and LMC ($L \sim 10^8$-$10^9 L_\odot$). (Figure 10 does not show the most massive subhalos which would correspond to the systems such as the Large Magellanic Clouds, which have luminosities $L > 10^8 L_\odot$ outside the range shown in the figure. This is justified because observational points shown in the figure include only the fainter dwarf spheroidal galaxies.) After all, the first order of business for all the models of satellite population is to reproduce the abundance and luminosities of the most massive ($V_{\mathrm{max}} \gtrsim 40$ km/s) satellites. The slope of the relation in (4) was set to reproduce the range of observed satellite luminosities and flatness of the $m_{0.3} - L$ relation. Note that this model does not assume any threshold for formation of galaxies. It simply implies that the efficiency with which baryons are converted into stars, $f_* = M_*/M_{\mathrm{vir}}$, steadily decreases with decreasing M_{vir} at the rate given by (4). The slope of 2.5 assumed in the equation above is on the lower end of the slopes suggested by matching of the faint end of galaxy luminosity function and small-mass end of halo mass functions discussed above, but is within the current uncertainties in the slope of the former [125]. Assuming such relation for field halos would therefore also reproduce the observed faint end of galaxy luminosity function within current uncertainties.

Figure 10 shows that the model with parameters of (4) is in agreement with observed measurements of the $m_{0.3} - L_V$ relation. The results will not change drastically if a somewhat steeper (≈3–3.5) slope is assumed. (The model of (4) is similar to the model 1B in the recent study by Koposov et al. [84], which assumes that stellar mass scales as $M_* = f_* M_0 (M_{\mathrm{vir,acc}}/M_0)^{1+\alpha}$, These authors find that the model reproduces the luminosity function of satellites for $f_* \approx 1.7 \times 10^{-4}$, $M_0 = 10^{10} M_\odot$, and $\alpha = 2$, which gives $M_* = 1.7 \times 10^3 (M_{\mathrm{sat}}/10^9 M_\odot)^3$, quite similar to the relation given by (4). Koposov et al. adjust parameters to match the observed luminosity function and then show that $L - m_{0.3}$ relation is reproduced, while I adopted the opposite route here. The key difference between the models is that their model assumes a ceiling on the value of $M_*/M_{\mathrm{vir,acc}}$, while I assume no such ceiling. Absence of the ceiling on star formation efficiency is actually important for bright satellites (see Figure 14).)

Having fixed the parameters of the $L - M_{\mathrm{vir,acc}}$ relation, we can then ask the question of whether the luminosity function of satellites would be reproduced self-consistently by such a model. We can use the observed luminosity functions corrected for completeness for the faintest dwarfs

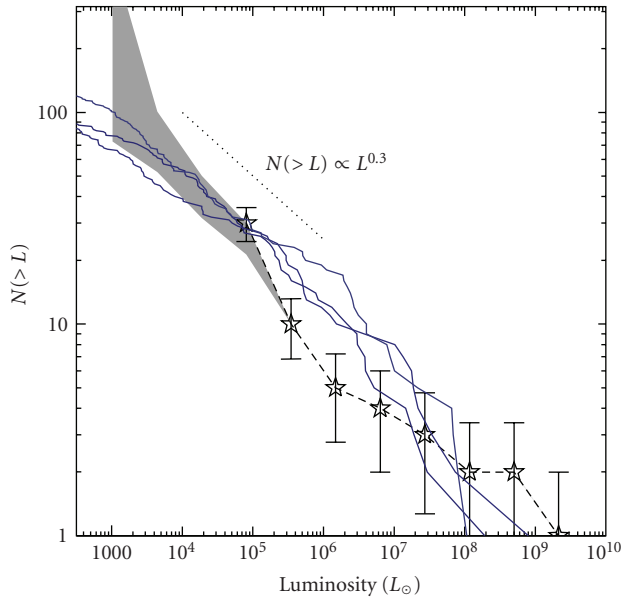

Figure 11: The cumulative luminosity function of subhalos in the three MW-sized halos shown in Figure 10 with the simple luminosity assignment ansatz of (4). The luminosity function includes all subhalos within 417 kpc from the center of each halo, the same radius as was used to construct the luminosity function of the observed satellites shown in Figure 6. The points with (Poisson) error bars, connected by the dashed line, and the shaded region show the observed and inferred satellite luminosity functions within the same radius for classical and ultra-faint dwarfs, respectively, as compiled by [56] (see text for details).

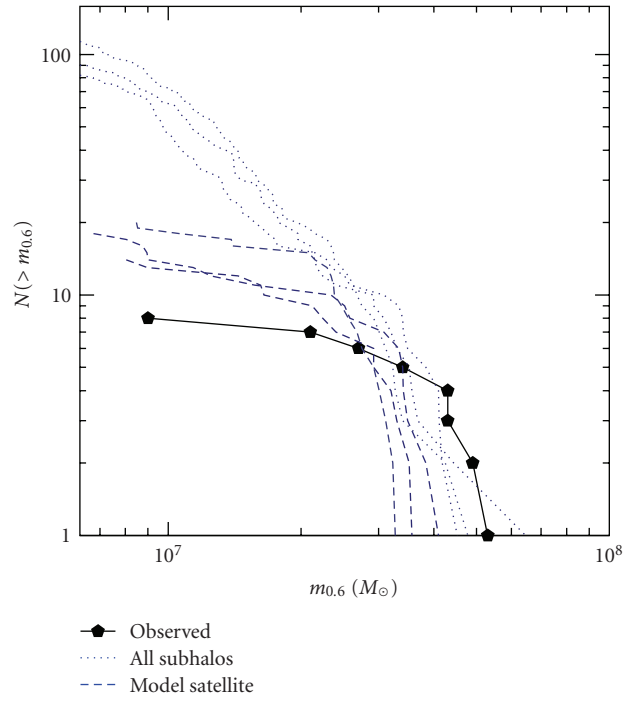

Figure 12: The cumulative $m_{0.6}$ function of subhalos in the ΛCDM simulations of three MW halos (dotted lines) and for the observed dSph Milky Way satellites (points, connected by solid line) Sagittarius was excluded due to its very large mass errors), as measured by [90]. The dashed lines show the mass function for subhalos with $L \geq 2.6 \times 10^5 L_\odot$ and $d < 270$ kpc (the same range of luminosities and distances as for the observed satellites) with luminosities assigned using (4). I have excluded the two most luminous objects from the model luminous satellites to account for the fact that SMC and LMC are not included in the observational sample and one additional object to account for noninclusion of the Sagittarius dwarf in the comparison.

from [56] (shown in Figure 6) to test this. Figure 11 shows the subhalo luminosity functions constructed using subhalos identified within 417 kpc (the same outer radius used in the construction of the observed luminosity function by [56]) in the simulations and the simple luminosity assignment scheme of (4). The points with (Poisson) error bars and the shaded region show the observed luminosity functions for the classical satellites and for ultra-faint dwarfs, as compiled by [56]. As I noted before, the current samples of the ultra-faint satellites exist only over a fraction of the sky and there are reasons to expect that they are incomplete for distances larger than ≈50 kpc. The shaded region, therefore, represents the likely bracket of the possibilities. The lower edge of the region is the luminosity function in the case when the observed luminosity function of the ultra-faints is simply corrected for the fractional sky coverage. The upper edge of the shaded region shows a combined correction for both the sky coverage and radial distribution assuming that ultra-faints have the same radial distribution as mass-selected subhalos in the Via Lactea I simulation [56].

Figure 11 shows that although the model and observed luminosity functions do not match perfectly, they are in reasonable agreement. One should remember a number of uncertainties in the model luminosity functions. First, the masses of host halos can be a factor of two or so larger than the mass of the Milky Way and the cosmology of the simulations may not be exactly correct. Second, the $L - M_{\rm acc}$ relation assumed in the model can be somewhat different from that assumed in the figure: for example, the slope can be somewhat steeper and normalization lower, which would make both the $m_{0.3} - L$ relation flatter and the luminosity functions closer to observations. The fiducial relation in (4) was chosen to have the shallowest slope (2.5) still reasonably consistent with observations.

Figure 12 shows comparison of the $m_{0.6}$ mass functions for the observed "classical" dwarf spheroidal satellites of the Milky Way [90] and predicted mass function for the entire subhalo population of the MW-sized halos within 270 kpc (the largest distance of the observed satellite included in the comparison) and the subhalos with $L > 2.6 \times 10^5 L_\odot$ (the smallest dSph luminosity included in the observed sample) with luminosities assigned using (4). I have excluded the Sagittarius dwarf from this comparison as its $m_{0.6}$ mass has very large errors [90]. The number of the predicted luminous satellites was reduced by three to account for exclusion of the Sagittarius, SMC, and LMC from the comparison. The figure shows that the model predicts the range of $m_{0.6}$ quite similar to that measured for the observed luminous dSphs. The shape of the mass function is also in reasonably good

agreement with the data. Although there are somewhat more predicted satellites at small masses, this is likely due to the somewhat larger virial mass of the simulated halos ($\approx 2 - 3 \times 10^{12} M_\odot$) compared to the mass of the Milky Way ($\approx 10^{12} M_\odot$). We expect the number of subhalos to scale approximately linearly with host mass and so the difference in the virial mass of the Milky Way and simulated halos can account for the difference with observations in Figure 12. There is some discrepancy at the largest $m_{0.6}$ values, but it is not clear just how significant the discrepancy is given that the typical errors on the $m_{0.6}$ measurements for these galaxies are ≈20%–40%.

Finally, Figure 13 compares cumulative radial distribution of the observed "classical" Milky Way satellites within 280 kpc and satellites with similar luminosities and within the same distance from their host halo in the model of (4). The figure also shows the cumulative distribution of all subhalos selected using their current $V_{\max}$. The predicted distribution of bright luminous satellites is somewhat more radially concentrated than the distribution of the $V_{\max}$-selected subhalos and is in reasonable agreement with the observed distribution both in its median and in the overall shape.

Thus, the observed $m_{0.3} - L$ relation, the luminosity function, the $m_{0.6}$ mass function, and the radial distribution of the observed satellites can all be reproduced simultaneously with such a simple dwarf galaxy formation scenario. The observational uncertainties in these statistics are still quite large, which leaves significant freedom in the parameters of (4) and in its functional form. (It is quite possible that relation between luminosity and mass is more complicated than (4). For example, the normalization of the $L - M_{\rm vir,acc}$ relation can evolve with redshift because luminosity may be determined both by the mass of the halo at the accretion epoch and by the period of time before its accretion during which it was sufficiently massive to withstand star formation suppressing processes. Such redshift dependence would be an extra parameter which would generate scatter in the $L - M_{\rm vir,acc}$ relation.) It is also possible that all of these statistics may be reproduced in a drastically different scenario. Nevertheless, the success of such simple model is encouraging and it is interesting to discuss its potential implications.

First of all, (4) implies that all of the observed Milky Way dSph satellites had virial masses $M_{\rm vir,acc} \gtrsim 5 \times 10^8 M_\odot$ when they were accreted and these masses may span the range up to $\sim 5 \times 10^{10} M_\odot$ (the actual range depends sensitively on the slope of the $L - M_{\rm vir,acc}$ relation). This shows that progenitors of the observed satellites could have had a wide range of virial masses, even though the range of their $m_{0.3}$ and $m_{0.6}$ masses is narrow.

An interesting implication of the value of lowest mass of the range of masses above is that whatever gas the small-mass halos ($M_{\rm vir} \lesssim 5 \times 10^8 M_\odot$) are able to accrete, it should remain largely unused for star formation, and of course would not be blown away by supernovae (given that the model implies that such objects should have no stars or supernovae). If some of this gas is neutral, it can contribute to HI absorption lines in the spectra of quasars and distant galaxies. If this gas is enriched, it can also produce absorption lines of heavier elements. At lower redshifts, the neutral gas in the otherwise starless or very faint halos could manifest itself in the form of the High Velocity Clouds (HVCs) abundant in the Local Group [169–172] and around other galaxies.

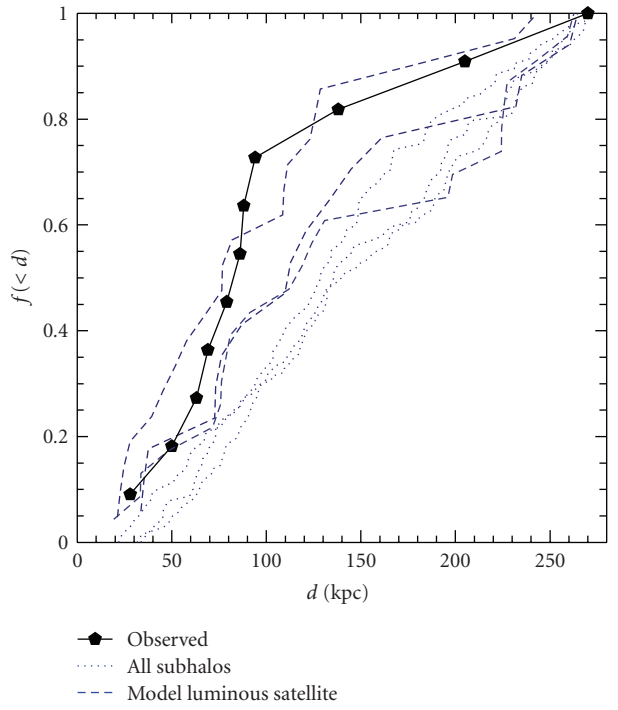

Figure 13: The cumulative radial distribution of the observed "classical" Milky Way satellites (solid points connected by the solid line) within 280 kpc and satellites with similar luminosities and within the same distance from their host halo in the model of (4) (dashed lines). The figure also shows the cumulative distribution of all subhalos selected using their current $V_{\max}$ (dotted lines).

Second, as I noted above the slope of the $L - M_{\rm vir}$ relation required to explain the weak dependence of $m_{0.3}$ on luminosity is not surprising, given what we know about the faint-end slope of galaxy luminosity function and what we expect about the slope of the mass function of their host halos in CDM scenario [173]. The implied *normalization* of the $L - M_{\rm vir}$ relation, however, is quite interesting. For example, it indicates that halo of $M_{\rm vir,acc} = 10^{10} M_\odot$ should have luminosity of $L_V = 1.6 \times 10^6 L_\odot$. Converting it to stellar mass assuming $M_*/L_V = 1$ (appropriate for old populations, e.g., [174]) gives $M_* = 1.6 \times 10^6 M_\odot$. Results of cosmological simulations with UV heating of gas show that halos of $M \sim 10^{10} M_\odot$ should have been able to accrete almost all of their universal share of baryons, $M_b = (\Omega_b/\Omega_m) M_{\rm vir,acc} \approx 1.7 \times 10^9 M_\odot$ (assuming $\Omega_b/\Omega_m \approx 0.17$ suggested by the WMAP measurements [10]), even in the presence of realistic UV heating [133, 134]. The derived stellar mass thus implies that only $F_* \equiv M_*/M_{\rm vir,acc} \times (\Omega_m/\Omega_b) \approx 0.001$ (i.e., 0.1%) of the expected baryon mass was converted into stars in such objects. Such small efficiency F_* for systems accretion onto which is not suppressed by the UV heating implies that *star formation is dramatically suppressed by some other mechanism.*

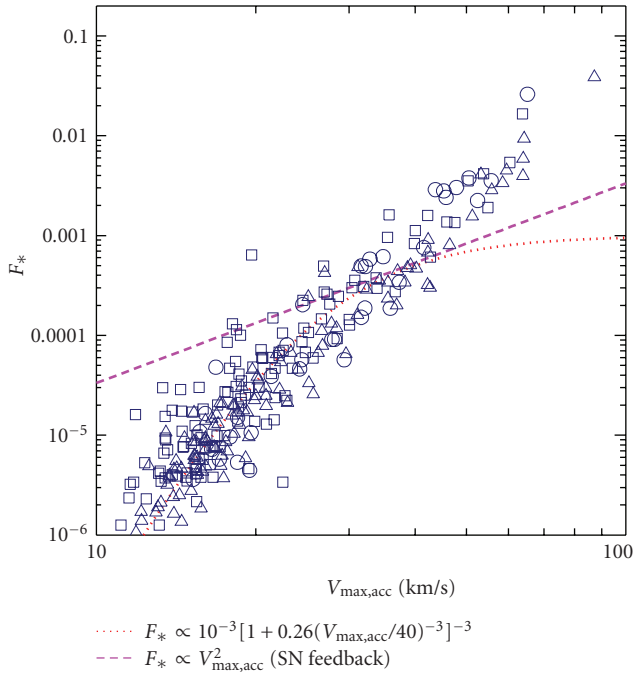

FIGURE 14: The efficiency of gas conversion into stars, defined as the fraction of baryon mass, expected if the halo accreted its universal fraction of baryons, converted into stars: $F_* = (\Omega_m/\Omega_b)(M_*/M_{\mathrm{vir,acc}})$. The points (as before different symbols correspond to subhalos in three different simulated host halos) show the dependence of F_* on the maximum circular velocity of each subhalo at accretion according to luminosity assignment model of (4). The short-dashed line shows the functional form expected if F_* was controlled by the suppression of gas accretion due to UV heating of intergalactic gas (model 3B of [84]), while long-dashed line shows scaling expected in efficiency was set by supernova feedback (e.g., [140]).

In fact, the implied efficiency of baryon conversion into the stars, F_*, in this model is a steep, power law function of mass and circular velocity ($F_* \approx V^{8\div9}_{\mathrm{max,acc}}$), as shown in Figure 14. The figure also shows the functional form one would have expected if the dependence of the efficiency F_* on circular velocity was determined by the fraction of gas halos are able to accrete in the presence of the UV radiation. This functional form is almost identical to the fiducial model 3B of Koposov et al. [84] (I used slightly larger value for critical velocity because I use V_{max} rather than the virial circular velocity used by these authors). The two models have similar behavior at $V_{\mathrm{max,acc}} \lesssim 30$ km/s, but the UV heating model asymptotes to a fixed value of $F_* = 10^{-3}$ for more massive systems. This model would therefore underpredict luminosities of the most massive satellites in MW-sized halos, which was noticed by Koposov et al. in its failure to reproduce the bright end of the satellite luminosity function. Moreover, the estimates of the efficiency F_* for more luminous galaxies, such as the Milky Way, are in the range $F_* \sim 0.05$–0.2 [175–178], which would lie roughly on the continuation of the relation in Figure 14 to larger circular velocities shown by symbols. (The $F_* - V_{\mathrm{max}}$ relation could plausibly flatten at larger V_{max}, as expected from the halo modeling of the galaxy population, e.g., [173].)

These considerations indicate a very interesting possibility that while the UV heating can mediate accretion of gas into very small mass halos, the efficiency with which the accreted gas is converted into stars in the known luminous galaxies is dramatically suppressed by some other *mass-dependent* mechanism. This strong suppression operates not only for halos in which gas accretion is suppressed but for halos of larger masses as well. Note that this suppression mechanism is unlikely to be due to blowout of gas by supernovae, which is expected to give $F_* \propto V^2_{\mathrm{max}}$ (e.g., [140]), a much shallower relation than the scaling in Figure 14.

While discussion of the nature of this suppression mechanism is outside the scope of this paper, the rapidly improving observational data on the satellite population should shed light on the possible mechanisms.

The exercise presented in this section illustrates just how powerful the combination of luminosity function and radial distribution of satellites, high-quality resolved kinematics data and inferred dynamical constraints on the total mass profile, measurements of star formation histories and enrichment histories can be in understanding formation of dwarf galaxies. The rapidly improving constraints on the mass profiles of the dSph galaxies down to the smallest luminosities [79, 88] should further constrain the range of subhalo masses hosting the observed satellites and, by inference, the efficiency of star formation in such small halos. The hints that star formation efficiency is actually a monotonic function of halo mass from galaxies such as the Milky Way to the faintest known galaxies, such as Segue 1, indicates that the physics learned from the "near-field cosmology" studies of the nearest dwarfs can potentially give us important insights into formation of more massive galaxies as well.

Acknowledgments

The author would like to thank Brant Robertson, Anatoly Klypin, Nick Gnedin, Jorge Peñarrubia, Erik Tollerud, and James Bullock for useful comments on the manuscript and stimulating discussions on the topics related to the subject of this paper. This work was partially funded by the NSF grants AST-0507666, and AST-0708154. The research was also partially supported by the Kavli Institute for Cosmological Physics at the University of Chicago through grant NSF PHY-0551142 and an endowment from the Kavli Foundation. He also would like to thank Kavli Institute for Theoretical Physics (KITP) in Santa Barbara and organizers of the 2008 KITP workshop "Back to the Galaxy II" where some of the work presented here was carried out, for hospitality and wonderful atmosphere. He has made extensive use of the NASA Astrophysics Data System and arXiv.org preprint server during writing of this paper.

References

[1] S. D. M. White and M. J. Rees, "Core condensation in heavy halos—a two-stage theory for galaxy formation and clustering," *Monthly Notices of the Royal Astronomical Society*, vol. 183, pp. 341–358, 1978.

[2] G. R. Blumenthal, S. M. Faber, J. R. Primack, and M. J. Rees, "Formation of galaxies and large-scale structure with cold dark matter," *Nature*, vol. 311, no. 5986, pp. 517–525, 1984.

[3] A. Loeb and M. Zaldarriaga, "Small-scale power spectrum of cold dark matter," *Physical Review D*, vol. 71, no. 10, Article ID 103520, 2005.

[4] S. D. M. White, "Formation and evolution of galaxies," in *Cosmology and Large Scale Structure*, R. Schaeffer, J. Silk, M. Spiro, and J. Zinn-Justin, Eds., pp. 349–430, Elsevier Scientific, Amsterdam, The Netherlands, 1996.

[5] B. Moore, S. Ghigna, F. Governato, G. Lake, T. Quinn, and J. Stadel, "The structure of cold dark matter halos," in *Large Scale Structure: Tracks and Traces*, V. Mueller, S. Gottloeber, J. P. Muecket, and J. Wambsganss, Eds., pp. 37–40, World Scientific, Singapore, 1998.

[6] S. Ghigna, B. Moore, F. Governato, G. Lake, T. Quinn, and J. Stadel, "Dark matter haloes within clusters," *Monthly Notices of the Royal Astronomical Society*, vol. 300, no. 1, pp. 146–162, 1998.

[7] G. Tormen, A. Diaferio, and D. Syer, "Survival of substructure within dark matter haloes," *Monthly Notices of the Royal Astronomical Society*, vol. 299, no. 3, pp. 728–742, 1998.

[8] B. Moore, S. Ghigna, F. Governato, et al., "Dark matter substructure within galactic halos," *The Astrophysical Journal*, vol. 524, no. 1, pp. L19–L22, 1999.

[9] A. Klypin, S. Gottlöber, A. V. Kravtsov, and A. M. Khokhlov, "Galaxies in N-body simulations: overcoming the overmerging problem," *The Astrophysical Journal*, vol. 516, no. 2, pp. 530–551, 1999.

[10] J. Dunkley, E. Komatsu, M. R. Nolta, et al., "Five-year wilkinson microwave anisotropy probe observations: likelihoods and parameters from the WMAP data," *The Astrophysical Journal*, vol. 180, no. 2, pp. 306–329, 2009.

[11] A. Kravtsov, "Modeling galaxy clustering with cosmological simulations," in *Proceedings of the 41st Rencontres de Moriond*, 2006.

[12] Y. Birnboim and A. Dekel, "Virial shocks in galactic haloes?" *Monthly Notices of the Royal Astronomical Society*, vol. 345, no. 1, pp. 349–364, 2003.

[13] D. Kereš, N. Katz, D. H. Weinberg, and R. Davé, "How do galaxies get their gas?" *Monthly Notices of the Royal Astronomical Society*, vol. 363, no. 1, pp. 2–28, 2005.

[14] W. J. G. de Blok, F. Walter, E. Brinks, C. Trachternach, and R. C. Kennicutt, "High-resolution rotation curves and galaxy mass models from things," *The Astronomical Journal*, vol. 136, no. 6, pp. 2648–2719, 2008.

[15] W. J. G. de Blok, "The Core-Cusp problem," *Advances in Astronomy*, 2009.

[16] A. A. Dutton, F. C. van den Bosch, A. Dekel, and S. Courteau, "A revised model for the formation of disk galaxies: low spin and dark halo expansion," *The Astrophysical Journal*, vol. 654, no. 1, pp. 27–52, 2007.

[17] L. Mayer, F. Governato, and T. Kaufmann, "The formation of disk galaxies in computer simulations," *Advanced Science Letters*, vol. 1, no. 1, pp. 7–27, 2008.

[18] J. F. Navarro, C. S. Frenk, and S. D. M. White, "A universal density profile from hierarchical clustering," *The Astrophysical Journal*, vol. 490, no. 2, pp. 493–508, 1997.

[19] A. V. Kravtsov, A. A. Berlind, R. H. Wechsler, et al., "The dark side of the halo occupation distribution," *The Astrophysical Journal*, vol. 609, no. 1, pp. 35–49, 2004.

[20] L. Gao, S. D. M. White, A. Jenkins, F. Stoehr, and V. Springel, "The subhalo populations of ΛCDM dark haloes," *Monthly Notices of the Royal Astronomical Society*, vol. 355, no. 3, pp. 819–834, 2004.

[21] F. C. van den Bosch, G. Tormen, and C. Giocoli, "The mass function and average mass-loss rate of dark matter subhaloes," *Monthly Notices of the Royal Astronomical Society*, vol. 359, no. 3, pp. 1029–1040, 2005.

[22] C. Giocoli, G. Tormen, and F. C. van den Bosch, "The population of dark matter subhaloes: mass functions and average mass-loss rates," *Monthly Notices of the Royal Astronomical Society*, vol. 386, no. 4, pp. 2135–2144, 2008.

[23] G. Kauffmann, S. D. M. White, and B. Guiderdoni, "The formation and evolution of galaxies within merging dark matter haloes," *Monthly Notices of the Royal Astronomical Society*, vol. 264, no. 1, pp. 201–218, 1993.

[24] A. Klypin, A. Kravtsov, O. Valenzuela, and F. Prada, "Where are the missing galactic satellites?" *The Astrophysical Journal*, vol. 522, no. 1, pp. 82–92, 1999.

[25] V. Springel, S. D. M. White, G. Tormen, and G. Kauffmann, "Populating a cluster of galaxies: I. Results at $z = 0$," *Monthly Notices of the Royal Astronomical Society*, vol. 328, no. 3, pp. 726–750, 2001.

[26] J. Diemand, B. Moore, and J. Stadel, "Velocity and spatial biases in cold dark matter subhalo distributions," *Monthly Notices of the Royal Astronomical Society*, vol. 352, no. 2, pp. 535–546, 2004.

[27] S. P. D. Gill, A. Kneb, and B. K. Gibson, "The evolution of substructure: I. A new identification method," *Monthly Notices of the Royal Astronomical Society*, vol. 351, no. 2, pp. 399–409, 2004.

[28] J. Weller, J. P. Ostriker, P. Bode, and L. Shaw, "Fast identification of bound structures in large N-body simulations," *Monthly Notices of the Royal Astronomical Society*, vol. 364, no. 3, pp. 823–832, 2005.

[29] S. R. Knollmann and A. Knebe, "AHF: Amiga's halo finder," *The Astrophysical Journal*, vol. 182, no. 2, pp. 608–624, 2009.

[30] O. Lahav, P. B. Lilje, J. R. Primack, and M. J. Rees, "Dynamical effects of the cosmological constant," *Monthly Notices of the Royal Astronomical Society*, vol. 251, pp. 128–136, 1991.

[31] J. Diemand, M. Kuhlen, P. Madau, et al., "Clumps and streams in the local dark matter distribution," *Nature*, vol. 454, no. 7205, pp. 735–738, 2008.

[32] V. Springel, J. Wang, M. Vogelsberger, et al., "The Aquarius Project: the subhaloes of galactic haloes," *Monthly Notices of the Royal Astronomical Society*, vol. 391, no. 4, pp. 1685–1711, 2008.

[33] J. Stadel, D. Potter, B. Moore, et al., "Quantifying the heart of darkness with GHALO—a multibillion particle simulation of a galactic halo," *Monthly Notices of the Royal Astronomical Society*, vol. 398, no. 1, pp. L21–L25, 2009.

[34] A. Jenkins, C. S. Frenk, S. D. M. White, et al., "The mass function of dark matter haloes," *Monthly Notices of the Royal Astronomical Society*, vol. 321, no. 2, pp. 372–384, 2001.

[35] J. Tinker, A. V. Kravtsov, A. Klypin, et al., "Toward a halo mass function for precision cosmology: the limits of universality," *The Astrophysical Journal*, vol. 688, no. 2, pp. 709–728, 2008.

[36] A. R. Zentner and J. S. Bullock, "Halo substructure and the power spectrum," *The Astrophysical Journal*, vol. 598, no. 1, pp. 49–72, 2003.

[37] J. Diemand, B. Moore, and J. Stadel, "Earth-mass dark-matter haloes as the first structures in the early universe," *Nature*, vol. 433, no. 7024, pp. 389–391, 2005.

[38] D. Nagai and A. V. Kravtsov, "The radial distribution of galaxies in Λ cold dark matter clusters," *The Astrophysical Journal*, vol. 618, no. 2, pp. 557–568, 2005.

[39] A. V. Kravtsov, O. Y. Gnedin, and A. A. Klypin, "The tumultuous lives of galactic dwarfs and the missing satellites problem," *The Astrophysical Journal*, vol. 609, no. 2, pp. 482–497, 2004.

[40] P. Colín, A. A. Klypin, A. V. Kravtsov, and A. M. Khokhlov, "Evolution of bias in different cosmological models," *The Astrophysical Journal*, vol. 523, no. 1, pp. 32–53, 1999.

[41] L. Gao, G. de Lucia, S. D. M. White, and A. Jenkins, "Galaxies and subhaloes in ACDM galaxy clusters," *Monthly Notices of the Royal Astronomical Society*, vol. 352, no. 2, pp. L1–L5, 2004.

[42] A. V. Macciò, B. Moore, J. Stadel, and J. Diemand, "Radial distribution and strong lensing statistics of satellite galaxies and substructure using high-resolution ACDM hydrodynamical simulations," *Monthly Notices of the Royal Astronomical Society*, vol. 366, no. 4, pp. 1529–1538, 2006.

[43] J. Peñarrubia, J. F. Navarro, and A. W. McConnachie, "The tidal evolution of Local Group dwarf spheroidals," *The Astrophysical Journal*, vol. 673, no. 1, pp. 226–240, 2008.

[44] A. R. Zentner, A. V. Kravtsov, O. Y. Gnedin, and A. A. Klypin, "The anisotropic distribution of galactic satellites," *The Astrophysical Journal*, vol. 629, no. 1, pp. 219–232, 2005.

[45] N. I. Libeskind, C. S. Frenk, S. Cole, et al., "The distribution of satellite galaxies: the great pancake," *Monthly Notices of the Royal Astronomical Society*, vol. 363, no. 1, pp. 146–152, 2005.

[46] X. Kang, F. C. van den Bosch, X. Yang, et al., "The alignment between satellites and central galaxies: theory versus observations," *Monthly Notices of the Royal Astronomical Society*, vol. 378, no. 4, pp. 1531–1542, 2007.

[47] V. Belokurov, D. B. Zucker, N. W. Evans, et al., "Cats and dogs, hair and a hero: a quintet of new Milky Way companions," *The Astrophysical Journal*, vol. 654, no. 2, pp. 897–906, 2007.

[48] M. Geha, B. Willman, J. D. Simon, et al., "The least-luminous galaxy: spectroscopy of the Milky Way satellite segue 1," *The Astrophysical Journal*, vol. 692, no. 2, pp. 1464–1475, 2009.

[49] M. Mateo, "Dwarf galaxies of the Local Group," *Annual Review of Astronomy and Astrophysics*, vol. 36, no. 1, pp. 435–506, 1998.

[50] S. Stierwalt, M. P. Haynes, R. Giovanelli, et al., "The arecibo legacy fast alfa survey. IX. The Leo region H I catalog, group membership, and the H I mass function for the Leo I group," *The Astrophysical Journal*, vol. 138, no. 2, pp. 338–361, 2009.

[51] J. Woo, S. Courteau, and A. Dekel, "Scaling relations and the fundamental line of the Local Group dwarf galaxies," *Monthly Notices of the Royal Astronomical Society*, vol. 390, no. 4, pp. 1453–1469, 2008.

[52] E. K. Grebel and J. S. Gallagher III, "The impact of reionization on the stellar populations of nearby dwarf galaxies," *The Astrophysical Journal*, vol. 610, no. 2, pp. L89–L92, 2004.

[53] A. E. Dolphin, D. R. Weisz, E. D. Skillman, and J. A. Holtzman, "Star formation histories of Local Group dwarf galaxies," http://arxiv.org/abs/astroph/0506430.

[54] C. Orban, O. Y. Gnedin, D. R. Weisz, E. D. Skillman, A. E. Dolphin, and J. A. Holtzman, "Delving deeper into the tumultuous lives of galactic dwarfs: modeling star formation histories," *The Astrophysical Journal*, vol. 686, no. 2, pp. 1030–1044, 2008.

[55] E. Tolstoy, V. Hill, and M. Tosi, "Star-formation histories, abundances, and kinematics of dwarf galaxies in the Local Group," *Annual Review of Astronomy and Astrophysics*, vol. 47, pp. 371–425, 2009.

[56] E. J. Tollerud, J. S. Bullock, L. E. Strigari, and B. Willman, "Hundreds of Milky Way satellites? Luminosity bias in the satellite luminosity function," *The Astrophysical Journal*, vol. 688, no. 1, pp. 277–289, 2008.

[57] B. Willman, F. Governato, J. J. Dalcanton, D. Reed, and T. Quinn, "The observed and predicted spatial distribution of Milky Way satellite galaxies," *Monthly Notices of the Royal Astronomical Society*, vol. 353, no. 2, pp. 639–646, 2004.

[58] D. Lynden-Bell, "The Fornax-Leo-Sculptor system," *The Observatory*, vol. 102, pp. 202–208, 1982.

[59] S. R. Majewski, "The Fornax-Leo-Sculptor stream revisited," *The Astrophysical Journal*, vol. 431, no. 1, pp. L17–L21, 1994.

[60] F. D. A. Hartwick, "The structure of the outer halo of the galaxy and its relationship to nearby large-scale structure," *The Astronomical Journal*, vol. 119, no. 5, pp. 2248–2253, 2000.

[61] P. Kroupa, C. Theis, and C. M. Boily, "The great disk of Milky-Way satellites and cosmological sub-structures," *Astronomy & Astrophysics*, vol. 431, no. 2, pp. 517–521, 2005.

[62] M. Metz, P. Kroupa, and H. Jerjen, "Discs of satellites: the new dwarf spheroidals," *Monthly Notices of the Royal Astronomical Society*, vol. 394, no. 4, pp. 2223–2228, 2009.

[63] R. A. Ibata, G. Gilmore, and M. J. Irwin, "A dwarf satellite galaxy in Sagittarius," *Nature*, vol. 370, no. 6486, pp. 194–196, 1994.

[64] D. R. Law, K. V. Johnston, and S. R. Majewski, "A two micron all-sky survey view of the Sagittarius dwarf galaxy. IV. Modeling the Sagittarius tidal tails," *The Astrophysical Journal*, vol. 619, no. 2, pp. 807–823, 2005.

[65] B. Willman, M. R. Blanton, A. A. West, et al., "A new Milky Way companion: unusual globular cluster or extreme dwarf satellite?" *The Astronomical Journal*, vol. 129, no. 6, pp. 2692–2700, 2005.

[66] V. Belokurov, D. B. Zucker, N. W. Evans, et al., "A faint new Milky Way satellite in bootes," *The Astrophysical Journal*, vol. 647, no. 2, pp. L111–L114, 2006.

[67] D. B. Zucker, V. Belokurov, N. W. Evans, et al., "A curious Milky Way satellite in Ursa Major," *The Astrophysical Journal*, vol. 650, no. 1, pp. L41–L44, 2006.

[68] D. B. Zucker, V. Belokurov, N. W. Evans, et al., "A new Milky Way dwarf satellite in canes venatici," *The Astrophysical Journal*, vol. 643, no. 2, pp. L103–L106, 2006.

[69] M. J. Irwin, V. Belokurov, N. W. Evans, et al., "Discovery of an unusual dwarf galaxy in the outskirts of the Milky Way," *The Astrophysical Journal*, vol. 656, no. 1, pp. L13–L16, 2007.

[70] S. Koposov, J. T. A. de Jong, V. Belokurov, et al., "The discovery of two extremely low luminosity Milky Way globular clusters," *The Astrophysical Journal*, vol. 669, no. 1, pp. 337–342, 2007.

[71] S. M. Walsh, H. Jerjen, and B. Willman, "A pair of boötes: a new Milky Way satellite," *The Astrophysical Journal*, vol. 662, no. 2, pp. L83–L86, 2007.

[72] B. Willman, "In pursuit of the least luminous galaxies," *Advances in Astronomy*, vol. 2010, Article ID 285454, 11 pages, 2010.

[73] E. N. Kirby, J. D. Simon, M. Geha, P. Guhathakurta, and A. Frebel, "Uncovering extremely metal-poor stars in the

Milky Way's ultrafaint dwarf spheroidal satellite galaxies," *The Astrophysical Journal*, vol. 685, no. 1, pp. L43–L46, 2008.

[74] S. Koposov, V. Belokurov, N. W. Evans, et al., "The luminosity function of the Milky Way satellites," *The Astrophysical Journal*, vol. 686, no. 1, pp. 279–291, 2008.

[75] L. E. Strigari, J. S. Bullock, M. Kaplinghat, et al., "A large dark matter core in the Fornax dwarf spheroidal galaxy?" *The Astrophysical Journal*, vol. 652, no. 1, pp. 306–312, 2006.

[76] J. Klimentowski, E. L. Łokas, S. Kazantzidis, F. Prada, L. Mayer, and G. A. Mamon, "Mass modelling of dwarf spheroidal galaxies: the effect of unbound stars from tidal tails and the Milky Way," *Monthly Notices of the Royal Astronomical Society*, vol. 378, no. 1, pp. 353–368, 2007.

[77] R. F. G. Wyse and G. Gilmore, "Observed properties of dark matter on small spatial scales," in *Proceedings of the International Astronomical Union*, J. Davies and M. Disney, Eds., vol. 244 of *IAU Symposium*, pp. 44–52, Cambridge University Press, 2008.

[78] J. Peñarrubia, A. W. McConnachie, and J. F. Navarro, "The cold dark matter halos of Local Group dwarf spheroidals," *The Astrophysical Journal*, vol. 672, no. 2, pp. 904–913, 2008.

[79] M. G. Walker, M. Mateo, E. W. Olszewski, J. Peñarrubia, N. W. Evans, and G. Gilmore, "A universal mass profile for dwarf spheroidal galaxies?" *The Astrophysical Journal*, vol. 704, no. 2, pp. 1274–1287, 2009.

[80] L. E. Strigari, "Kinematics of Milky Way satellites: rotational limits and mass estimation," *Advances in Astronomy*, 2009.

[81] J. S. Bullock, A. V. Kravtsov, and D. H. Weinberg, "Reionization and the abundance of galactic satellites," *The Astrophysical Journal*, vol. 539, no. 2, pp. 517–521, 2000.

[82] R. S. Somerville, "Can photoionization squelching resolve the substructure crisis?" *The Astrophysical Journal*, vol. 572, no. 1, pp. L23–L26, 2002.

[83] A. J. Benson, C. S. Frenk, C. G. Lacey, C. M. Baugh, and S. Cole, "The effects of photoionization on galaxy formation. II. Satellite galaxies in the Local Group," *Monthly Notices of the Royal Astronomical Society*, vol. 333, no. 1, pp. 177–190, 2002.

[84] S. E. Koposov, J. Yoo, H.-W. Rix, D. H. Weinberg, A. V. Macciò, and J. M. Escudé, "A quantitative explanation of the observed population of Milky Way satellite galaxies," *The Astrophysical Journal*, vol. 696, no. 2, pp. 2179–2194, 2009.

[85] Y.-S. Li, A. Helmi, G. De Lucia, and F. Stoehr, "On the common mass scale of the Milky Way satellites," *Monthly Notices of the Royal Astronomical Society*, vol. 397, no. 1, pp. L87–L91, 2009.

[86] A. V. Macciò, X. Kang, and B. Moore, "Central mass and luminosity of Milky Way satellites in the λ cold dark matter model," *The Astrophysical Journal*, vol. 692, no. 2, pp. L109–L112, 2009.

[87] M. T. Busha, M. A. Alvarez, R. H. Wechsler, T. Abel, and L. E. Strigari, "The impact of inhomogeneous reionization on the satellite galaxy population of the Milky Way," http://arxiv.org/abs/0901.3553.

[88] L. E. Strigari, J. S. Bullock, M. Kaplinghat, et al., "A common mass scale for satellite galaxies of the Milky Way," *Nature*, vol. 454, no. 7208, pp. 1096–1097, 2008.

[89] F. Stoehr, S. D. M. White, G. Tormen, and V. Springel, "The satellite population of the Milky Way in a ACDM universe," *Monthly Notices of the Royal Astronomical Society*, vol. 335, no. 4, pp. L84–L88, 2002.

[90] L. E. Strigari, J. S. Bullock, M. Kaplinghat, J. Diemand, M. Kuhlen, and P. Madau, "Redefining the missing satellites problem," *The Astrophysical Journal*, vol. 669, no. 2, pp. 676–683, 2007.

[91] E. Hayashi, J. F. Navarro, J. E. Taylor, J. Stadel, and T. Quinn, "The structural evolution of substructure," *The Astrophysical Journal*, vol. 584, no. 2, pp. 541–558, 2003.

[92] S. Kazantzidis, L. Mayer, C. Mastropietro, J. Diemand, J. Stadel, and B. Moore, "Density profiles of cold dark matter substructure: implications for the missing-satellites problem," *The Astrophysical Journal*, vol. 608, no. 2, pp. 663–679, 2004.

[93] O. Y. Gnedin, A. V. Kravtsov, A. A. Klypin, and D. Nagai, "Response of dark matter halos to condensation of baryons: cosmological simulations and improved adiabatic contraction model," *The Astrophysical Journal*, vol. 616, no. 1, pp. 16–26, 2004.

[94] J. Diemand, M. Kuhlen, and P. Madau, "Formation and evolution of galaxy dark matter halos and their substructure," *The Astrophysical Journal*, vol. 667, no. 2, pp. 859–877, 2007.

[95] A. R. Zentner, A. A. Berlind, J. S. Bullock, A. V. Kravtsov, and R. H. Wechsler, "The physics of galaxy clustering. I. A model for subhalo populations," *The Astrophysical Journal*, vol. 624, no. 2, pp. 505–525, 2005.

[96] M. Colpi, L. Mayer, and F. Governato, "Dynamical friction and the evolution of satellites in virialized halos: the theory of linear response," *The Astrophysical Journal*, vol. 525, no. 2, pp. 720–733, 1999.

[97] Y. Hashimoto, Y. Funato, and J. Making, "To circularize or not to circularize?—Orbital evolution of satellite galaxies," *The Astrophysical Journal*, vol. 582, no. 1, pp. 196–201, 2003.

[98] M. Boylan-Kolchin, C.-P. Ma, and E. Quataert, "Dynamical friction and galaxy merging time-scales," *Monthly Notices of the Royal Astronomical Society*, vol. 383, no. 1, pp. 93–101, 2008.

[99] C. Y. Jiang, Y. P. Jing, A. Faltenbacher, W. P. Lin, and C. Li, "A fitting formula for the merger timescale of galaxies in hierarchical clustering," *The Astrophysical Journal*, vol. 675, no. 2, pp. 1095–1105, 2008.

[100] S. Naoz, R. Barkana, and A. Mesinger, "Gas in simulations of high redshift galaxies and minihalos," *Monthly Notices of the Royal Astronomical Society*, vol. 399, p. 369, 2009, http://adsabs.harvard.edu/abs/2009MNRAS.399..369N.

[101] T. Abel, G. L. Bryan, and M. L. Norman, "The formation of the first star in the universe," *Science*, vol. 295, no. 5552, pp. 93–98, 2002.

[102] J. E. Taylor, J. Silk, and A. Babul, "Clues to dwarf galaxy formation from clustering and kinematics," in *Near-Fields Cosmology with Dwarf Elliptical Galaxies*, H. Jerjen and B. Binggeli, Eds., vol. 198 of *IAU Symposium and Colloquium*, pp. 185–188, CUP, Cambridge, UK, 2005.

[103] E. D'Onghia and G. Lake, "Small dwarf galaxies within larger dwarfs: why some are luminous while most go dark," *The Astrophysical Journal*, vol. 686, no. 2, pp. L61–L65, 2008.

[104] J. Bailin, C. Power, P. Norberg, D. Zaritsky, and B. K. Gibson, "The anisotropic distribution of satellite galaxies," *Monthly Notices of the Royal Astronomical Society*, vol. 390, no. 3, pp. 1133–1156, 2008.

[105] J. Chen, A. V. Kravtsov, F. Prada, et al., "Constraining the projected radial distribution of galactic satellites with the sloan digital sky survey," *The Astrophysical Journal*, vol. 647, no. 1, pp. 86–101, 2006.

[106] M. Kamionkowski and A. R. Liddle, "The dearth of halo dwarf galaxies: is there power on short scales?" *Physical Review Letters*, vol. 84, no. 20, pp. 4525–4528, 2000.

[107] P. Colín, V. Avila-Reese, and O. Valenzuela, "Substructure and halo density profiles in a warm dark matter cosmology," *The Astrophysical Journal*, vol. 542, no. 2, pp. 622–630, 2000.

[108] P. Bode, J. P. Ostriker, and N. Turok, "Halo formation in warm dark matter models," *The Astrophysical Journal*, vol. 556, no. 1, pp. 93–107, 2001.

[109] P. Colín, O. Valenzuela, and V. Avila-Reese, "On the structure of dark matter halos at the damping scale of the power spectrum with and without relict velocities," *The Astrophysical Journal*, vol. 673, no. 1, pp. 203–214, 2008.

[110] D. N. Spergel and P. J. Steinhardt, "Observational evidence for self-interacting cold dark matter," *Physical Review Letters*, vol. 84, no. 17, pp. 3760–3763, 2000.

[111] B. Moore, S. Gelato, A. Jenkins, F. R. Pearce, and V. Quilis, "Collisional versus collisionless dark matter," *The Astrophysical Journal*, vol. 535, no. 1, pp. L21–L24, 2000.

[112] C. S. Kochanek and M. White, "A quantitative study of interacting dark matter in halos," *The Astrophysical Journal*, vol. 543, no. 2, pp. 514–520, 2000.

[113] N. Yoshida, V. Springel, S. D. M. White, and G. Tormen, "Weakly self-interacting dark matter and the structure of dark halos," *The Astrophysical Journal*, vol. 544, no. 2, pp. L87–L90, 2000.

[114] J. Miralda-Escudé, "A test of the collisional dark matter hypothesis from cluster lensing," *The Astrophysical Journal*, vol. 564, no. 1, pp. 60–64, 2002.

[115] O. Y. Gnedin and J. P. Ostriker, "Limits on collisional dark matter from elliptical galaxies in clusters," *The Astrophysical Journal*, vol. 561, no. 1, pp. 61–68, 2001.

[116] D. Clowe, M. Bradač, A. H. Gonzalez, et al., "A direct empirical proof of the existence of dark matter," *The Astrophysical Journal*, vol. 648, no. 2, pp. L109–L113, 2006.

[117] K. Abazajian, "Linear cosmological structure limits on warm dark matter," *Physical Review D*, vol. 73, no. 6, Article ID 063513, 6 pages, 2006.

[118] U. Seljak, A. Makarov, P. McDonald, and H. Trac, "Can sterile neutrinos be the dark matter?" *Physical Review Letters*, vol. 97, no. 19, Article ID 191303, 4 pages, 2006.

[119] S. Mao and P. Schneider, "Evidence for substructure in lens galaxies?" *Monthly Notices of the Royal Astronomical Society*, vol. 295, no. 3, pp. 587–594, 1998.

[120] N. Dalal and C. S. Kochanek, "Direct detection of cold dark matter substructure," *The Astrophysical Journal*, vol. 572, no. 1, pp. 25–33, 2002.

[121] C. S. Kochanek and N. Dalal, "Tests for substructure in gravitational lenses," *The Astrophysical Journal*, vol. 610, no. 1, pp. 69–79, 2004.

[122] S. D. M. White and C. S. Frenk, "Galaxy formation through hierarchical clustering," *The Astrophysical Journal*, vol. 379, no. 1, pp. 52–79, 1991.

[123] A. H. Gonzalez, K. A. Williams, J. S. Bullock, T. S. Kolatt, and J. R. Primack, "The velocity function of galaxies," *The Astrophysical Journal*, vol. 528, no. 1, pp. 145–155, 2000.

[124] A. J. Benson, R. G. Bower, C. S. Frenk, C. G. Lacey, C. M. Baugh, and S. Cole, "What shapes the luminosity function of galaxies?" *The Astrophysical Journal*, vol. 599, no. 1, pp. 38–49, 2003.

[125] I. K. Baldry, K. Glazebrook, and S. P. Driver, "On the galaxy stellar mass function, the mass-metallicity relation and the implied baryonic mass function," *Monthly Notices of the Royal Astronomical Society*, vol. 388, no. 3, pp. 945–959, 2008.

[126] A. V. Tikhonov and A. Klypin, "The emptiness of voids: yet another overabundance problem for the Λ cold dark matter model," *Monthly Notices of the Royal Astronomical Society*, vol. 395, no. 4, pp. 1915–1924, 2009.

[127] A. A. Thoul and D. H. Weinberg, "Hydrodynamic simulations of galaxy formation. II. Photoionization and the formation of low-mass galaxies," *The Astrophysical Journal*, vol. 465, no. 2, pp. 608–616, 1996.

[128] T. Quinn, N. Katz, and G. Efstathiou, "Photoionization and the formation of dwarf galaxies," *Monthly Notices of the Royal Astronomical Society*, vol. 278, no. 4, pp. L49–L54, 1996.

[129] N. Y. Gnedin and L. Hui, "Probing the Universe with the Lyα forest-I. Hydrodynamics of the low-density intergalactic medium," *Monthly Notices of the Royal Astronomical Society*, vol. 296, no. 1, pp. 44–55, 1998.

[130] T. Kitayama and S. Ikeuchi, "Formation of subgalactic clouds under ultraviolet background radiation," *The Astrophysical Journal*, vol. 529, no. 2, pp. 615–634, 2000.

[131] N. Y. Gnedin, "Effect of reionization on structure formation in the universe," *The Astrophysical Journal*, vol. 542, no. 2, pp. 535–541, 2000.

[132] M. Dijkstra, Z. Haiman, M. J. Rees, and D. H. Weinberg, "Photoionization feedback in low-mass galaxies at high redshift," *The Astrophysical Journal*, vol. 601, no. 2, pp. 666–675, 2004.

[133] M. Hoeft, G. Yepes, S. Gottlöber, and V. Springel, "Dwarf galaxies in voids: suppressing star formation with photoheating," *Monthly Notices of the Royal Astronomical Society*, vol. 371, no. 1, pp. 401–414, 2006.

[134] T. Okamoto, L. Gao, and T. Theuns, "Mass loss of galaxies due to an ultraviolet background," *Monthly Notices of the Royal Astronomical Society*, vol. 390, no. 3, pp. 920–928, 2008.

[135] R. Barkana and A. Loeb, "The photoevaporation of dwarf galaxies during reionization," *The Astrophysical Journal*, vol. 523, no. 1, pp. 54–65, 1999.

[136] N. J. Shaviv and A. Dekel, "Photo-evaporation by thermal winds in dwarf galaxies," submitted to *Monthly Notices of the Royal Astronomical Society*.

[137] P. R. Shapiro, I. T. Iliev, and A. C. Raga, "Photoevaporation of cosmological minihaloes during reionization," *Monthly Notices of the Royal Astronomical Society*, vol. 348, no. 3, pp. 753–782, 2004.

[138] A. Dekel and J. Silk, "The origin of dwarf galaxies, cold dark matter, and biased galaxy formation," *The Astrophysical Journal*, vol. 303, pp. 39–55, 1986.

[139] M.-M. Mac Low and A. Ferrara, "Starburst-driven mass loss from dwarf galaxies: efficiency and metal ejection," *The Astrophysical Journal*, vol. 513, no. 1, pp. 142–155, 1999.

[140] A. Dekel and J. Woo, "Feedback and the fundamental line of low-luminosity low-surface-brightness/dwarf galaxies," *Monthly Notices of the Royal Astronomical Society*, vol. 344, no. 4, pp. 1131–1144, 2003.

[141] S. Mashchenko, J. Wadsley, and H. M. P. Couchman, "Stellar feedback in dwarf galaxy formation," *Science*, vol. 319, no. 5860, pp. 174–177, 2008.

[142] A. Marcolini, A. D'Ercole, F. Brighenti, and S. Recchi, "Star formation feedback and metal enrichment by types Ia and II supernovae in dwarf spheroidal galaxies: the case of Draco," *Monthly Notices of the Royal Astronomical Society*, vol. 371, no. 2, pp. 643–658, 2006.

[143] Z. Haiman, M. J. Rees, and A. Loeb, "Destruction of molecular hydrogen during cosmological reionization," *The Astrophysical Journal*, vol. 476, no. 2, pp. 458–463, 1997.

[144] Z. Haiman, T. Abel, and M. J. Rees, "The radiative feedback of the first cosmological objects," *The Astrophysical Journal*, vol. 534, no. 1, pp. 11–24, 2000.

[145] E. Scannapieco, R. J. Thacker, and M. Davis, "High-redshift galaxy outflows and the formation of dwarf galaxies," *The Astrophysical Journal*, vol. 557, no. 2, pp. 605–615, 2001.

[146] F. Sigward, A. Ferrara, and E. Scannapieco, "Suppression of dwarf galaxy formation by cosmic shocks," *Monthly Notices of the Royal Astronomical Society*, vol. 358, no. 3, pp. 755–764, 2005.

[147] T. Kaufmann, C. Wheeler, and J. S. Bullock, "On the morphologies, gas fractions, and star formation rates of small galaxies," *Monthly Notices of the Royal Astronomical Society*, vol. 382, no. 3, pp. 1187–1195, 2007.

[148] K. Tassis, A. V. Kravtsov, and N. Y. Gnedin, "Scaling relations of dwarf galaxies without supernova-driven winds," *The Astrophysical Journal*, vol. 672, no. 2, pp. 888–903, 2008.

[149] B. E. Robertson and A. V. Kravtsov, "Molecular hydrogen and global star formation relations in galaxies," *The Astrophysical Journal*, vol. 680, no. 2, pp. 1083–1111, 2008.

[150] N. Y. Gnedin, K. Tassis, and A. V. Kravtsov, "Modeling molecular hydrogen and star formation in cosmological simulations," *The Astrophysical Journal*, vol. 697, no. 1, pp. 55–67, 2009.

[151] N. Y. Gnedin and A. V. Kravtsov, "Fossils of reionization in the local group," *The Astrophysical Journal*, vol. 645, no. 2, pp. 1054–1061, 2006.

[152] B. Moore, J. Diemand, P. Madau, M. Zemp, and J. Stadel, "Globular clusters, satellite galaxies and stellar haloes from early dark matter peaks," *Monthly Notices of the Royal Astronomical Society*, vol. 368, no. 2, pp. 553–570, 2006.

[153] P. Madau, M. Kuhlen, J. Diemand, et al., "Fossil remnants of reionization in the halo of the Milky Way," *The Astrophysical Journal*, vol. 689, no. 1, pp. L41–L44, 2008.

[154] M. Ricotti and N. Y. Gnedin, "Formation histories of dwarf galaxies in the Local Group," *The Astrophysical Journal*, vol. 629, no. 1, pp. 259–267, 2005.

[155] M. S. Bovill and M. Ricotti, "Pre-reionization fossils, ultra-faint dwarfs and the missing galactic satellite problem," *The Astrophysical Journal*, vol. 693, no. 2, pp. 1859–1870, 2009.

[156] M. Ricotti, *Advances in Astronomy*, vol. 2009, 2009.

[157] F. Stoehr, S. D. M. White, V. Springel, G. Tormen, and N. Yoshida, "Dark matter annihilation in the halo of the Milky Way," *Monthly Notices of the Royal Astronomical Society*, vol. 345, no. 4, pp. 1313–1322, 2003.

[158] S. Salvadori, A. Ferrara, and R. Schneider, "Life and times of dwarf spheroidal galaxies," *Monthly Notices of the Royal Astronomical Society*, vol. 386, no. 1, pp. 348–358, 2008.

[159] E. K. Grebel, J. S. Gallagher III, and D. Harbeck, "The progenitors of dwarf spheroidal galaxies," *The Astronomical Journal*, vol. 125, no. 4, pp. 1926–1939, 2003.

[160] Y. Fenner, B. K. Gibson, R. Gallino, and M. Lugaro, "Cosmological implications of dwarf spheroidal chemical evolution," *The Astrophysical Journal*, vol. 646, no. 1, pp. 184–191, 2006.

[161] J. I. Read, A. P. Pontzen, and M. Viel, "On the formation of dwarf galaxies and stellar haloes," *Monthly Notices of the Royal Astronomical Society*, vol. 371, no. 2, pp. 885–897, 2006.

[162] S. Salvadori and A. Ferrara, "Ultra faint dwarfs: probing early cosmic star formation," *Monthly Notices of the Royal Astronomical Society*, vol. 395, no. 1, pp. L6–L10, 2009.

[163] M. Mateo, E. W. Olszewski, C. Pryor, D. L. Welch, and P. Fischer, "The Carina dwarf spheroidal galaxy: how dark is it?" *The Astronomical Journal*, vol. 105, no. 2, pp. 510–526, 1993.

[164] G. Gilmore, M. I. Wilkinson, R. F. G. Wyse, et al., "The observed properties of dark matter on small spatial scales," *The Astrophysical Journal*, vol. 663, no. 2, pp. 948–959, 2007.

[165] J. S. Bullock, T. S. Kolatt, Y. Sigad, et al., "Profiles of dark haloes: evolution, scatter and environment," *Monthly Notices of the Royal Astronomical Society*, vol. 321, no. 3, pp. 559–575, 2001.

[166] C. Conroy, R. H. Wechsler, and A. V. Kravtsov, "Modeling luminosity-dependent galaxy clustering through cosmic time," *The Astrophysical Journal*, vol. 647, no. 1, pp. 201–214, 2006.

[167] C. Conroy and R. H. Wechsler, "Connecting galaxies, halos, and star formation rates across cosmic time," *The Astrophysical Journal*, vol. 696, no. 1, pp. 620–635, 2009.

[168] J. L. Tinker and C. Conroy, "The void phenomenon explained," *The Astrophysical Journal*, vol. 691, pp. 633–639, 2009.

[169] R. Braun and W. B. Burton, "The kinematic and spatial deployment of compact, isolated high-velocity clouds," *Astronomy & Astrophysics*, vol. 341, no. 2, pp. 437–450, 1999.

[170] V. de Heij, R. Braun, and W. B. Burton, "An all-sky study of compact, isolated high-velocity clouds," *Astronomy & Astrophysics*, vol. 392, no. 2, pp. 417–451, 2002.

[171] D. A. Thilker, R. Braun, R. A. M. Walterbos, et al., "On the continuing formation of the Andromeda galaxy: detection of H I clouds in the M31 halo," *The Astrophysical Journal*, vol. 601, no. 1, pp. L39–L42, 2004.

[172] M. Grossi, C. Giovanardi, E. Corbelli, et al., "H I clouds in the proximity of M 33," *Astronomy & Astrophysics*, vol. 487, no. 1, pp. 161–175, 2008.

[173] F. C. van den Bosch, X. Yang, H. J. Mo, et al., "Towards a concordant model of halo occupation statistics," *Monthly Notices of the Royal Astronomical Society*, vol. 376, no. 2, pp. 841–860, 2007.

[174] N. F. Martin, J. T. A. de Jong, and H.-W. Rix, "A comprehensive maximum likelihood analysis of the structural properties of faint Milky Way satellites," *The Astrophysical Journal*, vol. 684, no. 2, pp. 1075–1092, 2008.

[175] J. Pizagno, F. Prada, D. H. Weinberg, et al., "Dark matter and stellar mass in the luminous regions of disk galaxies," *The Astrophysical Journal*, vol. 633, no. 2, pp. 844–856, 2005.

[176] R. Mandelbaum, U. Seljak, G. Kauffmann, C. M. Hirata, and J. Brinkmann, "Galaxy halo masses and satellite fractions from galaxy-galaxy lensing in the Sloan Digital Sky Survey: stellar mass, luminosity, morphology and environment dependencies," *Monthly Notices of the Royal Astronomical Society*, vol. 368, no. 2, pp. 715–731, 2006.

[177] C. Conroy, F. Prada, J. A. Newman, et al., "Evolution in the halo masses of isolated galaxies between $z \sim 1$ and $z \sim 0$: from DEEP2 to SDSS," *The Astrophysical Journal*, vol. 654, no. 1, pp. 153–171, 2007.

[178] A. Klypin, F. Prada, and A. Montero-Dorta, submitted to *Astrophysical Journal*.

Hindawi Publishing Corporation
Advances in Astronomy
Volume 2010, Article ID 285454, 11 pages
doi:10.1155/2010/285454

Review Article

In Pursuit of the Least Luminous Galaxies

Beth Willman

Department of Astronomy, Haverford College, 370 Lancaster Avenue, Haverford, PA 19041, USA

Correspondence should be addressed to Beth Willman, bwillman@haverford.edu

Received 11 May 2009; Accepted 23 July 2009

Academic Editor: Regina Schulte-Ladbeck

The dwarf galaxy companions to the Milky Way are unique cosmological laboratories. With luminosities as low as $10^{-7}L_{\rm MW}$, they inhabit the lowest mass dark matter halos known to host stars and are presently the most direct tracers of the distribution, mass spectrum, and clustering scale of dark matter. Their resolved stellar populations also facilitate detailed studies of their history and mass content. To fully exploit this potential requires a well-defined census of virtually invisible galaxies to the faintest possible limits and to the largest possible distances. I review the past and present impacts of survey astronomy on the census of Milky Way dwarf galaxy companions and discuss the future of finding ultra-faint dwarf galaxies around the Milky Way and beyond in wide-field survey data.

1. Introduction

The least luminous known galaxies have historically been those closest to the Milky Way. Whether visually or with automated searches, resolved stars reveal the presence of nearby dwarf galaxies with surface brightnesses too low to be discovered by diffuse light alone. Even until recently, nearly all cataloged dwarfs fainter than $M_V = -11$ resided within the Local Group of galaxies (LG) [1]. In 1999 the LG contained 36 known members, of which eleven are Milky Way (MW) satellites [2]. Four of these eleven MW dwarf galaxies are less luminous than $M_V = -10$, more than 10 000 times less luminous than the Milky Way itself. Although such low luminosity dwarfs almost certainly contribute a cosmologically insignificant amount to the luminosity budget of the Universe, all eight of the Milky Way's classical dwarf spheroidal companions ($-9 > M_v > -13$, not including Sagittarius or the Magellanic Clouds) have been studied in extensive detail. ("Classical" will be used in the paper to refer to the Milky Way dwarf companions known prior to 2003.) There is now a new class of "ultra-faint" dwarf companions to the Milky Way known to have absolute magnitudes as low as $M_V \sim -2$ ([3], see Section 3). The resolved stellar populations of these near-field cosmological laboratories have been used to derive their star formation and chemical evolution histories [4] and to model their dark mass content in detail (see article by Strigari in this volume and references therein). These complete histories of individual systems complement studies that rely on high redshift observations to stitch together an average view of the Universe's evolution with time.

The need for an automated, "systematic, statistically complete, and homogeneous search" for LG dwarf galaxies has been known for some time [5]. A combination of theoretical results and the advent of digital sky surveys have initiated a renaissance in the pursuit of a well-measured sample of the least luminous galaxies. This renaissance began in 1999, when simulations were used to highlight the discrepancy between the number of dark matter halos predicted to orbit the MW and the eleven observed to be lit up by dwarf galaxies orbiting the MW [6, 7]. As the resolution of simulations has increased over the last ten years, so has the magnitude of this apparent discrepancy. The most recent simulations predict tens ($M_{\rm halo} > 10^6 M_\odot$, [8]) or even hundreds of thousands ($M_{\rm halo} > 10^5 M_\odot$, [9]) of dark matter halos around the Milky Way. In light of this "missing satellite problem", great attention has been paid to the total number of Milky Way dwarf galaxies. However, this is only one metric with which to learn about the properties of dark matter. The intrinsically faintest dwarfs (which can only be found and studied close to the Milky Way) likely inhabit the least massive dark matter halos that can host stars. Such dwarfs may thus provide

the most direct measurement of the mass spectrum, spatial distribution, and clustering scale of dark matter.

What was initially viewed as a problem now provides an opportunity to simultaneously learn about dark matter and galaxy formation physics. Many studies have invoked simple models of galaxy formation within low-mass dark matter halos to successfully resolve the apparent satellite discrepancy within the context of ΛCDM (e.g., [10–13]). See the review article in this volume on "Dark matter substructure and dwarf galactic satellites" by A. Kravtsov for more details on the original missing satellite problem and on resolutions to this problem based on models of star formation in low-mass halos.

To untangle the extent to which dark matter physics, galaxy formation physics, and incompleteness in the census of dwarf galaxies contribute to this missing satellite "opportunity" requires a *well-defined* dwarf galaxy census that is as *uniform* as possible to the *faintest limits*. For example– *Well defined:* to compare observations of the MW dwarf population with models requires a detailed, quantitative description of the current census. Quantitative assessments of the detectability of MW dwarfs in recent survey data, plus an assumed spatial distribution of dwarfs, enabled extrapolation of the known population to predict a total number of ∼100–500 dwarf satellites [14, 15]. *Uniform:* because the very least luminous MW dwarfs ($M_V \sim -2$) can currently only be found within 50 kpc, it is presently unclear whether dwarfs can form with such intrinsically low luminosities, or whether the tidal field of the Milky Way has removed stars from these nearby objects. The epoch of reionization and its effect on the formation of stars in low-mass dark matter halos also leaves an imprint on both the spatial distribution [16, 17] and mass function of MW satellites [13, 18]. Other studies have claimed that the spatial distribution of MW satellites is inconsistent with that expected in a Cold Dark Matter-dominated model [19, 20]. Robust tests of these models are not possible without improving the uniformity of the MW census with direction and with distance. *Faintest limits:* reaching the low luminosity limit of galaxy formation is necessary to probe the smallest possible scales of dark matter, the scales on which the model faces the greatest challenges. Moreover, a census to faint limits over a large fraction of the MW's virial volume may yield enough dwarfs to rule out dark matter models with reduced power on small scales, although numerical effects presently inhibit concrete predictions of such models [21].

The specific observational requirements to fully exploit the population of MW dwarfs (and beyond) to effectively test dark matter theories and/or to learn about galaxy formation therefore include the following:

(i) a census of dwarfs (we apply the term "dwarf" only to stellar systems that, through direct or indirect evidence, are known to be dark matter dominated either now or at any point in the past) that is minimally biased with respect to Galactic latitude, distance (at least out to the virial radius of the Milky Way), star formation history, and structural parameters,

(ii) a statistically significant sample of lowest luminosity dwarfs,

(iii) a sample of the least luminous dwarfs in a range of environments.

This article focuses on the roles of wide-field, optical imaging surveys of the past, present, and future in the pursuit of a minimally biased census of the least luminous galaxies. In particular, it focuses on automated analyses of resolved star counts as a method to reveal these systems. Since the visual searches of the 20th century, new digital sky survey data have substantially progressed the completeness and uniformity of the MW satellite census. Although this progress has already revolutionized the landscape of dwarf galaxy cosmology, it has also revealed great incompleteness in our knowledge of the least luminous galaxies. Imminent and future surveys such as the Southern Sky Survey [22], PanSTARRS 1 (http://pan-starrs.ifa.hawaii.edu/public/) the Dark Energy Survey [23], and the Large Synoptic Survey Telescope [24] are poised to ultimately achieve the observational requirements needed for MW dwarf galaxy cosmology.

2. Discovering Milky Way Dwarf Galaxies, Pre-SDSS

All Milky Way dwarf galaxies known prior to 1990 were discovered in visual inspections of photographic survey data. Sculptor ($M_V = -11.1$) and Fornax ($M_V = -13.1$) were discovered in 1938 by Shapley [25, 26] in images obtained with a 24-inch telescope at Harvard's Boyden Station. Leo I ($M_V = -11.9$), Leo II ($M_V = -10.1$), Ursa Minor ($M_V = -8.9$), and Draco ($M_V = -9.4$) were discovered in the 1950's in the images obtained with a 48-inch Schmidt telescope as part of the original Palomar Observatory Sky Survey (POSS) [27, 28]. The last Milky Way companion discovered by an eyeball search was Carina (1977, $M_V = -9.4$), found on photographic plates obtained in the Southern hemisphere counterpart to the Palmar Observatory surveys—the ESO/SRC Southern Sky Survey [29]. Magnitudes listed above are from [30], except for Sculptor [1].

At the time of Carina's discovery, it was hypothesized that "The only possibility for detecting new systems of this type would seem to be in regions of relatively high foreground stars density and will probably require careful scanning under low-power magnification or detailed star counts" [29]. This hypothesis was validated by the discovery of Sextans in 1990 ($M_V = -9.5$) [31] as an overdensity of star counts from automated plate machine (APM) scans of the same POSS and ESO/SRC survey data that had been carefully inspected decades earlier. Sextans was discovered as part of the first large-scale, automated search for Milky Way companions [32]. The serendipitous discovery of the eleventh Milky Way companion, Sagittarius, in 1994 [33] as a moving group of stars was the final Milky Way dwarf discovered in the photographic survey data of the 20th century.

Since the discoveries of the eleven classical Milky Way dwarf satellites, Kleyna et al. [34] and Whiting et al. [35] conducted systematic searches of the COSMOS/UKST survey of the southern sky and the POSS-II and ESO/SRC survey data, respectively. Whiting's eyeball, all-sky search resulted in the discoveries of the Local Group dwarfs Antlia ($M_V = -11.2$) and Cetus ($M_V = -11.3$), but not new Milky Way satellites. The closest predecessor to the modern searches described in Section 3, Kleyna et al. searched for overdensities of resolved stars in spatially smoothed, pixellated maps of star counts. Although their survey revealed no new dwarf galaxies, they performed the first detailed characterization of the Milky Way dwarf satellite census. The detection limits of these searches are discussed in Section 4.

3. Mining for the Lowest Iuminosity Dwarfs in the SDSS Era

Although the searches for dwarfs in the survey data available in the 20th century were impressively successful, empirical evidence suggested that the census of Milky Way dwarf galaxies may not yet be complete [2, 16]. Since then, the Sloan Digital Sky Survey (SDSS, [36]) revolutionized the field of dwarf galaxy cosmology with the discoveries of 14 MW dwarfs (and possible dwarfs) as overdensities of resolved stars: 2005—Ursa Major [37] and Willman 1 (originally known as SDSSJ1049+5103, [38]); 2006—Boötes I [39], Ursa Major II [40], Canes Venatici I [41]; 2007—Segue 1, Coma Berenices, Leo IV, Canes Venatici II, Hercules (all announced in [42]), Leo T [43], Boötes II [44]; 2008—Leo V [45]; 2009—Segue 2 [46]. Follow-up observations confirmed most of these to be the most dark matter dominated (central M/L up to 1000 [3, 13]), least luminous ($-1.5 > M_V > -8.6$ [47]), and among the least chemically evolved galaxies known in the Universe [48, 49]. Among these 14, Willman 1, Segue 2, and Boötes II have not yet been shown to be dwarf galaxies rather than star clusters or unbound remnants thereof. The ultra-faint dwarfs are also predicted to be the most detectable sources of gamma-rays from dark matter annihilation [50, 51]. In parallel with these Milky Way discoveries, 11 new M31 satellite galaxies have been discovered, primarily in large INT and CFHT surveys of M31 (And IX - And XX, $-6.3 > M_v > -9$ [52–58]).

The accomplishments of the SDSS dataset seem particularly remarkable given that the data were obtained with 1-minute exposures taken on a 2.5 m telescope, with a resulting r-magnitude limit of 22.2. In general, pushing the census of resolved dwarf galaxies to lower luminosities and greater distances can be accomplished by (1) obtaining photometry of stars to fainter apparent magnitudes, (2) more efficiently suppressing the noise from point sources contaminating the signal from stars belonging to a dwarf galaxy, and/or (3) reducing spurious detections, the primary source of which had been cluster galaxies misclassified as point sources [32, 34]. The features of the SDSS that facilitated (2) and (3) were its multiband photometry and accurate star-galaxy separation. The digital camera and uniformity of the survey also played key roles in its richness as a hunting ground for dwarfs.

With a median luminosity of $M_V \sim -5$ ($10^4 L_\odot$), the ultra-faints are up to ten million times less luminous than the Milky Way. All but Willman 1 and Leo T of the new Milky Way satellites are invisible in the SDSS images, even in hindsight. How was the presence of these invisible galaxies revealed? The seventh data release of SDSS, DR 7 [59], includes 11 663 deg^2 of imaging and over 100 million cataloged stars. The searches that resulted in the discoveries of the ultra-faint dwarfs were based only on analyses of these cataloged stars. The methods applied were all similar in spirit, starting with the search of Willman et al. [60]. The search technique summarized here is the specific method used in the most recent automated search, that of Walsh et al. (WWJ [61]).

(i) *Apply a Color-Magnitude Filter to Point Sources.* The primary source of noise in searches for dwarfs in SDSS-depth data is MW stars. Figure 1(b) shows that MW stars are smeared out in color and magnitude. The red plume contains thin disk main sequence stars, the bright blue plume contains thick disk main sequence turnoff (MSTO) stars, and the faint blue plume contains halo MSTO and MS stars. However, the stars belonging to a dwarf galaxy will occupy a well-defined region of color-magnitude space. All stars with colors and magnitudes inconsistent with a dwarf galaxy (at a particular distance) can thus be filtered out. WWJ used Girardi isochrones to define a color-magnitude (CM) filter for stars between 8 and 14 Gyr old and with $-1.5 <$ [Fe/H] < -2.3. This filter is shown Figure 1(a) for a dwarf galaxy with $d = 20$ kpc. Unlike the matched filter technique of [62], stars outside of the filter are simply removed from the analysis. No weighting is done, because the filter is not intended to exactly match stars from a specific stellar population. The CM filter was shifted to 16 values of m–M between 16.5 and 24.0 to search for dwarfs with $20 \lesssim d \lesssim 600$ kpc. Figure 1(a) shows that a 20 kpc color-magnitude filter contains substantial noise from both thick disk and halo stars. Figure 1(d) shows that a 100 kpc filter resides primarily between the two plumes and includes contamination from faint halo stars. The horizontal branch (HB) extension of this 100 kpc filter passes through MSTO halo stars, suggesting that this HB extension may include more noise than signal from the least luminous systems. Although the analysis of WWJ was automated and included no visual component, the result of this processing step is illustrated in Figures 2(a) and 2(b). The Ursa Major I ultra-faint dwarf ($M_V = -5.5$, $d = 100$ kpc) is not visible in the star count map on the left. After CM filtering, a slight overdensity of point sources becomes visible.

(ii) *Create Spatially Smoothed Image of Stellar Surface Density.* As originally done in searches for nearby dwarf galaxies performed in the 1990's [32, 34], the number density map of stars passing CM filtering is smoothed with a spatial kernel to enhance the signals from resolved objects with angular scale sizes expected for nearby dwarf galaxies. WWJ used only a 4.5′ scale length filter, while [14] applied filters of two different angular sizes. The result of this analysis step is illustrated Figure 2(c), which shows that Ursa Major I appears prominent in a spatially smoothed map of CM-filtered stars.

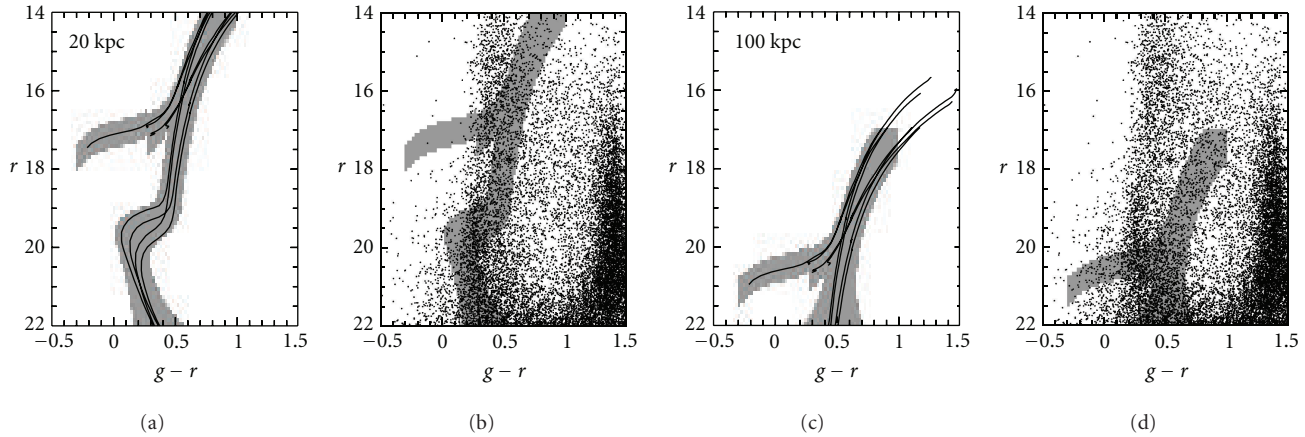

Figure 1: A color-magnitude (CM) filter used to suppress the noise from foreground stars while preserving the signal from dwarf galaxy stars at a specific distance. (a) and (c) CM filters for an old and metal-poor stellar population at a distance modulus of 16.5 and 20.0, respectively. The solid lines show Girardi isochrones for 8 and 14 Gyr populations with [Fe/H] = −1.5 and −2.3. (b) and (d) These CM filters overplotted on stars from a 1 deg^2 field to illustrate the character of the foreground contamination as a function of dwarf distance. Data are from SDSS DR7.

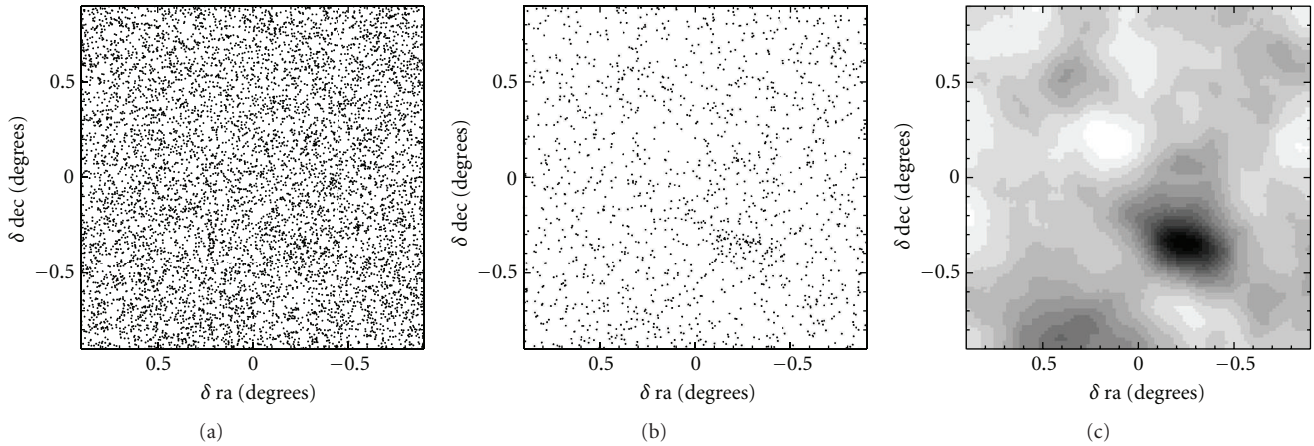

Figure 2: (a) Map of all stars in the field around the Ursa Major I dwarf satellite, $M_V = -5.5$, $d = 100$ kpc. (b) Map of stars passing the CM filter projected to $m - M = 20.0$ shown in Figure 1(c). (c) Spatially smoothed number density map of the stars in (b). The Ursa Major I dwarf galaxy has a $\mu_{V,0}$ of only 27.5 mag arcsec^2 [63]. Data are from SDSS DR7.

(iii) *Identify Statistically Significant Overdensities.* A search of 10 000 deg^2 of SDSS data, optimized for dwarfs at 16 different distances, and a single choice of stellar population and scale size require evaluating the statistical significance of 600 million data pixels that do not necessarily follow a Gaussian distribution of signal. Setting the detection threshold to select candidate dwarf galaxies was done by simulating numerous realizations of the search, assuming a random distribution of point sources and permitting only one completely spurious detection. The threshold is set to be a function of point source number density after CM filtering.

(iv) *Follow-up Candidates.* Regions detected above the detection threshold are considered candidates for MW dwarf galaxies. Although the threshold is set to prevent the detection of any stochastic fluctuations of a randomly distributed set of point sources [61], the detections are only "candidates" because resolved dwarf galaxies are not the only possible overdensities of point sources expected in the sky. For example, fluctuations in the abundant tidal debris in the Milky Way's halo or (un)bound star clusters could be detected. It is essential to obtain follow-up photometry to find the color-magnitude sequence of stars expected for a dwarf galaxy and also follow-up spectroscopy to measure the dark mass content (dark matter is required to be classified as a galaxy) based on the observed line-of-sight velocities.

This search algorithm is very efficient. In the WWJ search, the eleven strongest detections of sources unclassified prior to SDSS were 11 of the 14 (probable) ultra-faint Milky Way dwarfs. All of these but Boötes II were known prior to the WWJ search. See references in Section 3 for details of the follow-up observations that confirmed these objects to be dwarf galaxies. Follow-up observations of as-yet unclassified SDSS dwarf galaxy candidates are ongoing by several groups, including a group at the IoA at

Cambridge (M. Walker, private communication) and at the MPIA (N. Martin, private communication). The *Stromlo Missing Satellites* team (PI H. Jerjen) is also now obtaining and analyzing observations of the ∼ two dozen candidates from the WWJ search of 9500 square degrees of SDSS DR6.

Because most probable candidates for dwarf galaxies have already been followed up, it is possible that SDSS I has already been completely mined for ultra-faint dwarfs. Nevertheless, it is essential to concretely classify all objects identified down to the detection threshold used to quantify the limits of a survey. If there are dwarf galaxies hiding in the low significance detections, then they must be included when interpreting the properties of the global population down to the observational limits. If there are no dwarf galaxies anywhere close to the detection thresholds, then there may not be many unseen dwarfs with luminosities (distances) slightly fainter than (a bit more distant than) those of similar dwarfs in the known population.

4. Current Limitations of the Census of Milky Way Dwarfs

As discussed in Section 1, a well-defined census of dwarfs is essential to use the MW dwarf galaxy population as a probe of dark matter and galaxy formation physics. Astronomers have used a variety of approaches to characterize the completeness of the Milky Way dwarf census for more than 50 years, beginning with Wilson [28] in 1955 who observed that "The uniform coverage of the sky provided by the (Palomar Observatory) Sky Survey allows an estimate to be made of the probable total number of Sculptor-type galaxies in the local group."

Until this day, little is known about the possible population of MW dwarfs at $|b| < 20^\circ$ [32, 34], which includes 1/3 of the volume around our galaxy, owing to obscuration by the Galaxy's disk. A substantial fraction of the SDSS footprint is at $b > 30^\circ$; so no progress has yet been made on this severe observational bias at optical wavelengths. Searches for satellites near the Galactic plane at radio and near-infrared wavelengths (2MASS) are less affected by disk obscuration than optical studies. Although two satellites have tentatively been discovered at these wavelengths (high-velocity cloud Complex H in HI survey data [64], Canis Major in 2MASS [65]), searches for MW dwarfs at nonoptical wavelengths have not yet been very fruitful or quantified in detail.

Likewise, the limitations of the Southern hemisphere dwarf galaxy census remain unchanged since the searches conducted with photographic plate data. Kleyna et al. [34] derived detailed detection limits for their search by inserting simulated galaxies with the physical scale size of Sculptor into the COSMOS survey data. They found that the Southern sky at $b < -15^\circ$ was complete to dwarfs closer than 180 kpc and as faint as 1/8 L_{Sculptor}, corresponding to $M_v = -8.8$. Whiting et al. also quantitatively characterized the completeness of their visual search for dwarfs in the Southern Sky and estimated a limiting surface brightness ($25 < \mu_{\text{lim}} < 26$ mag arcsec^{-2}), with a 77% completeness of dwarfs above this surface brightness limit [35].

It is thus likely that no dwarf similar to any of the 14 ultra-faints discovered in SDSS I data could have been found outside of the SDSS footprint. Within the SDSS footprint, the most extensive calculation of the limitations of the ultra-faint dwarf census is that of WWJ. WWJ simulated the detectability of nearly 4 million artificial galaxies with a range of luminosity, scale size, distance, and Galactic latitude [61]. They estimate that the SDSS MW dwarf census is more than 99% complete within 300 kpc to dwarfs brighter than $M_V = -6.5$ with scale sizes up to 1 kpc. Although this is a tremendous improvement, only four of the 14 new MW satellites are brighter than this limit. d_{90}, the distance *at* which 90% of dwarfs with some set of properties can be detected, is independent of the distribution of objects. d_{90} is ∼35, 60, and 100 kpc for dwarfs with $M_V \sim -2, -3$, and -4 with scale sizes similar to those of the known ultra-faints at like absolute magnitude. (This is smaller than the distance *within* which 90% of dwarfs with some set of properties can be detected.) Larger scale length (lower surface brightness) systems are less detectable. For example, systems with $M_v = -2$ and a scale size of 100 pc or with $M_v = -4$ and a scale size of 500 pc would have been undetectable in SDSS. Koposov et al. [14] derived quantitative detection limits for their SDSS search for ultra-faint dwarfs and found similar results.

The luminosity bias still present in the MW dwarf census as a function of distance has several major implications. First, the unknown underlying radial distribution of MW dwarfs prevents assumption-free predictions of their total number or luminosity function. Second, assumption-free comparisons between the observed and predicted spatial distribution of MW dwarfs are still not possible. However, studies of the spatial distribution that only include the brighter MW dwarfs ($M_V < -5.5$) would provide initial insight into models. Finally, four of the MW ultra-faint companions (Willman 1, Boötes II, Segue 1 and 2) have $L < 10^3 L_\odot$ ($M_V \gtrsim -2.5$). At present, only ∼1/200 of the volume within the SDSS footprint has been mined for such ultra-faints. Are there pristine dwarfs in other environments with such low luminosities? Answering this question will be critical for determining whether they have extremely low luminosities because of nature (they formed that way) or nurture (e.g., the tidal field of the Milky Way removed previously bound stars). Preliminary morphological studies suggest that the properties of the nearest ultra-faints may have been affected by the MW's tidal field.

These limitations and achievements do not substantively vary across most of the SDSS footprint. ∼50% of the SDSS DR6 footprint resides at $b > 50^\circ$ and only ∼10% at $b < 30^\circ$. d_{90} is almost identical for dwarfs with $b = 53^\circ$ and $b = 73^\circ$ and is up to ∼25% less for $b \sim 30^\circ$, depending on $M_{V,\text{dwarf}}$. The relatively weak variation with latitude is owing to the CM filter (Figure 1) that does not include stars with $g - r > 1.0$, cutting the majority of thin disk stars from analysis. Although the spatial variation is weak *on average*, regions of lower Galactic latitude plus longitude or regions containing substantial Sagittarius stream debris do have a lower sensitivity for dwarfs. For searches extending to $b \lesssim 30^\circ$, careful attention must be paid to the dependence of detectability on Galactic direction.

5. Mining for Ultra-Faint Dwarfs Post-SDSS

To move from the excitement of discovery to more concrete comparisons between observations and predictions will require progress on the observational limitations described in Section 4. Here we highlight several new and upcoming wide-field optical surveys that contain the qualities necessary to make this progress.

The Southern Sky Survey (SSS) [22] and PanSTARRs (PS1) are optical surveys of the entire Southern and Northern skies, respectively. The SSS is anticipated to begin survey operations at the end of 2009, and PS1 has already begun obtaining survey data. The SDSS filter set [66] plus a Strömgren u filter will be used for the SSS, while SDSS *griz* plus a y filter at 1 micron is being used for PS1. These surveys are both conducted on small aperture telescopes (1.3 m for SSS, 1.8 m for PS1), with images of the sky obtained repeatedly over a period of about 5 years. The coadded point source catalogs anticipated from these surveys will be 0.5 (SSS) to 1 (PS1) magnitude deeper than the SDSS catalog.

Searches for resolved dwarf galaxies in the SSS will be led by H. Jerjen and the *Stromlo Missing Satellites* team and in PS1 will be lead by N. Martin at MPIA. Between the SSS and PS1, a full digital picture of the sky at optical wavelengths will be obtained, nearly 75% of it for the very first time. The region of sky at $b < -20^\circ$ to be observed by the SSS should contain many discoverable ultra-faint galaxies – perhaps a dozen by comparison with those already known in the North. These new surveys will also substantially progress our understanding of the distribution of dwarfs close to the disk. However, mining for dwarfs at low b will require careful adjustments to the search techniques applied to SDSS data owing to severe Galactic contamination and obscuration at low Galactic latitudes. For example, it has been common to use a $1^\circ \times 1^\circ$ running windows to measure the local density of the foreground [14, 61]. The steep spatial gradient in the number density of disk stars at low b will demand a more careful characterization of the average point source counts when searching for localized overdensities.

These imminent surveys will also reveal ultra-faint dwarfs throughout a greater fraction of the Milky Way's virial volume. A naive extrapolation from the detectability of dwarfs in the SDSS yields $d_{\mathrm{max,PS1}}/d_{\mathrm{max,SDSS}} = (f_{\mathrm{lim,PS1}}/f_{\mathrm{lim,SDSS}})^{0.5}$. In this approximation, analyzing the PS1 star catalog with methods analogous to those applied to SDSS data will reveal dwarfs (at $|b| > 20^\circ$) to distances $\sim$1.6 times farther, which is a factor of 4 in volume. Despite this anticipated improvement, these surveys will not provide an unbiased measurement of the ultra-faint dwarf galaxy population all the way out to the virial radius of the Milky Way ($\sim$300 kpc).

Only a survey such as the planned Large Synoptic Survey Telescope (LSST (http://www.lsst.org/)) project, currently scheduled to begin survey operations in 2016, will potentially yield a measurement of the ultra-faint dwarf galaxy population that truly satisfies all of the observational requirements needed to fully exploit these objects for dark matter and galaxy formation science. LSST's primary mode will be the planned "deep-wide-fast" survey that will observe 20 000 deg^2 of sky at $\delta < 34^\circ$ roughly 1000 times over 6 bands (SDSS *ugriz* plus y). Single 15-second exposures have an anticipated 5σ limit of $r = 24.5$, and the final 10-year co-added catalog has an anticipated limit of $r = 27.5$ [24].

Using the same naive extrapolation of the detectability of dwarfs in SDSS applied above to the PS1 survey, Tollerud et al. [15] showed that an SDSS-like analysis of a 10-year LSST-like catalog of stars would reveal $M_V = -2.0$ dwarfs to distances of at least 400 kpc. More luminous ultra-faints would be detectable throughout the entire Local Group, and even beyond, based on this sort of extrapolation. Such a calculation assumes that the number density of contaminating point sources passing color-magnitude filtering (such as shown in Figure 1) does not substantially vary with distance. However, the landscape of the point source population at magnitudes fainter than $r \sim 24$ does differ greatly from that in the SDSS-depth data shown in Figure 1.

Figure 1 showed that thick disk and halo main sequence and main sequence turnoff stars in the Milky Way were the primary noise in SDSS searches. At fainter apparent magnitudes, the number density of unresolved galaxies, galaxies at high redshift that cannot be distinguished from individual stars by morphology alone, rapidly increases. Figure 3 shows the $(V - I, V)$ color-magnitude diagram of galaxies in the 9 arcmin^2 Hubble Ultra Deep Field (HUDF) with an angular full-width half-max size smaller than $0.8''$, the expected average image quality of LSST. Overplotted in red are the stellar sources in the HUDF; they are outnumbered by galaxies by a factor of 75.

The CMDs in Figure 4 illustrate in more detail the point source contamination expected in deep searches for resolved ultra-faint dwarfs. Figure 4(a) displays a TRILEGAL (http://stev.oapd.inaf.it/cgi-bin/trilegal) [68] simulation of Milky Way stars in a one square deg field at $(l, b) = (45,40)$. Figure 4(b) displays a simulation of the galaxy population as it will be observed by LSST. The LSST image simulation project (led by A. Connolly at UW) was based on a mock catalog generated from the Millennium simulation [69]. The isochrone of an old and metal-poor stellar population overplotted on Figure 4(a) shows that red giant branch stars belonging to a system $\sim$300 kpc away will be contaminated by MW halo dwarf and subdwarf stars (the plume at $g - r \sim 1.0$). In multicolor survey data of sufficient depth and photometric precision, colors can be used to select stars based on temperature, metallicity, and surface gravity [70]. For example, it has been shown that $g-r$ combined with $u-g$ separates metal-poor red giants at halo distances from red dwarf stars in the disk of the Milky Way, but only to $r \sim 17$ in SDSS-depth data [71]. SDSS was not deep enough in all filters to utilize photometric stellar classification to distances beyond 25 kpc. LSST will have small enough photometric errors to photometrically select red giant stars at outer halo distances. Therefore, color-color selection of red giant stars at outer halo distance may reveal both bound and unbound structure at MW halo distances to unprecedentedly low surface brightnesses.

The overploted isochrone on Figure 4(b) shows that the main sequence turnoff of stars in an old and metal-poor stellar population in the MW's outer halo will be

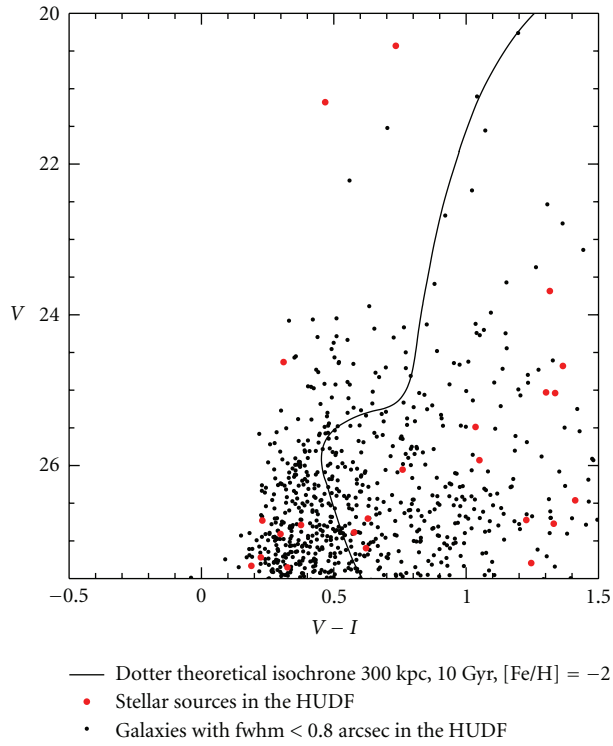

FIGURE 3: Color-magnitude diagram of galaxies with small angular sizes and stellar sources in the Hubble Ultra Deep Field [67]. Galaxies outnumber stellar objects by a factor of 75 in this figure, suggesting that unresolved galaxies will be the primary source of contamination in searches for ultra-faint dwarfs in deep survey data. Objects designated "stellar" in this image are those with *type* > 0.3 in the HUDF catalog.

severely contaminated by unresolved galaxies. The mock galaxy catalog predicts ~700 000 galaxies per deg^2 with $r < 27.5$ and $g - r < 1.5$. By contrast, the Trilegal model predicts ~35 000 stars per deg^2 with those same colors and magnitudes. Based on the HUDF catalog, roughly half of the galaxies at the faint magnitudes to be accessible by LSST have angular sizes smaller than the expected median image quality of 0.8″. Unresolved galaxies thus outnumber stars by a factor of 100 in observations down to $r = 27.5$ when only angular size is used to morphologically classify objects, consistent with the results obtained from the small HUDF field-of-view.

The very least luminous ($M_V \gtrsim -3$) systems can only be discovered by their MSTO and main sequence stars, because they have few, if any, red giant branch stars. The contamination by unresolved galaxies could therefore be catastrophic for discoveries of such systems at large distances, particularly because galaxies themselves are clustered and thus do not provide a smooth background that can easily be removed. However, a combination of careful morphological classification and color-color-magnitude filtering can be used to drastically reduce the noise from unresolved galaxies. In reality, star-galaxy separation is not performed by a simple measurement of angular size; the extended shapes of the light profiles of sources are often used to discriminate between stars and galaxies. For example, [72] describes a method to use the curve-of-growth of the light profile of individual objects to yield a morphological star-galaxy classification. This type of classification will still yield a star catalog that is dominated by faint galaxies. Galaxies also have colors that differ from those of stars. For example, color-color information has been used to distinguish Milky Way stars from unresolved galaxies at very faint magnitudes in the Deep Lens Survey, a deep, ground-based, survey in multiple optical filters [73].

An important consideration for dwarf searches in LSST-depth data is prospects for meaningful follow-up observations. Follow-up imaging to obtain deep CMDs has been needed to confirm many of the 14 known ultra-faint dwarfs. However, color-magnitude diagrams deeper than the expected LSST limiting r-magnitude of 27.5 could likely not be obtained from the ground. Space-based follow-up to confirm new dwarfs with JWST will probably also not be feasible, because the number of dwarfs may be in the hundreds (with a higher number of candidates) and because the fields-of-view of the cameras on JWST (~2.2′ × 2.2′) are smaller than the angular sizes expected for all but the smallest scale size dwarfs. With a half-degree field-of-view, the camera on the Supernova Acceleration Probe (SNAP) could provide the imaging needed to confirm the presence of relatively distant dwarfs tentatively detected in LSST data. There are not currently plans for SNAP to be a pointed tool for such science. Therefore the number of resolved stars required for a certain ultra-faint detection in very deep survey data will necessarily be higher than in SDSS-depth data. The spectroscopic resources now being used to measure the masses of new ultra-faint objects (e.g., DEIMOS on Keck II, Hectochelle on the MMT) are also already being pushed to their limits with the dwarfs discovered in SDSS. Much fainter or more distant dwarfs could not be effectively studied with these resources but instead will require next generation 30 m class telescopes (such as a Giant Magellan Telescope or Thirty Meter Telescope) and/or instrumentation.

A final consideration for searches is based on resolved stars in an LSST-depth dataset—the possible crowding of stars belonging to more distant satellites. Although fewer stars are resolved in more distant galaxies, the apparent angular separation of resolved stars decreases with increasing distance. If the average star separation is small relative to the average full-width half-max of stars in the image, then an object may be confusion limited and its individual stars not identified in a standard photometric pipeline. Could ultra-faint dwarf galaxies become confusion limited before they are, in theory, too distant to detect as overdensities of resolved stars? Using the Dotter stellar luminosity functions (http://stellar.dartmouth.edu/) [74] and assuming a star catalog as deep as the LSST 10-year coadd, the average spacing between resolved stars in a 10 Gyr, [Fe/H] = −2.0 stellar population is roughly constant with distance for 100 kpc—$d_{\rm lim}$. $d_{\rm lim}$ is the optimistic limiting detection distance for dwarfs with $-2.5 > M_V > -7.5$. For ultra-faint Milky Way satellites with scales sizes ~50% smaller (and thus smaller angular separation between stars) than those of ultra-faints

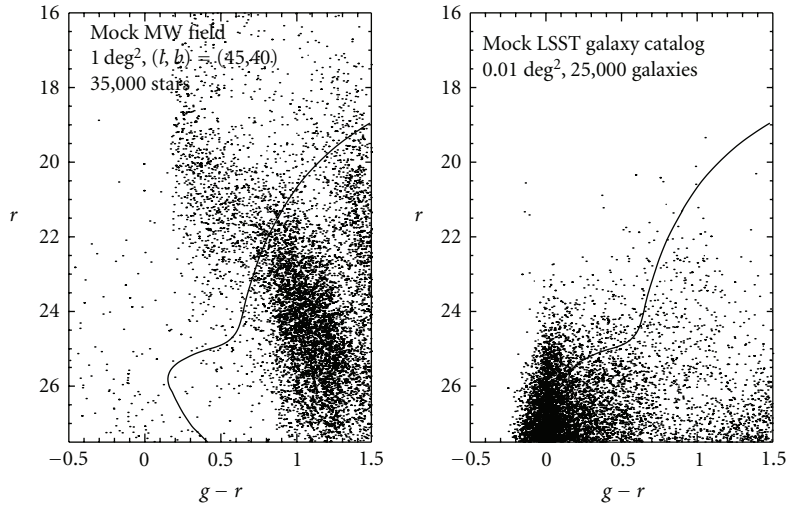

Figure 4: Simulated observations of Milky Way stars and galaxies in an LSST-like survey. (a) TRILEGAL simulated observation of Milky Way stars in a one deg^2 field at $(l, b) = (45,40)$. (b) Simulated observation of galaxies in a 0.01 deg^2 field based on [69] (A. Connolly, private communication). A Dotter isochrone for a 10 Gyr, [Fe/H] = −2.0 stellar population at a distance of 300 kpc ($m - M \sim 22$) is overplotted on both panels. For clarity, only 1/4 of sources in each panel are plotted. LSST-like photometric uncertainties have not been added to the simulated data.

with similar magnitudes, this average separation is expected to range between 1″ and 2″. Because this separation is larger than the average image quality expected for LSST and because LSST will likely reach its coadded depths by simultaneous photometering of numerous exposures, rather than photometering a single stacked image, crowding should not be a technical issue that will inhibit future dwarf searches.

6. Conclusion

The next 15 years will be an exciting time for near-field dwarf galaxy cosmology. A lot hinges on the new class of ultra-faint galaxies that was only discovered in the last 5 years but that may be the most numerous and cosmologically important class of galaxies. However, to effectively exploit these dwarfs as cosmological barometers will require improvements on many observational limitations. Several wide-field, optical surveys are planned that may finally reveal the true nature of the MW's satellite population and the true nature of ultra-faint dwarfs. Careful statistical analyses of star counts will continue to be a primary method to identify ultra-faints, which are known to have surface brightnesses as low as ∼27.5 mag arcsec^{-2}. Future surveys could possibly reveal such objects at Mpc and greater distances by their diffuse light, rather than just by individual stars. Planned and current surveys at infrared wavelengths will at minimum complement searches for dwarf galaxies done with optical datasets and will provide important support for dwarf searches near the Galactic plane. The upcoming Vista Hemisphere Survey (PI Richard McMahon) will image the entire Southern Sky in J and K_S 4 magnitudes deeper than 2MASS. UKIDSS is in the middle of survey operations and is obtaining 7000 deg^2 of IR imaging in the North to a depth of $K \sim 18$, including part of the Galactic plane. These surveys have the promise to open up enough new dwarf discovery space to reveal systems not yet accessible in optical datasets.

Pointed surveys will also reveal low luminosity galaxies in other systems, although they cannot yet reveal objects as low luminosity as many of the MW's ultra-faints. Recently, [75] identified 22 dwarf galaxy candidates as faint as $r = -10$ around M81. They used both eyeball evaluation and automated analysis of resolved stars in 65 square degrees of deep imaging. The on-going PAndAS survey (PI A. McConnachie) of 350 square degrees around M31 and M33 is expected to reveal diffuse objects around these galaxies as faint as 32 magnitudes per square arcsecond.

The future will reveal whether we have yet seen the ultimate limit of galaxy formation. The possibilities remain that either (1) the low luminosities of the ultra-faint dwarfs are an artifact of nature, rather than nurture, and/or (2) the present survey data are not deep enough to reveal the very least luminous systems and a vast population of ultra-faint dwarfs lie just beyond our fingertips. Regardless, at least dozens of ultra-faint satellites will be discovered in the near future, with the possibility of hundreds or more.

Acknowledgments

The author thanks both referees for comments that improved the clarity and the quality of this paper. She also thanks Joe Cammisa at Haverford for computing support, Marla Geha for inspiring Figure 2, and NSF AST-0908193 for supporting this work.

References

[1] M. Mateo, "Dwarf galaxies of the local group," *Annual Review of Astronomy and Astrophysics*, vol. 36, no. 1, pp. 435–506, 1998.

[2] S. G. van den Bergh, "The local group of galaxies," *The Astronomy and Astrophysics Review*, vol. 9, pp. 273–318, 1999.

[3] M. Geha, B. Willman, J. D. Simon, et al., "The least-Luminous galaxy: spectroscopy of the Milky Way satellite segue 1," *Astrophysical Journal*, vol. 692, pp. 1464–1475, 2009.

[4] A. E. Dolphin, D. R. Weisz, E. D. Skillman, and J. A. Holtzman, "Star formation histories of local group dwarf galaxies," in *Proceedings of the International Conference on Resolved Stellar Populations*, Cancun, Mexico, April-June 2005.

[5] H. T. MacGillivray, R. K. Bhatia, S. M. Beard, and R. J. Dodd, "An automated search for halo star clusters and Local Group dwarf galaxies," in *Proceedings of the European Southern Observatory Astrophysics Symposia*, M. Azzopardi and F. Matteucci, Eds., vol. 27 of *European Southern Observatory Astrophysics Symposia*, pp. 477–479, 1987.

[6] A. Klypin, A. V. Kravtsov, O. Valenzuela, and F. Prada, "Where are the missing galactic satellites?" *Astrophysical Journal*, vol. 522, no. 1, pp. 82–92, 1999.

[7] B. Moore, S. Ghigna, F. Governato, et al., "Dark matter substructure within galactic halos," *Astrophysical Journal*, vol. 524, no. 1, pp. L19–L22, 1999.

[8] J. Diemand, M. Kuhlen, P. Madau, et al., "Clumps and streams in the local dark matter distribution," *Nature*, vol. 454, no. 7205, pp. 735–738, 2008.

[9] V. Springel, J. Wang, M. Vogelsberger, et al., "The aquarius project: the subhaloes of galactic haloes," *Monthly Notices of the Royal Astronomical Society*, vol. 391, no. 4, pp. 1685–1711, 2008.

[10] J. S. Bullock, A. V. Kravtsov, and D. H. Weinberg, "Reionization and the abundance of galactic satellites," *Astrophysical Journal*, vol. 539, no. 2, pp. 517–521, 2000.

[11] A. J. Benson, C. S. Frenk, C. G. Lacey, C. M. Baugh, and S. Cole, "The effects of photoionization on galaxy formation—II: satellite galaxies in the local group," *Monthly Notices of the Royal Astronomical Society*, vol. 333, no. 1, pp. 177–190, 2002.

[12] A. V. Kravtsov, O. Y. Gnedin, and A. A. Klypin, "The tumultuous lives of galactic dwarfs and the missing satellites problem," *Astrophysical Journal*, vol. 609, no. 2, pp. 482–497, 2004.

[13] J. D. Simon and M. Geha, "The kinematics of the ultra-faint Milky Way satellites: solving the missing satellite problem," *Astrophysical Journal*, vol. 670, no. 1, pp. 313–331, 2007.

[14] S. Koposov, V. Belokurov, N. W. Evans, et al., "The luminosity function of the Milky Way satellites," *Astrophysical Journal*, vol. 686, no. 1, pp. 279–291, 2008.

[15] E. J. Tollerud, J. S. Bullock, L. E. Strigari, and B. Willman, "Hundreds of Milky Way satellites? Luminosity bias in the satellite luminosity function," *Astrophysical Journal*, vol. 688, no. 1, pp. 277–289, 2008.

[16] B. Willman, F. Governato, J. J. Dalcanton, D. Reed, and T. Quinn, "The observed and predicted spatial distribution of Milky Way satellite galaxies," *Monthly Notices of the Royal Astronomical Society*, vol. 353, no. 2, pp. 639–646, 2004.

[17] M. T. Busha, M. A. Alvarez, R. H. Wechsler, T. Abel, and L. E. Strigari, "The impact of inhomogeneous reionization on the satellite galaxy population of the Milky Way," submitted to *Astrophysical Journal*.

[18] L. E. Strigari, J. S. Bullock, M. Kaplinghat, J. Diemand, M. Kuhlen, and P. Madau, "Redefining the missing satellites problem," *Astrophysical Journal*, vol. 669, no. 2, pp. 676–683, 2007.

[19] P. Kroupa, C. Theis, and C. M. Boily, "The great disk of Milky-Way satellites and cosmological sub-structures," *Astronomy and Astrophysics*, vol. 431, no. 2, pp. 517–521, 2005.

[20] M. Metz, P. Kroupa, and N. I. Libeskind, "The orbital poles of Milky Way satellite galaxies: a rotationally supported disk of satellites," *Astrophysical Journal*, vol. 680, no. 1, pp. 287–294, 2008.

[21] J. Wang and S. D. M. White, "Discreteness effects in simulations of hot/warm dark matter," *Monthly Notices of the Royal Astronomical Society*, vol. 380, no. 1, pp. 93–103, 2007.

[22] S. C. Keller, B. P. Schmidt, M. S. Bessell, et al., "The SkyMapper telescope and the southern sky survey," *Publications of the Astronomical Society of Australia*, vol. 24, no. 1, pp. 1–12, 2007.

[23] The Dark Energy Survey Collaboration, "The dark energy survey," White Paper submitted to *Dark Energy Task Force*, http://arxiv.org/abs/astro-ph/0510346.

[24] Z. Ivezic, J. A. Tyson, R. Allsman, et al., "LSST: from science drivers to reference design and anticipated data products," submitted, http://arxiv.org/abs/0805.2366, http://www.lsst.org/overview.

[25] H. Shapley, "A stellar system of a new type," *Harvard College Observatory Bulletin*, vol. 908, pp. 1–11, 1938.

[26] H. Shapley, "Two stellar systems of a new kind," *Nature*, vol. 142, no. 3598, pp. 715–716, 1938.

[27] R. G. Harrington and A. G. Wilson, "Two new stellar systems in Leo," *Publications of the Astronomical Society of the Pacific*, vol. 62, pp. 118–120, 1950.

[28] A. G. Wilson, "Sculptor-type systems in the local group of galaxies," *Publications of the Astronomical Society of the Pacific*, vol. 67, pp. 27–29, 1955.

[29] R. D. Cannon, T. G. Hawarden, and S. B. Tritton, "A new sculptor-type dwarf elliptical galaxy in Carina," *Monthly Notices of the Royal Astronomical Society*, vol. 180, pp. 81P–82P, 1977.

[30] E. K. Grebel, J. S. Gallagher III, and D. Harbeck, "The progenitors of dwarf spheroidal galaxies," *The Astronomical Journal*, vol. 125, no. 4, pp. 1926–1939, 2003.

[31] M. J. Irwin, P. S. Bunclark, M. T. Bridgeland, and R. G. McMahon, "A new satellite galaxy of the Milky Way in the constellation of Sextans," *Monthly Notices of the Royal Astronomical Society*, vol. 244, pp. 16P–19P, 1990.

[32] M. J. Irwin, "Searches for galactic dwarf spheroidal satellites," in *Proceedings of the European Southern Observatory Astrophysics Symposia*, G. Meylan and P. Prugniel, Eds., vol. 49 of *European Southern Observatory Astrophysics Symposia*, p. 27, January 1994.

[33] R. A. Ibata, G. Gilmore, and M. J. Irwin, "A dwarf satellite galaxy in Sagittarius," *Nature*, vol. 370, no. 6486, pp. 194–196, 1994.

[34] J. T. Kleyna, M. J. Geller, S. J. Kenyon, and M. J. Kurtz, "An adaptive kernel approach to finding DSPH galaxies around the Milky Way," *The Astronomical Journal*, vol. 113, no. 2, pp. 624–633, 1997.

[35] A. B. Whiting, G. K. T. Hau, M. Irwin, and M. Verdugo, "An observational limit on the dwarf galaxy population of the local group," *The Astronomical Journal*, vol. 133, no. 2, pp. 715–733, 2007.

[36] D. G. York, J. Adelman, J. E. Anderson Jr., et al., "The sloan digital sky survey: technical summary," *The Astronomical Journal*, vol. 120, pp. 1579–1587, 2000.

[37] B. Willman, M. R. Blanton, A. A. West, et al., "A new Milky Way companion: unusual globular cluster or extreme dwarf satellite?" *The Astronomical Journal*, vol. 129, no. 6, pp. 2692–2700, 2005.

[38] B. Willman, J. J. Dalcanton, D. Martinez-Delgado, et al., "A new Milky Way dwarf galaxy in URSA major," *Astrophysical Journal*, vol. 626, no. 2, pp. L85–L88, 2005.

[39] V. Belokurov, D. B. Zucker, N. W. Evans, et al., "A faint new Milky Way satellite in bootes," *Astrophysical Journal*, vol. 647, no. 2, pp. L111–L114, 2006.

[40] D. B. Zucker, V. Belokurov, N. W. Evans, et al., "A curious Milky Way satellite in Ursa Major," *Astrophysical Journal*, vol. 650, no. 1, pp. L41–L44, 2006.

[41] D. B. Zucker, V. Belokurov, N. W. Evans, et al., "A new Milky Way dwarf satellite in canes venatici," *Astrophysical Journal*, vol. 643, no. 2, pp. L103–L106, 2006.

[42] V. Belokurov, D. B. Zucker, N. W. Evans, et al., "Cats and dogs, hair and a hero: a quintet of new Milky Way companions," *Astrophysical Journal*, vol. 654, no. 2, pp. 897–906, 2007.

[43] M. J. Irwin, V. Belokurov, N. W. Evans, et al., "Discovery of an unusual dwarf galaxy in the outskirts of the Milky Way," *Astrophysical Journal*, vol. 656, no. 1, pp. L13–L16, 2007.

[44] S. M. Walsh, H. Jerjen, and B. Willman, "A pair of boötes: a new Milky Way satellite," *Astrophysical Journal*, vol. 662, no. 2, pp. L83–L86, 2007.

[45] V. Belokurov, M. G. Walker, N. W. Evans, et al., "Leo V: a companion of a companion of the Milky Way galaxy?" *Astrophysical Journal*, vol. 686, no. 2, part 2, pp. L83–L86, 2008.

[46] V. Belokurov, M. G. Walker, N. W. Evans, et al., "The discovery of segue 2: a prototype of the population of satellites of satellites," *Monthly Notices of the Royal Astronomical Society*, p. 903, 2009.

[47] N. F. Martin, J. T. A. de Jong, and H.-W. Rix, "A comprehensive maximum likelihood analysis of the structural properties of faint Milky Way satellites," *Astrophysical Journal*, vol. 684, no. 2, pp. 1075–1092, 2008.

[48] E. N. Kirby, J. D. Simon, M. Geha, P. Guhathakurta, and A. Frebel, "Uncovering extremely metal-poor stars in the Milky Way's ultrafaint dwarf spheroidal satellite galaxies," *Astrophysical Journal*, vol. 685, no. 1, pp. L43–L46, 2008.

[49] A. Frebel, J. D. Simon, M. Geha, and B. Willman, "High-resolution spectroscopy of extremely metal-poor stars in the least evolved galaxies: Ursa major II and coma berenices," submitted to *The Astrophysical Journal*, http://arxiv.org/abs/0902.2395.

[50] G. D. Martinez, J. S. Bullock, M. Kaplinghat, L. E. Strigari, and R. Trotta, "Indirect dark matter detection from dwarf satellites: joint expectations from astrophysics and supersymmetry," *Journal of Cosmology and Astro-Particle Physics*, vol. 6, p. 14, 2009.

[51] L. E. Strigari, S. M. Koushiappas, J. S. Bullock, et al., "The most dark-matter-dominated galaxies: predicted gamma-ray signals from the faintest Milky Way dwarfs," *Astrophysical Journal*, vol. 678, no. 2, pp. 614–620, 2008.

[52] D. B. Zucker, A. Y. Kniazev, E. F. Bell, et al., "Andromeda IX: a new dwarf spheroidal satellite of M31," *Astrophysical Journal*, vol. 612, no. 2, pp. L121–L124, 2004.

[53] N. F. Martin, R. A. Ibata, M. J. Irwin, et al., "Discovery and analysis of three faint dwarf galaxies and a globular cluster in the outer halo of the Andromeda galaxy," *Monthly Notices of the Royal Astronomical Society*, vol. 371, no. 4, pp. 1983–1991, 2006.

[54] S. R. Majewski, R. L. Beaton, R. J. Patterson, et al., "Discovery of andromeda XIV: a dwarf spheroidal dynamical rogue in the local group?" *Astrophysical Journal*, vol. 670, no. 1, pp. L9–L12, 2007.

[55] D. B. Zucker, A. Y. Kniazev, D. Martínez-Delgado, et al., "Andromeda X, a new dwarf spheroidal satellite of M31: photometry," *Astrophysical Journal*, vol. 659, no. 1, pp. L21–L24, 2007.

[56] R. Ibata, N. F. Martin, M. Irwin, et al., "The haunted halos of andromeda and triangulum: a panorama of galaxy formation in action," *Astrophysical Journal*, vol. 671, no. 2, pp. 1591–1623, 2007.

[57] M. J. Irwin, A. M. N. Ferguson, A. P. Huxor, N. R. Tanvir, R. A. Ibata, and G. F. Lewis, "Andromeda XVII: a new low-luminosity satellite of M31," *Astrophysical Journal*, vol. 676, no. 1, pp. L17–L20, 2008.

[58] A. W. McConnachie, A. Huxor, N. F. Martin, et al., "A trio of new local group galaxies with extreme properties," *Astrophysical Journal*, vol. 688, no. 2, pp. 1009–1020, 2008.

[59] K. N. Abazajian, J. K. Adelman-Mccarthy, M. A. Agüeros, et al., "The seventh data release of the sloan digital sky survey," *Astrophysical Journal, Supplement Series*, vol. 182, no. 2, pp. 543–558, 2009.

[60] B. Willman, J. Dalcanton, Ž. Ivezić, et al., "An SDSS survey for resolved Milky Way satellite galaxies. I. Detection limits," *The Astronomical Journal*, vol. 123, no. 2, pp. 848–854, 2002.

[61] S. M. Walsh, B. Willman, and H. Jerjen, "The invisibles: a detection algorithm to trace the faintest Milky Way satellites," *The Astronomical Journal*, vol. 137, no. 1, pp. 450–469, 2009.

[62] C. M. Rockosi, M. Odenkirchen, E. K. Grebel, et al., "A matched-filter analysis of the tidal tails of the globular cluster palomar 5," *The Astronomical Journal*, vol. 124, no. 1, pp. 349–363, 2002.

[63] N. F. Martin, M. G. Coleman, J. T. A. de Jong, et al., "A deep large binocular telescope view of the Canes Venatici I dwarf galaxy," *Astrophysical Journal*, vol. 672, no. 1, pp. L13–L16, 2008.

[64] F. J. Lockman, "High-velocity cloud complex H: a satellite of the Milky Way in a retrograde orbit?" *Astrophysical Journal*, vol. 591, no. 1, pp. L33–L36, 2003.

[65] N. F. Martin, R. A. Ibata, M. Bellazzini, M. J. Irwin, G. F. Lewis, and W. Dehnen, "A dwarf galaxy remnant in Canis Major: the fossil of an in-plane accretion on to the Milky Way," *Monthly Notices of the Royal Astronomical Society*, vol. 348, no. 1, pp. 12–23, 2004.

[66] T. X. Thuan and J. E. Gunn, "A new four-color intermediate-band photometric system," *Publications of the Astronomical Society of the Pacific*, vol. 88, pp. 543–547, 1976.

[67] S. V. W. Beckwith, M. Stiavelli, A. M. Koekemoer, et al., "The hubble ultra deep field," *The Astronomical Journal*, vol. 132, no. 5, pp. 1729–1755, 2006.

[68] L. Girardi, M. A. T. Groenewegen, E. Hatziminaoglou, and L. da Costa, "Star counts in the galaxy simulating from very deep to very shallow photometric surveys with the TRILEGAL code," *Astronomy and Astrophysics*, vol. 436, no. 3, pp. 895–915, 2005.

[69] M. G. Kitzbichler and S. D. M. White, "The high-redshift galaxy population in hierarchical galaxy formation models," *Monthly Notices of the Royal Astronomical Society*, vol. 376, no. 1, pp. 2–12, 2007.

[70] D. D. Lenz, J. Newberg, R. Rosner, G. T. Richards, and C. Stoughton, "Photometric separation of stellar properties using SDSS filters," *Astrophysical Journal, Supplement Series*, vol. 119, no. 2, pp. 121–140, 1998.

[71] A. Helmi, Ž. Ivezić, F. Prada, et al., "Selection of metal-poor giant stars using the sloan digital sky survey photometric system," *Astrophysical Journal*, vol. 586, no. 1, pp. 195–200, 2003.

[72] H. K. C. Yee, "A faint-galaxy photometry and image-analysis system," *Publications of the Astronomical Society of the Pacific*, vol. 103, pp. 396–411, 1991.

[73] P. C. Boeshaar, V. Margoniner, and The Deep Lens Survey Team, "Ground-based optical deep pencil beam surveys," in *Brown Dwarfs*, E. Martín, Ed., vol. 211 of *IAU Symposium*, p. 203, 2003.

[74] A. Dotter, B. Chaboyer, D. Jevremovic, V. Kostov, E. Baron, and J. W. Ferguson, "The dartmouth stellar evolution database," *Astrophysical Journal, Supplement Series*, vol. 178, no. 1, pp. 89–101, 2008.

[75] K. Chiboucas, I. D. Karachentsev, and R. B. Tully, "Discovery of new dwarf galaxies in the M81 group," *The Astronomical Journal*, vol. 137, no. 2, pp. 3009–3037, 2009.

Hindawi Publishing Corporation
Advances in Astronomy
Volume 2010, Article ID 434390, 9 pages
doi:10.1155/2010/434390

Review Article

Dwarf Cosmology with the Stromlo Missing Satellites Survey

Helmut Jerjen

Research School of Astronomy & Astrophysics, Mt Stromlo Observatory Australian National University, Cotter Road, Weston ACT 2611, Australia

Correspondence should be addressed to Helmut Jerjen, jerjen@mso.anu.edu.au

Received 11 May 2009; Accepted 30 July 2009

Academic Editor: Regina Schulte-Ladbeck

The standard Lambda Cold Dark Matter model is considered to be a triumph of theoretical astrophysics but observations of the Milky Way and its system of satellite galaxies irresistibly signal that theory is incomplete on galactic and subgalactic scales. The Stromlo Missing Satellites (SMS) Survey is a critical endeavor to investigate at what level predictions of CDM cosmology are consistent with the observed matter distribution in the Milky Way halo. It will be the deepest, most extended search for optically elusive satellite galaxies to date, covering 20 000 square degrees of sky. The international SMS Survey collaboration will exploit 150 TB of CCD images in six filters acquired by the new SkyMapper telescope of the Australian National University over the next five years, expecting on completion photometric limits 0.5–1.0 mag fainter than the Sloan Digital Sky Survey. The primary objective of the program is to characterise the baryonic and dark matter components of a complete sample of MW satellites in the Southern hemisphere to provide stringent observational constraints for improving our understanding of how the Milky Way formed and what physical processes governed galaxy formation and evolution in general.

1. Satellite Galaxies

According to cosmological theory, overdensities of cold dark matter gravitationally collapsed and formed the first structures in the Universe one billion years after the Big Bang. The gravitational pull of those dark matter clumps drew in primordial baryons in the form of hydrogen gas, providing the seeds for galaxy formation. The observational Universe today is populated with galaxies, the prime repositories of stars, the shining baryonic matter. For obvious reasons, most of the detected and catalogued galaxies are intrinsically the largest and the brightest, those that can be seen from the greatest distance and are most easily studied against the night sky. Ironically, a major limitation on our ability to develop a physically consistent model that describes how galaxies evolved out of the dark matter and baryonic ingredients comes from our incomplete picture of the vicinity of the Milky Way, in particular from the lack of a good understanding of the phenomenon "satellite galaxies." This term is broadly used for dwarf galaxy companions of the Milky Way (Figure 1), some of which contain only a few thousand stars. They cover a stellar mass range of $10^{3-7}\mathcal{M}_{\odot}$ and consist of up to 99.9% of dark matter (e.g., [1–7]). At the low end of the mass scale, satellites exhibit extreme low star densities so they are completely resolved, that is, transparent, and hard to detect against the screen of MW foreground stars. A few examples of such ultrafaint satellites have been discovered around the Milky Way in the recent years. Cold Dark Matter theory tells us that those are the survivors of the accretion/merger process that assembled larger galaxies. Hence, if we want to shed light on the nature of dark matter and understand how galaxies formed we have to spend a much greater amount of effort on finding and physically characterising these faintest, most elusive galaxies that exist in the Universe.

2. Cold Dark Matter Theory to the Test

While the cold dark matter paradigm successfully explains the large-scale distribution of bright baryons (i.e., luminous galaxies) in the Universe (e.g., [8]), one crucial test of the model lies in its ability to predict the properties of dark matter on subgalactic scales, most fundamentally the number and distribution of substructures around the Milky Way and their optical manifestation, the satellite galaxies.

A generic result of high-resolution numerical simulations of large galaxies [9–12] is that the dark matter halo of the Milky Way must be filled with hundreds or even thousands of smaller dark matter condensations [13]. It is thought that the majority of these subhalos will gravitationally collect sufficient primordial hydrogen gas, turn it into stars, and form MW satellite galaxies observable today. However, the number of bound dark matter subhaloes exceeds the entire population of currently known MW satellites by at least one order of magnitude. This discrepancy is discussed in the literature as the "missing satellites" or "substructure" problem [9, 14]. There has been no shortage of solutions proposed, ranging from a drastic modification of the dark matter power spectrum [15] or self-interacting dark matter [16] to the reduction of the amount of small-scale features through warm dark matter-like models (e.g., [17–20]) to careful estimates of the effects of the epoch of photoionization on the ability of subhalos to retain baryons and evolve into luminous satellite galaxies (e.g., [21]).

More recently focus has shifted to the question whether the known Milky Way satellites can actually originate from a population of dark matter subhalos. Even if the suppression of star formation by cosmic reionization and other mechanisms was quite effective in the early Universe and thus the observed satellite galaxies today are comprising only a subset of the actually present CDM substructures, their number-density distribution should be still consistent with an isotropic or mildly triaxial parent distribution. However, Kroupa and collaborators [22–24] showed that the spatial distribution of the luminous Milky Way satellites that was known to be anisotropic for more than 30 years [25–29] is well described by a plane of finite thickness, statistically inconsistent with the distribution of a cosmological dark matter substructure population at the 99.5% confidence level (see Figure 1). First evidence for a similar disc-of-satellites in M31 has been found by [24] that is now awaiting further testing with the results from the Pan-Andromeda Archaeological Survey (PI McConnachie; http://www.nrc-cnrc.gc.ca/eng/projects/hia/pandas.html).

Although theoretical cosmologists argue that the distribution of the few galaxies in such a "Great Disk of Satellites" almost perpendicular to the MW plane is not improbable (e.g., [30]), debating this issue remains difficult due to the incompleteness of the census of Milky Way satellites, particularly in the crucial parts of the sky away from the proposed plane, regions that are coincidently not covered by the SDSS Survey. Currently, little is known about what physics is concealed behind the "missing satellites" and "Great Disk of Satellites" phenomena but researchers agree that resolving the mystery is going to have a major impact on our understanding of dark matter and its role in the formation process and evolution of galaxies over the lifetime of the Universe.

For example, Kroupa [31] showed that dSph satellite solutions are obtained from ancient tidal dwarf galaxies, implying that the disc-of-satellites can be naturally understood as the remnant of ancient tidal arms that formed during the early assembly of the Milky Way. The almost exact match of one of the author's models with the Hercules satellite [32] is noteworthy. If a significant number of MW dSphs are confirmed to be of tidal origin this would also imply the substructure crisis to become even more severe. Alternative explanations have been put forward to reconcile this anisotropic distribution within the ΛCDM paradigm. So Li and Helmi [33] and D'Onghia and Lake [34] proposed a scenario where the majority of satellites entered the Milky Way halo in a group rather than individually to explain the spatial and dynamical peculiarities of its satellite distribution. However, no dwarf galaxy associations exist in the vicinity of the Local Group today that are sufficiently compact to produce a disc-of-satellites [35]. On the theoretical side, Libeskind et al. [36] found that one third of their N-body simulations of MW-type halos are in agreement with the observed flattened spatial arrangement and the coherence of angular momenta of the Milky Way satellites. Accurate proper motion estimates for more satellites are needed to properly test the consistency within CDM galaxy formation model.

3. Searching for the Invisibles

Because incompleteness in the census of Milky Way satellites prevents any serious scrutiny of the currently best cosmological model, a breakthrough can only be expected once observers established the number and spatial distribution of satellite galaxies around the Milky Way including accurate estimates of those that remain hidden due to detection limits [37, 38]. Indirect evidence for a large number of undetected Milky Way, satellites was provided by Willman et al. [39]. The comparison of the spatial distributions of satellites around M31, the Milky Way and a simulated galaxy showed that the radial distribution of M31 satellites and the 15 oldest subhaloes of the simulated galaxy are in agreement, while the Milky Way satellites fall below expectations within the limits of observational completeness. Moreover, if one looks at the distribution of satellites as a function of Galactic latitude, the number of Milky Way satellites is less than the simulation predicts at low latitudes.

Northern Hemisphere. Willman et al. [40, 41] conduced a first systematic modern search for Milky Way satellites based on the Sloan Digital Sky Survey (SDSS; [42]) covering 20 percent of the entire sky. The analyses of resolved stars in both the SDSS and the Two Micron All Sky Survey (2MASS) uncovered the Willman 1 and Ursa Major galaxies. Since then, the SDSS collaboration [43–48] and other groups [49, 50] have found already more new Milky Way satellites than were detected in the previous 70 years while the exploitation of the SDSS data is still in process. In an attempt to reach to even lower luminosity systems, Walsh et al. [38, Figure 5] identified a total of 30 ultrafaint candidates in the DR6 footprint (see Figure 2). Establishing the true nature of these stellar overdensities will deeply probe into unknown territory of the galaxy luminosity function.

Southern Hemisphere. This part of the sky remains completely unexplored to faint magnitude levels with modern digital imaging data. The great potential of finding new

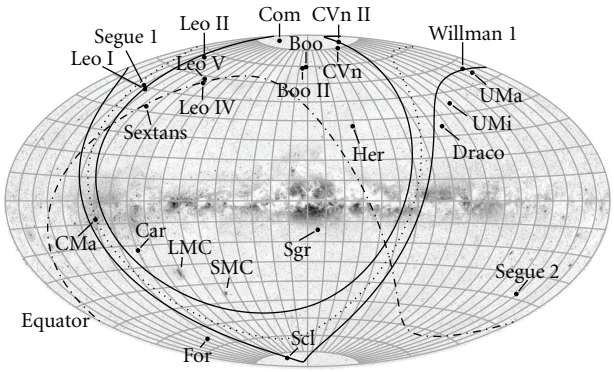

Figure 1: The distribution of currently known Milky Way satellites out to the 250 kpc virial radius from the center of the Milky Way. The arrangement of the galaxies in a "Great Disk of Satellites" almost perpendicular to the Galactic plane is highlighted by the dotted line and the arbitrarily chosen ±15 degree band. Half of the sky will be searched for satellites by the SMS survey (area south of the celestial equator).

Milky Way satellites in the Southern hemisphere was demonstrated when the analysis of stars from 2MASS led to the discovery of the Canis Major dwarf galaxy (see [51–53]; but see [54] for an update on the controversy of the nature of the CMa phenomenon). Covering twice the area of the SDSS footprint, the Southern hemisphere is expected to conceal at least 30 satellites more luminous than Boo II, Willman 1, or Segue 2.

4. The Stromlo Missing Satellites Survey

The Stromlo Missing Satellites (SMS) Survey (see http://msowww.anu.edu.au/~jerjen/SMS_Survey.html) was initiated to carry out the deepest, most extended search for Milky Way satellites over the next five years, covering the entire 20 000 square degrees of the Southern hemisphere. The international SMS Survey collaboration will analyse the digital images obtained by the Australian National University (ANU) SkyMapper Telescope and will use specialized data mining tools on the catalogues produced from the images by the SkyMapper team. Extensive follow-up observations of newly detected satellite candidates are absolutely essential and require the most powerful telescopes to gain an accurate picture of their physical nature. Recent follow-up works on one of the most luminous MW satellites, the CMa dwarf [54, and references therein], and the least luminous Segue 1 [55, 56] highlight some of the many challenges.

4.1. The ANU SkyMapper Telescope. Large CCD arrays are finally becoming available to construct wide-field CCD cameras at optical telescopes. Given this new research window of wide-field astronomy it is not surprising that almost every major observatory worldwide is in the process of developing survey telescopes base on that technology: Pan-STARRS of the University of Hawaii, the near-infrared 4 m Survey Telescope VISTA of the European Southern Observatory, and on an even larger financial and time scale, the 8.4 m Large Synoptic Survey Telescope (http://www.lsst.org/lsst), a wide-field telescope facility that is planned to have first light in 2015.

In this latest development, the ANU 1.35 m SkyMapper telescope (http://www.mso.anu.edu.au/skymapper/) at Siding Spring Observatory represents an investment in Australian frontier technologies of A$13 million. It is among the first of this new breed of specialised telescopes capable of scanning the night sky more quickly and sensitively than ever before featuring a 32 × 4k × 2k CCD mosaic camera with 0.5 arcsec pixels and a 5.7-sq degree field of view. The primary goal of the facility is to perform the Southern Sky Survey (hereafter S3) over the next five years, producing 150 Terabytes of CCD images and a reference catalogue for one billion stars and galaxies. This program is a six-colour photometry survey based on the SDSS filter set (u, g, r, i, and z) plus a Strömgren-like v filter. It will cover all 20 000 square degrees south of the celestial equator in 3845 individual pointings with photometric limits 0.5–1.0 magnitudes fainter than SDSS. The absolute stellar photometry accuracy is expected to be three percent. The S3 is carried out in six full scans of the sky each pointing of 90 seconds duration and a total integration time of 540 seconds. On completion, the S3 is expected to be 70 times more sensitive than 2MASS and 1.5 times deeper than the northern hemisphere SDSS. A single S3 epoch requires approximately six months to complete. For a detailed description of the SkyMapper observing cadence, the reduction pipeline, photometric and astrometry calibration, and accuracy we refer to Keller et al. [57].

4.2. Needles in the Haystack. The S3 catalogue is the ideal data set to continue the success story of finding new dwarf galaxies in the Milky Way halo. Out to the virial radius of 250 kpc, Milky Way satellites are completely resolved into stars. Hence, a satellite initially reveals its presence only through an unusual concentration of faint stars in the sky behind a foreground screen of disk stars, embedded in halo and possibly tidal stream stars, and superimposed on a sea of mid-to-high redshift galaxies. This excess of stars will also populate a well-defined locus in the colour-magnitude diagram depending on the satellite's star formation history (see Figure 3).

In practice, searching for new satellites in the multidimensional parameter space of galactocentric distance, satellite SFH, star density, and angular size is a computer intensive process; the S3 catalogue will contain coordinates and photometric parameters for approximately one billion stars but only about 1 : 100 000 belong to a satellite galaxy. The SMS team has already a working data mining algorithm in place that was originally developed by Willman et al. [41] and subsequently extended and improved by Walsh et al. [38]. In essence, it is a cluster detection algorithm with capabilities to analyse colour-magnitude diagrams of any given patch of sky. The important preselection of stars in the colour-magnitude diagram employs a comprehensive library of isochrone filters based on Padova evolutionary tracks [58, 59]. This selection process is repeated to scan through various distance slices. The concept of this search

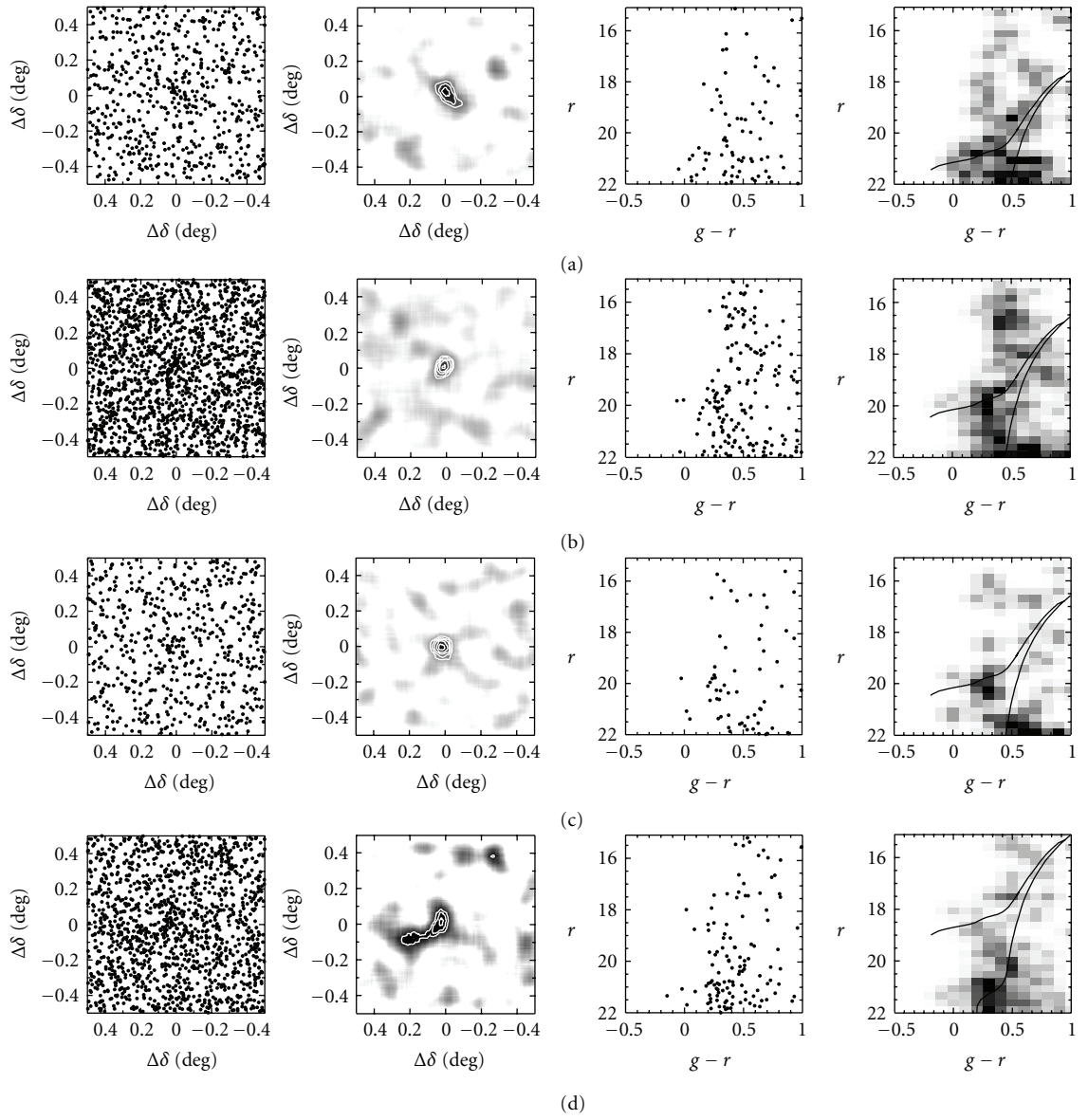

Figure 2: Four stellar overdensities found in SDSS-DR6 with detection significances equal to or greater than known MW satellites. Candidates were found (from top to bottom) in the constellations Canes Venatici, Hercules, Ursa Major, and Virgo. Isochrones in the Hess diagrams (right panel) show at what heliocentric distances those overdensities produced the strongest signal (figures from [38]).

strategy has been extensively tested [38] by taking advantage of the publicly available Sloan Digital Sky Survey data (DR5 and DR6). In single-blind experiments every Northern Hemisphere Milky Way satellite was recovered as well as the previously unknown satellite Boötes II [50, 60].

4.3. Satellites, Light Beacons, or Extreme Globular Clusters. Stochastic fluctuations in the distribution of MW halo stars are one of the major sources of confusion in the search for satellite candidates. Our algorithm has been carefully calibrated to separate these unwanted sources from true stellar overdensities. Detection thesholds were set above the 1 in 10 000 chance for a false positive. However, we cannot exclude a priori the possibility that some of the stellar overdensities turn out to be extremely low luminosity globular clusters, such as Koposov 1 and 2 [61], or stellar condensations in large-scale stellar streams [45, 62, 63]. Any of these alternatives would be equally important to confirm.

Ultrafaint satellites such as Willman 1, Boo II, and Segue 2 with absolute magnitudes $M_{V,\mathrm{tot}} \sim -2.7$ [48, 66] are less luminous than the median Milky Way globular cluster. Hence, the expected numbers of RGB and HB stars are naturally small (see Figure 3) making it necessary to obtain accurate photometry fainter than the Main Sequence Turnoff (MSTO) to confirm/negate spurious detections to

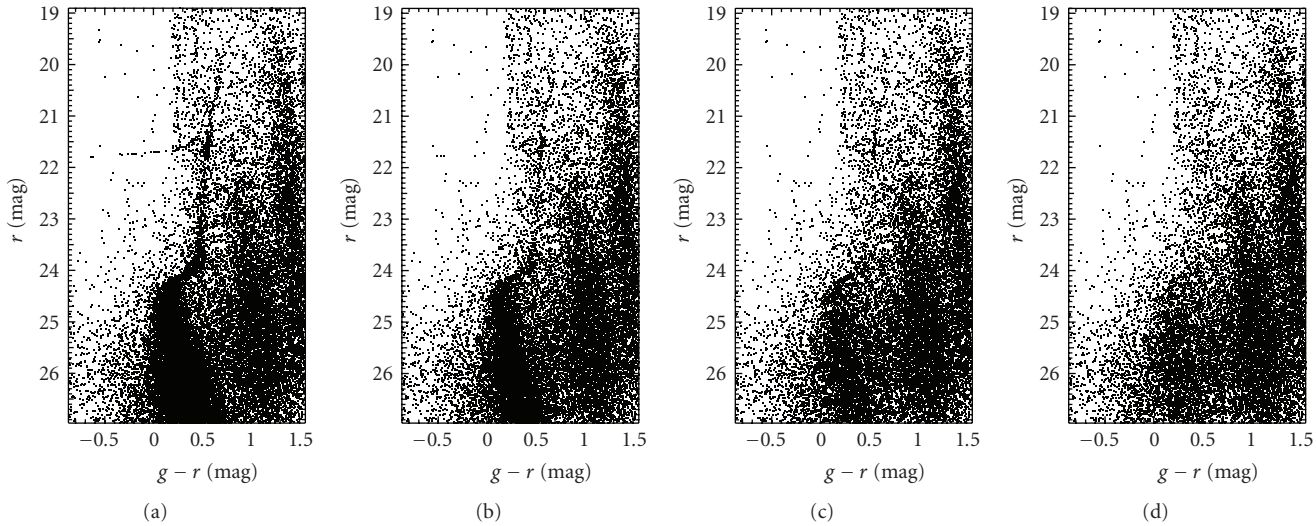

FIGURE 3: A series of four $(g-r, r)$ mock colour-magnitude diagrams of a 10 Gyr old, [Fe/H] $= -2.0$ single burst stellar population (Padua library) at 150 kpc with realistic Galactic foreground (TRILEGAL; [64]), background galaxies (ACS; [65]) and photometric errors as expected from observations at an 8-m class telescope. Each stellar population has its total luminosity decreased by one magnitude from left to right. The top of the main sequence and the MSTO remain the only visible features that reveal the presence of an ultrafaint dwarf.

the highest possible degree. As a point of reference, the MSTO of a 10 Gyr old, [Fe/H] $= -2.0$ stellar population at 150 kpc, is at $r \sim 24.2$ magnitude. Ideally, one aims at 1.0 mag below the MSTO (S/N $\sim$ 10) in both photometric bands to have a sufficiently large number of stars available for deriving a mean age and metallicity of the population from isochrone fitting and to measure the distance modulus. Deep photometry combined with the fact that these stellar systems have a typical half-light angular size of 10–20 arcmin (see Figure 2) demands a large aperture telescope and an CCD camera with a wide field of view. Imagers like IMACS at the 6.5 m Magellan telescope (27×27 sq arcmin FOV) or Suprime-Cam at the 8m Subaru Telescope (34×27 sq arcmin FOV) come immediately to mind.

4.4. Kinematics and Dark Matter Contents. The importance of Milky Way satellites extends far beyond the simple construction of a complete list with spatial coordinates. Stellar velocity measurements over the last 20 years continue to show that the luminous satellites all have central velocity dispersions of the order of 10 km s^{-1} (e.g., Sculptor [67, 68]; Fornax [69]; Carina [70]; Sextans [71]; Ursa Minor [72–74]; Draco [73–75]; Leo II [76]). These results support the picture that those stellar systems are completely governed by dark matter—up to 99.9% of the total mass (e.g., [1–7]). Consequently, each individual satellite represents a prime laboratory to study dark matter physics in great details.

Once a candidate has been confirmed with deep imaging, red-giant candidates in the satellite will be targeted to the faintest possible limit employing multiobject spectrographs such as AAOmega at the AAT and the Michigan/MIKE Fiber Spectrograph on 6.5 m Magellan telescope. Measuring routinely radial velocities of stars ($V \lesssim 20.5$) to 2-3 km s^{-1} precision over the last couple of years enabled not only to measure the systemic velocity of a satellite but also its internal velocity dispersion (dynamical mass) assuming spherical symmetry, dynamic equilibrium, velocity isotropy, and a constant stellar mass-to-light ratio [4, 5, 55, 77, and references therein]. After the SMS Survey completion we hope to have measured these quantities for as many as 30 satellites providing a stringent test for the notion that dwarf satellites have a common total mass of $10^7 \mathcal{M}_\odot$ within the central 300 parsec [7, 70, 78, 79].

In cases where sufficient stellar spectra can be measured across the surface of the dwarf satellite, its projected velocity dispersion profile and the underlying mass density profile can also be derived [39, 50]. These results will allow a statistically robust comparison with the dark matter halo profiles determined from high-resolution N-body simulations to address the core-cusp problem, that observed galactic dark matter haloes show a density profile with a flat core (e.g., [80, 81]) while CDM haloes have divergent density (a cusp) at the centre [82, 83].

As a valuable byproduct of radial velocity measurements the high resolution spectra of the more luminous stars in these dwarf satellites will be very useful for a chemical abundance analysis (e.g., [84–87]). This will enable to test the "galactic building block" hypothesis in which the Milky Way galaxy grew through the merging of smaller dwarf galaxies. Current observations of the four dwarf satellites Sculptor, Sextans, Fornax, and Carina have shown a significantly different chemical composition from stars in the Milky Way halo (e.g., [88, 89]), leading to the suggestion that not the bright, but rather the newly discovered ultrafaint MW satellites are the predicted building blocks (e.g., [90]).

5. Possible Outcomes

A cosmological model is only as good as it is capable of describing what is observed. On galaxy scales these are the internal and external physical properties of dwarf satellite galaxies. From cold dark matter simulations we expect the virialized extent of the Milky Way's halo (radius < 250 kpc), which has an almost spherically symmetric shape [91, 92] to contain hundreds of subhalos following a power-law radial distribution. After the accomplishment of a full analysis of the SDSS, SkyMapper, and Pan-STARRS data, a highly complete census of MW satellites over the entire sky will be available, based on data mining algorithms that reliably pick up $M_V = -5$ dwarfs out to that galactocentric distance. If the number of satellites will be still relatively small and their spatial configuration isotropic, the conclusion would be that they comprise indeed only a subset of the existing low-mass DM halos orbiting the Milky Way [93–97]. The ratio of observed satellites to dark matter subhalo numbers would tell us about the effectiveness of processes such as gas physics, photoionization, and stellar feedback to suppress or evacuate baryons from low mass dark matter halos. First attempts of detailed comparisons between the Milky Way satellite luminosity function down to its faint end and subhalo predictions from ΛCDM simulations have been presented over the last year [98–102]. On the one hand, the MW dwarf satellites would be superb targets to discriminate between competing dark matter particle models including the search for annihilation signals (e.g., [11, 103]) using the upcoming new generation of ground-based Imaging Air Cherenkov Telescopes like MAGIC II and CTA. On the other hand, the reconciliation of CDM theory and observations at that level would prompt the development of innovative techniques to search for the "missing" pure dark CDM substructures in the Milky Way halo (e.g., [104]).

However, if after all the observational effort the sky distribution of any number of genuine satellites is still consistent with a planar or highly anisotropic configuration, the result would be severely at odds with the apparent sphericity of the Milky Way dark matter halo, and even more at odds with an oblate halo having the same orientation as the MW disk. Such a finding would lend strong support to the hypothesis that the majority of MW dwarf satellites have a noncosmological origin and thus lack significant amounts of dark matter. They could have formed from a gas-rich parent satellite on an eccentric near-polar orbit that interacted with the proto-MW [22] or during the dense early stages of the Universe, when the proto-Milky Way and M31 were pulled apart by the general cosmological expansion [105].

In this debate it is interesting to note that the list of the most luminous Milky Way satellites is essentially complete, modulo the possibility of a bright satellite lurking behind the Galactic disk. Accordingly, these "classical" satellites will always show a disk-like arrangement independently of how many low luminous systems will be added to the population in the future. Hence there is a fair chance that the MW dwarf satellites may themselves be divided into two subclasses with different origins. While we look forward in great anticipation to the Stromlo Missing Satellites Survey and similar programs there is no doubt that MW dwarf satellites will play a central role in near-field cosmology for decades to come.

Acknowledgments

The author thanks both referees for their comments that helped to improve the presentation and the quality of this paper. He also acknowledges the financial support from the Go8-DAAD-Australia/Germany Joint Research Co-operation Scheme and from the Access to Major Research Facilities Programme which is a component of the International Science Linkages established under the Australian Government Innovation Statement, Backing Australia's Ability.

References

[1] M. Mateo, "Dwarf galaxies of the Local Group," *Annual Review of Astronomy and Astrophysics*, vol. 36, no. 1, pp. 435–506, 1998.

[2] J. T. Kleyna, M. I. Wilkinson, N. Evans, and G. Gilmore, "Ursa Major: a missing low-mass CDM halo?" *The Astrophysical Journal*, vol. 630, no. 2, pp. L141–L144, 2005.

[3] N. F. Martin, R. A. Ibata, S. C. Chapman, M. Irwin, and G. F. Lewis, "A Keck/DEIMOS spectroscopic survey of faint Galactic satellites: searching for the least massive dwarf galaxies," *Monthly Notices of the Royal Astronomical Society*, vol. 380, no. 1, pp. 281–300, 2007.

[4] J. D. Simon and M. Geha, "The kinematics of the ultra-faint Milky Way satellites: solving the missing satellite problem," *The Astrophysical Journal*, vol. 670, no. 1, pp. 313–331, 2007.

[5] M. G. Walker, M. Mateo, E. W. Olszewski, et al., "Velocity dispersion profiles of seven dwarf spheroidal galaxies," *The Astrophysical Journal*, vol. 667, pp. L53–L56, 2007.

[6] A. Koch, M. I. Wilkinson, J. T. Kleyna, et al., "Stellar kinematics and metallicities in the Leo I dwarf spheroidal galaxy—wide-field implications for galactic evolution," *The Astrophysical Journal*, vol. 657, no. 1, pp. 241–261, 2007.

[7] L. E. Strigari, J. S. Bullock, M. Kaplinghat, et al., "A common mass scale for satellite galaxies of the Milky Way," *Nature*, vol. 454, no. 7208, pp. 1096–1097, 2008.

[8] V. Springel, S. D. M. White, A. Jenkins, et al., "Simulations of the formation, evolution and clustering of galaxies and quasars," *Nature*, vol. 435, no. 7042, pp. 629–636, 2005.

[9] A. Klypin, A. V. Kravtsov, O. Valenzuela, and F. Prada, "Where are the missing galactic satellites?" *The Astrophysical Journal*, vol. 522, no. 1, pp. 82–92, 1999.

[10] B. Moore, S. Ghigna, F. Governato, et al., "Dark matter substructure within galactic halos," *The Astrophysical Journal*, vol. 524, no. 1, pp. L19–L22, 1999.

[11] J. Diemand, M. Kuhlen, and P. Madau, "Dark matter substructure and gamma-ray annihilation in the Milky Way halo," *The Astrophysical Journal*, vol. 657, no. 1, pp. 262–270, 2007.

[12] V. Springel, J. Wang, M. Vogelsberger, et al., "The Aquarius Project: the subhaloes of galactic haloes," *Monthly Notices of the Royal Astronomical Society*, vol. 391, no. 4, pp. 1685–1711, 2008.

[13] J. Diemand, M. Kuhlen, and P. Madau, "Formation and evolution of galaxy dark matter halos and their substructure," *The Astrophysical Journal*, vol. 667, no. 2, pp. 859–877, 2007.

[14] E. D'Onghia and G. Lake, "Cold dark matter's small-scale crisis grows up," *The Astrophysical Journal*, vol. 612, no. 2, pp. 628–632, 2004.

[15] M. White and R. A. C. Croft, "Suppressing linear power on dwarf galaxy halo scales," *The Astrophysical Journal*, vol. 539, no. 2, pp. 497–504, 2000.

[16] D. N. Spergel and P. J. Steinhardt, "Observational evidence for self-interacting cold dark matter," *Physical Review Letters*, vol. 84, no. 17, pp. 3760–3763, 2000.

[17] P. Colin, V. Avila-Reese, and O. Valenzuela, "Substructure and Halo Density Profiles in a Warm Dark Matter Cosmology," *The Astrophysical Journal*, vol. 542, p. 622, 2000.

[18] P. Bode, J. P. Ostriker, and N. Turok, "Halo formation in warm dark matter models," *The Astrophysical Journal*, vol. 556, no. 1, pp. 93–107, 2001.

[19] A. R. Zentner and J. S. Bullock, "Halo substructure and the power spectrum," *The Astrophysical Journal*, vol. 598, no. 1, pp. 49–72, 2003.

[20] M. T. Busha, A. E. Evrard, and F. C. Adams, "The asymptotic form of cosmic structure: small-scale power and accretion history," *The Astrophysical Journal*, vol. 665, no. 1, pp. 1–13, 2007.

[21] J. S. B. Wyithe and A. Loeb, "Suppression of dwarf galaxy formation by cosmic reionization," *Nature*, vol. 441, no. 7091, pp. 322–324, 2006.

[22] P. Kroupa, C. Theis, and C. M. Boily, "The great disk of Milky-Way satellites and cosmological sub-structures," *Astronomy and Astrophysics*, vol. 431, no. 2, pp. 517–521, 2005.

[23] M. Metz, P. Kroupa, and H. Jerjen, "The spatial distribution of the Milky Way and Andromeda satellite galaxies," *Monthly Notices of the Royal Astronomical Society*, vol. 374, no. 3, pp. 1125–1145, 2007.

[24] M. Metz, P. Kroupa, and H. Jerjen, "Discs of satellites: the new dwarf spheroidals," *Monthly Notices of the Royal Astronomical Society*, vol. 394, p. 2223, 2009.

[25] W. E. Kunkel and S. Demers, "The Magellanic Plane," *Royal Greenwich Observatory Bulletins*, vol. 182, p. 241, 1976.

[26] D. Lynden-Bell, "Dwarf galaxies and globular clusters in high velocity hydrogen streams," *Monthly Notices of the Royal Astronomical Society*, vol. 174, pp. 695–710, 1976.

[27] D. Lynden-Bell, "Internal kinematics and dynamics of galaxies," in *Proceedings of the IAU Symposium*, vol. 100, p. 89, D. Reidel, Dordrecht, The Netherlands, 1983.

[28] S. R. Majewski, "The Fornax-Leo-Sculptor stream revisited," *The Astrophysical Journal*, vol. 431, no. 1, pp. L17–L21, 1994.

[29] F. D. A. Hartwick, "The Structure of the Outer Halo of the Galaxy and its Relationship to Nearby Large-Scale Structure," *The Astronomical Journal*, vol. 119, p. 2248, 2000.

[30] X. Kang, S. Mao, L. Gao, and Y. P. Jing, "Are great disks defined by satellite galaxies in Milky-Way type halos rare in ΛCDM?" *Astronomy and Astrophysics*, vol. 437, no. 2, pp. 383–388, 2005.

[31] P. Kroupa, "Dwarf spheroidal satellite galaxies without dark matter," *New Astronomy*, vol. 2, no. 2, pp. 139–164, 1997.

[32] M. G. Coleman, J. T. A. de Jong, N. F. Martin, et al., "The elongated structure of the Hercules dwarf spheroidal galaxy from deep Large Binocular Telescope imaging," *The Astrophysical Journal*, vol. 668, no. 1, pp. L43–L46, 2007.

[33] Y.-S. Li and A. Helmi, "Infall of substructures on to a Milky Way-like dark halo," *Monthly Notices of the Royal Astronomical Society*, vol. 385, no. 3, pp. 1365–1373, 2008.

[34] E. D'Onghia and G. Lake, "Small Dwarf Galaxies within Larger Dwarfs: Why Some Are Luminous while Most Go Dark," *The Astrophysical Journal*, vol. 686, p. L61, 2008.

[35] M. Metz, P. Kroupa, C. Theis, G. Hensler, and H. Jerjen, "Did the Milky Way dwarf satellites enter the halo as a group?" *The Astrophysical Journal*, vol. 697, no. 1, pp. 269–274, 2009.

[36] N. I. Libeskind, C. S. Frenk, S. Cole, A. Jenkins, and J. C. Helly, "How common is the Milky Way—satellite system alignment?" http://arxiv.org/abs/0905.1696.

[37] S. Koposov, V. Belokurov, N. W. Evans, et al., "The luminosity function of the Milky Way satellites," *The Astrophysical Journal*, vol. 686, no. 1, pp. 279–291, 2008.

[38] S. M. Walsh, B. Willman, and H. Jerjen, "The invisibles: a detection algorithm to trace the faintest Milky Way satellites," *Astronomical Journal*, vol. 137, no. 1, pp. 450–469, 2009.

[39] B. Willman, F. Governato, J. J. Dalcanton, D. Reed, and T. Quinn, "The observed and predicted spatial distribution of Milky Way satellite galaxies," *Monthly Notices of the Royal Astronomical Society*, vol. 353, no. 2, pp. 639–646, 2004.

[40] B. Willman, J. J. Dalcanton, D. Martinez-Delgado, et al., "A new Milky Way dwarf galaxy in URSA major," *The Astrophysical Journal*, vol. 626, no. 2, pp. L85–L88, 2005.

[41] B. Willman, M. R. Blanton, A. A. West, et al., "A new Milky Way companion: unusual globular cluster or extreme dwarf satellite?" *Astronomical Journal*, vol. 129, no. 6, pp. 2692–2700, 2005.

[42] D. G. York, J. Adelman, J. E. Anderson Jr., et al., "The sloan digital sky survey: technical summary," *The Astronomical Journal*, vol. 120, p. 1579, 2000.

[43] D. B. Zucker, V. Belokurov, N. W. Evans, et al., "A new Milky Way dwarf satellite in canes venatici," *The Astrophysical Journal*, vol. 643, no. 2, pp. L103–L106, 2006.

[44] D. B. Zucker, V. Belokurov, N. W. Evans, et al., "A curious Milky Way satellite in Ursa Major," *The Astrophysical Journal*, vol. 650, no. 1, pp. L41–L44, 2006.

[45] V. Belokurov, D. B. Zucker, N. W. Evans, et al., "The field of streams: sagittarius and its siblings," *The Astrophysical Journal*, vol. 642, no. 2, pp. L137–L140, 2006.

[46] V. Belokurov, D. B. Zucker, N. W. Evans, et al., "Cats and dogs, hair and a hero: a quintet of new Milky Way companions," *The Astrophysical Journal*, vol. 654, no. 2, pp. 897–906, 2007.

[47] V. Belokurov, M. G. Walker, N. W. Evans, et al., "Leo V: a companion of a companion of the Milky Way galaxy?" *The Astrophysical Journal*, vol. 686, no. 2, pp. L83–L86, 2008.

[48] V. Belokurov, M. G. Walker, N. W. Evans, et al., "The discovery of Segue 2: a prototype of the population of satellites of satellites," *Monthly Notices of the Royal Astronomical Society*, vol. 397, no. 4, pp. 1748–1755, 2009.

[49] T. Sakamoto and T. Hasegawa, "Discovery of a faint old stellar system at 150 kpc," *The Astrophysical Journal*, vol. 653, no. 1, pp. L29–L32, 2006.

[50] S. Walsh, H. Jerjen, and B. Willman, "A Pair of Bootes: A New Milky Way Satellite," *The Astrophysical Journal*, vol. 83, p. L662, 2007.

[51] N. F. Martin, R. A. Ibata, M. Bellazzini, M. J. Irwin, G. F. Lewis, and W. Dehnen, "A dwarf galaxy remnant in Canis Major: the fossil of an in-plane accretion on to the Milky Way," *Monthly Notices of the Royal Astronomical Society*, vol. 348, no. 1, pp. 12–23, 2004.

[52] N. F. Martin, R. A. Ibata, B. C. Conn, G. F. Lewis, M. Bellazzini, and M. J. Irwin, "A radial velocity survey of low Galactic latitude structures: I. Kinematics of the Canis Major dwarf galaxy," *Monthly Notices of the Royal Astronomical Society*, vol. 362, no. 3, pp. 906–914, 2005.

[53] M. Bellazzini, R. Ibata, N. Martin, G. F. Lewis, B. Conn, and M. J. Irwin, "The core of the Canis Major galaxy as traced by red clump stars," *Monthly Notices of the Royal Astronomical Society*, vol. 366, no. 3, pp. 865–883, 2006.

[54] C. Mateu, A. K. Vivas, R. Zinn, L. R. Miller, and C. Abad, "No excess of RR lyrae stars in the Canis Major overdensity," *The Astronomical Journal*, vol. 137, pp. 4412–4423, 2009.

[55] M. Geha, B. Willman, J. D. Simon, et al., "The least luminous galaxy: spectroscopy of the Milky Way satellite segue 1," *The Astrophysical Journal*, vol. 692, pp. 1464–1475, 2009.

[56] M. Niederste-Ostholt, V. Belokurov, N. W. Evans, G. Gilmore, R. F. G. Wyse, and J. E. Norris, "The origin of segue 1," *Monthly Notices of the Royal Astronomical Society*, vol. 398, no. 4, pp. 1771–1781, 2009.

[57] S. C. Keller, B. P. Schmidt, M. S. Bessell, et al., "The SkyMapper telescope and the southern sky survey," *Publications of the Astronomical Society of Australia*, vol. 24, no. 1, pp. 1–12, 2007.

[58] L. Girardi, G. Bertelli, A. Bressan, et al., "Theoretical isochrones in several photometric systems I. Johnson-Cousins-Glass, HST/WFPC2, HST/NICMOS, Washington, and ESO imaging survey filter sets," *Astronomy and Astrophysics*, vol. 391, no. 1, pp. 195–212, 2002.

[59] P. Marigo, L. Girardi, A. Bressan, M. A. T. Groenewegen, L. Silva, and G. L. Granato, "Evolution of asymptotic giant branch stars: II. Optical to far-infrared isochrones with improved TP-AGB models," *Astronomy and Astrophysics*, vol. 482, no. 3, pp. 883–905, 2008.

[60] S. M. Walsh, B. Willman, D. Sand, et al., "Boötes II reBoöted: an MMT/Megacam study of an ultrafaint Milky Way satellite," *The Astrophysical Journal*, vol. 688, no. 1, pp. 245–253, 2008.

[61] S. Koposov, J. T. A. de Jong, V. Belokurov, et al., "The discovery of two extremely low luminosity Milky Way globular clusters," *The Astrophysical Journal*, vol. 669, no. 1, pp. 337–342, 2007.

[62] D. Martínez-Delgado, A. Aparicio, M. A. Gómez-Flechoso, and R. Carrera, "Tidal streams in the galactic halo: evidence for the sagittarius northern stream or traces of a new nearby dwarf galaxy," *The Astrophysical Journal*, vol. 549, no. 2, pp. L199–L202, 2001.

[63] C. J. Grillmair, "Four new stellar debris streams in the galactic halo," *The Astrophysical Journal*, vol. 693, pp. 1118–1127, 2009.

[64] L. Girardi, M. A. T. Groenewegen, E. Hatziminaoglou, and L. da Costa, "Star counts in the galaxy simulating from very deep to very shallow photometric surveys with the TRILEGAL code," *Astronomy and Astrophysics*, vol. 436, no. 3, pp. 895–915, 2005.

[65] D. Harsono and R. De Propris, "The luminosity function of galaxies to $M_{BgVriz} \sim -14$ in $z \sim 0.3$ Clusters," *Astronomical Journal*, vol. 137, no. 2, pp. 3091–3099, 2009.

[66] N. F. Martin, J. T. A. de Jong, and H.-W. Rix, "A comprehensive maximum likelihood analysis of the structural properties of faint Milky Way satellites," *The Astrophysical Journal*, vol. 684, no. 2, pp. 1075–1092, 2008.

[67] M. Aaronson and E. W. Olszewski, "Accurate radial velocities for carbon stars in the Sculptor dwarf spheroidal," *The Astrophysical Journal*, vol. 94, p. 657, 1987.

[68] D. Queloz, P. Dubath, and L. Pasquini, "A kinematic study of the Sculptor dwarf spheroidal galaxy," *Astronomy and Astrophysics*, vol. 300, p. 31, 1995.

[69] M. Mateo, E. Olszewski, D. L. Welch, P. Fischer, and W. Kunkel, "A kinematic study of the fornax dwarf spheroidal galaxy," *Astronomical Journal*, vol. 102, no. 3, pp. 914–926, 1991.

[70] M. Mateo, E. W. Olszewski, C. Pryor, D. L. Welch, and P. Fischer, "The Carina dwarf spheroidal galaxy: how dark is it?" *Astronomical Journal*, vol. 105, no. 2, pp. 510–526, 1993.

[71] N. B. Suntzeff, M. Mateo, D. M. Terndrup, E. W. Olszewski, D. Geisler, and W. Weller, "Spectroscopy of giants in the Sextans dwarf spheroidal galaxy," *The Astrophysical Journal*, vol. 418, no. 1, pp. 208–228, 1993.

[72] J. C. Hargreaves, G. Gilmore, M. J. Irwin, and D. Carter, "A dynamical study of the Ursa-Minor dwarf spheroidal galaxy," *Monthly Notices of the Royal Astronomical Society*, vol. 271, p. 693, 1994.

[73] T. E. Armandroff, E. W. Olszewski, and C. Pryor, "The mass-to-light ratios of the draco and ursa minor dwarf spheroidal galaxies. I. Radial velocities from multifiber spectroscopy," *Astronomical Journal*, vol. 110, no. 5, pp. 2131–2165, 1995.

[74] E. W. Olszewski, M. Aaronson, and J. M. Hill, "Nine seasons of velocity measurements in the Draco and Ursa Minor dwarf spheroidal galaxies with the MMT echelle," *Astronomical Journal*, vol. 110, p. 2120, 1995.

[75] J. C. Hargreaves, G. Gilmore, and J. D. Annan, "The influence of binary stars on dwarf spheroidal galaxy kinematics," *Monthly Notices of the Royal Astronomical Society*, vol. 279, no. 1, pp. 108–120, 1996.

[76] S. S. Vogt, M. Mateo, E. W. Olszewski, and M. J. Keane, "Internal kinematics of the Leo II dwarf spheroidal galaxy," *Astronomical Journal*, vol. 109, no. 1, pp. 151–163, 1995.

[77] M. Mateo, E. W. Olszewski, S. S. Vogt, and M. J. Keane, "The internal kinematics of the Leo I dwarf spheroidal galaxy: dark matter at the fringe of the Milky Way," *Astronomical Journal*, vol. 116, no. 5, pp. 2315–2327, 1998.

[78] G. Gilmore, M. I. Wilkinson, R. F. G. Wyse, et al., "The observed properties of dark matter on small spatial scales," *The Astrophysical Journal*, vol. 663, no. 2, pp. 948–959, 2007.

[79] J. Peñarrubia, A. W. McConnachie, and J. F. Navarro, "The cold dark matter halos of local group dwarf spheroidals," *The Astrophysical Journal*, vol. 672, no. 2, pp. 904–913, 2008.

[80] W. J. G. de Blok, S. S. McGaugh, A. Bosma, and V. C. Rubin, "Mass density profiles of low surface brightness galaxies," *The Astrophysical Journal*, vol. 552, no. 1, pp. L23–L26, 2001.

[81] G. Gentile, A. Burkert, P. Salucci, and U. Klein, "The dwarf galaxy DDO 47 as a dark matter laboratory: testing cusps hiding in triaxial halos," *The Astrophysical Journal*, vol. 634, no. 2, pp. L145–L148, 2005.

[82] J. F. Navarro, C. S. Frenk, and S. D. M. White, "A universal density profile from hierarchical clustering," *The Astrophysical Journal*, vol. 490, no. 2, pp. 493–508, 1997.

[83] J. F. Navarro, E. Hayashi, C. Power, et al., "The inner structure of ΛCDM haloes: III. Universality and asymptotic slopes," *Monthly Notices of the Royal Astronomical Society*, vol. 349, no. 3, pp. 1039–1051, 2004.

[84] A. Koch, E. K. Grebel, R. F. G. Wyse, et al., "Complexity on small scales: the metallicity distribution of the Carina dwarf spheroidal galaxy," *Astronomical Journal*, vol. 131, no. 2, pp. 895–911, 2006.

[85] A. Koch, A. McWilliam, E. K. Grebel, D. B. Zucker, and V. Belokurov, "The highly unusual chemical composition of the hercules dwarf spheroidal galaxy," *The Astrophysical Journal*, vol. 688, pp. L13–L16, 2008.

[86] E. N. Kirby, P. Guhathakurta, and C. Sneden, "Metallicity and alpha-element abundance measurement in red giant stars from medium-resolution spectra," *The Astrophysical Journal*, vol. 682, no. 2, pp. 1217–1233, 2008.

[87] J. E. Norris, G. Gilmore, R. F. G. Wyse, et al., "The abundance spread in the boötes I dwarf spheroidal galaxy," *The Astrophysical Journal*, vol. 689, no. 2, pp. L113–L116, 2008.

[88] A. Helmi, M. J. Irwin, E. Tolstoy, et al., "A new view of the dwarf spheroidal satellites of the Milky Way from VLT flames: where are the very metal-poor stars?" *The Astrophysical Journal*, vol. 651, no. 2, pp. L121–L124, 2006.

[89] W. Aoki, N. Arimoto, K. Sadakane, et al., "Chemical composition of extremely metal-poor stars in the sextans dwarf spheroidal galaxy," *Astronomy & Astrophysics*, vol. 502, no. 2, pp. 569–578, 2009.

[90] E. N. Kirby, J. D. Simon, M. Geha, P. Guhathakurta, and A. Frebel, "Uncovering extremely metal-poor stars in the Milky Way's ultrafaint dwarf spheroidal satellite galaxies," *The Astrophysical Journal*, vol. 685, no. 1, pp. L43–L46, 2008.

[91] R. P. Olling and M. R. Merrifield, "Two measures of the shape of the dark halo of the Milky Way," *Monthly Notices of the Royal Astronomical Society*, vol. 311, no. 2, pp. 361–369, 2000.

[92] S. Kazantzidis, A. V. Kravtsov, A. R. Zentner, B. Allgood, D. Nagai, and B. Moore, "The effect of gas cooling on the shapes of dark matter halos," *The Astrophysical Journal*, vol. 611, no. 2, pp. L73–L76, 2004.

[93] F. Stoehr, S. D. M. White, G. Tormen, and V. Springel, "The satellite population of the Milky Way in a ΛCDM universe," *Monthly Notices of the Royal Astronomical Society*, vol. 335, no. 4, pp. L84–L88, 2002.

[94] E. Hayashi, J. F. Navarro, J. E. Taylor, J. Stadel, and T. Quinn, "The structural evolution of substructure," *The Astrophysical Journal*, vol. 584, no. 2, pp. 541–558, 2003.

[95] J. S. Bullock, A. V. Kravtsov, and D. H. Weinberg, "Reionization and the abundance of galactic satellites," *The Astrophysical Journal*, vol. 539, no. 2, pp. 517–521, 2000.

[96] H. Susa and M. Umemura, "Formation of dwarf galaxies during the cosmic reionization," *The Astrophysical Journal*, vol. 600, no. 1, pp. 1–16, 2004.

[97] A. V. Kravtsov, O. Y. Gnedin, and A. A. Klypin, "The tumultuous lives of galactic dwarfs and the missing satellites problem," *The Astrophysical Journal*, vol. 609, no. 2, pp. 482–497, 2004.

[98] P. Madau, M. Kuhlen, J. Diemand, et al., "Fossil remnants of reionization in the halo of the Milky Way," *The Astrophysical Journal*, vol. 689, no. 1, pp. L41–L44, 2008.

[99] A. V. Macciò, X. Kang, and B. Moore, "Central mass and luminosity of Milky Way satellites in the Λ cold dark matter model," *The Astrophysical Journal*, vol. 692, pp. L109–L112, 2009.

[100] A. V. Macciò, X. Kang, F. Fontanot, R. S. Somerville, S. E. Koposov, and P. Monaco, "On the origin and properties of Ultrafaint Milky Way Satellites in a LCDM Universe," submitted to *Monthly Notices of the Royal Astronomical Society*.

[101] Y.-S. Li, A. Helmi, G. De Lucia, and F. Stoehr, "On the common mass scale of the Milky Way satellites," *Monthly Notices of the Royal Astronomical Society*, vol. 397, p. L87, 2009.

[102] S. E. Koposov, J. Yoo, H.-W. Rix, D. H. Weinberg, A. V. Macciò, and J. M. Escudé, "A quantitative explanation of the observed population of Milky Way satellite galaxies," *The Astrophysical Journal*, vol. 696, pp. 2179–2194, 2009.

[103] T. Bringmann, M. Doro, and M. Fornasa, "Dark matter signals from Draco and Willman 1: prospects for MAGIC II and CTA," *Journal of Cosmology and Astroparticle Physics*, vol. 1, p. 16, 2009.

[104] L. V. E. Koopmans, "Gravitational imaging of cold dark matter substructures," *Monthly Notices of the Royal Astronomical Society*, vol. 363, no. 4, pp. 1136–1144, 2005.

[105] T. Sawa and M. Fujimoto, "A dynamical model for the orbit of the andromeda galaxy M31 and the origin of the local group of galaxies," *Publication of the Astronomical Society of Japan*, vol. 57, no. 3, pp. 429–446, 2005.

Hindawi Publishing Corporation
Advances in Astronomy
Volume 2010, Article ID 478910, 14 pages
doi:10.1155/2010/478910

Review Article

Gravitational Lensing as a Probe of Cold Dark Matter Subhalos

Erik Zackrisson and Teresa Riehm

Department of Astronomy, Oskar Klein Centre for Cosmoparticle Physics, Stockholm University, 10691 Stockholm, Sweden

Correspondence should be addressed to Erik Zackrisson, ez@astro.su.se

Received 30 April 2009; Accepted 10 September 2009

Academic Editor: Regina Schulte-Ladbeck

In the cold dark matter scenario, dark matter halos are assembled hierarchically from smaller subunits. Some of these subunits are disrupted during the merging process, whereas others survive temporarily in the form of subhalos. A long-standing problem with this picture is that the number of subhalos predicted by simulations exceeds the number of luminous dwarf galaxies seen in the vicinity of large galaxies like the Milky Way. Many of the subhalos must therefore have remained dark or very faint. If cold dark matter subhalos are as common as predicted, gravitational lensing may in principle offer a promising route to detection. In this paper, we describe the many ways through which lensing by subhalos can manifest itself, and summarize the results from current efforts to constrain the properties of cold dark matter subhalos using such effects.

1. Introduction: Subhalos and Satellite Galaxies

The cold dark matter (CDM) model is based on the hypothesis that a significant fraction (around 23% [1]) of the energy content of the Universe is made up of nonbaryonic particles, which interact predominantly through gravity and have moved with nonrelativistic velocities since the earliest epochs of structure formation. While this scenario has been very successful in explaining the formation of large-scale structures in the Universe (galaxies, galaxy groups, and galaxy clusters), its predictions on subgalactic scales have not yet been observationally confirmed in any convincing way. On the contrary, there are at least two features of current CDM simulations that appear to be in conflict with empirical data: the existence of high-density cusps in the centres of dark matter halos, and a rich spectrum of substructures within each halo. There is, however, no consensus on how serious these problems really are for the CDM paradigm.

Massive CDM halos are assembled hierarchically from smaller halos. As these subunits fall into the potential well of larger halos, they suffer tidal stripping of material which ends up in the smooth dark matter component of the halo that swallowed them. Since this is a process that may take several billion years to complete, many of these smaller halos temporarily survive in the form of subhalos (also known as halo substructures or subclumps) within the larger halo. According to current simulations, around 10% of the virial mass of a Milky Way-sized CDM halo should be in the form of subhalos at the current epoch [2, 3]. Naively, one might expect dwarf galaxies to form in these low-mass halos prior to merging, which would result in large numbers of satellite galaxies within the CDM halo of each large galaxy. A long-standing problem with this picture is that the number of subhalos predicted by simulations greatly exceeds the number of dwarf galaxies seen in the the vicinity of large galaxies like the Milky Way and Andromeda [4, 5]. This has become known as the "missing satellite problem." A similar lack of dwarf galaxies compared to the number of dark halos predicted is also evident within group-sized dark matter halos [6]. While most studies have focused on the discrepancy between the number of subhalos and observed satellite galaxies, the discrepancy persists in the field population as well. In a sense, the missing satellites are just one aspect of a more general problem—the mismatch between the low-mass end of the dark matter mass function and the luminosity function of dwarf galaxies [7].

A number of potential solutions to the missing satellites problem have been suggested in the literature. These can be sorted into three different categories, depending on how they

propose to answer the question "Do subhalos exist in the numbers predicted by CDM simulations?"

(i) *No*. In the first category, we find modifications of the properties of dark matter that act to reduce the numbers of low-mass halos and subhalos, including warm dark matter [8], self-interacting dark matter [9], fuzzy dark matter [10], and dark matter in the form of superWIMPs [11], but also models of inflation that produce the required cutoff in the primordial density fluctuation spectrum [12].

(ii) *Yes*. Here, we find processes for inhibiting star formation in low-mass halos [13–17] and observational biases that would put the resulting "dark galaxies" [7, 18] outside the reach of current surveys [19–23]. While these mechanisms may be able to solve the missing satellites problem as it was originally defined, solutions of this type imply that a vast population of low-mass CDM subhalos (hosting very faint stellar populations or none at all) should still be awaiting discovery.

(iii) *Yes, but not in our neighbourhood*. The final possibility is that the large halo-to-halo scatter in subhalo mass fraction may have left the Milky Way and Andromeda sitting inside CDM halos with unusually few subhalos compared to the cosmic average [24, 25]. This would imply that large numbers of CDM subhalos (either bright or dark) should be awaiting discovery in the vicinity of more distant galaxies.

Gravitational lensing may play an important role in the quest to determine which of these different solutions is the correct one. If subhalos do exist, lensing can in principle be used to detect even those that are too faint to be observed through other means. If subhalos do not exist, the absence of subhalo-induced lensing effects should be able to tell us so. The goal of this paper is to explain how this can be achieved and to point out some potential pitfalls along the way. The material will be described at a level comprehensible even for beginning PhD students, with focus on the big picture rather than the computational details of lensing.

In Section 2, we review the properties of the CDM subhalo population, as inferred by current N-body simulations. Section 3 outlines the four expected effects of lensing by CDM subhalos—flux ratio anomalies, astrometric effects, small-scale image distortions, and time delay effects—which are then covered in more detail in Sections 4–7. A number of open questions and future prospects are discussed in Section 8.

2. The Properties of Cold Dark Matter Subhalos

N-body simulations indicate that the subhalos within a galaxy-sized CDM halo follow a mass function of the type:

$$\frac{\mathrm{d}N}{\mathrm{d}M_{\mathrm{sub}}} \propto M_{\mathrm{sub}}^{-\alpha}, \tag{1}$$

with $\alpha \approx 1.9$ [2, 26], albeit with nonnegligible halo-to-halo scatter at the high-mass end ($M_{\mathrm{sub}} \gtrsim 5 \times 10^8\, M_\odot$) [2, 25]. Current simulations of entire galaxy-sized dark matter halos can resolve subhalos with masses down to $M_{\mathrm{sub}} \sim 10^5\ M_\odot$, but the mass function may extend all the way down to the cutoff in the density fluctuation power spectrum, which is set by the detailed properties of the CDM particles. For many types of WIMPs (e.g., neutralinos) this cut-off lies at $\sim 10^{-6}\, M_\odot$ [27–32], but other CDM candidates may alter this truncation mass considerably. As an example, axions may allow the existence of halos with masses as low as $10^{-12}\, M_\odot$ [33]), whereas very few halos with masses below $10^4 - 10^7\, M_\odot$ are expected in the case of MeV mass dark matter [34]. The overall mass contained in resolved subhalos (i.e., $M_{\mathrm{sub}} \gtrsim 10^5\, M_\odot$) within a galaxy-sized CDM halo amounts to a subhalo mass fraction around $f_{\mathrm{sub}} \approx 0.1$, and extrapolating the mass function given by (1) towards lower masses does not boost this by much [2].

Since subhalos are more easily disrupted in the central regions of their parent halo, the subhalo population tends to be less centrally concentrated than the smooth CDM component. The spatial distribution of subhalos within r_{200}, the radius at which the density of the halo drops below 200 times the critical density of the Universe, can be described by [35]

$$N(<x) = N(<r_{200})\frac{12x^3}{1+11x^2}, \tag{2}$$

where $x = r/r_{200}$ and N denotes the number of subhalos within a specific radius. It should be noted that this result is based on CDM-only simulations, and that the presence of baryons within the subhalos may make them more resistant to tidal disruption, thereby boosting their number densities in the inner regions of their parent halos [36]. Some simulations of cluster-mass halos have indicated that the spatial distribution of subhalos may be a function of subhalo mass, in the sense that high-mass subhalos would tend to avoid the central regions more than low-mass ones [37, 38], but this has not been confirmed by the latest simulations of galaxy-sized halos [2, 39].

While the term subhalo is typically used to denote clumps located within the virial radius (or, alternatively, r_{200}) of a large CDM halo, there is also a large number of low-mass clumps located just outside this limit [39, 40]. Some of these have previously been bona fide subhalos, and others are bound to venture inside the virial radius in the near future. Such objects can through projection appear close to lines of sight passing through the centres of large galaxies and may therefore be important in certain lensing situations.

The internal structure of subhalos is still a matter of much debate. As low-mass halos are accreted by more massive ones and become subhalos, substantial mass loss occurs, preferentially from their outer regions. The shape of the outer part of the subhalo density profile may therefore be seriously affected by stripping whereas the inner profile is left more or less intact. In many lensing studies, CDM subhalos are considered to be singular isothermal spheres (SIS) or even point masses. This is mainly for simplicity—the lensing properties of such objects are well-known, but neither observations, theory, nor simulations favour models

of this types for the subhalos predicted by CDM (see [41] for references).

An SIS has a density profile given by,

$$\rho_{\rm SIS} = \frac{\sigma_{\rm v}^2}{2\pi G r^2}, \tag{3}$$

where $\sigma_{\rm v}$ is the line-of-sight velocity dispersion. This model has proved to be successful for the massive galaxies responsible for strong lensing (see Section 3.1) on arcsecond scales [42, 43]. The SIS density profile has a steep inner slope ($\rho \propto r^{\beta}$ with $\beta = -2$), which in the case of massive galaxies is believed to be due to the luminous baryons residing in their inner regions. This baryonic component contributes substantially to the overall mass density in the centre, and its formation over cosmological time scales may also have caused the CDM halo itself to contract, thereby steepening the inner slope of its density profile [44–47].

Low-mass CDM halos which never formed many stars are unlikely to have density profiles this steep. Instead, they should resemble the halo density profiles derived from CDM-only simulations. The NFW density profile [48], with an inner slope of $\beta = -1$, has for a number of years served as the standard density profile for CDM halos, and is given by

$$\rho_{\rm NFW}(r) = \frac{\rho_{\rm i}}{(r/r_{\rm S})(1 + r/r_{\rm S})^2}, \tag{4}$$

where $r_{\rm S}$ is the characteristic-scale radius of the halo and $\rho_{\rm i}$ is related to the density of the Universe at the time of collapse. Modifications of this formula are required once halos become subhalos and are tidally stripped. Attempts to quantify the effects of this mass loss on their density profile have been made by Hayashi et al. [49] and Kazantzidis et al. [50].

Controversy remains, however, over whether the NFW profile gives the best representation of CDM halos (and, consequently, of subhalos prior to stripping). Based on recent high-resolution simulations, some have argued for a slightly steeper inner slope ($\beta \approx -1.2$; see [51]) with significant halo-to-halo variations, whereas other have favoured a far shallower inner slope [2, 52–54]. Inner density profiles as steep as that of the SIS model (3) are, however, unanimously ruled out. While the internal structure of subhalos may be relatively unimportant in certain lensing situations, it can be crucial in others [55]. For lensing tests that are sensitive to the exact slope of the inner density profile of subhalos [41], the subhalo-to-subhalo scatter in this quantity may also be a very important.

3. Gravitational Lensing by Cold Dark Matter Subhalos

The majority of methods aiming to probe CDM subhalos through gravitational lensing focus on detecting subhalos outside the Local Group (typically at redshifts $z \approx 0.5$–1.0). Whereas the subhalos sitting within the dark matter halo of the Milky Way will also give rise to lensing, these effects would be very difficult to detect and separate from other phenomena. It has been suggested that CDM subhalos around the Milky Way may be detectable through the gravitational time delay they impose on millisecond pulsars [56, 57], but the time scales and probabilities for such events indicate that this is only viable for the very low-mass end of the subhalo mass function ($M < 1\ M_{\odot}$). In what follows, we will therefore focus on the lensing situations relevant for subhalos at cosmological distances.

3.1. Strong and Weak Lensing. Gravitational lensing effects can be divided into two regimes, strong and weak lensing, depending on the level of image distortions produced. Strong lensing can occur when the surface mass density along a given sightline exceeds a certain (redshift-dependent) critical value and is associated with high magnifications, multiple images, arcs and rings in the lens plane. In practice, strong lensing tends to take place when the line of sight from the observer to source lies very close to the centre of a galaxy or a galaxy cluster, since it is only there that sufficiently high surface mass densities are attained. Weak lensing occurs in regions of subcritical surface mass density—in practice when the lens is located further away from the line of sight—and gives rise to small magnifications and mild image distortions. The two situations are schematically illustrated in Figure 1.

Generally speaking, weak lensing is extremely common in the cosmos (at some level, every single light source is affected) but inconspicuous and can only be detected statistically by studying a large number of lensed light sources. Strong lensing effects, on the other hand, are rare but dramatic, and can readily be spotted in individual sources. All published strategies for detecting CDM subhalos (in the mass range relevant for the missing satellite problem) through lensing belong to the strong lensing category.

3.2. Macrolensing and Millilensing. Strong lensing can be further divided into subcategories, depending on the typical angular separation of the multiple images produced: macrolensing ($\gtrsim$ 0.1 arcseconds), millilensing ($\sim 10^{-3}$ arcseconds), microlensing ($\sim 10^{-6}$ arcseconds), nanolensing ($\sim 10^{-9}$ arcseconds), and so on. When large galaxies ($M \sim 10^{12}\ M_{\odot}$) are responsible for the lensing, the image separation typically falls in the macrolensing range, whereas individual solar-mass stars give image separations in the microlensing regime. Since all objects with resolved multiple images due to gravitational lensing have image separations of $\gtrsim$ 0.1 arcseconds, the term strong lensing is often used synonymously with macrolensing. Lensing by objects of dwarf-galaxy masses ($\sim 10^6 - 10^{10}\ M_{\odot}$), like the CDM subhalos relevant for the missing satellite problem, has been estimated to give rise to millilensing, although the exact image separation depends on the internal structure of such objects. In this paper, we will for simplicity use the term millilensing for *all* lensing effects associated with dwarf-galaxy mass subhalos, regardless of whether multiple images are produced or not. The term mesolensing is sometimes also used to denote this type of lensing (with angular scales intermediate between microlensing and macrolensing), but since this word also has an alternative meaning in the gravitational lensing literature [58], we will avoid it here.

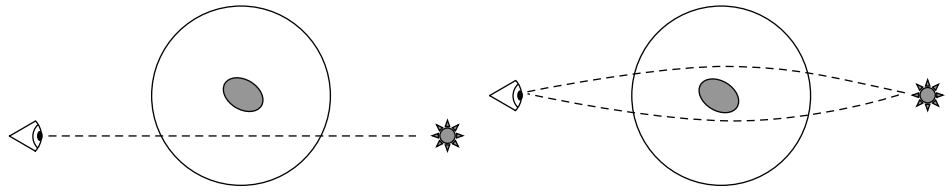

Figure 1: Weak and strong lensing. (a) Weak lensing occurs when the lens (here illustrated by a gray elliptical galaxy, surrounded by a dark matter halo which extends to the outer circle) lies relatively far from the line of sight between the observer (eye) and the background light source (star). In this case, where the sightline misses the central galaxy, only a single image is produced, subject to mild magnification and distortion. The signatures of this are only detectable in a statistical sense, by studying the weak lensing effects on large numbers of background light sources. (b) Strong lensing can occur when the dense central region of the lens galaxy is well-aligned with the line of sight. The light from the background light source may then reach the observer along different paths, corresponding to separate images in the sky. This case is also associated with high magnifications and strong image distortions. The angular deflection in this figure, as in all subsequent ones, has been greatly exaggerated for clarity.

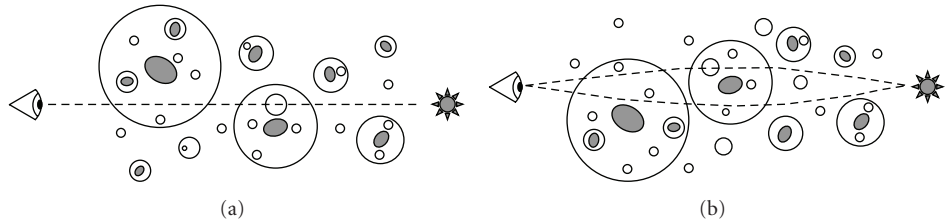

Figure 2: Macrolensed and singly imaged sources. (a) The sightline towards a distant light source passes through many dark matter halos with subhalos, but too far from the dense galaxies in the centres of halos for macrolensing to occur. A subhalo in one of these halos happens to intersect the line of sight, thereby potentially producing millilensing effects in a singly imaged light source. (b) One of the halos happens to lie almost exactly on the line of sight, thereby splitting the background light source into separate macroimages. Furthermore, one of the subhalos in the main lens lies on the sightline towards one of the macroimages, thereby producing millilensing effects in this macroimage.

3.3. Suitable Light Sources. In principle, any distant light source may be affected by subhalos along the line of sight. The situation is schematically illustrated in Figure 2(a). A random line of sight towards a light source outside the local volume passes within the virial radius of numerous galaxy-sized CDM halos [59] and may hence intersect subhalos anywhere along the line of sight. The probability of hitting a subhalo is, however, rather small in this situation, and sightlines of this type may also pass through low-mass field halos (i.e., the progenitors of subhalos) [60–63]. It will therefore be difficult to distinguish between the lensing effects produced by these two types of lenses. While the low-mass end of the field halo population may be very interesting in its own right, lensing by such objects is more often considered an unwanted "background" when attempting to address the missing satellite problem as it is currently defined. It may also be hard to distinguish complicated intrinsic source structure from extrinsic distortions due to lensing (by either subhalos or low-mass field halos) in this case.

Instead, the main targets for attempts to constrain the CDM subhalo population using lensing have so far been sources that are already known to be macrolensed (see Figure 2(b)), which in practice means observing either multiply imaged quasars or galaxies lensed into arcs or Einstein rings. By doing so, one preselects a sightline where one knows that there is a massive dark matter halo (and supposedly subhalos) located along the line of sight. Whether one sees several distinct, point-like images, or elongated arcs that approach the form of an Einstein ring, mainly depends on the source size: point-like sources (quasars in the optical, but potentially also supernovae, gamma-ray bursts, and their afterglows) give distinct images whereas extended sources (galaxies) give rise to arcs and rings (see Figure 3). The strong magnification produced by the macrolens (large foreground galaxy plus dark halo) acts to boost the probability for lensing by the subhalo and typically augments the observable consequences of such secondary lensing. In the case of multiple images, millilensing by subhalos can moreover be distinguished from intrinsic source features, since any structure intrinsic to the source should be imprinted in all macroimages, whereas millilensing effects will be unique to each image. Transient light sources like supernovae or gamma-ray bursts can in principle also be used for this endeavour, but no macrolensed sources of this type have so far been detected.

Lensing by subhalos can give rise to a number of observable effects, which we describe in the following sections: flux ratio anomalies, astrometric effects, small-scale structure in macroimages, and time-delay effects. In what follows, we will

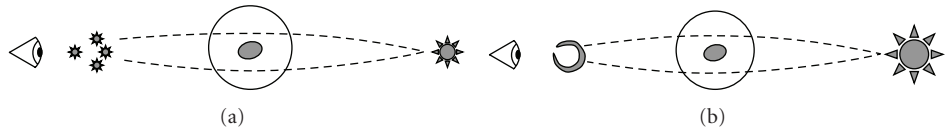

Figure 3: Small and large sources. (a) A galaxy surrounded by a dark matter halo produces multiple images of a small background light source (e.g., an optical quasar). (b) For a larger background source (e.g., a galaxy or a radio-loud quasar), the macroimages may be stretched into arcs or even a complete Einstein ring.

focus on subhalos in the mass range from globular clusters to dwarf galaxies ($\sim 10^5 - 10^{10}\ M_\odot$), since current predictions indicate that subhalos at lower masses may be very difficult to detect through lensing effects.

4. Flux Ratio Anomalies

It was noticed quite early that simple smooth models of galaxy lenses usually fit the image positions of macrolensed systems well, whereas the magnifications of the macroimages are more difficult to explain [64]. To see how this works, a bit of simple lens theory is required.

Specific relations are expected to apply for the magnifications of macroimages close to each other and a critical line. Formally, critical lines are the curves in the lens plane where the magnification tends to infinity. If critical curves are mapped into the source plane, a set of caustic curves is obtained. These separate regions in the source plane that give rise to different numbers of images (see Figure 4). The smooth portions of a caustic curve are called folds, while the points where two folds meet are referred to as cusps. For a background source which is close to either a fold (Figure 4(a)) or a cusp (Figure 4(b)) in the caustic of a smooth lens, two, respectively, three close images will be produced near the critical line in the lens plane. If the source is placed in the center of the caustic, the macroimages will form a cross configuration (Figure 4(c)).

All macroimages can furthermore be described as having either positive parity (meaning that the image has the same orientation as the source) or negative parity (the image is mirror flipped in one dimension relative to the source). When taking the image parity into account and assigning negative magnifications to negative parity images, the sum of the magnifications of the close images should approach zero [65–67]. The following relations should then apply for the flux ratio R of a fold configuration:

$$R_{\text{fold}} = \frac{|\mu_A| - |\mu_B|}{|\mu_A| + |\mu_B|} \longrightarrow 0, \tag{5}$$

when the separation between the close images (A and B in Figure 4(a)) is asymptotically small [68]. Here, μ represents the magnification of a specific image. For the cusp configuration (Figure 4(b)), the corresponding relation is

$$R_{\text{cusp}} = \frac{|\mu_A| - |\mu_B| + |\mu_C|}{|\mu_A| + |\mu_B| + |\mu_C|} \longrightarrow 0. \tag{6}$$

However, most observed lensing systems violate these relations. This has been interpreted as evidence of small-scale structure in the lens on approximately the scale of the image separations between the close images. Magnifications of individual macroimages due to millilensing by subhalos would indeed cause the values for R_{fold} and R_{cusp} to differ from zero fairly independently of the form of the rest of the lens [69–76].

A notable problem with this picture is that both semi-analytical structure formation models and high-resolution ΛCDM simulations seem to be unable to reproduce the observed flux ratio anomalies, since the surface mass density in substructure is lower than that required [45, 77–80].

4.1. Complications: Propagation Effects and Microlensing. Several alternative reasons for the observed flux anomalies have been discussed, such as propagation effects like absorption, scattering, or scintillation in the interstellar medium of the lens [81] and microlensing by stars in the lensing galaxy [82]. Since some sources, like quasars, can exhibit intrinsic flux variations on different timescales, flux ratios may also be difficult to interpret if the time delay between the macroimages (see Section 7) is not well known.

The relevance of propagation effects can be tested by supplementary observations of flux ratios at different wavelengths, since flux losses due to such mechanisms should vary as a function of wavelength. Microlensing by stars can be checked for using long-term monitoring, as this type of lensing is transient and expected to introduce extrinsic variability on the order of months. Millilensing by halo substructure can on the other hand be treated as stationary [70]. Extended sources (e.g., quasars at mid-infrared and radio wavelengths) should also be far less affected by microlensing than small point-like sources (quasars in the optical and at X-ray wavelengths). Even though it is often assumed that radio observations of quasars are essentially microlensing-free, some caution should be applied, since substantial short-term microlensing variability is possible in the special case of a relativistic radio jet oriented close to the line of sight. This phenomenon has been detected in at least one multiply imaged system [83].

Mid-infrared imaging of lenses is attractive since the flux at such wavelengths should be free from differences in extinction among the macroimages, in addition to being free from microlensing by stars due to the extended source size. Such observations can therefore be used to test some of the alternative causes for flux ratio anomalies. Recent studies have used this technique to examine several macrolensed

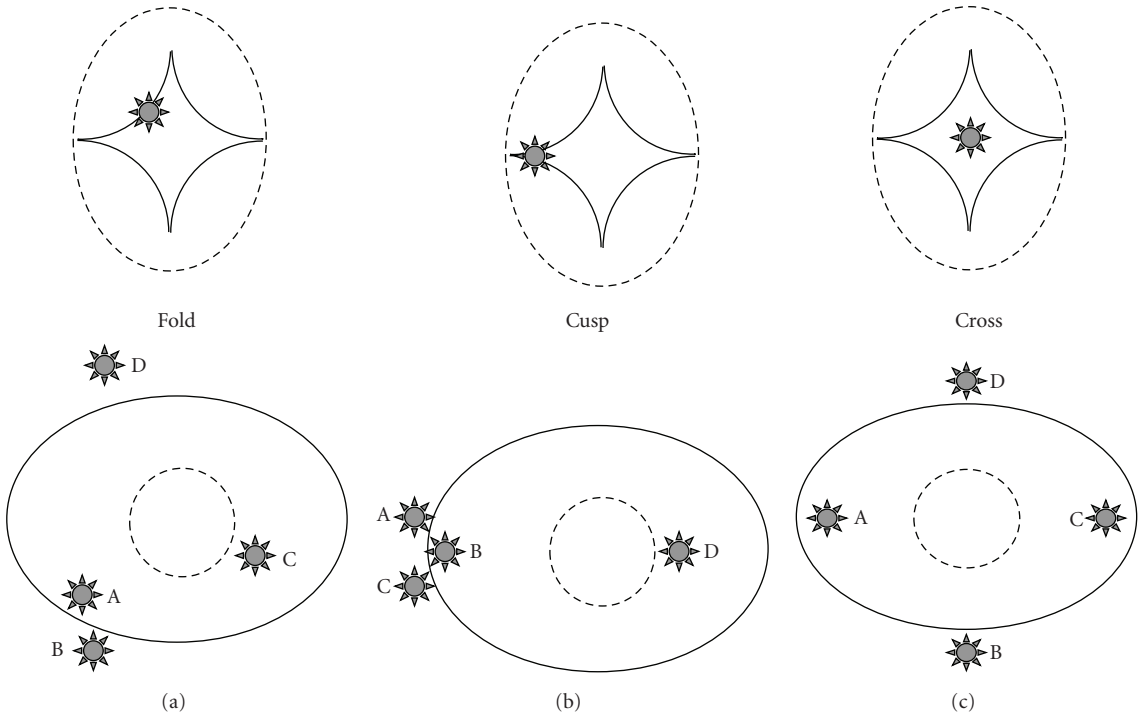

Figure 4: Different configurations of a four-image lens: (a) Fold, (b) Cusp, and (c) Cross. The upper row shows the caustics and position of the source (star) in the source plane. The solid line indicates the inner caustic and the dashed line the outer caustic. A source positioned inside the inner caustic produces five images; A source positioned between the inner and outer caustic produces three images, whereas a source positioned outside the outer caustic will not be multiply imaged. In the case of multiple images, one of the images is usually highly demagnified, so that only four- and two-image lens systems are observed, respectively. The lower row shows the corresponding critical lines and resulting observable images in the lens plane. The inner caustic maps on the outer critical line and vice versa. A close pair (A, B) and a close triplet (A, B, C) are produced in the fold (a) and cusp (b) configurations, respectively.

quasars with known flux ratio anomalies in the optical [84–87]. The mid-infrared flux ratios of about half of these systems can be fitted with smooth lensing models, which means that only the remaining half of these anomalies are due to millilensing by substructures.

There are also other observational features that argue for substructures as the cause of (at least some) flux ratio anomalies. Negative parity images (so-called saddle images, e.g., the middle image (B) of the close triplet in Figure 4(b)) are often fainter than predicted by smooth lens models. This is expected from millilensing, as the magnification perturbations induced by substructure lensing have been shown to depend on image parity [75, 76, 82, 88]. In contrast, such anomalies cannot be attributed to propagation effects since those should statistically affect all types of images similarly, regardless of their parity. Whether the lensing is due to luminous or dark substructures is, however, a different matter.

4.2. Luminous Substructures. Luminous substructures have been identified in many of the lens systems with known flux ratio anomalies. Including such substructures in the lens model tends to greatly improve the fit to observations. One example of such a lens system is the radio-loud quadruple quasar B2045+265 [89] which exhibits one of the most extreme anomalous flux ratios known. Recent deep imaging of this system has revealed the presence of a small satellite galaxy which is believed to cause the flux ratio anomaly [90]. Nearly half of the lenses detected in the Cosmic Lens All-Sky Survey (CLASS) also display luminous satellite galaxies within a few kpc of the primary lensing galaxy [80].

Recently, there have been studies combining the results from simulations and semianalytical models of galaxy formation to investigate if luminous dwarf galaxies might be able to explain the frequency of flux ratio anomalies observed [91, 92]. They find that the fraction of luminous satellites in group-sized halos is roughly consistent with the observational data within a factor of two, while the results for galaxy-sized halos seem too low to explain the frequency of luminous satellites within the observed systems. The lensing effect of these luminous dwarf galaxies is also somewhat unclear since most satellites found in the inner regions of larger galaxies are expected to be "orphan" galaxies stripped of their dark matter halos. To investigate this further, higher-resolution simulations involving a realistic treatment of the gas processes are required. Possible explanations for the discrepancy between the expected and observed fraction of luminous satellites include dwarf galaxies elsewhere along the line of sight mistakenly identified as the lens perturber [62]. Luminous substructures may moreover be more efficient in

producing flux ratio anomalies, since they are likely to be denser than dark substructures due to baryon cooling and condensation [92].

Projection effects are potentially also important for flux ratio anomalies caused by completely dark substructures as one expects a large amount of line-of-sight structure. Although those structures are less effective than substructures within the lens galaxy in inducing magnification perturbations, the overall effect of line-of-sight clumps may be significant [60, 62, 63, 93].

5. Astrometric Effects

In macrolensed systems, the presence of halo substructure may perturb the angular deflection caused by the lens galaxy and thereby the position of macroimages at observable levels, so-called astrometric perturbations (see Figure 5).

This method for detecting subhalos has the advantage of being relatively unaffected by propagation effects (absorption, scattering, or scintillation by the interstellar medium) that may contaminate flux ratio measurements. Since the astrometric perturbation is a steeper function of subhalo mass than flux ratio perturbations, it is mostly sensitive to intermediate and high-mass substructures and therefore probes a distinct part of the subhalo mass function [55, 94]. Stellar microlensing may complicate the interpretation by producing additional shifts of the positions of macroimages [95], but such shifts would be transient and predominantly affect point-like sources.

However, the overall size and probability of subhalo-induced astrometric perturbations are expected to be rather small. Metcalf and Madau [70] used lensing simulations of random realizations of substructure in regions near images and found that it would take substructures with masses $\gtrsim 10^8 M_\odot$ that are very closely aligned with the images to change the image positions by a few tens of milliarcseconds. Such an alignment would be rare in the CDM model. Therefore, they suggest to employ lensed jets of quasars observed at radio wavelengths, as such sources would cover more area on the lens plane. This would increase the probability of having a large subhalo nearby but still allow for pronounced distortions due to the thinness of the jet. Metcalf [96] investigated this technique further and used it to show that the lens system B1152+199 is likely to contain a substructure of mass $\sim 10^5 - 10^7\, M_\odot$.

Further observational evidence for astrometric perturbations from small-scale structure was found in the detailed image structures of B2016+112 [97, 98] and B0123+437 [99]. In the latter system, a substructure of at least $\sim 10^6\, M_\odot$ would be needed in order to reproduce the observed image positions.

The CDM scenario predicts that there are far more low-mass subhalos than high-mass ones (see (1)) and their summed effect could in principle add up to a substantial perturbation. Conversely, since perturbers positioned on opposite sides around the macrolens generate equal but opposite perturbations, the net effect of a large number of substructures may cancel out, ensuring that rare massive substructures dominate the position perturbation of the images. Chen et al. [94] have investigated this by modelling the effects of a wide range of subhalo masses and found that all residual distributions have very large peak perturbations ($\gtrsim 10$ milliarcseconds). Since the simulation models predict extremely few or no substructures in the inner region of the lens, the perturbers must be located further away. Therefore, it was also inferred that position perturbations of different images in any lens configuration may be strongly correlated. Although these results suggested that rare massive clumps may cause larger perturbations than the more abundant smaller clumps, the astrometric perturbations of the images were considerable even in models where no such massive substructures were present. On the other hand, these perturbations are at least partly degenerate with model parameters of the host halo.

Since astrometric perturbations are expected to manifest themselves at (sub-)milliarcsecond levels, high spatial resolution observations are required which so far are mainly achieved by Very Long Baseline Interferometry (VLBI) observations of radio-loud quasars.

However, recent studies have shown that perturbation effects of substructure should also be detectable on larger scales (~ 0.1 arcseconds) and at shorter wavelengths in extended Einstein rings and arcs produced by galaxy-galaxy lensing. Peirani et al. [100] used the perturbative method and lens distributions from toy models as well as cosmological simulations to predict the possible signatures of substructures. They show that when a substructure is positioned near the critical line, not only astrometric but also morphological effects, that is, breaking of the image, will occur which are approximately 10 times larger and should be easier to detect.

Other studies have suggested to use nonparametric source and lens potential reconstructions to probe small perturbations in the lens potential of highly magnified Einstein rings and arcs (e.g., [101, 102]). Vegetti and Koopmans [103] have used an adaptive-grid method and shown that for substructures located on or close to the Einstein ring, perturbations with masses $\gtrsim 10^7\, M_\odot$, respectively, $10^9\, M_\odot$ can be reconstructed. This technique may then be used to constrain the substructure mass fraction and their mass-function slope, once a larger sample of high-resolution lenses becomes available [104].

With the upcoming generation of telescopes—for example, the Large Synoptic Survey Telescope (LSST), the Joint Dark Energy Mission (JDEM), the James Webb Space Telescope (JWST), and the Atacama Large Millimeter Array (ALMA)— a significant increase in the number of macrolensed sources is expected which will allow the use of astrometric perturbations as a probe of the subhalo population.

6. Small-Scale Structure in Macroimages

When dark objects in the dwarf-galaxy mass range intersect the line of sight towards distant quasars, image-splitting, or distortion on characteristic scales of milliarcseconds may occur [105, 106]. As already mentioned, quasars can

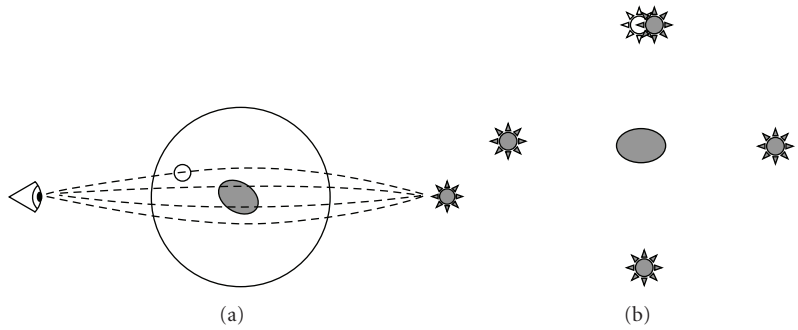

Figure 5: Astrometric perturbations. (a) One of the multiple sightlines towards a distant light source passes through a dark subhalo. (b) The images of the macrolensed source are observed at the positions of the gray source symbols. Modelling of the lens system with a smooth lens potential predicts the position of the upper image at the white source symbol. The subhalo close to the sightline of the image causes a deflection on the order of a few tens of milliarcseconds.

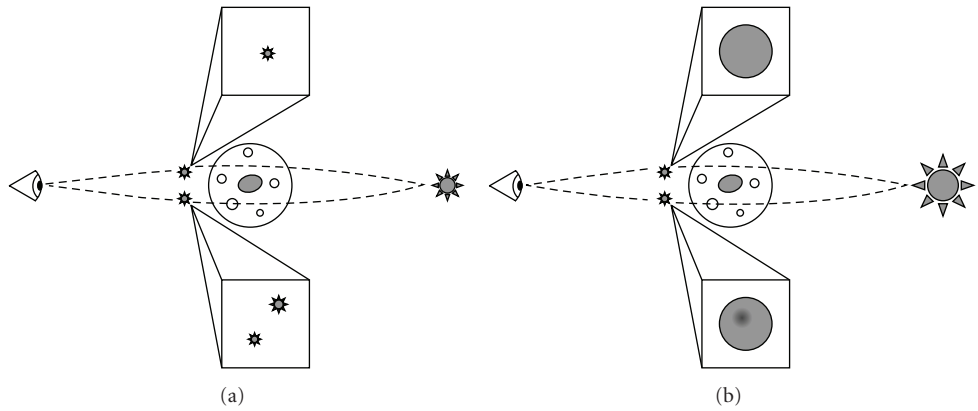

Figure 6: A foreground galaxy with a dark matter halo produces multiple macroimages of a background light source. A subhalo located in the dark halo intercepts one of these macroimages, which may give rise to (a) additional image small-scale splitting of the affected macroimage if the source is sufficiently small, or (b) a mild distortion in the affected macroimage, if the source is large.

currently only be probed on such small scales using VLBI techniques at radio wavelengths, but future telescopes and instruments may allow similar angular resolution at both optical and X-ray wavelengths [41].

Using VLBI, Wilkinson et al. [107] reported no detections of millilensing among 300 compact-radio sources and was able to impose an upper limit of $\Omega < 0.01$ on the cosmological density of point-mass objects (i.e., very compact objects, like black holes) in the $10^6 - 10^8\ M_\odot$ range. However, this does not convert into any strong limits on the subhalo population, since CDM halos and subhalos are not nearly as dense as black holes. Correcting for this would decrease the expected image separations for a millilens of a given mass and yield a probability for lensing that is much lower than assumed in their analysis. The sources used were moreover not macrolensed—this would have made it difficult to make the distinction between subhalos and low-mass field halos as the main culprits even if any signs of millilensing had been detected (see Figure 2(a)).

The effects that a subhalo can have on the internal structure of one of the macroimages in a multiply-imaged quasar (Figure 2(b)) are schematically illustrated in Figure 6. For a small point-like source (e.g., a quasar observed at optical wavelengths), the macroimage may split into several distinct images with small angular separations (Figure 6(a)). A larger source (e.g., a quasar at radio wavelengths) may instead exhibit small-scale image distortions (Figure 6(b)). Even though quasars may display complicated *intrinsic* structure when imaged with high spatial resolution, such effects can at least in principle be separated from the features imprinted by millilensing, since intrinsic structure will be reproduced in all macroimages, whereas millilensing effects are unique to each macroimage. The distinction between these small-scale changes in the morphologies of macroimages, and the astrometric effects discussed in Section 5, becomes somewhat arbitrary in some cases since image distortion may both shift the centroid of an image *and* alter its overall appearance (e.g. through the introduction of new small-scale images). The distortion of macrolensed jets is for instance usually referred to as an astrometric effect.

Yonehara et al. [108] have argued that a significant fraction of all macrolensed optical quasars may exhibit

secondary image splitting on milliarcsecond scales due to CDM subhalos. Inoue and Chiba [109, 110] have explored a similar scenario in the case of the extended images expected for macrolensed quasars at longer wavelengths and concluded that the small-scale macroimage distortions produced by CDM subhalos may be detectable with upcoming radio facilities such as ALMA or the VLBI Space Observatory Programme 2 (VSOP-2).

The merit of probing CDM subhalos through the small-scale structure of macroimages is that, contrary to the case for flux ratio anomalies, there is little risk of confusion due to microlensing by stars or propagation effects in the interstellar medium. Globular clusters may be able to produce similar effects [111], and so may luminous dwarf galaxies (i.e., the subset of CDM subhalos that happen to have experienced substantial star formation), but subhalos are expected to outnumber both of these populations, at least in most mass intervals. Instead, the main problem with this approach seems to be that CDM subhalos may not be sufficiently dense to produce multiple images on scales that can be resolved by current technology. Most studies of these effects have assumed that CDM subhalos can be treated as SIS lenses, resulting in a gross overprediction of the image separations compared to more realistic subhalo models [41]. The angular resolution by which macrolensed quasars can be probed is on the other hand likely to increase substantially in the coming years, in principle reaching ≈ 0.04 milliarcseconds with the VSOP-2 mission (scheduled to launch in 2013).

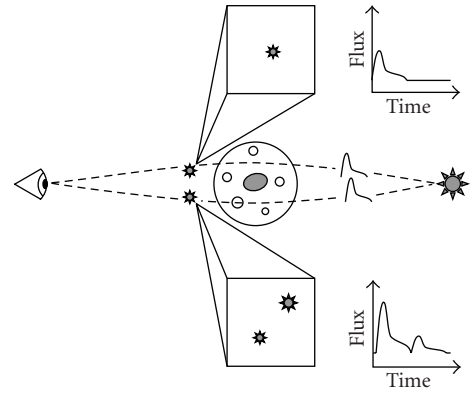

Figure 7: A galaxy with a dark matter halo produces distinct macroimages of a background light source. If this source displays intrinsic variability, observable time delays between the different macroimages may occur. If one of the macroimages experiences further small-scale image splitting due to a subhalo along the line of sight, a light echo may be observable in the affected macroimage. This may serve as a signature of millilensing in cases where the small-scale images blend into one due to insufficient angular resolution of the observations.

7. Time Delay Effects

The images of a macrolensed light source (see Figure 3(a)) are subject to different time delays, which become detectable when the source exhibits intrinsic temporal variability over observable time scales. These time delays stem from a combination of differences in the relativistic time delays (clocks running slower in deep gravitational fields, also known as Shapiro time delays) and the differences in photon path lengths (due to geometric deflection) among the macroimages. Since quasars are both nontransient and known to vary significantly in brightness on time scales of hours and upwards, they are very convenient targets for observing campaigns aiming to measure such time delays. At the current time, around 20 macrolensed quasars have measured time delays (with typical delays of $\Delta t \sim 0.1 - 400$ days; see Oguri [112] for a recent compilation). Time delays of this type have often been used to constrain the Hubble constant and the density profile of the macrolens (i.e., the overall gravitational potential of the lens galaxy and its associated dark halo) but can also potentially be used to probe the CDM subhalos of the lens galaxy.

As shown by Keeton and Moustakas [113], the presence of subhalos within the macrolens will perturb the time delays predicted by smooth lens models and may also violate the predicted arrival-time ordering of the images. Such violations would signal the presence of subhalos in a way that, unlike the case for optical flux ratio anomalies, cannot be mimicked by dust extinction or microlensing by stars. The time delay perturbations due to subhalos are typically on the order of a fraction of a day. By pushing the uncertainties in the observed time delays to this level, strong constraints on CDM subhalo populations may potentially be derived. One case of a time ordering reversal which may possibly be attributed to subhalos has already been identified in the macrolensed quasar RX J1131-1231 [113, 114].

If the subhalos themselves give rise to small-scale image splittings (as described in Section 6), short time lags between the light pulses of the separate small-scale images would be introduced. This imprints echo-like signatures in the overall light curve of astronomical objects with short-term variability (such as gamma-ray bursts and X-ray quasars), even if the small-scale images cannot be spatially resolved. These echos correspond to light signals transported through small-scale images with longer time delays than the leading image, and the flux ratios of the peaks are given by the different magnifications of these images. The light curves of gamma-ray bursts have been used to search for such light echos in the interval $\sim 1 - 60$ seconds, resulting in upper limits ($\Omega < 0.1$) on point-mass dark objects in the $10^5 - 10^9\ M_\odot$ range [115] and even a few candidate detections of repeating flares due to millilensing [116]. However, just like in the case of the search for spatial millilensing effects by Wilkinson et al. [107], current investigations of this kind have little bearing on CDM subhalos, since the probability for subhalo millilensing is too low when the target objects are not macrolensed. Yonehara et al. [108] instead suggested monitoring of macrolensed quasars, predicting that CDM subhalos may produce light echos separated by ~ 1000 seconds, which could potentially be detected in X-rays, where rapid intrinsic flares have been observed. This lensing situation is schematically illustrated in Figure 7.

8. Open Questions and Future Prospects

As we have argued, lensing can in principle be used to probe the CDM subhalo population but has so far not resulted in any strong constraints. Most studies have focused on flux ratio anomalies, but a number of studies now suggest that subhalos by themselves are unable to explain this phenomenon [63, 78–80, 93]. If correct, this would limit the usefulness of this diagnostic, since some other mechanism must also be affecting the flux ratios. Luckily, constraints from other techniques, such as astrometric perturbations, small-scale image distortions, and time delay perturbations may be just around the corner.

Observationally, the future for the study of strong gravitational lensing is looking bright. As of 2009, around 200 macrolensed systems have been detected with galaxies acting as the main lens. Planned observational facilities such as the Square Kilometer Array (SKA) and the LOw Frequency ARray for radio astronomy (LOFAR) at radio wavelengths and JDEM and LSST in the optical have the power to boost this number by orders of magnitude in the coming decade [117]. The spatial resolution by which these systems can be studied is also likely to become significantly better, approaching ~ 10 milliarcseconds in the optical and ~ 0.1 milliarcseconds at radio wavelenghts [41].

On the modelling side, there are still a number of issues that need to be properly addressed before strong constraints on the existence and properties of CDM subhalos can be extracted from such data.

8.1. Input Needed from Subhalo Simulations. The largest N-body simulations of galaxy-sized halos are now able to resolve CDM subhalos with masses down to $\sim 10^5\,M_\odot$, but there are still a number of aspects of the subhalo population that remain poorly quantified and could have a significant impact on its lensing signatures.

(i) What is the halo-to-halo scatter in the subhalo mass function and how does this evolve with redshift?

(ii) What are the density profiles of subhalos? How do they evolve with subhalo mass and subhalo position within the parent halo? How large is the difference from subhalo to subhalo?

(iii) What is the spatial distribution of subhalos as a function of subhalo mass within the parent halo? What is the corresponding distribution outside the virial radius?

(iv) How do baryons affect the properties of subhalos? Can baryons promote the survival of subhalos within the inner regions of their host halos?

The lensing effects discussed in Sections 4–7 are sensitive to the density profiles and mass function of subhalos, albeit to a varying degree [55]. Attempts to quantify the effects of different density profiles on the lensing signature have been made [41, 79, 92, 94, 113], but the models used are still far from realistic, and many of those active in this field still cling to SIS profiles for simplicity.

8.2. The Role of Other Small-Scale Structure. CDM subhalos are not the only objects along the line of sight to high-redshift light sources that are capable of producing millilensing effects. Many large galaxies are known to be surrounded by $10^2 - 10^3$ globular clusters with masses in the $10^5 - 10^6\ M_\odot$ range. While typically less numerous than CDM subhalos in the same mass range, they are concentrated within a smaller volume (the stellar halo) and have more centrally concentrated density profiles, thereby potentially making them more efficient lenses. We also expect a fair share of luminous dwarf galaxies within the dark halos of large galaxies. These dwarfs may well represent the subset of CDM subhalos inside which baryons were able to collapse and form stars, but if so, this means that they may have density profiles significantly more centrally concentrated than their dark siblings. While the role of globular clusters and luminous satellite galaxies has been studied in the case of flux ratio anomalies [71, 92], their effects on many of the other lensing situations discussed in the previous sections have not yet been addressed. Low-mass halos along the line of sight may also affect these lensing signatures, and sometimes appreciably so [62, 63].

Aside from dwarf galaxies and globulars, there may of course be other surprises hiding in the dark halos of galaxies. Intermediate mass ($M \sim 10^2 - 10^4\ M_\odot$) black holes formed either in the very early Universe or as the remnants of population III stars may inhabit the halo region [118–120] and could give rise to millilensing effects [121]. If accretion onto such objects is efficient, the predicted X-ray properties of such black holes already place very strong constraints on their contribution to the dark matter ($\Omega \lesssim 0.005$ [122]), but the more generalized dynamical [123–125] and lensing [115, 126] constraints on other types of dark objects in the star cluster mass range ($\sim 10^2 - 10^5\ M_\odot$) are otherwise rather weak ($\Omega \lesssim 0.1$). Lensing observations originally aimed to constrain the CDM subhalo population may therefore also lead to the detections of completely new types of halo substructure. As telescopes attain better sensitivity and higher angular resolution in the next decade, we can surely look forward to an exciting new era in the study of dark matter halos.

Acknowledgments

The first author acknowledges the support from the Swedish Research Council. The authors are indebted to Robert Cumming for a careful reading of the manuscript and to two anonymous referees for insightful comments.

References

[1] E. Komatsu, J. Dunkley, M. R. Nolta, et al., "Five-year *wilkinson microwave anisotropy probe* observations: cosmological interpretation," *The Astrophysical Journal, Supplement Series*, vol. 180, no. 2, pp. 330–376, 2009.

[2] V. Springel, J. Wang, M. Vogelsberger, et al., "The Aquarius project: the subhaloes of galactic haloes," *Monthly Notices of the Royal Astronomical Society*, vol. 391, no. 4, pp. 1685–1711, 2008.

[3] M. Zemp, J. Diemand, M. Kuhlen, et al., "The graininess of dark matter haloes," *Monthly Notices of the Royal Astronomical Society*, vol. 394, no. 2, pp. 641–659, 2009.

[4] A. Klypin, A. V. Kravtsov, O. Valenzuela, and F. Prada, "Where are the missing galactic satellites?" *The Astrophysical Journal*, vol. 522, no. 1, pp. 82–92, 1999.

[5] B. Moore, S. Ghigna, F. Governato, et al., "Dark matter substructure within galactic halos," *The Astrophysical Journal*, vol. 524, no. 1, pp. L19–L22, 1999.

[6] R. B. Tully, R. S. Somerville, N. Trentham, and M. A. W. Verheijen, "Squelched galaxies and dark halos," *The Astrophysical Journal*, vol. 569, no. 2, pp. 573–581, 2002.

[7] L. Verde, S. P. Oh, and R. Jimenez, "The abundance of dark galaxies," *Monthly Notices of the Royal Astronomical Society*, vol. 336, no. 2, pp. 541–549, 2002.

[8] P. Bode, J. P. Ostriker, and N. Turok, "Halo formation in warm dark matter models," *The Astrophysical Journal*, vol. 556, no. 1, pp. 93–107, 2001.

[9] D. N. Spergel and P. J. Steinhardt, "Observational evidence for self-Interacting cold dark matter," *Physical Review Letters*, vol. 84, no. 17, pp. 3760–3763, 2000.

[10] W. Hu, R. Barkana, and A. Gruzinov, "Fuzzy cold dark matter: the wave properties of ultralight particles," *Physical Review Letters*, vol. 85, no. 6, pp. 1158–1161, 2000.

[11] J. A. R. Cembranos, J. L. Feng, A. Rajaraman, and F. Takayama, "Superweakly interacting massive particle solutions to small scale structure problems," *Physical Review Letters*, vol. 95, no. 18, Article ID 181301, 4 pages, 2005.

[12] M. Kamionkowski and A. R. Liddle, "The dearth of halo dwarf galaxies: is there power on short scales?" *Physical Review Letters*, vol. 84, no. 20, pp. 4525–4528, 2000.

[13] J. S. Bullock, A. V. Kravtsov, and D. H. Weinberg, "Reionization and the abundance of galactic satellites," *The Astrophysical Journal*, vol. 539, no. 2, pp. 517–521, 2000.

[14] R. S. Somerville, "Can photoionization squelching resolve the substructure crisis?" *The Astrophysical Journal*, vol. 572, no. 1, pp. L23–L26, 2002.

[15] A. J. Benson, C. S. Frenk, C. G. Lacey, C. M. Baugh, and S. Cole, "The effects of photoionization on galaxy formation. II. Satellite galaxies in the Local Group," *Monthly Notices of the Royal Astronomical Society*, vol. 333, no. 1, pp. 177–190, 2002.

[16] A. V. Kravtsov, O. Y. Gnedin, and A. A. Klypin, "The tumultuous lives of galactic dwarfs and the missing satellites problem," *The Astrophysical Journal*, vol. 609, no. 2, pp. 482–497, 2004.

[17] B. Moore, J. Diemand, P. Madau, M. Zemp, and J. Stadel, "Globular clusters, satellite galaxies and stellar haloes from early dark matter peaks," *Monthly Notices of the Royal Astronomical Society*, vol. 368, no. 2, pp. 563–570, 2006.

[18] N. Trentham, O. Möller, and E. Ramirez-Ruiz, "Completely dark galaxies: their existence, properties and strategies for finding them," *Monthly Notices of the Royal Astronomical Society*, vol. 322, no. 3, pp. 658–668, 2001.

[19] J. D. Simon and M. Geha, "The kinematics of the ultra-faint Milky Way satellites: solving the missing satellite problem," *The Astrophysical Journal*, vol. 670, no. 1, pp. 313–331, 2007.

[20] E. J. Tollerud, J. S. Bullock, L. E. Strigari, and B. Willman, "Hundreds of Milky Way satellites? Luminosity bias in the satellite luminosity function," *The Astrophysical Journal*, vol. 688, no. 1, pp. 277–289, 2008.

[21] S. M. Walsh, B. Willman, and H. Jerjen, "The invisibles: a detection algorithm to trace the faintest Milky Way satellites," *The Astronomical Journal*, vol. 137, no. 1, pp. 450–469, 2009.

[22] S. E. Koposov, J. Yoo, H.-W. Rix, D. H. Weinberg, A. V. Macciò, and J. Miralda-Escudé, "A quantitative explanation of the observed population of Milky Way satellite galaxies," *The Astronomical Journal*, vol. 696, no. 2, pp. 2179–2194, 2009.

[23] A. V. Macciò, X. Kang, F. Fontanot, R. S. Somerville, S. E. Koposov, and P. Monaco, "Luminosity function and radial distribution of Milky Way Satellites in a LCDM Universe," http://arxiv.org/abs/0903.4681.

[24] T. Ishiyama, T. Fukushige, and J. Makino, "Environmental effect on the subhalo abundance—a solution to the missing dwarf problem," *Publications of the Astronomical Society of Japan*, vol. 60, no. 4, pp. L13–L18, 2008.

[25] T. Ishiyama, T. Fukushige, and J. Makino, "Variation of the subhalo abundance in dark matter halos," *The Astrophysical Journal*, vol. 696, no. 2, pp. 2115–2125, 2009.

[26] L. Gao, S. D. M. White, A. Jenkins, F. Stoehr, and V. Springel, "The subhalo populations of ΛCDM dark haloes," *Monthly Notices of the Royal Astronomical Society*, vol. 355, no. 3, pp. 819–834, 2004.

[27] A. M. Green, S. Hofmann, and D. J. Schwarz, "The first WIMPy halos," *Journal of Cosmology and Astroparticle Physics*, vol. 8, article 3, 2005.

[28] A. Loeb and M. Zaldarriaga, "Small-scale power spectrum of cold dark matter," *Physical Review D*, vol. 71, no. 10, Article ID 103520, 7 pages, 2005.

[29] J. Diemand, B. Moore, and J. Stadel, "Earth-mass dark-matter haloes as the first structures in the early Universe," *Nature*, vol. 433, no. 7024, pp. 389–391, 2005.

[30] S. Profumo, K. Sigurdson, and M. Kamionkowski, "What mass are the smallest protohalos?" *Physical Review Letters*, vol. 97, no. 3, Article ID 031301, 2006.

[31] V. Berezinsky, V. Dokuchaev, and Y. Eroshenko, "Remnants of dark matter clumps," *Physical Review D*, vol. 77, no. 8, Article ID 083519, 2008.

[32] T. Bringmann, "Particle models and the small-scale structure of dark matter," *New Journal of Physics*, vol. 11, no. 10, Article ID 105027, 18 pages, 2009.

[33] C. J. Hogan and M. J. Rees, "Axion miniclusters," *Physics Letters B*, vol. 205, no. 2-3, pp. 228–230, 1988.

[34] D. Hooper, M. Kaplinghat, L. E. Strigari, and K. M. Zurek, "MeV dark matter and small scale structure," *Physical Review D*, vol. 76, no. 10, Article ID 103515, 2007.

[35] P. Madau, J. Diemand, and M. Kuhlen, "Dark matter subhalos and the dwarf satellites of the Milky Way," *The Astrophysical Journal*, vol. 679, no. 2, pp. 1260–1271, 2008.

[36] D. H. Weinberg, S. Colombi, R. Davé, and N. Katz, "Baryon dynamics, dark matter substructure, and galaxies," *The Astrophysical Journal*, vol. 678, no. 1, pp. 6–21, 2008.

[37] S. Ghigna, B. Moore, F. Governato, G. Lake, T. Quinn, and J. Stadel, "Density profiles and substructure of dark matter halos: converging results at ultra-high numerical resolution," *The Astrophysical Journal*, vol. 544, no. 2, pp. 616–628, 2000.

[38] G. de Lucia, G. Kauffmann, V. Springel, et al., "Substructures in cold dark matter haloes," *Monthly Notices of the Royal Astronomical Society*, vol. 348, no. 1, pp. 333–344, 2004.

[39] A. D. Ludlow, J. F. Navarro, V. Springel, A. Jenkins, C. S. Frenk, and A. Helmi, "The unorthodox orbits of substructure halos ," *The Astrophysical Journal*, vol. 692, no. 1, pp. 931–941, 2009.

[40] J. Diemand, M. Kuhlen, and P. Madau, "Formation and evolution of galaxy dark matter halos and their substructure," *The Astrophysical Journal*, vol. 667, no. 2, pp. 859–877, 2007.

[41] E. Zackrisson, T. Riehm, O. Möller, K. Wiik, and P. Nurmi, "Strong lensing by subhalos in the dwarf galaxy mass range. I. Image separations," *The Astrophysical Journal*, vol. 684, no. 2, pp. 804–810, 2008.

[42] D. Rusin, C. S. Kochanek, and C. R. Keeton, "Self-similar models for the mass profiles of early-type lens galaxies," *The Astrophysical Journal*, vol. 595, no. 1, pp. 29–42, 2003.

[43] L. V. E. Koopmans, T. Treu, A. S. Bolton, S. Burles, and L. A. Moustakas, "The Sloan Lens ACS survey. III. The structure and formation of early-type galaxies and their evolution since $z \approx 1$," *The Astrophysical Journal*, vol. 649, no. 2, pp. 599–615, 2006.

[44] O. Y. Gnedin, A. V. Kravtsov, A. A. Klypin, and D. Nagai, "Response of dark matter halos to condensation of baryons: cosmological simulations and improved adiabatic contraction model," *The Astrophysical Journal*, vol. 616, no. 1, pp. 16–26, 2004.

[45] A. V. Macciò, B. Moore, J. Stadel, and J. Diemand, "Radial distribution and strong lensing statistics of satellite galaxies and substructure using high-resolution ΛCDM hydrodynamical simulations," *Monthly Notices of the Royal Astronomical Society*, vol. 366, no. 4, pp. 1529–1538, 2006.

[46] M. Gustafsson, M. Fairbairn, and J. Sommer-Larsen, "Baryonic pinching of galactic dark matter halos," *Physical Review D*, vol. 74, no. 12, Article ID 123522, 2006.

[47] M. Kampakoglou, "An improved model for contraction of dark matter haloes in response to condensation of baryons," *Monthly Notices of the Royal Astronomical Society*, vol. 369, no. 4, pp. 1988–1994, 2006.

[48] J. F. Navarro, C. S. Frenk, and S. D. M. White, "The structure of cold dark matter halos," *The Astrophysical Journal*, vol. 462, no. 2, pp. 563–575, 1996.

[49] E. Hayashi, J. F. Navarro, J. E. Taylor, J. Stadel, and T. Quinn, "The structural evolution of substructure," *The Astrophysical Journal*, vol. 584, no. 2, pp. 541–558, 2003.

[50] S. Kazantzidis, L. Mayer, C. Mastropietro, J. Diemand, J. Stadel, and B. Moore, "Density profiles of cold dark matter substructure: implications for the missing-satellites problem," *The Astrophysical Journal*, vol. 608, no. 2, pp. 663–679, 2004.

[51] J. Diemand, M. Kuhlen, P. Madau, et al., "Clumps and streams in the local dark matter distribution," *Nature*, vol. 454, no. 7205, pp. 735–738, 2008.

[52] J. F. Navarro, E. Hayashi, C. Power, et al., "The inner structure of ΛCDM haloes. III. Universality and asymptotic slopes," *Monthly Notices of the Royal Astronomical Society*, vol. 349, no. 3, pp. 1039–1051, 2004.

[53] J. Stadel, D. Potter, B. Moore, et al., "Quantifying the heart of darkness with GHALO—a multibillion particle simulation of a galactic halo," *Monthly Notices of the Royal Astronomical Society*, vol. 398, no. 1, pp. L21–L25, 2008.

[54] J. F. Navarro, A. Ludlow, V. Springel, et al., "The diversity and similarity of simulated cold dark matter halos," http://arxiv.org/abs/0810.1522.

[55] L. A. Moustakas, K. Abazajian, A. Benson, et al., "Strong gravitational lensing probes of the particle nature of dark matter," Astro2010: The Astronomy & Astrophysics Decadal Survey, Science White Papers, no. 214, http://arxiv.org/abs/0902.3219.

[56] E. R. Siegel, M. P. Hertzberg, and J. N. Fry, "Probing dark matter substructure with pulsar timing," *Monthly Notices of the Royal Astronomical Society*, vol. 382, no. 2, pp. 879–885, 2007.

[57] E. R. Siegel, "What millisecond pulsars can tell us about matter in the galaxy," http://arxiv.org/abs/0801.3458.

[58] R. Di Stefano, "Mesolensing: high-probability lensing without large optical depth," *The Astrophysical Journal*, vol. 684, no. 1, pp. 46–58, 2008.

[59] E. Zackrisson and T. Riehm, "High-redshift microlensing and the spatial distribution of dark matter in the form of MACHOs," *Astronomy & Astrophysics*, vol. 475, no. 2, pp. 453–465, 2007.

[60] J. Chen, A. V. Kravtsov, and C. R. Keeton, "Lensing optical depths for substructure and isolated dark matter halos," *The Astrophysical Journal*, vol. 592, no. 1, pp. 24–31, 2003.

[61] R. B. Metcalf, "Testing ΛCDM with gravitational lensing constraints on small-scale structure," *The Astrophysical Journal*, vol. 622, no. 1, pp. 72–80, 2005.

[62] R. B. Metcalf, "The importance of intergalactic structure to gravitationally lensed quasars," *The Astrophysical Journal*, vol. 629, no. 2, pp. 673–679, 2005.

[63] M. Miranda and A. V. Macciò, "Constraining warm dark matter using QSO gravitational lensing," *Monthly Notices of the Royal Astronomical Society*, vol. 382, no. 3, pp. 1225–1232, 2007.

[64] C. S. Kochanek, "The implications of lenses for galaxy structure," *The Astrophysical Journal*, vol. 373, no. 2, pp. 354–368, 1991.

[65] S. Mao, "Gravitational microlensing by a single star plus external shear," *The Astrophysical Journal*, vol. 389, no. 1, pp. 63–67, 1992.

[66] P. Schneider and A. Weiss, "The gravitational lens equation near cusps," *Astronomy & Astrophysics*, vol. 260, no. 1-2, pp. 1–13, 1992.

[67] A. F. Zakharov, "On the magnification of gravitational lens images near cusps," *Astronomy & Astrophysics*, vol. 293, no. 1, pp. 1–4, 1995.

[68] R. Blandford and R. Narayan, "Fermat's principle, caustics, and the classification of gravitational lens images," *The Astrophysical Journal*, vol. 310, pp. 568–582, 1986.

[69] S. Mao and P. Schneider, "Evidence for substructure in lens galaxies?" *Monthly Notices of the Royal Astronomical Society*, vol. 295, no. 3, pp. 587–594, 1998.

[70] R. B. Metcalf and P. Madau, "Compound gravitational lensing as a probe of dark matter substructure within galaxy halos," *The Astrophysical Journal*, vol. 563, no. 1, pp. 9–20, 2001.

[71] M. Chiba, "Probing dark matter substructure in lens galaxies," *The Astrophysical Journal*, vol. 565, no. 1, pp. 17–23, 2002.

[72] N. Dalal and C. S. Kochanek, "Direct detection of cold dark matter substructure," *The Astrophysical Journal*, vol. 572, no. 1, pp. 25–33, 2002.

[73] R. B. Metcalf and H. Zhao, "Flux ratios as a probe of dark substructures in quadruple-image gravitational lenses," *The Astrophysical Journal*, vol. 567, no. 1, pp. L5–L8, 2002.

[74] C. R. Keeton, B. S. Gaudi, and A. O. Petters, "Identifying lenses with small-scale structure. I. Cusp lenses," *The Astrophysical Journal*, vol. 598, no. 1, pp. 138–161, 2003.

[75] C. S. Kochanek and N. Dalal, "Tests for substructure in gravitational lenses," *The Astrophysical Journal*, vol. 610, no. 1, pp. 69–79, 2004.

[76] M. Bradač, P. Schneider, M. Lombardi, M. Steinmetz, L. V. E. Koopmans, and J. F. Navarro, "The signature of substructure on gravitational lensing in the ΛCDM cosmological model," *Astronomy & Astrophysics*, vol. 423, no. 3, pp. 797–809, 2004.

[77] A. R. Zentner and J. S. Bullock, "Halo substructure and the power spectrum," *The Astrophysical Journal*, vol. 598, no. 1, pp. 49–72, 2003.

[78] A. Amara, R. B. Metcalf, T. J. Cox, and J. P. Ostriker, "Simulations of strong gravitational lensing with substructure," *Monthly Notices of the Royal Astronomical Society*, vol. 367, no. 4, pp. 1367–1378, 2006.

[79] A. V. Macciò and M. Miranda, "The effect of low-mass substructures on the cusp lensing relation," *Monthly Notices of the Royal Astronomical Society*, vol. 368, no. 2, pp. 599–608, 2006.

[80] D. D. Xu, S. Mao, J. Wang, et al., "Effects of dark matter substructures on gravitational lensing: results from the Aquarius simulations," *Monthly Notices of the Royal Astronomical Society*, vol. 398, no. 3, pp. 1235–1253, 2009.

[81] R. Mittal, R. Porcas, and O. Wucknitz, "Free-free absorption in the gravitational lens JVAS B0218+357," *Astronomy & Astrophysics*, vol. 465, no. 2, pp. 405–415, 2007.

[82] P. L. Schechter and J. Wambsganss, "Quasar microlensing at high magnification and the role of dark matter: enhanced fluctuations and suppressed saddle points," *The Astrophysical Journal*, vol. 580, no. 2, pp. 685–695, 2002.

[83] L. V. E. Koopmans and A. G. de Bruyn, "Microlensing of multiply-imaged compact radio sources: evidence for compact halo objects in the disk galaxy of B1600 + 434," *Astronomy & Astrophysics*, vol. 358, no. 3, pp. 793–811, 2000.

[84] M. Chiba, T. Minezaki, N. Kashikawa, H. Kataza, and K. T. Inoue, "Subaru mid-infrared imaging of the quadruple lenses PG 1115 + 080 and B1422 + 231: limits on substructure lensing," *The Astrophysical Journal*, vol. 627, no. 1, pp. 53–61, 2005.

[85] H. Sugai, A. Kawai, A. Shimono, et al., "Integral field spectroscopy of the quadruply lensed quasar 1RXS J1131-1231: new light on lens substructures," *The Astrophysical Journal*, vol. 660, no. 2, pp. 1016–1022, 2007.

[86] T. Minezaki, M. Chiba, N. Kashikawa, K. T. Inoue, and H. Kataza, "Subaru mid-infrared imaging of the quadruple lenses. II. unveiling lens structure of MG0414 + 0534 and Q2237 + 030," *The Astrophysical Journal*, vol. 697, no. 1, pp. 610–618, 2009.

[87] C. L. MacLeod, C. S. Kochanek, and E. Agol, "Detection of a companion lens galaxy using the mid-infrared flux ratios of the gravitationally lensed quasar H1413 + 117," *The Astrophysical Journal*, vol. 699, no. 2, pp. 1578–1583, 2009.

[88] J. Chen, "Parity dependence in strong lens systems as a probe of dark matter substructure," *Astronomy & Astrophysics*, vol. 498, no. 1, pp. 49–60, 2009.

[89] C. D. Fassnacht, R. D. Blandford, J. G. Cohen, et al., "B2045 + 265: a new four-image gravitational lens from class," *The Astronomical Journal*, vol. 117, no. 2, pp. 658–670, 1999.

[90] J. P. McKean, L. V. E. Koopmans, C. E. Flack, et al., "High-resolution imaging of the anomalous flux ratio gravitational lens system CLASS B2045 + 265: dark or luminous satellites?" *Monthly Notices of the Royal Astronomical Society*, vol. 378, no. 1, pp. 109–118, 2007.

[91] S. E. Bryan, S. Mao, and S. T. Kay, "Luminous satellite galaxies in gravitational lenses," *Monthly Notices of the Royal Astronomical Society*, vol. 391, no. 2, pp. 959–966, 2008.

[92] E. M. Shin and N. W. Evans, "The effect of satellite galaxies on gravitational lensing flux ratios," *Monthly Notices of the Royal Astronomical Society*, vol. 385, no. 4, pp. 2107–2116, 2008.

[93] S. Mao, Y. Jing, J. P. Ostriker, and J. Weller, "Anomalous flux ratios in gravitational lenses: for or against cold dark matter?" *The Astrophysical Journal*, vol. 604, no. 1, pp. L5–L8, 2004.

[94] J. Chen, E. Rozo, N. Dalal, and J. E. Taylor, "Astrometric perturbations in substructure lensing," *The Astrophysical Journal*, vol. 659, no. 1, pp. 52–68, 2007.

[95] L. L. R. Williams and P. Saha, "Improper Motions in Lensed QSOs," *The Astronomical Journal*, vol. 110, p. 1471, 1995.

[96] R. B. Metcalf, "The detection of pure dark matter objects with bent multiply imaged radio jets," *The Astrophysical Journal*, vol. 580, no. 2, pp. 696–704, 2002.

[97] L. V. E. Koopmans, M. A. Garrett, R. D. Blandford, C. R. Lawrence, A. R. Patnaik, and R. W. Porcas, "2016 + 112: a gravitationally lensed type II quasar," *Monthly Notices of the Royal Astronomical Society*, vol. 334, no. 1, pp. 39–47, 2002.

[98] A. More, J. P. McKean, S. More, R. W. Porcas, L. V. E. Koopmans, and M. A. Garrett, "The role of luminous substructure in the gravitational lens system MG 2016 + 112," *Monthly Notices of the Royal Astronomical Society*, vol. 394, no. 1, pp. 174–190, 2009.

[99] A. D. Biggs, I. W. A. Browne, N. J. Jackson, et al., "Radio, optical and infrared observations of CLASS B0128 + 437," *Monthly Notices of the Royal Astronomical Society*, vol. 350, no. 3, pp. 949–961, 2004.

[100] S. Peirani, C. Alard, C. Pichon, R. Gavazzi, and D. Aubert, "Numerical investigation of lens models with substructures using the perturbative method," *Monthly Notices of the Royal Astronomical Society*, vol. 390, no. 3, pp. 945–957, 2008.

[101] R. Blandford, G. Surpi, and T. Kundić, "Modeling galaxy lenses," in *Gravitational Lensing: Recent Progress and Future Goals*, G. Tereasa, Brainerd, and C. S. Kochanek, Eds., vol. 237 of *ASP Conference Proceedings*, p. 65, Astronomical Society of the Pacific, 2001.

[102] L. V. E. Koopmans, "Gravitational imaging of cold dark matter substructures," *Monthly Notices of the Royal Astronomical Society*, vol. 363, no. 4, pp. 1136–1144, 2005.

[103] S. Vegetti and L. V. E. Koopmans, "Bayesian strong gravitational-lens modelling on adaptive grids: objective detection of mass substructure in Galaxies," *Monthly Notices of the Royal Astronomical Society*, vol. 392, no. 3, pp. 945–963, 2009.

[104] S. Vegetti and L. V. E. Koopmans, "Statistics of mass substructure from strong gravitational lensing: quantifying the mass fraction and mass function," *Monthly Notices of the Royal Astronomical Society*. In press.

[105] A. Kassiola, I. Kovner, and R. D. Blandford, "Bounds on intergalactic compact objects from observations of compact radio sources," *The Astrophysical Journal*, vol. 381, no. 1, pp. 6–13, 1991.

[106] J. Wambsganss and B. Paczyński, "A direct gravitational lensing test for $10^6 M_\odot$ black holes in halos of galaxies," *The Astrophysical Journal*, vol. 397, no. 1, pp. L1–L4, 1992.

[107] P. N. Wilkinson, D. R. Henstock, I. W. A. Browne, et al., "Limits on the cosmological abundance of supermassive compact objects from a search for multiple imaging in compact radio sources," *Physical Review Letters*, vol. 86, no. 4, pp. 584–587, 2001.

[108] A. Yonehara, M. Umemura, and H. Susa, "Quasar mesolensing—direct probe to substructures around galaxies," *Publications of the Astronomical Society of Japan*, vol. 55, no. 6, pp. 1059–1078, 2003.

[109] K. T. Inoue and M. Chiba, "Three-dimensional mapping of CDM substructure at submillimeter wavelengths," *The Astrophysical Journal*, vol. 633, no. 1, pp. 23–28, 2005.

[110] K. T. Inoue and M. Chiba, "Extended source effects in substructure lensing," *The Astrophysical Journal*, vol. 634, no. 1, pp. 77–89, 2005.

[111] Yu. V. Baryshev and Yu. L. Ezova, "Gravitational mesolensing by king objects and quasar-galaxy associations," *Astronomy Reports*, vol. 41, no. 4, pp. 436–446, 1997.

[112] M. Oguri, "Gravitational lens time delays: a statistical assessment of lens model dependences and implications for the global hubble constant," *The Astrophysical Journal*, vol. 660, no. 1, pp. 1–15, 2007.

[113] C. R. Keeton and L. A. Moustakas, "A new channel for detecting dark matter substructure in galaxies: gravitational lens time delays," *The Astrophysical Journal*, vol. 699, no. 2, pp. 1720–1731, 2009.

[114] N. D. Morgan, C. S. Kochanek, E. E. Falco, and X. Dai, "Time-delay measurement for the quadruple lens RX J1131-1231," http://arxiv.org/abs/astro-ph/0605321.

[115] R. J. Nemiroff, G. F. Marani, J. P. Norris, and J. T. Bonnell, "Limits on the cosmological abundance of supermassive compact objects from a millilensing search in gamma-ray burst data," *Physical Review Letters*, vol. 86, no. 4, pp. 580–583, 2001.

[116] O. S. Ougolnikov, "A search for possible mesolensing of cosmic gamma-ray bursts. II. Double and triple bursts in the BATSE catalog," *Cosmic Research*, vol. 41, no. 2, pp. 141–146, 2003.

[117] L. V. E. Koopmans, M. Auger, M. Barnabe, et al., "Strong gravitational lensing as a probe of gravity, dark-matter and super-massive black holes," Astro2010: The Astronomy and Astrophysics Decadal Survey, Science White Papers, no. 159, http://arxiv.org/abs/0902.3186.

[118] R. P. van der Marel, "Intermediate-mass black holes in the Universe: a review of formation theories and observational constraints," in *Coevolution of Black Holes and Galaxies*, L. C. Ho, Ed., p. 37, Cambridge University Press, London, UK, 2004.

[119] H. Zhao and J. Silk, "Dark minihalos with intermediate mass black holes," *Physical Review Letters*, vol. 95, no. 1, Article ID 011301, 4 pages, 2005.

[120] T. Kawaguchi, M. Kawasaki, T. Takayama, M. Yamaguchi, and J. Yokoyama, "Formation of intermediate-mass black holes as primordial black holes in the inflationary cosmology with running spectral index," *Monthly Notices of the Royal Astronomical Society*, vol. 388, no. 3, pp. 1426–1432, 2008.

[121] K. T. Inoue and M. Chiba, "Direct mapping of massive compact objects in extragalactic dark halos," *The Astrophysical Journal*, vol. 591, no. 2, pp. L83–L86, 2003.

[122] M. Mapelli, A. Ferrara, and N. Rea, "Constraints on Galactic intermediate mass black holes," *Monthly Notices of the Royal Astronomical Society*, vol. 368, no. 3, pp. 1340–1350, 2006.

[123] B. J. Carr and M. Sakellariadou, "Dynamical constraints on dark matter in compact objects," *The Astrophysical Journal*, vol. 516, no. 1, pp. 195–220, 1999.

[124] J. Yoo, J. Chanamé, and A. Gould, "The end of the MACHO era: limits on halo dark matter from stellar halo wide binaries," *The Astrophysical Journal*, vol. 601, no. 1, pp. 311–318, 2004.

[125] D. P. Quinn, M. I. Wilkinson, M. J. Irwin, J. Marshall, A. Koch, and V. Belokurov, "On the reported death of the MACHO era," *Monthly Notices of the Royal Astronomical Society*, vol. 396, no. 1, pp. L11–L15, 2009.

[126] R. B. Metcalf and J. Silk, "New constraints on macroscopic compact objects as dark matter candidates from gravitational lensing of type Ia supernovae," *Physical Review Letters*, vol. 98, no. 7, Article ID 071302, 2007.

Hindawi Publishing Corporation
Advances in Astronomy
Volume 2010, Article ID 271592, 21 pages
doi:10.1155/2010/271592

Review Article

The First Galaxies and the Likely Discovery of Their Fossils in the Local Group

Massimo Ricotti

Department of Astronomy, University of Maryland, College Park, MD 20742, USA

Correspondence should be addressed to Massimo Ricotti, ricotti@astro.umd.edu

Received 22 May 2009; Revised 17 September 2009; Accepted 5 November 2009

Academic Editor: Andrey V. Kravtsov

The lower bound for the mass of a galaxy is unknown, as are the typical luminosity of the smallest galaxies and their numbers. The answers depend on the extent to which star formation in the first population of small mass halos may be suppressed by radiative feedback loops. If early populations of dwarf galaxies did form in significant number before reionization, their "fossils" should be found today in the Local Group. This paper reviews our ongoing efforts to simulate and identify fossil dwarfs in the Local Group. It is widely believed that reionization stopped star formation in fossil dwarfs. However, here we dispute this idea and discuss a physical mechanism whereby recent episodes of star formation would be produced in some fossil dwarfs that, hence, may characterized by a bimodal star formation history. The same mechanism could turn dark halos that failed to form stars before reionization into gas-rich "dark galaxies". We believe that current observational data supports the thesis that a fraction of the new ultra-faint dwarfs discovered in the Local Group are fossil dwarfs and we predict the existence of a population of ultra-faint dwarfs with lower surface brightness than currently observed.

1. Introduction

There are many questions that remain open in cosmology with regard to the mass, number, and properties of the smallest galaxies in the universe. Have we already discovered the smallest galaxies in the universe or are we still missing an elusive but large population of ultrafaint dwarf galaxies?

In cold dark matter (CDM) cosmologies most of the dark halos that formed before reionization had masses smaller than 10^8-$10^9\,M_\odot$ (e.g., [1]). The small mass halos that survived tidal destruction to the modern epoch, were they able to form stars, would constitute a subpopulation of dwarf satellites orbiting larger halos. Small mass dark halos significantly outnumber more massive galaxies like the Milky Way and can be located in the voids between luminous galaxies (e.g., [2, 3]).

However, until recently (i.e., before 2005) observations did not show a large number of satellites around massive galaxies like the Milky Way and Andromeda. This became known as the "missing galactic satellite problem" [4, 5]. The voids between bright galaxies appear to be devoid of dwarf galaxies [6–8]. While the abundance of dwarfs in large voids may not pose a problem to CDM cosmology, as shown by Tinker and Conroy [9], it is unclear whether the predictions of the number of faint dwarfs in the Local Group are consistent with both the number of observed Milky Way dwarf satellites and the number of relatively isolated dwarfs in the local voids.

Historically, the discrepancy between observation and theory on the number of dwarf galaxies has been interpreted in two ways: (1) as a problem with the CDM paradigm that could be solved by a modification of the dark matter properties—for instance, by introducing warm dark matter (e.g., [10])—or (2) as an indicator of feedback processes that are exceptionally efficient in preventing star formation in small mass halos, which remain mostly dark (e.g., [11]).

The recently discovered population of ultrafaint dwarfs [12–22] in combination with a proper treatment of observational incompleteness [23–26] has increased the estimated number of Milky Way satellites to a level that can be more easily reconciled with theoretical expectations. For instance, the suppression of dwarf galaxy formation due to intergalactic medium (IGM) reheating during reionization [2, 3, 27–40], in conjunction with a strong suppression

of star formation in small mass pre-reionization dwarfs, may be sufficient to explain the observed number of Milky Way satellites. In the near future we can hope to answer perhaps a more interesting question: what is the minimum mass that a galaxy can have? This is a nontrivial and fundamental question in cosmology. Answering it requires a better understanding of the feedback mechanisms that regulate the formation of the first galaxies before reionization and the details of the process of reionization feedback itself.

The formation of the first dwarf galaxies—before reionization—is self-regulated on cosmological distance scales. This means that the fate of small mass halos (i.e., whether they remain dark or form stars) depends on local and global feedback effects. This type of galaxy feedback differs from the more familiar model operating in normal galaxies (e.g., SN explosions, AGN feedback, etc.), where the feedback is responsible for regulating the star formation rate within the galaxy itself but does not impact star formation in other distant galaxies. Rather, before reionization, each protodwarf galaxy reacts to the existence of all the others. Different theoretical assumptions and models for the cosmological self-regulation mechanisms will, of course, produce different predictions for the number and luminosity of the first dwarf galaxies [11, 41–44].

We now introduce the basic concepts on how feedback-regulated galaxy formation operates in the early universe (i.e., before reionization).

A cooling mechanism for the gas is required in order to initiate star formation in dark halos. In proto-galaxies that form after reionization this is initially provided by hydrogen Lyman-alpha emission. This cooling is efficient at gas temperatures of 20,000 K but becomes negligible below $T \sim 10,000$ K. Later, as the temperature drops below 10,000 K, the cooling is typically provided by metal line cooling. In the first galaxies, however, both these cooling mechanisms may be absent. This is because the first dwarf galaxies differ when compared to present-day galaxies in two respects: (1) they lack important coolants—such as carbon and oxygen, because the gas is nearly primordial in composition, and (2) due to the smaller typical masses of the first dark halos, the gas initially has a temperature that is too low to cool by Lyman-alpha emission.

The gas in small mass halos with circular velocity $v_{\rm vir} = (GM_{\rm tot}/r_{\rm vir})^{1/2} \lesssim 20\,{\rm km\,s^{-1}}$, where $r_{\rm vir}$ is the virial radius—roughly corresponding to a mass $M_{\rm tot} \lesssim 10^8\,{\rm M_\odot}$ at the typical redshift of virialization—has a temperature at virialization $T \lesssim 10,000$ K. Hence, if the gas has primordial composition, it is unable to cool by Lyman-alpha emission and initiate star formation unless it can form a sufficient amount of primordial H_2 (an abundance $x_{H_2} \gtrsim 10^{-4}$ is required). Because molecular hydrogen is easily destroyed by far-ultraviolet (FUV) radiation in the Lyman-Werner bands ($11.3 < h\nu < 13.6$ eV) emitted by the first stars, it is widely believed that the majority of galaxies with $v_{\rm vir} < 20\,{\rm km\,s^{-1}}$ remain dark (e.g., [11]). However, several studies show that even if the FUV radiation background is strong, a small amount of H_2 can always form, particularly in relatively massive halos with virial temperature of several thousands of degrees [43, 45]. Thus, negative feedback from FUV radiation may only delay star formation in the most massive pre-reionization dwarfs rather than fully suppress it [46, 47]. We will argue later that hydrogen ionizing radiation ($h\nu > 13.6$ eV) in the extreme-ultraviolet (EUV) plays a far more important role in regulating the formation of the first galaxies than FUV radiation. Thus, in our opinion, models that do not include 3D radiative transfer of H and He ionizing radiation cannot capture the most relevant feedback mechanism that regulates galaxy formation in the early universe [41, 48].

After reionization, the formation of dwarf galaxies with $v_{\rm vir} < 20\,{\rm km\,s^{-1}}$ is strongly inhibited by the increase in the Jeans mass in the IGM. Thus, according to this model, reionization feedback and negative feedback due to H_2 photodissociation by the FUV background (important before reionization) determine the mass of the smallest galactic building blocks. The resultant circular velocity of the smallest galactic building blocks is $v_{\rm vir} \sim 20\,{\rm km\,s^{-1}}$, roughly corresponding to masses $M_{\rm tot} \sim 10^8$-$10^9\,{\rm M_\odot}$. If this is what really happens in the early universe, the "missing Galactic satellite problem" can be considered qualitatively solved because the predicted number of Milky Way satellites with $v_{\rm vir} > 20\,{\rm km\,s^{-1}}$ is already comparable to the estimated number of observed satellites after applying completeness corrections (although this model may still have problems reproducing the observations in detail).

However, as briefly mentioned above, we have argued for some time that most simulations of the first galaxies cannot capture the main feedback mechanism operating in the early universe because they do not include a key physical ingredient: radiative transfer of H and He ionizing radiation. Our simulations of the formation of the first galaxies are to date the only simulations of a cosmologically representative volume of the universe (at $z \sim 10$) that include 3D radiative transfer of H and He ionizing radiation [41, 44, 48]. Figure 1 shows the evolution of ionized bubbles around the first galaxies in a cubic volume of 1.5 Mpc in size at redshifts $z = 21.2, 17.2, 15.7, 13.3$ from one of our simulations. The results suggest that negative feedback from the FUV background is not the dominant feedback mechanism that regulates galaxy formation before reionization. Rather, "positive feedback" on H_2 formation from ionizing radiation [30, 49] dominates over the negative feedback of H_2 dissociating radiation. Hence, a strong suppression of galaxy formation in halos with $v_{\rm vir} < 20\,{\rm km\,s^{-1}}$ does not take place. In this latter case, some galactic satellites would be the fossil remnants of the first galaxies. Comparisons of simulated pre-reionization fossils to dwarf spheroidals in the Local Group show remarkable agreement in properties (see [50], hereafter RG05). Based on the results of the simulations, we also suggested the existence of the ultrafaint population before it was discovered about a year later (see RG05 [51]).

1.1. Definition of "Pre-Reionization Fossils". Throughout this paper we define "pre-reionization fossils" as the dwarfs hosted in halos with a maximum circular velocity remaining below $20\,{\rm km\,s^{-1}}$ at all times during their evolution: $v_{\rm max}(t) < 20\,{\rm km\,s^{-1}}$. It will become clear in this paper that this definition is not directly related to the ability of fossils to

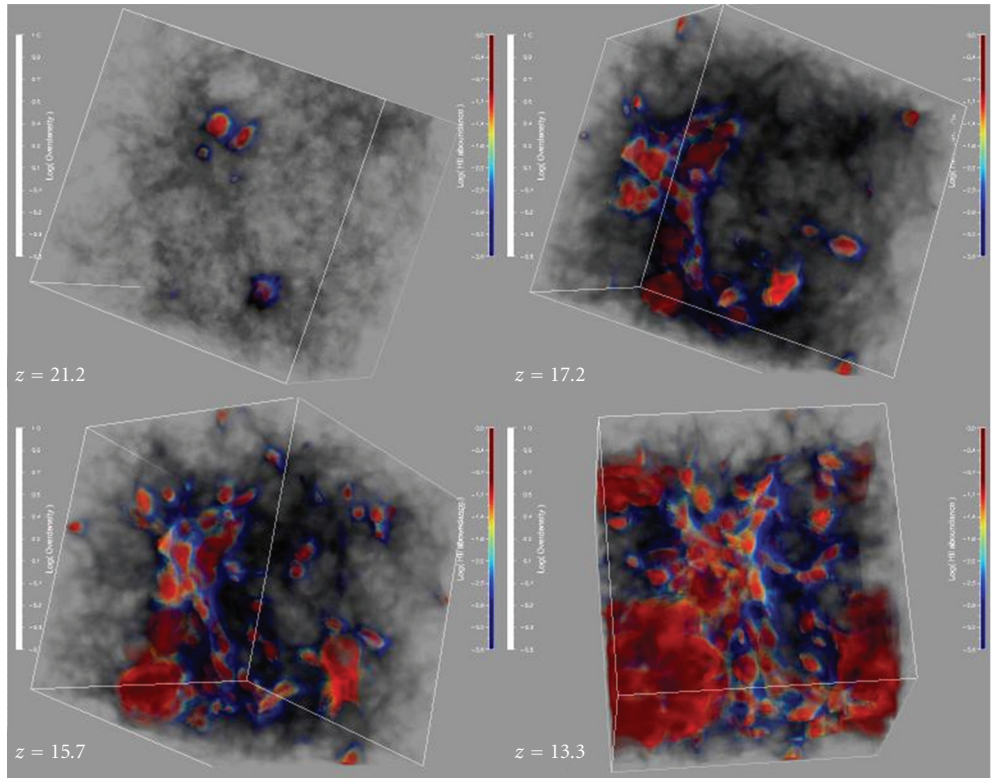

FIGURE 1: 3D rendering of cosmological H II regions (fully ionized gas is red and partially ionized gas is blue) around the first galaxies in a box of 1.5 Mpc. The four boxes show a time sequence at redshifts $z = 21.2, 17.2, 15.7, 13.3$ for the simulation S2 from Ricotti et al. [41]. The rendering shows several tens of small size H II regions around the first galaxies (there are a few hundreds of galaxies in this volume). A movie of the same simulation shows that the H II regions are short lived: they form and expand to a size comparable to the large-scale filamentary structure of the IGM and recombine, promoting the formation of molecular hydrogen inside the relic H II regions.

retain gas and form stars after reionization: in Section 4 we describe a mechanism in which small mass halos with $v_{\rm max}(t) < 20\,{\rm km\,s^{-1}}$ are able to have a late phase of gas accretion and possibly star formation.

Our definition of fossil reflects the *special cooling mechanisms and feedback processes* that regulate star formation and the number of luminous halos with $v_{\rm max}(t) < 20\,{\rm km\,s^{-1}}$, before and *after* reionization. In protofossil galaxies—even adopting the most conservative assumption of maximum efficiency of shock heating of the gas during virialization—the gas is heated to a temperature below $T \sim 10,000$ K. Thus the gas cannot cool by Lyman-alpha emission, a very efficient coolant. The cooling of the gas is dominated either by H_2 roto-vibrational line emission or by metal cooling, important if the metallicity exceeds $Z \sim 10^{-3}\,Z_\odot$ (e.g., [44, 52–54]). These coolants are much less efficient than Lyman-alpha emission. Moreover, H_2 abundance and cooling is modulated and often suppressed by the FUV and EUV radiation fields. The FUV radiation in the H_2 Lyman-Werner bands and hard ultraviolet radiation have large mean free paths with respect to the typical distances between galaxies; thus their feedback is global in nature. Qualitatively, this explains why the first galaxies have low luminosities and low surface-brightness, similar to dwarf spheroidal (dSph) galaxies in the Local Group (see RG05 [51, 55]).

Simulations also show that stars in the the first galaxies do not form in a disk but in a spheroid (see RG05 [44]). A thin galactic disk is not formed because of the high merger rates and the low masses of dark halos in the early universe. Roughly, pre-reionization fossils have a mass at virialization $M_{\rm tot} < 10^8\,{\rm M}_\odot$, assuming that they form at $z_{\rm vir} \sim 10$, but their mass may increase by up to one order of magnitude by $z = 0$ due to secondary infall (see RGS02a, b [44]). Secondary infall does not affect $v_{\rm max}$, which remains roughly constant after virialization.

1.2. Pre-Reionization Fossils and Reionization. The critical value of $v_{\rm max,crit}$ for which dwarf galaxy formation is suppressed by reionization feedback is close to the $20\,{\rm km\,s^{-1}}$ value that defines a fossil, but it is *not necessarily the same value*. Indeed, it can be significantly larger than $20\,{\rm km\,s^{-1}}$ if the IGM is heated to $T \gg 10,000$ K [56]. Thus, we expect that the virialization of new "pre-reionization fossils" is strongly suppressed after reionization due to IGM reheating (i.e., they mostly form before reionization). However, pre-reionization fossils and dark halos with $v_{\rm max} < 20\,{\rm km\,s^{-1}}$ that virialized before reionization may accrete gas and, in certain cases, form new stars after reionization at redshifts $z <$ 1-2 [3].

Unfortunately, the value of $v_{\rm max,crit}$ is uncertain due to our poor understanding of the thermal history of the IGM [56]. The uncertainty surrounding the IGM equation of state may partially explain the differences found in literature on the values for $v_{\rm max,crit}$ and the different levels of suppression of star formation as a function of the halo mass after reionization (e.g., [2, 33, 36, 40]). Regardless of assumptions for the reionization feedback model, one should bear in mind that no halo with $v_{\rm max} < 20\,{\rm km\,s^{-1}}$ can form stars after reionization unless the gas in those halos has been significantly pre-enriched with metals. For instance, the model by Koposov et al. [57] assumes star formation after reionization in halos as small as $v_{\rm max} \sim 10\,{\rm km\,s^{-1}}$. With this assumption they find that their model is consistent with observations of ultrafaint dwarfs but claim that fossils are not needed to explain the data. However, star formation in such small halos can only take place in a gas that was pre-enriched with metals, suggesting the existence of older populations of stars in those halos. Indeed, according to our definition, the smallest post-reionization dwarfs with $10\,{\rm km\,s^{-1}} < v_{\rm max} < 20\,{\rm km\,s^{-1}}$ in the Koposov et al. [57] model are "fossils." As stated above, fossils may also be able to form stars after reionization due to a late phase of cold gas accretion from the IGM [3].

1.3. Identification of Pre-Reionization Fossils in Observations. Pre-reionization fossils are not easily identifiable because $v_{\rm max}$ cannot be measured directly from observations. Understanding the star formation history of dwarf galaxies may help in this respect, as fossils likely show some degree of suppression of their star formation rate occurring about 12.5 Gyr ago due to reionization. However, their identification based on their star formation history may be complicated because some pre-reionization fossils in the last 10 Gyr may have had a late phase of gas accretion and star formation. The caveat is that star formation histories cannot be measured with accuracy better than to within 1-2 Gyr and the accuracy becomes increasingly poorer for old stellar populations. Thus, it is impossible to prove whether an old population of stars formed before reionization (which happened about 1 Gyr after the Big Bang) or at $z \sim 3$, when the Milky Way was assembled. Nevertheless, ultrafaint dwarfs that show some degree of bimodality in their star formation history are candidates for being pre-reionization fossils.

According to results by RG05 and Bovill and Ricotti [51], Willman 1, Bootes II, Segue 1, and Segue 2 do not lie on the luminosity-surface brightness relationship of simulated pre-reionization fossils. This result is based on the assumption that fossil properties are not modified by tides. Their surface brightness is larger than the model predictions for objects with such low-luminosity. Yet undiscovered population of ultrafaints with lower surface brightness is instead predicted by our simulations. It is likely that the properties of the lowest luminosity ultrafaints may have been modified by tidal forces due to their proximity to the Milky Way disk.

Although it is difficult to identify individual fossils, statistical arguments suggest that at least some ultrafaint dwarf galaxies are pre-reionization fossils. This is because the number of satellites from N-body simulations with $v_{\rm max}(t) > 20\,{\rm km\,s^{-1}}$ is substantially smaller than the estimated number of observed satellites after completeness corrections. Admittedly the current theoretical and observational uncertainties on the number of satellites are still large. However, if the estimated number (after completeness corrections) of ultrafaint dwarfs increases further, the existence of pre-reionization fossils will be inescapably proven. This is especially the case if a population of ultrafaint dwarfs with luminosities similar to Willman 1, Bootes II, Segue 1, and Segue 2 but surface brightness below the current sensitivity limit of the SDSS—as predicted by our simulations—is discovered.

The possibility of identifying the fossils of the first galaxies in our own backyard is very exciting. It would greatly improve our understanding of the physics involved in self-regulating the formation of the first galaxies before reionization. Clearly, even the launch of the James Webb Space Telescope (JWST) would not yield the wealth of observational data on the formation of the first galaxies that could be obtained by studying ultrafaint galaxies in the Local Group.

The rest of the paper is organized as follows. In Section 2 we briefly review and discuss observational data on Galactic satellites; in Section 3 we summarize the results of simulations of the formation of the first galaxies in a cosmological volume and the effect of reionization feedback on galaxy formation. In Section 4 we discuss a recently proposed model for "late gas accretion" from the IGM onto small mass halos. In Section 5 we compare the theoretical properties of simulated pre-reionization fossils to observations. In Section 6 we compare different ideas for the origin of classical and ultrafaint dwarf spheroidals. We present our conclusions in Section 7.

2. Observations

2.1. The Ultrafaint Satellites of the Milky Way and Andromeda. Prior to 2005, the number of observed dwarf satellites of the Milky Way and Andromeda was about 30 [58]. One of the most evident properties of the dwarfs in the Local Group is a type segregation, with "gas free" dwarf spheroidal (dSph) galaxies distributed near the center of their host galaxy and gas rich dwarf Irregulars (dIrr) at larger distances from the galactic centers. Notable exceptions are the Magellanic Clouds that are dIrr less than 100 kpc from the center of the Milky Way and a few isolated dSphs like Tucana and Antlia. One popular explanation for this segregation is the transformation of dIrr into dSph due to tidal and ram pressure stripping as dwarfs fall toward the Milky Way center [59, 60]. In addition, simulations showed that the number of dark matter satellites of the Milky Way with mass $> 10^8\,{\rm M}_\odot$ (i.e., with mass sufficiently large to expect star formation in them) was an order of magnitude larger than the number of known dwarf satellites [4, 5]. This posed a problem for CDM cosmologies.

Since 2005-2006 the number of known Local Group satellites has begun to increase dramatically, with the discovery of a new population of ultrafaint dwarfs. The new galaxies have been discovered by data mining the SDSS and other

surveys of the halo around M31, resulting in the discovery of 14 new ultrafaint Milky Way satellites [12–19, 24, 61] and 11 new companions for M31 [20–22, 62]. Unofficial reports from members of the SDSS collaboration state that there are actually at least 17 new ultrafaint Milky Way dwarfs, but several of them are as yet unpublished (anonymous referee's private communication).

The new Milky Way satellites have been slowly discovered since SDSS Data Release 2, with the most recent Segue 2 discovered in Data release 7 [63, 64]. Koposov et al. [24] and Walsh et al. [61] systematically searched Data Releases 5 and 6, respectively. Due to the partial sky coverage of the SDSS, and assuming isotropic distribution of satellites (but see [65, 66]), the total number of ultrafaint dwarfs in the Milky Way should be at least 5.15 times larger than the observed number [25]. With this simple but conservative correction, the number of Milky Way satellites within 400 kpc is about $12 + 5.15 \times (14 \pm 3.7) \sim 84 \pm 19$. The quoted uncertainty is simply Poisson error due to the relatively small number of known ultrafaint dwarfs.

In estimating the completeness correction for the number of Milky Way dwarfs, one should account for selection effects inherent in the method used to find the ultrafaints in the SDSS data. In addition to completeness corrections for the survey's coverage of the sky, the most important selection effect is the total number of stars from the object seen in the survey, that is, horizontal branch stars or main sequence and/or red giant stars for the lowest luminosity ultrafaints like Coma or Segue 1. This sets a limiting surface brightness cutoff at roughly 30 mag arcsec^{-2} for the SDSS [24] (but see Martin et al. [67] that find a limiting surface brightness about 6.4 times larger). There is also a distance-dependent absolute magnitude cutoff. The efficiency of finding ultrafaint dwarfs by data mining the SDSS typically drops rapidly at Galactocentric distances beyond 50–150 kpc for the ultrafaints (depending on their luminosity) [23–25, 61]. Of the new Milky Way dwarfs, only Leo T is well beyond this distance threshold, and 11 of the 14 new Milky Way satellites are within 200 kpc. (Leo T was found because it contains a young stellar population and gas. Otherwise, it would not have been identified as an ultrafaint dwarf due to its large Galactocentric distance.)

The luminous satellites can be radially biased. So, the abundance of the faintest satellites within 50 kpc, that is the most complete sample, may not be used to correct for incompleteness at larger distances from the Galactic center without prior knowledge of this bias. And, of course, satellites of different luminosity and surface brightness will have different completeness limits. These selection biases have been considered in a paper by Tollerud et al. [25]. Their study finds that there may be between 300 to 600 luminous satellites within 400 kpc. Their estimate for the number of luminous satellites within a Galactocentric distance of 200 kpc is between 176 to 330.

Recent surveys of M31 [20, 22, 62] have covered approximately a quarter of the space around the M31 spiral. The surveys have found 11 new M31 satellites, bringing the total number to 19. If we make a simple correction for the covered area of the survey, the estimated number of M31 satellites, including the new dwarfs, increases from 8 to 52 ± 13.

The sensitivity limits of the surveys for Andromeda do not allow the detection of ultrafaint dwarfs that would correspond with those with the lowest luminosity found in the Milky Way. However, despite the fact that Andromeda and the Milky Way are thought to have approximately the same mass (within a factor of two), their satellite systems show interesting differences for even the satellites at the brighter end of the luminosity function. For instance, there are small differences in the galactocentric distance distribution of satellites and in the morphology of the satellites (e.g., number of dIrr, dE, and dSphs).

2.2. Peculiar Ultrafaint Dwarfs. Many of the newly discovered dwarfs are dSphs with a dominant old population of stars and virtually no gas, which makes them candidates for being pre-reionization fossils. However, there are notable exceptions that we discuss below that may not perfectly fit the properties of simulated "fossils." For instance, the dwarf galaxy Leo T resembles all the other ultrafaints but has gas and recent star formation [14, 23]. We argue that Leo T could be a true "fossil" with $v_{\max}(t) < 20\,\mathrm{km\,s^{-1}}$ but may have experienced a late phase of gas accretion and star formation due to the mechanism discussed in Section 4.

Leo T has a stellar velocity dispersion of $\sigma_{\mathrm{LeoT}} = 7.5 \pm 1.6\,\mathrm{km\,s^{-1}}$ [23] or an estimated dynamical mass of $10^7\,\mathrm{M}_\odot$ within the stellar spheroid (although its total halo mass may be much larger). Leo T shows no sign of recent tidal destruction by either the Milky Way or M31 [68] and is located in the outskirts of the Milky Way at a Galactocentric distance of 400 kpc. Leo T photometric properties are consistent with those of pre-reionization fossils. On the other hand, the halo of Leo T could be sufficiently massive ($v_{\max}(t) > 20\,\mathrm{km\,s^{-1}}$) to retain or accrete mass after reionization and not be a pre-reionization fossil. However, as discussed in Section 4 it is also possible that Leo T is a pre-reionization fossil that has been able to accrete gas from the IGM at late times due to an increase in the concentration of its dark halo and a decrease in the IGM temperature [3]. Under this scenario, Leo T stopped forming stars after reionization but was able to start accreting gas again from the IGM at $z \lesssim 1 - 2$ and therefore would have a bimodal stellar population. De Jong et al. [68] have found evidence for bimodal star formation in Leo T. Our model would explain why Leo T does not resemble other dIrr and is similar to dSphs and pre-reionization fossils, while not suffering significant tidal stripping.

Willman 1, Bootes II, Segue1, and Segue2 are among the lowest luminosity ultrafaint dwarfs discovered so far; however, they do not fit the typical properties of pre-reionization fossils (see Section 5). For instance, Willman 1 has a dynamical mass within the largest stellar orbit ($r \sim 100$ pc) of $5 \times 10^5\,\mathrm{M}_\odot$ and a mass-to-light ratio ~470, similar to other ultrafaint dwarfs [17]. However, given its low luminosity, Willman 1 has central surface brightness that is too large when compared to simulated "fossils." Simulated fossils with luminosities $L_{\mathrm{V}} < 10^3\,\mathrm{L}_\odot$ should have a typical surface brightness that falls below the detection limit of ~30 mag arcsec^{-2} estimated for the SDSS [24]. Hence,

the lowest luminosity fossils may still be undiscovered. Although the nature of the lowest luminosity ultrafaints is unknown, due to selection effects they can only be found within ∼50 kpc of the Galactic center. Thus it is possible, and perhaps to be expected, that their properties have been affected by tidal forces [60, 69].

3. Formation of First Galaxies in CDM

The first episodes of star formation in the universe are thought to take place at redshift $z \sim 30$–50, in the center of dark matter halos with typical mass $M_{\rm tot} \sim 10^5$-$10^6\,{\rm M}_\odot$. The gas in these halos is metal free and simulations show that a single or binary massive star per halo is formed [70–77]. Such stars are called Pop III and their mass, although not well constrained by the simulations, is quite large: in the range between $20\,{\rm M}_\odot$ and a few $100\,{\rm M}_\odot$. Whether or not we can refer to minihalos containing a single massive star (or a binary star) in their center as the "first galaxies" is debatable. However, the crucial point to be made here is that there is a gap of 2 to 3 orders of magnitude between the typical halo mass in which Pop III stars are born (10^5-$10^6\,{\rm M}_\odot$) and the typical mass of the population of dwarf galaxies that are not strongly influenced by radiative and reionization feedback (10^8-$10^9\,{\rm M}_\odot$). The primordial dwarfs that fill the gap are those that we refer to as *pre-reionization fossils*.

If the formation of pre-reionization fossils is not drastically suppressed by radiative feedback, their number may be several orders of magnitude larger than the number of more massive dwarfs. This is because in CDM cosmologies the number of dark halos per unit comoving volume roughly scales with the mass as $N \propto M_{\rm dm}^{-2}$.

It is widely believed that nearly all halos with mass $M_{\rm tot} > 10^8$-$10^9\,{\rm M}_\odot$ host luminous galaxies, although there can be substantial disagreement among theorists on their luminosity. However, most of the theoretical controversy rests in understanding the fate of the halos with mass between 10^6–$10^8\,{\rm M}_\odot$ and the dominant feedback that determines whether they become luminous or remain dark. We will elaborate on this statement in the next sections.

3.1. Radiative Feedback. Simulating the formation of the first stars is a relatively well-defined initial condition problem, given the cosmological parameters. However, these simple initial conditions must soon be modified to take into account the effects of other newborn stars, whose properties are still quite uncertain. The physics becomes more complex as competing feedback effects determine the fate of the first galaxies: radiative feedback regulates the formation and destruction of H_2 and metals are injected into the IGM and into protogalaxies.

3.1.1. Negative Feedback from H_2 Photodissociating Radiation. The net effect of radiative feedback on the global star formation history of the universe before the redshift of reionization is uncertain. An FUV background (at energies between 11.34 eV and 13.6 eV) destroys H_2, the primary coolant at the start of galaxy formation. The FUV radiation emitted by the first few Pop III stars is sufficient to *suppress or delay* galaxy formation in halos with circular velocities $v_{\rm vir} < 20\,{\rm km\,s^{-1}}$ that are too small to cool by Lyman-alpha emission [11, 43, 78, 79]. Hence, according to this scenario, most halos with masses $< 10^8$-$10^9\,{\rm M}_\odot$ remain dark. More work is needed to quantify the level of suppression of galaxy formation and examine how these models compare to observations of Milky Way satellites.

Figure 2 illustrates the effect of H_2 dissociating radiation on the IGM. The two panels show slices through a simulation in Ricotti et al. [41] at $z = 19.44$ and $z = 18.5$. The top-right tiles in the two panels show H_2 abundance. At $z = 19.4$, the H_2 has its relic abundance everywhere in the IGM except inside the dissociation spheres around the first galaxies, where it is destroyed. At $z = 18.5$, the dissociation spheres are still visible, but the UV background starts to dissociate H_2 everywhere in the IGM except the denser filaments.

3.1.2. Positive Feedback Regions. Our main criticism for the "negative feedback" model is that it does not take into account the effect of hydrogen ionizing radiation [49, 80] that, according to simulations, may indeed play a dominant role in regulating galaxy formation before reionization [41, 48]. Simulations including 3D radiation transfer show that star formation in the first small mass halos is inefficient, partially due to winds produced by internal UV sources. This produces galaxies that are extremely faint and have very low surface brightnesses. However, our simulations show that a large number of ultrafaint dwarfs (a few hundred galaxies per comoving $\rm Mpc^3$) form before reionization at $z \sim 7 - 10$. Hence, according to this model, the Local Group may contain thousands of ultrafaint dwarf galaxies.

Ionizing radiation from the first stars enhances the production of H_2 (we refer to this as "positive feedback") by creating free electrons and promoting the formation of H^-, the main catalyst for the formation of H_2 in a low metallicity gas [30, 49, 81–83]. Ricotti et al. [49] found that shells of H_2 can be continuously created in precursors around the Strömgren spheres produced by ionizing sources and, for a bursting mode of star formation, inside recombining H II regions. We refer to these shells as "positive feedback regions." This is because the catalyst H^-, and hence H_2, is formed most efficiently in regions where the gas ionization fraction is about 50%. This local "positive feedback" is difficult to incorporate into cosmological simulations because the implementation of spatially inhomogeneous, time-dependent radiative transfer is computationally expensive.

Figure 3 shows "positive feedback regions" in one of our simulations. The figure shows a slice through a simulation at 4 different times (at $z = 17.3, 12.2, 11.3$, and 10.2). We recognize the two main processes that create H_2 in the filaments. In the top-left frame at $z = 17.3$ we can see a "positive feedback region" as an irregular shell of H_2 surrounding the H II region that is barely intersected by the slice. In the bottom-left frame ($z = 11.3$) two H II regions are clearly visible. Inside the H II regions, the H_2 is destroyed. In the bottom-right frame ($z = 10.2$) the H II regions are recombining (demonstrating that the star formation is

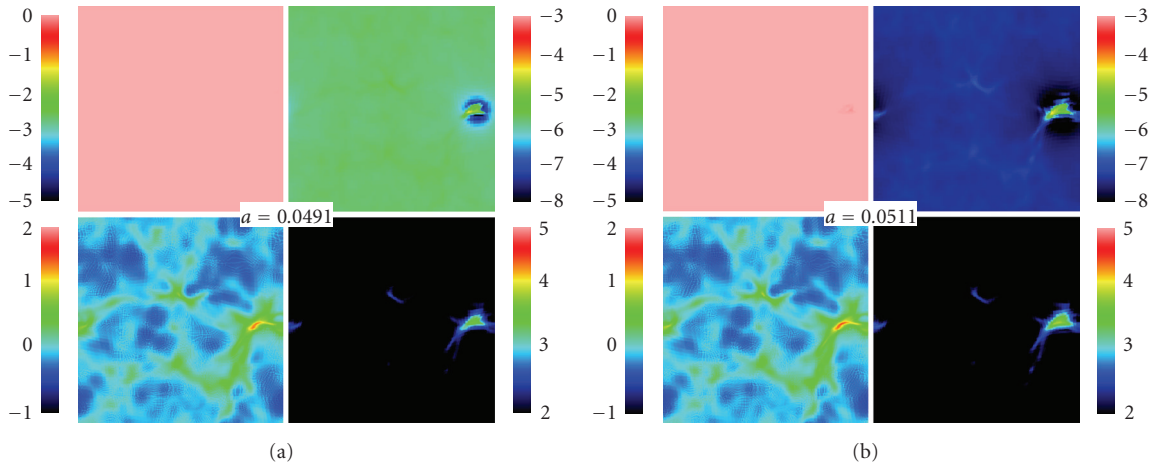

FIGURE 2: The two (2×2) panels show slices through the most massive object in the simulation 64L05p2 in RGS02b at $z = 19.4$ and 18.5. The box size is $L_{box} = 0.7$ comoving Mpc. Each one of the 2×2 panels shows in log-scale the neutral hydrogen fraction (top left), the molecular fraction (top right), the gas overdensity (bottom left), and the gas temperature (bottom right). The sequence illustrates the evolution of a H_2 dissociation sphere around a single source (panel at $z = 19.4$) and the dominance of the H_2 dissociating background at $z = 18.5$.

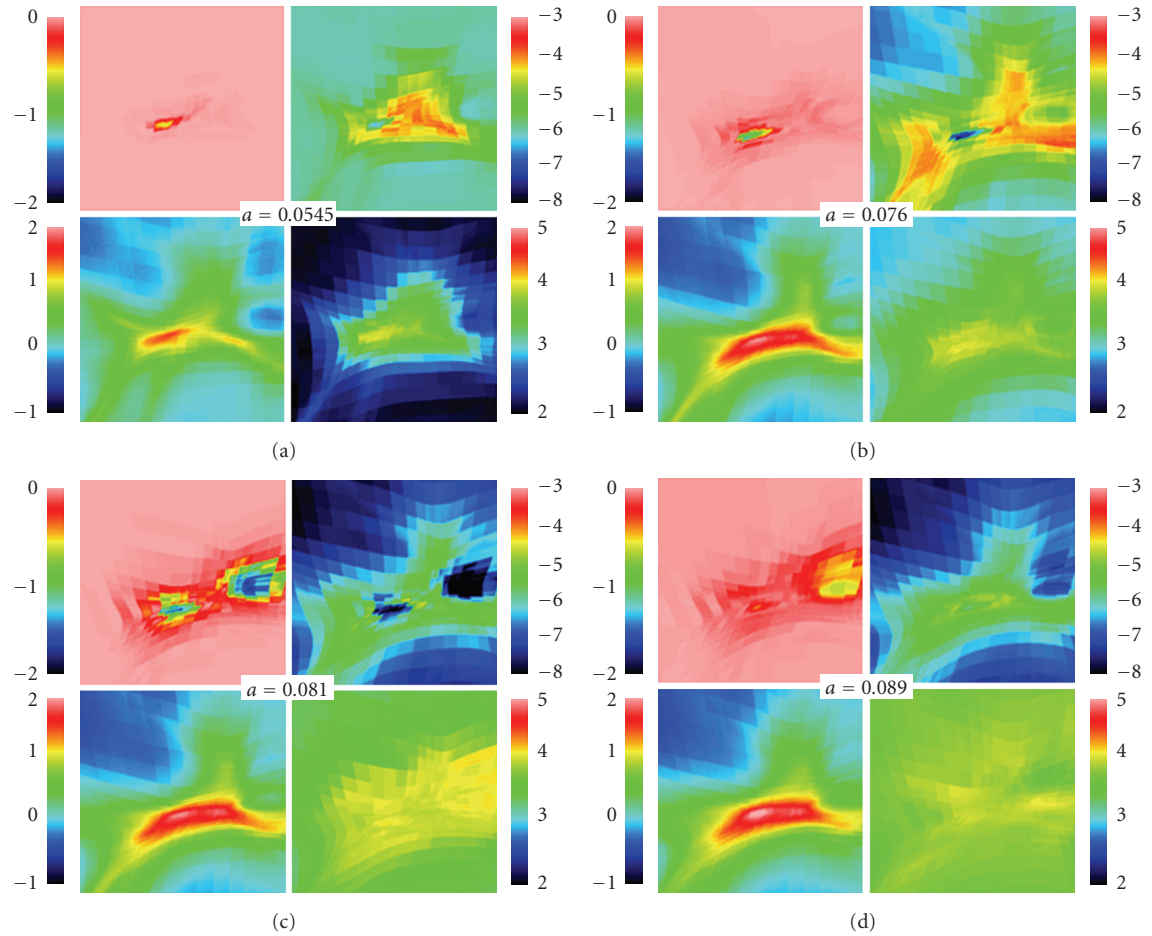

FIGURE 3: Same as in Figure 2 except for a zoomed region of $0.125^2\ h^{-2}$ Mpc^2 around the most massive object in the 64L05p3 simulation in RGS02b. In this time sequence of images (top: $z = 17.3, 12.2$ from left to right; bottom: $z = 11.3, 10.2$ from left to right) we recognize the two main processes that create H_2 in the filaments: "positive feedback regions" in front of H II regions and the reformation of H_2 inside relic H II regions. The bursting mode of the star formation is evident from the continuous formation and recombination of the H II regions in the time sequence of the slices.

bursting) and new H_2 is being reformed inside the relic H II regions. A finer inspection of the time evolution of this slice shows that at least five H II regions form and recombine between $z = 20$ and $z = 10$ in this small region of the simulation (Movies of 2D slices and 3D rendering of the simulations are publicly available on the web at the URL: http://www.astro.umd.edu/~ricotti/movies.html).

There are two reasons why our results are still controversial. First, our simulations do not yet have sufficient resolution to ensure their convergence. Second, there are no other published simulations to compare our results with. Only recently have some groups started to include the effect of 3D radiative transfer on hydrodynamics (e.g., [42, 45]). However, currently there are no other simulations of the formation of the first galaxies in a cosmological volume suited for comparison with observations of dwarfs in the Local Group other than our own [41, 44, 48, 50, 51]. Hence, our results may differ from other numerical studies because of the inclusion in the code of the effects of "positive feedback regions" and galactic winds from ionizing radiation.

Simulations by Wise and Abel [42] include a self-consistent treatment of hydro and 3D radiative transfer that is more accurate than our approximate, but faster method. However, because the authors use ray-tracing for the radiative transfer, only a few sources of radiation can be simulated at the same time. This limits the volume and number of galaxies that can be simulated. Due to these limitations the simulations are not suited for comparison between the primordial dwarf populations and the ultrafaint dwarfs. In addition, at the moment, the aforementioned simulations do not include metal cooling and the formation of normal stars (other than Pop III).

3.1.3. The Simulations. The simulation used for comparison to observations of ultrafaint dwarfs has been thoroughly described in Ricotti et al. [41, 48] as run "256L1p3." Here we remind the reader that the simulation includes 256^3 dark matter particles, an equal number of baryonic cells, and more than 700,000 stellar particles in a box of size ~ 1.5 comoving Mpc. The mass of the dark matter particles in our simulation is $4930\,M_\odot$, and real comoving spatial resolution (twice the Plummer softening length) is $150\,h^{-1}$ pc (which corresponds to a physical scale of 24 parsecs at $z = 8.3$). This resolution allows us to resolve cores of all simulated galaxies that would correspond to the observed Local Group dwarfs. The stellar masses are always smaller than the initial baryon mass in each cell but can vary from $\sim 0.6\,h^{-1}\,M_\odot$ to $600\,h^{-1}\,M_\odot$ with a mean of $6\,h^{-1}\,M_\odot$. Stellar particles do not represent individual stars but, in general, a collection of stars (e.g., OB associations).

The simulation includes most of the relevant physics, including time-dependent spatially-variable radiative transfer using the OTVET approximation [84], detailed radiative transfer in Lyman-Werner bands, and nonequilibrium ionization balance. In addition to primordial chemistry and 3D radiative transfer, the simulations include a subgrid recipe for star formation, metal production by SNe, and metal cooling. The code also includes mechanical feedback by SN explosions. However, we found that for a Salpeter IMF, the effect of SNe is not dominant when compared to feedback produced by ionizing radiation from massive stars (see [44], hereafter RGS08). The effect of SN explosions is somewhat model dependent and uncertain because it is treated using a subgrid recipe. Hence, the simulation analyzed in this work includes metal pollution but not mechanical feedback by SNe.

In RG05, we included the effect of reionization in the simulation 256L1p3. Because the size of the simulation box has been fixed at ~ 1.5 comoving Mpc, the simulation volume is too small to model the process of cosmological reionization with sufficient accuracy. We therefore assume that the simulation volume is located inside an H II region of a bright galaxy at a higher redshift. Specifically, we introduce a source of ionizing radiation within the computational box, properly biased, which corresponds to a star-forming galaxy with the constant star formation rate of 1 solar mass per year (similar to star formation rates of observed Lyman Break Galaxies at $z \sim 4$, Steidel et al. [85]). The source is switched on at $z = 9.0$, and by $z = 8.3$ the whole simulation box is completely ionized.

3.1.4. Summary of Main Results. The main results of the simulations are the following (see [44], for details).

(1) Negative Feedback. H_2 photodissociation from FUV radiation, the main negative feedback thought to suppress the formation of the first galaxies, is not the dominant feedback. If we modify the spectrum of the sources of radiation to artificially increase or decrease the FUV flux emitted by up to one order of magnitude, we do not find any appreciable effect on the global star formation history.

(2) Self-Regulation. Feedback by hydrogen ionizing radiation (EUV) plays the key role. Galactic outflows, produced by UV photoheating from massive stars, and H_2 formation/photodissociation induces a bursting star formation mode in the first galaxies that acts as the catalyst for H_2 reformation inside relic (recombining) H II regions and in the "precursors" of cosmological Strömgren spheres (i.e., positive feedback regions). As a result, the formation of the first galaxies is self-regulated on a cosmological distance scale. It is significantly reduced by radiative feedback but it is not completely suppressed, even in halos with $v_{\max} \sim 5$–$10\,\mathrm{km\,s^{-1}}$. Note that our subgrid recipe for star formation assumes a Schmidt law with a tunable efficiency parameter ϵ_* (the fraction of gas converted into stars per crossing time). We find that the global star formation history and the fraction of baryons converted into stars in each galaxy, $f_* = M_*/M_{\mathrm{bar}}$, are nearly independent on the assumed value of ϵ_*. This is typical for feedback regulated star formation. Hence, the star formation efficiency, f_*, is not an assumed parameter but it is extracted from the simulations. Thus, the derived star formation efficiency f_* is a very generic prediction of our feedback model because it is nearly independent of the assumed value of ϵ_*, that is instead quite uncertain.

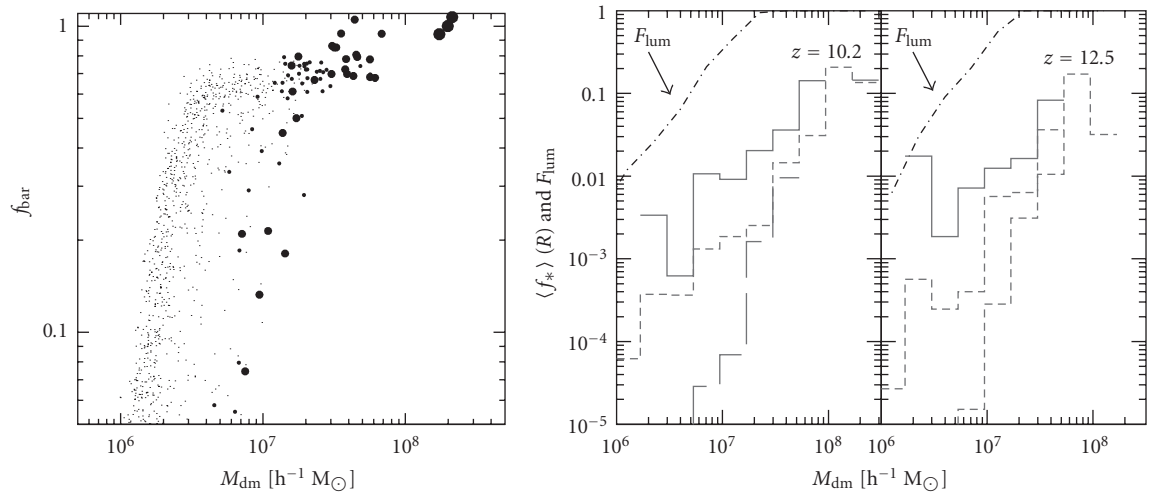

FIGURE 4: (a) Fraction of baryons retained by each galaxy (normalized to the cosmic mean value, $M_{\rm bar} = f_{\rm bar}^{\rm max} M_{\rm dm}$, where $f_{\rm bar}^{\rm max} = \Omega_b/\Omega_m = 0.136$) as function of the halo mass $M_{\rm dm}$ for run S1 in RGS08 at $z = 10$. The size of the dots is proportional to the fraction of stars $f_* = M_*/M_{\rm bar}$ in each halo: from the largest to the smallest dots we have $f_* > 10\%$, $1 < f_* < 10\%$, $0.1 < f_* < 1\%$ and $f_* < 0.1\%$, respectively. The plot illustrates the role of internal and external sources of ionizing radiation in reducing the gas retained by small mass halos. Luminous sources (with larger f_*) retain less gas than dark halos due to winds driven by internal sources of radiation. (b) Average star formation efficiency $\langle f_* \rangle$ as a function of halo mass at $z = 10.2$ (left panel) and 12.5 (right panel) for run S1. We divide all halos into three groups: those at distance $d < 8$ kpc from the nearest luminous halo (solid histograms), those with 8 kpc $< d <$ 50 kpc (dashed histogram), and those with $d > 50$ kpc (long-dashed histograms). The dot-dashed curve shows the fraction of luminous halos $F_{\rm lum}(M_{\rm dm})$ as a function of the halo mass.

(3) Contribution to Reionization. Due to the feedback-induced bursting mode of star formation in pre-reionization dwarfs, the cosmological H II regions that they produce remain confined in size and never reach the overlap phase (e.g., Figure 1). Reionization is completed by more massive galaxies.

(4) Gas Photoevaporation and Metallicity. Star-forming dwarf galaxies show large variations in their gas content because of the combined effects of stellar feedback from internal sources and IGM reheating. Ratios of gas to dark matter lie below the cosmic mean in halos with masses $M_{\rm dm} < 10^8\,{\rm M}_\odot$. Figure 4(a) shows the fraction of baryons retained by dark and luminous halos. It is clear that small mass luminous halos lose most of their gas before reionization due to internal radiation sources. Dark halos instead are able to retain gas for a longer time (see also [2]). Gas depletion increases with decreasing redshift: the lower-mass halos lose all their gas first but, as the universe evolves, larger halos with $M_{\rm dm} \sim 10^8\,{\rm M}_\odot$ also lose a large fraction of their gas. Gas photoevaporation reduces the metallicity of pre-reionization dwarfs to levels consistent with observations of dSph galaxies.

(5) Number of Luminous Galaxies. Only about 1% of dwarf dark matter halos with mass $M_{\rm dm} \sim 5 \times 10^6\,{\rm M}_\odot$, assembled prior to reionization, are able to form stars. The fraction of luminous halos scales with the halo mass as $F_{\rm lum} \propto M_{\rm dm}^2$. Thus, most halos with mass $\gtrsim 5 \times 10^7\,{\rm M}_\odot$ are luminous. Figure 4(b) shows $F_{\rm lum}$ as a function of the halo mass at redshifts $z = 12.5$ and $z = 10.2$. The figure also illustrated that f_* depends on the environment. Namely, it depends on the proximity of the pre-reionization dwarfs to other luminous galaxies. We find ∼450 dwarf galaxies per Mpc^3 with bolometric luminosity between 10^4 and $10^8\,{\rm L}_\odot$. The luminosity function is rather flat at low luminosities, with about 10 galaxies per Mpc^3 in the range $10^7 < L < 10^8\,{\rm L}_\odot$, and about 220 Mpc^{-3} in the ranges $10^4 < L < 10^5\,{\rm L}_\odot$ and $10^5 < L < 10^6\,{\rm L}_\odot$.

(6) Star Formation Efficiency and Mass-to-Light. The mean star formation efficiency $\langle f_* \rangle = \langle M_*/M_{\rm bar}^{\rm max} \rangle$, where $M_{\rm bar}^{\rm max} \simeq M_{\rm dm}/7$, is found to be *nearly independent of redshift* and to depend on total mass as $\langle f_* \rangle \propto M_{\rm dm}^\alpha$ with $\alpha = 2$ if the radiative feedback is strong (i.e., top heavy IMF and/or large $\langle f_{\rm esc} \rangle$) and $\alpha = 1.5$ if the feedback is weak. This is shown in Figure 5(a), where we plot the mean star formation efficiency, $\langle f_* \rangle$ and the mean gas fraction $\langle f_g \rangle$ in halos of mass $M_{\rm dm}$.

(7) Scatter of the Mass-to-Light Ratio. A tight relationship between the star formation efficiency f_* and the total mass of halos holds only for galaxies with $M_{\rm dm} > 5 \times 10^7\,{\rm M}_\odot$. In lower-mass halos, the scatter around the mean $\langle f_* \rangle$ is increasingly large (see Figure 5(b)). For a given halo mass, the galaxy can be without stars (dark galaxy) or have star formation efficiency $f_* \sim 0.1$. However, only a few dark galaxies with mass at formation $M_{\rm dm} \sim 1-5\times10^7\,{\rm M}_\odot$ should exist in the Local Group.

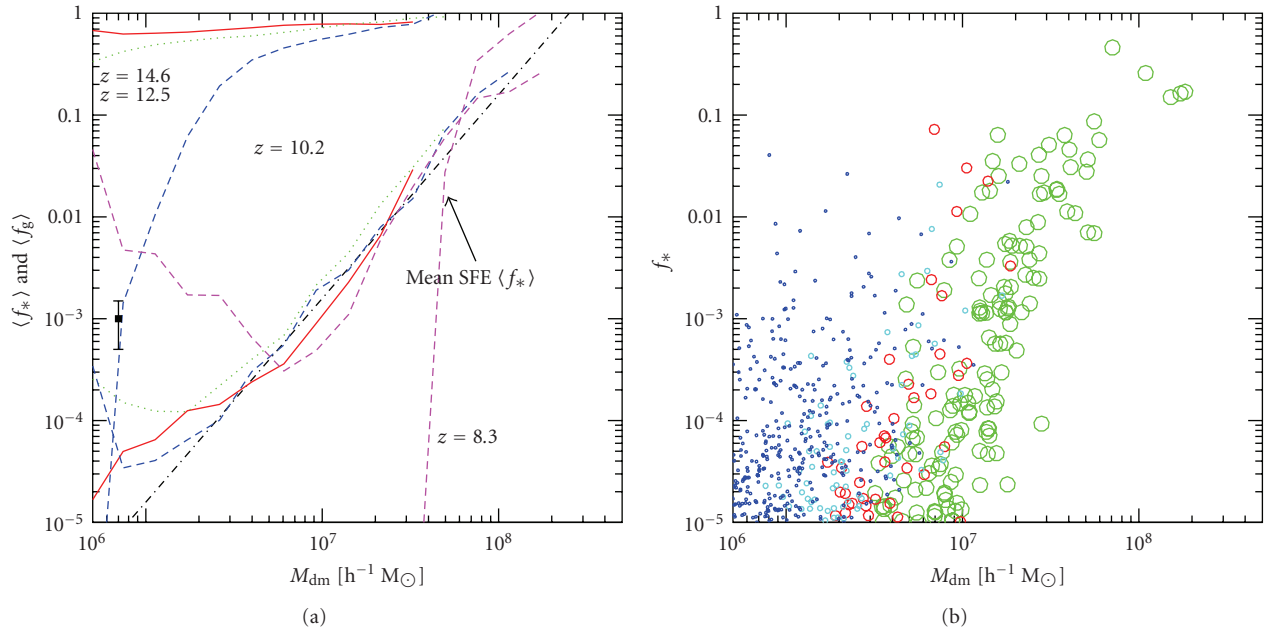

FIGURE 5: (a) Average star formation efficiency (i.e., fraction of the collapsed baryon mass converted into stars), $\langle f_* \rangle = \langle M_*/M_{\rm bar} \rangle$ (thick curves), and gas fraction (i.e., fraction of the collapsed baryon mass retained in the gas phase) $\langle f_{\rm g} \rangle = \langle M_{\rm g}/M_{\rm bar} \rangle$ (thin curves), of the first galaxies as a function of their halo mass for run S2 in RGS08 at $z = 14.5, 12.5, 10.2$, and 8.3. For comparison, the symbol with error bar shows the expected star formation efficiency (roughly $M_* \sim 30$–$300\,{\rm M}_\odot$ divided by the baryonic mass of the halo) in the first mini halo of mass $10^6\,{\rm M}_\odot$ simulated by Abel et al. [71]. The dot-dashed line shows a power-law fit for the mean SFE, $\langle f_* \rangle (M_{\rm dm}, z) \propto M_{\rm dm}^2$. The SFE is nearly independent of redshift apart from an increase in halos with $M_{\rm dm} < 10^7\,{\rm M}_\odot$ at $z \sim 8$. (b) Same as (a) but showing the star formation efficiency, f_*, for individual galaxies in the simulation at $z = 10.2$. Circles, from smaller to the larger, refer to galaxies with gas fractions $f_{\rm g} < 0.1\%$ (blue), $0.1\% < f_{\rm g} < 1\%$ (cyan), $1\% < f_{\rm g} < 10\%$ (red), and $f_{\rm g} > 10\%$ (green), respectively.

(8) Size and Morphology of Stellar Component. Galaxies with masses $M_{\rm dm} < 10^8\,{\rm M}_\odot$ have a low surface brightness and extended stellar spheroid. At $z \sim 10$, the outer edges of the stellar spheroid nearly reach the virial radius. In more massive galaxies that cool more efficiently by Lyman-alpha radiation, the stars and light are more centrally concentrated. Figure 6 shows the structural properties of the dark matter and stellar halo in three of the most massive galaxies in our simulation. These dwarf galaxies have properties similar to Draco and Umi dSphs. The figure also shows that the velocity dispersion of the stars in these dwarfs is about a factor of two smaller than $v_{\rm max}$.

3.1.5. Photoevaporation and Reionization Feedback. The small total mass of the first galaxies has two other implications. First, the ionizing radiation emitted by massive stars can blow out most of the gas before SN-driven winds become important, further reducing star formation rates (see RGS08). Second, the increase in temperature of the IGM to 10,000–20,000 K due to H I reionization prevents the gas from condensing into newly virialized halos with circular velocities smaller than 10–$20\,{\rm km\,s^{-1}}$ (e.g., [2, 27, 28, 35, 40, 86]). It follows that dwarf galaxies with $v_{\rm max} < 10$–$20\,{\rm km\,s^{-1}}$ lose most of their gas before reionization and stop accreting new gas and forming stars after reionization.

The value $v_{\rm max} \sim 20\,{\rm km\,s^{-1}}$ that we use to define a fossil is motivated by the fundamental differences in cooling and feedback processes discussed above that regulate star formation in the early universe. It is not the critical value for suppression of gas accretion due to reionization. Indeed, we discuss in Section 4 that pre-reionization fossils may have a late phase of gas accretion and star formation well after reionization, at redshift $z <$ 1-2. Thus, a complete suppression of star formation after reionization (about 12 Gyr ago) is not the defining property of a fossil dwarf.

4. Late Time Cold Accretion from the IGM

The ability of the IGM gas to condense at the center of dark halos depends on the ratio, $\Gamma = v_{\rm vir}/c_{\rm s,igm}$, of the circular velocity to the IGM sound speed and also on the dark halo concentration, c [3]. Typically, the concentration of a halo is $c_{\rm vir} \sim 4$ at the redshift of virialization [87, 88] but, as the halo evolves in the expanding universe, its concentration increases $\propto (1 + z_{\rm vir})/(1 + z)$. The evolution of the halo concentration with redshift can be understood in the context of the theory of cosmological secondary infall of dark matter [89] and has been quantified using N-body simulations [87, 88]. Thus, primordial halos with $v_{\rm vir} < 10$–$20\,{\rm km\,s^{-1}}$ stop accreting gas immediately after reionization, but, in virtue of their increasing concentration and the decreasing temperature of the IGM at $z < 3$ (after He II reionization), they may start accreting gas from the IGM at later times (see [3]). As a result, we expect that if the fossils of the first galaxies exist in

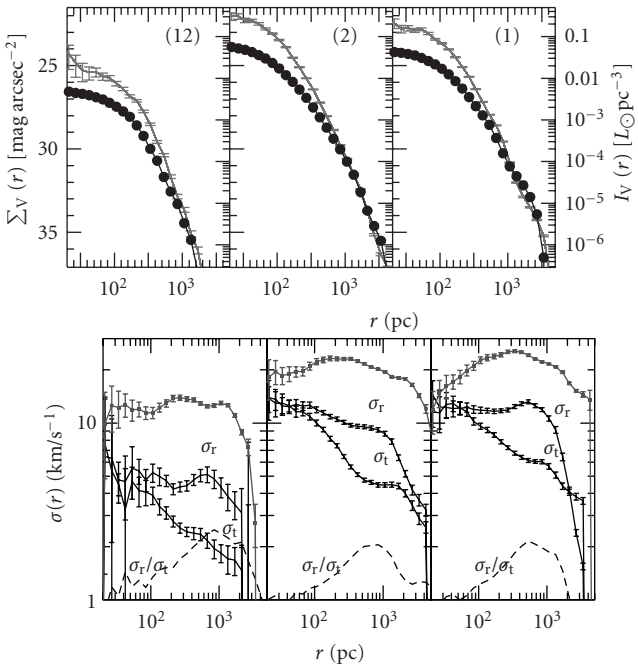

FIGURE 6: The top panels show the surface brightness (black point) and luminosity density (gray points) radial profiles for 3 galaxies from among the most massive dwarf galaxies extracted from the RG05 simulation at $z = 8.3$. We have evolved the stellar population passively to $z = 0$. The simulated galaxies shown in this figure have a stellar spheroid similar to Draco and Umi already in place at the time of formation (i.e., the spheroid is not produced by tidal effects). The bottom panels show the velocity dispersion profiles of the dark matter (gray points) and of the stars (black points) for the same 3 galaxies. The velocity dispersion of the stars is split in the radial and tangential components. All quantities are spherically averaged because the dark matter and stars have nearly spherical symmetry.

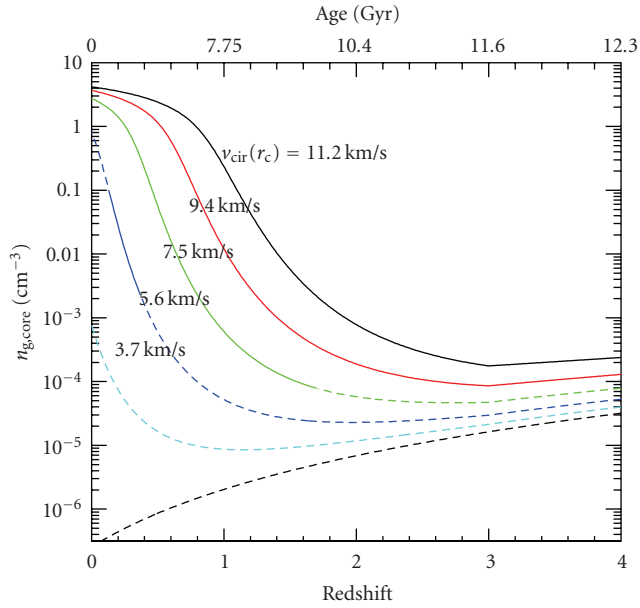

FIGURE 7: The evolution of the gas density in the core of dark halos due to cold accretion from the IGM for halos with $v_{vir} = 18, 15, 12, 9$ and 6 km s^{-1} (from the top to the bottom), and corresponding to the circular velocities at the core radius $v_{cir}(r_{core}) = 0.66 v_{vir}$ (shown by the labels). The curves are assuming isothermal equation of state of the gas but the dashed portions show the parameter space in which such assumption fails because the gas cannot cool sufficiently fast as it is compressed toward the center of the halo.

the Local Group (RG05), they may have a more complex star formation history than previously envisioned. A signature of this model is a bimodal star formation history with an old (~13 Gyr) and a younger ($\lesssim$ 5–10 Gyr, depending on the halo mass) population of stars. Leo T properties can be reproduced by this simple model for late gas accretion [3]. In addition, Leo T seems to show a bimodal star formation history [68] as expected in our model. Still, other models may also explain the observed star formation history of Leo T [90].

Perhaps more important is the possible existence of dark galaxies: small mass halos containing only gas but no stars. Dark galaxies are most likely to exist if pre-reionization fossils do not form efficiently due to dominant negative feedback in the early universe (e.g., H_2 photodissociation by the FUV background).

The late gas accretion from the IGM is shown in Figure 7 for dark halos with circular velocity at virialization $v_{vir} = 18, 15, 12, 9$ and 6 km s^{-1} (lines from the top to the bottom). The lines show the evolution of the gas density in the core of the halo as a function of redshift. The core radius is typically 100 pc and the labels show the circular velocity at the core radius ($v_{cir}(r_{core}) \approx 0.66 v_{vir} \approx 0.624 v_{max}$, where v_{vir} is circular velocities at the virial radius and v_{max} is the maximum circular velocity). We show the evolution of the gas density only for halos that are affected by reionization feedback. More massive halos will also accrete gas from the IGM as they evolve in isolation after virialization, but the gas accretion is continuous and not affected by reionization.

Under the scenario in which halos with masses smaller than the critical value of 10^8-10^9 $M_\odot$ remain dark due to feedback effects, the increase in their dark matter concentration and the temperature evolution of the IGM will produce a late phase of gas accretion at redshift $z < 1 - 2$. If the gas has very low metallicity or is metal free, it is unlikely that the accreted gas will be able to form stars in the smallest mass halos. This is why we envisioned the possible existence of dark galaxies. However, their mass would be smaller than the mass of any luminous galaxy and their discovery would be challenging.

The level of metal pre-enrichment necessary to initiate star formation in minihalos that experience a late phase of gas accretion can be roughly estimated from the cooling function from hyperfine transitions of oxygen and carbon: $\Lambda_{23} \sim 10^{-3}\ (Z/Z_\odot)$, where $\Lambda_{23} = 10^{-23}$ erg s^{-1} cm^3 and Z is the gas metallicity. A necessary condition for star formation is $t_{cool} \approx (0.7\,\mathrm{yr})\ T/(n_{g,core}\Lambda_{-23}) < t_H$, that can be written as $n_{g,core} > 0.03\,\mathrm{cm}^{-3}(Z/10^{-2}Z_\odot)^{-1}$. Figure 8(a) shows $n_{g,core}$ and N_H in minihalos that evolve isothermally at $T \sim 10^4$ K but that do not form stars (i.e., candidates for extragalactic

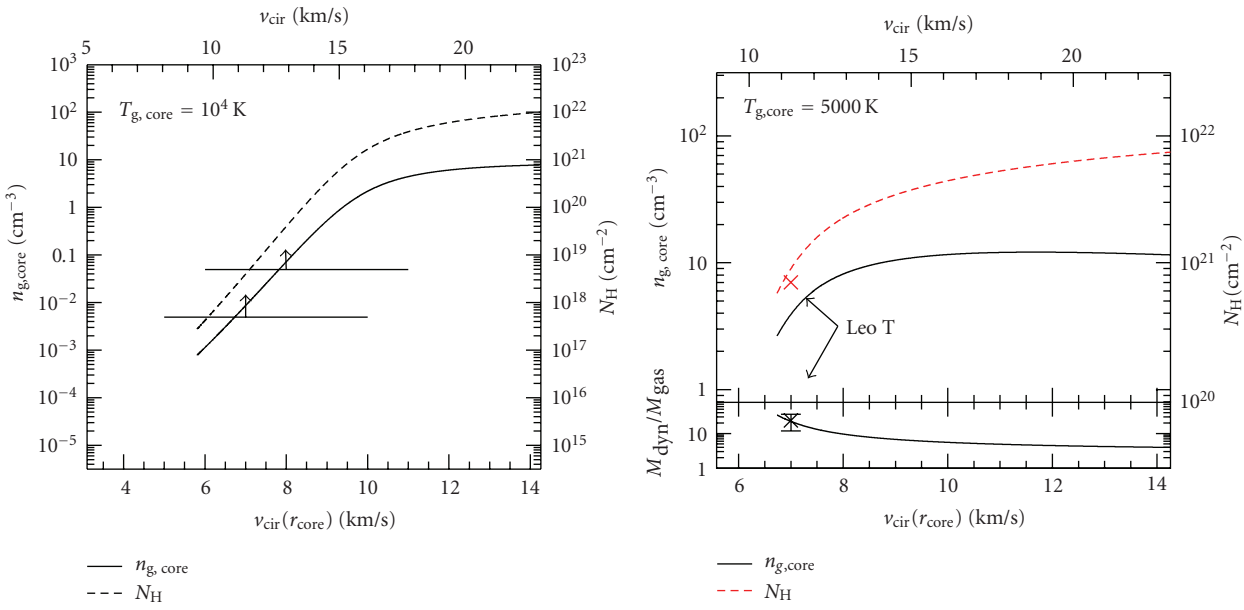

FIGURE 8: (a) The gas density, $n_{g,core}$ (solid curves), and hydrogen column density, $N_H = 2r_c n_{g,core}$ (dashed curves), within the core, r_c, of a minihalo at redshift $z = 0$ as a function its circular velocity at r_c. The minimum v_{cir} in each curve is determined by the condition $t_{rec}/t_H < 1$, necessary for cooling to $T_{gas} \sim 10^4$ K. The horizontal lines with arrows show the requirement for cooling to temperatures below 10^4 K, necessary for initiate star formation, for gas metallicity $Z = 0.1$ (lower line) and $0.01\,Z_\odot$ (higher line). (b) Same as (a) but for minihalos whose gas is able to cool to $T_{g,core} = 5000$ K due to metal pre-enrichment ($Z = 0.1\,Z_\odot$). These halos are likely able to sustain a multi-phase ISM and form stars.

CHVCs and dark galaxies). The horizontal lines show the requirement for metal cooling and star formation assuming gas metallicity $Z = 0.1$ and $0.01\,Z_\odot$. Figure 8(b) shows $n_{g,core}$, N_H and M_{dyn}/M_{gas} (the dynamical mass to gas mass ratio) in the core of minihalos that are able to cool to $T_{g,core} = 5000$ K (roughly the temperature of the ISM in Leo T), and thus form stars. The symbols show the observed value for Leo T.

5. Comparison of Theory and Observations

5.1. Number of Fossils and Nonfossil Satellites in the Milky Way. N-body simulations can be used to estimate the number of dark halos in the Milky Way with maximum circular velocity $v_{max} > 20\,km\,s^{-1}$. However, there is a complication to this naive calculation. A significant fraction of dark halos that today have $v_{max} < 20\,km\,s^{-1}$ were once more massive, due to tidal stripping [91]. According to our definition, dwarf galaxies formed in these dark halos would not be pre-reionization fossils if they had at any time during their evolution $v_{max}(t) > 20\,km\,s^{-1}$ (see Section 3.1.5). If the number of observed Milky Way satellites exceeds the estimated number of these massive halos we must conclude that at least a fraction of the observed Milky Way satellites are pre-reionization fossils.

However, there is an assumption in this scenario. One must assume that the stars in these halos survive tidal stripping for as long as the dark matter. In this case tidally stripped halos may indeed account for a fraction or all of the newly discovered ultrafaint dwarfs. However, Peñarrubia et al. [60] find that tidally stripped dark halos lose their stars more rapidly than they lose their dark matter. Thus, they may become dark halos even though they were initially luminous satellites. These dark halos should not be counted as ultrafaint dwarfs.

Using results of published N-body simulations of the Milky Way, Bovill and Ricotti [51] have estimated the number of dark halos that have or had in the past $v_{max}(t) > 20\,km\,s^{-1}$ (i.e., non pre-reionization fossils). In Table 1 we summarize the results of the counts for dark matter and luminous satellites for two large N-body simulations of a Milky Way type halo: the "Aquarius" simulation [92] and the Via Lactea I simulation [93].

The number of luminous satellites that exist within the Milky Way is highly uncertain beyond a distance from the Galactic center of 200 kpc. Tollerud et al. [25], after applying incompleteness corrections, estimated 304–576 satellites within 417 kpc and about 176–330 within 200 kpc (the numbers are from their Table 3). As shown in Table 1, the existence of some pre-reionization fossils among the ultrafaint dwarfs appears to be favored by the data. However, the current uncertainties on the completeness corrections of observations and on the simulations are too large to deem the existence of fossils as necessary.

The error bars on the theoretical estimate of the number of fossils in the Milky Way shown in Table 1 come from uncertainties in the fraction of halos that were more massive in the past. This fraction was derived from simulations by [91]. Another uncertainty in the simulation results can

Table 1: Number of observed satellites versus number of dark halos with $v_{max}(t) > 20\,km\,s^{-1}$ (i.e., non pre-reionization fossils) for the Milky Way.

Distance from center	Luminous dwarfs	Dark halos with $v_{max}(t) > 20\,km\,s^{-1}$ via			
		Lactea I sim.		Aquarius sim.	
		Today	Any time	Today	Any time
<200 kpc	176 to 330	14	36 ± 8	34	91 ± 20
<417 kpc	304 to 576	28	73 ± 16	69	182 ± 40

be attributed to the different predictions for the number of Milky Way satellites in the Via Lactea I and II and Aquarius simulations. The discrepancy can be partially attributed to different cosmology in the simulations but mostly because the Via Lactea I simulation likely used erroneous initial conditions. Finally, Tollerud et al. [25] corrections on the number of observed satellites also rely on the radial distribution of dark matter sub halos extracted from Via Lactea I simulations that may be erroneous. Once the discrepancies among different simulations are better understood the number of simulated satellites of the Milky Way may be known with greater certainty.

Using comparisons between the predicted and observed Galactocentric distributions of dwarf satellites around the Milky Way, Gnedin and Kravtsov [94], hereafter GK06, have estimated that pre-reionization fossils may constitute about 1/3 of Milky Way dwarfs. GK06 estimated the number of fossils in the Milky Way using data from the simulations of the first galaxies in RG05. GK06 defined a fossil as a simulated halo which survives at $z = 0$ and remains below the critical circular velocity of $20\,km\,s^{-1}$ with no appreciable tidal stripping (the usual definition of fossil adopted in this paper as well). They calculate the probability, $P_S(v_{max}, r)$, of a luminous halo with a given maximum circular velocity v_{max} to survive from $z = 8$ (the final redshift of the RG05 simulation) to $z = 0$. The surviving halos are assigned a luminosity based on the L_V versus v_{max} relationship from RG05. At $z = 0$, GK06 has a population of dwarf galaxies with a resolution limit of $v_{max} = 13\,km\,s^{-1}$. This limit corresponds to a lower luminosity limit of $L_V \sim 10^5\,L_\odot$, which includes Leo T and Canes Venatici I, but excludes all the other new ultrafaint Milky Way satellites.

In Figure 9, we show the cumulative luminosity function from GK06 for the Milky Way and M31 satellites. Figure 9(c) shows satellites with distance from their host $d < 100\,kpc$, Figure 9(b) $d < 300\,kpc$, and Figure 9(a) $d < 1\,Mpc$. The gray lines show the GK06 predictions, and the shaded region encompasses the error bars. The resolution limits in GK06 cause halos with $v_{max} < 17\,km\,s^{-1}$ to be preferentially destroyed by tidal effects. The dashed line show the predicted luminosity function corrected for the resolution effects. Both the uncorrected (solid lines) and corrected (dashed lines) luminosity functions are plotted in Figure 9(c). The points with error bars show the observed luminosity function of dSph galaxies around the Milky Way and M31 corrected only for limits in sky coverage of the SDSS survey. The plot is from GK06 but has been updated to include the new ultrafaint dwarfs with $L_V \gtrsim 10^5\,L_\odot$.

The results of this model are consistent with the observations. The model reproduces the Galactocentric distribution of the most luminous dSphs, even though in this model dSphs are not tidally stripped dIrrs. It also shows a good agreement with observations for luminosities that can be considered nearly complete within a given Galactocentric distance.

5.2. Statistical Properties of Pre-Reionization Fossils. In this section, we compare the properties of the new dwarf galaxies discovered in the Local Group to the theoretical predictions of simulations of primordial galaxies formed before reionization. The argument that justifies this comparison is that star formation stops or is greatly reduced after reionization (but see Section 4). We do not expect two perfectly distinct populations of fossil galaxies with $v_{max} < 20\,km\,s^{-1}$ and nonfossils with $v_{max} \geq 20\,km\,s^{-1}$, but a gradual transition of properties from one population to the other. Some fossils may become more massive than $v_{max} \sim 20\,km\,s^{-1}$ after reionization, accrete some gas from the IGM, and form a younger stellar population. These dwarfs are no longer defined as "fossils". However, if the dark halo circular velocity remains close to $20\,km\,s^{-1}$ the young stellar population is likely to be small with respect to the old one. In RG05 we call these galaxies "polluted fossils" because they have the same basic properties of "fossils" with a sub-dominant young stellar population. A similar argument can be made regarding the late phase of gas accretion that may produce objects similar to Leo T.

In Figures 10 and 11, we compare the RG05 predictions for the fossils of primordial galaxies to the observed properties of the new Milky Way and M31 dwarfs. The symbols and lines in Figures 10 and 11 have the following meanings. All known Milky Way dSphs are shown by circles; Andromeda's dSphs satellites are shown by triangles; simulated fossils are shown by the small solid squares. The solid and open symbols refer to previously known and new dSphs, respectively. The transition between fossils and nonfossil galaxies is gradual. In order to illustrate the different statistical trends of "nonfossil" galaxies we show dwarf irregulars (dIrr) as asterisks and the dwarf ellipticals (dEs) as crosses, and we show the statistical trends for more luminous galaxies as thick dashed lines on the right side of each panel.

Figure 10(a) shows how the surface brightness (top panel) and half light radius (bottom panel) of all known Milky Way and Andromeda satellites as a function of V-band luminosity compares to the simulated fossils. The surface

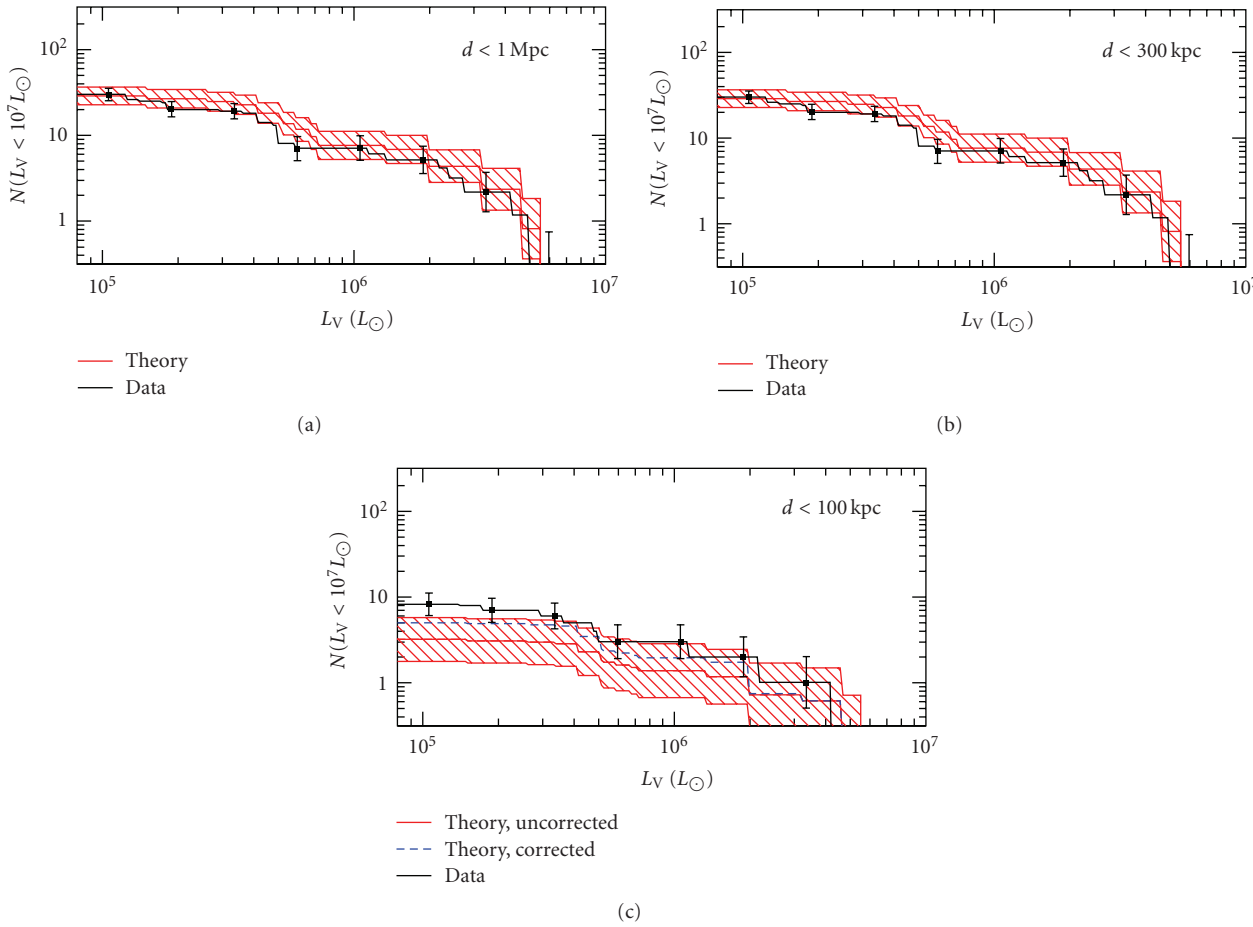

FIGURE 9: Luminosity function of pre-reionization fossil dwarfs predicted in GK06 (red bands) plotted with the luminosity function for Local Group dSphs (points with error bars). The data from observations are corrected only for limits in sky coverage of the SDSS survey.

brightness limit of the SDSS is shown by the thin solid lines in both panels of the figure. The new dwarfs agree with the predictions up to this threshold, suggesting the possible existence of an undetected population of dwarfs with Σ_V below the SDSS sensitivity limit. The new M31 satellites have properties similar to their previously known Milky Way counterparts (e.g., Ursa Minor and Draco). Given the similar host masses and environments, further assuming similar formation histories for the halos of M31 and the Milky Way, we may be tempted to speculate on the existence of an undiscovered population of dwarfs orbiting M31 equivalent to the new SDSS dwarfs.

The large mass outflows due to photo-heating by massive stars and the subsequent suppression of star formation after an initial burst make reionization fossils among the most dark matter dominated objects in the universe, with predicted mass-to-light ratios as high as 10^4 and $L_V \sim 10^3$–10^4 $L_\odot$. Figure 10(b) shows the velocity dispersion (bottom panel) and mass-to-light ratios, M_σ/L_V (top panel), as a function of V-band luminosity of the new and old dwarfs from observations in comparison to simulated fossils. The symbols are the same as in the previous figures. Theoretical and observed dynamical masses are calculated from the velocity dispersions of stars (i.e., $M_\sigma = 2r_{1/2}\sigma^2/G$), and do not necessarily reflect the total mass of the dark halo at virialization.

Observations show that the value of the dynamical mass within the stellar spheroid, $M \sim (1 \pm 5) \times 10^7$ $M_\odot$, remains relatively constant as a function of L_V [58]. Recent work by Strigari et al. [97] shows analogous results to the one found by Mateo [58]. The dynamical mass of dwarf spheroidals within a radius of 300 pc is relatively constant: $M \sim 10^7$ $M_\odot$. The radii of the stellar spheroids in these dwarf galaxies may be either larger or smaller than 300 pc. In the later case, the determination of the mass of the dwarfs is uncertain.

Our simulation provides some insight into the reason why the dynamical mass remains roughly constant in dSphs. The simulations show that in pre-reionization dwarfs, the ratio of the radius of the stellar spheroid to the virial radius of the dark halo decreases with increasing dark halo mass (i.e., the stellar profile becomes more concentrated for more luminous dwarfs). Thus, as the halo mass and virial radius increases, the stellar spheroid becomes increasingly concentrated in the deepest part of the potential well. If follows that the ratio, $f_\sigma \equiv M_\sigma/M_{\rm dm}$, of the dynamical mass within the largest stellar orbits to total dark matter mass is

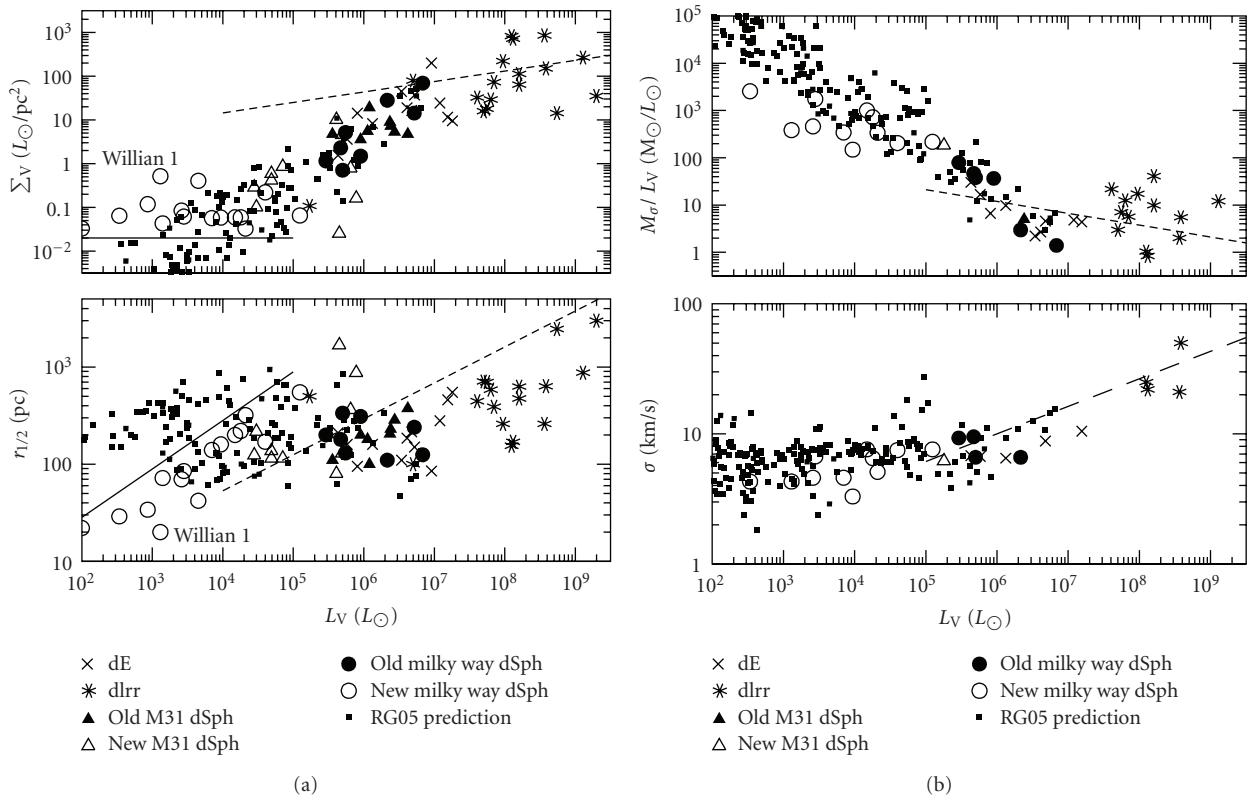

Figure 10: (a) Surface brightness and core radius versus. V-band luminosities. Small filled squares are simulated pre-reionization fossils from RG05, asterisks are dIrrs, crosses are dEs, closed circles are the previously known dSph around the Milky Way, closed triangles are previously known dSph around M31, and open circles and triangles are new dSph around the Milky Way and M31 respectively. The solid lines roughly show the detection limits inherent to the methods used to find the ultrafaints in the SDSS data [24] and the dashed lines show the scaling relationships for more luminous Sc-Im galaxies ($10^8 L_\odot \lesssim L_B \lesssim 10^{11} L_\odot$) derived by Kormendy and Freeman [95]. (b) Mass-to-light ratio and velocity dispersion of a subset of the new dwarfs [23, 96] versus V-band luminosity. The symbols and lines are as in (a).

also reduced. Thus, the decrease of f_σ for increasing dark matter mass of halos maintains the value of the dynamical mass $M_\sigma = f_\sigma M_{\rm dm}$ (measured by the velocity dispersion of the stars) almost constant, even though the total mass of the halo increases. The extent of the stellar spheroids in the lowest mass dwarfs is comparable in size to their virial radii at formation (see Section 3.1).

The metallicity-luminosity relation of the observed and simulated dwarfs is shown in Figure 11(a). [Fe/H] is plotted against V-band luminosity in solar units. Symbols for the previously known dwarfs, the new, ultrafaint dwarfs, and simulated fossils are the same as in Figure 10. In this plot we color code simulated fossils according to their star formation efficiency, f_*. Red symbols show simulated dwarfs with $f_* < 0.003$, blue $0.003 \leq f_* \leq 0.03$ and green $f_* > 0.03$.

Using the data for the metallicity collected in Bovill and Ricotti [51], the new ultrafaint dwarfs do not appear to follow the tight luminosity-metallicity relationship observed in more luminous galaxies (although error bars are large). Note that here, as well as in Bovill and Ricotti [51] (although Table 3 in that paper was erroneously not updated), we have plotted data from Kirby et al. [98] for the 6 ultrafaint Milky Way satellites provided in that paper. There are several physical mechanisms that may produce the observed scatter in metallicities of dwarfs at a given constant luminosity. The large spread of star formation efficiencies producing a dwarf of a given luminosity in our simulations is responsible for at least part of the large spread of the luminosity-metallicity relation. At this point it is unclear whether our simulations can reproduce the scatter of metallicities of simulated fossils, or if perhaps the luminosity of the lowest luminosity ultrafaint dwarfs has been reduced due to tidal interactions. As mentioned before we have suggested that the lowest luminosity ultrafaint dwarfs have not yet been discovered because their surface brightness lies below the SDSS detection limits.

Figure 11(b) shows the scatter of the metallicity of the stars, $\sigma_{\rm [Fe/H]}$, plotted against V-band luminosity and [Fe/H] respectively. The various point types and colors are the same used in Figure 11(a). The large spread in the metallicity of the stars is a natural consequence of the hierarchical assembly of dwarf galaxies in cosmological simulations. It is not necessarily an indication that star formation in dwarf satellites was protracted for longer than 1 Gyr, as argued in Grebel and Gallagher III [99] to prove that star formation in dwarf spheroidals is not stopped by reionization feedback.

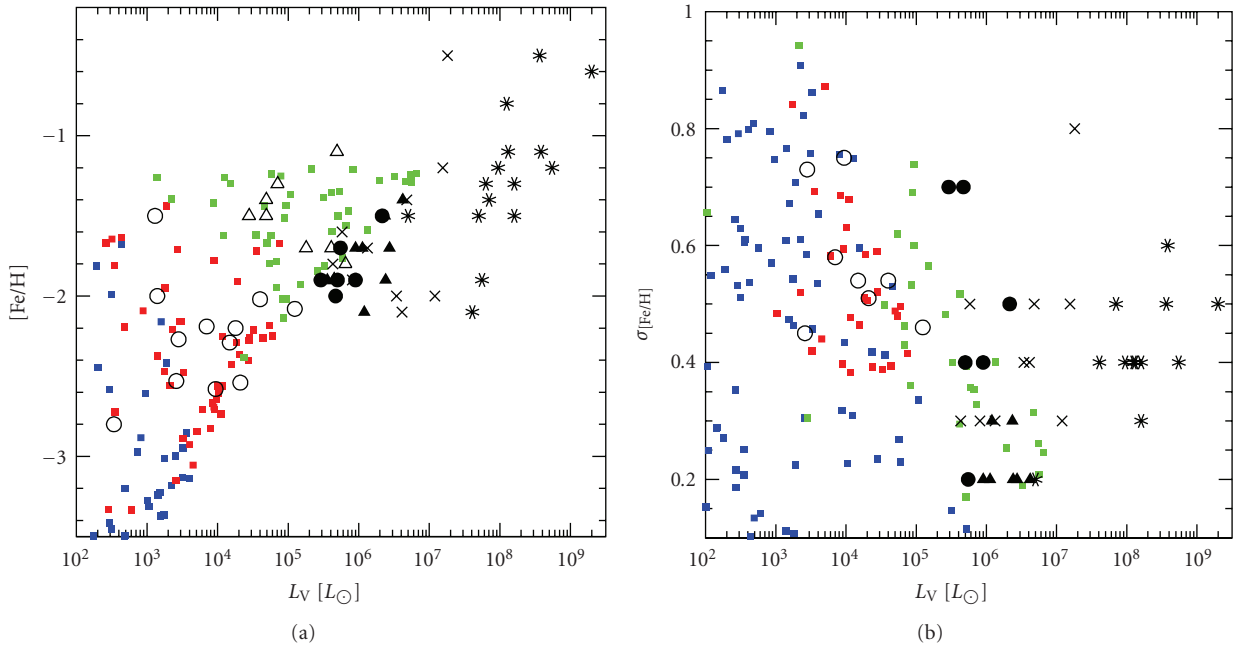

Figure 11: (a) Mean metallicity of the stars versus. V-band luminosity for Local Group dSphs plotted against RG05 predictions. They symbols have the same meaning as in Figure 8. In this plot simulated fossils (shown as small squares) are color coded according to their star formation efficiency, f_*: red symbols show simulated dwarfs with $f_* < 0.003$, blue $0.003 \leq f_* \leq 0.03$ and green $f_* > 0.03$. (b) Same as (a) but showing the spread of the stellar metallicities in each dwarf (i.e., variance of the metallicity distribution) versus. their V-band luminosity.

6. Discussion: The Tidal Scenario versus Fossil Hypothesis

According to the results summarized above in Table 1, the number of dark matter satellites of the Milky Way that have or had in the past $v_{\max} > 20\,\mathrm{km\,s^{-1}}$ is smaller than the number of observed luminous satellites (after applying completeness corrections). This implies that nonfossil galaxies cannot account for all the observed satellites. Thus, pre-reionization fossils should exist.

However, we have already discussed the several uncertainties in estimating the numbers summarized in Table 1. Additional uncertainties that render the identification of fossils uncertain are the following. The mass and circular velocity of the dark matter halo of the Milky Way are not known precisely. Simulations should take into account the effect of baryons in modifying the density profile and the radial distribution of satellites. The effect of tidal stripping on the properties of the stars in the satellites is not well understood, thus we do not know if the tidal scenario is consistent with observations of ultrafaint dwarfs. The luminosity and stellar properties of nonfossil dwarf satellites are not known.

Nonfossil galaxies with $v_{\max} > 20\,\mathrm{km\,s^{-1}}$ may lose a substantial fraction of their mass due to tidal interactions. If they survive the interaction, their properties, such as surface brightness and half light radius, may be modified. Kravtsov et al. [91] estimate that about 10% of Milky Way dark matter satellites were at least ten times more massive at their formation than they are today. Although their simulation does not include stars, they favor the idea that the stellar properties of these halos would remain unchanged (i.e., dSphs are not tidally stripped dIrr). In their model the majority of brighter dwarf satellites have been considerably more massive in the past and could have formed their stars undisturbed after reionization. More precisely, the redshift of reionization does not affect the results of their model for classic dwarfs because the probability of these to be fossils is low.

This version of the tidal model may be hard to distinguish observationally from the model we propose for the fossils because in both models the properties of the dwarfs are not modified by tidal forces (i.e., their properties are those at formation). In addition, fossil dwarfs may stop forming stars for only about 2 to 4 Gyr after reionization, before starting to accrete gas again from the IGM. Thus, reionization may imprint a bimodal star formation history in some fossils, but this signature is not a robust discriminant because the star formation history of dwarfs cannot be determined with sufficient accuracy.

Observations seem to suggest that star formation in dwarf galaxies slightly more massive than 10^8-10^9 $M_\odot$ may be similar to star formation in fossils and thus fit the observed properties of classical dSphs without requiring significant tidal stripping of stars. If star formation was included in Kravtsov et al. [91], their model may have reproduced the properties of observed dwarf satellites that our simulations of pre-reionization dwarf galaxies already does. The differences between the two models will depend on whether fossil galaxies are allowed to form and on their properties.

In other words, the two models may differ on the assumed mass of the smallest dark halo that can host luminous satellites. This critical mass cannot be directly observed in dwarf galaxies but, in principle, can be constrained by comparing the observed number of luminous satellites to the model predictions. Determining the minimum mass for a dark halo to become luminous is of great importance in understanding galaxy formation in the early universe.

To summarize, there are a few observational tests that can be used to distinguish true fossils from dSphs or dEs that form in more massive halos and form stars unaffected by IGM reionization. True fossils should have either a single old stellar population or have a bimodal star formation history produced by a temporary suppression of star formation after reionization and late gas accretion. In addition, if the number of observed Milky Way satellites (or the number of isolated dwarfs) exceeds some critical value determined using N-body simulations (e.g., see Table 1), we may conclude that some pre-reionization fossils do exist in the Local Group.

It is likely that these tests will prove inconclusive for some time to come, unless the number (after corrections for completeness) of new ultrafaint galaxies surges in the coming years. The weakness of the star formation history test is that it requires measurements with precision of 1-2 Gyr of the stellar populations in order to be really discriminating between models that are quite similar to each other. This is hard to achieve especially for ultrafaint dwarfs with few stars. If the number of ultrafaint dwarfs remains about the same as today, the number argument may also remain controversial until more detailed theoretical modeling can reduce the current uncertainties surrounding the expected number of dark halos in the Milky Way and the completeness corrections of the observations. Ultimately, the case for the origin of ultrafaint dwarfs must be made on the basis of the model that does the best job of reproducing available observations.

Finally, even if pre-reionization fossils do not exist (i.e., halos with $v_{\max} < 20\,\mathrm{km\,s^{-1}}$ are all dark), a fraction of them should be able to accrete some gas at redshift $z < 1-2$ and might be discoverable in the outer parts of the Local Group using Hα or 21 cm surveys (e.g., ALFALFA survey [100, 101]). Of course, one should prove that the gas clouds are embedded in dark halos. Measurements of the gas cloud size, column density, and velocity broadening of the emission/absorption lines can be used to discriminate between "dark galaxies" and tidal debris. This is because the gas in dark galaxies is confined by the gravitational potential of the dark matter halo, while tidal debris or clouds formed via thermal instability are confined by the external gas pressure [3]. This is another promising direction for determining the minimum mass of luminous galaxies in the universe.

Another variant of the tidal hypothesis for the origin of dSphs is a scenario in which dIrr galaxies transform into dSphs as they fall into the Milky Way and Andromeda, due to tidal and ram pressure stripping [59, 102]. A work by Peñarrubia et al. [60] explores the idea that ultrafaint dSphs are tidally stripped dIrrs. They achieve some success in reproducing observed properties of ultrafaint dwarfs. While this type of tidal stripping can reproduce properties of an individual galaxy, it is unable to completely reproduce all the trends in the ultrafaint population. This is primarily seen in the kinematics of the ultrafaint dwarfs. Tidal stripping predicts a steeper than observed drop in the velocity dispersion of the stars with decreasing L_V [60]. In addition several dSph do not show signs of strong tidal stripping. And XII and And XIV may be on their first approach to the Local Group [22, 103]. Other examples of dSphs that are found distant from the center of their host galaxies are And XVIII, Cetus and Tucana [104].

Finally, another interesting case study is Leo T, that we have discussed extensively above in Sections 2.2 and 4. Leo T properties can be explained in some detail as being a fossil that experienced a late phase of gas accretion [3]. However, another possibility that should be explored quantitatively with simulations is that Leo T is more massive than a fossil but less massive than dIrr galaxies.

7. Conclusions and Future Work

We have summarized our work on the formation of the first galaxies before reionization (i.e., pre-reionization dwarfs) and the quest to identify the fossils of these first galaxies in the Local Group. The definition of a pre-reionization fossil is not directly related to the suppression of star formation experienced by these galaxies due to reionization feedback. Indeed, we discussed how pre-reionization fossils may experience a late phase of gas accretion and possibly star formation at redshift $z < 1-2$. Most importantly, fossils are a population of dwarf galaxies whose formation (i.e., the fraction of halos that are luminous) is self-regulated on cosmological distance scales by radiative processes. Their existence is not certain due to a possible strong negative feedback that may prevent the majority of these halos from ever forming stars. In addition, if negative feedback heavily suppresses the number and luminosity of these first galaxies, more massive halos with $v_{\max} > 20\,\mathrm{km\,s^{-1}}$ will evolve differently because of the lower level of metal pre-enrichment of the IGM. To summarize, the critical circular velocity $v_{\max} \sim 20\,\mathrm{km\,s^{-1}}$ that we adopt to define a fossil is primarily motivated by fundamental differences in cooling and feedback processes that regulate star formation in these halos in the early universe. However, it is also close to the critical value for continued gas accretion after IGM reionization [2, 40, 86].

The number of Milky Way and M31 satellites provides an indirect test of galaxy formation and the importance of positive and negative feedback in the early universe. This test, although the uncertainties are large, supports the idea that a fraction of the new ultrafaint dwarfs are fossils. The good agreement of the SDSS and new M31 ultrafaint dwarf properties with predictions of our simulations (RG05, GK06, [51]) does not prove the primordial origin of the new ultrafaint dwarfs, but it supports this possibility.

More theoretical work and more observational data are needed to prove that some dwarfs in the Local Group are true fossils of the first galaxies. Future theoretical work should focus on improving the accuracy of predictions on

the properties of dwarf galaxies formed before reionization and their evolution to the present day. Modeling the evolution of the baryonic component after reionization in dwarf satellites and in the Milky Way—Andromeda system may be necessary to make robust predictions. More observational data will certainly be available in the near future. A large number of surveys, both at optical and radio wavelengths will be online in the near future (e.g., *Pan-STARRS, LSST, ALMA, EVLA, JWST, SKA* to mention a few). Different survey strategies may be used to find and characterize fossil dwarf galaxies. A deep pencil beam survey would be useful to find the faintest dwarf satellites of the Milky Way and determine more precisely their Galactocentric distribution. A willower all sky survey could be used to quantify the degree of anisotropy in the distribution of satellites around the Milky Way.

The star formation history of the dwarf galaxies is not strongly discriminatory because fossil galaxies may have a late phase of gas accretion and star formation during the last 9-10 Gyrs [3]. The distinction between fossils and nonfossil galaxies may be quite elusive but it is nevertheless important to understand galaxy formation and feedback in the early universe. Arguments based on counting the number of dwarfs in the Local universe are among the more solid arguments that could be used to prove the existence of fossil galaxies (see Table 1).

Future tests may be provided by deep surveys looking for ultrafaint galaxies in the local voids or looking for gas in dark galaxies (i.e., dark halos that have been able to accrete gas from the IGM at $z < 1 - 2$). Ultra-faint dwarfs should be present in the voids if dwarf galaxies formed in large numbers before reionization (Bovill & Ricotti, in preparation). If pre-reionization dwarfs never formed due to dominant negative feedback in the early universe, it is possible that a faint (in Hα and 21 cm emission) population of dark galaxies exists in the outer parts of the Local Group. Hence, another way to detect fossil galaxies in the outer parts of the Milky Way or outside the super-galactic plane would be to search for neutral or ionized gas that they may have accreted from the IGM. Future radio telescopes (e.g., *ALMA, EVLA, SKA*) may be able to detect neutral hydrogen in dark galaxies or in ultrafaint dwarfs. Ionized gas in the outer parts of dark halos may be observed in absorption along the line of sight of distant quasars (e.g., in O VI or O IV with *COS* on the *HST*). However, the probability that a line of sight toward a quasar intersects the ionized gas collected from the IGM by dark or fossil galaxies might be small. Additional theoretical work is required to address these issues.

References

[1] N. Y. Gnedin and J. P. Ostriker, "Reionization of the universe and the early production of metals," *The Astrophysical Journal*, vol. 486, no. 2, pp. 581–598, 1997.

[2] M. Hoeft, G. Yepes, S. Gottlöber, and V. Springel, "Dwarf galaxies in voids: suppressing star formation with photoheating," *Monthly Notices of the Royal Astronomical Society*, vol. 371, no. 1, pp. 401–414, 2006.

[3] M. Ricotti, "Late gas accretion on to primordial minihaloes: a model for Leo T, dark galaxies and extragalactic high-velocity clouds," *Monthly Notices of the Royal Astronomical Society*, vol. 392, pp. L45–L49, 2009.

[4] A. Klypin, A. V. Kravtsov, O. Valenzuela, and F. Prada, "Where are the missing galactic satellites?" *The Astrophysical Journal*, vol. 522, no. 1, pp. 82–92, 1999.

[5] B. Moore, T. Quinn, F. Governato, J. Stadel, and G. Lake, "Cold collapse and the core catastrophe," *Monthly Notices of the Royal Astronomical Society*, vol. 310, no. 4, pp. 1147–1152, 1999.

[6] I. D. Karachentsev, V. E. Karachentseva, W. K. Huchtmeier, and D. I. Makarov, "A catalog of neighboring galaxies," *The Astronomical Journal*, vol. 127, no. 4, pp. 2031–2068, 2004.

[7] I. D. Karachentsev, A. Dolphin, R. B. Tully, et al., "Advanced camera for surveys imaging of 25 galaxies in nearby groups and in the field," *The Astronomical Journal*, vol. 131, no. 3, pp. 1361–1376, 2006.

[8] R. B. Tully, L. Rizzi, A. E. Dolphin, et al., "Associations of dwarf galaxies," *Astronomical Journal*, vol. 132, no. 2, pp. 729–748, 2006.

[9] J. L. Tinker and C. Conroy, "The void phenomenon explained," *The Astrophysical Journal*, vol. 691, pp. 633–639, 2009.

[10] P. Bode, J. P. Ostriker, and N. Turok, "Halo formation in warm dark matter models," *The Astrophysical Journal*, vol. 556, no. 1, pp. 93–107, 2001.

[11] Z. Haiman, T. Abel, and M. J. Rees, "The radiative feedback of the first cosmological objects," *The Astrophysical Journal*, vol. 534, no. 1, pp. 11–24, 2000.

[12] V. Belokurov, D. B. Zucker, N. W. Evans, et al., "A faint new Milky Way satellite in bootes," *The Astrophysical Journal*, vol. 647, no. 2, pp. L111–L114, 2006.

[13] V. Belokurov, D. B. Zucker, N. W. Evans, et al., "Cats and dogs, hair and a hero: a quintet of new Milky Way companions," *The Astrophysical Journal*, vol. 654, no. 2, pp. 897–906, 2007.

[14] M. J. Irwin, V. Belokurov, N. W. Evans, et al., "Discovery of an unusual dwarf galaxy in the outskirts of the Milky Way," *The Astrophysical Journal*, vol. 656, no. 1, pp. L13–L16, 2007.

[15] S. M. Walsh, H. Jerjen, and B. Willman, "A pair of boötes: a new Milky Way satellite," *The Astrophysical Journal*, vol. 662, no. 2, pp. L83–L86, 2007.

[16] B. Willman, J. J. Dalcanton, D. Martinez-Delgado, et al., "A new Milky Way dwarf galaxy in URSA major," *The Astrophysical Journal*, vol. 626, no. 2, pp. L85–L88, 2005.

[17] B. Willman, M. R. Blanton, A. A. West, et al., "A new Milky Way companion: Unusual globular cluster or extreme dwarf satellite?" *The Astronomical Journal*, vol. 129, no. 6, pp. 2692–2700, 2005.

[18] D. B. Zucker, V. Belokurov, N. W. Evans, et al., "A new Milky Way dwarf satellite in canes venatici," *The Astrophysical Journal*, vol. 643, no. 2, pp. L103–L106, 2006.

[19] D. B. Zucker, V. Belokurov, N. W. Evans, et al., "A curious Milky Way satellite in Ursa Major," *The Astrophysical Journal*, vol. 650, no. 1, pp. L41–L44, 2006.

[20] R. Ibata, N. F. Martin, M. Irwin, et al., "The haunted halos of andromeda and triangulumml: a panorama of galaxy formation in action," *The Astrophysical Journal*, vol. 671, no. 2, pp. 1591–1623, 2007.

[21] S. R. Majewski, R. L. Beaton, R. J. Patterson, et al., "Discovery of andromeda XIV: a dwarf spheroidal dynamical rogue in the local group?" *The Astrophysical Journal*, vol. 670, no. 1, pp. L9–L12, 2007.

[22] N. F. Martin, R. A. Ibata, M. J. Irwin, et al., "Discovery and analysis of three faint dwarf galaxies and a globular cluster in

the outer halo of the Andromeda galaxy," *Monthly Notices of the Royal Astronomical Society*, vol. 371, no. 4, pp. 1983–1991, 2006.

[23] J. D. Simon and M. Geha, "The kinematics of the ultra-faint Milky Way satellites: solving the missing satellite problem," *The Astrophysical Journal*, vol. 670, no. 1, pp. 313–331, 2007.

[24] S. Koposov, V. Belokurov, N. W. Evans, et al., "The luminosity function of the Milky Way satellites," *The Astrophysical Journal*, vol. 686, no. 1, pp. 279–291, 2008.

[25] E. J. Tollerud, J. S. Bullock, L. E. Strigari, and B. Willman, "Hundreds of Milky Way satellites? Luminosity bias in the satellite luminosity function," *The Astrophysical Journal*, vol. 688, no. 1, pp. 277–289, 2008.

[26] M. Geha, B. Willman, J. D. Simon, et al., "The least-luminous galaxy: spectroscopy of the Milky Way satellite segue 1," *The Astrophysical Journal*, vol. 692, no. 2, pp. 1464–1475, 2009.

[27] A. Babul and M. J. Rees, "On dwarf elliptical galaxies and the faint blue counts," *Monthly Notices of the Royal Astronomical Society*, vol. 255, pp. 346–350, 1992.

[28] G. Efstathiou, "Suppressing the formation of dwarf galaxies via photoionization," *Monthly Notices of the Royal Astronomical Society*, vol. 256, no. 2, pp. 43P–47P, 1992.

[29] P. R. Shapiro, M. L. Giroux, and A. Babul, "Reionization in a cold dark matter universe: the feedback of galaxy formation on the intergalactic medium," *The Astrophysical Journal*, vol. 427, no. 1, pp. 25–50, 1994.

[30] Z. Haiman, M. J. Rees, and A. Loeb, "H_2 cooling of primordial gas triggered by UV irradiation," *The Astrophysical Journal*, vol. 467, no. 2, pp. 522–531, 1996.

[31] A. A. Thoul and D. H. Weinberg, "Hydrodynamic simulations of galaxy formation. II. Photoionization and the formation of low-mass galaxies," *The Astrophysical Journal*, vol. 465, no. 2, pp. 608–616, 1996.

[32] T. Quinn, N. Katz, and G. Efstathiou, "Photoionization and the formation of dwarf galaxies," *Monthly Notices of the Royal Astronomical Society*, vol. 278, no. 4, pp. L49–L54, 1996.

[33] D. H. Weinberg, L. Hernquist, and N. Katz, "Photoionization, numerical resolution, and galaxy formation," *The Astrophysical Journal*, vol. 477, no. 1, pp. 8–20, 1997.

[34] J. F. Navarro and M. Steinmetz, "The effects of a photoionizing ultraviolet background on the formation of disk galaxies," *The Astrophysical Journal*, vol. 478, no. 1, pp. 13–28, 1997.

[35] J. S. Bullock, A. V. Kravtsov, and D. H. Weinberg, "Reionization and the abundance of galactic satellites," *The Astrophysical Journal*, vol. 539, no. 2, pp. 517–521, 2000.

[36] N. Y. Gnedin, "Cosmological reionization by stellar sources," *The Astrophysical Journal*, vol. 535, no. 2, pp. 530–554, 2000.

[37] R. S. Somerville, "Can photoionization squelching resolve the substructure crisis?" *The Astrophysical Journal*, vol. 572, no. 1, pp. L23–L26, 2002.

[38] M. Dijkstra, Z. Haiman, and A. Loeb, "A limit from the X-ray background on the contribution of quasars to reionization," *The Astrophysical Journal*, vol. 613, no. 2, pp. 646–654, 2004.

[39] P. R. Shapiro, I. T. Iliev, and A. C. Raga, "Photoevaporation of cosmological minihaloes during reionization," *Monthly Notices of the Royal Astronomical Society*, vol. 348, no. 3, pp. 753–782, 2004.

[40] T. Okamoto, L. Gao, and T. Theuns, "Mass loss of galaxies due to an ultraviolet background," *Monthly Notices of the Royal Astronomical Society*, vol. 390, no. 3, pp. 920–928, 2008.

[41] M. Ricotti, N. Y. Gnedin, and J. M. Shull, "The fate of the first galaxies. II. Effects of radiative feedback," *The Astrophysical Journal*, vol. 575, no. 1, pp. 49–67, 2002.

[42] J. H. Wise and T. Abel, "Resolving the formation of protogalaxies. III. Feedback from the first stars," *The Astrophysical Journal*, vol. 685, no. 1, pp. 40–56, 2008.

[43] B. W. O'Shea and M. L. Norman, "Population III star formation in a ΛCDM universe. II. Effects of a photodissociating background," *The Astrophysical Journal*, vol. 673, no. 1, pp. 14–33, 2008.

[44] M. Ricotti, N. Y. Gnedin, and J. M. Shull, "The fate of the first galaxies. III. Properties of primordial dwarf galaxies and their impact on the intergalactic medium," *The Astrophysical Journal*, vol. 685, no. 1, pp. 21–39, 2008.

[45] J. H. Wise and T. Abel, "Suppression of H_2 cooling in the ultraviolet background," *The Astrophysical Journal*, vol. 671, no. 2, pp. 1559–1567, 2007.

[46] M. E. Machacek, G. L. Bryan, and T. Abel, "Simulations of pregalactic structure formation with radiative feedback," *The Astrophysical Journal*, vol. 548, no. 2, pp. 509–521, 2001.

[47] M. E. Machacek, G. L. Bryan, and T. Abel, "Effects of a soft X-ray background on structure formation at high redshift," *Monthly Notices of the Royal Astronomical Society*, vol. 338, no. 2, pp. 273–286, 2003.

[48] M. Ricotti, N. Y. Gnedin, and J. M. Shull, "The fate of the first galaxies. I. Self-consistent cosmological simulations with radiative transfer," *The Astrophysical Journal*, vol. 575, no. 1, pp. 33–48, 2002.

[49] M. Ricotti, N. Y. Gnedin, and J. M. Shull, "Feedback from galaxy formation: production and photodissociation of primordial H_2," *The Astrophysical Journal*, vol. 560, no. 2, pp. 580–591, 2001.

[50] M. Ricotti and N. Y. Gnedin, "Formation histories of dwarf galaxies in the local group," *The Astrophysical Journal*, vol. 629, no. 1, pp. 259–267, 2005.

[51] M. S. Bovill and M. Ricotti, "Pre-reionization fossils, ultra-faint dwarfs, and the missing galactic satellite problem," *The Astrophysical Journal*, vol. 693, pp. 1859–1870, 2009.

[52] V. Bromm, A. Ferrara, P. S. Coppi, and R. B. Larson, "The fragmentation of pre-enriched primordial objects," *Monthly Notices of the Royal Astronomical Society*, vol. 328, no. 3, pp. 969–976, 2001.

[53] F. Santoro and J. M. Shuli, "Critical metallicity and fine-structure emission of primordial gas enriched by the first stars," *The Astrophysical Journal*, vol. 643, no. 1, pp. 26–37, 2006.

[54] B. D. Smith, M. J. Turk, S. Sigurdsson, B. W. O'Shea, and M. L. Norman, "Three modes of metal-enriched star formation in the early universe," *The Astrophysical Journal*, vol. 691, pp. 441–451, 2009.

[55] S. Salvadori and A. Ferrara, "Ultra faint dwarfs: probing early cosmic star formation," *Monthly Notices of the Royal Astronomical Society*, vol. 395, pp. L6–L10, 2009.

[56] M. Ricotti, N. Y. Gnedin, and J. M. Shull, "The evolution of the effective equation of state of the intergalactic medium," *The Astrophysical Journal*, vol. 534, no. 1, pp. 41–56, 2000.

[57] S. E. Koposov, J. Yoo, H.-W. Rix, D. H. Weinberg, A. V. Macciò, and J. M. Escudé, "A quantitative explanation of the observed population of Milky Way satellite galaxies," *The Astrophysical Journal*, vol. 696, pp. 2179–2194, 2009.

[58] M. Mateo, "Dwarf galaxies of the local group," *Annual Review of Astronomy and Astrophysics*, vol. 36, no. 1, pp. 435–506, 1998.

[59] L. Mayer, S. Kazantzidis, C. Mastropietro, and J. Wadsley, "Early gas stripping as the origin of the darkest galaxies in the universe," *Nature*, vol. 445, no. 7129, pp. 738–740, 2007.

[60] J. Peñarrubia, J. F. Navarro, and A. W. McConnachie, "The tidal evolution of local group dwarf spheroidals," *The Astrophysical Journal*, vol. 673, no. 1, pp. 226–240, 2008.

[61] S. M. Walsh, B. Willman, and H. Jerjen, "The invisibles: a detection algorithm to trace the faintest Milky Way satellites," *The Astronomical Journal*, vol. 137, no. 1, pp. 450–469, 2009.

[62] N. F. Martin, A. W. McConnachie, M. Irwin, L. M. Widrow, A. M.N. Ferguson, R. A. Ibata, J. Dubinski, A. Babul, S. Chapman, M. Fardal, G. F. Lewis, J. Navarro, and R. M. Rich, "PandAS' Cubs: discovery of two new dwarf galaxies in the surroundings of the Andromeda and triangulum galaxies," *Astrophysical Journal*, vol. 705, no. 1, pp. 758–765, 2009.

[63] J. K. Adelman-McCarthy, M. A. Agüeros, S. S. Allam, et al., "The fourth data release of the sloan digital sky survey," *The Astrophysical Journal, Supplement Series*, vol. 162, no. 1, pp. 38–48, 2006.

[64] J. K. Adelman-McCarthy, M. A. Agüeros, S. S. Allam, et al., "The fifth data release of the sloan digital sky survey," *The Astrophysical Journal, Supplement Series*, vol. 172, no. 2, pp. 634–644, 2007.

[65] P. Kroupa, C. Theis, and C. M. Boily, "The great disk of Milky-Way satellites and cosmological sub-structures," *Astronomy & Astrophysics*, vol. 431, no. 2, pp. 517–521, 2005.

[66] A. R. Zentner, A. V. Kravtsov, O. Y. Gnedin, and A. A. Klypin, "The anisotropic distribution of galactic satellites," *The Astrophysical Journal*, vol. 629, no. 1, pp. 219–232, 2005.

[67] N. F. Martin, M. G. Coleman, J. T. A. de Jong, et al., "A deep large binocular telescope view of the Canes Venatici I dwarf galaxy," *The Astrophysical Journal*, vol. 672, no. 1, pp. L13–L16, 2008.

[68] J. T. A. de Jong, J. Harris, M. G. Coleman, et al., "The structural properties and star formation history of Leo T from deep LBT photometry," *The Astrophysical Journal*, vol. 680, no. 2, pp. 1112–1119, 2008.

[69] N. F. Martin, J. T. A. de Jong, and H.-W. Rix, "A comprehensive maximum likelihood analysis of the structural properties of faint Milky Way satellites," *The Astrophysical Journal*, vol. 684, no. 2, pp. 1075–1092, 2008.

[70] V. Bromm, P. S. Coppi, and R. B. Larson, "The formation of the first stars—I: the primordial star-forming cloud," *The Astrophysical Journal*, vol. 564, no. 1, pp. 23–51, 2002.

[71] T. Abel, G. L. Bryan, and M. L. Norman, "The formation of the first star in the universe," *Science*, vol. 295, no. 5552, pp. 93–98, 2002.

[72] K. Saigo, T. Matsumoto, and M. Umemura, "The formation of population III binaries," *The Astrophysical Journal*, vol. 615, no. 2, pp. L65–L68, 2004.

[73] L. Gao, S. D. M. White, A. Jenkins, C. S. Frenk, and V. Springel, "Early structure in ΛCDM," *Monthly Notices of the Royal Astronomical Society*, vol. 363, no. 2, pp. 379–392, 2005.

[74] B. W. O'Shea and M. L. Norman, "Population III star formation in a ACDM universe. I. The effect of formation redshift and environment on protostellar accretion rate," *The Astrophysical Journal*, vol. 654, no. 1, pp. 66–92, 2007.

[75] N. Yoshida, K. Omukai, and L. Hernquist, "Protostar formation in the early universe," *Science*, vol. 321, no. 5889, pp. 669–671, 2008.

[76] M. J. Turk, T. Abel, and B. O'Shea, "The formation of population III binaries from cosmological initial conditions," *Science*, vol. 325, no. 5940, pp. 601–605, 2009.

[77] A. Stacy, T. H. Greif, and V. Bromm, "The first stars: formation of binaries and small multiple systems," *Monthly Notices of the Royal Astronomical Society*, 12 pages, January 2010.

[78] B. Ciardi, A. Ferrara, and T. Abel, "Intergalactic H_2 photodissociation and the soft ultraviolet background produced by population III objects," *The Astrophysical Journal*, vol. 533, no. 2, pp. 594–600, 2000.

[79] M. E. Machacek, G. L. Bryan, A. Meiksin, et al., "Hydrodynamical simulations of the Lyα forest: model comparisons," *The Astrophysical Journal*, vol. 532, no. 1, pp. 118–135, 2000.

[80] D. Whalen, B. W. O'Shea, J. Smidt, and M. L. Norman, "Photoionization of clustered halos by the first stars," in *First Stars III*, vol. 990 of *AIP Conference Proceedings*, pp. 381–385, Santa Fe, NM, USA, 2007.

[81] P. R. Shapiro and H. Kang, "Hydrogen molecules and the radiative cooling of pregalactic shocks," *The Astrophysical Journal*, vol. 318, pp. 32–65, 1987.

[82] M. A. Alvarez, V. Bromm, and P. R. Shapiro, "The H II region of the first star," *The Astrophysical Journal*, vol. 639, no. 2, pp. 621–632, 2006.

[83] B. Ciardi, E. Scannapieco, F. Stoehr, A. Ferrara, I. T. Iliev, and P. R. Shapiro, "The effect of minihaloes on cosmic reionization," *Monthly Notices of the Royal Astronomical Society*, vol. 366, no. 2, pp. 689–696, 2006.

[84] N. Y. Gnedin and T. Abel, "Multi-dimensional cosmological radiative transfer with a variable Eddington tensor formalism," *New Astronomy*, vol. 6, no. 7, pp. 437–455, 2001.

[85] C. C. Steidel, K. L. Adelberger, M. Giavalisco, M. Dickinson, and M. Pettini, "Lyman-break galaxies at $z > 4$ and the evolution of the ultraviolet luminosity density at high redshift," *Astrophysical Journal*, vol. 519, no. 1, pp. 1–17, 1999.

[86] N. Y. Gnedin, "Effect of reionization on structure formation in the universe," *The Astrophysical Journal*, vol. 542, no. 2, pp. 535–541, 2000.

[87] J. S. Bullock, T. S. Kolatt, Y. Sigad, et al., "Profiles of dark haloes: evolution, scatter and environment," *Monthly Notices of the Royal Astronomical Society*, vol. 321, no. 3, pp. 559–575, 2001.

[88] R. H. Wechsler, J. S. Bullock, J. R. Primack, A. V. Kravtsov, and A. Dekel, "Concentrations of dark halos from their assembly histories," *The Astrophysical Journal*, vol. 568, no. 1, pp. 52–70, 2002.

[89] E. Bertschinger, "Self-similar secondary infall and accretion in an Einstein-de Sitter universe," *The Astrophysical Journal, Supplement Series*, vol. 58, p. 39, 1985.

[90] G. S. Stinson, J. J. Dalcanton, T. Quinn, T. Kaufmann, and J. Wadsley, "Breathing in low-mass galaxies: a study of episodic star formation," *The Astrophysical Journal*, vol. 667, no. 1, pp. 170–175, 2007.

[91] A. V. Kravtsov, O. Y. Gnedin, and A. A. Klypin, "The tumultuous lives of galactic dwarfs and the missing satellites problem," *The Astrophysical Journal*, vol. 609, no. 2, pp. 482–497, 2004.

[92] V. Springel, J. Wang, M. Vogelsberger, et al., "The Aquarius Project: the subhaloes of galactic haloes," *Monthly Notices of the Royal Astronomical Society*, vol. 391, no. 4, pp. 1685–1711, 2008.

[93] J. Diemand, M. Kuhlen, and P. Madau, "Formation and evolution of galaxy dark matter halos and their substructure," *The Astrophysical Journal*, vol. 667, no. 2, pp. 859–877, 2007.

[94] N. Y. Gnedin and A. V. Kravtsov, "Fossils of reionization in the local group," *The Astrophysical Journal*, vol. 645, no. 2, pp. 1054–1061, 2006.

[95] J. Kormendy and K. C. Freeman, "Scaling laws for dark matter halos in late-type and dwarf spheroidal galaxies," in

Proceedings of the IAU Symposium, p. 377, San Francisco, Calif, USA, 2004.

[96] N. F. Martin, R. A. Ibata, S. C. Chapman, M. Irwin, and G. F. Lewis, "A Keck/DEIMOS spectroscopic survey of faint Galactic satellites: searching for the least massive dwarf galaxies," *Monthly Notices of the Royal Astronomical Society*, vol. 380, no. 1, pp. 281–300, 2007.

[97] L. E. Strigari, J. S. Bullock, M. Kaplinghat, et al., "A common mass scale for satellite galaxies of the Milky Way," *Nature*, vol. 454, no. 7208, pp. 1096–1097, 2008.

[98] E. N. Kirby, J. D. Simon, M. Geha, P. Guhathakurta, and A. Frebel, "Uncovering extremely metal-poor stars in the Milky Way's ultrafaint dwarf spheroidal satellite galaxies," *The Astrophysical Journal*, vol. 685, no. 1, pp. L43–L46, 2008.

[99] E. K. Grebel and J. S. Gallagher III, "The impact of reionization on the stellar populations of nearby dwarf galaxies," *The Astrophysical Journal*, vol. 610, no. 2, pp. L89–L92, 2004.

[100] R. Giovanelli, M. P. Haynes, B. R. Kent, et al., "The arecibo legacy fast ALFA survey. I. Science goals, survey design, and strategy," *The Astronomical Journal*, vol. 130, no. 6, pp. 2598–2612, 2005.

[101] R. Giovanelli, M. P. Haynes, B. R. Kent, et al., "The arecibo legacy fast alfa survey. III. H I source catalog of the northern virgo cluster region," *The Astronomical Journal*, vol. 133, no. 6, pp. 2569–2583, 2007.

[102] L. Mayer, C. Mastropietro, J. Wadsley, J. Stadel, and B. Moore, "Simultaneous ram pressure and tidal stripping; how dwarf spheroidals lost their gas," *Monthly Notices of the Royal Astronomical Society*, vol. 369, no. 3, pp. 1021–1038, 2006.

[103] S. C. Chapman, J. Peñarrubia, R. Ibata, et al., "Strangers in the night: discovery of a dwarf spheroidal galaxy on its first local group infall," *The Astrophysical Journal*, vol. 662, no. 2, pp. L78–L82, 2007.

[104] A. W. McConnachie, A. Huxor, N. F. Martin, et al., "A trio of new local group galaxies with extreme properties," *Astrophysical Journal*, vol. 688, no. 2, pp. 1009–1020, 2008.

Hindawi Publishing Corporation
Advances in Astronomy
Volume 2010, Article ID 693968, 16 pages
doi:10.1155/2010/693968

Review Article

Dwarf Galaxies in Voids: Dark Matter Halos and Gas Cooling

Matthias Hoeft[1] and Stefan Gottlöber[2]

[1] *Thüringer Landessternwarte Tautenburg, 07778 Tautenburg, Germany*
[2] *Astrophysikalisches Institut Potsdam, 14482 Potsdam, Germany*

Correspondence should be addressed to Matthias Hoeft, hoeft@tls-tautenburg.de

Received 7 July 2009; Accepted 14 January 2010

Academic Editor: Ulrich Hopp

Galaxy surveys have shown that luminous galaxies are mainly distributed in large filaments and galaxy clusters. The remaining large volumes are virtually devoid of luminous galaxies. This is in concordance with the formation of the large-scale structure in the universe as derived from cosmological simulations. However, the numerical results indicate that cosmological voids are abundantly populated with dark matter haloes which may in principle host dwarf galaxies. Observational efforts have in contrast revealed that voids are apparently devoid of dwarf galaxies. We investigate the formation of dwarf galaxies in voids by hydrodynamical cosmological simulations. Due to the cosmic ultraviolet background radiation low-mass haloes show generally a reduced baryon fraction. We determine the characteristic mass below which dwarf galaxies are baryon deficient. We show that the circular velocity below which the accretion of baryons is suppressed is approximately 40 kms^{-1}. The suppressed baryon accretion is caused by the photo-heating due to the UV background. We set up a spherical halo model and show that the effective equation of the state of the gas in the periphery of dwarf galaxies determines the characteristic mass. This implies that any process which heats the gas around dwarf galaxies increases the characteristic mass and thus reduces the number of observable dwarf galaxies.

1. Introduction: Formation of Structure in the Universe

During the last couple of decades new extensive observations of the universe were made using both ground-based telescopes and space instruments. These measurements have provided new insights into the structure of the universe on various scales. A wide range of the electromagnetic spectrum emitted by cosmic objects has been studied. The wavelengths extend from very long radio wavelengths to energetic gamma rays. This observational progress has been accompanied by considerable effort in our theoretical understanding of the formation of different components of the observed structure of the Universe from small scales (galaxies and their satellites) up to the largest scales (clusters of galaxies and superclusters).

The standard picture of structure formation was suggested by White and Rees [1] more than 30 years ago. It suggests that gravitational instability drives the dark matter (DM) to cluster hierarchically in a bottom-up fashion. The gaseous baryons settle into the DM haloes (namely, bound virial DM structures) and via gas-dynamical dissipative processes cool, fragment, and form stars. This simple picture prevails today although our knowledge of the details and of the actual processes has evolved dramatically since then. The nonlinear nature of the gravitational dynamics and the gas-astrophysical processes makes the problem of structure formation virtually intractable analytically, and therefore the fiecp..ld relies on numerical simulations. A substantial part of the progress in understanding structure formation of the universe is due to the increasing possibilities to make numerical experiments using the largest massive parallel supercomputers. In the eighties the best simulations handled 32^3 particles, whereas at present 1024^3 particles became a standard for numerical simulations, a increase of 2^{15} roughly in agreement with Moore's law.

The effort of observers and theorists brought about the so called standard cosmological model. This model is based on the idea that some kind of dark energy contributes about 70% of the total energy density of the spatially flat universe in which the total energy density equals the critical one. The dark energy is responsible for the observed

accelerated expansion of the universe. The simplest form of the dark energy is the cosmological constant, which was introduced already in 1917 by Albert Einstein in his paper about the cosmological solutions of the field equations of general relativity. The remaining about 30% of energy density consists of matter. About 85% of this matter is made of unknown dark matter particles, the remaining 15% is the contribution of "normal" baryonic particles well known to particle physicists. This means that the nature of more than 95% of the matter in the universe is not yet understood.

According to this standard cosmological model, the main process responsible for the formation of the observed structures is gravitational instability. The initial seeds, which eventually became galaxies and superclusters and all other structures, came from the quantum fluctuations generated during the early inflationary phase: $\sim 10^{-35}$ sec or so from the beginning of the Big Bang. The power spectrum of these primordial fluctuations has been confirmed by measuring the temperature fluctuations of the cosmic microwave background radiation. These temperature fluctuations tell us the magnitude of the small fluctuations in the universe about 300 000 years after the Big Bang.

One of the key features of the standard model is its simplicity. The expansion rate and the clustering properties are described by only few parameters which are measured at present with quite high accuracy. These parameters are the current rate of universal expansion, $H_0 = h \times 100\,\mathrm{km\,s^{-1}\,Mpc^{-1}}$, the mass density parameter, Ω_{mat}, the value of the cosmological constant, Ω_Λ, the primordial baryon abundance, Ω_{b}, and the overall normalisation of the power spectrum of initial density fluctuations, typically characterised by σ_8, the present-day r.m.s. mass fluctuations on spheres of radius 8 h^{-1} Mpc.

The initial power spectrum (created during the inflationary phase) does not contain preferred length scales. However, the horizon size at matter-radiation equality is mapped on this scale-free spectrum. Since this scale (today around 100 Mpc) is well above the typical scales of observed objects, structure formation is predicted to be essentially scale invariant: in a statistical sense the structures on scales of galaxy clusters are repeated on scales of galaxies. Typically, small objects merge together and form more and more massive objects. However, the small objects do not disappear within those larger objects but rather form a complex hierarchy of substructures. This hierarchical scenario predicts that our Milky Way galaxy is expected to have as many satellites (many hundreds) as a cluster of galaxies has galaxies. However, only a few dozen satellite of the Milky Way have been observed yet: this is the well-known missing satellite problem [2, 3]. Other manifestations of the scale-free power spectrum are the predicted large number of dwarfs in low density regions of the universe [4, 5] or the predicted spectrum of mini-voids in the Local Universe [6].

A better understanding of the physics of structure formation on small scales, in particular of the correct modelling of baryonic physics, could solve these problems [7]. Based on semianalytical models recently Macciò et al. [8] (see also [9]) claimed that the long standing problem of missing satellites can be solved within the ΛCDM scenario. The basic idea behind this solution of the problem is that the haloes which host a galaxy of a given measured rotational velocity are more massive than expected by the direct association of rotational velocity and the haloes maximum circular velocity. Since more massive haloes are less frequent, the problem of missing satellites is solved. However, any nonbaryonic physics that reduces power on small scales compared to the standard model will also improve the situation. It is well known that warm dark matter acts in this direction by erasing power at short scales due to free streaming [10, 11].

Altogether, we arrive at a picture in which dark matter particles form the backbone structure for all objects in the universe from clusters of galaxies to dwarf galaxies. Normal matter (baryons) falls into the potential wells formed by the dark matter particles and forms the luminous objects. The details of this formation process must be followed using hydrodynamical simulations. Galaxy formation depends on many physical processes, some of which are very poorly understood, and some of which take place on subgrid scales and therefore cannot be modelled fully and consistently and need to be fudged numerically by ad hoc recipes. For example, the formation of stars and the feedback of stars on the intergalactic medium take place on scales orders of magnitudes below the present day resolution. In cosmological simulations of galaxy formation typical masses of "stellar particles" are $10^4\ h^{-1}\ M_\odot$ or more. Thus such a particle represents the formation and evolution of a large number of real stars.

The paper is organised as follows. In Section 2 we introduce briefly the method of cosmological simulations and discuss observational facts about voids and how they are defined in simulations. In Section 3 we present the baryon fraction in low mass dark matter haloes and introduce the characteristic mass. In Section 4 we introduce a spherical model for the halo gas and discuss the relation between photo-heating of the halo gas and gas accretion. Our findings are summarised in Section 5.

2. Cosmological Simulations

The cosmic microwave background (CMB) originates from the recombination of the hydrogen in the universe at redshift about 1000. Primordial small density fluctuations are imprinted on the spectrum of the CMB temperature fluctuations which is closely related to the initial power spectrum of density fluctuations. The observed unique features of CMB temperature fluctuations constrain the cosmological parameters as well as the normalisation of the power spectrum of density fluctuations. The most recent results of the WMAP experiment combined with the measurements of the baryonic oscillations and supernova data [12] yield a Hubble parameter $h = 7.01$, the density of dark matter $\Omega_{\mathrm{DM}} = 0.228$, the baryonic density $\Omega_{\mathrm{bar}} = 0.046$, the cosmological constant $\Omega_\Lambda = 0.726$, the normalisation of the power spectrum $\sigma_8 = 0.82$, and its slope $n = 0.96$. These parameters fix the cosmological model and also the power spectrum of the initial perturbations. Starting with the initial conditions the simulations follow the growth of the perturbation in a universe that

expands according to the chosen cosmological parameters. In this expanding universe the gravitational interaction is Newtonian.

2.1. Initial Conditions. The first step of running cosmological simulations is to set up the initial conditions, namely, amplitudes and phases of small perturbations at a very high redshift. Having in mind that the largest structures in the universe—superclusters and voids—have sizes of 10 to 50 Mpc, the simulated volume should be significantly larger. However, we may be interested in the structure of a much smaller object such as our Milky Way galaxy or its satellites. In N-body simulations each mass element is represented by a point-like particle. The mass resolution is limited by the total number of particles computers can handle at a given time. Thus, increasing the representative cosmological volume decreases the mass resolution. To overcome this problem mass refinement techniques have been developed. Here we follow the algorithm proposed in [13]. To construct suitable initial conditions, we first create a random realisation at the highest possible resolution. This depends on the available computers; at present we reach 4096^3 particles. The initial displacements and velocities of N particles are calculated using all waves ranging from the fundamental mode $k = 2\pi/L_{\rm box}$ to the Nyquist frequency $k_{\rm Ny} = 2\pi/L_{\rm box} \times N^{1/3}/2$. Then the resolution can be decreased by replacing 8^i ($i = 1, 5$) neighbouring particles by one particle with 8^i higher mass which results in a distribution of 2048^3, 1024^3, 512^3, 256^3, or 128^3 particles. Using a smaller number of more massive particles we first run low-resolution simulations until the present epoch. In this simulation we select the regions of interest. Then we repeat the simulation but this time we preserve low mass particles inside the region of interest. Outside of this region we progressively replace small particles by massive ones creating shells of more and more massive particles until we reach the low resolution region of 128^3 particles. This procedure ensures that our object evolves in the proper cosmological environment and with the right gravitational tidal fields.

Based on the power spectrum of density fluctuations we set up the initial conditions of our simulation at an early redshift which depends on the size of the box and the required resolution. To move the particles from the original Lagrangian point on a regular grid to their Eulerian position we use the Zeldovich approximation. The power spectrum of the generated Gaussian stochastic density field corresponds to the input power spectrum. The random nature of the realisation manifests itself on scales comparable to the box size where the spectrum is sampled only by a few modes. By this procedure the cosmological parameters and the normalisation of the density power spectrum fully determine the initial conditions of the cosmological simulations, except of a random number which characterises the starting point of the random number generator. Thus, on scales comparable to the box size cosmic variance enters through this number which characterises a given simulation. On smaller scales—typically a quarter of the box size—the realisation follows very closely the input power spectrum. Starting from the initial matter distribution we simulate the formation of cosmological structures. More precisely, we integrate the Poisson equation by the help of particle methods (Gadget and ART).

2.2. The Simulation Method. Our hydrodynamical simulations have been run with an updated version of the parallel Tree-SPH code Gadget [14, 15]. The dark and baryonic matter distributions are represented by particles. The gravitational forces are computed by a new algorithm based on the Tree-PM method which speeds up the force computation significantly compared with a pure tree algorithm. The hydrodynamical equations are solved by a Smoothed-Particle Hydrodynamics (SPH) method. The code uses an entropy-conserving formulation of SPH [14] which alleviates problems due to numerical over-cooling.

The code also includes photo-ionisation and radiative cooling processes for an optically thin primordial mix of helium and hydrogen. For computing the thermal evolution it uses ionisation, recombination and cooling rates as given in [16]. Since we will set up later in this paper an analytic model for the evolution of the intergalactic medium (IGM) we give here in detail the processes which affect the temperature, T, of the IGM. It primarily changes due to photo-heating, $\mathcal{H}$, and radiative cooling, Γ. Moreover, it decreases due to the adiabatic Hubble expansion, $\mathrm{d}T \propto H\mathrm{d}t$, where H is the time-dependent Hubble constant. Cosmological structure formation changes the temperature adiabatically, $\mathrm{d}T \propto \mathrm{d}\rho$. Finally, changes of the chemical composition also affect the temperature, $\mathrm{d}T \propto \mathrm{d}\Sigma_i X_i$, where X_i denotes the abundance of the atomic species i with respect to the cosmic baryon density, $X_i = n_i/n_{\rm b}$. In summary, the temperature evolution is given by

$$\mathrm{d}T = \frac{2}{3}\frac{(\mathcal{H}-\Gamma)\,\mathrm{d}t}{k_{\rm B} n_{\rm b} \Sigma_i X_i} - 2HT\mathrm{d}t + \frac{2}{3}\frac{T\mathrm{d}\Delta}{\Delta} - \frac{T\mathrm{d}(\Sigma_i X_i)}{\Sigma_i X_i}, \tag{1}$$

where Δ denotes the overdensity, $\Delta = \rho/\langle\rho\rangle$. We take the atomic hydrogen and helium species, {HI, HII, HeI, HeII, HeIII}, into account. We assume a constant, primordial helium mass fraction of $Y_{\rm p} = 0.24$.

The physics of star formation is treated in the code by means of a sub-resolution model in which the gas of the interstellar medium (ISM) is described as a multiphase medium of hot and cold gas [17, 18]. Cold gas clouds are generated due to cooling and they are the material out of which stars can be formed in regions that are sufficiently dense. Supernova feedback heats the hot phase of the ISM and evaporates cold clouds, thereby establishing a self-regulation cycle for star formation. The heat input due to the supernovae also leads to a net pressurisation of the ISM, such that its effective equation of state becomes stiffer than isothermal. This stabilises the dense star forming gas in galaxies against further gravitational collapse, and allows converged numerical results for star formation even at moderate resolution. See [17] for a more detailed description of the star formation model implemented in the Gadget code.

2.3. Dark Matter Haloes. During the cosmological evolution dark matter haloes are formed which accrete more and more matter or merge with other ones. Within a simulation with one billion particles it is a challenge to find structures and substructures. To find structures at virial over-density one can use a friends-of-friends algorithm with a certain linking length (0.17 of the mean inter-particle distance for the ΛCDM model at redshift zero). The resulting particle clusters are in general tri-axial objects. Substructures can be identified as particle clusters at smaller linking lengths (higher over-densities). The more different linking lengths are used the better substructures will be resolved. Thus a whole hierarchy of friends-of-friends clusters have to be calculated. To this end we have developed a hierarchical friends-of-friends algorithm which is based on the calculation of the minimum spanning tree of the given particle distribution. We use also the bound-density-maxima (BDM) algorithm [19] which determines spherical haloes and their subhaloes. The code removes unbound particles which is particularly important for subhaloes.

At all redshifts the sample of haloes is characterised by the mass function of the isolated haloes. This number density of haloes of a given mass depends on the power spectrum. A first very successful analytical ansatz to predict the mass function of haloes has been made by Press and Schechter [20]. Later on this has been improved by Bond et al. [21] and Sheth and Tormen [22]. The search for an accurate and universal function which describes the number density of haloes found in simulation at different redshifts led to a set of fitting functions proposed by different authors [23–25].

2.4. Voids. With the first available large galaxy surveys it became clear that there exist large regions in the Universe which are not occupied by bright galaxies [26–28]. Regions of all possible sizes devoid of galaxies can be seen in all redshift surveys. The observational discovery was soon followed by the theoretical understanding that voids constitute a natural outcome of structure formation via gravitational instability [29, 30]. Together with clusters, filaments, and superclusters, giant voids constitute the large-scale structure of the Universe.

More than 20 years ago, for the first time the sizes of voids have been estimated in different samples of galaxies with measured redshifts [31]. Later on voids in the CfA redshift catalogues were studied by [32], in the Las Campanas redshift survey by [33], in the Optical Redshift Survey and in the IRAS 1.2-Jy survey by [34, 35] and in the PSCz catalogue by Plionis and Basilakos [36] and Hoyle and Vogeley [37]. For a review of early observational efforts see Peebles [5]. More recently voids have been studied by many authors using the Two-Degree Field Galaxy Redshift Survey [38–41] and the Sloan Digital Sky Survey [42–45].

There were several attempts to find dwarf galaxies in few individual voids [46–49]. The overall conclusion is that faint galaxies do not show a strong tendency to fill up voids defined by bright galaxies. The strongest arguments that voids are not populated by dwarf galaxies were given by Peebles [5] who points out that the dwarf galaxies in the ORS catalogue follow remarkably close the distribution of bright galaxies: there are no indications that they fill voids in the distribution of bright galaxies. To summarise, observations indicate that large voids found in the distribution of bright ($\sim M_*$) galaxies are empty of galaxies, which are two magnitudes below M_*. Recently, Tikhonov and Klypin [6] studied the properties of mini-voids in the nearby universe.

The void phenomenon was already the target of many theoretical studies [50–59]. Using a set of DM only simulations [4] have studied the inner structure of voids. The haloes in voids are arranged in a pattern, which looks like a miniature Universe with the same structural elements as the large-scale structure of the galactic distribution of the Universe. There are filaments and voids; larger haloes are at the intersections of filaments. The mass function of haloes in voids is much steeper for high masses resulting in very few galaxies with circular velocities $v_{\rm circ} \approx 100\,{\rm km\,s^{-1}}$. Note, however, that in DM simulations it has been usually assumed that each dark matter halo hosts at least one galaxy. This may not be true. Physical processes of galaxy formation are not well known and there could be processes that strongly suppress the formation of stars inside small haloes, which collapse relatively late in voids. This issue will be discussed in detail in the following sections.

There is a lot of interest in the void phenomena. However, there is no clear definition of a void. Almost every study uses its own definition of a void and its own void finder. Recently, the different approaches have been compared within the Aspen-Amsterdam Void Finder Comparison Project [60]. Here we use a rather simple and direct definition. In order to identify voids, we start with a selection of point like objects in 3D. These objects can be haloes above a certain mass or a certain circular velocity or galaxies above a certain luminosity. Thus the voids are characterised by the threshold mass or luminosity. The void finding algorithm can be applied both to numerical and observational data. In numerical simulations it takes into account periodic boundary conditions. At first it searches the largest empty sphere which is completely inside the given volume. The radius of this empty region is $R_{\rm void}$. Then we extend this region to an empty region with irregular shape. We define this empty region as union of all spheres with radius $r_{\rm ext} \geq 0.789\ R_{\rm void}$ (thus with a volume greater or equal half of the volume of the original void sphere) which can be moved to their place without crossing any object or the box boundary. To find the other voids we repeat this procedure however taking into account the previously found voids. We now search the largest empty sphere which is completely inside the volume and does not intersect with any already known void. The voids are characterised by volume, shape and orientation.

For the resimulation we selected a void region from a larger periodic computational box. To construct suitable initial conditions, at first we replaced in a box of side-length $50\ h^{-1}$ Mpc with 2048^3 particles the low mass particles by 256^3 massive ones. After running the simulation at this low mass resolution we determined a void region of interest and, finally, we were rerunning the simulation with the original set of particles inside the void (2048^3) and replacing only outside the void the low mass particles by more massive ones.

Table 1: Main characteristics of the two simulations analysed for determining the characteristic mass.

Refined region	Simulation bos size	Mass resolution (dark matter)
void	$50\,h^{-1}$ Mpc	$1.03 \times 10^6\,h^{-1}\,M_\odot$
filament	$80\,h^{-1}$ Mpc	$8.24 \times 10^6\,h^{-1}\,M_\odot$

3. The Baryon Content of Dwarf Galaxy Haloes

The number density of dwarf galaxies observed in the Universe is apparently smaller than the predicted number density of low mass dark matter haloes [61]. The missing galaxies are either not formed because the corresponding dark matter haloes do not exist, or no stars are formed in small haloes. As shown by Hoeft et al. [7] and Okamoto et al. [62], the optically thin UV-background already causes baryon deficiency in small haloes. In this section we determine the mass scale below which photo-heating causes baryon deficiency.

3.1. Mass Accretion History. The gravitationally bound structures, that is, galaxies and clusters of galaxies, grow in two ways: they accrete surrounding matter and they merge with other galaxies or clusters. Numerical simulations allow us to follow the merging history of the haloes. Every massive halo at the end of the simulation has a large number of progenitors which subsequently merge to the final structure.

We compute the mass accretion history for all haloes in our two simulations, see Table 1. To this end we determine the haloes in each simulation snapshot. Then we go backward from the final snapshot and search for the most massive progenitor in the previous snapshot. Since we have stored more than one hundred snapshots for each simulation we can simply search for the most massive progenitor in the vicinity of a given halo. However, during merger events the halo finder sometimes fails to identify the halo at all, since two approaching haloes appear spuriously gravitationally unbound. Figure 1 shows the mass accretion histories of ten sample haloes, where the jumps are caused by merger events.

3.2. Characteristic Mass. We determine for all distinct haloes in our simulations the baryon fraction within the virial radius, $f_\mathrm{b} = M_\mathrm{bar}/M_\mathrm{tot} = (M_\mathrm{star} + M_\mathrm{gas})/(M_\mathrm{star} + M_\mathrm{gas} + M_\mathrm{dm})$, where M_bar denotes the baryonic mass, M_tot the total mass, M_dm the dark matter mass, M_gas the gas mass and M_star in stellar mass. We take those haloes into account which consist of more than 180 dark matter particles. The resulting lowest halo mass is $1.9 \times 10^8\,h^{-1}\,M_\odot$ and $1.5 \times 10^9\,h^{-1}\,M_\odot$ for the void and for the filament region, respectively. Moreover, we exclude all haloes which have been within the virial radius of a more massive halo in the past, because the dark matter and baryonic masses may be affected by stripping. Figure 2 shows the resulting baryon fraction for both the low density region simulation the filament region simulation. The low mass haloes evidently have a baryon fraction much smaller than the cosmic baryon fraction. Since the transition from "cosmic mean baryon fraction" to "baryon deficient" occurs within a rather small mass range this phenomenon can be characterised by a single parameter, namely the mass at which the baryon fraction amounts in average to half of the cosmic mean, $M_{1/2}$. We determine the characteristic mass computing the average baryon fraction in mass bins and approximating the resulting curve by the following analytic expression

$$f_\mathrm{b} = \langle f_\mathrm{b} \rangle \left\{ \frac{1}{2} + \frac{1}{\pi} \arctan\left(\frac{\log M_\mathrm{tot} - \log M_{1/2}}{w_M} \right) \right\}. \quad (2)$$

We use a different expression than in [7] to make the fitting procedure more robust, in particular when a second free parameter is included, here the width w_M. Moreover, we expect that the halo gas, which is present independently from the halo size, leads to a floor in the baryon fraction. As we have shown in [7] the characteristic mass depends very little on the mass resolution used in our simulations. This indicates that the physical processes causing the baryon deficiency are reasonably resolved even if there are only a few tens of gas particles in small mass haloes.

In [7] we focussed on the baryon content of dwarf galaxies in cosmological voids. The result we obtained might be affected by restricting to void dwarf galaxies. To investigate also the effect of the cosmological environment we include here dwarf galaxies in a cosmological filament. These galaxies have a higher merger rate than void dwarf galaxies with a similar mass but they do accrete less diffuse gas, see [63] and references therein. We have excluded all galaxies which have passed through the halo of a more massive galaxy since their dark matter and baryonic mass could be affected by stripping. Despite the cosmologically quite different environments, the characteristic mass of both regions coincide well, see Figure 2(top row). In conclusion, the general mass accretion history of a dwarf galaxy has only little effect on their baryon content, that is, there is universal characteristic mass for all dwarf galaxies. Note, this result is obtained with a homogeneous UV-background. We will argue later that the UV-heating may have a crucial impact on the baryon accretion in dwarf galaxies.

Observationally, the total mass of a galaxy is difficult to determine. Galaxies are preferably characterised by the maximum circular velocity, v_max. One should note that also v_max is difficult to measure in dwarf galaxies since most rotation curves do not approach a maximum, that is, the maximum of the circular velocity lies outside the observable gas distribution. However, we will characterise haloes mainly by v_max. Figure 2(middle row) shows the baryon fractions in distinct haloes as a function of the maximum circular velocity.

Our aim is to determine what makes haloes below the characteristic mass baryon deficient. The baryon content at a given time is accumulated over the history of the halo. To assess what prevents at a given time haloes from accreting baryonic mass we determine the baryon fraction of newly accreted matter

$$f_\mathrm{b}^\mathrm{accr} = \frac{M_\mathrm{cond}(t_{i+1}) - M_\mathrm{cond}(t_{i-1})}{M_\mathrm{tot}(t_{i+1}) - M_\mathrm{tot}(t_{i-1})}, \quad (3)$$

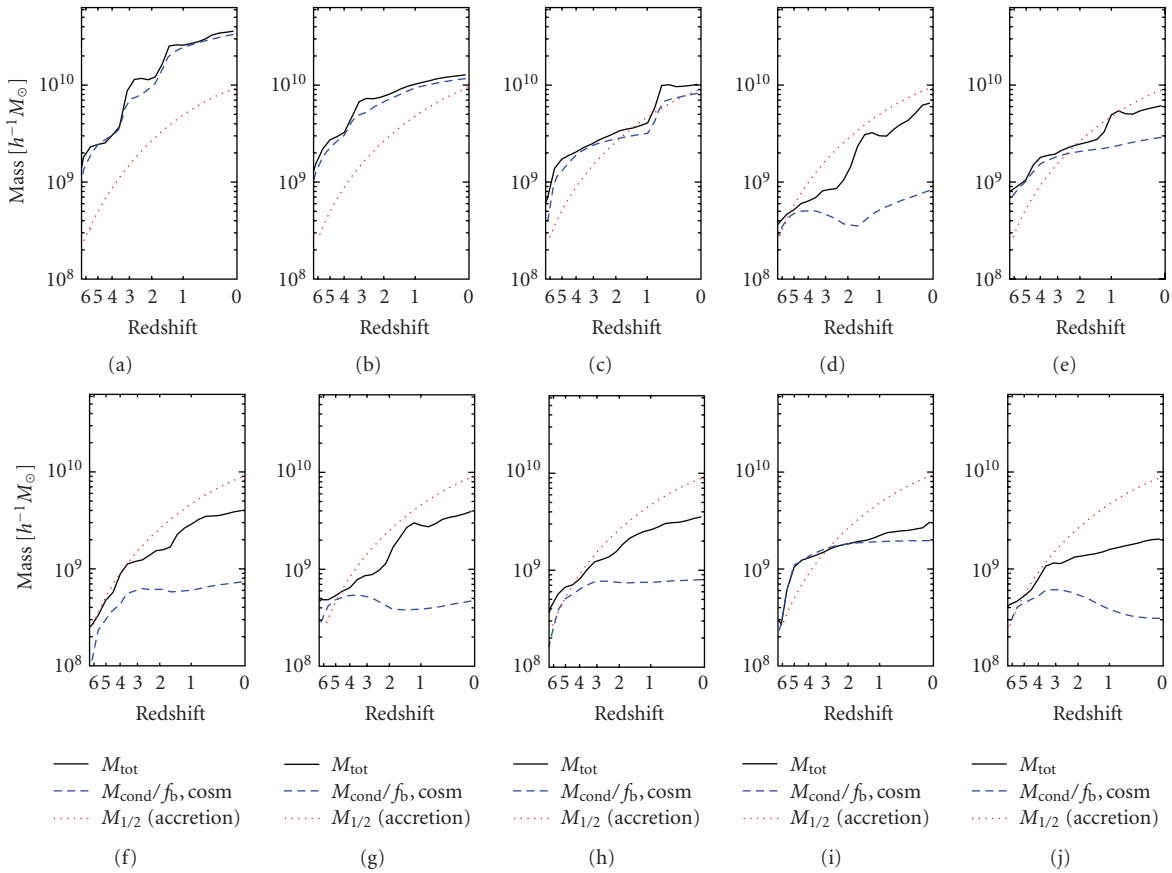

FIGURE 1: The mass accretion histories for several haloes. In each panel the total mass (solid line) and the condensed mass (dashed line) of one halo is shown. We have divided the condensed mass by the mean cosmic baryon fraction, $\langle f_{\rm b}\rangle$, to highlight when the condensed mass does not follow the expectation according to the mean baryon density. In addition, the characteristic mass (dotted line) is shown as derived from baryon fraction in newly accreted matter. One can clearly see that haloes cease to condense baryons when their total mass falls below the characteristic mass.

where t_{i-1} and t_{i+1} denote the masses of a given halo at an earlier and at a later time, respectively. Figure 2(bottom row) shows that small haloes do not accrete baryonic mass. Since we consider the differential evolution of the dark matter and the baryonic masses we have a large scatter in the characteristic mass of newly accreted matter. However, similar to the baryon fraction in haloes there is a clear separation between low mass haloes which accrete virtually no baryonic matter and high mass haloes which accrete matter with the mean cosmic baryon fraction.

3.3. Evolution of the Characteristic Mass. Figure 2 shows that the characteristic mass decreases with redshift. For instance, at redshift $z = 4$ the characteristic mass is about $3 \times 10^8\, h^{-1}\, M_\odot$, while it amounts to $6 \times 10^9\, h^{-1}\, M_\odot$ at $z = 0$. Figure 3 shows the redshift evolution of the characteristic mass as obtained from combined halo lists from our two simulations. For comparison also a few mass accretion histories from Figure 1 are shown.

Plotted as a function of circular velocity the evolution of the characteristic mass of the newly accreted matter has a rather simple behaviour: after a steep increase it is almost constant at $\sim 40\,\mathrm{km\,s^{-1}}$ for $z \lesssim 3$. Note that in [7] we found a lower value since we used the circular velocity at the virial radius, $v(r_{\rm vir})$, instead of $v_{\rm max}$. Moreover, we considered only the baryon fraction in haloes. Since semianalytic models of galaxy formation assume a low-mass cut-off for gas accretion, see, for example, [64, 65], we investigate here also the characteristic mass of newly accreted matter.

Because the circular velocity of most of the dwarf galaxy haloes is almost constant with time, except a major merger occurs, one can separate two types of evolutionary scenarios for dwarf galaxies: (i) small galaxies with $v_{\rm max} \ll 40\,\mathrm{km\,s^{-1}}$ accrete baryons only for $z \gtrsim 4$ and (ii) galaxies with $v_{\rm max} \gg 40\,\mathrm{km\,s^{-1}}$ are not affected at all. In Figure 1 we have also depicted for each halo the evolution of $M_{1/2}^{\rm accr}$ as shown in Figure 3(a). One can see nicely that haloes get baryon deficient when their halo mass is below $M_{1/2}^{\rm accr}$.

3.4. Can the Characteristic Mass Explain the Void Phenomenon? The void phenomenon comprises two observational findings [5]: first, the distribution of massive galaxies ($\geq L_*$) shows large empty regions, the "voids", see Section 2.4. Low-luminosity galaxies populate the voids but

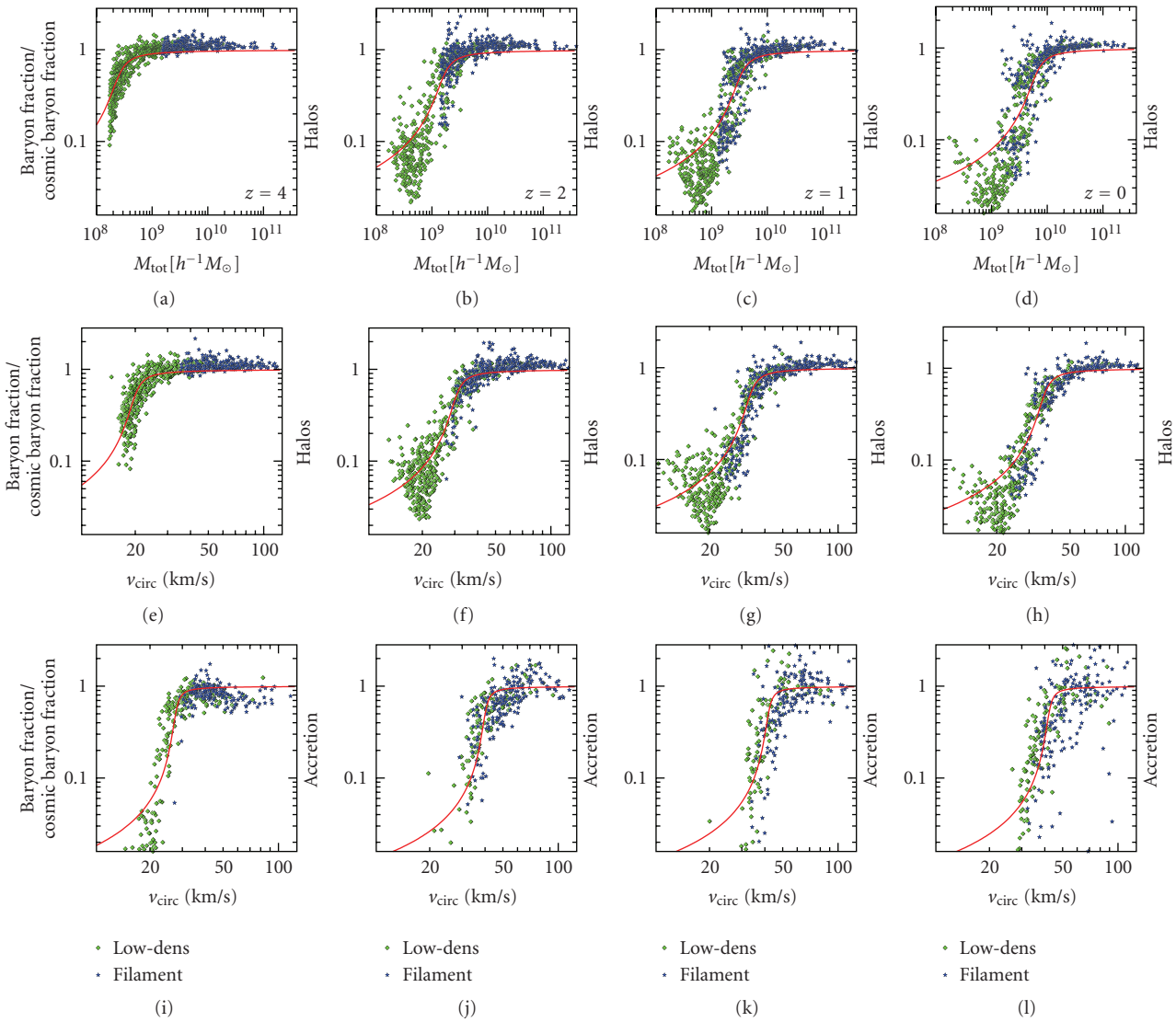

Figure 2: The baryonic mass fraction in units of the cosmic mean, $\Omega_{\rm b}/\Omega_{\rm m}$. Filled squares refer to the simulation of low density region while stars refer to the filament region. Only haloes with more than 180 dark matter are taken into account. The top row shows the baryon fraction at different redshifts as a function of total halo mass. The middle row gives the baryon fraction as a function of maximum circular velocity. The bottom row shows the baryon fraction of newly accreted matter (see text for a more detailed description).

with a low volume density compared to the dense regions [43]. Secondly, the galaxies found in voids are not special at all. According to the concordance ΛCDM cosmology voids are filled by dark matter haloes with the size of dwarf galaxies [4]. To judge if this is at odds with the void phenomenon in observations one has to assign a luminosity to the dark matter haloes. Recently, Tinker and Conroy [66] applied a Halo Occupations Distribution (HOD) to a large dark matter simulation and analysed void regions. They found that the haloes in void regions which host galaxies with an absolute magnitude $M_r > -10$ are located close to the walls of the voids. Only even fainter galaxies, that is, galaxies which are significantly below the current detection limit of surveys covering large void regions [43], populate the entire void volume. According to Tinker and Conroy galaxies with $M_r = -10$ reside in haloes with a mass $\sim 10^{10}\,h^{-1}\,M_\odot$. Hence, the photo-heating discussed here would reduce the luminosity of the haloes filling the entire void volume rendering those galaxies even more difficult to detect.

The HOD used by Tinker and Conroy implies that the mass-to-light ratio increases by a factor of ten from haloes with a mass of $10^{13}\,h^{-1}\,M_\odot$ to haloes with $10^{10}\,h^{-1}\,M_\odot$, independent of the environment. This is consistent with the compilation of the baryon content of galaxies by McGaugh [67]. Haloes with the mass of $10^{10}\,h^{-1}\,M_\odot$ seem to host only 5% of the baryonic mass corresponding to the cosmic mean. In our simulations we do not find any indication that the UV-background reduces the baryon fraction in galaxies significantly more massive than the characteristic mass. Therefore, we speculate that stellar feedback plays a key

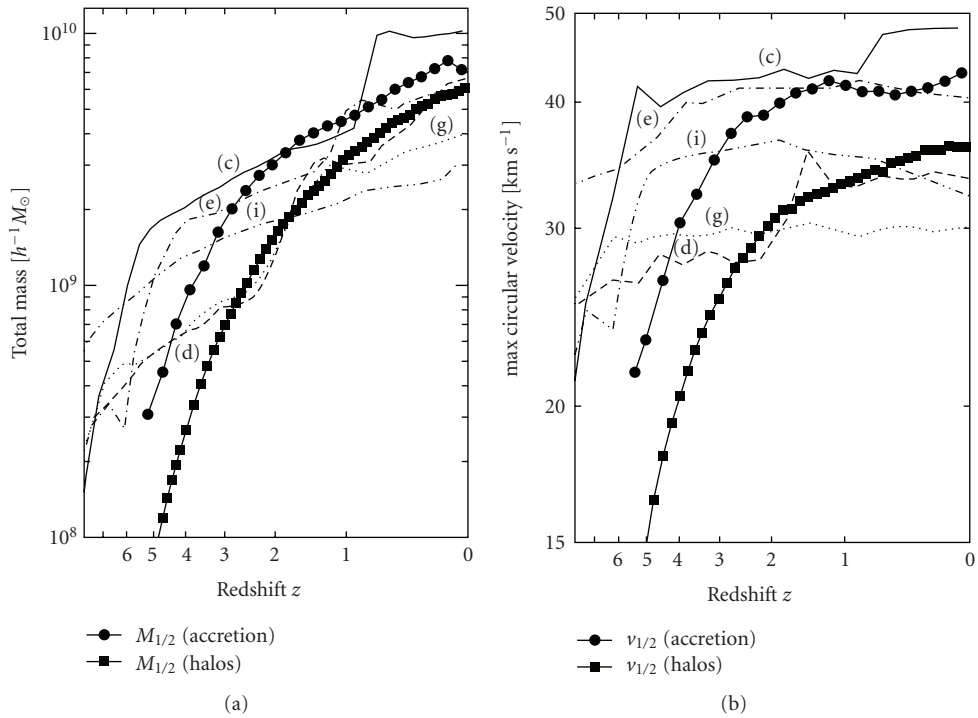

FIGURE 3: (a) Evolution of the characteristic mass of the baryon fraction in distinct haloes (squares) and in newly accreted matter (circles). For comparison the mass accretion histories of five haloes, as depicted in Figure 1, are shown. (b) Evolution of the characteristic circular velocity in distinct haloes and in newly accreted matter. Additionally, the circular velocity histories of the haloes in the left panel is shown.

role in reducing the baryon fraction galaxies with $M_{\rm tot} > M_{1/2}$. Note that the baryon fractions in [67] shows indeed a break at $v_{\rm circ} \approx 30\,{\rm km\,s^{-1}}$, consistent with our findings for the characteristic mass.

In summary, the surprising low number of low-luminosity galaxies in voids can be explained by a mass-dependent mass-to-light ratio, as obtained from a global Halo Occupation Distribution and from a proper mass modelling of galaxies. Haloes above the characteristic mass are expected to reside close to the walls of voids. The photo-heating discussed here reduces the luminosity of the low-mass and low-luminosity galaxies which can populate the entire void volume. Current surveys are limited to detect galaxies close to the walls due to the sensitivity limits of the surveys.

4. Why Small Haloes Fail to Accrete Gas

In the previous section we have shown that dark matter haloes with $v_{\rm max} \ll 40\,{\rm km\,s^{-1}}$ do accrete dark matter for $z \lesssim 4$ while they do not accrete baryons for smaller redshifts. Halos with $v_{\rm max} < 35\,{\rm km\,s^{-1}}$ are generally baryon deficient for $z = 0$. These results are obtained for high-resolution hydrodynamical cosmological simulations including a homogeneous photo-heating of an optically thin medium and including radiative cooling for a primordial chemical composition. In this section we investigate in detail the origin of the baryon deficiency which is evidently related to the photoheating by the UV background. To this end we set up an analytic model and investigate how baryons cool in dwarf galaxies.

4.1. Outline of the Analytic Model. Our simple model is constructed as follows: In the beginning the gas in the universe is homogeneously distributed. In the process of structure formation gas is accreted by galaxies, that is, its density increases.

Starting from a homogenous distribution the gas in the periphery of haloes and in the IGM follows the evolution of the dark matter. For our model here we assume that there is universal evolution of the overdensity, $\Delta(t, \Delta_0)$, which only depends on the time and on the final overdensity, see Figure 4. By the help of (1) we can determine the temperature as a function of the overdensity. For a given temperature-density relation we can determine the gas density profile of NFW-type haloes. Assuming that the gas density in the periphery of the halo is given by the mean cosmic baryon fraction we can determine the central gas density and temperature. If the resulting cooling time is short the halo would accrete baryonic matter, if the cooling time is long the halo would fail to accrete baryonic matter.

4.2. Effective Equation of State of the IGM. For a known overdensity evolution, $\Delta(t, \Delta_0)$, we can integrate the thermal evolution of the IGM, (1). To determine the heating and the cooling, $\mathcal{H}(t)$ and $\Gamma(t)$, respectively, we have to know the abundance of each species, that is, the ionisation state of hydrogen and helium. As in the cosmological simulations we

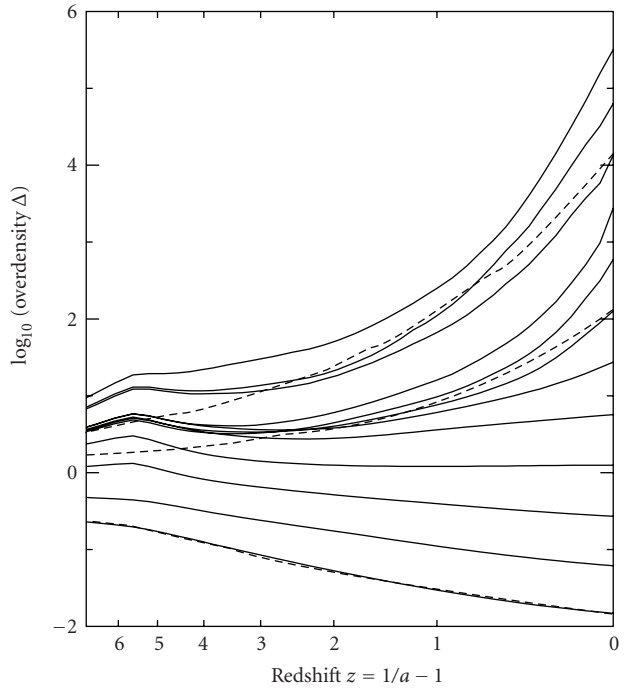

FIGURE 4: The overdensity evolution $\Delta(a, \Delta_0)$. We group in the simulation snapshot for $z = 0$ all particles according to their overdensity. Then trace back the density of the SPH-particles and compute the average density of the groups for earlier redshifts (solid lines). Moreover, we show three approximated overdensity evolutions (dashed lines) according to (4). See Section 4.2 for details. The peak-like structures at $z \approx 6$ are caused by photo-evaporation and are neglected in our approximation.

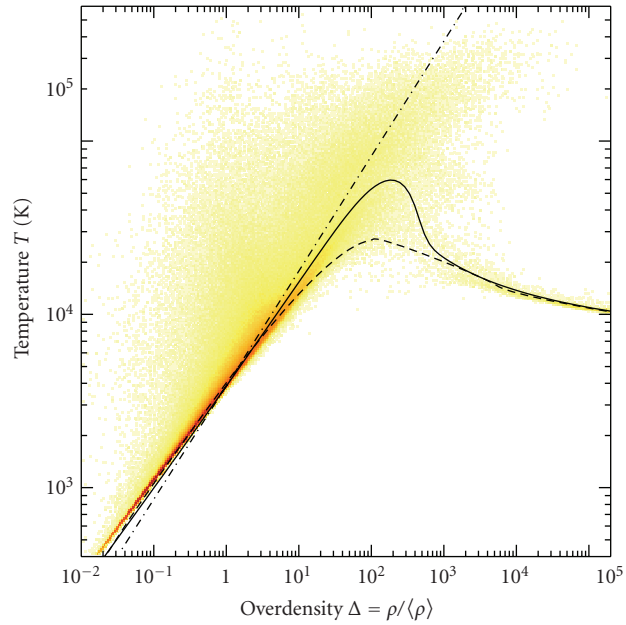

FIGURE 5: Temperature-density relation, $T(\Delta, t_0)$ for the overdensity histories as given in (4) (thick solid line). In addition two extreme scenarios for the overdensity history are shown. First, all gas is compressed or decompressed to its final overdensity, Δ_0, at the very beginning, that is, before reionisation takes place (dashed-dotted line). Secondly, all gas evolves at cosmic mean density until $z = 0$ and is then instantaneously compressed or decompressed to its final overdensity. The latter clearly results in an adiabatic relation (dash-dotted line). Finally, the distribution of the SPH-particles in the simulation is shown.

adopt collisional equilibrium, hence, we can determine for a given time and a given temperature the relative abundances. We solve the rate equations for collisional ionisation, for recombination, and for photo-ionisation. Now we can compute the photo-heating and cooling of the gas. Time-dependent specific energy injection rates, ϵ_i, are tabulated according to the UV-background model. As a result, the total photoheating can be written as $\mathcal{H} = n_{\mathrm{HI}}\epsilon_{\mathrm{HI}} + n_{\mathrm{HeI}}\epsilon_{\mathrm{HeI}} + n_{\mathrm{HeII}}\epsilon_{\mathrm{HeII}}$. Cooling rates are used as given in [16]. Hence, for a given overdensity evolution, $\Delta(t, \Delta_0)$ and UV-background model we can compute the final gas temperature, $T(t_0, \Delta_0)$.

We use our numerical simulations to estimate the overdensity evolution, $\Delta(t, \Delta_0)$. In Gadget the hydrodynamical equations are solved by the SPH method, hence, the fluid is represented by mass elements. The SPH-particles can be traced through the simulation. We group SPH-particles according to their overdensity at the end of the simulation, Δ_0, regardless if they are located in a galaxy, in a cosmological filament or in the field. Then, we trace back the density of the particles and compute the average density of each group, see Figure 4. For the integration of the thermal evolution of the IGM we approximate the overdensity evolution by an analytic expression, namely,

$$\log \Delta(t, \Delta_0) = \log \Delta_0 \cdot \left| \frac{G(a, \Delta_0)}{G(1, \Delta_0)} \right|, \tag{4}$$

where we use the cosmic expansion factor, $a = 1/(z + 1)$, as time variable. We approximate the time evolution by $G(a, \Delta_0) = |(a + 1)^{m(\log \Delta_0)} - 1|$, and determine for each final overdensity the exponent $m(\log \Delta_0)$. We fit (4) to each curve in Figure 4, where we take only the data for $z \leq 3$ into account. In the overdensity range $-2 < \log \Delta_0 < 6$ the resulting exponents are reasonably reproduced by $m(\log \Delta_0) = 1.3 \log \Delta_0 - 0.26(\log \Delta_0)^2$. This finally provides an analytic model for the overdensity evolution, $\Delta(t, \Delta_0)$.

In Figure 5 the temperature-density relation, $T(\Delta, t_0)$, obtained by integrating (1) using the analytic formula for the overdensity evolution described above, is shown. For comparison the density-temperature phase-space, as obtained from the numerical simulation, is also depicted. For high densities, $\Delta \gtrsim 10^3$, the analytic result, $T(\Delta, t_0)$, and the distribution of the SPH-particle coincides very well, because the thermal state is determined by thermal equilibrium. For low densities, most of the SPH-particles also follow $T(\Delta, t_0)$. Finally, a significant fraction of the SPH-particles has temperatures substantially above $T(\Delta, t_0)$, since in the numerical simulation particles are also heated by dissipation at shock fronts.

Which impact has the overdensity evolution? To answer this question we investigate two extreme scenarios. First, gas stays at mean cosmic density until $z = 0$ and is then instantaneously compressed or decompressed to the final

overdensity. This clearly leads to an adiabatic temperature-density relation, see Figure 5 (dash-dotted line). Secondly, gas is brought to the final overdensity before reionisation takes place and has then constant overdensity. The resulting temperature-density (dashed line) relation is only slightly different from the result for the average cosmic density evolution (solid line); the transition to thermal balance occurs at lower overdensities, since the compressed gas has more time to cool.

For the overdensity history introduced in (4) we find for low overdensities, $\Delta \lesssim 100$, an effective equation-of-state, that is, the temperature-density relation follows a power-law,

$$T_{\rm eos}(\Delta, t = t_0) = T_0 \Delta^{\alpha}, \tag{5}$$

with $T_0 = 3.85 \times 10^3$ K and $\alpha = 0.59$.

By plotting the cooling times in the temperature-density phase-space we can clearly see at which overdensities the gas is in thermal balance, see Figure 6. For low overdensities, $\Delta \lesssim 10^2$, cooling has only a negligible effect, that is, the thermal state of the gas is determined by the cumulative photo-heating. In contrast, at high overdensities, $\Delta \gtrsim 10^3$, the temperature lies exactly at the boundary between heating and cooling, that is, it is in thermal balance. Therefore, in the range $10^2 < \Delta < 10^3$ the transition from the pure photo-heating to the equilibrium between heating and cooling takes place.

4.3. The Halo Density Profile. We now set up the second part of our toy model, namely, the spherical halo model, with the aim to estimate the innermost gas density as a function of halo mass.

For a spherically symmetric halo in hydrostatic equilibrium the pressure force and the gravitational force are in balance:

$$\frac{1}{\rho}\frac{{\rm d}P}{{\rm d}r} = -\frac{GM_{\rm tot}(< r)}{r^2}, \tag{6}$$

where G is the gravitational constant and $M_{\rm tot}(< r)$ is the total mass enclosed by the radius r. Assuming an effective equation-of-state, as given in (5), we can write the left-hand side of (6) in terms of the gas overdensity. To this end we expand the gas density, $\rho = \Delta n_{\rm b} m_{\rm p}$, where $m_{\rm p}$ is the proton mass. The pressure can be written as $P = \Sigma_i n_i k_{\rm B} T = (\Delta n_{\rm b}/\mu)\, k_{\rm B} T_0 \Delta^{\alpha}$, where we have used the molecular weight, $\mu = n_{\rm b}/\Sigma_i n_i$, and (5). Now we rewrite the left-hand side of (6):

$$\frac{k_{\rm B} T_0}{\mu m_{\rm p}} (\alpha + 1) \Delta^{\alpha - 1} \frac{{\rm d}\Delta}{{\rm d}r}. \tag{7}$$

We simplify the right-hand side of (6) by assuming that the distribution of the total mass is determined by the dark matter. For the density profile of the latter we follow [68]

$$\rho_{\rm dm} = \rho_{\rm s} \frac{4}{x(1+x)^2}, \tag{8}$$

with $x = r/r_{\rm s}$. The scaling radius, $r_{\rm s}$, is related to the virial radius, $r_{\rm vir}$, of a halo by $r_{\rm s} = r_{\rm vir}/c$, where c is the concentration parameter. The mass enclosed by the scaled radius x is

$$\begin{aligned} M(< x) &= 16\pi r_{\rm s}^3 \rho_{\rm s} \left\{ \ln(1+x) - \frac{x}{1+x} \right\} \\ &= 16\pi r_{\rm s}^3 \rho_{\rm s} F(x). \end{aligned} \tag{9}$$

Evidently, the virial radius encloses the virial mass, $M_{\rm vir} = M(< c)$. Dividing (9) by the virial mass leads to

$$M(< x) = M_{\rm vir} \frac{F(x)}{F(c)}. \tag{10}$$

Using $r = r_{\rm vir} x/c$ and the expression (7) we can rewrite (6)

$$\frac{k_{\rm B} T_0}{\mu m_{\rm p}} (\alpha + 1) \Delta^{\alpha - 1} {\rm d}\Delta = \frac{GM_{\rm vir}}{r_{\rm vir}} \frac{F(x)}{F(c)} \frac{c}{x^2} {\rm d}x. \tag{11}$$

We can further simplify the expression on the right-hand side by introducing the maximum circular velocity. The circular velocity is given by

$$\begin{aligned} v_{\rm circ}(r) &= \sqrt{\frac{GM(< r)}{r}} \\ &= \sqrt{\frac{GM_{\rm vir}}{r_{\rm vir}} \frac{c}{x} \frac{F(x)}{F(c)}}. \end{aligned} \tag{12}$$

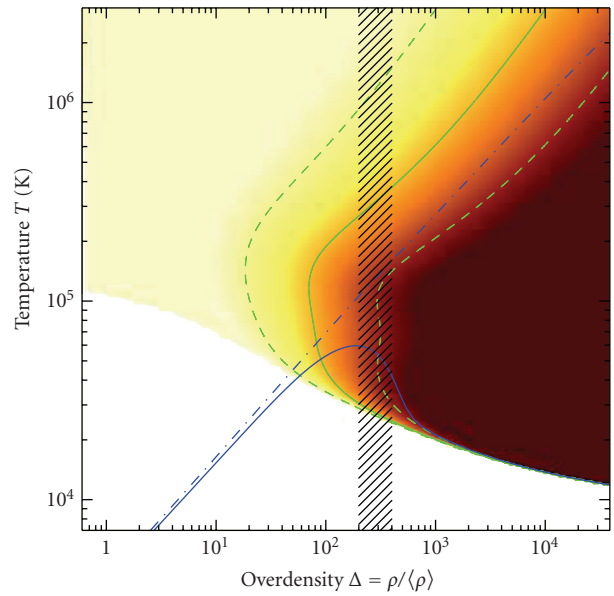

Figure 6: Theoretical result for $T(\Delta)$ with cooling (solid line) and without (dash-dotted line). The result without cooling follows the power-law $T = 3.85\,{\rm K}\,(\delta + 1)^{0.595}$. Cooling times are indicated by colours and contour lines. Contours from left to right are at 10x Hubble time (dashed line), Hubble time (solid line), and 0.1x Hubble time (dashed line). Cooling times are also indicated by colours, the blank area indicate the regime of UV heating. The hashed area highlights the transition region from cumulative photo-heating to thermal balance.

The quotient $F(x)/x$ is independent from the halo properties and has a maximum value of ∼0.22. Therefore, we can write for the maximum circular velocity

$$v_{\max}^2 = \frac{GM_{\rm vir}}{r_{\rm vir}} \frac{0.22c}{F(c)}. \tag{13}$$

Equation (11) is now independent from the concentration parameter of the halo, namely,

$$\frac{k_{\rm B}T_0}{\mu m_{\rm p}}(\alpha+1)\Delta^{\alpha-1}{\rm d}\Delta = \frac{v_{\max}^2}{0.22}\frac{F(x)}{x^2}{\rm d}x. \tag{14}$$

To determine the innermost gas overdensity we integrate (14) starting from the periphery of the halo, $x = x_{\rm out}$, to the center, $x = 0$. Since the halo gas is highly ionised we adopt $\mu = 0.59$. The resulting central overdensity is

$$\Delta_{\rm centre}^{\alpha} = \left(\frac{T_0}{10^4\,{\rm K}}\right)^{-1}\left(\frac{v_{\max}}{5.6\,{\rm km\ s^{-1}}}\right)^2 \times \frac{\alpha}{(\alpha+1)}\left(1-\frac{\ln(1+x_{\rm out})}{x_{\rm out}}\right)+\Delta_{\rm out}^{\alpha}, \tag{15}$$

where $\Delta_{\rm out}$ is the gas overdensity at $x_{\rm out}$. We estimate the outer overdensity by assuming that it is identical to the dark matter overdensity.

From (8) we get

$$\Delta_{\rm dm} = \frac{\rho_{\rm dm}}{\langle\rho_{\rm dm}\rangle} = \frac{\rho_{\rm s}}{\langle\rho_{\rm dm}\rangle}\frac{4}{x(1+x)^2}. \tag{16}$$

The virial radius is determined by the cumulative overdensity, $\Delta_{\rm c}(z)$, at which virialisation is expected. We use the approximation of [69] for $\Delta_{\rm c}(z)$. For the virial mass we write now

$$M_{\rm vir} = \frac{4}{3}\pi r_{\rm vir}^3\Delta_{\rm c}\langle\rho_{\rm dm}\rangle = 16\pi r_{\rm s}^3\rho_{\rm s}F(c), \tag{17}$$

where we have used (9) for the last equality. Substituting $r_{\rm s}/\langle\rho_{\rm dm}\rangle$ we can write for (16) that

$$\Delta_{\rm dm}(x_{\rm out}) = \frac{\Delta_{\rm c}(z)}{3}\frac{c^3}{F(c)}\frac{1}{x_{\rm out}(1+x_{\rm out})^2}, \tag{18}$$

which allows us to estimate $\Delta_{\rm out}$ in (15).

We wish to give the central gas overdensity as a function of the maximum circular velocity. To utilise (18) we have to find a relation between $v_{\max}$ and the concentration parameter. Macciò et al. [70] give an relation between c and the virial mass of a halo for $z = 0$:

$$c(M_{\rm vir}) = 10.47\times\left(\frac{M_{\rm vir}}{10^{12}\,h^{-1}M_\odot}\right)^{-0.109}. \tag{19}$$

From our simulations we find that $M_{\rm vir}$ and the maximum circular velocity are on average related by

$$\frac{M_{\rm vir}}{10^{12}\,h^{-1}M_\odot} = \left(\frac{v_{\max}}{210\,{\rm km\,s^{-1}}}\right)^{2.9}. \tag{20}$$

Moreover, the concentration parameter is expected to scale with redshift according to $c \sim (1+z)^{-1}$ [71, 72]. Thus, we obtain an relation between concentration parameter and $v_{\max}$, namely,

$$c(v_{\max}) = 10.47\left(\frac{v_{\max}}{210\,{\rm km\,s^{-1}}}\right)^{-0.32}\frac{1}{(z+1)}, \tag{21}$$

which allows us finally to evaluate (15).

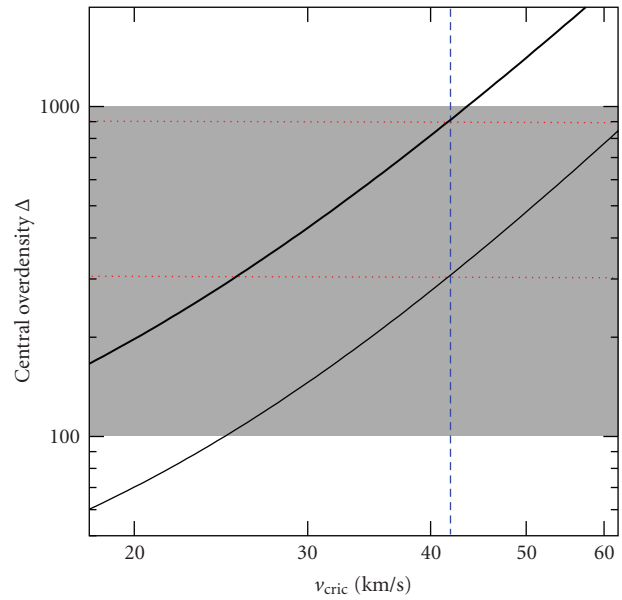

Figure 7: Central gas overdensity as a function of the halo circular velocity. We compute the central overdensity according to (15) (thick solid line). Moreover, we plot the overdensity at the scaling radius, $r_{\rm s}$ (thin solid line). The grey area indicates the transition region from pure UV heating to thermal balance, see Section 4.2 or Figure 6. The blue dashed line indicates the characteristic circular velocity obtained from the numerical simulations. The thick and the thin red dotted lines indicate a condensation criterion of $\Delta = 900$ and 300, respectively.

Finally, we compute the central gas overdensity as follows: For a given circular velocity we determine the concentration parameter of the halo by (21). Then we estimate the outer gas density, here we assume that $\Delta(x_{\rm out}) = \Delta_{\rm dm}(x_{\rm out})$, see (18), at three times the virial radius, $x_{\rm out} = 3c$. Finally, we compute the central gas overdensity, (15), as a function of the circular velocity, see Figure 7.

To estimate the characteristic circular velocity by our analytic model we have to give a criterion at which central overdensity gas condenses in a halo centre. The transition from the effective equation-of-state to the thermal balance takes place in the overdensity range of $10^2 < \Delta < 10^3$. For an overdensity of 900 our analytic model would match the characteristic circular velocity obtained from the numerical simulations. However, the resolution in the numerical simulation is not sufficient to reach the innermost gas density as assumed in our model. To mimic the numerical resolution we integrate (15) only up to the scaling radius, see thin line in Figure 7. In this case an overdensity of 300 corresponds to the characteristic circular velocity. This leads to two conclusions: First, the analytic model matches the numerical result very well. Secondly, better resolved simulations may

result in a lower characteristic velocity. However, gas mixing in the halo centre may generally prohibit an ideal hydrostatic equilibrium.

4.4. Evolution of the Characteristic Mass. In the previous section we have shown that our model well reproduces the characteristic circular velocity at $z = 0$. We can easily extend the model to other redshifts by determining the effective e.o.s and the criterion for condensation as a function of redshift. We derive the time-dependent e.o.s. by integrating (1), see Section 4.2. To obtain a time-dependent condensation criterion we determine the position of the maximum in the density-temperature relation, see the solid line in Figure 5. To compensate for the discrepancy between $\Delta_{\max}$ and the actual overdensity for condensation we introduce a correction factor. To match the characteristic circular velocity obtained from the simulations this factor also comprises the effect of the limited numerical resolution. Equation (15) can be now rewritten:

$$\left(\frac{v_{1/2}}{5.6\,\mathrm{km\,s^{-1}}}\right)^2 = \Delta_{\max}^{\alpha} f_{\mathrm{corr}} \frac{T_0}{10^4\,\mathrm{K}} \frac{\alpha+1}{\alpha}, \tag{22}$$

where we have neglected the contribution of the outer halo boundary. To match the characteristic circular velocity at $z = 0$ we choose $f_{\mathrm{corr}} = 2.5$. Equation (22) indicates that the characteristic circular velocity is essentially determined by the density-temperature relation at any time. All parameters on the r.h.s., namely slope and normalisation of the e.o.s. and $\Delta_{\max}$, are derived from $T(\Delta, t)$. Figure 8(upper row) shows how the characteristic circular velocity is composed of three parameters of the temperature-density relation. The upper left panel shows $T(\Delta)$ for several redshifts. The next three panels show the evolution of the parameters of $T(\Delta, t)$: The temperature T_0, the overdensity at the maximal temperature, $\Delta_{\max}$, and the slope $\mathrm{dlog}T(\Delta, t)/\mathrm{dlog}\Delta$ at $\Delta = 1$. The right panel shows the resulting $v_{1/2}$, which nicely matches the characteristic circular velocity obtained from the numerical simulations. In the range $3 \gtrsim z \geq 0$ the circular velocity is virtually constant. This is the result of the decreasing T_0 and the increasing $\Delta_{\max}$.

The redshift evolution of the characteristic mass can be derived from characteristic circular and (13) and (17). Combining these equations and using $\langle\rho\rangle \propto (z+1)^3$ we find

$$M_{1/2} \propto v_{1/2}^3 \Delta_{\mathrm{c}}^{-1/2}(z)(z+1)^{-3/2}. \tag{23}$$

This is in agreement with the results found earlier [7]. More precisely, the dominating terms in $M_{1/2}$ are introduced by the redshift dependence in the definition of the virial radius, (17).

4.5. Variations in the UV Background. As shown above the cumulative heating of the IGM by the UV background prevents the gas cooling in the centre of small mass haloes. It is therefore evident that the characteristic mass depends on the UV background and its evolution over cosmic times. We use our model worked out above to assess the impact of modifications of the UV background model on the characteristic circular velocity. We first consider changes of the UV flux density and secondly of the UV spectrum.

4.5.1. UV Flux Density. The flux density of the UV background has only a small effect on the temperature of the IGM. The reason is that a higher flux reduces the fraction of neutral hydrogen in the tenuous IGM, hence, the higher flux finds fewer neutral atoms to ionise. As a result the heating rate is essentially independent from the flux density, when photo-ionisation dominates over collisional ionisation and as long as the spectrum remains unchanged. In this case the fraction of neutral hydrogen, $x_{\mathrm{HI}} = 1 - x_{\mathrm{HII}}$, can be derived from the balance between photo-ionisation and recombination

$$\Gamma_{\gamma\mathrm{HI}} x_{\mathrm{HI}} n_{\mathrm{H}} = \alpha_{\mathrm{HII}}(T) x_{\mathrm{HII}} n_{\mathrm{H}} n_{\mathrm{e}}. \tag{24}$$

The IGM is generally highly ionised, hence $x_{\mathrm{HII}} \sim 1$. In this case the electron density is proportional to the hydrogen density, $n_{\mathrm{e}} \sim n_{\mathrm{H}}$. As a result the heating due to hydrogen ionisation becomes

$$\mathcal{H}_{\mathrm{HI}} = n_{\mathrm{HI}} \epsilon_{\mathrm{HI}} \sim \alpha_{\mathrm{HII}}(T) \frac{\epsilon_{\mathrm{HII}}}{\Gamma_{\gamma\mathrm{HI}}} n_{\mathrm{H}}^2. \tag{25}$$

The heating therefore depends only on the ratio $\epsilon_{\mathrm{HII}}/\Gamma_{\gamma\mathrm{HI}}$, that is, only on the average energy input per ionisation event. In the limits made above the heat input is independent from the actual flux density. In accordance with this result we have found in [7] that the characteristic mass depends only little on the UV background flux density. Even very strong variations of the flux causes only a small shift of the characteristic mass, showing that the latter is sensitive only to the thermal state of the IGM which is little affected by the actual flux density.

4.5.2. UV Spectrum. Significantly more important for the thermal evolution of the IGM is the spectrum of the UV background. As a first guess one may expect that the final temperature of the IGM is directly proportional to the energy per ionising photon. However, since the recombination rate, $\alpha_{\mathrm{HII}}(T)$, decreases with increasing temperature the effect is not that strong. Figure 9 shows the results for increased energies per ionising photon compared to the [73] model. We have computed models with four times and with eight times increased energy per ionisation event. The higher average energy shifts the effective equation-of-state to higher temperatures. Also the shape of the temperature-density relation changes. The maximum in the relation shifts to higher densities. In particular, the maximum changes significantly between the four times and eight times increased model. The effective equation-of-state runs in the cooling regime virtually parallel to lines of constant cooling times. When $T_0 \gtrsim 1.5 \times 10^4\,\mathrm{K}$ these cooling times are above the Hubble time. In those cases the cases the transition to thermal balance appears at very high overdensities.

We use the models introduced above to estimate the impact of the UV spectrum on the characteristic circular velocity. To this end we compute the evolution of the characteristics of the temperature-density relation, see Figure 8. For the four times increased energy per ionising photon we find that the characteristic circular velocity amounts to $\sim 60\,\mathrm{km\,s^{-1}}$ for $z \lesssim 2$. For the eight times increased model

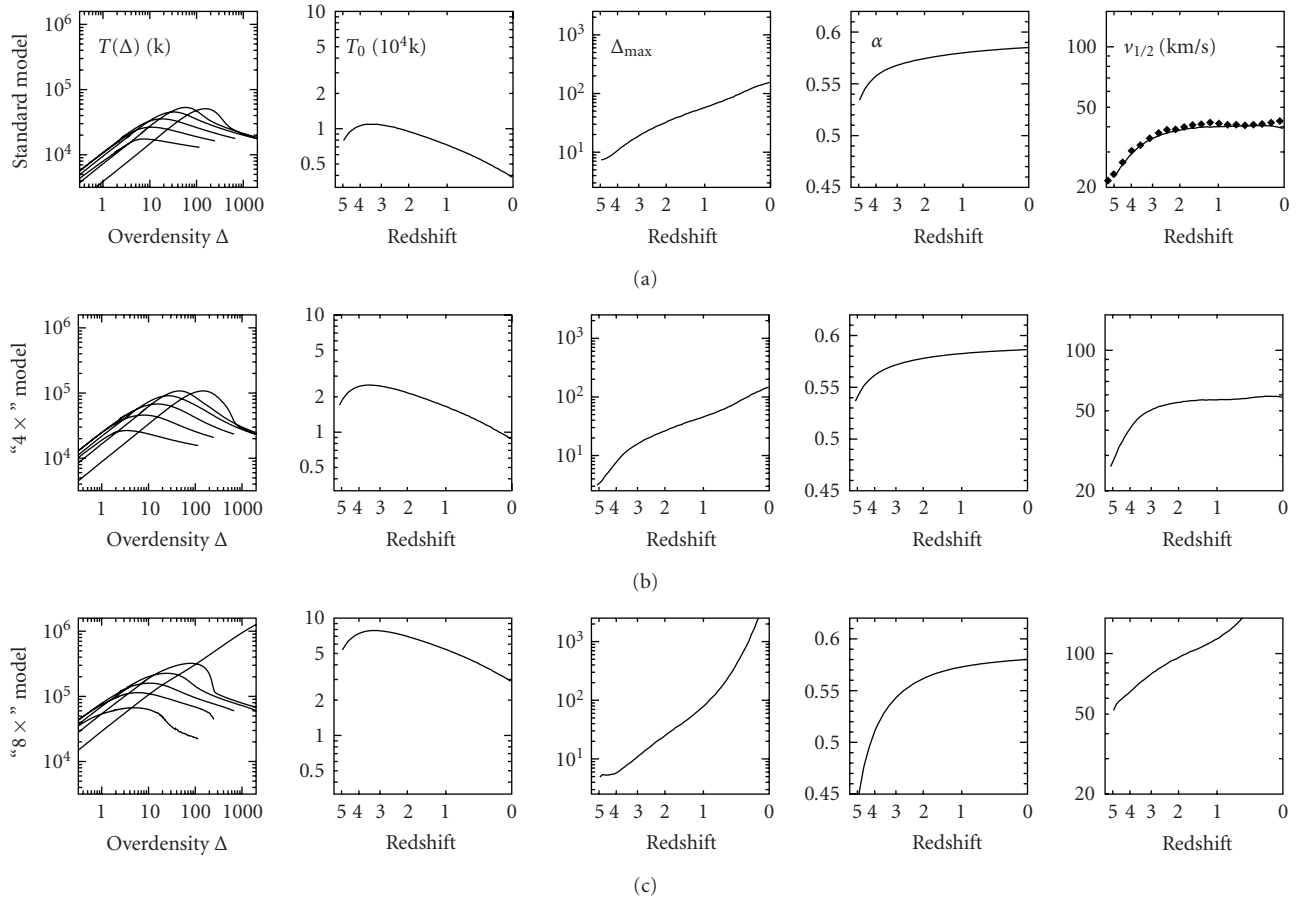

FIGURE 8: *Left panels*: The density-temperature $T(\Delta, t)$ for several redshifts and three different UV-background models. The next three columns show the redshift evolution of the parameters of $T(\Delta, t)$: The normalisation and the effective e.o.s., T_0, the position of the maximum, $\Delta_{\max}$, and the slope of the e.o.s., α. Finally, for each UV-background model the resulting characteristic circular velocity is shown, see (22). The upper right panel shows also the characteristic velocity obtained from the numerical simulations.

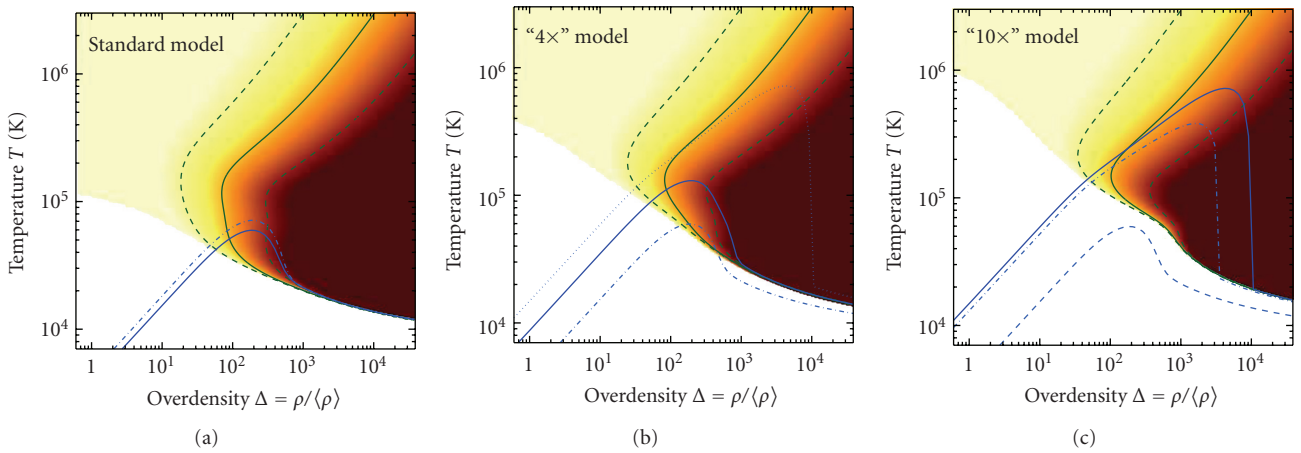

FIGURE 9: Theoretical results for temperature distribution in the IGM as a result of different UVB heating models. (a) The thick solid line indicate the result for our standard model according to [73]. Color coded is the cooling time. The blank area indicates the region where the gas is heated. Three contour lines are shown, they indicate from the left to right a cooling time 10x, 1x, and 0.1x the Hubble time. The dashed blue line indicates a four times increased energy per ionising photon only for $z > 2$. (b) Results for four times increased energy per ionising photon for all redshifts. For comparison the dashed blue line indicates temperature distribution resulting from the standard model as shown in (a). (c) Results for ten times increased energy per ionising photon for all redshifts. For comparison also the eight times increased energy and the standard heating as shown in (a) are indicated.

the characteristic velocity get very high, since $\Delta_{\max}$ shifts to very high overdensities.

5. Summary

We discuss high-resolution simulations including radiative cooling and photoheating. We focus on the baryon content of dwarf galaxy-sized dark matter haloes. To this end, we have simulated the structure formation in two distinct cosmological environments and we found that the characteristic mass below which haloes are baryon deficient does not depend on the environment. Moreover, we found that in haloes in the mass range of $\sim 10^9$ to $10^{10}\, h^{-1}\, M_\odot$ in general gas condensation stops at some redshift between reionisation and today. In our simulation those haloes are able to retain the already condensed gas, allowing further star formation. We have derived the characteristic mass in newly accreted matter, which is somewhat higher than the characteristic mass of the baryon fraction in the haloes. The former is more appropriate for semianalytic modelling.

Tinker and Conroy [66] found by a Halo Occupation Distribution analysis that the magnitude of galaxies which reside in haloes with a mass about the characteristic mass is $M_r \sim -10$. Moreover, they found that more luminous void galaxies, that is, $M_r > -10$, are preferably located close to the walls of the voids. Therefore, photo-heating would reduce the baryon content of the small-mass haloes populating the entire void volume, rendering these galaxies even more dark. Current surveys which cover large void volumes are not sensitive enough to detect the galaxies affected by photo-heating.

The failure of condensing gas can be traced back to the cooling time in the halo centre, which may exceed the Hubble time. We have set up a spherical model for the haloes gas density profile. Crucial for this model is the effective equation of state which we have derived by integrating the thermal history of the IGM using an approximation for the overdensity evolution as a function of the final overdensity We have justified this model by considering the density contrast evolution in the simulation. This spherical model allows us to derive the characteristic mass for different heating histories of the IGM.

We find that the mass at which galaxy formation seems to fade can be explained by a heating model which incorporates 6–8 times more energy per ionising photon than given in the Haardt and Madau model [73]. For redshift $z \gtrsim 3$ it is known from analyses of the Lymanα forest that the temperature of the IGM is higher than obtained by a naive application of the Haardt and Madau model. The derived temperature implies a 3-4 times increased energy per ionising photon, or a more efficient heating due to non-equilibrium effects or radiative transfer effects. We found that if the average temperature of the IGM is today as high as $\gtrsim 10^4$ K dwarf galaxy formation would be suppressed at a mass scale consistent with that derived, for example, by the conditional luminosity function. Therefore, the mass scale for suppression of dwarf galaxy formation may be considered as a measure for the temperature of gas in the surroundings of dwarf galaxies. The heat source could be the UV background or alternatively any feedback of the galaxy.

Acknowledgments

The simulations discussed here have been performed at the LRZ Munich and the NIC Jülich. The authors would like to thank Gustavo Yepes and Volker Springel for many comments and discussions during the last years. Finally, they would like to thank their referees, in particular Michael Vogeley, who read the paper very carefully and provided many comments which improved this text.

References

[1] S. D. M. White and M. J. Rees, "Core condensation in heavy halos—a two-stage theory for galaxy formation and clustering," *Monthly Notices of the Royal Astronomical Society*, vol. 183, pp. 341–358, 1978.

[2] A. Klypin, A. V. Kravtsov, O. Valenzuela, and F. Prada, "Where are the missing galactic satellites?" *The Astrophysical Journal*, vol. 522, no. 1, pp. 82–92, 1999.

[3] B. Moore, S. Ghigna, F. Governato, et al., "Dark matter substructure within galactic halos," *The Astrophysical Journal*, vol. 524, no. 1, pp. L19–L22, 1999.

[4] S. Gottlöber, E. L. Łokas, A. Klypin, and Y. Hoffman, "The structure of voids," *Monthly Notices of the Royal Astronomical Society*, vol. 344, no. 3, pp. 715–724, 2003.

[5] P. J. E. Peebles, "The void phenomenon," *The Astrophysical Journal*, vol. 557, no. 2, pp. 495–504, 2001.

[6] A. V. Tikhonov and A. Klypin, "The emptiness of voids: yet another overabundance problem for the Λ cold dark matter model," *Monthly Notices of the Royal Astronomical Society*, vol. 395, no. 4, pp. 1915–1924, 2009.

[7] M. Hoeft, G. Yepes, S. Gottlöber, and V. Springel, "Dwarf galaxies in voids: suppressing star formation with photoheating," *Monthly Notices of the Royal Astronomical Society*, vol. 371, no. 1, pp. 401–414, 2006.

[8] A. V. Macciò, X. Kang, F. Fontanot, R. S. Somerville, S. E. Koposov, and P. Monaco, "Luminosity function and radial distribution of Milky Way satellites in a LCDM universe," *Monthly Notices of the Royal Astronomical Society*, vol. 402, no. 4, pp. 1995–2008, 2010.

[9] S. E. Koposov, J. Yoo, H.-W. Rix, D. H. Weinberg, A. V. Macciò, and J. M. Escudé, "A quantitative explanation of the observed population of Milky Way satellite galaxies," *The Astrophysical Journal*, vol. 696, no. 2, pp. 2179–2194, 2009.

[10] A. V. Tikhonov, S. Gottlöber, G. Yepes, and Y. Hoffman, "The sizes of minivoids in the local universe: an argument in favour of a warm dark matter model?" *Monthly Notices of the Royal Astronomical Society*, vol. 399, no. 3, pp. 1611–1621, 2009.

[11] J. Zavala, Y. P. Jing, A. Faltenbacher, et al., "The velocity function in the local environment from ΛCDM and ΛWDM constrained simulations," *The Astrophysical Journal*, vol. 700, no. 2, pp. 1779–1793, 2009.

[12] G. Hinshaw, J. L. Weiland, R. S. Hill, et al., "Five-year wilkinson microwave anisotropy probe observations: data processing, sky maps and basic results," *Astrophysical Journal, Supplement Series*, vol. 180, no. 2, pp. 225–245, 2009.

[13] A. Klypin, A. V. Kravtsov, J. S. Bullock, and J. R. Primack, "Resolving the structure of cold dark matter halos," *The Astrophysical Journal*, vol. 554, no. 2, pp. 903–915, 2001.

[14] V. Springel and L. Hernquist, "Cosmological smoothed particle hydrodynamics simulations: the entropy equation," *Monthly Notices of the Royal Astronomical Society*, vol. 333, no. 3, pp. 649–664, 2002.

[15] V. Springel, N. Yoshida, and S. D. M. White, "GADGET: a code for collisionless and gasdynamical cosmological simulations," *New Astronomy*, vol. 6, no. 2, pp. 79–117, 2001.

[16] N. Katz, D. H. Weinberg, and L. Hernquist, "Cosmological simulations with TreeSPH," *Astrophysical Journal, Supplement Series*, vol. 105, no. 1, pp. 19–35, 1996.

[17] V. Springel and L. Hernquist, "Cosmological smoothed particle hydrodynamics simulations: a hybrid multiphase model for star formation," *Monthly Notices of the Royal Astronomical Society*, vol. 339, no. 2, pp. 289–311, 2003.

[18] G. Yepes, R. Kates, A. Khokhlov, and A. Klypin, "Hydrodynamical simulations of galaxy formation: effects of supernova feedback," *Monthly Notices of the Royal Astronomical Society*, vol. 284, no. 1, pp. 235–256, 1997.

[19] A. Klypin, S. Gottlöber, A. V. Kravtsov, and A. M. Khokhlov, "Galaxies in N-body simulations: overcoming the overmerging problem," *The Astrophysical Journal*, vol. 516, no. 2, pp. 530–551, 1999.

[20] W. H. Press and P. Schechter, "Formation of galaxies and clusters of galaxies by self-similar gravitational condensation," *The Astrophysical Journal*, vol. 187, pp. 425–438, 1974.

[21] J. R. Bond, S. Cole, G. Efstathiou, and N. Kaiser, "Excursion set mass functions for hierarchical Gaussian fluctuations," *The Astrophysical Journal*, vol. 379, no. 2, pp. 440–460, 1991.

[22] R. K. Sheth and G. Tormen, "Large-scale bias and the peak background split," *Monthly Notices of the Royal Astronomical Society*, vol. 308, no. 1, pp. 119–126, 1999.

[23] A. Jenkins, C. S. Frenk, S. D. M. White, et al., "The mass function of dark matter haloes," *Monthly Notices of the Royal Astronomical Society*, vol. 321, no. 2, pp. 372–384, 2001.

[24] J. Tinker, A. V. Kravtsov, A. Klypin, et al., "Toward a halo mass function for precision cosmology: the limits of universality," *The Astrophysical Journal*, vol. 688, no. 2, pp. 709–728, 2008.

[25] M. S. Warren, K. Abazajian, D. E. Holz, and L. Teodoro, "Precision determination of the mass function of dark matter halos," *The Astrophysical Journal*, vol. 646, no. 2, pp. 881–885, 2006.

[26] S. A. Gregory and L. A. Thompson, "The Coma/A1367 supercluster and its environs," *The Astrophysical Journal*, vol. 222, pp. 784–799, 1978.

[27] M. Joeveer, J. Einasto, and E. Tago, "Spatial distribution of galaxies and of clusters of galaxies in the southern galactic hemisphere," *Monthly Notices of the Royal Astronomical Society*, vol. 185, pp. 357–370, 1978.

[28] R. P. Kirshner, A. Oemler, P. L. Schechter, and S. A. Shectman, "A million cubic megaparsec void in Bootes," *The Astrophysical Journal Letters*, vol. 248, no. 5, pp. L57–L60, 1981.

[29] Y. Hoffman and J. Shaham, "On the origin of the voids in the galaxy distribution," *The Astrophysical Journal Letters*, vol. 262, pp. L23–L26, 1982.

[30] P. J. E. Peebles, "Large-scale background temperature and mass fluctuations due to scaleinvariant primeval perturbations," *The Astrophysical Journal Letters*, vol. 263, pp. L1–L5, 1982.

[31] J. Einasto, M. Einasto, and M. Gramann, "Structure and formation of superclusters. IX. Selfsimilarity of voids," *Monthly Notices of the Royal Astronomical Society*, vol. 238, pp. 155–177, 1989.

[32] M. S. Vogeley, M. J. Geller, C. Park, and J. P. Huchra, "Voids and constraints on nonlinear clustering of galaxies," *Astronomical Journal*, vol. 108, no. 3, pp. 745–758, 1994.

[33] V. Müller, S. Arbabi-Bidgoli, J. Einasto, and D. Tucker, "Voids in the Las Campanas Redshift Survey versus cold dark matter models," *Monthly Notices of the Royal Astronomical Society*, vol. 318, no. 1, pp. 280–288, 2000.

[34] H. El-Ad and T. Piran, "Voids in the large-scale structure," *The Astrophysical Journal*, vol. 491, no. 2, pp. 421–435, 1997.

[35] H. El-Ad and T. Piran, "A case devoid of bias: optical redshift survey voids versus IRAS voids," *Monthly Notices of the Royal Astronomical Society*, vol. 313, no. 3, pp. 553–558, 2000.

[36] M. Plionis and S. Basilakos, "The size and shape of local voids," *Monthly Notices of the Royal Astronomical Society*, vol. 330, no. 2, pp. 399–404, 2002.

[37] F. Hoyle and M. S. Vogeley, "Voids in the point source catalogue survey and the updated zwicky catalog," *The Astrophysical Journal*, vol. 566, no. 2, pp. 641–651, 2002.

[38] L. Ceccarelli, N. D. Padilla, C. Valotto, and D. G. Lambas, "Voids in the 2dFGRS and ACDM simulations: spatial and dynamical properties," *Monthly Notices of the Royal Astronomical Society*, vol. 373, no. 4, pp. 1440–1450, 2006.

[39] D. J. Croton, E. Gaztañaga, C. M. Baugh, et al., "The 2dF Galaxy Redshift Survey: higher-order galaxy correlation functions," *Monthly Notices of the Royal Astronomical Society*, vol. 352, no. 4, pp. 1232–1244, 2004.

[40] F. Hoyle and M. S. Vogeley, "Voids in the two-degree field galaxy redshift survey," *The Astrophysical Journal*, vol. 607, no. 2, pp. 751–764, 2004.

[41] S. G. Patiri, J. E. Betancort-Rijo, F. Prada, A. Klypin, and S. Gottlöber, "Statistics of voids in the two-degree Field Galaxy Redshift Survey," *Monthly Notices of the Royal Astronomical Society*, vol. 369, no. 1, pp. 335–348, 2006.

[42] D. M. Goldberg, T. D. Jones, F. Hoyle, R. R. Rojas, M. S. Vogeley, and M. R. Blanton, "The mass function of void galaxies in the sloan digital sky survey data release 2," *The Astrophysical Journal*, vol. 621, no. 2, pp. 643–650, 2005.

[43] F. Hoyle, R. R. Rojas, M. S. Vogeley, and J. Brinkmann, "The luminosity function of void galaxies in the sloan digital sky survey," *The Astrophysical Journal*, vol. 620, no. 2, pp. 618–628, 2005.

[44] R. R. Rojas, M. S. Vogeley, F. Hoyle, and J. Brinkmann, "Photometric properties of void galaxies in the sloan digital sky survey," *The Astrophysical Journal*, vol. 617, no. 1, pp. 50–63, 2004.

[45] M. S. Vogeley, F. Hoyle, R. R. Rojas, and D. Goldberg, "The void spectrum and properties of void galaxies in the SDSS," *Bulletin of the American Astronomical Society*, vol. 36, p. 1496, 2004.

[46] N. A. Grogin and M. J. Geller, "An imaging and spectroscopic survey of galaxies within prominent nearby voids. I. The sample and luminosity distribution," *Astronomical Journal*, vol. 118, no. 6, pp. 2561–2580, 1999.

[47] B. Kuhn, U. Hopp, and H. Elsässer, "Results of a search for faint galaxies in voids," *Astronomy & Astrophysics*, vol. 318, no. 2, pp. 405–415, 1997.

[48] U. Lindner, M. Einasto, J. Einasto, et al., "The distribution of galaxies in voids," *Astronomy & Astrophysics*, vol. 314, no. 3, pp. 1–12, 1996.

[49] C. C. Popescu, U. Hopp, and H. Elsässer, "Results of a search for emission-line galaxies towards nearby voids. The spatial distribution," *Astronomy & Astrophysics*, vol. 325, no. 3, pp. 881–892, 1997.

[50] A. J. Benson, C. S. Frenk, C. G. Lacey, C. M. Baugh, and S. Cole, "The effects of photoionization on galaxy formation. II. Satellite galaxies in the Local Group," *Monthly Notices of the Royal Astronomical Society*, vol. 333, no. 1, pp. 177–190, 2002.

[51] J. Einasto, M. Einasto, M. Gramann, and E. Saar, "Structure and formation of superclusters. XIII. The void probability function," *Monthly Notices of the Royal Astronomical Society*, vol. 248, pp. 593–605, 1991.

[52] Y. Friedmann and T. Piran, "A model of void formation," *The Astrophysical Journal*, vol. 548, no. 1, pp. 1–6, 2001.

[53] S. R. Furlanetto and T. Piran, "The evidence of absence: galaxy voids in the excursion set formalism," *Monthly Notices of the Royal Astronomical Society*, vol. 366, no. 2, pp. 467–479, 2006.

[54] S. Ghigna, S. A. Bonometto, J. Retzlaff, S. Gottlöber, and G. Murante, "Void analysis as a test for dark matter composition?" *The Astrophysical Journal*, vol. 469, no. 1, pp. 40–47, 1996.

[55] S. Ghigna, S. Borgani, S. A. Bonometto, et al., "Sizes of voids as a test for dark matter models," *The Astrophysical Journal*, vol. 437, no. 2, pp. L71–L74, 1994.

[56] J. Lee and D. Park, "Rotation of cosmic voids and void spin statistics," *The Astrophysical Journal*, vol. 652, no. 1, pp. 1–5, 2006.

[57] H. Mathis and S. D. M. White, "Voids in the simulated local universe," *Monthly Notices of the Royal Astronomical Society*, vol. 337, no. 4, pp. 1193–1206, 2002.

[58] V. Sahni, B. S. Sathyaprakash, and S. F. Shandarin, "The evolution of voids in the adhesion approximation," *The Astrophysical Journal*, vol. 431, no. 1, pp. 20–40, 1994.

[59] S. Shandarin, H. A. Feldman, K. Heitmann, and S. Habib, "Shapes and sizes of voids in the Lambda cold dark matter universe: excursion set approach," *Monthly Notices of the Royal Astronomical Society*, vol. 367, no. 4, pp. 1629–1640, 2006.

[60] J. M. Colberg, F. Pearce, C. Foster, et al., "The Aspen-Amsterdam void finder comparison project," *Monthly Notices of the Royal Astronomical Society*, vol. 387, no. 2, pp. 933–944, 2008.

[61] F. C. van den Bosch, X. Yang, H. J. Mo, et al., "Towards a concordant model of halo occupation statistics," *Monthly Notices of the Royal Astronomical Society*, vol. 376, no. 2, pp. 841–860, 2007.

[62] T. Okamoto, L. Gao, and T. Theuns, "Mass loss of galaxies due to an ultraviolet background," *Monthly Notices of the Royal Astronomical Society*, vol. 390, no. 3, pp. 920–928, 2008.

[63] O. Fakhouri and C.-P. Ma, "Dark matter halo growth. II. Diffuse accretion and its environmental dependence," *Monthly Notices of the Royal Astronomical Society*, vol. 401, no. 4, pp. 2245–2256, 2010.

[64] R. S. Somerville, "Can photoionization squelching resolve the substructure crisis?" *The Astrophysical Journal*, vol. 572, no. 1, pp. L23–L26, 2002.

[65] Y.-S. Li, G. De Lucia, and A. Helmi, "On the nature of the Milky Way satellites," *Monthly Notices of the Royal Astronomical Society*, vol. 401, no. 3, pp. 2036–2052, 2010.

[66] J. L. Tinker and C. Conroy, "The void phenomenon explained," *The Astrophysical Journal*, vol. 691, pp. 633–639, 2009.

[67] S. S. McGaugh, J. M. Schombert, W. J. G. de Blok, and M. J. Zagursky, "The baryon content of cosmic structures," *The Astrophysical Journal Letters*, vol. 708, no. 1, pp. L14–L17, 2010.

[68] J. F. Navarro, C. S. Frenk, and S. D. M. White, "A universal density profile from hierarchical clustering," *The Astrophysical Journal*, vol. 490, no. 2, pp. 493–508, 1997.

[69] G. L. Bryan and M. L. Norman, "Statistical properties of X-ray clusters: analytic and numerical comparisons," *The Astrophysical Journal*, vol. 495, no. 1, pp. 80–99, 1998.

[70] A. V. Macciò, A. A. Dutton, F. C. van den Bosch, B. Moore, D. Potter, and J. Stadel, "Concentration, spin and shape of dark matter haloes: scatter and the dependence on mass and environment," *Monthly Notices of the Royal Astronomical Society*, vol. 378, no. 1, pp. 55–71, 2007.

[71] R. H. Wechsler, J. S. Bullock, J. R. Primack, A. V. Kravtsov, and A. Dekel, "Concentrations of dark halos from their assembly histories," *The Astrophysical Journal*, vol. 568, no. 1, pp. 52–70, 2002.

[72] D. H. Zhao, Y. P. Jing, H. J. Mo, and G. Börner, "Mass and redshift dependence of dark halo structure," *The Astrophysical Journal*, vol. 597, no. 1, pp. L9–L12, 2003.

[73] F. Haardt and P. Madau, "Radiative transfer in a clumpy universe. II. The ultraviolet extragalactic background," *The Astrophysical Journal*, vol. 461, no. 1, pp. 20–37, 1996.

Hindawi Publishing Corporation
Advances in Astronomy
Volume 2010, Article ID 651621, 5 pages
doi:10.1155/2010/651621

Review Article

Star Formation History of Dwarf Galaxies in Cosmological Hydrodynamic Simulations

Kentaro Nagamine

Department of Physics and Astronomy, University of Nevada, Las Vegas 4505 S. Maryland Pkwy, Box 454002, Las Vegas, NV 89154-4002, USA

Correspondence should be addressed to Kentaro Nagamine, kn@physics.unlv.edu

Received 8 May 2009; Revised 31 August 2009; Accepted 30 September 2009

Academic Editor: Andrey V. Kravtsov

We examine the past and current work on the star formation (SF) histories of dwarf galaxies in cosmological hydrodynamic simulations. The results obtained from different numerical methods are still somewhat mixed, but the differences are understandable if we consider the numerical and resolution effects. It remains a challenge to simulate the episodic nature of SF history in dwarf galaxies at late times within the cosmological context of a cold dark matter model. More work is needed to solve the mysteries of SF history of dwarf galaxies employing large-scale hydrodynamic simulations on the next generation of supercomputers.

1. Introduction

Dwarf galaxies play unique roles in the cosmological studies of galaxy formation. Low-mass galaxies contribute the most to the cosmic star formation rate (SFR) density at low redshift, and in contrast the star formation in high-mass galaxies seems to cease at $z \gtrsim 1$ [1, 2]: the so-called "downsizing" effect in galaxy formation. This global trend of star formation is presumably driven by the feedback effects by supernovae (SNe) and supermassive black holes as well as the cosmological effects such as the expansion and the reionization of the Universe. All of these effects can suppress the star formation, eventually giving rise to the characteristic shape of galaxy luminosity function. The question that is not fully answered yet is "which physical processes have the strongest impact, and which galaxies are affected the most?" Studying the star formation in dwarf galaxies gives us useful clues not only on the physics of star formation but also on the feedback processes that cause the downsizing in galaxy formation and how the galaxy luminosity function has been shaped over time.

Observations of stellar populations suggest that the star formation in dwarf galaxies [3–7] is sporadic, separated by millions to billions of years, even in isolated systems. What causes the episodic SF history? Past interaction with other galaxies or merger events are obvious possibilities to explain the SF activity in these systems, but the lack of tidal debris in the outer regions of dwarf galaxies argues against such scenarios [8]. Then the remaining likely possibility is the instability in the local interstellar medium (ISM); however, many interesting questions remain. For example, why is it *now* that they are undergoing active star formation? What determines the epoch and the duration of star formation? Is it the local physics or the cosmological processes that are more important in determining the downsizing effect?

While the recent episodic SF activity is observed in dwarf galaxies, most dwarf galaxies in the Local Group are also dominated by the old stellar populations (ages of $\gtrsim$10 Gyr) with an occasional mixture of younger stars [9–12]. This suggests that the main formation epoch of those dwarf galaxies was before $z \sim 6$.

It is important to address the above questions using the *ab initio* cosmological hydrodynamic simulations, in which the gas dynamics is simulated self-consistently from early universe to the present time. Although there has been much numerical work on the formation of dwarf galaxies [13–20], usually the work is presented in the context of reionization or the missing satellite problem, and most publications do not present the SF histories of dwarf galaxies in their simulations.

As we describe in the next section, explaining the episodic nature of SF history in low-mass systems remains a challenge for many reasons in the framework of cold dark matter (CDM) model. The purpose of this short article is to record what we know on the SF history of dwarf galaxies in the past and current cosmological hydrodynamic simulations.

2. Cosmological Hydrodynamic Simulations

2.1. Star Formation Model. In order to simulate the formation and evolution of dwarf galaxies, one has to model the collapse of gas clouds and subsequent star formation. In most cosmological simulations, the star formation is modeled by creating a star particle from a parcel of gas (either the gas in an Eulerian cell or a gas particle in the case of smoothed particle hydrodynamics [SPH]) when the following criteria are satisfied [21, 22]: (i) the region is overdense ($\delta > \delta_c$), (ii) converging gas flow ($\nabla \cdot \mathbf{v} < 0$), (iii) cooling rapidly ($t_{\rm cool} < t_{\rm dyn}$), and (iv) Jeans unstable ($m_{\rm gas} > m_{\rm Jeans}$). One would expect that if the condition (iii) or (iv) is satisfied, the other conditions are also likely to be met, but more rigorous analyses would be required to assess which criterion is the most important one. There are other variants of SF models, but the discussion will be deferred to another place [23].

Simulations of galaxy formation require vast dynamic ranges in both mass and space: from molecular clouds (~parsecs) to groups/clusters of galaxies (~mega-parsecs). With the currently available computational resources, it is still difficult to resolve the details of molecular clouds while simultaneously simulating the formation of thousands of galaxies on the scales of $\gtrsim$10 Mpc. In other words, we can reliably identify the sites of galaxy formation on large scales and simulate the average SFR of each galaxy, but the small-scale instabilities of multiphase ISM on subparsec scales caused by, for example, turbulence, cannot be followed in detail in cosmological simulations. As we will describe in the next section in more detail, the earlier Eulerian cosmological simulation [24] was not able to reproduce the episodic nature of SF history, even though it properly simulated the gas dynamics on large scales ($\gtrsim$20 kpc). This suggests that the sporadic star formation in dwarf galaxies is driven by the instabilities on small scales, which is difficult to simulate properly with the current resolution limits.

The above limitation is a typical criticism directed towards cosmological simulations; however, the cosmological simulations can calculate the amount of gas that fall into the region correctly. Combined with a star formation law, we can calculate the overall SFR of the system, which is valid within the limitations of the model and still is relevant to the subject of this article. We simulate the gas dynamics at intermediate scales (~kpc) as accurately as possible and treat the small-scale physics with a subgrid/particle model for star formation and SN feedback based on our astrophysical knowledge. In this approach, the SFR is calculated as $\dot{\rho}_\star = c_\star(\rho_{\rm gas}/t_\star)$, where $c_\star$ is the SF efficiency and $t_\star$ is the SF time-scale. Both of these parameters are usually adjusted so that the simulation result matches the observed Kennicutt-Schmidt law [25, 26]. One can further adopt a subgrid/particle model [27, 28] to calculate the cold gas density $\rho_{\rm cold}$ and use this in place of $\rho_{\rm gas}$ in the above SF law. The projected SFR generally follows the Kennicutt law well [27, 29–31], but the consequences of the adopted SF model (e.g., the SF threshold density or the equation of state) must be studied further [23].

2.2. Past and Current Work. The work in [24] showed that, using an Eulerian cosmological hydrodynamic simulation, the star formation ceased at high redshift in the dwarf galaxies that survived to $z = 0$. In their simulation, only 7% of stars formed below $z = 1$ in galaxies with stellar masses $2\times10^8 < M_\star(z=0) < 2\times10^9 h^{-1}M_\odot$, and no stars formed at $z < 1$ in galaxies with $M_\star(z=0) < 2\times10^8 h^{-1}M_\odot$. This result is consistent with the general expectation in the CDM model, in which the small systems form early on and the accretion of material stops thereafter, as the residual gas is easily swept out by the SN feedback or evaporated by photoionization [13, 32–36]. The conclusion of [24] was that, in a CDM universe, dwarf galaxies found today are dominated by old stars; they consist predominantly of stars 10 Gyrs old and do not show recent SF activity.

However, as we outlined in Section 1, the observed SF histories of dwarf galaxies exhibit sporadic SF activity at late times, and we wonder whether the result of [24] was affected by the resolution limitation. Eulerian mesh simulations lose the physical spatial resolution at late times owing to the cosmic expansion. On the other hand, they generally have a larger mesh number compared to the number of particles employed in cosmological SPH simulations; hence they have higher baryonic mass resolution at early times than SPH simulations. (If the number of dark matter particles and the box sizes are comparable, then the resolution in the initial gravitational field would be similar in the two methods.) This numerical trend could explain the efficient conversion of gas into stars at early times and the lack of SF activity at late times in the Eulerian mesh simulation of [24], because the simulation may underestimate the cooling rate of gas when it cannot resolve the density fluctuation of gas on scales below the physical mesh size, as they approach to the present time. A related notable advantage of the Eulerian mesh simulation over the SPH method is that it is better at modeling the gas in low-density regions; therefore it is more suitable for the study of Ly-α forest [37].

In contrast to the Eulerian mesh simulation, the SPH simulation is more suitable to simulate the late-time evolution of high-density regions owing to its Lagrangian nature. Therefore one might expect that the SPH simulations perform better in modeling the sporadic SF history at late times in dwarf galaxies. In the left panel of Figure 1, we compare some examples of SF history in a cosmological SPH simulation of a comoving box size $L_{\rm box} = 100\,h^{-1}$ Mpc and 2×400^3 (gas and dark matter) particles. The adopted cosmological parameters are consistent with the latest WMAP5 results [38]: $(\Omega_{\rm m}, \Omega_\Lambda, \Omega_{\rm b}, \sigma_8, h) = (0.26, 0.74, 0.044, 0.80, 0.72)$, where $h = H_0/(100\,{\rm km\,s^{-1}\,Mpc^{-1}})$. The masses of dark matter, gas, and star particles are $(m_{\rm dm}, m_{\rm gas}, m_{\rm star}) = (9.4\times10^8, 1.9\times10^8, 8.5\times10^7)\ h^{-1}M_\odot$. In each panel, we indicate the

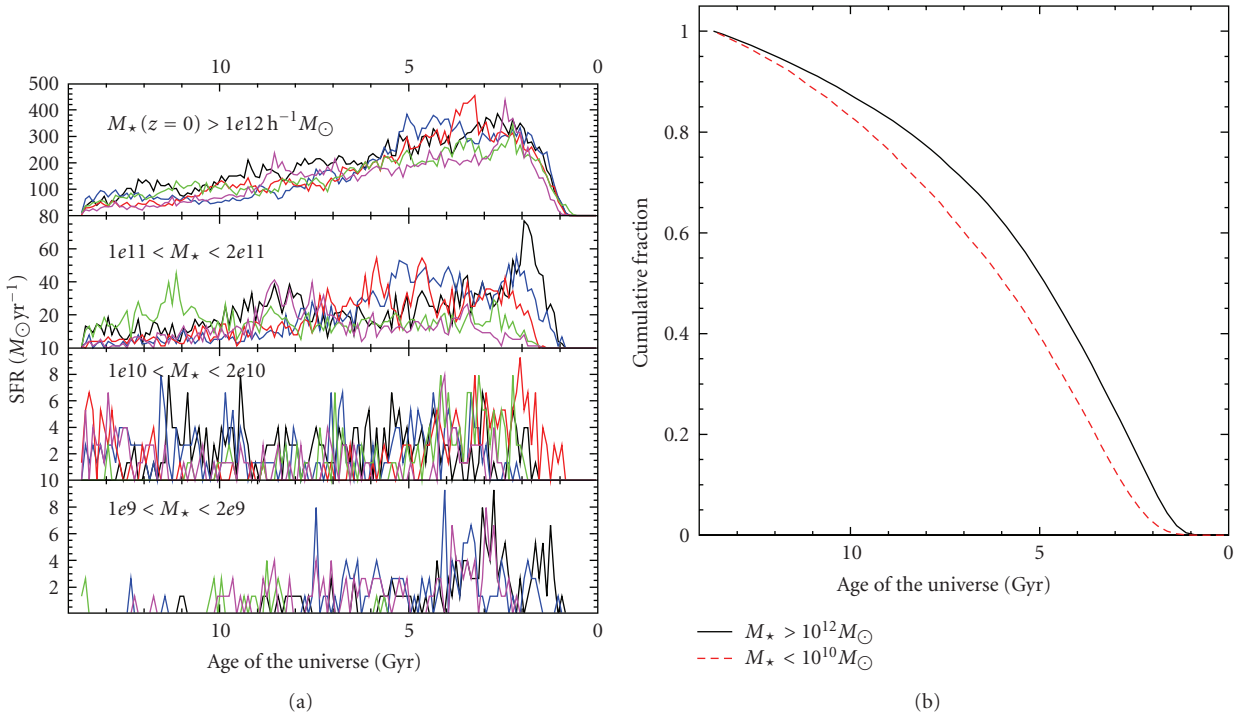

(a) (b)

Figure 1: (a) We compare some examples of star formation histories with 10^8 yr bins in a cosmological SPH simulation of a comoving box size $L_{\rm box} = 100\,h^{-1}$ Mpc and 2×400^3 (gas and dark matter) particles. In each panel, five different galaxies in the indicated stellar mass ranges (in units of $h^{-1}M_\odot$) at $z = 0$ are shown with different colors. Stars formed in all the progenitors are coadded for each galaxy. (b) Cumulative stellar mass fraction as a function of cosmic time for all the galaxies with $M_\star(z=0) > 10^{12}\,h^{-1}M_\odot$ and $M_\star(z=0) < 10^{10}\,h^{-1}M_\odot$.

range of stellar masses of the selected galaxies at $z = 0$. Each SF history includes all the stars formed in the progenitors of the current galaxy. The SF histories of the most massive galaxies with $M_\star > 10^{12}\,h^{-1}M_\odot$ peak at $t = 2-3$ Gyr and gradually decline thereafter in a roughly exponential manner, consistently with the results of [24]. In the bottom panel, the SF histories of dwarf galaxies with $1\times10^9 < M_\star < 2\times10^9\,h^{-1}M_\odot$ are shown. In this simulation, the dwarf galaxies continue to form stars sporadically at late times, even at $t > 10$ Gyrs.

In the right panel of Figure 1, we compare the cumulative stellar mass fraction that formed in galaxies with $M_\star(z = 0) > 10^{12}\,h^{-1}M_\odot$ and $M_\star(z=0) < 10^{10}\,h^{-1}M_\odot$ as a function of the age of the universe. This figure shows that, in a relative sense, the more massive galaxies form their stars earlier than the lower mass galaxies, in qualitative agreement with the observational trend (e.g., [39]) of downsizing.

Even though our new SPH simulations [23] seem to be more successful in modeling the qualitative trend of star formation in different galaxies, we may still have difficulties in reproducing the correct number density of "red and dead" massive galaxies at $z = 1-2$ or the ultraluminous infrared galaxies (ULIRGs), as examined in [40, 41]. Interestingly, their work showed that the Eulerian simulation exhibited more sporadic SF history for the massive galaxies than the SPH simulation at intermediate redshifts of $z = 1-3$. The difference in the nature of SF history was perhaps due to a combination of differences in the SF models and the effectiveness of feedback as well as the numerical resolution reached in the different simulations.

3. Discussion and Conclusion

As described in the previous section, the results from different numerical methods are still somewhat mixed, but we understand their qualitative differences when we consider the resolution and numerical effects. The main factor seems to be the numerical resolution, and one way to get around this problem might be to utilize the adaptive mesh refinement (AMR) technique (e.g., [20]). However, as we pointed out in [42], current AMR codes require substantially larger computational resources to obtain an equivalent result on the dark matter halo mass function as the SPH codes do at early times. Therefore it is difficult to simulate a large sample of dwarf galaxies in a large cosmological volume, and the simulation is usually not run down to $z = 0$ [20, 43].

Perhaps the best way to view the current situation is that each code captures the essence of dwarf galaxy formation at different epochs. The Eulerian mesh codes can capture the very early starbursts in low-mass halos better than the SPH codes, whereas the SPH codes can capture the gas infall and star formation in dwarf galaxies at late times owing to their higher spatial resolution in high-density regions. Both of these processes (i.e., early and late star formation) probably

took place in the real Universe as [18] proposed: some dwarf galaxies being the true fossils of the pre-reionization era, some being dominated by the late star formation at low redshift, and the rest being the mixture of the two.

Our hope is that, within the next decade, the results from different numerical techniques (Eulerian mesh, SPH, and AMR) will converge and provide a consistent picture of dwarf galaxy formation. Then we will have a much better idea on the physical processes that shaped the galaxy luminosity function and how the downsizing effect of galaxy formation is caused. To achieve this goal, we still have to overcome a huge dynamic range from subparsec to Mpc scales, and it will require a petascale supercomputer of next generation, such as *Blue Waters* [44].

Acknowledgments

The author is grateful to Jun-Hwan Choi who kindly allowed him to present the results of his cosmological SPH simulations that he is collaborating on. The full results of our work will be presented elsewhere [23]. This work is supported in part by the National Science Foundation Grant AST-0807491, the National Aeronautics and Space Administration under Grant/Cooperative Agreement no. NNX08AE57A issued by the Nevada NASA EPSCoR program, the National Science Foundation through TeraGrid resources provided by the Texas Advanced Computing Center and the San Diego Supercomputer Center, and the President's Infrastructure Award at UNLV.

References

[1] S. Juneau, K. Glazebrook, D. Champton, et al., "Cosmic star formation history and its dependence on galaxy stellar mass," *The Astrophysical Journal*, vol. 619, no. 2, pp. L135–L138, 2005.

[2] E. Le Floc'h, C. Papovich, H. Dole, et al., "Infrared luminosity functions from the chandra deep field-south: the *Spitzer* view on the history of dusty star formation at $0 \lesssim z \lesssim 1$," *Astrophysical Journal*, vol. 632, no. 1, pp. 169–190, 2005.

[3] A. E. Dolphin, A. Saha, E. D. Skillman, et al., "Deep hubble space telescope imaging of sextans A. III. The star formation history," *Astronomical Journal*, vol. 126, pp. 187–196, 2003.

[4] A. E. Dolphin, D. R. Weisz, E. Skillman, et al., "Star formation histories in local group dwarf galaxies," *New Astronomy Reviews*, vol. 49, no. 7–9, pp. 453–460, 2005.

[5] K. B. W. McQuinn, E. D. Skillman, J. M. Cannon, et al., "The true durations of starbursts: *hubble space telescope* observations of three nearby dwarf starburst galaxies," *The Astrophysical Journal*, vol. 695, pp. 561–573, 2009.

[6] L. Searle, W. L. W. Sargent, and W. G. Bagnuolo, "The history of star formation and the colors of late-type galaxies," *The Astrophysical Journal*, vol. 179, pp. 427–438, 1973.

[7] D. R. Weisz, E. D. Skillman, J. M. Cannon, et al., "The recent star formation histories of M81 group dwarf irregular galaxies," *The Astrophysical Journal*, vol. 689, no. 1, pp. 160–183, 2008.

[8] K. E. Dellenbusch, J. S. Gallagher III, P. M. Knezek, and A. G. Noble, "Deep optical imaging of starbursting "transition" dwarf galaxies," *The Astronomical Journal*, vol. 135, no. 1, pp. 326–332, 2008.

[9] N. Y. Gnedin, "Local group dwarf galaxies and the star formation law at high redshift," *The Astrophysical Journal*, vol. 535, no. 2, pp. L75–L78, 2000.

[10] E. K. Grebel, "Star formation histories of local group dwarf galaxies," *Reviews in Modern Astronomy*, vol. 10, pp. 29–60, 1997.

[11] M. Mateo, "Dwarf galaxies of the Local Group," *Annual Review of Astronomy and Astrophysics*, vol. 36, no. 1, pp. 435–506, 1998.

[12] S. van den Bergh, "The local group of galaxies," *Astronomy and Astrophysics Review*, vol. 9, no. 3-4, pp. 273–318, 1999.

[13] N. Y. Gnedin, "Effect of reionization on structure formation in the universe," *The Astrophysical Journal*, vol. 542, pp. 535–541, 2000.

[14] N. Y. Gnedin and A. V. Kravtsov, "Fossils of reionization in the local group," *The Astrophysical Journal*, vol. 645, no. 2, pp. 1054–1061, 2006.

[15] M. Hoeft, G. Yepes, S. Gottlöber, and V. Springel, "Dwarf galaxies in voids: suppressing star formation with photoheating," *Monthly Notices of the Royal Astronomical Society*, vol. 371, no. 1, pp. 401–414, 2006.

[16] A. V. Kravtsov, O. Y. Gnedin, and A. A. Klypin, "The tumultuous lives of galactic dwarfs and the missing satellites problem," *The Astrophysical Journal*, vol. 609, no. 2, pp. 482–497, 2004.

[17] S. Mashchenko, H. M. P. Couchman, and A. Sills, "Modeling star formation in dwarf spheroidal galaxies: a case for extended dark matter halos," *The Astrophysical Journal*, vol. 624, no. 2, pp. 726–741, 2005.

[18] M. Ricotti and N. Y. Gnedin, "Formation histories of dwarf galaxies in the Local Group," *The Astrophysical Journal*, vol. 629, no. 1, pp. 259–267, 2005.

[19] K. Tassis, A. V. Kravtsov, and N. Y. Gnedin, "Scaling relations of dwarf galaxies without supernova-driven winds," *The Astrophysical Journal*, vol. 672, no. 2, pp. 888–903, 2008.

[20] K. Tassis, T. Abel, G. L. Bryan, and M. L. Norman, "Numerical simulations of high-redshift star formation in dwarf galaxies," *The Astrophysical Journal*, vol. 587, no. 1, pp. 13–24, 2003.

[21] R. Cen and J. P. Ostriker, "Galaxy formation and physical bias," *The Astrophysical Journal*, vol. 399, no. 2, part 2, pp. L113–L116, 1992.

[22] N. Katz, "Dissipational galaxy formation. II. Effects of star formation," *The Astrophysical Journal*, vol. 391, no. 2, pp. 502–517, 1992.

[23] J.-H. Choi and K. Nagamine, "Effects of cosmological parameters and star formation models on the cosmic star formation history in LambdaCDM cosmological simulations," *Monthly Notices of the Royal Astronomical Society*, http://lanl.arxiv.org/abs/0909.5425.

[24] K. Nagamine, M. Fukugita, R. Cen, and J. P. Ostriker, "Star formation history and stellar metallicity distribution in a cold dark matter universe," *The Astrophysical Journal*, vol. 558, no. 2, pp. 497–504, 2001.

[25] R. C. Kennicutt Jr., "The global schmidt law in star-forming galaxies," *The Astrophysical Journal*, vol. 498, pp. 541–552, 1998.

[26] M. Schmidt, "The rate of star formation," *The Astrophysical Journal*, vol. 129, p. 243, 1959.

[27] V. Springel and L. Hernquist, "Cosmological smoothed particle hydrodynamics simulations: a hybrid multiphase model for star formation," *Monthly Notices of the Royal Astronomical Society*, vol. 339, no. 2, pp. 289–311, 2003.

[28] G. Yepes, R. Kates, A. Khokhlov, and A. Klypin, "Hydrodynamical simulations of galaxy formation: effects of supernova

feedback," *Monthly Notices of the Royal Astronomical Society*, vol. 284, no. 1, pp. 235–236, 1997.

[29] J.-H. Choi and K. Nagamine, "Effects of metal enrichment and metal cooling in galaxy growth and cosmic star formation history," *Monthly Notices of the Royal Astronomical Society*, vol. 393, no. 4, pp. 1595–1607, 2009.

[30] K. Nagamine, V. Springel, and L. Hernquist, "Star formation rate and metallicity of damped Lyman α absorbers in cosmological smoothed particle hydrodynamics simulations," *Monthly Notices of the Royal Astronomical Society*, vol. 348, no. 2, pp. 435–450, 2004.

[31] J. Schaye and C. Dalla Vecchia, "On the relation between the Schmidt and Kennicutt-Schmidt star formation laws and its implications for numerical simulations," *Monthly Notices of the Royal Astronomical Society*, vol. 383, no. 3, pp. 1210–1222, 2008.

[32] A. Dekel and J. Silk, "The origin of dwarf galaxies, cold dark matter, and biased galaxy formation," *The Astrophysical Journal*, vol. 303, part1, pp. 39–55, 1986.

[33] G. Efstathiou, "Suppressing the formation of dwarf galaxies via photoionization," *Monthly Notices of the Royal Astronomical Society*, vol. 256, no. 2, pp. 43P–47P, 1992.

[34] J. F. Navarro and M. Steinmetz, "The effects of a photoionizing ultraviolet background on the formation of disk galaxies," *The Astrophysical Journal*, vol. 478, no. 1, pp. 13–28, 1997.

[35] T. Quinn, N. Katz, and G. Efstathiou, "Photoionization and the formation of dwarf galaxies," *Monthly Notices of the Royal Astronomical Society*, vol. 278, no. 4, pp. L49–L54, 1996.

[36] D. H. Weinberg, L. Hernquist, and N. Katz, "Photoionization, numerical resolution, and galaxy formation," *The Astrophysical Journal*, vol. 477, no. 1, pp. 8–20, 1997.

[37] R. Cen, J. Miralda-Escudé, J. P. Ostriker, and M. Rauch, "Gravitational collapse of small-scale structure as the origin of the Lyman-alpha forest," *The Astrophysical Journal*, vol. 437, no. 1, part 2, pp. L9–L12, 1994.

[38] E. Komatsu, J. Dunkley, M. R. Nolta, et al., "Five-year wilkinson microwave anisotropy probe observations: cosmological interpretation," *The Astrophysical Journal, Supplement Series*, vol. 180, no. 2, pp. 330–376, 2009.

[39] D. Thomas, C. Maraston, R. Bender, and C. M. de Oliveira, "The epochs of early-type galaxy formation as a function of environment," *The Astrophysical Journal*, vol. 621, no. 2, pp. 673–694, 2005.

[40] K. Nagamine, R. Cen, L. Hernquist, J. P. Ostriker, and V. Springel, "Massive galaxies and extremely red objects at $z = 1-3$ in cosmological hydrodynamic simulations: near-infrared properties," *The Astrophysical Journal*, vol. 627, no. 2, pp. 608–620, 2005.

[41] K. Nagamine, R. Cen, L. Hernquist, J. P. Ostriker, and V. Springel, "Massive galaxies in cosmological simulations: ultraviolet-selected sample at redshift $z = 2$," *The Astrophysical Journal*, vol. 618, pp. 23–37, 2005.

[42] B. W. O'Shea, K. Nagamine, V. Springel, L. Hernquist, and M. L. Norman, "Comparing AMR and SPH cosmological simulations. I. Dark matter and adiabatic simulations," *The Astrophysical Journal, Supplement Series*, vol. 160, no. 1, pp. 1–27, 2005.

[43] N. Y. Gnedin, K. Tassis, and A. V. Kravtsov, "Modeling molecular hydrogen and star formation in cosmological simulations," *The Astrophysical Journal*, vol. 697, no. 1, pp. 55–67, 2009.

[44] http://www.ncsa.illinois.edu/BlueWaters/.

Hindawi Publishing Corporation
Advances in Astronomy
Volume 2010, Article ID 158568, 25 pages
doi:10.1155/2010/158568

Review Article

Star Formation Histories of Dwarf Galaxies from the Colour-Magnitude Diagrams of Their Resolved Stellar Populations

Michele Cignoni[1,2] and Monica Tosi[2]

[1] *Astronomy Department, Bologna University, Via Ranzani 1, 40127 Bologna, Italy*
[2] *Osservatorio Astronomico di Bologna, INAF, Via Ranzani 1, 40127 Bologna, Italy*

Correspondence should be addressed to Michele Cignoni, michele.cignoni@unibo.it

Received 5 May 2009; Accepted 12 August 2009

Academic Editor: Ulrich Hopp

In this tutorial paper we summarize how the star formation (SF) history of a galactic region can be derived from the colour-magnitude diagram (CMD) of its resolved stars. The procedures to build synthetic CMDs and to exploit them to derive the SF histories (SFHs) are described, as well as the corresponding uncertainties. The SFHs of resolved dwarf galaxies of all morphological types, obtained from the application of the synthetic CMD method, are reviewed and discussed. To summarize: (1) only early-type galaxies show evidence of long interruptions in the SF activity; late-type dwarfs present rather continuous, or *gasping*, SF regimes; (2) a few early-type dwarfs have experienced only one episode of SF activity concentrated at the earliest epochs, whilst many others show extended or recurrent SF activity; (3) no galaxy experiencing now its first SF episode has been found yet; (4) no frequent evidence of strong SF bursts is found; (5) there is no significant difference in the SFH of dwarf irregulars and blue compact dwarfs, except for the current SF rates. Implications of these results on the galaxy formation scenarios are briefly discussed.

1. Introduction

Dwarf galaxies are the most diffused type of galaxies in the Universe and were probably even more numerous in the past, when they might have contributed to the population of blue systems overabundant in deep galaxy counts (e.g., [1, 2]) and more likely to the assembling of larger baryonic systems. In spite of having received less attention than spiral and elliptical galaxies, dwarf galaxies have probably more cosmological relevance. For instance, late-type dwarfs are the preferred targets for cosmologists interested in Big Bang Nucleosynthesis, because their low metal and helium contents allow the derivation of the primordial helium abundance from HII regions spectra with minimum extrapolation (e.g., [3–5]). Moreover, their low metallicity and high gas content make them apparently less evolved than spirals and ellipticals, thus more similar to what primeval galaxies may have been.

One of the main cosmological interests is related to the possibility that today's dwarfs are the survivors of the building blocks of massive galaxies. Cold Dark Matter (CDM) cosmology predicts that dwarf systems are the first ones to form after the Big Bang, since only dark matter halos of mass smaller than $10^8 M_\odot$ are able to condense from primordial density perturbations. In this framework, more massive systems are assembled by subsequent merging of these protogalactic fragments (the hierarchical formation scenario; e.g., [6, 7]), and dwarfs have a pivotal role in the evolution of massive galaxies.

Observations show that galaxies merge in the local Universe and that big galaxies accrete their satellites. We know the cases of the Magellanic Stream and of other streams connected to the Sagittarius dwarf spheroidal (dSph) and other satellites falling on the Milky Way (e.g., [8, 9]). Andromeda is quite similar in this respect (e.g., [10–12]), with streams and clumps just as, or even more than, our own

Galaxy. The question is whether big galaxies form only by successive mergers of smaller building blocks, as proposed by the hierarchical formation scenario, or satellite accretion is a frequent but not necessary and dominant event, consistent with a downsizing formation scenario. Downsizing [13] in principle does not concern the hierarchy or the epoch of galaxy formation, it simply reflects the observational evidence that the bulk of stars in more massive galaxies formed earlier and at a higher rate than those in less massive systems. If mechanisms are found allowing for these star formation properties in the bottom-up scenario (e.g., [14–16]), then downsizing is not incompatible either with CDM or with the hierarchical scenario. However, downsizing is often seen as the alternative to hierarchical formation, replacing in this role the monolithical scenario, where each galaxy forms from the collapse (dissipative or dissipationless) of its protogalactic gas cloud. In the monolithical scenario more massive galaxies form much earlier than less massive ones for simple gravitational arguments [17], with timescales for the collapse of the protogalactic cloud originally suggested to be of the order of 100 Myr and now more often considered of the order of 1 Gyr.

One of the effective ways to check whether or not big galaxies are made *only* by successive accretions of satellites like the current ones is to observe the resolved stellar populations of massive and dwarf systems and compare their properties with each other. If chemical abundances, kinematics, and star formation histories of the resolved stars of massive galaxies are all consistent with those of dwarf galaxies, then the former can be the result of successive merging of the latter; otherwise, either satellite accretion is not the only means to build up spirals and ellipticals or the actual building blocks are not alike today's dwarfs.

An updated review of the chemical, kinematical, and star formation properties of nearby dwarfs can be found in [18]. In this tutorial paper, we describe how the star formation history of a galactic region can be derived from the colour-magnitude diagram of its resolved stars, and we summarize what people have learnt on the SFHs of dwarf galaxies from the application of the most popular approach based on the CMD. In Section 2 we introduce the method; in Section 3 we describe in detail procedures and uncertainties; in Section 4 we report on the results of its application on the SFH of dwarf galaxies. A discussion on how these results may affect our understanding of galaxy evolution which is presented in Section 5.

2. Star Formation Histories from Colour-Magnitude Diagrams: The Method

The need for understanding the star formation histories of dwarf galaxies was recognized long ago and over the years many approaches have been followed to infer the SFH of different galaxies. Among the many studies devoted to the field, we recall the seminal paper [19] and the extensive and detailed analyses performed by Gallagher, Hunter and collaborators (see [20, 21], and references therein), who used various indicators to estimate the star formation rates at different epochs of large samples of dwarfs. The quantum leap in the field occurred two decades ago, when the power and resolution of new generation telescopes and detectors allowed people to resolve and measure individual stars even in the crowded fields of external galaxies and to draw their CMDs. The CMD of a stellar system is in fact the best information desk on the system evolution, because it preserves the imprinting of all the relevant evolution parameters (age, mass, chemical composition, initial mass function).

Twenty years ago, stellar age dating was done with isochrone fitting, a handy tool for simple stellar populations, such as those of stellar clusters, but inadequate to interpret the composite populations of galaxies, where many subsequent generations of stars, with possibly different initial mass function, metallicity, reddening, and distance, contribute to the morphology of the observational CMD. With CCD detectors and new reduction packages for PSF fitting photometry allowing for the first time to measure accurately individual stars in Local Group (LG) galaxies, the time had come to develop a reliable tool to quantitatively derive their SFHs. The best tool is based on CMDs, and is the extrapolation of the standard isochrone fitting method to the complicated CMDs of composite stellar populations: the synthetic CMD method.

2.1. Building a Synthetic Population. The synthetic CMD method allows us to derive all the SFH parameters within the lookback time reached by the available photometry. To do this, a synthesizer works with classical ingredients:

(i) star formation law and rate, SFR(t), which regulate the astrated mass at each time t;

(ii) initial mass function (IMF), which gives the number N of stars in each generation per unit stellar mass interval, a useful form is a power-law:

$$dN \propto M^{-\alpha} dM, \tag{1}$$

the IMF is usually assumed to be independent of time;

(iii) chemical enrichment due to the galaxy chemical evolution, the metallicity of the gas from which stars form changes with time, this is described by an age-metalicity relation (AMR) $Z(t)$;

(iv) stellar evolution tracks, giving the temperature and luminosity of stars of given mass and metallicity at any time after their birth;

(v) stellar atmosphere models, to transform the bolometric magnitudes and temperatures into the observational plane;

(vi) binary fraction and mass ratio.

The standard procedure is the following. Using a Monte Carlo algorithm, masses and ages are extracted according to the IMF and the SF law (e.g., constant or exponentially decreasing with time, proportional to some power of the gas density, etc.). The metallicity follows suitable AMRs.

The extracted synthetic stars are placed in the CMD by interpolation among the adopted stellar evolution tracks of the assumed metallicity. In order to take into account the presence of unresolved binary stars, a chosen fraction of stars are assumed to be binaries and coupled with a companion star. The fake population is put at the distance of the galaxy we want to analyze, simultaneously correcting for reddening and extinction. Finally, photometric errors, incompleteness, and blending factors, as accurately estimated from artificial star tests on the actual photometric images of the examined field, are applied to the synthetic CMD.

Different combinations of the parameter choices provide the whole variety of CMDs observed in real galaxies. As an example, Figure 1 shows the CMDs resulting from 6 representative, although simplistic, cases.

Figures 1(a)–1(f) illustrate the effect of different SFHs on the synthetic CMD of a hypothetical galactic region with a number of resolved individual stars, photometric errors, as well as blending and incompleteness factors typical of a region in the SMC imaged with HST/WFPC2. Figures 1(a)–1(c) show examples of CMDs typical of late-type galaxies, with ongoing or recent star formation activity. If the SFR has been constant for all the galaxy lifetime, the CMD of the region is expected to have the morphology of Figure 1(b), with a prominent blue plume mostly populated by main-sequence (MS) stars and an equally prominent red plume resulting from the overposition of increasingly bright and massive stars in the red giant branch (RGB), asymptotic giant branch (AGB), and red supergiant phases. At intermediate colours, for decreasing brightness, stars in the blue loops, red clump, and subgiant phases are visible, as well as the stars at the oldest MS turnoff (MSTO) and on the faint MS of low mass stars. Stars of all ages are present, from those as old as the Hubble time to the brightest ones a few tens Myr old.

If we leave the SFH unchanged except for the addition of a burst ten times stronger concentrated in the last 20 Myr, the CMD (Figure 1(a)) has a much brighter and more populated blue plume, now containing many stars a few Myr old. In Figure 1(c) the same constant SFR as in the first case is assumed, but with a quiescent interval between 3 and 2 Gyrs ago: a gap is clearly visible in the CMD region corresponding to isochrones with the age of the missing stars.

The three bottom panels of Figure 1 show CMDs typical of early-type galaxies, whose SF activity is concentrated at earlier epochs. If only one SF episode has occurred from 13 to 10 Gyr ago, with a constant metallicity $Z = 0.004$ as in Figures 1(a)–1(c) , the resulting CMD is shown in Figure 1(e). If the SF has occurred at the same epoch, but with a metallicity ten times lower, the evolutionary phases in the resulting CMD (Figure 1(f)) have colours and luminosities quite different from the previous case. Finally, Figure 1(d) shows the case of two bursts, the first from 13 to 11 Gyr ago and the second from 5 to 4 Gyr ago. The gap corresponding to the quiescent interval is visible in the CMD although not as much as the more recent gap of Figure 1(c).

Once a synthetic CMD is built, the challenging part of the method is the comparison with the observational CMD. The best values of the parameters (IMF, AMR, SFR, binary fraction, reddening, and distance modulus) are found by selecting the cases providing synthetic CMDs with morphology, colours, number of stars in the various evolutionary phases, and luminosity functions consistent with the observed ones. Independently of the specific method, any approach is unavoidably statistical and does not provide a unique solution for the SFH of the examined region. Nevertheless, the synthetic CMD method is quite powerful, thanks to the wealth of independent constraints available in a good CMD, and it strongly reduces the range of possible scenarios.

In what follows, we will describe what are the major uncertainties in the method. Before diving into details, however, it is crucial to understand which parts of a CMD are the most reliable clocks.

2.2. Stellar Ages from a CMD. What can be learnt from a CMD? All the evolutionary sequences are witness of the same SFH, but some sequences are specifically sensitive to age more than to any other ingredient (e.g., metallicity, convection, etc.). In order to track the history of a galaxy, it is necessary to select the safest age indicators. Because different evolutionary phases populate different CMD regions, one must then know which parts of the CMD are more informative.

The best indicators share a useful feature: the age is related to the luminosity, which depends on the burning rate and on the available fuel. The MS is the archetype of this class of phases, since in this stage the stars obey a mass-luminosity relation $L \propto M^n$ (where n varies from 3 to 4). This relationship has strong implications. Adopting a mean value $n = 3.5$ and considering that the available fuel is proportional to the stellar mass M, the time spent in MS is proportional to $M^{-2.5}$: massive stars live for short times (50 Myr for a 8 $M_\odot$), mapping *only* the recent SFH, while objects smaller than 1.5 $M_\odot$ can survive for many Gyr, mapping the recent as well as the ancient star formation history. From the point of view of the CMD, this one-to-one correspondence of luminosity and mass/age allows, for a given metallicity, a direct conversion of the MS information into the SFH.

Beyond the MS, a mass-luminosity relation does not hold anymore, and the luminosity is rather sensitive to the core mass growth. The phases between the MS and the red giant are so fast (thermodynamical evolution) that the probability of observing their stars is low (compared to that for nuclear phases). This causes the so-called Hertzsprung gap, that is, the observed lack (or paucity) of stars in the evolutionary phase right after the MS. However, for stars smaller than about 2–2.5 $M_\odot$, the evolutionary times are long enough (because the degeneracy pressure prevents a rapid core contraction) to define another useful age indicator: the *subgiant branch* (SGB). Like the MS turn-off, the SGB fades as the the age increases.

Later evolutionary phases, namely, the RGB, the horizontal branch (HB), the red clump (RC), and the asymptotic giant branch, with the exception of the blue loop (BL) stage, are questionable age indicators. In fact, the CMD position of such objects mostly reveals the age through the colour, which can be influenced by several factors. As an example, aging the stars makes the RGB redder, but theoretical uncertainties like the colour transformations and the super-adiabatic convection can lead to higher colour shifts. The RGB is

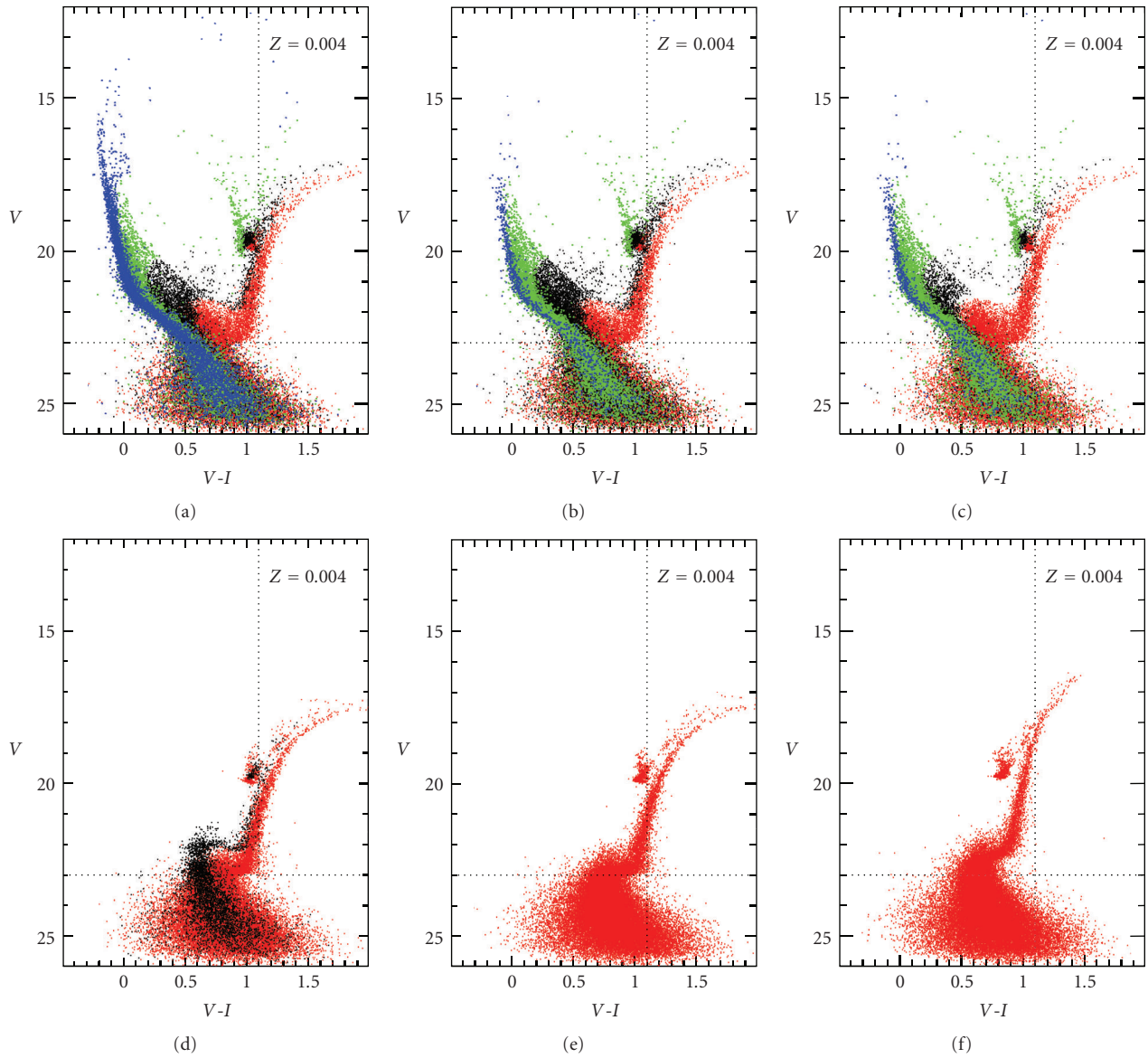

FIGURE 1: The effect of the SFH on the theoretical CMD of a hypothetical galactic region with $(m - M)_0 = 19$, $E(B - V) = 0.08$, and with the photometric errors and incompleteness typical of HST/WFPC2 photometry. All the shown synthetic CMDs contain 50 000 stars and are based on the Padova models [22, 23] with the labelled metallicities. (b) The case of an SFR constant from 13 Gyr ago to the present epoch. (a) The effect of adding a burst 10 times stronger in the last 20 Myr to the constant SFR. The CMD has a much brighter and thicker blue plume. (c) The same constant SFR as in the first case, but with a quiescence interval between 3 and 2 Gyrs ago; a gap appears in the CMD region corresponding to stars 2-3 Gyr old, which are completely missing. (e) SF activity only between 13 and 10 Gyr ago with $Z = 0.004$. (f) SF activity only between 13 and 10 Gyr ago with $Z = 0.0004$: notice how colour and luminosity of turnoff, subgiant, and red giant branches differ from the previous case. (d) SF activity between 13 and 11 Gyr ago, followed by a second episode of activity between 5 and 4 Gyr ago: a gap separates the two populations in the CMD, but less evident than in (c) case, when the quiescent interval was more recent.

undoubtedly more sensitive to the metallicity. On the other hand, all these phases are indisputable signature of stars older than a limiting age and extremely useful in the age dating of galaxies too distant to have the MSTO reachable by any photometry: HB stars are always older than 10 Gyr, RGBs at least 1-2 Gyr old, and AGBs older than 100 Myr. Moreover, as thoroughly discussed by Greggio [24], the relations existing between the number counts of post-MS stars and their mass helps in constraining the SFH.

Among core helium burning stars, the HB and the RC phases are composed by stars of initial mass smaller than about 2 solar masses, whose luminosity depends on the helium core mass and is quite independent of the stellar mass. In particular, the HB colour frequently shows a correlation with metallicity (the "first parameter"), while age is only one of the possible secondary parameters. Quite different is the behavior of intermediate mass stars (over 2 $M_\odot$): during the core helium burning these objects describe

a large loop in colour (the so-called blue loops) and their luminosities are critically sensitive to the mass; this is because the core mass is connected to the extension of the convective cores in the previous MS structures. Thanks to this feature, for ages of 100–500 Myr, the luminosity of the loops fades with age and the BL is an excellent age indicator.

After the core helium burning phase, low and intermediate mass stars experience the AGB phase. As for the RGB, a relation between the luminosity and the core mass holds. In addition, many phenomena occur (e.g., mixing and extra mixing of convective layers, thermal pulses, etc.) which are not yet understood in detail, and this leaves considerable uncertainty.

The very first and the final stages of stellar evolution, namely, the pre-main sequence (PMS) and the white dwarf (WD) regimes, also deserve some comments. As for the former, prior to reaching the MS, the star's energy source is a contraction on thermodynamical timescales (tenths of Myr). While aging, PMS stars fade and become hotter. Figure 2 shows the HST/ACS images and the corresponding CMDs of two star forming regions in the Small Magellanic Cloud, NGC602 (left-hand panels, [25]) and NGC346 (right-hand panels, [26]). The well-defined sequence well separated from the canonical main sequence, which appears on the right-hand side of these CMDs, is composed by PMS stars. Were not this phase affected by several theoretical and observational uncertainties, the PMS would be a powerful clock for the most recent Myrs (see, e.g.,[27], and references therein).

On the other hand, WDs represent the final fate of all stars with masses below 8 $M_\odot$. These stars share a useful feature: the peak of the WD luminosity function fades with age. Unfortunately, the presence of theoretical uncertainties (e.g., crystallization processes, nuclear reaction rates, convection, mass loss, and initial chemical composition) together with an intrinsic low luminosity ($10 < M_V < 18$) tend to invalidate its reliability.

In conclusion, MS and SGB stars are certainly the most reliable age indicators. If we add that in these phases faint objects live longer, a deeper CMD gives a better chance to robustly trace the past star formation history. It is important to underline that quantitative and qualitative indicators can be combined and typically complement each other. In other words, when a deep CMD is not available, evolved stars can be used very profitably to recover the SFH although with higher uncertainty and within shorter lookback times.

2.3. Deep is Better. The presence of a completeness limit (due to both the intrinsic crowding and distance of the examined galaxy and to the instrumental capabilities) hinders the possibility to exploit all the information contained in a CMD. To visualize this effect, we built age-frequency plots for various stellar mass ranges, assuming different completeness limits (see Figure 3) and using an artificial population generated from the Padova stellar models [22] with $Z = 0.004$, no binaries, and constant SFR. In order to be as general as possible, all the results are shown using absolute magnitudes. In all panels of Figure 3 we plot with different colours the fraction of stars of various mass ranges visible in the CMD above the assumed completeness limit as a function of their age.

In Figure 3(a) the completeness limit is set to $M_V = 2.5$: we see that on the MS only stellar masses higher than 1.5 $M_\odot$ are brighter than this limit and usable witnesses of the last 2 Gyr. On the other hand, the long-lived nature of lower masses guarantees to trace long periods of star formation, but not the recent SFR. The explanation comes from the limit $M_V = 2.5$ itself: it cuts off the MS, so for stars below 1.5 $M_\odot$, we see only later (i.e., brighter) evolutionary phases, represented by the RGB and the central helium burning (the dotted lines for the mass ranges $0.6-1.0$ $M_\odot$ and $1.0-1.5$ $M_\odot$ represent the contribution of PMS, MS, and SGB stars).

Moving the limit to $V = 3.5$ (Figure 3(b)), the mass interval 1–1.5 $M_\odot$ is visible in the CMD and informative of the star formation history between now and ~8 Gyr ago. However, only masses over 1.2-1.3 $M_\odot$ are on the MS. Lower masses or, equivalently, older epochs, must refer to RGB and He burning phases. The situation improves when the completeness limit is set at $M_V = 4.5$ (Figure 3(c)), and the MS phase is visible for all stars down to ~0.8 $M_\odot$. This limit represents a very good level for studying the history of a resolved galaxy, since it guarantees age-sensitive tracers (MS and SGB stars) covering the entire Hubble time (13 Gyr).

Finally, Figure 3(d) shows the age plots for a completeness limit $M_V = 5.5$: at this luminosity, the zero age main sequence is reached for subsolar masses, whose lifetimes are longer than the age of the Universe. With respect to $M_V = 4.5$ case, the advantages here are (1) a much more reliable photometry of the turn-off and SGB stars; (2) further information on the IMF, thanks to a better coverage of the lowest/faintest mass intervals, where the IMF slope may significantly change (see, e.g., [28, 29], and references therein); (3) a better constraint on $Z(t)$, given the mild influence of the SF law on the CMD position of low mass stars.

These results depend on the assumed chemical composition. This is important when one considers that in galaxies some chemical enrichment must always be at work. Following this paradigm, the oldest stars in a galaxy are expected to be metal poor. Changing the metallicity has two main effects on the model; namely, changes in the evolutionary lifetimes and changes in the stellar luminosity, which in turn can sensibly modify the relation between CMD and SFH. To investigate this phenomenon, in Figure 4, the frequency-age plot for the completeness limit $M_V = 4.5$ is shown for two different metallicities, $Z = 0.004$ (thick lines in the figure) and $Z = 0.0004$ (thin lines). Lowering the metallicity accelerates the evolution, and the age distribution for all the mass intervals (except 0.6–1 $M_\odot$) is shifted by, at least, 1 Gyr with respect to the $Z = 0.004$ cases. The age plot for masses 0.6–1 $M_\odot$ has a different genesis: part of these stars live more than 13 Gyr, so the evolutionary effect is not visible. In contrast, the mass range 0.6–1 $M_\odot$ emphasizes the luminosity effect: a lower metallicity pushes MS stars over the completeness limit $M_V = 4.5$, injecting younger stars in the age distribution that now involves ages between 0 and 13 Gyr. In practice, a lower metallicity mimics what happens with a more favorable completeness limit.

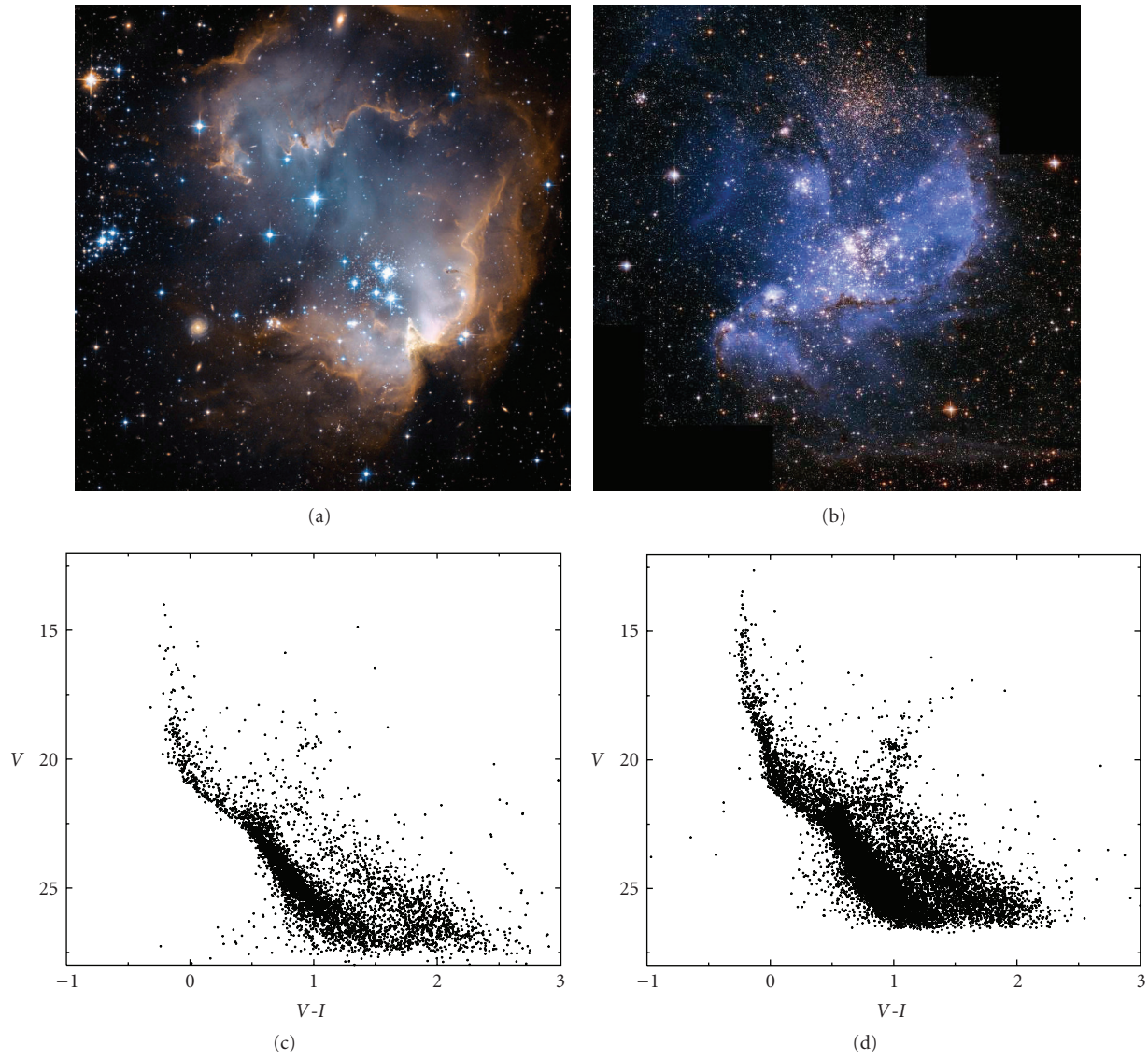

Figure 2: (a, b) HST/ACS true colour images of NGC602 (a), a very young cluster in the wing of the SMC and NGC346 (b), a populous young cluster in the main body of the SMC. Images credit NASA, ESA, and A. Nota (STScI, ESA). (c, d) CMD of NGC602 (c) and of NGC346 (d). PMS stars are clearly visible at the right of the Main Sequence.

This implies the following rule: in order to safely use the CMD for an estimate of the oldest star formation history we need to resolve all the stars down to $M_V = 4.5$. Since this magnitude can be reached only in the closest galaxies, this implies that in most cases the information on the earliest SF activity is either completely lacking or very uncertain.

3. Deducing the SFH: Guidelines

3.1. A Changing Landscape. The first procedures to derive the SFH of nearby galaxies from synthetic CMDs were developed by the Bologna and the Padova groups about 20 years ago [30–34], with the latter then combining with the Canary group [35–37]. These works used luminosity functions, colour distributions and the general CMD morphology to constrain the underlying SFH. In particular, the ratio of star counts in several regions of the CMD was used to determine both the SFR and the IMF [32]. The drawback of these procedures is the lack of a robust statistical criterion to evaluate the best solution and the corresponding uncertainties. On the other hand, these authors made an optimal use of all the CMD phases and took into careful account all the properties and uncertainties of stellar evolution models, thus avoiding blind statistical approaches, which can lead to misleading results.

Later on, several methods have been proposed to statistically compare simulated and observed CMDs. In this framework, some groups have derived the SFHs of galaxies in the LG (see, e.g., [37–44]). Others (see, e.g., [45–48]) have tackled the question of the SFH in the solar neighborhood. To the same class of investigators we can assign also

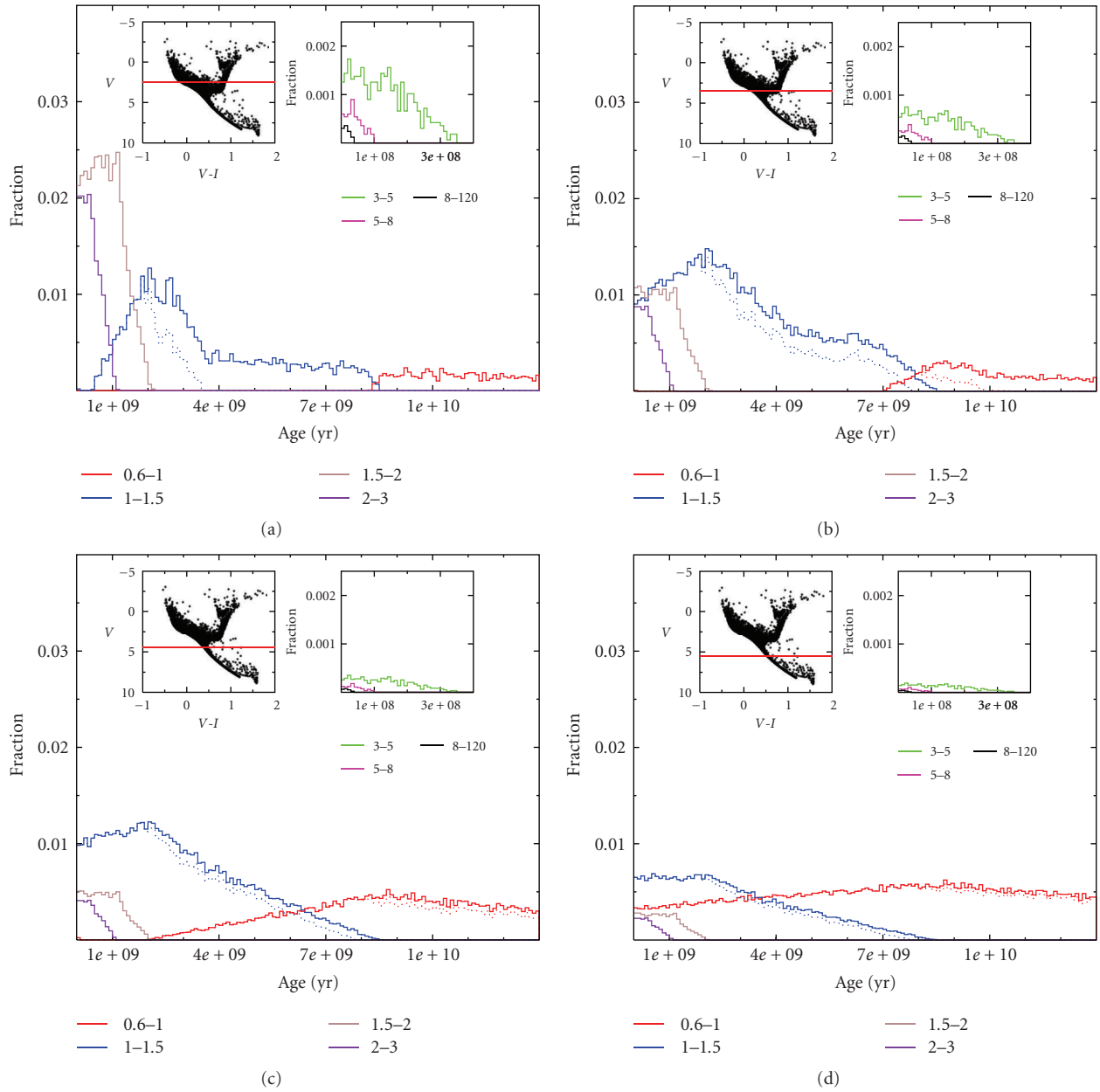

Figure 3: Fractional age distributions of stars generated with a constant SFR (0–13 Gyr) for four different completeness limits. In different colours (solid lines) are plotted the contributions from different mass ranges. In (a), only stars with absolute magnitude brighter than 2.5 are plotted, while in (b), (c), and (d), this limit is, respectively, $M_V = 3.5$, $M_V = 4.5$, and $M_V = 5.5$. The dotted lines represent the contribution of PMS, MS, SGB. In each panel, the left and right subfigures show, respectively, the adopted simulated population (with the limiting magnitude marked by a red line) and a blow-up with the contribution of intermediate and massive stars in the last 300 Myr.

the study by [49] focussing on star clusters. In all these works, the emphasis is transferred from the stellar evolution properties to the problem of selecting the most appropriate model through decision making criteria: here, the likelihood between observed and model CMD is evaluated on statistical bases. There are subtle differences among different groups, reflecting how these authors define the likelihood and how they solve it. The advantages are mainly three: the possibility to exploit each star of the CMD, and not only few strategic ratios; the evaluation of the uncertainty on the retrieved SFH, which is robust; the explorability of a wide parameter space. However, a blind statistical approach is not risk-free. Although significant advances have been made in stellar evolution and atmosphere theories, several processes (only to cite the most infamous ones, the HB morphology, RGB and AGB features, convection in general) remain poorly understood and affect the statistical tests. If some parts of the CMDs have a low reliability and others are statistically weak, but very informative (like the helium burning loops), any blind algorithm may miss something crucial. In this case,

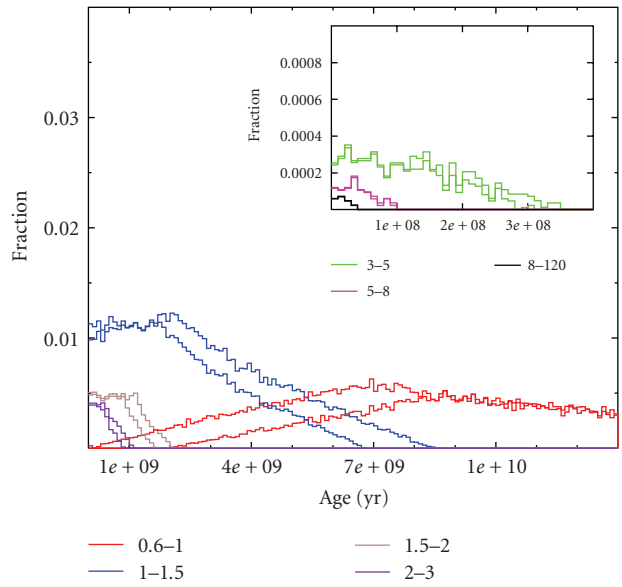

FIGURE 4: Fractional age distributions for stars brighter than $M_V = 4.5$ at two different metallicities. The thick line represents $Z = 0.004$, while the thin line represents $Z = 0.0004$.

a careful inspection of the CMD morphology, in particular the ratios of stellar number counts in different evolutionary phases is the irrenounceable and necessary complement to the statistical approach. Finally, whatever the adopted procedure, the absolute rate of star formation must be obtained normalizing the best model to the observed number of stars.

The major differences among the various procedures concern the approach to select the best solutions and the treatment of metallicity variations. In 2001, the predictions of the synthetic CMD method from about ten different groups were compared with each other, showing that within the uncertainties, most procedures provided consistent results (the *Coimbra Experiment*, see [50], and references therein).

In the following section we describe the main steps to rank the likelihood among CMDs.

3.2. To Grid or Not to Grid. In order to decide if a synthetic CMD is a good representation of the data, the observed and the model star-counts can be compared in a number of CMD regions. In [40], these regions are large and strategically chosen to sample stars of different ages or specific stellar evolutionary phases and to take into account uncertainties in the stellar models: this solution guarantees an optimal statistics, but has the drawback of underexploiting the fine structure of the CMD. Another possibility is to choose a fine grid of regions (see, e.g., [51, 52]), counting how many predicted and observed stars fall in each region: the temporal resolution is higher, but the Poisson noise is the new drawback. An intermediate solution is to build a variable grid, coarser where the density of stars is lower and finer when the density is higher (see, e.g., [45, 53]). At this level, ad-hoc weighting of some regions can be introduced both to emphasize CMD regions of particular significance for the determination of age, and to mask those regions where stellar evolutionary theory is not robust.

Other authors avoid to grid the CMD: for instance, in [38] each model point (apparent magnitude and colour) is replaced with a box with a Gaussian distributed probability density (the photometric error). The total likelihood of a model is the product of the probabilities of observing the data in each box. The idea of this method is equivalent to use blurred isochrones (each point is weighted by the Gaussian spread), so that the photometric uncertainty is embodied in the theoretical model.

3.3. Maximum Likelihood. The next step is to choose a criterion for the comparison between synthetic and observational CMDs. For any grid scheme, once binned, data and synthetic CMDs are converted in colour-magnitude *histograms*. So, the new problem is to quantify the similarity among 2D histograms. One possibility is to minimize a χ^2 likelihood function: when the residuals (differences among theoretical and observed star-counts in the CMD regions) are normally distributed, all models that have a χ^2 greater than the best fit plus one are rejected. However, when the distribution is not normal, a χ^2 minimization leads to a wrong solution. This motivates the use of the Poisson likelihood function instead of the least-squares fit-to-data function. In order to determine the uncertainties around the best model, a valid alternative is to use a bootstrap test: the original data are randomly resampled with replacements to produce pseudoreplicated datasets. This mimics the observational process: if the observational data are representative of the underlying distribution, the data produced with replacements are copies of the original one with local crowding or sparseness. The star formation recovery algorithm is performed on each of these replicated datasets. The result will be a set of "best" parameters. The confidence interval is then the interval that contains a defined percentage of this parameter distribution.

One aspect deserves closer inspection: the minimization of a merit function of residuals (χ^2 or Poisson likelihood) is a global measure of the fit quality. The first side effect is purely statistical: low-density regions of the CMD may be ignored in the extremization process, whereas well-populated phases (as the MS) are usually well reproduced. This is a problem of contrast: low-density regions are Poisson dominated, thus, they are much easier to match with respect to the well populated regions.

A Monte Carlo method can be used with great success to evaluate this bias: building synthetic CMDs from the best set of parameters and re-recovering the SFH can allow to remark any statistical discrepancy. Then, a straightforward solution is to enhance the significance of the discrepant regions of the CMD (with appropriate weights).

Another problem is connected with the theoretical ingredients we have used in the models: first of all, stellar evolution models are not perfect and computations by different groups show systematic differences (see, e.g., for a review [54]). Model atmospheres are often unreliable for cool and metal rich stars. Moreover, our models are only covering a part of the possible parameter space and some degree of freedom

(additional metallicities, mass loss, overshooting, etc.) may have been neglected. In this case, our best model is only the best (in a relative sense) of the explored parameter space, not necessarily a good one.

In order to deal with these undesirable effects, the residuals can be placed in the CMD, identifying all the regions where the discrepancy between observed and predicted star-counts is larger. If the residuals are larger and concentrated in some part of the CMD, we may understand what is the reason for the discrepancy and take it into account. For instance, a poor fit in the red giant branch, less populated than the main sequence but morphologically well defined in colour (and for this reason often neglected in χ^2 minimization), may suggest a wrong metallicity, a different mixing length parameter, or a wrong colour transformations.

3.4. Wondering in the Parameter Space. The main drawback of Maximum Likelihood (ML) approaches is the computational burden. Algorithms that find the ML score must search through a multidimensional space of parameters, using, for instance, derivative methods, like Powell's routine, or nonderivative ones, like the downhill simplex routine, or genetic approaches (see, e.g., [53]).

These techniques are not guaranteed to find the peak, but work relatively well for a limited number of parameters. Traditionally, this question has been tackled by constructing synthetic CMDs from an SFH built as a series of contiguous bursts and finding the amplitudes of each burst that give the maximum probability to have produced the data: the synthetic CMD is now a linear sum of the partial CMDs produced from a single realization for each burst. In this way, a huge parameter space can be explored: rather than calculating a complete CMD for each SFR(t), the partial CMDs can be linearly combined to build a CMD for any SFR(t). In order to reduce the Poisson noise, the partial CMDs are simulated with many more stars than observed (typically, 100 times more).

The computer time spent for building the final CMD is only that needed to go through a finite number of models, simply equal to the number of combinations of $Z(t)$ relations, IMF slopes, reddenings, and distance moduli *times* the number of age bins in the solution.

Age Bins: disentangling a stellar population showing both very recent (Myr) and very old (Gyr) episodes of star formation is not straightforward. Only low-mass stars survive from ancient episodes because their evolutionary timescales are very long: small CMD displacements, for example, due to photometric errors, can bias their age estimates up to some Gyr. In this case, increasing the time resolution, besides being time-consuming, may produce unrealistic star formation rates due to misinterpretations. Hence, the choice of temporal resolution must follow both the time scale of the underlying stellar populations and the data scatter (photometric errors, incompleteness, etc.). A practical way out is to use a coarser temporal resolution for the older epochs, which (1) allows us to avoid SFH artifacts at early epochs, (2) reduces the Poisson noise, and (3) reduces the parameter space. Figure 5 shows a possible time stepping (see, [27]). Finally, it is worth noting that the choice of each set of age bins will prevent to identify any SF episode shorter than the bin duration: for instance, the 1 Gyr lull (between 2 and 3 Gyr ago) in the star formation history, as simulated in the Figure 1(c), will result in a lower (half) activity in the 7th age bin (1–3 Gyr).

In the following sections we describe some numerical experiments illustrating the reliability of a typical ML algorithm. In particular, the sensitivity of such algorithm to several physical uncertainties is outlined. These examples expand the discussions and results by [46]. The experiments described here are based on different set of tracks, mass spectrum, and photometric errors/completeness, but the results are the same as in [46], thus showing that they are independent of these assumptions. Other instructive examples can be found in [40, 54, 55].

3.5. A Practical Example. To describe how an ML procedure works, let us build a fake galaxy assuming for the sake of simplicity a constant star formation rate between now and 13 Gyr ago and a metallicity fixed at $Z = 0.004$. We put it at the distance of the closest dwarf irregular galaxy, the Small Magellanic Cloud (SMC), $(m - M)_0 = 18.9$, and adopt the SMC mean foreground reddening $E(B - V) = 0.08$. To minimize statistical fluctuations, the Monte Carlo extractions are iterated until we have 30 000 stars brighter than $V = 23$, which roughly corresponds to about 100 000 stars in the entire CMD. Photometric errors and incompleteness as obtained in actual HST/ACS SMC campaigns [27] are convolved with the synthetic data, producing a realistic artificial population. This fake galaxy will be used as a reference set in all the following exercises.

To recover its SFH, we have gridded the CMD in small bins of colour and magnitude (0.1 mags large) and we have minimized a Poisson likelihood. The time stepping for the partial CMDs is as follows (going backward in time from the present epoch to 13 Gyr ago): 100 Myr, 400 Myr, 500 Myr, 1 Gyr, 2 Gyr, 3 Gyr, 3 Gyr, 3 Gyr. A bootstrap technique is implemented to determine the final uncertainties.

Figure 6(a) shows the CMD of our reference fake galaxy, and Figure 6(b) the SFH recovered from it, using only stars brighter than $V = 23$ (i.e., $M_V = 3.85$), for a self-consistency check. As expected, the retrieved SFR is fitted by a constant value. We will use this basic experiment as a starting point for a series of exercises aimed at describing the major uncertainties affecting the synthetic CMD method.

3.6. Uncertainties Affecting the Synthetic CMD Procedures. Contrary to real cases, in the reference case of Figure 6 we have all the information: all parameters are known and the data are complete down to 23 ($M_V = 3.85$). Real galaxies are far from this ideal condition. Inadequate information or uncertainty about the assumed parameters can influence the identification of the best SFH. The major sources of uncertainty are primarily the IMF, the binary fraction, and the chemical composition. From the observational point of view, the completeness level is another important factor. Moreover, population synthesis methods make a number of simplifications to reduce significantly the computational load; for example, reddening constant across the data, same

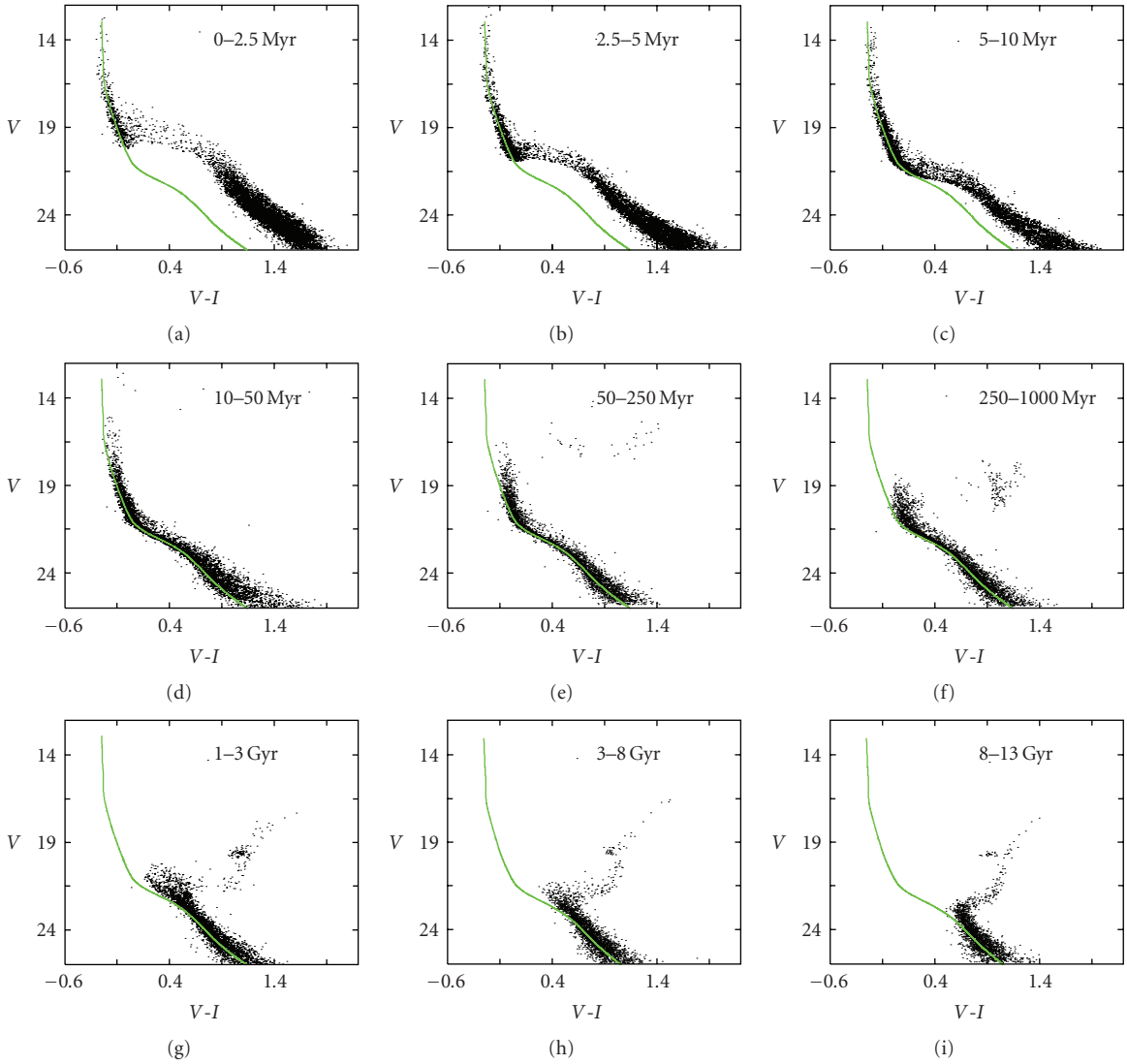

Figure 5: Partial theoretical CMDs. Each one is generated with a constant star formation rate, for the age interval pointed out in the label. The bright part of the main sequence is dominated by high-mass stars so the CMD time step has to be shorter.

distance for all stars, linear age-metallicity relation, and so forth. Dropping these simplifying assumptions considerably complicates all analyses of the CMD properties.

There are two main strategies to face the complexity of the problem. One is to increase the number of free parameters in the model. For example, the work in [56] recovers simultaneously distance, enrichment history, and SFR of the local dwarf LGS 3. The other is to reduce the data complexity by means of additional information; for instance, the metallicity may be estimated from appropriate spectroscopy and multiband observations may help to disentangle the reddening.

In the following subsections we test the reliability of the star formation recovery when the uncertainties related to each parameter are taken into account individually. A word of caution is necessary for the interpretation of these exercises: in each case, we show how the recovery of the SFH of the reference fake galaxy is affected by forcing the procedure to adopt a specific (and in most cases wrong) value for the tested parameter. This is aimed at emphasizing the effect of that parameter. In the derivations of the SFH of real galaxies, the parameter values are all unknown (which complicates the derivation), but the selection procedure is allowed to cover all the meaningful ranges of values and can therefore distinguish which combinations allow to maximize the agreement with the data.

3.7. Completeness. The numerical experiment seen in Section 3.5 represents an ideal situation: (1) the SMC is one of the closest galaxies, (2) HST/ACS currently provides the top level photometry in terms of spatial resolution and depth. At the distance of the SMC (60 kpc), ACS photometry can be 100% complete to $V \approx 24 - 25$. Farther galaxies and/or images from ground-based telescopes have larger photometric errors and more severe incompleteness. For comparison, the optical survey conducted at the Las

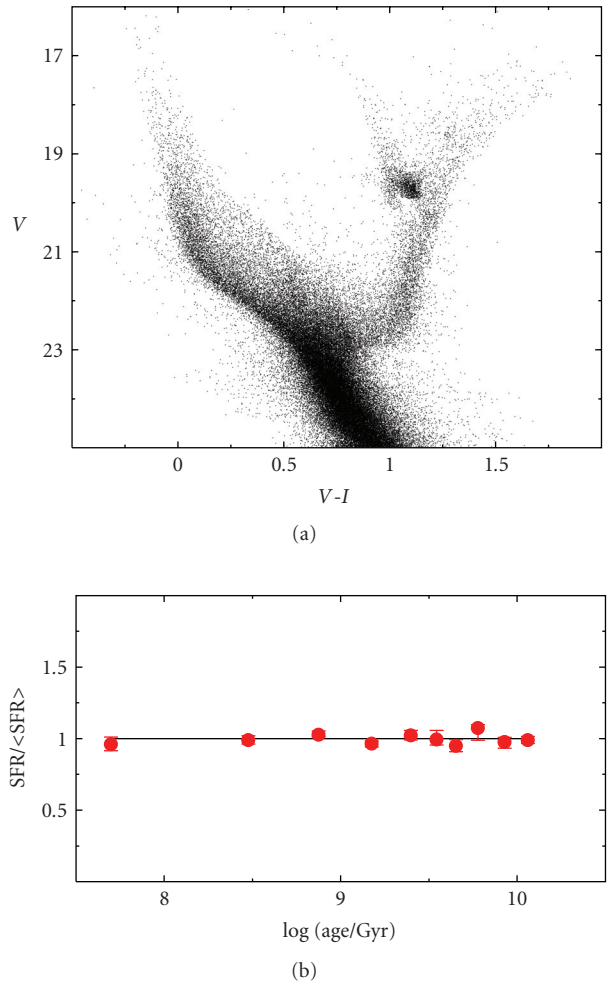

Figure 6: Starting case for the experiments on the uncertainties on the retrieved SFH due to different factors. In (a) we show an artificial population of stars generated with constant SFR, Salpeter IMF, constant metallicity $Z = 0.004$ [23], $(m - M)_0 = 18.9$, $E(B - V) = 0.08$, and the HST/ACS errors and completeness of the photometry in the SMC field NGC602 [27]. In (b) the input (solid line) and the recovered (dotted) SFH are compared.

Campanas Observatory 1 mt Swope Telescope, to trace the bright stellar population in the Magellanic Clouds, is 50% complete to $V \sim 21 - 22$ (see [57]).

To demonstrate the importance of the completeness limit, we perform the star formation recovery using only stars brighter than $V = 21$ and $V = 22$. The results are displayed in Figure 7. It is evident that the deeper the CMD, the higher the chance to properly derive the old star formation activity. Compared to $V = 23$ case, where the SFR recovery is accurate and precise at any age, the quality already drops when the completeness limit is at $V = 22$: the larger error bars at old epochs reflect the fact that the only signature of the oldest activity comes from evolved stars, less frequent, and much more packed in the CMD than the corresponding MS stars. Rising the limiting magnitude at $V = 21$ further worsens the result, and the recovered SFH is a factor of 2 uncertain for ages older than 1-2 Gyr.

These results are actually optimistic: we have analyzed different levels of completeness with the same photometric errors (HST/ACS), but this is an utopic situation. More distant galaxies have a less favorable completeness limit, and also the photometric error is larger. In these cases, an additional blurring occurs.

3.8. IMF. A large body of evidence seems to indicate that (1) the stellar IMF has a rather universal slope, (2) above 1 $M_\odot$ the IMF is well approximated by a power law with Salpeter-like exponent [58], (3) below 1 $M_\odot$ the IMF flattens.

According to [28], the average IMF (as derived from local Milky Way star-counts and OB associations) is a three-part power law, with exponent $\alpha = 2.7 \pm 0.7$ for $m > 1\ M_\odot$, $\alpha = 2.3 \pm 0.3$ for $0.5\ M_\odot < m < 1\ M_\odot$, $\alpha = 1.3 \pm 0.5$ for $0.08\ M_\odot < m < 0.5\ M_\odot$. Other authors, in the past, have proposed different (although somewhat similar) slopes for the IMF of various stellar mass ranges (e.g., [29, 59, 60]). Given these uncertainties, it is necessary to evaluate how this impacts the possibility to infer the SFH. In fact, we have the degeneracy condition that false combinations of IMF and SFH can match as well the present day mass function (the current distribution of stellar masses) of MS stars. To quantify it, three fake populations were generated with different IMF exponents (α =2, 2.35 and 2.7), but the SFH searched using always 2.35. The results are shown in Figure 8.

To interpret these results, one must recall that recent steps of star formation are still populated by the entire mass spectrum, while old steps see only low-mass stars because the more massive stars born at those epochs have already died. For old stars, a steeper IMF is almost indiscernible from a more intense star formation. In fact, even if evolved stars are included in the SFH derivation, the mass difference between a star at the RGB tip and those at the MS turn-off is only few hundredths of solar masses: too small for allowing the identification of any IMF effect.

For young stars the situation in different. Any attempt to reproduce with an IMF steeper than that of the reference population the number of stars on the lower MS requires a stronger SF activity, but this (wrong) solution leads to overestimating the number of massive stars. Hence, for young stars, IMF and SFH are not degenerate. However, an automatic optimization algorithm, if not allowed to search better solutions including also the IMF among the free parameters, inevitably faces the impossibility to accommodate the number of both massive and low-mass stars, by choosing a compromising recent SFH giving higher weight to the more populated (although less reliable) CMD region.

As shown in Figure 8 the automatic fit tends to overestimate the age of any population whose IMF is actually steeper than the adopted one, and vice versa, for a flatter IMF. Again, we remark that the automatic solution is only the best solution in a parameter space where the IMF is fixed, not necessarily a good one: if the CMD of the recovered SFH is compared with the reference CMD, we immediately recognize that the ratio between low and massive stars is wrong. In other words, to figure out whether our "best"

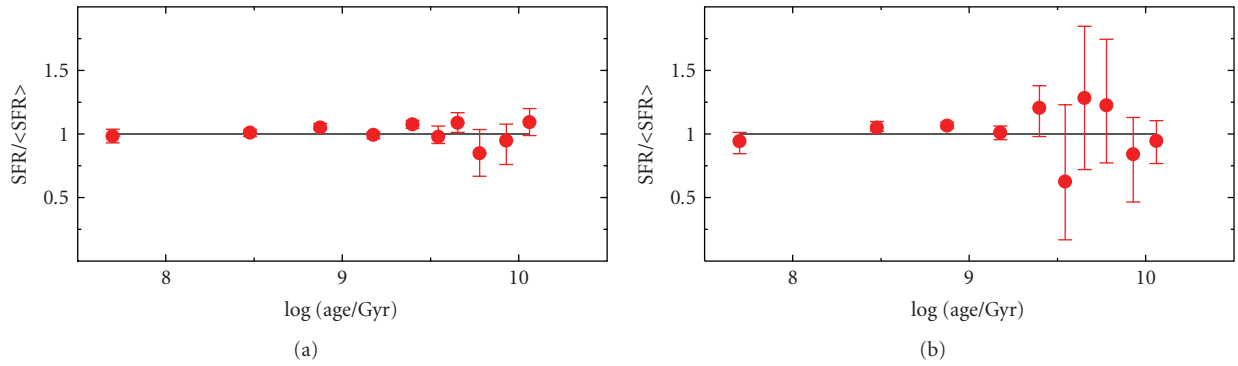

FIGURE 7: Effect of different completeness limits: in Figure 7(a) the SFH is recovered using only stars brighter than $V = 22$. In this case, most of the information is still retrieved. In (b) this limit is lowered at $V = 21$ as expected, most of the old star formation (older than 1 Gyr) is much more uncertain.

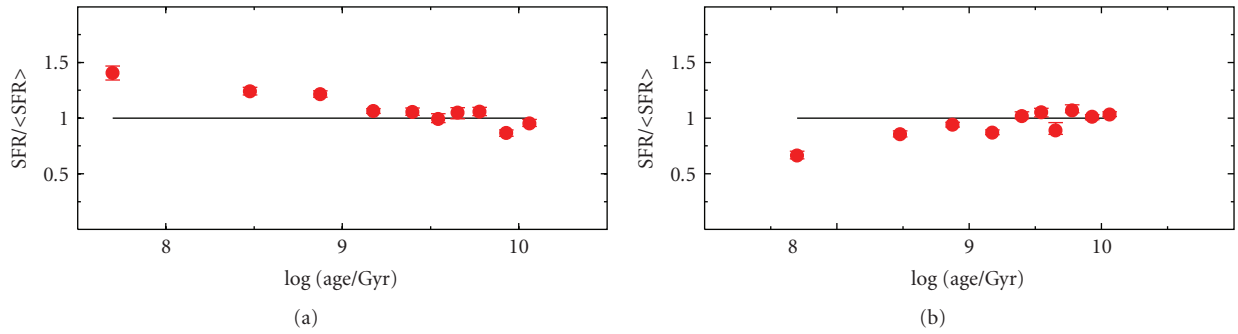

FIGURE 8: Effect of different IMFs. SFH recovered assuming Salpeter's IMF exponent (2.35) for synthetic stellar populations actually generated adopting different IMF (labeled in each panel) and a constant SFR.

solution is actually acceptable, it is always crucial to compare all its CMD results with the observed one.

3.9. Binaries. Another source of uncertainty is the percentage of stars in unresolved binary systems and the relative mass ratio. The presence of a given percentage of not resolved binary systems affects the CMD morphology. The aim, here, is to see if these effects can destroy or alter the recovered information on the SFH. In order to perform this analysis, we build fake populations using different prescriptions for the binary population (10%, 20%, and 30% of binaries with random mass ratio), but the SFH is searched ignoring any binary population (i.e., assuming only single stars). Our models do not include binary evolution with mass exchange, thus we assume that each star in a double system evolves as a single star.

Figure 9 shows the results, as for the IMF, also in this case a modest systematic effect is visible. This is because the stars in binary systems are brighter and redder than the average single star population (for an in depth analysis see, e.g., [61]). For the recent SFH, this corresponds to moving lower MS stars from a star formation step to the contiguous *older* step: in this way, the most recent star formation step is emptied of stars, mimicking a lower activity. Intermediate SF epochs are progressively less affected, because some stars get in and some stars get out of the step bin. For the oldest epochs, the situation is opposite: the binary effect is to move stars toward younger bins. Here, the SGB, that is, the main signature of any old population, is brighter because of the binaries, mimicking a younger system.

3.10. Metallicity and Metallicity Spread. The precise position of a star on the CMD depends on the chemical composition, namely, the mass fraction of hydrogen, helium, and metals (X, Y, Z , respectively). The Z content mainly changes the radiative opacity and the CNO burning efficiency: the result of a decreasing Z is to increase the surface temperature and the luminosity of the stars. This has two consequences of relevance for us: (a) metal poor stars have a shorter lifetime compared to the metal-rich ones (because overluminous and hotter), (b) a metal-poorer stellar population is bluer but can be mistaken for a younger but metal-richer population.

To test these effects, the first stars (ages older than 5 Gyr) in our reference fake population are built with a slightly different metallicity ($Z = 0.002$) than the younger objects, which have the usual $Z = 0.004$. Then, we recover the SFH by adopting a model with $Z = 0.004$ independently of age. The results are shown in Figure 10: neglecting that the oldest population of our galaxy was slightly metal poorer, systematic, nonnegligible discrepancies appear in the recovered SFH. It is the classical age-metallicity degeneracy: to match the blue-shifted sequences of old metal poorer stars,

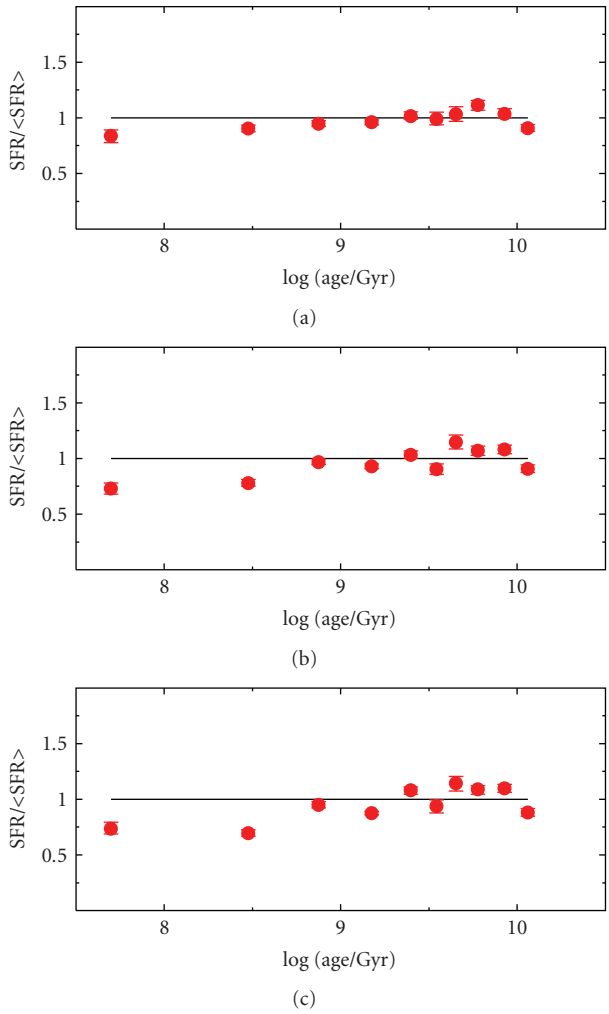

Figure 9: Effect of unresolved binaries. Three fake populations are built with different percentage of binary stars (10%, 20%, and 30%). The SFR is recovered using only single stars.

our models with wrong metallicity must be younger. Note that the overall trend of the young SFR is not significantly biased, while the old SFR is now significantly different.

This result is a strong warning against any blind attempt to match the CMD with a single (average) metallicity, especially considering that many galaxies exhibit a pronounced age metallicity relation.

During and at the end of their life, stars pollute the surrounding medium, so we expect that more recently formed stars have higher metallicity and helium abundance than those formed at earlier epochs. The progressive chemical enrichment with time results from the combined contribution of stellar yields, gas infall and outflows, mixing among different regions of a galaxy. Observational studies have shown that several galaxies reveal a metallicity spread at each given age.

In [46], the SFH sensitivity to a metallicity dispersion is tested: several fake populations were generated with a mean metallicity $Z = 0.02$ plus a variable dispersion from

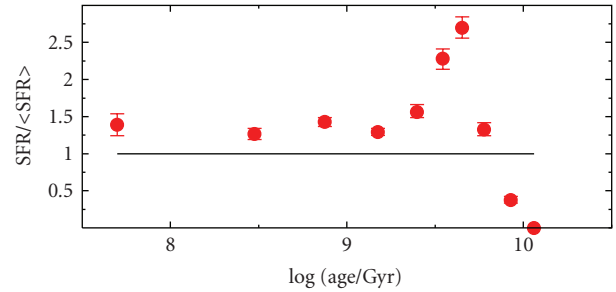

Figure 10: Sensitivity test to metallicity. The reference fake galaxy has a variable composition: $Z = 0.004$ for stars younger than 5 Gyr, $Z = 0.002$ for older stars. The red dots represent the SFR as recovered using a single metallicity $Z = 0.004$ for all epochs.

$\sigma = 0.01$ dex to $\sigma = 0.2$ dex in $[Fe/H]$. Then, the SFH was searched adopting in the model the same mean metallicity of the artificial data, but *without metallicity spread*. The results are shown in Figure 11. As described earlier, $\sigma = 0.1$ dex, the retrieved SFH differs significantly from the true one: this numerical experiment points out that the metallicity dispersion can be a non negligible factor.

3.11. Helium Content. The SFH retrieval must be also tested against possible variations of the helium abundance for a given metallicity. The abundance of He and metallicity influence the stellar structure through the molecular weight. Increasing Y corresponds to increasing the molecular weight and affects the hydrostatic equilibrium. The pressure decreases and the star shrinks (producing heat), reaching a new equilibrium characterized by a smaller radius and a higher central temperature. As a consequence, the efficiency of the central burning increases and this makes the star brighter and hotter.

Helium absorption lines appear only in the spectra of very hot stars. Hence, the traditional procedure to infer the helium abundance of a standard stellar population cannot be via direct measures and is instead based on the correlation (which is assumed linear) between the helium mass fraction Y and the metal abundance Z.

In order to explore the effects of a wrong choice of the helium content, we have built a reference fake population with $Z = 0.004$ and $Y = 0.27$ and we have tried to recover its SFH using a $Z = 0.004$ model coupled with $Y = 0.23$, which is obviously a very extreme assumption and, therefore, provides a stringent upper limit to the possible Y effects on the SFH. The result is shown in Figure 12: there are a number of small variations, but the general morphology is well reproduced. The small features of the recovered SFR are blended (the peaks are attenuated) but the overall trend is still recovered.

3.12. Reddening and Distance. In order to test how wrong choices of reddening and distance invalidate the possibility to recover the right SFH, we consider two extreme situations: first, the fake galaxy is put at $(m - M)_0 = 18.6$, with the models still assuming $(m - M)_0 = 18.9$ second, the fake

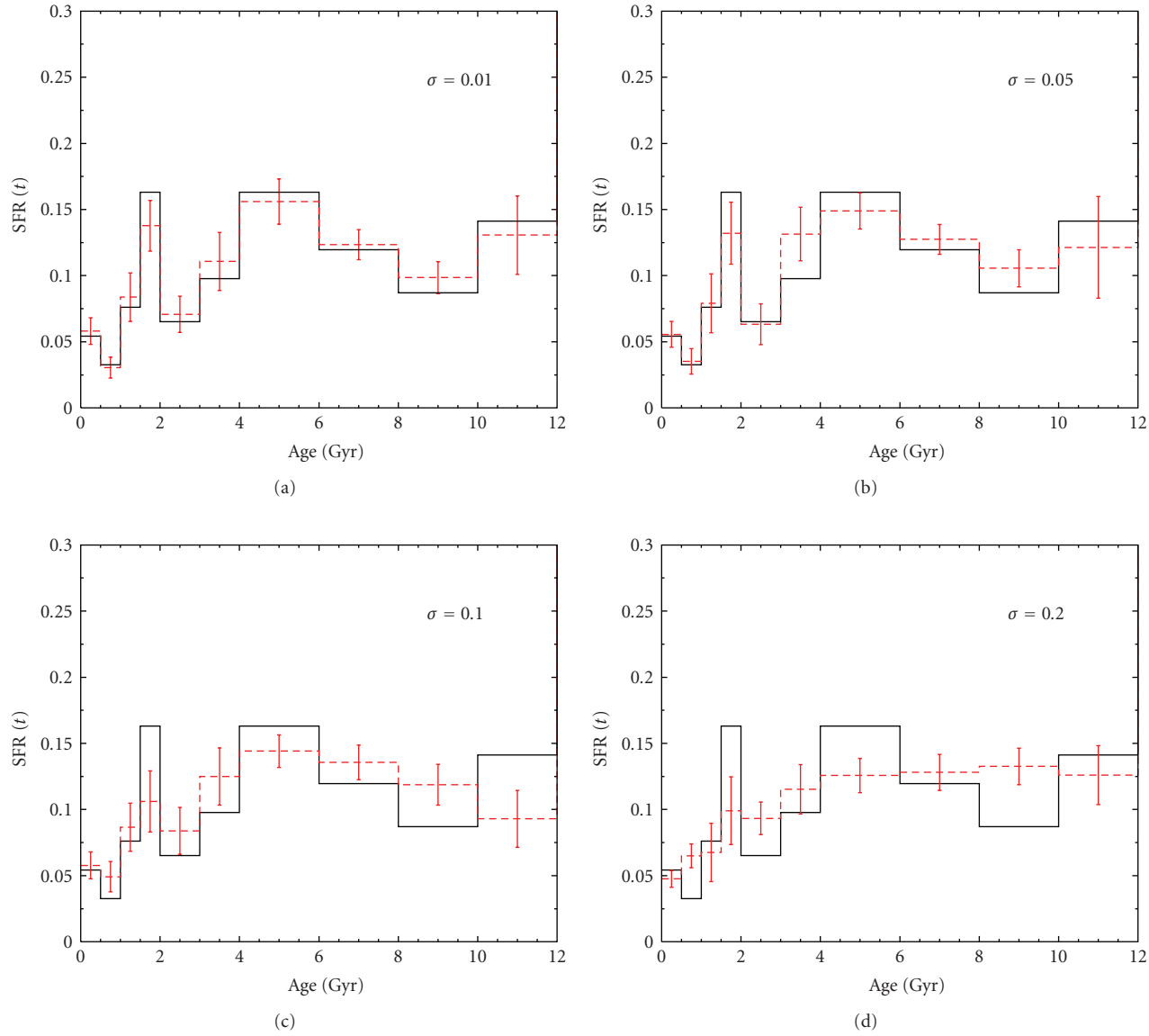

FIGURE 11: Sensitivity test to the metallicity dispersion. Solid line: SFH assumed for the fake population. Dashed line: recovered SFH. The σ value indicates the dispersion in $[Fe/H]$, used for the reference artificial data. The model has the same mean metallicity, but no dispersion.

galaxy is reddened using $E(B-V) = 0.16$ mag, while the models adopt $E(B-V) = 0.08$. The results are shown in Figure 13: it is evident that the SFH is not recovered, and shows large deviations from the reference case at any epoch. However, it is worth to remind that we have derived the best models from a blind χ^2 minimization: it is clear that at the distance of SMC, with the beautiful HST photometry available, both a visual inspection of the CMD morphology (in particular the blue MS envelope) and the evaluation of the χ^2 probability would be effective to reject all the models with wrong distance and reddening. The problem is more challenging for more distant galaxies, where the only observables are massive stars and reddening and distance are difficult to constrain.

Other potential problems are related to differential reddening and line-of-sight depth. There are several indications that some galaxies or portions of them are affected by differential reddening. For instance, young stars can be still surrounded by relics of their birthing cocoon material and suffer an additional amount of absorption. The first signature of a differential reddening is the red clump morphology when it appears elongated and/or tilted (see, e.g., [62]). Another effect is a smeared appearance of colour and magnitude in any stellar evolution sequence of the CMD.

A finite line-of-sight depth is a natural expectation, at least for nearby galaxies where the physical extension can be a nonnegligible fraction of their distance from us. As an example, according to [63], the SMC may have a depth of 14–17 kpc, corresponding to a spread in magnitude of few tenths of magnitude. This effect may alter the evolutionary information from the clump and the RGB. A correct description of the stellar populations thus requires analyses

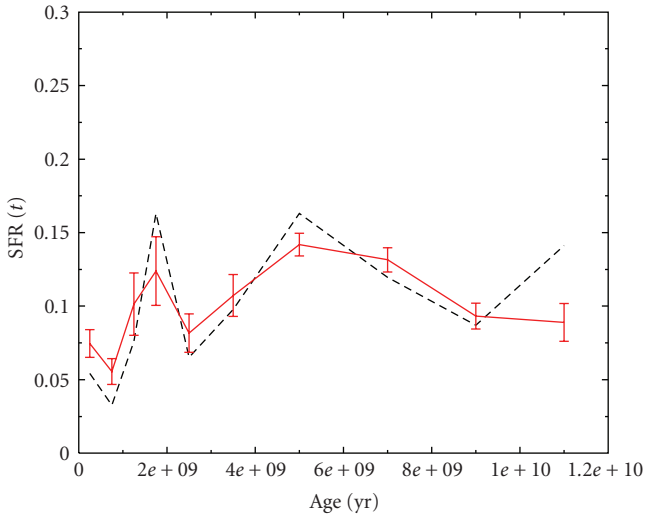

FIGURE 12: Experiment of the helium effect on the SFH: reference fake population and model have the same metallicity $Z = 0.004$, but different helium content ($Y = 0.23$ for the model and $Y = 0.27$ for the artificial data). The black dashed line is the input SFH. The red solid line is the recovered SFH.

involving the spatial structure. Both differential reddening and line-of-sight effects can be dealt with as additional free parameters.

In order to check how the recovered SFH is influenced by differential reddening and line-of-sight spread, we built two fake populations with the following features: the first has a reddening dispersion $E(B-V) = 0.08 \pm 0.04$, the second has a distance spread $(m-M)_0 = 18.9 \pm 0.2$. Figure 14 shows the result when the SFH is searched using the canonical combination $E(B-V) = 0.08$ and $(m-M)_0 = 18.9$. The reference SFH is still fully recovered. The reason is in the random nature of these uncertainties that produce a blurred CMD, but not a systematic trend.

3.13. Additional Issues. The previous experiments do not exhaust all the possible sources of uncertainty. Rather, they represent the best understood and manageable ones: among others, convection, atmospheres, and colour transformations, stellar rotation, mass exchange in binary systems may be relevant as well. Moreover, we have explored each single bias separately, while in a real galaxy, several uncertainties may be at work simultaneously with different intensities. In this case, the final effect may not be the simple summation of the previous results: some of the effects may compensate each other or conspire to build an uncertainty larger than the sum of the individual uncertainties.

For example, in the metallicity experiment, when the reference old population was metal poorer than in the search procedure, the retrieved SFH resulted younger. However, this is true *only* if the best SFH is searched with fixed reddening. Letting the reddening vary could lead to a different SFH (and reddening).

To summarize, the final uncertainty on the recovered SFH strongly depends on which parameter space is explored. Generally speaking, when the best photometric conditions are achieved and all the parameter space is properly covered, within the reached lookback time the error on the epochs of the SF activities is around ten percent of their age and that on the SFR is of the order of a few. With poorer photometry or with coarser procedures the uncertainties obviously increase, but the qualitative scenario is usually reliably derived.

4. Star Formation Histories of Resolved Dwarfs from Synthetic CMD Analyses: Results

In spite of the uncertainties described earlier in the identification of the *best solution* for the SFH, the synthetic CMD method is extremely powerful in reducing the range of acceptable scenarios, that is, the range of values of the various parameters. As demonstrated every time different synthetic CMD procedures have been applied to the same galaxy region, all the solutions come out consistent with each other (see, e.g., the *Coimbra experiment* on the LMC bar [50], and IC1613 [64]). We can, therefore, dare drawing some general conclusions from the results obtained so far with this method.

Since the dawn of its application, the method immediately proved its power. First, it was found that the SFH differs significantly from one galactic region to the other even in tiny systems such as WLM, the first dwarf irregular (dIrr) in the Local Group to which the method was applied [30]. As soon as a few other nearby irregulars were studied, it turned out that, contrary to the common belief of the time, the SF activity in late-type dwarfs within the lookback time spanned by the available photometry has occurred in long episodes of moderate intensity, separated by short quiescent phases, rather than in short episodes of strong intensity, separated by long quiescent intervals [31, 33–35, 66]. In other words, a *gasping* [34] rather than a *bursting* regime.

Nowadays, one can resolve individual faint/old stars in galaxies of the LG and its immediate vicinities, and infer their SFHs over long lookback times. In the (still few) cases when the oldest MSTO is reached, the SFH can be derived over the entire Hubble time, as already achieved in some regions of the LMC [43, 62, 67–70], of the SMC [27, 71, 72] and in Leo A [65]. As an example, Figure 15 shows the CMD obtained by [65] from ACS imaging of the dIrr Leo A, located at 800 kpc from us [52], and the resulting SFH. In Leo A the star formation activity was present, although quite low at the earliest epochs, and 90% of the activity occurred in the last 8 Gyr, with the main peak around 2 Gyr ago and a secondary peak a few hundreds Myr ago. This SFH is very similar to that of fields in the LMC, SMC, IC1613 [73], and other late-type galaxies and we can consider it typical of dIrrs: a rather continuous star formation since the earliest epochs, but with significant peaks and gasps. Notice that the main SFR peak in dIrrs rarely occurs at the most recent epochs.

The high spatial resolution of HST cameras also allows to spatially resolve the SF activity, at least within relatively recent epochs. For instance, the work in [74, 75] has measured the SF activity over the last 0.5 Gyr in all the subregions of the dIrrs Gr8 and Sextans A, close to the

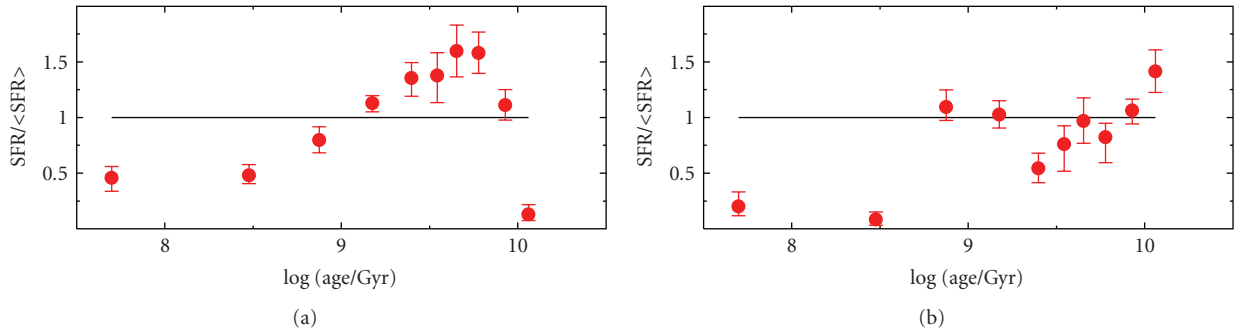

Figure 13: Sensitivity test to reddening and distance. Red dots represent the recovered SFH. In (a), the reference fake population is built with a distance spread $(m - M)_0 = 18.6$, while the model used to retrieve the SFH adopts $(m - M)_0 = 18.9$. In (b),the reference fake population is built with reddening $E(B - V) = 0.16$, while the model used to retrieve the SFH adopts reddening $E(B - V) = 0.08$.

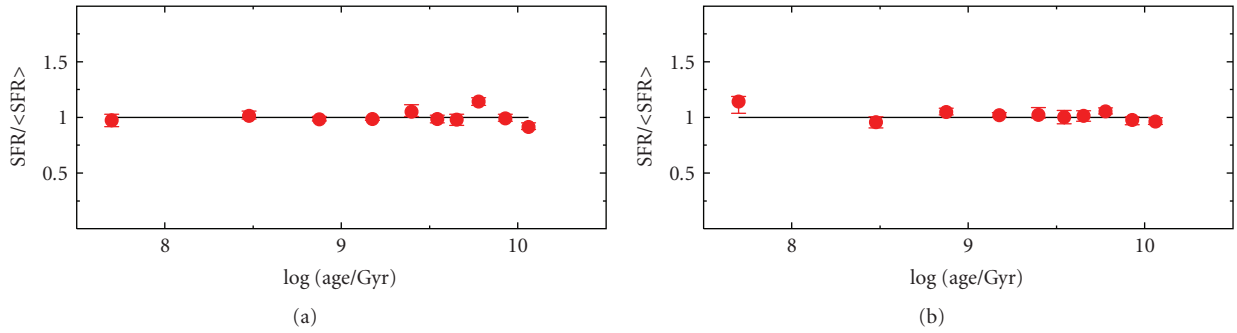

Figure 14: Sensitivity test to differential reddening and line-of-sight spread. Red dots represent the recovered SFH. In (a), the reference fake population is built with a distance spread $(m - M)_0 = 18.9 \pm 0.2$, while the model used to retrieve the SFH has a single distance $(m - M)_0 = 18.9$. In (b), the reference fake population is built with a differential reddening $E(B - V) = 0.08 \pm 0.04$, while the model used to retrieve the SFH has a single reddening $E(B - V) = 0.08$.

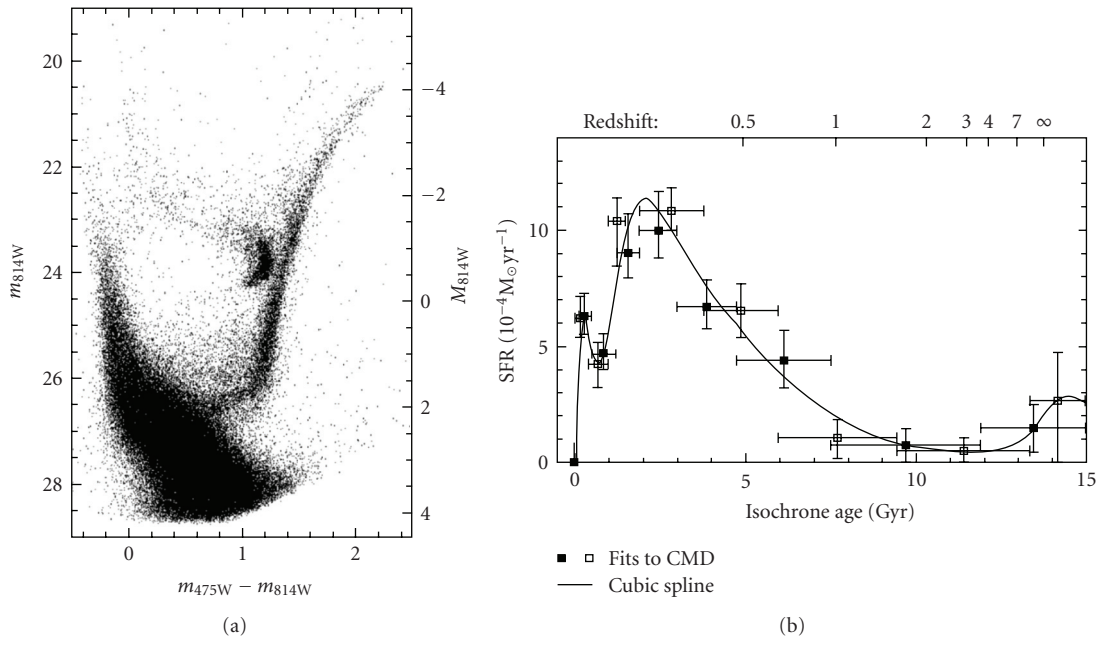

Figure 15: CMD and SFH of Leo A as derived by [65] from HST/ACS data. Notice the impressive depth and tightness of the CMD, allowing to infer the SFH even at the earliest epochs. Courtesy A. Cole.

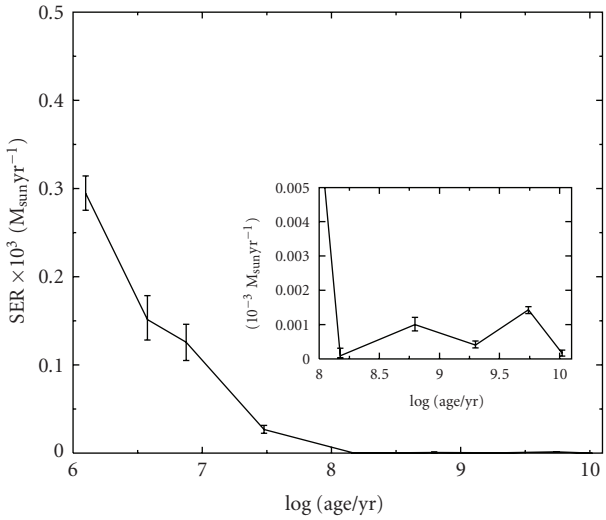

Figure 16: SFH of the ACS field centered on the SMC young cluster NGC602 as derived by [27]. The oldest part of the SFH is zoomed-in in the upper right inset. The ACS image and the CMD of the field are shown in Figure 2(a).

borders of the LG. The resulting space and time distribution of the SF, with lightening and fading of adjacent cells, once again shows a gasping regime, and is intriguingly reminiscent of the predictions of the stochastic self-propagating SF theory proposed by [76] almost 30 years ago.

In the Magellanic Clouds, the conditions are clearly optimal, thanks to their proximity. Figure 16 displays the SFH of the ACS field centered on the very young cluster NGC602 in the Wing of the SMC. It shows that the cluster has formed most of its stars around 2.5 Myr ago, while the surrounding field has formed stars continuously since the earliest epochs. All the studies on the MC fields have found that the SFHs of their different regions differ from one another in the details (e.g., epoch of activity peaks, enrichment history, etc.) but are always characterized by a gasping regime. In the LMC a clear difference has been found between the SFH of field stars and of star clusters, the latter showing a long quiescence phase absent in the field. This difference is not found in the SMC.

To find SFHs peaked at earlier epochs, one needs to look at early-type dwarfs: dwarf ellipticals (dEs), dSphs, and even transition-type dwarfs clearly underwent their major activity around or beyond 10 Gyr ago [73]. The latter also have significat activity at recent epochs (e.g., [77]). The former have few (or no) episodes of moderate activity in the last several Gyrs (e.g., [40, 52, 78–81]). A beautiful example of CMDs and SFH of a dSph is shown in Figure 17. It is the Cetus dSph, observed with HST/ACS by the L-CID group [82] and to be published by Monelli et al. (in preparation). Here the SF activity in the last several Gyrs is negligible and the strongest peak occurred about 11 Gyr ago (interestingly, not at the earliest epoch, though).

To date, a large fraction of LG galaxies have been studied to infer the SFH of at least some of their regions with the synthetic CMD method (see, [18, 83] and references therein, for updated reviews): the two spirals, M31 and M33, the two Magellanic Clouds, a dozen dIrrs, 5 transition-type dwarfs and about 20 early-type dwarfs (dwarf spheroidals and dwarf ellipticals). In some of these fields, the photometry has allowed to reach the oldest MSTO, in others the HB, that is, the unmistakable signature of SF activity earlier than 10 Gyr ago (e.g., [84–86]). Attention is being payed [87] also to the ultra-faint dwarfs (uFds) recently discovered by the Sloan Digital Sky Survey around the Milky Way (e.g., [88]), for their interest as possible Galactic building blocks. Additional efforts by various groups are in progress to obtain deeper and more accurate photometry in these and other galaxies and derive reliable SFHs over longer lookback times. For instance, very interesting results are expected from the L-CID HST program [82] on the SFH of 6 LG dwarfs of different type (two dIrrs, two dSphs, and two transition type) observed by the ACS with unprecedented depth and resolution.

In galaxies beyond the LG, distance makes crowding more severe, and even HST cannot resolve stars as faint as the MSTO of old populations. The higher the distance, the worse the crowding conditions, and the shorter the lookback time τ reachable even with the deepest, highest-resolution photometry. Depending on distance and intrinsic crowding, the reachable lookback time in galaxies more than 1 Mpc away ranges from several Gyrs (in the best cases, when the RGB or even the HB are clearly identified) to several hundreds Myr (when AGB stars are recognized) to a few tens Myr (when only the brightest supergiants are resolved). The effect of distance on the possibility of resolving individual stars, and therefore on the reachable τ, is displayed in Figure 18, where the CMDs of three late-type galaxies are shown, as resulting from WFPC2 photometry in equivalent observing conditions: the LMC bar [68], with a distance modulus of 18.47 (50 kpc) and a CMD reaching a few mags below the old MSTO; NGC1705 [91], with distance modulus 28.54 (5.1 Mpc) and a CMD reaching a few mags below the tip of the RGB; and IZw18 [92]), with the new distance modulus 31.3 (18 Mpc) derived by [89] and AGB stars being the faintest/older resolved stars.

Notice that the new modulus of IZw18 is inferred from the periods and luminosities of a few classical Cepheids measured from ACS time-series photometry, which also allowed to obtain a much deeper CMD [89]. The WFPC2 data shown in Figure 18 reach only the AGB, while the CMD obtained from the ACS (shown in Figure 19 together with the ACS image) reaches below the tip of the RGB. Indeed, the unique performances of the ACS have allowed people to resolve individual stars on the RGB of some of the most metal-poor Blue Compact Dwarfs (BCDs), such as SBS 1415 + 437 at 13.6 Mpc [93] and IZw18 at 18 Mpc [89]. The discovery of stars several Gyrs old in these extremely metal-poor systems is a key information for galaxy formation and evolution studies. It has allowed to detect in BCDs population gradients, the central concentration of most of the SF activity, the existence of old, metal-poor halos (e.g., [94], and subsequent papers).

With an amazing success rate, the ACS has allowed people to resolve individual stars from the brightest and youngest to those as faint and old as the red giants in an

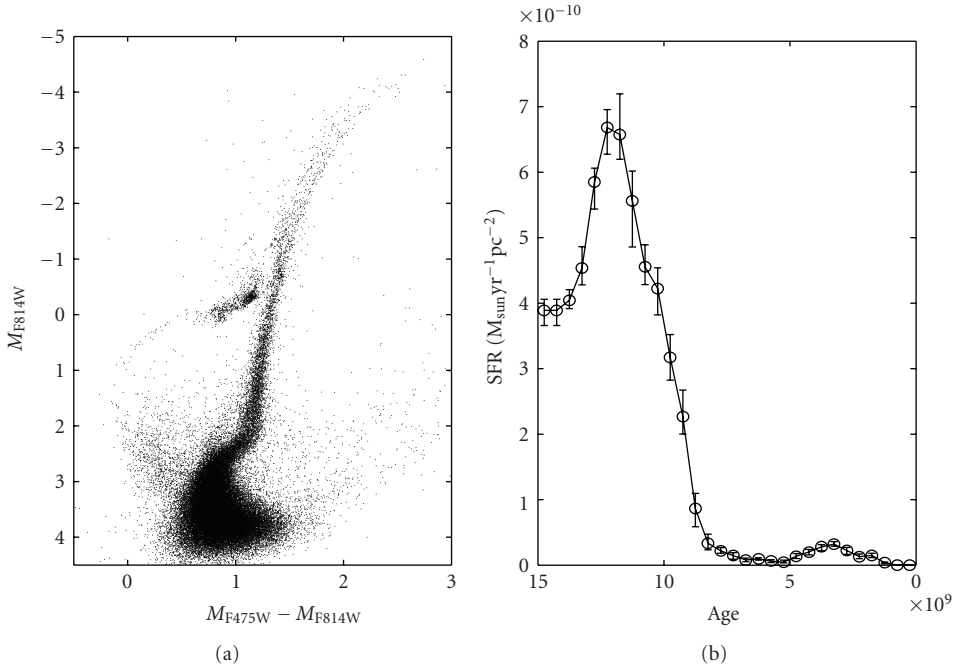

FIGURE 17: CMD and SFH of Cetus as derived by Monelli et al. (in preparation) from HST/ACS data in the framework of the L-CID project [82]. Notice again the impressive depth and tightness of the CMD, allowing to infer the SFH even at the earliest epochs. Courtesy M. Monelli and C. Gallart.

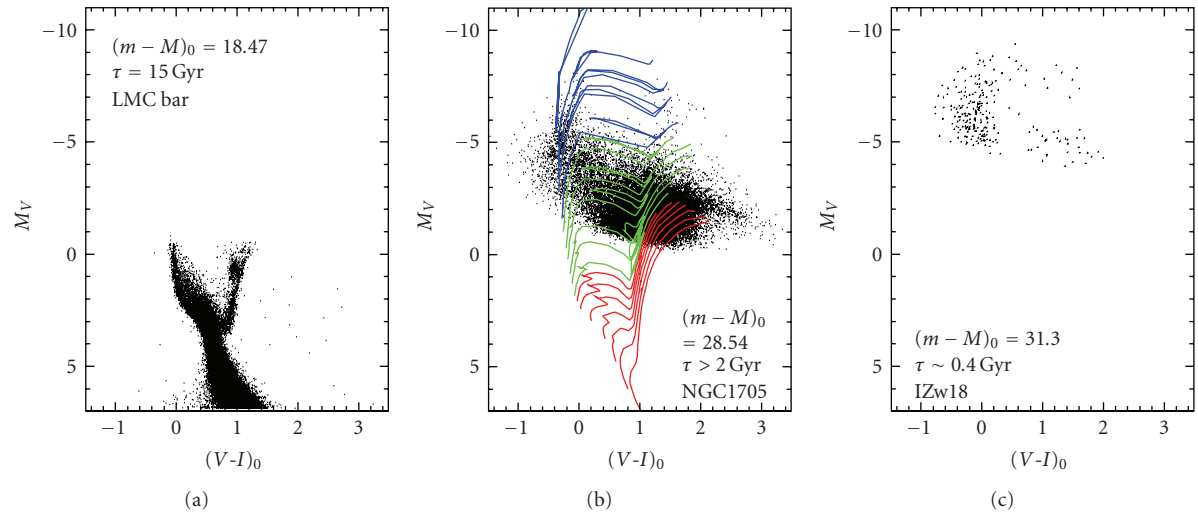

FIGURE 18: Effect of distance on the resolution of individual stars and on the corresponding lookback time τ for the SFH. CMD in absolute magnitude and colour of systems observed with the HST/WFPC2 and analysed with the same techniques, but at different distances; from (a) to (c): 50 Kpc (LMC bar), 5.1 Mpc (NGC1705), and 18 Mpc (IZw18); (b) also shows stellar evolution tracks from [23] for reference: red lines refer to low-mass stars, green lines to intermediate mass stars, and blue lines to massive stars.

increasing number of dwarfs outside the LG, in the distance range 2–20 Mpc. This allows to study the SFH of isolated and interacting dwarfs. People are becoming able to compare the SFHs of LG dwarfs with those of other groups of galaxies, such as the M81 (e.g., [95]) and the IC342 (Grocholski et al. in preparation) groups. The resulting CMDs lead to the derivation of their SFHs over a lookback time of at least a few Gyrs and, often, to a more accurate estimate of their distance (e.g., [89, 96])

Only few groups have embarked in the more challenging application of the synthetic CMD method beyond the LG, and most of them have concentrated their efforts on star-bursting late-type dwarfs [92, 94, 97–99, 101–108]. However, HST (new observations and archive) is still providing a

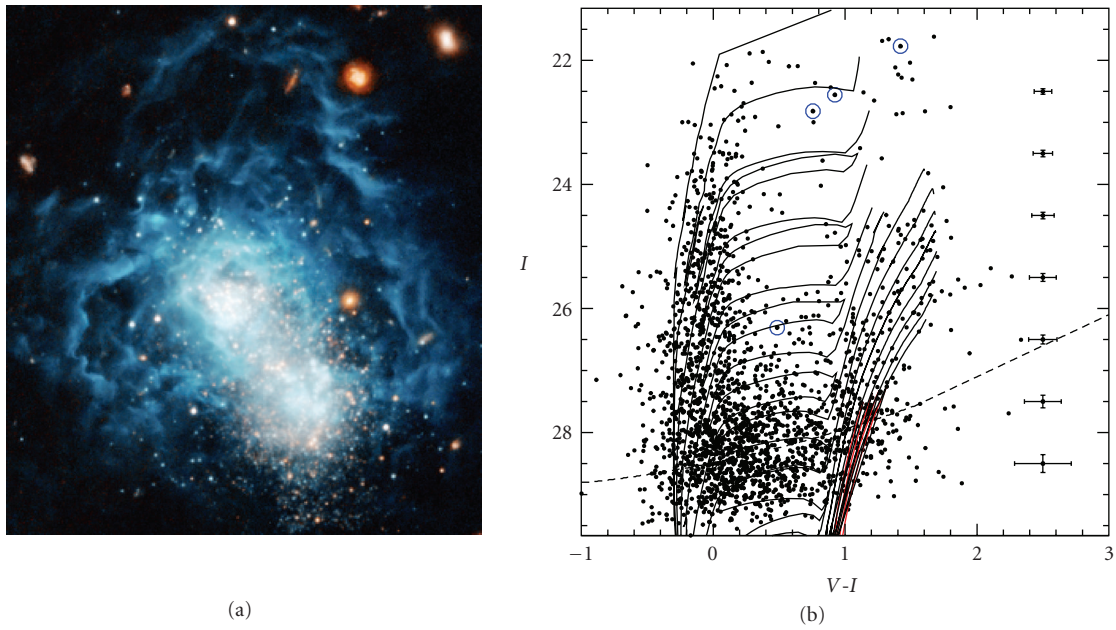

Figure 19: Image and CMD of IZw18, obtained from HST/ACS imaging [89]. Overimposed on the CMD are the $Z = 0.0004$ isochrones by [90] with the RGB in red. Also shown is the average position of the 4 classical Cepheids with reliable light curves obtained from these data. Image credit: NASA, ESA, and A. Aloisi (STScI, ESA).

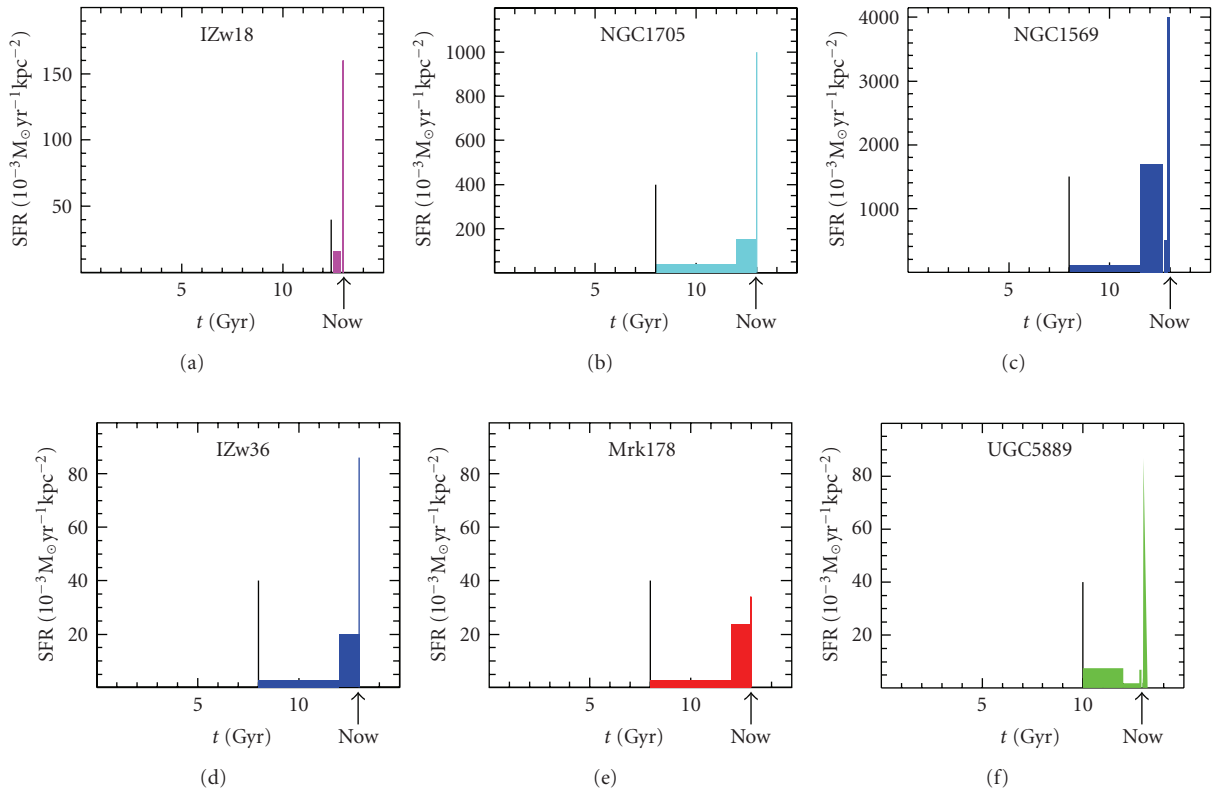

Figure 20: SFHs of late-type dwarfs outside the Local Group observed with WFPC2 or NICMOS. In all panels, the SFR per unit area as a function of time is plotted. The thin vertical line indicates the lookback time reached by the adopted photometry. Notice that for those galaxies that have been subsequently observed also with the ACS, the lookback time is actually quite older, and always with indisputable evidence of SF activity already in place. References: NGC 1569, [97, 98]; NGC 1705, [99, 100]; I Zw 18, [92]; I Zw 36, [101]; Mrk 178, [102]; UGC 5889, [103].

wealth of excellent images of external dwarfs. In particular, the ACS Nearby Galaxy Survey Treasury is promising an unprecedented data base for these purposes [109], and we can expect a flourishing of applications of the synthetic CMD method to many more galaxies beyond the LG boundaries in the near future.

All the studies performed so far have shown that all the examined galaxies were already active at the reached lookback time, including the BCDs that in the past had been suggested to be genuinely young galaxies, experiencing now their first episode of SF. All late-type dwarfs present a recent SF burst, which lets people discover them in spite of the distance, and none of them exhibits long quiescent phases within the reached lookback time. On the other hand, the SFR differs significantly from one galaxy to the other.

These results can be visualized in Figure 20, where some examples of SFH of external late-type dwarfs are given. All these SFHs have been derived with the synthetic CMD method applied to HST/WFPC2 or NICMOS photometry. The lookback time reached by the photometry is indicated by the thin vertical line in each panel, and in all cases stars of that age were detected. As shown by [100] for NGC1705, the available data allow to rule out that these galaxies have had short-duration, intermediate-age bursts like the current one within the covered lookback time. The sample of displayed galaxies contains various types of dwarfs: UGC 5889 is a low surface brightness galaxy (LSB), NGC 1705, IZw18, IZw36, and Mrk178 are BCDs, while NGC 1569 is classified as dIrr. Nonetheless, they all show a qualitatively similar behavior: a stronger current burst overimposed on a moderate and rather continuous SF activity. Quantitatively, instead, the SFRs differ from each other by orders of magnitude.

The general results drawn from all the SFHs derived so far from CMDs in and beyond the LG can be schematically summarized as follows:

(i) evidence of long interruptions in the SF activity is found only in early-type galaxies;

(ii) few early-type dwarfs have experienced only one episode of SF activity concentrated at the earliest epochs: many show instead extended or recurrent SF activity;

(iii) no galaxy currently at its first SF episode has been found yet;

(iv) no frequent evidence of strong SF bursts is found;

(v) there is no significant difference in the SFH of dIrrs and BCDs, except for the current SFR.

5. Concluding Remarks

By comparing the results on the SFHs described in the previous section, one can infer interesting conclusions and attempt some speculations.

An interesting result of the SFH studies both in the LG and beyond is that all dwarfs have, and have had, fairly moderate SF activity. None of the dwarfs SFRs from the CMDs studied so far ever reaches values as high as $1\,M_\odot$/yr, and only one (NGC 1569) gets close to it [96–98]. Since $1\,M_\odot$/yr is the minimum rate required to let a galaxy contribute to the overabundance of faint blue objects in deep galaxy counts (see the models by [2]), this makes it quite unlikely that dwarfs are responsible for the blue excess.

If we look at the dwarfs shown in Figure 20, we notice that the least active system is one of the BCDs and the most active one is the dIrr. This is not inconsistent with the findings from an extensive H_α study of 94 late-type galaxies [110], showing that the typical SFR of irregular galaxies is $10^{-3} M_\odot \mathrm{yr}^{-1}\mathrm{kpc}^{-2}$ and that of BCDs is generally higher. From that survey, Hunter and Elmegreen [110] indeed conclude that NGC 1569 and NGC 1705 are among the few systems with unusually high star formation, and that the star formation regions are not intrinsically different in the various galaxy types, except for a significantly higher spatial concentration in BCDs.

In our view, this suggests that either the morphological classification does not strictly correspond to the intensity of the SF activity, or that, most likely, the traditional classification, based in most cases on photographic plates, is rather uncertain for systems too distant to be properly resolved before the advent of HST. Probably an active dwarf such as NGC1569, hosting three Super Star Clusters and a huge number of HII regions, would have been classified as BCD, had it been just a few Mpc farther away.

If we compare the SFHs of late-type dwarfs inside and outside the LG (e.g., Figures 15 and 20), we see that the overall scenario is quite similar, but the latter galaxies are always more active than the former at very recent epochs. Part of this is presumably due to the selection effect resulting from the difficulty of finding distant dwarf, faint galaxies, unless currently active. This effect is also the reason why early-type and quiescent dwarfs are so rare in the surveys performed so far outside the LG except for deep surveys devoted to individual galaxy clusters and groups, where they preferentially reside in central regions. Indeed, most often the HII region emission is what led to the discovery of distant dwarfs (recall that BCDs were originally called "extragalactic HII regions") and it is thus inevitable that these sytems have recent SF activity. From this point of view, it is interesting to note that the SFH of the external dwarfs of Figure 20 is very similar in shape to that of the NGC 602 region in the SMC [27], consistent with the circumstance that NGC 602 is also associated with an HII region (N90).

How do the Results on SFHs Affect Our Understanding of Galaxy Formation? The circumstance that all dwarfs contain stars as old as the reached lookback time, independently of their metallicity, gas content, or morphological classification suggests that their SF activity started at the earliest epochs. This is absolutely coherent with both the hierarchical formation scenario and the monolithical scenario. It is also consistent with downsizing if their early SFR was lower than that of more massive systems. For the (few) early-type dwarfs with studied SFH, we know that this is indeed the case; how about late-type dwarfs? We do not have direct evidences due to the large distance of most of these systems which prevents us to reach epochs older than a few Gyrs. However, all indirect arguments go in this direction: only

with quite moderate early SF activity can dIrrs and BCDs have managed to remain as metal-poor and gas-rich as they actually are. SFRs as high as the recent ones would have inevitably consumed all their gas in much less than a Hubble time and would have led to a significant chemical enrichment.

As mentioned in Section 1, to select the most viable scenario, it is the combination of the SFH with the chemical and kinematic properties of the candidate building blocks that needs to be compared with the properties of massive galaxies. In the case of local dwarfs, these properties have been recently reviewed by [18]. Stars in *classical* dwarfs do not resemble those in the halo of the Milky Way, most notably their metallicity distribution functions [111–113] and the abundance ratios of α elements over iron (see [18], and references therein). Moreover, if all early-type dwarfs have had the relatively moderate SF activity shown in Figure 17 for Cetus, with a rather long duration and the peak some Gyr after the beginning, there is no way to let them provide the iron-poor stars with high $[\alpha/Fe]$ typical of our halo, since the SF peak forms most of the stars when SNeIa have already had the time to pollute the medium with their iron.

On the other hand, the current knowledge of the outer Galaxy is far from complete. We know that the stellar halo hosts two distinct populations (see, e.g., [114, 115], and references therein). The work in [116] finds that the so-called "inner halo" selected among halo stars with prograde rotation and low apogalactic maximum distance from the galactic center is different for several aspects from the "outer halo" selected among stars with high retrograde rotation and high apogalactic maximum distance. In particular, the following hold. (1) The inner halo is characterized by a tight correlation between $[\alpha/Fe]$ versus $[Fe/H]$, suggesting that either the abundance ratios in distant regions of the inner halo are very similar or the inner halo developed from a well-homogenized interstellar medium. In contrast, the outer halo shows a much larger scatter in $[\alpha/Fe]$ for a given $[Fe/H]$, signature that the star formation was spatially inhomogeneous or these stars have been accreted from outside (from dwarf galaxies). (2) The inner halo shows an average $[\alpha/Fe]$ slightly higher than observed in the outer halo, providing a clue for a more intense and short-lasting star formation activity. (3)The inner halo is only found with metallicities in the range $-2.5 < [Fe/H] < -0.5$, while most of the outer halo is in the range $-3.5 < [Fe/H] < -1.5$.

Unfortunately, the outer halo is still mostly inaccessible: current high-resolution abundances rely mainly on halo stars that pass near the Sun. If these stars are formed in the outer halo, their selection is biased towards higher eccentricity orbits. Avoiding this bias implies a new class of surveys able to trace α variations in situ. In this context, the Gaia mission will provide a quantum leap in the ability to obtain highly precise astrometry, photometry and metallicity for a volume of several Kpc.

If the outer halo is a natural place to search for possible accretion events, the recent discovery of ultra-faint dwarfs promises to complete the picture: containing extremely metal-poor stars, probably with high $[\alpha/\mathrm{Fe}]$ like in our halo [117–119], these galaxies are ideal candidates for Galactic building blocks. The problem in this case is the extreme uncertainty still affecting their measures, due to both faintness and high Galactic contamination. Overcoming these limits will be a challenge only suitable for wide-field spectrographs mounted on giant ground-based telescopes.

Acknowledgments

Over the years several interesting conversations with A. Aparicio, C. Chiosi, S. DeglâInnocenti, J. Gallagher, C. Gallart, P.G. Prada Moroni, R. Schulte-Ladbeck, S. N. Shore, E. Skillman, E. Tolstoy, and in particular L. Greggio, have been fruitful to dig into the secrets of synthetic CMD building and exploitation. We thank A. Cole for providing the Leo A figure in appropriate format and M. Monelli for the Cetus figure. We also thank Laura Greggio and the anonymous referees for detailed and constructive comments helpful to make this paper clearer. We acknowledge the financial support from ASI through contract ASI-INAF I/016/07/0 and from the Italian MIUR through contract PRIN-2007JJC53X-001.

References

[1] S. J. Lilly, L. Tresse, F. Hammer, D. Crampton, and O. Le Fèvre, "The canada-france redshift survey. VI. Evolution of the galaxy luminosity function to z approximately 1," *The Astrophysical Journal*, vol. 455, no. 1, pp. 108–124, 1995.

[2] A. Babul and H. C. Ferguson, "Faint blue galaxies and the epoch of dwarf galaxy formation," *The Astrophysical Journal*, vol. 458, no. 1, pp. 100–119, 1996.

[3] M. Peimbert and S. Torres-Peimbert, "Chemical composition of H II regions in the Large Magellanic Cloud and its cosmological implications," *The Astrophysical Journal*, vol. 193, pp. 327–333, 1974.

[4] K. A. Olive, G. Steigman, and E. D. Skillman, "The primordial abundance of4He: an update," *The Astrophysical Journal*, vol. 483, no. 2, part 1, pp. 788–797, 1997.

[5] Y. I. Izotov and T. X. Thuan, "The primordial abundance of 4He revisited," *The Astrophysical Journal*, vol. 500, p. 188, 1998.

[6] S. D. M. White and M. J. Rees, "Core condensation in heavy halos—a two-stage theory for galaxy formation and clustering," *Monthly Notices of the Royal Astronomical Society*, vol. 183, pp. 341–358, 1978.

[7] C. S. Frenk, S. D. M. White, M. Davis, and G. Efstathiou, "The formation of dark halos in a universe dominated by cold dark matter," *The Astrophysical Journal*, vol. 327, pp. 507–525, 1988.

[8] M. Bellazzini, R. Ibata, F. R. Ferraro, and V. Testa, "Tracing the Sgr stream with 2MASS: detection of stream stars around outer halo globular clusters," *Astronomy and Astrophysics*, vol. 405, no. 2, pp. 577–583, 2003.

[9] V. Belokurov, D. B. Zucker, N. W. Evans, et al., "Cats and dogs, hair and a hero: a quintet of new milky way companions," *Astrophysical Journal*, vol. 654, no. 2, pp. 897–906, 2007.

[10] A. M. N. Ferguson, M. J. Irwin, R. A. Ibata, G. F. Lewis, and N. R. Tanvir, "Evidence for stellar substructure in the halo

and outer disk of M31," *The Astronomical Journal*, vol. 124, pp. 1452–1463, 2002.

[11] R. Ibata, S. Chapman, A. M. N. Ferguson, M. Irwin, G. Lewis, and A. McConnachie, "Taking measure of the Andromeda halo: a kinematic analysis of the giant stream surrounding M31," *Monthly Notices of the Royal Astronomical Society*, vol. 351, no. 1, pp. 117–124, 2004.

[12] A. M. N. Ferguson, R. A. Johnson, D. C. Faria, et al., "The stellar populations of the M31 Halo substructure," *The Astrophysical Journal*, vol. 622, no. 2, part 2, pp. L109–L112, 2005.

[13] L. L. Cowie, A. Songaila, E. M. Hu, and J. G. Cohen, "New insight on galaxy formation and evolution from keck spectroscopy of the Hawaii deep fields," *The Astronomical Journal*, vol. 112, no. 3, pp. 839–864, 1996.

[14] H. Mouri and Y. Taniguchi, "Downsizing of star-forming galaxies by gravitational processes," *Astronomy and Astrophysics*, vol. 459, no. 2, pp. 371–374, 2006.

[15] E. Neistein, F. C. van den Bosch, and A. Dekel, "Natural downsizing in hierarchical galaxy formation," *Monthly Notices of the Royal Astronomical Society*, vol. 372, no. 2, pp. 933–948, 2006.

[16] A. Cattaneo, A. Dekel, S. M. Faber, and B. Guiderdoni, "Downsizing by shutdown in red galaxies," *Monthly Notices of the Royal Astronomical Society*, vol. 389, no. 2, pp. 567–584, 2008.

[17] O. J. Eggen, D. Lynden-Bell, and A. R. Sandage, "Evidence from the motions of old stars that the galaxy collapsed," *The Astrophysical Journal*, vol. 136, p. 748, 1962.

[18] E. Tolstoy, V. Hill, and M. Tosi, "Star formation histories, abundances and kinematics of dwarf galaxies in the local group," *Annual Review of Astronomy and Astrophysics*, vol. 47, pp. 371–425, 2009.

[19] L. Searle, W. L. W. Sargent, and W. G. Bagnuolo, "The history of star formation and the colors of late-type galaxies," *The Astrophysical Journal*, vol. 179, pp. 427–438, 1973.

[20] J. S. Gallagherc III, D. A. Hunter, and A. V. Tutukov, "Star formation histories of irregular galaxies," *The Astrophysical Journal*, vol. 284, pp. 544–556, 1984.

[21] J. S. Gallagher III and D. A. Hunter, "Structure and evolution of irregular galaxies," *Annual Review of Astronomy and Astrophysics*, vol. 22, pp. 37–74, 1984.

[22] F. Fagotto, A. Bressan, G. Bertelli, and C. Chios, "Evolutionary sequences of stellar models with new radiative opacities. Z = .0004 and Z = .05," *Astronomy and Astrophysics Supplement Series*, vol. 104, pp. 365–376, 1996.

[23] F. Fagotto, A. Bressan, G. Bertelli, and C. Chios, "Evolutionary sequences of stellar models with new radiative opacities. VI. Z = .004 and Z = .008," *Astronomy and Astrophysics Supplement Series*, vol. 105, pp. 29–38, 1996.

[24] L. Greggio, "The color-magnitude diagram of composite stellar populations," in *Observed HR Diagrams and Stellar Evolution*, T. Lejeune and J. Fernandes, Eds., vol. 274 of *Astronomical Society of the Pacific Conference Series*, p. 444, 2002.

[25] L. R. Carlson, E. Sabbi, M. Sirianni, et al., "Progressive star formation in the young SMC cluster NGC 602," *The Astrophysical Journal*, vol. 665, no. 2, part 2, pp. L109–L114, 2007.

[26] E. Sabbi, M. Sirianni, A. Nota, et al., "Past and present star formation in the SMC: NGC 346 and its neighborhood," *The Astronomical Journal*, vol. 133, no. 1, pp. 44–57, 2007.

[27] M. Cignoni, E. Sabbi, A. Nota, et al., "Star formation history in the small magellanic cloud: the case of NGC 602," *The Astronomical Journal*, vol. 137, no. 3, pp. 3668–3684, 2009.

[28] P. Kroupa, "On the variation of the initial mass function," *Monthly Notices of the Royal Astronomical Society*, vol. 322, no. 2, pp. 231–246, 2001.

[29] G. Chabrier, "Galactic stellar and substellar initial mass function," *Publications of the Astronomical Society of the Pacific*, vol. 115, no. 809, pp. 763–795, 2003.

[30] F. R. Ferraro, F. Fusi Pecci, M. Tosi, and R. Buonanno, "A method for studying the star formation history of dwarf irregular galaxies. I - CCD photometry of WLM," *Monthly Notices of the Royal Astronomical Society*, vol. 241, pp. 433–452, 1989.

[31] M. Tosi, L. Greggio, G. Marconi, and P. Focardi, "Star formation in dwarf irregular galaxies: sextans B," *The Astronomical Journal*, vol. 102, no. 3, pp. 951–974, 1991.

[32] G. Bertelli, M. Mateo, C. Chiosi, and A. Bressan, "The star formation history of the large magellanic cloud," *The Astrophysical Journal*, vol. 388, no. 2, pp. 400–414, 1992.

[33] L. Greggio, G. Marconi, M. Tosi, and P. Focardi, "Star formation in dwarf irregular galaxies—DDO 210 and NGC 3109," *The Astronomical Journal*, vol. 105, no. 3, pp. 894–932, 1993.

[34] G. Marconi, M. Tosi, L. Greggio, and P. Focardi, "Star formation in dwarf irregular galaxies: NGC 6822," *The Astronomical Journal*, vol. 109, no. 1, pp. 173–199, 1995.

[35] C. Gallart, A. Aparicio, G. Bertelli, and C. Chiosi, "The Local Group dwarf irregular galaxy NGC 6822. II. The old and intermediate-age star formation history," *The Astronomical Journal*, vol. 112, no. 5, pp. 1950–1968, 1996.

[36] C. Gallart, A. Aparicio, G. Bertelli, and C. Chiosi, "The local group dwarf irregular galaxy NGC 6822. III. The recent star formation history," *The Astronomical Journal*, vol. 112, no. 6, pp. 2596–2606, 1996.

[37] A. Aparicio, C. Gallart, and G. Bertelli, "The star formation history of the pegasus dwarf irregular galaxy," *The Astronomical Journal*, vol. 114, no. 2, pp. 669–679, 1997.

[38] E. Tolstoy and A. Saha, "The interpretation of color-magnitude diagrams through numerical simulation and bayesian inference," *The Astrophysical Journal*, vol. 462, no. 2, part 1, pp. 672–683, 1996.

[39] A. Dolphin, "A new method to determine star formation histories of nearby galaxies," *New Astronomy*, vol. 2, no. 5, pp. 397–409, 1997.

[40] C. Gallart, W. L. Freedman, A. Aparicio, G. Bertelli, and C. Chiosi, "The star formation history of the local group dwarf galaxy Leo I," *The Astronomical Journal*, vol. 118, no. 5, pp. 2245–2261, 1999.

[41] A. A. Cole, E. Tolstoy, J. S. Gallagher III, et al., "Stellar populations at the center of IC 1613," *The Astronomical Journal*, vol. 118, no. 4, pp. 1657–1670, 1999.

[42] X. Hernandez, D. Valls-Gabaud, and G. Gilmore, "Deriving star formation histories: inverting Hertzsprung-Russell diagrams through a variational calculus maximum likelihood method," *Monthly Notices of the Royal Astronomical Society*, vol. 304, no. 4, pp. 705–719, 1999.

[43] J. A. Holtzman, J. S. Gallagher III, A. A. Cole, et al., "Observations and implications of the star formation history of the large magellanic cloud," *The Astronomical Journal*, vol. 118, no. 5, pp. 2262–2279, 1999.

[44] J. Harris and D. Zaritsky, "A method for determining the star formation history of a mixed stellar population," *Astrophysical Journal, Supplement Series*, vol. 136, no. 1, pp. 25–40, 2001.

[45] J.-L. Vergely, J. Köppen, D. Egret, and O. Bienaymé, "An inverse method to interpret colour-magnitude diagrams," *Astronomy and Astrophysics*, vol. 390, no. 3, pp. 917–929, 2002.

[46] M. Cignoni, S. Degl'Innocenti, P. G. Prada Moroni, and S. N. Shore, "Recovering the star formation rate in the solar neighborhood," *Astronomy and Astrophysics*, vol. 459, no. 3, pp. 783–796, 2006.

[47] K.-P. Schröder and B. E. J. Pagel, "Galactic archaeology: initial mass function and depletion in the 'thin disc'," *Monthly Notices of the Royal Astronomical Society*, vol. 343, no. 4, pp. 1231–1240, 2003.

[48] X. Hernandez, D. Valls-Gabaud, and G. Gilmore, "The recent star formation history of the Hipparcos solar neighbourhood," *Monthly Notices of the Royal Astronomical Society*, vol. 316, no. 3, pp. 605–612, 2000.

[49] T. Naylor and R. D. Jeffries, "A maximum-likelihood method for fitting colour-magnitude diagrams," *Monthly Notices of the Royal Astronomical Society*, vol. 373, no. 3, pp. 1251–1263, 2006.

[50] E. D. Skillman and C. Gallart, "First results of the coimbra experiment," in *Observed HR Diagrams and Stellar Evolution*, T. Lejeune and J. Fernandes, Eds., vol. 274 of *Astronomical Society of the Pacific Conference Series*, p. 535, 2002.

[51] M. Cignoni, S. Degl'Innocenti, P. G. Prada Moroni, and S. N. Shore, "Recovering the star formation rate in the solar neighborhood," *Astronomy and Astrophysics*, vol. 459, no. 3, pp. 783–796, 2006.

[52] A. E. Dolphin, "Numerical methods of star formation history measurement and applications to seven dwarf spheroidals," *Monthly Notices of the Royal Astronomical Society*, vol. 332, no. 1, pp. 91–108, 2002.

[53] A. Aparicio and S. L. Hidalgo, "IAC-pop: finding the star formation history of resolved galaxies," *The Astronomical Journal*, vol. 138, no. 2, pp. 558–567, 2009.

[54] C. Gallart, M. Zoccali, and A. Aparicio, "The adequacy of stellar evolution models for the interpretation of the color-magnitude diagrams of resolved stellar populations," *Annual Review of Astronomy and Astrophysics*, vol. 43, pp. 387–434, 2005.

[55] L. O. Kerber, L. Girardi, S. Rubele, and M.-R. Cioni, "Recovery of the star formation history of the LMC from the VISTA survey of the Magellanic system," *Astronomy and Astrophysics*, vol. 499, no. 3, pp. 697–710, 2009.

[56] A. Aparicio, C. Gallart, and G. Bertelli, "The stellar content and the star formation history of the local group dwarf galaxy LGS 3," *The Astronomical Journal*, vol. 114, no. 2, pp. 680–693, 1997.

[57] J. Harris and D. Zaritsky, "The star formation history of the small magellanic cloud," *The Astronomical Journal*, vol. 127, no. 3 1779, pp. 1531–1544, 2004.

[58] E. E. Salpeter, "The luminosity function and stellar evolution," *The Astrophysical Journal*, vol. 121, p. 161, 1955.

[59] B. M. Tinsley, "Evolution of the stars and gas in galaxies," *Fundamentals of Cosmic Physics*, vol. 5, pp. 287–388, 1980.

[60] J. Scalo, "The IMF revisited: a case for variations," in *The Stellar Initial Mass Function (38th Herstmonceux Conference)*, G. Gilmore and D. Howell, Eds., vol. 142 of *Astronomical Society of the Pacific Conference Series*, p. 201, 1998.

[61] J. Hurley and C. A. Tout, "The binary second sequence in cluster colour-magnitude diagrams," *Monthly Notices of the Royal Astronomical Society*, vol. 300, no. 4, pp. 977–980, 1998.

[62] K. A. G. Olsen, "Star formation histories from hubble space telescope color-magnitude diagrams of six fields of the large magellanic cloud," *The Astronomical Journal*, vol. 117, no. 5, pp. 2244–2267, 1999.

[63] S. Stanimirović, L. Staveley-Smith, and P. A. Jones, "A new look at the kinematics of neutral hydrogen in the small magellanic cloud," *Astrophysical Journal*, vol. 604, pp. 176–186, 2004.

[64] E. D. Skillman, E. Tolstoy, A. A. Cole, et al., "Deep hubble space telescope imaging of IC 1613. II. The star formation history," *Astrophysical Journal*, vol. 596, pp. 253–272, 2003.

[65] A. A. Cole, E. D. Skillman, E. Tolstoy, et al., "Leo A: a late-blooming survivor of the epoch of reionization in the local group," *The Astrophysical Journal*, vol. 659, no. 1, part 2, pp. L17–L20, 2007.

[66] E. Tolstoy, "The resolved stellar population of leo A," *The Astrophysical Journal*, vol. 462, no. 2, part 1, pp. 684–704, 1996.

[67] A. E. Dolphin, "The star formation histories of two northern LMC fields," *Monthly Notices of the Royal Astronomical Society*, vol. 313, no. 2, pp. 281–290, 2000.

[68] T. A. Smecker-Hane, A. A. Cole, J. S. Gallagher III, and P. B. Stetson, "The star formation history of the large magellanic cloud," *The Astrophysical Journal*, vol. 566, no. 1, part 1, pp. 239–244, 2002.

[69] S. C. Javiel, B. X. Santiago, and L. O. Kerber, "Constraints on the star formation history of the large magellanic cloud," *Astronomy and Astrophysics*, vol. 431, no. 1, pp. 73–85, 2005.

[70] C. Gallart, P. B. Stetson, I. P. Meschin, F. Pont, and E. Hardy, "Outside-in disk evolution in the large magellanic cloud," *The Astrophysical Journal*, vol. 682, no. 2, part 2, pp. L89–L92, 2008.

[71] A. E. Dolphin, A. R. Walker, P. W. Hodge, et al., "Old stellar populations of the small magellanic cloud," *The Astrophysical Journal*, vol. 562, no. 1 ,part 1, pp. 303–313, 2001.

[72] N. E. D. Noël, C. Gallart, E. Costa, and R. A. Mèndez, "Old main-sequence turnoff photometry in the small magellanic cloud. I. Constraints on the star formation history in different fields," *The Astronomical Journal*, vol. 133, no. 5, pp. 2037–2052, 2007.

[73] S. L. Hidalgo, A. Aparicio, and C. Gallart, "Recovering the ages and metallicities of stars of a complex stellar population system," in *The Ages of Stars*, E. E. Mamajek, D. R. Soderblom, and R. F. G. Wyse, Eds., vol. 258 of *International Astronomical Union Symposium*, pp. 245–252, June 2009.

[74] R. C. Dohm-Palmer, E. D. Skillman, J. Gallagher, et al., "The recent star formation history of GR 8 from hubble space telescope photometry of the resolved stars," *The Astronomical Journal*, vol. 116, no. 3, pp. 1227–1243, 1998.

[75] R. C. Dohm-Palmer, E. D. Skillman, M. Mateo, et al., "Deep hubble space telescope imaging of Sextans A. I. The spatially resolved recent star formation history," *The Astronomical Journal*, vol. 123, no. 2, pp. 813–831, 2002.

[76] P. E. Seiden, L. S. Schulman, and H. Gerola, "Stochastic star formation and the evolution of galaxies," *The Astrophysical Journal*, vol. 232, pp. 702–706, 1979.

[77] L. M. Young, E. D. Skillman, D. R. Weisz, and A. E. Dolphin, "The aptly named phoenix dwarf galaxy," *The Astrophysical Journal*, vol. 659, no. 1, part 1, pp. 331–338, 2007.

[78] T. A. Smecker-Hane, P. B. Stetson, J. E. Hesser, and D. A. Vandenberg, "Episodic star formation in the carina dSph galaxy," in *From Stars to Galaxies: The Impact of Stellar Physics on Galaxy Evolution*, C. Leitherer, U. Fritze-von-Alvensleben, and J. Huchra, Eds., vol. 98 of *Astronomical Society of the Pacific Conference Series*, pp. 328–332, 1996.

[79] D. Hurley-Keller, M. Mateo, and J. Nemec, "The star formation history of the Carina dwarf galaxy," *The Astronomical Journal*, vol. 115, no. 5, pp. 1840–1855, 1998.

[80] X. Hernandez, G. Gilmore, and D. Valls-Gabaud, "Non-parametric star formation histories for four dwarf spheroidal galaxies of the local group," *Monthly Notices of the Royal Astronomical Society*, vol. 317, no. 4, pp. 831–842, 2000.

[81] A. E. Dolphin, D. R. Weisz, E. D. Skillman, and J. A. Holtzman, "Star formation histories of local group dwarf galaxies," *Astrophysics and Space Science*, vol. 284, no. 2, pp. 589–594, 2003.

[82] C. Gallart and The Lcid Team, "The ACS LCID project: overview and first results," in *Proceedings of the International Astronomical Union*, A. Vazdekis and R. F. Peletier, Eds., vol. 241 of *International Astronomical Union Symposium*, pp. 290–294, August 2007.

[83] M. Tosi, "Star formation histories of resolved galaxies," in *Proceedings of the International Astronomical Union*, E. E. Mamajek, D. R. Soderblom, and R. F. G. Wyse, Eds., vol. 258 of *International Astronomical Union Symposium*, pp. 61–72, June 2009.

[84] E. V. Held, I. Saviane, Y. Momany, and G. Carraro, "The elusive old population of the dwarf spheroidal galaxy Leo I," *The Astrophysical Journal*, vol. 530, no. 2, part 2, pp. L85–L88, 2000.

[85] L. Baldacci, L. Rizzi, G. Clementini, and E. V. Held, "Variable stars in the dwarf irregular galaxy NGC 6822: thephotometric catalogue," *Astronomy & Astrophysics*, vol. 431, pp. 1189–1201, 2005.

[86] Y. Momany, E. V. Held, I. Saviane, et al., "HST/ACS observations of the old and metal-poor Sagittarius dwarf irregular galaxy," *Astronomy and Astrophysics*, vol. 439, no. 1, pp. 111–127, 2005.

[87] J. T. A. de Jong, J. Harris, M. G. Coleman, et al., "The structural properties and star formation history of Leo T from deep LBT photometry," *The Astrophysical Journal*, vol. 680, no. 2, pp. 1112–1119, 2008.

[88] V. Belokurov, M. G. Walker, N. W. Evans, et al., "Leo V: a companion of a companion of the milky way galaxy?" *The Astrophysical Journal*, vol. 686, pp. L83–L86, 2008.

[89] A. Aloisi, G. Clementini, M. Tosi, et al., "I Zw 18 revisited with HST ACS and Cepheids: new distance and age," *The Astrophysical Journal*, vol. 667, no. 2, part 2, pp. L151–L154, 2007.

[90] G. Bertelli, A. Bressan, C. Chiosi, F. Fagotto, and E. Nasi, "Theoretical isochrones from models with new radiative opacities," *Astronomy & Astrophysics*, vol. 106, pp. 275–302, 1994.

[91] M. Tosi, E. Sabbi, M. Bellazzini, et al., "The resolved stellar populations in NGC 1705," *The Astronomical Journal*, vol. 122, no. 3, pp. 1271–1288, 2001.

[92] A. Aloisi, M. Tosi, and L. Greggio, "The star formation history of I Zw 18," *The Astronomical Journal*, vol. 118, no. 1, pp. 302–322, 1999.

[93] A. Aloisi, R. P. van der Marel, J. Mack, C. Leitherer, M. Sirianni, and M. Tosi, "Do young galaxies exist in the local universe? red giant branch detection in the metal-poor dwarf galaxy SBS 1415+437," *The Astrophysical Journal*, vol. 631, pp. L45–L48, 2005.

[94] R. E. Schulte-Ladbeck, U. Hopp, L. Greggio, and M. M. Crone, "A near-infrared stellar census of the blue compact dwarf galaxy VII Zw 403," *The Astronomical Journal*, vol. 118, no. 6, pp. 2705–2722, 1999.

[95] D. R. Weisz, E. D. Skillman, J. M. Cannon, et al., "The recent star formation histories of M81 group dwarf irregular galaxies," *The Astrophysical Journal*, vol. 689, no. 1, pp. 160–183, 2008.

[96] A. J. Grocholski, A. Aloisi, R. P. van der Marel, et al., "A new hubble space telescope distance to NGC 1569: starburst properties and IC 342 group membership," *The Astrophysical Journal*, vol. 686, no. 2, part 2, pp. L79–L82, 2008.

[97] L. Gregoio, M. Tosi, et al., "The resolved stellar population of the poststarburst galaxy NGC 1569," *The Astrophysical Journal*, vol. 504, no. 2, part 1, pp. 725–742, 1998.

[98] L. Angeretti, M. Tosi, L. Greggio, E. Sabbi, A. Aloisi, and C. Leitherer, "The complex star formation history of NGC 1569," *The Astronomical Journal*, vol. 129, no. 5, pp. 2203–2216, 2005.

[99] F. Annibali, L. Greggio, M. Tosi, A. Aloisi, and C. Leitherer, "The star formation history of NGC 1705: a poststarburst galaxy on the verge of activity," *The Astronomical Journal*, vol. 126, pp. 2752–2773, 2003.

[100] F. Annibali, M. Tosi, M. Monelli, et al., "Young stellar populations and star clusters in NGC 1705," *The Astronomical Journal*, vol. 138, no. 1, pp. 169–183, 2009.

[101] R. E. Schulte-Ladbeck, U. Hopp, L. Greggio, M. M. Crone, and I. O. Drozdovsky, "A near-infrared stellar census of blue compact dwarf galaxies: the Wolf-Rayet galaxy I Zw 36," *The Astronomical Journal*, vol. 121, no. 6, pp. 3007–3025, 2001.

[102] R. E. Schulte-Ladbeck, U. Hopp, L. Greggio, and M. M. Crone, "A near-infrared stellar census of blue compact dwarf galaxies: nicmos detection of red giant stars in the Wolf-Rayet galaxy Markarian 178," *Astronomical Journal*, vol. 120, no. 4, pp. 1713–1730, 2000.

[103] A. Vallenari, L. Schmidtobreick, and D. J. Bomans, "The star formation history of the LSB galaxy UGC 5889," *Astronomy and Astrophysics*, vol. 435, no. 3, pp. 821–829, 2005.

[104] A. Vallenari and D. J. Bomans, "Star formation history of the post starburst galaxy NGC 1569," *Astronomy and Astrophysics*, vol. 313, no. 3, pp. 713–722, 1996.

[105] R. Lynds, E. Tolstoy, E. J. O'Neil Jr., and D. A. Hunter, "Star formation in and evolution of the blue compact dwarf galaxy UGC 6456 determined from Hubble space telescope images," *The Astronomical Journal*, vol. 116, no. 1, pp. 146–162, 1998.

[106] A. E. Dolphin, L. Makarova, I. D. Karachentsev, et al., "The stellar content and distance of UGC 4483," *Monthly Notices of the Royal Astronomical Society*, vol. 324, no. 1, pp. 249–256, 2001.

[107] M. M. Crone, R. E. Schulte-Ladbeck, L. Greggio, and U. Hopp, "The star formation history of the blue compact dwarf galaxy UGCA 290," *The Astrophysical Journal*, vol. 567, no. 1 ,part 1, pp. 258–276, 2002.

[108] K. B. W. McQuinn, E. D. Skillman, J. M. Cannon, et al., "The true durations of starbursts: HST observations of three nearby dwarf starburst galaxies," *The Astrophysical Journal*, vol. 695, no. 1, pp. 561–573, 2009.

[109] B. F. Williams, J. J. Dalcanton, A. C. Seth, et al., "The acs nearby galaxy survey treasury. I. the star formation history of the M81 outer disk," *The Astronomical Journal*, vol. 137, no. 1, pp. 419–430, 2009.

[110] D. A. Hunter and B. G. Elmegreen, "Star formation properties of a large sample of irregular galaxies," *The Astronomical Journal*, vol. 128, no. 5, pp. 2170–2205, 2004.

[111] K. A. Venn, M. Irwin, M. D. Shetrone, C. A. Tout, V. Hill, and E. Tolstoy, "Stellar chemical signatures and hierarchical galaxy formation," *The Astronomical Journal*, vol. 128, no. 3, pp. 1177–1195, 2004.

[112] A. Helmi, M. J. Irwin, E. Tolstoy, et al., "A new view of the dwarf spheroidal satellites of the milky way from VLT FLAMES: where are the very metal-poor stars?" *The Astrophysical Journal*, vol. 651, pp. L121–L124, 2006.

[113] T. Schoerck, N. Christlieb, J. G. Cohen, et al., "The stellar content of the Hamburg/ESO survey. V. The metallicity distribution function of the Galactic halo," http://arxiv.org/abs/0809.1172.

[114] D. Carollo, T. C. Beers, Y. S. Lee, et al., "Two stellar components in the halo of the Milky Way," *Nature*, vol. 450, no. 7172, pp. 1020–1025, 2007.

[115] R. G. Gratton, E. Carretta, S. Desidera, S. Lucatello, P. Mazzei, and M. Barbieri, "Abundances for metal-poor stars with accurate parallaxes. II. alpha -elements in the halo," *Astronomy & Astrophysics*, vol. 406, pp. 131–140, 2003.

[116] I. U. Roederer, "Chemical inhomogeneities in the milky way stellar halo," *The Astronomical Journal*, vol. 137, no. 1, pp. 272–295, 2009.

[117] E. N. Kirby, J. D. Simon, M. Geha, P. Guhathakurta, and A. Frebel, "Uncovering extremely metal-poor stars in the Milky way's ultrafaint dwarf spheroidal satellite galaxies," *The Astrophysical Journal*, vol. 685, no. 1, part 2, pp. L43–L46, 2008.

[118] A. Koch, A. McWilliam, E. K. Grebel, D. B. Zucker, and V. Belokurov, "The highly unusual chemical composition of the hercules dwarf spheroidal galaxy," *The Astrophysical Journal*, vol. 687, no. 1, part 2, pp. L13–L16, 2008.

[119] A. Frebel, J. D. Simon, M. Geha, and B. Willman, "High-resolution spectroscopy of extremely metal-poor stars in the least evolved galaxies: ursa major II and coma berenices," http://arxiv.org/abs/0902.2395.

Hindawi Publishing Corporation
Advances in Astronomy
Volume 2010, Article ID 278434, 21 pages
doi:10.1155/2010/278434

Review Article

Environmental Mechanisms Shaping the Nature of Dwarf Spheroidal Galaxies: The View of Computer Simulations

Lucio Mayer

Institute for Theoretical Physics, University of Zürich, Winterthurerstrasse 190, 8057 Zürich, Switzerland

Correspondence should be addressed to Lucio Mayer, lmayer@physik.unizh.ch

Received 14 June 2009; Revised 17 September 2009; Accepted 1 October 2009

Academic Editor: Andrey V. Kravtsov

We review numerical works carried out over the last decade on the role of environmental mechanisms in shaping nature of the faintest galaxies known, dwarf spheroidals (dSphs). The combination of tidally induced morphological transformation, termed tidal stirring, with mass loss due to tidal and ram-pressure stripping aided by heating due to the cosmic ionizing background can turn late-type dwarfs resembling present-day dIrrs into classic dSphs. The time of infall into the primary halo is shown to be a key parameter. Dwarfs accreting at $z > 1$, when the cosmic ultraviolet ionizing flux was much higher than today, and was thus able to keep the gas in the dwarfs warm and diffuse, were rapidly stripped of their baryons via ram pressure and tidal forces, producing very dark-matter-dominated objects with truncated star-formation histories, such as the Draco dSph. The low star-formation efficiency expected in such low-metallicity objects prior to their infall was crucial for keeping their disks gas dominated until stripping took over. *Therefore gas stripping along with inefficient star-formation provides a new feedback mechanism, alternative to photoevaporation or supernovae feedback, playing a crucial role in dwarf galaxy formation and evolution*. We also discuss how the ultra-faint dSphs belong to a different population of lower-mass dwarf satellites that were mostly shaped by reionization rather than by environmental mechanisms ("reionization fossils"). Finally, we scrutinize the various caveats in the current understanding of environmental effects as well as other recent ideas on the origin of Local Group dSphs.

1. Introduction

Dwarf spheroidals (dSphs) in the Local Group are the faintest galaxies known. Including the ultrafaint dwarf spheroidals discovered in the last few years, they span luminosities in the range $-3 < M_B < -14$. They are gas poor and have pressure supported stellar components [1]. Among them, some stopped forming stars about 10 Gyr ago and others have extended star-formation histories [2–4]. They are typically clustered around the largest galaxy in a group, although a few of them are found also at significantly larger distances from the primary galaxy [1]. These properties of dSphs, while best studied and known in the Local Group due to its proximity, are also typical of this class of galaxies in nearby groups and clusters. Chiboucas, Karachentsev, and Tully [5] have recently uncovered a population of dSphs in the M81 group having a range of luminosities comparable to the LG dwarfs and which share with the latter the same scaling relations between fundamental structural properties, such as the relation between luminosity and effective radius. Recent studies of early-type dwarfs in clusters [6] show that there is overlap in the structural properties between the faint spheroidals in clusters and the classic dSphs in the LG, as shown by the size-luminosity and the surface brightness-luminosity relations. Strong similarities between dSphs in the LG and in clusters are also found by Penny et al. [7] in their study of the Perseus cluster. Hence, LG dSphs can be considered a representative laboratory for the study of dSphs in the Universe. Mass loss from supernovae winds [8], environmental mechanisms such as tidal and ram pressure strippings [9, 10] and suppression, of gas accretion and/or photoevaporation during the reionization epoch [11, 12] have all been invoked to explain their origin and present-day properties. In this paper we review the current status of theoretical models attempting to explain dwarf spheroidals as the end product of environmentally induced morphological transformations from larger, gas-rich disky galaxies [13, 14]. The transformation scenario is suggested by the fact that

gas-rich, disky dwarf irregular galaxies (dIrrs) and dSphs have similar stellar density profiles, close to exponential laws [10], and obey the morphology-density relation whereby dIrrs are found in the outskirts of groups while dSphs are mainly clustered around the main galaxy [1, 15]. In hierarchical structure formation, subhalos nearer to the center of a virialized group halo or galaxy-sized halo were accreted earlier [16]; they were once beyond the edge of the primary halo removed from its tidal influence. We discuss how the combination of tidal effects, ram pressure stripping and the cosmic ultraviolet background radiation at high redshift may provide an explanation to both the similarities and differences among the many known Local Group dwarf spheroidal galaxies. We place our analysis in the context of the current paradigm for structure formation, the ΛCDM model. In this review we will always distinguish between *classic* dSphs [1], those that were known even before the advent of the SDSS deep photometric survey and have luminosities $M_B < -7$, and the *ultrafaint* dwarfs discovered by the SDSS, whose luminosities reach as low as $M_B \sim -3$ (e.g., [17]). The classic dwarfs include Draco, Ursa Minor, Sculptor, Sextans, Leo I and Leo II, Carina, Sagittarius, Cetus, and Tucana among the companions of the Milky Way, and the many "And" satellites of M31. Based on the current measures of their internal stellar velocity dispersions and on theoretical predictions on tidal mass loss of subhalos, we will argue that classic dwarf spheroidals were assembled in fairly massive halos, with masses in the range 10^8–$10^{10} M_\odot$. For these dwarfs, reionization played some role in depleting their baryonic content enhancing the effect of gas removal mechanisms such as tidal stripping and tidal stirring as well as ram pressure stripping. Such mechanisms were the major drivers of their evolution. On the contrary, the low halo masses of ultrafaint dwarfs make them likely candidates for reionization fossils. The theoretical models that we present here are based on the results of N-Body+hydrodynamical simulations of the detailed interaction of individual dwarf galaxies with a primary host, as well as of high-resolution cosmological simulations of Milky-Way-sized galaxies.In the interaction simulations, the model galaxies and the choice of the orbits are consistent with the predictions of ΛCDM models [18–20, hereafter MA06].

2. Current and Past Masses of Dwarf Spheroidals: Why Tides Are Important

Knowing the present and past masses of dSphs is crucial in order to compute the effects of both environmental and internal mechanisms that might affect their evolution. Moreover, determining the mass of dSphs, or, equivalently, their circular velocity, plays a crucial role in the context of the missing satellites problem [21, 22]. Here we will concentrate on the effects that tides have on the evolution of the mass and circular velocity of subhalos of Milky-Way-sized halos, and we will discuss how this folds in with the interpretation of the mass and circular velocity measured for observed dwarf spheroidals.

In cold dark matter models, subhalos are accreted on highly eccentric orbits, with a mean apocenter-to-pericenter ratio of 5-6 [16, 23–25]. Since the orbits are eccentric, subhalos feel a time-dependent tidal force whose intensity is strongest close to pericenter of their orbit. The system undergoes an increase of internal kinetic energy as a result of the tidal forcing, which modifies the energy and mass profile of the subhalo, eventually unbinding some of its stars or dark matter, namely producing tidal stripping. The system will then attempt to reach a new virial equilibrium with a lower gravitational binding energy, which in turn can make it more susceptible to the effect of subsequent tidal shocks as its internal orbital/dynamical time increases (see Binney & Tremaine 1987). If a new equilibrium cannot be achieved, the system will continue to expand, lower its gravitational binding energy, and lose mass, until it is eventually completely disrupted. At low eccentricities, the heating is reduced significantly, until it becomes completely absent for a strictly circular orbit [26].

Tidal heating in an extended mass distribution is most effective when the internal dynamical time of the satellite is larger or at least commensurate with the characteristic timescale associated with the galaxy's orbit [26–28]. In this case it can be described using an extension of the impulsive approximation valid for a generic elliptical orbit of the satellite [26], while the original impulsive approximation was derived for a pointlike perturber and a target (the satellite) moving on a straight-line path (Binney & Tremaine 1987). Following Gnedin et al. [26], the expression for the heating term per unit mass for an extended perturber, but approximating the orbit to a straight-line path, is $\langle \Delta E \rangle = (2GM_0/V_{\rm peri}{R_{\rm peri}}^2)(r^2/3)\chi_{\rm st}(R_{\rm peri})$, where G is the gravitational constant, M_0 is the mass of the perturber, $R_{\rm peri}$ and $V_{\rm peri}$ are, respectively, the pericenter distance and pericenter velocity, r is the distance of a member star from the center of the satellite, and $\chi_{\rm st}$ is function that accounts for the form of the mass distribution of the perturber (it would be unity for a point mass). A more complex expression, but with similar scaling on the relevant variables, can be obtained for elliptical orbits. If, instead, the reverse condition applies to the two timescales, the system can readjust quickly to the perturbation and remain close to its original equilibrium configuration. This second situation can be described analytically by introducing the socalled adiabatic corrections. These are functions that reduce the mean relative increase of internal energy $\langle \Delta E \rangle / E$ derived via the impulsive approximation, their value being proportional to the internal orbital frequency of the system. Based on the same formalism, it is easy to see that the innermost region of any system, that has the highest density and thus the shortest dynamical time/orbital frequency, is also the one that responds more adiabatically to the tidal perturbation. The instantaneous orbital timescale, $t_{\rm orb} = 2\pi R_{\rm orb}/V_{\rm orb}$, is shortest at pericenter of the orbit, that is, when $R_{\rm orb} = R_{\rm peri}$ and $V_{\rm orb} = V_{\rm peri}$, which naturally implies that the effect of the tidal perturbation will be stronger there. Since the instantaneous orbital timescale, and thus the effect of the tidal perturbation, varies the most when the galaxy approaches or leaves pericenter, this is where the tidal force

varies more strongly (recall that the tidal force is relatively short range, being proportional to r^{-3}, where r is the distance from the center of the perturbing potential), hence the term "tidal shock". If the orbit of the dwarf is circular, there is no tidal shock.

Even before suffering the first tidal shock, a subhalo falling into the potential of the primary halo for the first time would lose mass located at a radius r larger than its instantaneous tidal radius r_t (the tidal radius of the subhalo decreases as it plunges closer to the center of the primary halo). This other stripping mode is often termed "tidal truncation". There are thus two mechanisms of tidal mass loss, tidal truncation, which typically shrinks the subhalo to a radius of order r_t evaluated at the pericenter of its orbit, and tidal shocks [27, 29–31]. For subhalos with masses $< 1/50$ of the mass of the primary halo, as true for most satellites of the Milky Way and M31 except perhaps the Large Magellanic Cloud, dynamical friction has a negligible effect [32], thereby one can assume that their orbits did not change since infall. The growth in mass and size of the primary halo over time also has been shown to have a negligible effect on the orbits of satellites in the case of a smoothly evolving analytical potential [33], although the clumpy and more erratic character of halo accretion and growth observed in cosmological simulations may still have an impact on orbital dynamics that should be investigated. With the assumption of a subhalo orbit constant over time, the tidal field of the primary near the pericenter of orbit is fixed over time. Tidal truncation thus occurs only on the first orbit. On the contrary, tidal shocks lead to continued mass loss on a fixed orbit since each subsequent shock can heat the satellite and alter progressively its internal structure. The process will cease to be effective only when the region heated by the shock is dense enough to respond adiabatically to the external perturbation or when the satellite is completely disrupted by tides. As shown in Figure 1, analytical models using a combination of tidal truncation on the first orbit and repeated tidal shocks describe well the mass loss seen in numerical simulations [27].

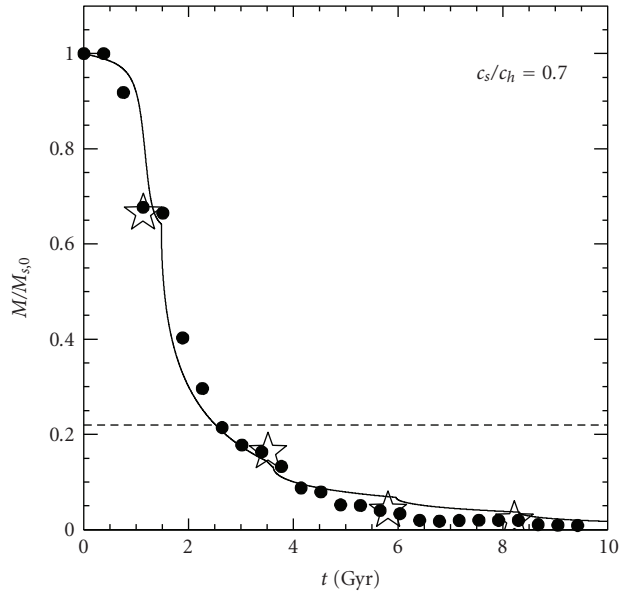

Figure 1: Bound mass in units of the initial mass as a function of time, for a (dark-matter-only) satellite moving on an eccentric orbit within a Milky Way halo potential (see [27] for details). The mass of the satellite is 1/50 of the mass of the primary and both are modeled with NFW halos. The ratio between the concentration parameter of the halo and satellite is $c_s/c_h = 0.7$, where $c_h = 10$ is the concentration of the primary halo. The symbols are the N-Body data and the solid line shows the results of the semianalytical model described in Taffoni et al. [27], that includes both tidal truncation and tidal shocks (see text). Stars identify each pericentre passage. The dashed line is the bound mass that would remain if only tidal truncation is applied.

The amount of tidal mass loss of subhalos in numerical simulations can be remarkable. Kazantzidis et al. [34] have studied the disruption of CDM subhalos within a Milky-Way-sized primary with as many as 10^7 particles. This approach has the advantage of allowing much higher resolution in subhalos relative to a fully cosmological simulation that has to cope with modeling many objects simultaneously. Tidal mass loss was found to be more severe in less concentrated halos (where the concentration parameter is defined as the ratio $c = r_{\rm vir}/r_s$, where $r_{\rm vir}$ is the virial radius of the subhalo and r_s is its scale radius, assuming an initial NFW profile) because they respond more impulsively owing to their lower characteristic density and, correspondingly, longer internal dynamical times. Subhalos typically lose between 70% and 95% of their mass depending on orbits and concentration. Correspondingly, their peak circular velocity, $V_{\rm peak}$, decreases by a factor 2-3 over ten billion years of tidal mass loss. $V_{\rm peak}$ reflects the inner mass distribution of the subhalo, at radii of order r_s, and is commonly used as a measure of the characteristic subhalo mass throughout literature. Its evolution over time is less strongly affected by tidal mass loss compared to the circular velocity of the subhalo at the virial radius. Subhalos initialized with cuspy NFW profiles maintain cuspy profiles with inner slopes close to -1 down to the force resolution, which in Kazantzidis et al. [34] was smaller than the core radius of dSphs ($\sim$100 pc) [35]. This result contradicts previous attempts to place dSphs within cored subhalos with the highest masses and $V_{\rm peak}$ among the satellites' population in an attempt to solve the substructure problem [24, 36, 37].

Kravtsov et al. [24], using fully cosmological dark matter-only simulations, found that $V_{\rm peak}$ of the subhalos drops on average by a factor of 1.5–2 in 10 Gyr of tidal evolution. More recently, Diemand et al. [16] and Madau et al. [38], using the high-resolution Via Lactea simulation of the formation of a Milky-Way-sized halo, found that satellites lose between 30% and 99% of their preinfall mass and that $V_{\rm peak}$ decreases typically by a factor of 2-3. This is consistent with the recent results of Klimentowski et al. [39, 40] on the mass loss of an ultra-high-resolution subhalo with embedded stellar disk (see Figure 3, top panel). Quantitatively similar results are obtained also in individual subhalo-primary interaction simulations in which gas dynamics with cooling and heating are included ([19, 20, 41], see also Section 5). Therefore

there is now strong consensus on how tidal mass loss affects subhalos, both qualitatively and quantitatively.

Peak velocities for the best fit models to observed dSphs are at most a factor of 2 higher than those used in Moore et al. [22] for subhalos, with the consequence that little changes for the missing satellite problem. Measurements of $V_{\rm peak}$, in both simulated subhalos and real satellite galaxies of the Local Group, are extremely important since they are used to express the missing satellite problem, namely, the excess in the number counts of subhalos at a given $V_{\rm peak}$ compared to the counts of observed dSph satellites of the Milky Way and M31 ([21], Moore et al. 1998, [24]). However, in observed dSph satellites, one measures stellar velocity dispersions rather than the $V_{\rm peak}$ of the subhalo. Going from stellar velocity dispersion to $V_{\rm peak}$ requires assumptions when the only information available from simulations is that provided by the dark matter component. Typically (e.g., [34, 42]) one uses the radial moment of the Jeans equations to compute the relation between the circular velocity of the halo of the satellite and the velocity dispersion of the stars, using the simulated subhalo dark matter profile but adopting a simple functional form for a spherically symmetric stellar profile (typically a King model). In this approach it is also necessary to assume a value for the velocity anisotropy of the stellar system. As first shown by Lokas [42], anisotropy can play an important role in determining masses of dSphs from the data. By varying assumptions in the Jeans modeling, including anisotropy, S.Kazantzidis et al. [34] found that the observed stellar velocity dispersions of Draco and Fornax ($\sigma \sim$ 10–14 km/s) can be reproduced in subhalos with $V_{\rm peak} \sim$ 20–30 km/s. Similar results were obtained by Zentner and Bullock [43]. Finally, this range is confirmed also by a more recent analysis that adopts a similar methodology but takes advantage of the cosmological Via Lactea simulation [38, 44]. The latter work finds values closer to 15–20 km/s for some of the other dSphs (e.g., Carina and Sextans). In Madau et al. [38] a match between individual Local Group (LG) dwarf spheroidals and individual subhalos is achieved by considering information on the distances and spatial distribution of dwarfs. In any case, the values of $V_{\rm peak}$ obtained by these recent works for dSphs are within a factor of 2 from those originally used in Klypin et al. [21] and Moore et al. [22] to formulate the substructure problem (note also that these two works did not use exactly the same conversion between circular velocity and stellar velocity dispersion, see Kravtsov in this volume).

Recently, Klimentowski et al. [39, 40] have addressed the question of relating the observed line-of-sight stellar velocity dispersion σ_{1D} of dSphs to the $V_{\rm peak}$ of their halo using simulations that, albeit not fully cosmological, model both the baryonic and dark matter component of a disky dwarf subject to the tidal perturbation from a Milky-Way-sized galaxy (see below). They have found that the simple assumption that $Vc \sim \sqrt{3}\sigma_{1D}$, formally valid for a tracer stellar population in an isotropic dark matter halo and used by Klypin et al. [21], correctly describes the relation between the local stellar dispersion and the local halo circular velocity over a wide range of radii after 10 Gyr of evolution in the Milky Way potential (see Figure 3), as explained in the next section (intermediate phases in which the stellar velocity dispersion tensor is more anisotropic produce temporary deviations from this relation).

In summary, the substantial simulation work carried out in the last few years suggests that stellar velocity dispersions of present-day classic dSphs of the MW and M31 in the range $\sigma \sim$ 7–13 km/s (7–20 km/s if we include the bright dwarf elliptical satellites of M31, NGC187, and NGC205) imply present-day halo $V_{\rm peak}$ in the range 12–22 km/s, and original halo $V_{\rm peak}$, that is, before infall and tidal mass loss, in the range 24–44 km/s [24, 38]. These last numbers are quite important. In fact, with such relatively high values of the original $V_{\rm peak}$, photoevaporation by cosmic ultraviolet background at high redshift and supernovae feedback cannot be what shaped the baryonic content and nature of dwarf spheroidal as often advocated. In fact photoevaporation would remove most of the gas only for $V_{\rm peak} < 20$ km/s [12]. This is consistent with the lack of a clear signature of the reionization epoch in the star-formation histories of dSphs [45, 46]. Second, substantial blowout of the gas of dSphs due to supernovae winds cannot have occurred since it requires $V_{\rm peak} < 10$ km/s (e.g., [47, 48]). A caveat in the last line of reasoning is that in LCDM the progenitors of todays' dSphs formed by hierarchical accretion of smaller sublumps as any other galaxy and such sublumps might have had a mass low enough to be affected by both reionization and feedback. However, the old ages of the bulk of the stars in the majority of dwarf spheroidals mean that their star-formation epoch occurred more than 10 Gyr ago ($z > 2$). While dating of stars is nonaccurate enough to establish how much of the old stellar component was formed before or after reionization, which occurred at $z > 6$, the cosmic UV background was still close to its peak intensity at $z = 2$ according to standard models [49, 2000], and yet star formation was clearly happening. This argues against an important effect of the cosmic UV background arising from reioinization, perhaps owing to self-shielding (see [12]). Note that, conversely, there are examples of low mass LG dIrrs bearing a likely imprint of reionization in their star-formation history (e.g.; Leo A, see [50]).

The same argument does not apply to the ultrafaint dwarf spheroidals discovered in the last few years using deep photometry from the Sloan Digital Sky Survey (SDSS) (e.g., [51, Belokurov et al. 2008, 53]). With a few exceptions, most of the extremely faint dwarfs have very low velocity dispersions in the range 3–8 km/s [52], implying masses much lower than those of classic dSphs. We will discuss them in Section 8.

For the classic dSphs, we advocated that physical processes associated with the environment, such as tidal forces and ram-pressure stripping, were the major players in setting their current properties and shaping their evolution. The remainder of this review will be devoted to summarizing in quite some detail the work done in this direction. In the next two sections, we will discuss how tidal interactions can completely reshape dwarf galaxies, presenting a plausible model for the origin of dwarf spheroidals in which such galaxies started out with a configuration and properties similar to gas-rich dwarf irregulars, and how these tidal

interactions were subsequently transformed. We will also discuss the issue of measuring the masses of dwarf spheroidals from the observed stellar velocity dispersions, highlighting how tidal effects may produce contaminated samples with a fraction of unbound stars projected along the line of sight.

3. Morphological Evolution of Disky Dwarfs into dSphs: Tidal Stirring

Aside from the different gas content, three other facts have to be considered when comparing dSphs and the other known type of dwarfs, namely, gas-rich, similarly faint dwarf irregular galaxies (dIrrs) (see [1] for a review on the subject). First, except for the faintest among them, all dIrrs in the Local Group and nearby groups exhibit substantial rotation while dSphs do not. Second, stellar profiles in the two classes of galaxies are similarly close to exponential. Third, a morphology density relation exists such that dSphs are clustered around the primary galaxies while dIrrs are found at much larger distances from them. Interestingly, Karachentsev [53] finds that the fraction of dSphs over the total number of dwarfs in several nearby groups (including the Local Group) decreases markedly at distances larger than about 250 kpc from the primary galaxies, comparable to the virial radius of halos hosting bright spiral galaxies in ΛCDM models. Clear trends of dwarf galaxy morphology with environment for nearby groups (Centaurus A and Sculptor) are also found by Bouchard et al. [54]. The quantitative correlation found by Karachentsev [53] strongly suggests, although it does not prove, that dSphs are bound satellites of bright spirals. It follows then automatically that the environment provided by the extended halo of such massive hosts must be playing a crucial role in differentiating dIrrs from dSphs. Of course there are outliers like the Local Group dSphs Cetus and Tucana, located at more than 500 kpc from, respectively, M31 and the MW. However, cosmological simulations provide a potential explanation for those few distant dSphs; a few satellite halos on very plunging orbits can have apocenters exceeding the virial radius of the primary [23], or can be on tighter orbits and subsequently be ejected out to much larger distances via three-body interactions (Sales et al. 2009). The outgoing radial velocity of Tucana further supports this possibility [55]. Overall, there are various effects that could make the orbital dynamics of satellites much more complex than in our simulation setup and accomodate such a case (see page 17-18).

Mayer et al. [13, 14], Mayer [19], MA06, Mayer et al. [41], and Klimentowski et al. [39, 57] have shown that repeated tidal shocks at pericenters of their orbits within the halo of a massive spiral can transform infalling disky dwarfs into objects resembling dSphs. The timescale of the transformation is a few orbital times (several Gyr). The mechanism behind the transformation is tidally induced nonaxisymmetric instabilities of stellar disks combined with impulsive tidal heating of the stellar distribution. We recall that the time-dependent tidal field varies on a timescale proportional to the orbital timescale of the galaxy.

The tidal forcing induces a perturbation to the internal energy and velocity distribution of the system, which results into a perturbation of its mass and density distribution as it attempts to acquire a new equilibrium configuration. Through the density perturbation tidal heating can thus excite modes in a self-gravitating system that would otherwise have a negligible amplitude. If the induced velocity and density perturbation are considerable, a strong mode might be seeded and be subsequently amplified by the self-gravity of the system. An example of such induced mode amplification is the triggering of a bar instability, which corresponds to an $m = 2$ mode for the planar density field of the galaxy, of a warp, which corresponds to an $m = 1$ in the vertical density field (i.e., perpendicular to the disk plane), or of a bending or buckling instability, which corresponds to an $m = 2$ mode in the vertical density field [58]. Numerical experiments, starting from the early 90s, have shown that the buckling instability can be triggered by a preceding bar instability. A bar is supported by families of centrophilic stellar orbits, whose collective effect is to increase the radial velocity dispersion along the plane of the galaxy. Raha et al. [58] first showed that above some critical value of the radial velocity anisotropy, a system would become unstable to the buckling instability; the whole disk bends above and below, and, as a result, stars acquire a larger vertical velocity dispersion. The instability saturates when the system has reached a new, nearly isotropic configuration in velocity space. This picture has been confirmed by more recent simulations with much higher resolution and physical complexity [59]. As it reaches a new, nearly isotropic configuration, the system undergoes a transition from a cold disk into a spheroid. This mechanism has indeed been proposed as a possible channel for the formation of bulges starting from cold stellar disks [60].

In simulations of disky dwarfs on eccentric orbits interacting with a Milky-Way-sized halo, the following sequence of events is typically observed. First, tidal shocks induce strong bar instabilities in otherwise stable, light disks resembling those of present-day dIrrs. Second, the bar buckles due to the amplification of vertical bending modes and turns into a spheroidal component in disks with relatively high stellar surface density (Mayer et al.) [13, 14], or else subsequent shocks destroy the centrophilic orbits supporting the bar which then loses its elongation and heats up into a more isotropic diffuse spheroid [39, 41]. An example of the first channel of transformation is shown in Figure 2 (top). The second channel for the transformation is favored in systems with lower mass, lower surface density disks, for these tidal heating is particularly efficient because the dynamical response of the stellar system is impulsive rather than adiabatic. As shown in Mayer et al. [41], the latter conditions likely apply to the progenitors of the faintest classic dwarf spheroidals (dSphs) such as Draco, Sculptor or Leo I, or the And satellites of M31, while the bar-buckling sequence might have been more likely for the progenitors of the brightest dSphs such as Fornax and Sagittarius, and even more so for those of the bright dwarf elliptical satellites (dEs) of M31, such as NGC185 and NGC167 (but not M32 whose unusually high surface density for a dwarf suggests that it is

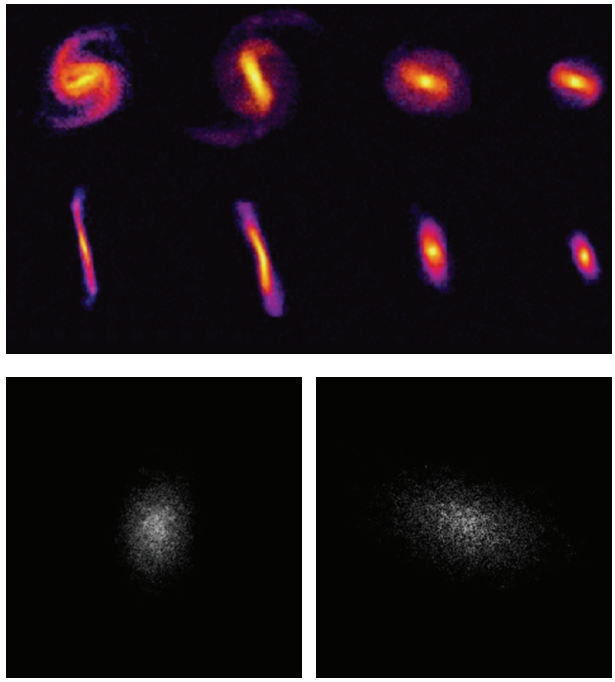

Figure 2: Top: color-coded logarithmic density maps of a tidally stirred dwarf seen face-on (i.e., with the line-of-sight perpendicular to the initial disk orientation, on the top) and edge-on (i.e., with the line-of-sight parallel to the initial disk orientation, on the bottom). The time increases from the left to right; each snapshot is separated by about half an orbital time (the orbital time is ∼2 Gyr in this simulation), starting with the time corresponding to the first pericenter passage, when the bar first appears. Boxes are 10 kpc on a side. The edge-on view shows clearly the buckling of the bar occurring on the second orbit, and the subsequent transformation into a diffuse spheroidal. Bottom: gray-scale surface brightness maps of the remnant of the simulation shown after 10 billion years of evolution (about 5 orbits). Two perpendicular viewing projections are shown. The limiting B band surface brightness shown in the images corresponds to $\mu_B = 32$ mag arcsec^{-2}, and a B band stellar mass-to-light ratio of 5 was adopted for converting surface mass density into surface brightness (see [14] on models for the evolution of the luminosity and stellar mass-to-light ratio in the tidally stirred dwarf). The faint simulated remnant resembles classic dSphs such as Draco or Carina in both apparent shape and luminosity and surface brightness distribution.

the "threshed" core of a low luminosity elliptical–see Bekki 2001. The bar-buckling sequence of instabilities also occurs for the progenitors of bright dwarf spheroidals and dwarf S0s in galaxy clusters, where both tidal stirring and harassment, that is, repeated flybies with the brightest cluster members, are at play [61]. Tidal heating/tidal mass losses remove the disk outside the region that goes bar unstable. Removal of the outer region, which contains most of the angular momentum in the original disk, can be complete or partial, depending on the number and strength of tidal shocks. Within this scenario, the LMC and SMC, and perhaps the two bright dEs of M31 which show fairly elliptical outer isophotes, are in earlier stages of the transformation, but may also be sufficiently massive and dense to limit the tidal damage and never end up into spheroidals [14]. Some of the faint dSphs, that show markedly elongated isophotes, such as Ursa Minor and some of the newly discovered ultrafaint dwarfs (e.g., Bootes; see [62], and Leo V; see [63]), may owe such elongation to a residual bar-like component rather than to tidal deformation.

It is important to stress that tidal stirring operates independently of tidal mass loss of the baryonic component. While systems that undergo substantial tidal mass loss are also effectively transformed, the transformation can occur even when stellar tidal mass loss is marginal (see, for example, the GR8 model presented in Mayer et al. [13, 14]). This implies that the detection of tidal tails in dSphs should not be used as a direct way to test the feasibility of tidal stirring. Instead, the deep structural analysis of dSphs and also of the socalled transition dwarfs, a class with intermediate properties between dSphs and dIrrs [15], offers a much better test of the predictions of tidal stirring for the different stages of the transformation mechanism. In clusters, the discovery of disk-like features and bars in some dwarfs previously classified as dSphs [64] matches very well the expectations of the tidal stirring and harassment models. While in the Milky Way halo the main epoch of interaction between the primary and the satellite may be over, as suggested by the the Sagittarius stream that is the only bright stellar stream present today in the Milky Way halo, the study of other groups with more recent assembly histories may unfold a population of satellites in the process of being transformed.

The remnants left behind by tidal stirring have nearly exponential profiles and very low surface brightness (Figure 2). Tidal features typically lie at very low surface brightness levels, below 32 mag arcsec^{-2} (Figure 2). The brightest among the remnants, those coming from

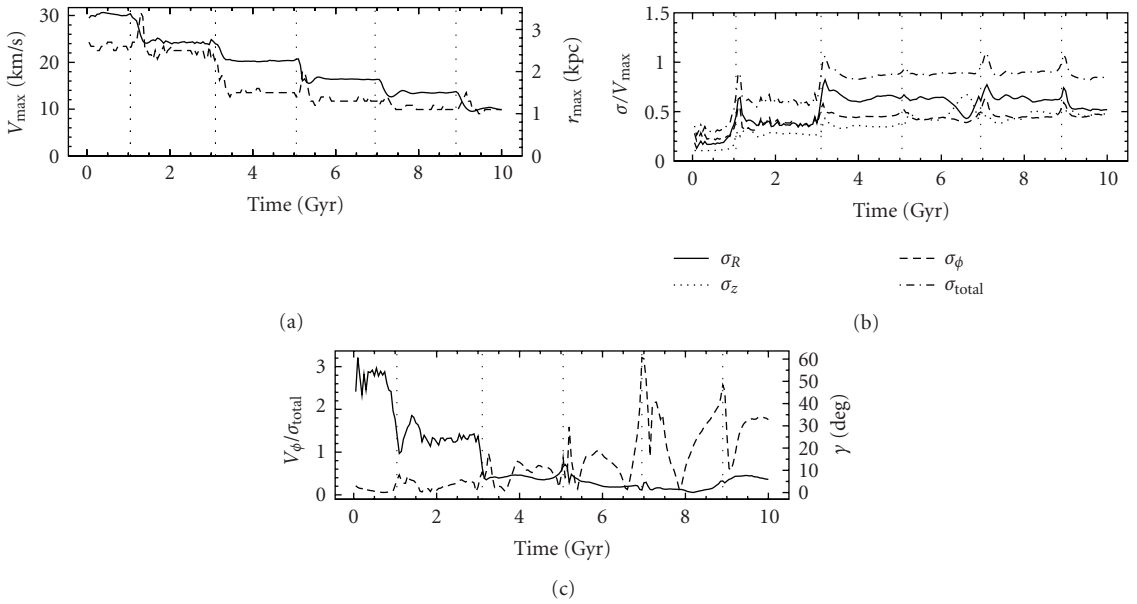

Figure 3: Evolution of structural parameters of a tidally stirred dwarf in a high resolution numerical simulation. The plot shows the results for one of the models studied by Klimentowski et al. [39], whose initial disk was oriented at 90 degrees with respect to the orbital plane (this is a conservative case since other orientations leave almost no residual angular momentum, see text in Section 3). Upper panel: the maximum circular velocity (solid line, left axis) and the radius at which the maximum circular velocity occurs (dashed line, right axis). Middle panel: the velocity dispersion (total 3D, and 1D along three different cylindrcal axes) expressed in units of the maximum circular velocity (indicated as V_{peak} in the text). Lower panel: evolution of the ratio of the mean rotation velocity to the total (3D) velocity dispersion and the angle γ between the total angular momentum vector of the stars and the orbital plane (dashed line, right axis).In all panels vertical dotted lines indicate pericentre passages. Loss of angular momentum due to tidally induced instabilities and simultaneous increase of stellar velocity dispersion owing to tidal heating lead to a low v/σ ratio comparable to that of dSphs. See Klimentowski et al. [39] for details on how internal angular momentum is lost.

progenitors having relatively massive disks ($> 10^8 M_\odot$) and high surface density disks, develop a central steepening of the profile during the bar stage that persists even after buckling, and overall their profile resembles that of the bright dwarf elliptical satellites of M31, like NGC205 [13, 14]. Most importantly, both "tidally heated" and "buckled" remnants have a very low angular momentum, consistent with what is seen in dSphs and dEs, despite being descendants of disk-like systems. The loss of angular momemtum is a by product of the bar instability. The bar sheds angular momentum outwards to the outer stellar disk and dark matter, which are stripped after repeated shocks, thus leaving behind a surviving stellar and dark matter core with very low rotation, having a typical final $v/\sigma < 0.5$. The gradual loss of internal angular momentum and decrease of v/σ can be inspected in Figure 3. Some residual rotation may be present at the end depending on the initial structural properties and orbits of the dwarfs [13, 14]. Klimentowski et al. [39] have also shown that for the same inital disky dwarf model, the initial orientation of the disk angular momentum of the dwarf with respect to the orbit also matters. In orbits with high inclination, for example, polar orbits, $v/\sigma \sim 0.4$, perhaps consistent with what is found in Leo I [65], as opposed to close to zero in coplanar or moderately inclined orbits. How likely is one or the other configuration in CDM? The answer still awaits us since it is likely that inclusion of the disk of the primary may have played a significant role, for example, by dragging satellites towards its orbital plane and thus yielding a preferential bias towards a coplanar configuration [66]. This would explain why most dSphs do not show sign of residual rotation. In Lokas et al. [67], we analyzed the velocity structure of the remnants. In some cases we find radial anisotropy in the velocity ellipsoid. This can be significant in remnants that have some residual rotation and are triaxial due to a residual bar-like structure in the remnant, or can be negligible in those that have been efficiently heated, turning into nearly isotropic spheroids with negligible rotation. In other words, when tidal stirring produces a good match to a dSph, anisotropy in the kinematics is not important.

The transformation mechanism that we have studied requires the dwarf to be on a bound orbit; for the mean apocenter/pericenter ratio found in cosmological simulations, ~5, Mayer et al. [14] determine that an apocenter distance comparable to the distance of Leo I (250 kpc), the farthest dSph satellite of the MW, is a limiting case for producing a dSph from a disky dwarf in less than 10 Gyr. However, this estimate is very conservative and should be revised. In fact,in the meantime we have learned that some satellites enter the primary system in subgroups and thereby might have already felt significant tidal perturbations before entering the primaries [24, 68]. Kravtsov et al. [24] find that, at least in some cases, most of the tidal heating in cosmological subhalos occurs before they enter the primary

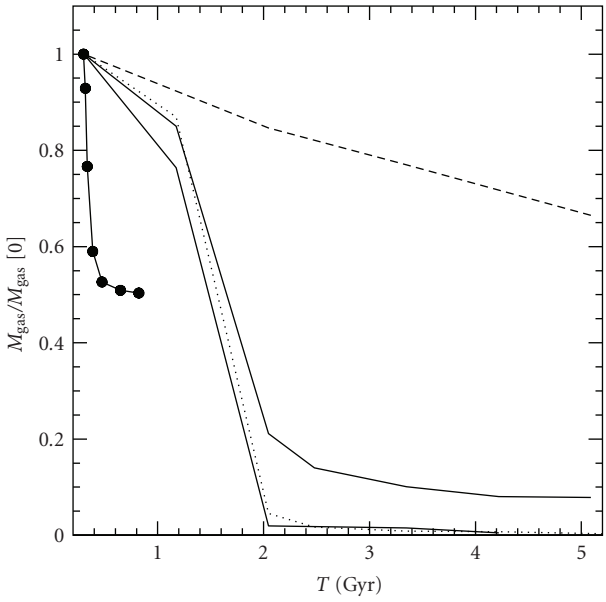

Figure 4: Time evolution of the bound gas mass for a disky dwarf galaxy model(initial $V_{peak} = 42$) km/s within a Milky-Way-sized dark matter halo ($M_{vir} \backsim 10^{12} M_{\odot}$) having a hot gaseous halo about 1% of its total mass (see [20] for details on the modeling). The dwarf's orbit has an apocenter of 150 kpc and a pericenter of 30 kpc. The same model has been run with adiabatic gas conditions (thin solid line), radiative cooling with no heating (thick solid line), and radiative cooling plus heating by the cosmic ionizing UV background (dashed line), assuming that when the simulation is started, the time corresponds to $z = 2$. The long-dashed line shows the results for a run in which the hot gaseous halo of the Milky Way was absent to isolate the effect of tides from that of ram pressure. Stripping from ram pressure only is instead shown by the thick solid with dots; in this run, the same dwarf model was evolved in a "wind tunnel", moving with a speed comparable to the orbital velocity at pericenter in the other runs. In the "wind tunnel" the dwarf moves within a static gas distribution along a straight trajectory withe specified velocity (periodic boundary conditions are used for the gaseous background), but responds only to the ram-pressure force. The latter curve spans less than a Gyr of evolution since ram-pressure stripping saturates quickly without tidal mass loss.

halo. Furthermore, we have assumed that the only thing that could affect the orbit of the dwarf within the primary halo is dynamical friction, and, moreover, that its effect can be neglected for the typical low masses of subhalos. While this would be a reasonable picture for dwarfs orbiting in a spherical, nonevolving primary halo, cold dark matter halos are triaxial and accrete mass via both smooth accretion and mergers. Triaxial halos are populated by families of chaotic orbits whose pericenters can fluctuate over time. Yet, baryonic infall makes the potential of the primary halo very close to spherical [69], which also agrees with current observational limits on the shape of the MW halo [70], thus suggesting that triaxiality should not be an important effect. Instead, dwarfs infalling at very early epochs, when the primary halo is still undergoing substantial growth via merging of relatively massive subgroups, might undergo rapid changes in their orbits as the global potential changes. Another effect, which is seen to take place in simulations, is orbit scattering via the interaction with another satellite, which can not only modify the parameters of the orbit of the satellites but even cause ejections when a three-body interaction takes place [71].

All simulations conducted to study the dwarf-primary interactions neglect the effect of the disk of the primary. The disk of the Milky Way was likely in place already at z =1.5–2, hence during most of the time during which satellites were accreted and evolved within the primary halo. While the tidal effect of the disk is not expected to be important for typical pericenter distances of satellites accreted below $z < 1$, because these should be larger than 20–30 kpc (see [14]), satellites accreting earlier had smaller pericenters that would graze the disk and could even be quickly reduced by the additional dynamical friction provided by the disk itself [72] if satellites accrete more frequently on a prograde rather than retrograde orbit [66, + in prep.]. D'Onghia et al. [73] find that disk shocking, namely, tidal shocks induced by passages through the disk, can affect significantly the evolution of satellites having masses $<10^9 M_{\odot}$ and pericenters < 20 kpc, causing the disruption of a fraction of them and thus playing a role in the missing satellites problem (which normally neglects disk shocking) as well as in determining the radial distribution of satellites inside primary halos.

This "tidal stirring" accounts for most of the similarities and differences between dIrrs and dSphs, including the existence of the morphology-density relation, by postulating progenitors of dSphs with light, low surface brightness disks embedded in massive halos. This, however, does not mean that such progenitors were identical to present-day gas-rich dIrrs. Indeed, since they formed at high z, they likely had assembly histories quite different from present-day dIrrs, and thus their stellar populations and metallicities were different (this is an aspect that will be addressed by new, ongoing simulations that start from a gas-rich dwarf galaxy formed self-consistently in a cosmological simulation). The next step would be to verify the model within a fully cosmological simulation, and thus extend the analysis directly to the implications for the star, formation and metallicity histories of the dwarfs. Unfortunately, to date cosmological simulations with hydrodynamics have not allowed a robust analysis of the structural evolution of satellites due to their limited resolution (typically the force resolution is of order a few hundred parsecs, see Mayer et al. [74] for a review, so the tiniest dSphs like Draco are not resolved at all). Satellites, in addition, are too bright and dense in published cosmological galaxy formation simulations due to numerical loss of angular momentum and overcooling [75]. Searching for evidence of tidal stirring in these simulations is thus quite hard, but it can be done in a qualitative sense for a few well-resolved dwarfs. We selected the brightest satellites ($M_B > -14$) of the large spiral galaxy in the cosmological hydrodynamical simulation of Governato, Mayer et al. [76], as well as similarly bright dwarfs outside the virial radius of the same galaxy. Figure 5 shows their v/σ within the effective radius versus the number of orbits performed within the main system. Clearly v/σ correlates well with the number of orbits as expected within the tidal stirring scenario. We also

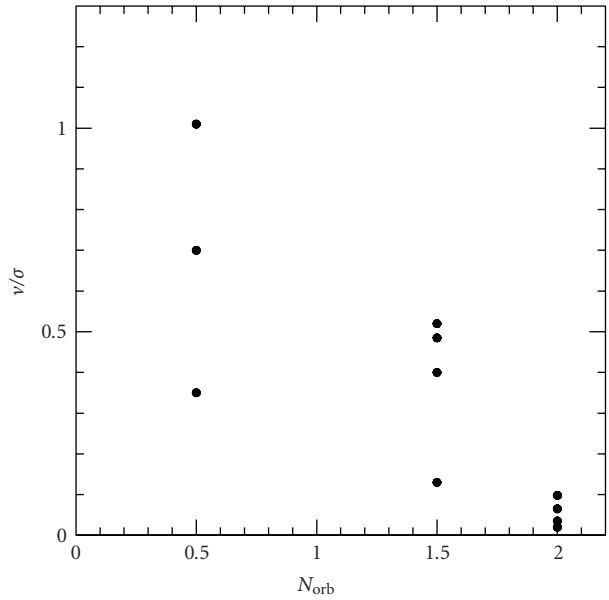

FIGURE 5: v/σ as a function of the number of orbits for the satellites in the cosmological hydrodynamical simulation of Governato, Mayer et al. [56]. v/σ is measured within the half mass radius of the dwarfs at the end of the simulation, namely, after 13 billion years of evolution. The mean number of orbits for each of the three groups of dwarfs appears on the horizontal axis.

found that the shape of the stellar components of the dwarfs goes from more disky to more spheroidal with increasing number of orbits. The absolute values of the v/σ have to be taken with caution because numerical two-body heating (e.g., Mayer [76]) is certainly an issue for these objects (halos have only a few thousand particles at this scale). However the trend is evident. A similar result, more recently, has been obtained in a much higher-resolution cosmological simulation of the formation of a massive early-type galaxy (Feldmann et al., in prep.) as well as in newer, higher-resolution simulations of the formation of a Milky-Way-sized galaxy (Callegari et al., in prep.).

4. Tidal Tails in Disky Dwarfs and Line-of-Sight Stellar Velocity Dispersions

As the dwarf is tidally perturbed and gradually transforms into a dwarf spheroidal, it also loses mass. In Mayer et al. [18] tidal mass loss and the formation of tidal tails in dark-matter-dominated, tidally stirred disky dwarfs was studied using a range of initial models embedded in an NFW halo and a range of cosmologically motivated orbits, that is, spanning and apocenter-to-pericenter ratio of 3 to 10. The main conclusions were that (1) tidal tails projecting along the line of sight could lead to an overestimate of the velocity dispersion (and thus an overestimate of the mass-to-light ratio) by at most a factor of 2 and (2) the most important contribution to the measured mass-to-light ratio is always the intrinsic dark-matter content of the dwarf. The corollary of the second point is that the most dark-matter-dominated dwarfs have the faintest tails, just lying at the detection limit of photometric surveys. However, the role of projections effects, especially how likely tidal tails lie perpendicular to the observer and thus can be more easily detected, was not clarified. Klimentowski et al. [57, 77] and Lokas et al. [65] confirmed, in a much more detailed study, that velocity dispersion profiles in dSphs can be affected by contamination from unbound stars in the tails. While the central velocity dispersion is not changed (the contamination from unbound stars is statistically too weak since most of the stars projected towards the inner core of the dwarfs are indeed bound), the outer velocity dispersion can increase by nearly a factor of 2, with consequences on the measurements of the total mass and mass-to-light ratio of the dwarf. The same authors present a method of interloper removal to clean observed samples from unbound stars contamination. In Klimentowski et al. [78] tidal tails disky dwarfs were revisited. The interesting conclusion is that on typical cosmological orbits (apocenter/pericenter ~5-6), tails point towards the observer for the largest fraction of an orbital revolution of the dwarf within the Milky Way halo, especially where it spends most of the time, namely, near apocenter. This renders the detection of tails extremely difficult and maximizes the enhancement of the line-of-sight velocity dispersion because it implies that unbound stars belonging to the tails would be normally projected along the line-of-sight, contaminating observed samples, although the effect is complicated by variations in the intrinsic line-of-sight velocity dispersions along the different axes of the dwarfs, see [57, 77]. The difficulty in separating the tails from the bound core of the dwarfs due to this biased projection effect may explain why in only a few of the dSphs, for example, Carina [79] and Ursa Minor [80], tails have been tentatively detected. This effect adds to the most important requisite for tidal tail detection, namely, the need of an exceptional photometric technique [81].

5. Gas Stripping; Ram Pressure, Tides, and the Cosmic Ultraviolet Radiation

Mayer et al. [14] showed that tidal stripping alone cannot produce the low gas fractions found in dSphs starting from a gas-rich disky dwarf. Bar instabilities drive gas towards the center, making it tightly bound. Such inner gas distribution is not stripped by tides for the same reason of why an inner stellar core always survives in the tidally stirred dwarfs, namely, because its binding energy is too high and the response to tidal shocks is nearly adiabatic. Gas consumption by star-formation does not solve the problem if one adopts the mean star formation rates inferred for dSphs [2, 4]; too much gas is left even after billions of years [14]. In addition, gas turning into stars during the orbital evolution gives rise to an extended star formation history, a feature that is seen only in a subset of dSphs [3, 15]. Therefore a mechanism that selectively removes the gas while leaving the stars unaffected seems required. Mayer et al. [20] studied the combined effect of ram-pressure and tidal stripping. Ram pressure-stripping occurs when the pressure force exerted

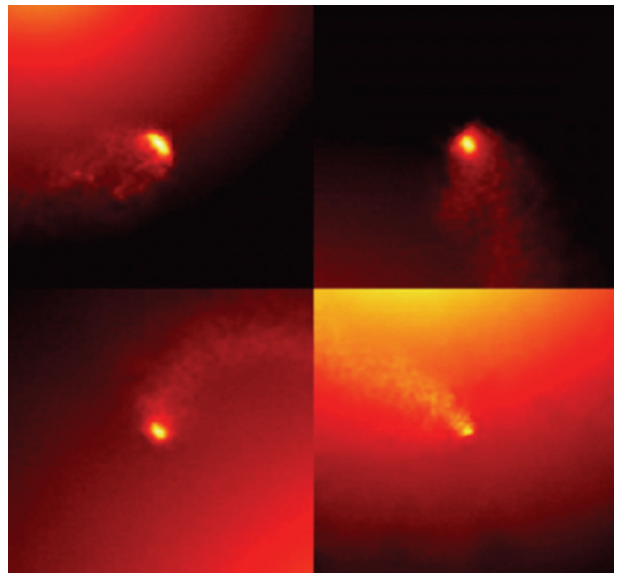

Figure 6: Evolution of the gas-dominated disky dwarf model studied in Mayer et al. [41], which produces a dark-matter-dominated dwarf resembling Draco after 10 Gyr of evolution. This N-Body + SPH simulation employed millions of dark matter, gas, and star particles. It included tidal mass loss due to a live Milky Way halo, ram-pressure stripping in a tenuous gaseous halo, radiative cooling, and a time-varying cosmic ionizing UV background consistent with the Haardt and Madau (2000) model. The snapshots show the color-coded logarithmic density maps (the brighter the color, the higher will be the density, with densities in the range $10^{-32} - 10^{-23}$ g cm^{-3}) for the first 2.5 Gyr of evolution. Boxes are 30 kpc on a side. The dwarf begins falling into the Milky Way halo on a typical eccentric cosmological orbit (apo/per= 5 at the beginning of the simulation, which corresponds to $z = 2$). At the first pericenter passage ($R_{\rm peri} = 30$ kpc) a prominent ram-pressure tail is evident (top left), and once the dwarf comes to first apocenter (top right), it has lost already more than half of its gas. As it begins the second orbit, ram-pressure stripping continues to remove gas (bottom left), until all gas is stripped at second pericenter (bottom right).

by the ambient gaseous medium exceeds the gravitational restoring force felt by the gas inside the dwarf. The ram-pressure is given by $P_{\rm ram} = \rho_{\rm gh} {V_{\rm orb}}^2$, where $\rho_{\rm gh}$ is the density of the ambient halo gas and $V_{\rm orb}$ is the orbital velocity of the galaxy (Gunn & Gott 1972). Assuming a constant ram pressure, there will be a characteristic radius at which the ram pressure force $F_{\rm rp} = P_{\rm ram} S_{\rm gd}$ (where $S_{\rm gd}$ is the surface area of the gas disk) is equal to the gravitational restoring force $F_{\rm gr}(r) = \nabla\phi(r)$, where $\phi(r)$ is the gravitational potential of the galaxy. The gravitational restoring force will indeed vary with radius since in galaxies the potential is a function of radius. Since the gravitational restoring force will increase with decreasing radius in a typical galactic potential (e.g., see Abadi et al. 1999) the gas located at or outside the radius at which $F_{\rm rp} = F_{\rm gr}$ will be stripped.

Mayer et al. [20] constructed two-component models for the Milky Way halo in which a dark matter halo consistent with the results of ΛCDM simulations has an embedded diffuse gaseous component with a temperature of $\sim 10^6$ K and a density of about $\sim 10^{-4}$ atoms/cm^3 at 30 kpc from the center, consistent with the values inferred from OVI absorption measurements and the existence of the Magellanic Stream [82]. Dwarf galaxies are placed on eccentric orbits (apo/peri= 5-6) with pericenters of 30 or 50 kpc. The initial models were gas-rich disky dwarfs ($M_{\rm gas}/M_{stars} \geq 0.4$). It was found that ram pressure increases by a factor up to 10 the amount of stripped gas mass compared to the case in which only tides are considered (Figure 4). Ram pressure strongly depends on the depth of the potential well of the dwarfs. While for dwarfs with $V_{\rm peak} \leq 30$ km/s most of the gas content is easily removed, for more massive dwarfs the end result depends a lot on the orbit and on gas thermodynamics (the effect of thermodynamics is seen in Figure 4, where we compare results for an adiabatic run, a run with radiative cooling, and one with both radiative cooling and the cosmic ionizing background).

For a galaxy moving on a noncircular orbit, the ram-pressure is not constant but varies with time as both the galaxy's orbital velocity and the density of the ambient medium change along its trajectory within the primary. The pericenter distance sets the maximum strength of the ram-pressure force since $P_{\rm ram} = \rho_{\rm gh} {V_{\rm orb}}^2$, and both $\rho_{\rm gh}$ and $V_{\rm orb}$ are maximum at pericenter. Moreover, there is another important time-dependent effect for galaxies on eccentric orbits. Repeated tidal shocks lower progressively the depth of the potential well of the dwarf at each pericenter passage, reducing the gravitational restoring force, and thus allowing gas removal towards increasingly smaller radii as time advances (this would be the case even if the ram-pressure wind was constant). This explains why ram pressure stripping can continue over several billion years (Figure 4) rather than saturating after the first pericenter passage. However, when gas can cool down radiatively but cannot be heated, the stripping process saturates after two orbits; this is because the gas torqued by the bar flows towards the central region of the dwarf, increasing its central density and rendering the response of the potential to tidal shocks more adiabatic (see Section 7).

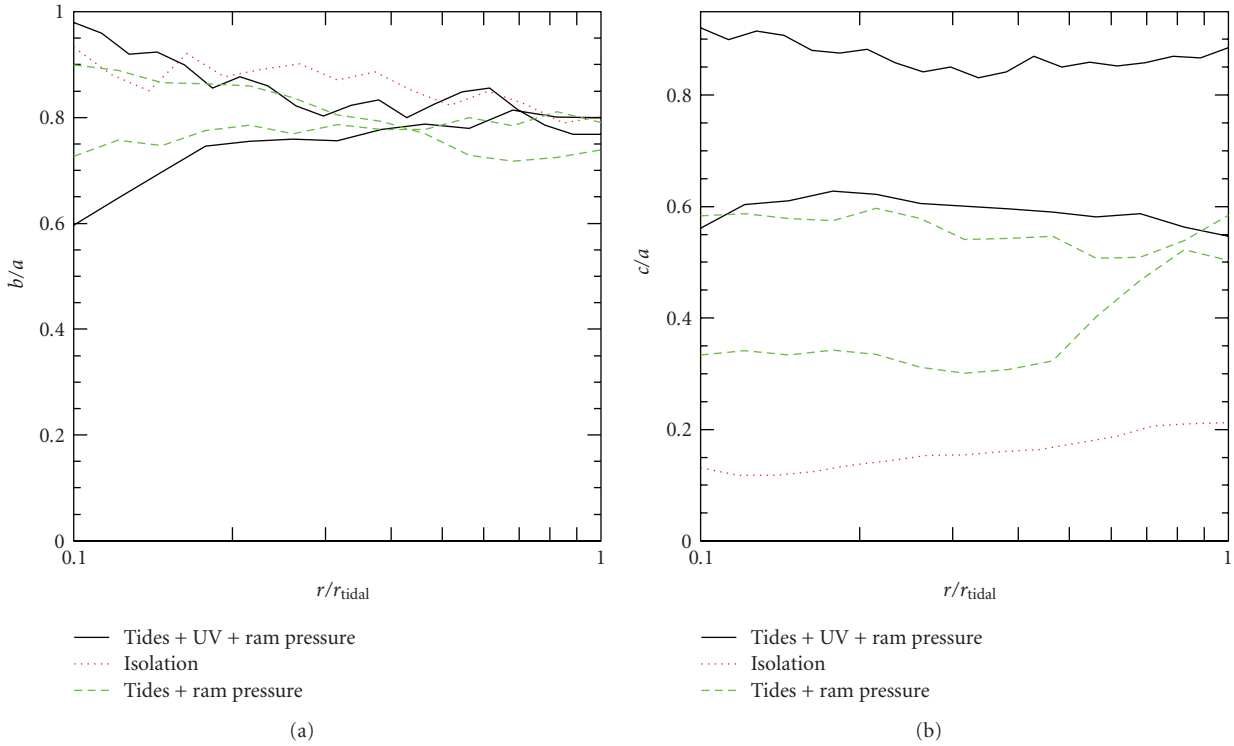

Figure 7: Shape evolution of the stellar component. The upper panel shows the intermediate-to-major axis ratio, b/a, and the bottom panel presents the minor-to-major axis ratio, c/a. Solid lines correspond to the self-consistent simulation in which tides, ram pressure stripping, and UV background were included throughout the orbital evolution of the dwarf. Dotted lines correspond to the case where the dwarf galaxy was extracted from the simulation just after the gas was removed and evolved in isolation. Dashed lines show results of a test in which approximately 30% of the initial gas mass remains in the galaxy because the absence of the UV background reduces significantly the effectiveness of ram pressure stripping. Thick and thin lines correspond to 10 and 5 Gyr of orbital evolution, respectively (for the extracted dwarf we only show the result after 10 Gyr). The shape of the stellar component changes gradually over time and the presence of UV heating is essential for the shape transformation of thedwarf.

In principle stripping may still occur after the saturation induced by the bar inflow via a mechanism that is not correctly captured by the SPH simulations discussed throughout this paper, namely, turbulent stripping by ablation due to Kelvin-Helmoltz instabilities at the interface between the gas in the dwarf and the surrounding hot diffuse halo ([83, 84], but see how simple modifications of standard SPH can solve the problem in [85]). In hydrodynamical flows two shearing fluids moving with relative velocity $V_{\rm rel}$ are subject to an instability (the Kelvin-Helmoltz instability) that tends to ablate their interface; a wave-like perturbation will grow proportionally to the density contrast and relative velocity of the fluids, but could be damped with increasing viscosity or if an external force, such as a gravitational field, is applied to the system.

We can show that Kelvin-Helmoltz instabilities will not occur for dwarfs embedded in a massive dark halo because of the stabilizing effect of the gravity of the halo. We neglect the effect of SPH artificial viscosity in the following calculation; this is a conservative assumption since viscosity would stabilize the system further. Following existing analytical predictions [83], we estimate that the critical value of the gravitational acceleration necessary to stabilize the dwarf gas disk against Kelvin-Helmoltz in dwarf galaxy models with $V_{\rm peak} = 40$ km/s used in Mayer et al. [20] and Mayer et al. [41] is $g_{\rm cr} \sim 0.1$ initially, where $g_{\rm cr} = 2\pi V^2/DR_g$ ($V \sim 200$ km/s is the average orbital velocity of the galaxy, $R_g = 0.5$ kpc is the scale length of the gas component, and $D = \rho_g/\rho_{\rm gh}$ is the ratio between the density of the gaseous disk at $R \sim R_g$ and the time averaged density of gaseous halo along the orbit of the dwarf; and for simplicity we express the gravitational acceleration in the adimensional system of units of our simulations, in which we assume $G = 1$ for the gravitational constant G). The self-gravity of the dwarf galaxy within R_g, which is mainly provided by the dark halo, is instead $g \sim 2.5 > g_{\rm cr}$, where $g = GM_{\rm halo}/{R_g}^2$. We note that $g > g_{\rm cr}$ holds down to about 1/5 of the disk scale length, and also for $R > R_g$. Hence the gaseous disk of the dwarf is initially stable to Kelvin-Helmoltz instabilities. However, on subsequent orbits the situation can change. For the simulation presented in Mayer et al. [41] after the second pericenter passage, the density of the dwarf within 0.5 kpc, decreases by a factor of 4 as a result of the tidal shocks, so that g drops to ~0.6 at one disk scale length, now being very close to $g_{\rm cr}$ (the latter has also decreased in the meantime, $g_{\rm cr} \sim 0.3$, since the mean density of the gas has dropped). The gas component of the dwarf is now only marginally stable to Kelvin-Helmoltz instabilities, but using the formula to

calculate the mass loss rate due to Kelvin-Helmoltz [83] for $R_g = 0.5$ kpc one derives a characteristic stripping timescale still quite long, that is, comparable to the Hubble time.

There is then one more stripping mode to examine. Although formally standard SPH solves the equations for an inviscid fluid, de facto the necessity of artificial viscosity renders the fluid model viscid. It thus makes sense to consider laminar viscous stripping as another possible stripping mechanism. The mass loss rate in this case is given by $\dot{M} \sim 12/2.8\pi {R_g}^2 V_{\rm rel}\rho_{\rm gh}(\lambda_{\rm max}/R_g)(c_1/V_{\rm rel})$ [83, 86], where $\lambda_{\rm max}$ is the longest wavelength not stabilized by gravity. Assuming that, at second pericenter, the longest unstable wavelength is $\lambda_{\rm max} \sim 0.5$ kpc, one obtains a laminar viscous timescale of $\sim$2 Gyr for the typical ambient gas densities and relative velocities in our simulations ($V_{\rm rel} = V_{\rm orb}$). The gas is indeed completely stripped $\sim$1 Gyr later in cases in which the gas component remains diffuse and extended because cooling is inefficient (e.g., the run with adiabatic gas and with added cosmic UV background presented in Figure 4; see also next paragraph). In runs where only radiative cooling is considered, the longest unstable wavelength is much smaller than the radius of the residual gas, which implies a laminar viscous timescale close to the Hubble time. This explains why the gas is not completely stripped in cooling-only runs (see Figure 4). In conclusion, despite the strongly time-dependent behaviour of all the variables involved in the problem, both the action and the saturation of stripping seen in the simulations is consistent with the expected characteristic timescales and relative importance of the various ram-pressure stripping modes.

The next point to discuss in order to understand the different mass loss curves shown in Figure 4 is the effect of radiation physics/thermodynamics, which we have just hinted during the description of the stripping process above. The temperature evolution determines whether the gas component stays extended or becomes concentrated in the central, deeper part of the potential well as a result of tidally induced bar-driven inflows. Compression from the outer medium heats the gas. The gas is rapidly heated to 10^5 K, where the cooling function peaks (the initial temperature of the gas disk in the dwarf models is in the range $\sim$3000–8000 K depending on the initial mass and is set by hydrostatic equilibrium requirements) at which point it cools radiatively to 10^4 K in a fraction of a dynamical time; such cold gas easily sinks towards the center due to the torque exerted by the bar and cannot be removed by ram pressure. Instead, if compressional heating is not radiated away, as when the gas evolves adiabatically, the increased pressure opposes the bar-driven inflow, keeping more gas at larger radii where it can easily be stripped. For stripping to be very effective for dwarfs with initial $V_{\rm peak} \sim$ 30–60 km/s, it is sufficient that the temperature of the gas is kept above 10^4 K (the virial temperature of these halos is $3–5\times10^4$ K). This requires some heating source to counteract radiative cooling. Mayer et al. [20] find that for $V_{\rm peak} \sim$ 30–40 km/s such temperature increase can be achieved owing to heating by the (uniform) cosmic UV background at $z > 1.5$–2, where the heating rate and ionizing flux rates are based on standard models for the time evolution of the intensity of the cosmic ionizing background [49, 2000].

For even higher values of the circular velocity ($V_{\rm peak} \sim$ 40–60 km/s), complete stripping would require an even higher heating rate. This is likely to be provided by the local ionizing radiation originating from the primary galaxy (the Milky Way or M31 for the case of the Local Group). Mashchenko et al. [87] calculate that the FUV flux of M31 derived from its H_α luminosity is higher than these of the present-day value of the cosmic UV background out to 10–20 kpc from its center. Current starbursts have FUV luminosities 10^3–10^4 higher than the MW and M31, in the range 10^{44}–10^{45} erg/s [88]. According to cosmological simulations at z = 2-3 Milky-Way-sized galaxies were hosting a major central starburst, forming stars at a rate of $\sim$20–30$M_\odot$/yr [75, 89]. This is consistent with the star-formation rates measured for $z = 2$ galaxies that should evolve into L_* galaxies by the present epoch (Conroy et al. 2007). Determining the escape fraction of ultraviolet photons that will contribute to heating and ionizing, the gas of the dwarf is a complex task, with the estimated escape fraction varying between a few percent to more than 10% (e.g., Fernandez-Soto et al. [90], Shapley et al. [91]). We choose a simpler approach by assuming that the FUV luminosity of the primary galaxy in the starbursting phase is comparable to that of a major present-day starburst ($L_{FUV} = 10^{45}$ erg/s). At higher redshift, dust absorption should be lower since the metallicity should also be lower, thereby our estimate, while crude, should be on the conservative side. Under this hypothesis we obtain that at 30 kpc from the center the heating rate was 10 times higher than that associated with the metagalactic UV background at $z \sim 2$. We have run new simulations including such a local, time-dependent UV background (the intensity of the flux is modulated by the orbital distance of the dwarf) and found that ram-pressure stripping is greatly enhanced, leading to complete gas removal after a couple of orbits even for $V_{\rm peak} \sim 50$ km/s [19]. A systematic exploration of the effect of the local ionizing radiation over a range of mass scales of dwarf galaxies will help assess the overall relevance of the effect in the context of the evolution of dwarf galaxy satellites.

The implications of these simulations on the enhanced gas stripping resulting when the ionizing background at high redshift is taken into account are quite important. Indeed we can argue that if the progenitors of Draco or Ursa Minor fell into the Milky Way at $z > 1.5$–2, then ram pressure combined with tides was able to remove their entire gas content in a couple of orbits. This translates into a timescale of about 2-3 Gyr after infall assuming a range of orbital times consistent with their current distance from the Milky Way. Therefore, in this scenario the observed truncation of the star formation in Draco and Ursa Minor more than 10 Gyr ago occurred as a consequence of the infall of these galaxies into the Milky Way halo. Draco would have formed most of its stars before infall since most of the gas becomes ionized while approaching pericenter for the first time. This scenario, however, would still be unable to explain the very high dark matter content of a galaxy like Draco nor why do other dSphs, such as Fornax, appear to have a similar total mass (baryons plus

dark matter) but a much lower dark matter content. We will see in the next section that these other properties of dSph satellites of the Milky Way can also be explained once proper assumptions on the structure of their disky progenitors are made, and the time-dependent nature of the cosmic ionizing background is taken into account.

6. A Scenario for the Origin of Classic Dwarf Spheroidals in a Hierarchical Universe: The Timing of Infall into the Primary

In Mayer et al. [41] we built on the results of the previous section and we proposed a coherent scenario that explains at the same time the origin of the common properties of dSphs (low gas content, exponential profiles, low luminosity and surface brightness, and low angular momentum content) and their differences (different star-formation histories and mass-to-light ratios). In this model the key parameter is the epoch of accretion onto the Milky Way and a key assumption is that the progenitors of present-day classic dSphs were not simply gas-rich but extremely gas dominated, consistent with what is found in most present-day dIrrs in the Local Group and elsewhere in the nearby Universe [92]. The large gas fractions found in field dwarfs can be understood in terms of a decreasing star-formation efficiency towards decreasing galaxy mass. Recently, the THINGS survey [93] has confirmed that disky dwarfs have a star-formation efficiency, defined as the fraction of gas (atomic+molecular) that is converted into stars, well below that of normal spirals, of order 1% or less. The low gas surface densities typically found in dwarfs likely imply a low conversion efficiency between atomic hydrogen and the star-forming molecular hydrogen phase [94], probably explaining the low star-formation efficiency (note that the conversion between molecular gas and stars does not seem to be lower in dwarf compared to normal spirals, see [95]). Such conversion can be even less efficient in presence of the ionizing ultraviolet flux arising during reionization, which can dissociate molecular hydrogen [94]. Therefore for field dwarfs that were accreted by the Milky Way or M31 at $z > 1$, the assumption of mostly gaseous baryonic disk is even more well grounded.

The initial conditions, including the orbits of the satellites, were chosen based on a hydrodynamical cosmological simulation of the formation of a Milky-Way-type galaxy [75]. We found that satellites that were accreted when the cosmic ionizing background was still high, roughly before $z = 1$, were completely ram pressure stripped of their gas in one to two pericenter passsages (Figure 6). As a result their star formation was truncated. As explained in Section 5, the effect of the ionizing radiation is to heat and ionize the gas, making it more diffuse because of the increased pressure support, and to suppress star formation. This, in turn, makes it easier to strip even from the central regions of the dwarf, essentially having the same effect of a reduced binding energy. Hence gas-rich dwarfs accreted when the UV radiation background was at its peak lost most of their baryonic content because this was initially in gaseous form, thus naturally ending up with a very low luminosity. While their baryonic content dropped orders of magnitude below the cosmic mean as a result of gas stripping, their original central dark matter mass in the central region around the surviving baryonic core was largely preserved because dark matter is affected only by tides, not by ram pressure. This automatically produced very high mass-to-light ratios, of order 100 (see Mayer et al. [80, Figure 2]). We showed that all the final properties of such systems after 10 billion years of evolution, including the stellar velocity dispersion profiles, resemble those of the classic strongly dark-matter-dominated dwarfs such as Draco, Ursa Minor, or And IX. Even the brightest among the ultrafaint dwarfs, that have velocity dispersions > 5 km/s (e.g., Ursa Major) may be explained by this model. However, the very low characteristic mass scale of most ultrafaint dwarfs suggests that other formation paths might indeed be more likely (see Section 8). Dwarfs that fell into halos of bright galaxies below $z = 1$, when the cosmic UV radiation dropped by more than an order of magnitude, retained some gas because tides and ram pressure could not strip it completely and underwent subsequent episodes of star formation at pericenter passages due to bar-driven inflows and tidal compression [13, 14]. These ended up in dSphs that are brighter for a given halo mass (or given central stellar velocity dispersion) compared to the ones that were accreted earlier. This should be case with, for example, Fornax, Carina, or Leo I. The two regimes of infall epochs explain why Fornax and Draco have roughly the same halo peak circular velocities (and thus mass) despite having a luminosity and mass-to-light ratio that differ by about an order of magnitude. Likewise, Carina and Leo I, these being prototypical cases of dSphs with an extended (episodic) star-formation history, have a luminosity comparable to Draco but a mass-to-light ratio 5–10 times lower than that of Draco [1].

As a final remark, we note that Madau et al. [38] argue that a very low efficiency of star formation, corrresponding to less than 0.1% of their total mass being converted into stars, would offer a solution to the excess in number counts of subhalos with $V_c > 20$ km/s in dark-matter-only simulations (see also [78] for a similar interpretation). Our model for the origin of Local Group dwarf spheroidals provides a clue to why dSphs were so inefficient at producing a stellar component, thus pointing to a solution of the substructure problem at the bright end of the mass function of dwarf satellites of the Milky Way, which essentially contains all the classic dSphs. Instead of relating the low efficiency of star-formation to photoevaporation and/or suppression of gas accretion by the cosmic ultraviolet background, we argue that it arose naturally from intrinsic low star-formation efficiency in the progenitor gas-rich dwarfs (well below 1%) combined with copious gas stripping after they were accreted in the potential of the primary galaxy. Our mechanism is absolutely general in hierarchical structure formation and should thus apply to dwarf galaxy satellites of any galaxy group. The combination of an intrinsic low star-formation efficiency prior to infall with ram pressure and tidal stripping can be thought of as an effective feedback mechanism alternative to reionization and supernovae feedback. Recent

models that relate star-formation directly to the formation of molecular hydrogen and to its dependence on metallicity [96, 97] show convincingly that the star-formation efficiency was at the low levels assumed by us, and invoked by Madau et al. [38], when the metallicity was below 0.1 of the solar value. This is because both molecular hydrogen formation and self-shielding from the dissociating UV radiation depend on the dust content, which drops with decreasing metallicity. Interestingly, the *current* metallicity dSphs, both of the ultrafaint ones and of the classic ones, is comparable to or smaller than a tenth of the solar value [52], suggesting that these objects likely spent a significant fraction of their assembly history at metallicity lower than such critical threshold. Therefore inefficient star formation played a key role in delivering gas-dominated dwarfs at the time of their infall into the halo of the primary and at the same time is key to understand the missing satellites problem.

7. The Interplay between Gas Stripping and the Tidally-Induced Transformation of the Stellar Component

The removal of gas due to ram pressure can in principle have effects on the dynamical evolution of the other components of the dwarf, dark-matter and stars, since it is initially a nonnegligible fraction of the total mass within the central kiloparsec. We have performed a number of tests to explore in detail the nature of the transformation of the baryonic component in the simulations presented by Mayer et al. [41], where both stars and gas are present in the initial disky dwarf. The main goal was to determine the relative role of the rapid removal of the gas (Figure 6), which comprises most of the baryons initially, and that of the repeated tidal shocks in changing the shape of the stellar component. Although the initial dwarf model is dark matter dominated by construction, baryons comprise as much as 30% of the total mass within the initial exponential disk scale length. Their rapid removal due to ram-pressure stripping might in principle affect the dark matter potential, possibly lowering its density as found in previous studies where baryonic stripping occurs as a result of powerful supernovae winds [98–100].

Figure 7 shows principle axis ratios $s = b/a$ and $q = c/a$ ($a > b > c$) of stars, calculated from the eigenvalues of a modified inertia tensor [101]: $I_{ij} = \sum_\alpha x_i^\alpha x_j^\alpha / r_\alpha^2$, where x_i^α is the i coordinate of the αth particle, $r_\alpha^2 = (y_1^\alpha)^2 + (y_2^\alpha/s)^2 + (y_3^\alpha/q)^2$, and y_i^α are coordinates with respect to the principle axes. We use an iterative algorithm starting with a spherical configuration ($a = b = c$) and use the results of the previous iteration to define the principle axes of the next iteration until the results converge to a fractional difference of 10^{-2}. Results are shown for three experiments. The comparison between the red and the black lines clearly shows that repeated tidal shocks are necessary for the transformation of the stellar component to occur; c/a increases by more than a factor of 6 when the dwarf is continuously tidally shocked relative to a case in which it just loses most of its baryons owing to ram pressure and then evolves without any tidal perturbation (in the latter case we removed the primary halo from the simulation after the gas was stripped). The green lines in Figure 7 show a test in which about 30% of the initial gas content is retained until the end because the UV background is absent and thus the effect of ram pressure is reduced (we tested that not including the cosmic UV background at all or including it with the low amplitude expected at $z < 1$ from the Haardt and Madau model yields the same result, see Mayer [19] and Mayer et al. [20]). The residual gas is funneled to the center by the bar, where it forms a very dense knot [20]. We notice that despite the fact that this is a small fraction of the initial gas content, it represents a nonnegligible contribution to the central potential because it all ends up in the inner 0.5 kpc (corresponding to the initial disk scale length). In this case the dwarf maintains a bar-like, prolate shape even after 10 Gyr, hence the lower c/a. After 5 Gyr the central density is 8 times higher compared to the simulation in which complete gas stripping occurs. As a result $t_{\rm shock} > t_{\rm orb}$ within 0.5 kpc, where $t_{\rm shock}$ is $R_{\rm peri}/V_{\rm peri}$, $R_{\rm peri}$ and $V_{\rm peri}$ being, respectively, the pericentric distance and the velocity at pericenter, and $t_{\rm orb}$ is the orbital time at 0.5 kpc from the center of the dwarf; the response of the system to the tidal forcing is thus adiabatic instead of impulsive, hence further morphological changes are inhibited. This demonstrates that while gas removal does not drive the transformation, it represents a crucial step for the evolution of the stellar component because the effect of the tidal shocks is considerably weakened when a dense central gas component is retained.

Figure 7 also shows that c/a does not grow beyond 0.2 in isolation, even after a few Gyr of evolution. The average (apparent) ellipticity measured for late-type dIrrs in the Local Group is larger, ∼0.58, for the 8 dwarfs having a range of rotational velocities comparable with those of our initial dwarf galaxy model ($V_{\rm peak} \sim$ 30–40 km/s) [1]. Similar values are found for dwarf irregular galaxies in clusters [102]. However, comparing with observed values of ellipticity one must take into account inclination effects, since the c/a discussed for our simulated dwarf is the intrinsic value, that is, the value that would be measured by an observer viewing the dwarf exactly edge-on. By viewing the dwarf at inclinations in the range 30–60 degrees, which statistically are a much more representative situation, the mean apparent c/a varies in the range ∼0.4–0.7 within 3 disk scale lengths (it is 0.55 at 45 degrees of inclination), hence perfectly consistent with the observed values. This indicates that initial conditions used in tidal stirring experiments are a reasonable match to gas-rich dIrrs.

To summarize, these experiments indicate that the repeated tidal shocks in the impulsive regime drive the transformation of the shape and mass distribution of the dwarf galaxy, and that gas removal is a necessary condition for them to be effective. Prolonged impulsive tidal heating is one of the ways by which tidal stirring can induce the morphological transformation from disk into spheroid, the other being bar-buckling (see Section 3). The former is naturally favored for low mass, low density stellar disks that are naturally prone to an impulsive response and also less

self-gravitating, while the latter is favored at higher stellar densities and thus higher self-gravity since it is based on the growth of unstable modes [14, 61].

8. The Ultrafaint Dwarfs in the Tidal-Stirring Scenario

In the last five years deep photometry with the Sloan Digital Sky Survey (SDSS) has unveiled a new class of ultrafaint dwarfs with structural properties (e.g., low angular momentum, no gas content) analogous to classic dwarf spheroidals (dSphs) but with masses and luminosities 1-2 orders of lower magnitude [17, 51, 52, 103] Indeed with velocity dispersions in the range 2–6 km/s and luminosities in the range $-2 < M_B < -7$, these objects are fainter than most known Globular Clusters, but clearly differ from them because of their lower stellar surface densities, larger optical radii, and much higher mass-to-light ratios. The dozen ultrafaint dSphs detected so far all have $M/L \sim 100$–1000, hence they are even more dark matter dominated than the darkest among the classic dSphs, such as Draco and Ursa Minor. Like most classic dSphs, they are found at distances well within the virial radius of the Milky Way halo (at galactocentric distances < 300 kpc). The brightest of them, such as Ursa Major, may be the product of the same transformation mechanism elucidated in the previous sections. In this case the initial progenitor managed to form just a minuscule stellar component before ram pressure aided by the UV background removed most of the baryons. But the low masses inferred for most of the ultrafaint dwarfs are below the critical mass threshold for "surviving" reionization ([104], Bullock, Kravtsov & Weinberg 2001, [12, 105]); they would have been below the threshold even before being accreted by the Milky Way assuming a factor of 2-3 decrease in their peak velocity dispersion/circular velocity (thus a factor ∼8–30 in mass) due to tidal mass loss over billions of years. This implies that at $z \sim 7$–12, when reionization began, they could not hold onto their gas and form stars, rather they suffered complete photoevaporation. The most plausible explanation for the origin of the ultrafaint dwarfs is that they formed their stellar components entirely before the onset of reionization (later gas accretion at $z > 1$ would be difficult with such shallow potential wells). They are thus the natural candidates for being the "reionization fossils" predicted in the models of Ricotti and Gnedin [106] and Gnedin and Kravtsov [107]. High-resolution cosmological simulations of galaxy-sized halos indeed find about a thousand subhalos with virial masses $>10^6 M_\odot$ prior to reionization, hence massive enough for cooling via molecular hydrogen to lead to gas collapse and star formation before they are accreted onto the primary galaxy [108]. A low intrinsic efficiency of star formation due to inefficient formation of molecular hydrogen is expected for these low mass, low metallicty systems (see Section 6). In addition, even modest star formation would strongly affect these systems via supernovae feedback, keeping the star-formation efficiency low [100]. Inefficient star formation might thus be the main cause of the extremely low stellar content of the ultrafaint dwarfs. Moreover, gas photoevaporation owing to the rising ionizing background would remove most of their gas, hence most of their baryons, leading naturally to very high mass-to-light ratios without the need of additional environmental processes such as ram pressure and/or tidal stripping.

On the other end, with original masses likely below $10^7 M_\odot$, up to two orders of magnitude less than those of classic dSphs, tidal stirring and tidal mass loss were also very effective in the progenitors of ultrafaint dwarfs. What we detect today is probably the surviving inner core of the original dwarf, which responded more adiabatically to the tidal shocks owing to the high halo concentration/central density expected in very low mass satellites [34, 69, 109]. However, such tiny subhalos were likely never disky in the first place. In fact for standard values of spin parameters expected in cosmological halos, their initial angular momentum content was too low to provide more support than thermal pressure against the low gravity of their tiny halo potential wells, especially in the presence of the cosmic ionizing UV background [77]. Therefore ultrafaint dwarfs do not owe their current diffuse, spheroidal appearance and pressure-supported kinematics to the effect of tidal stirring, rather these structural properties were established before infall.

Finally, an emerging feature of the ultrafaint dwarfs is that some of them appear to be associated with other classic dSphs such as Sagittarius or Fornax. One example is the very recently discovered Segue 2 [110], where the kinematics support the association with the Sagittarius stream and with other similarly faint dwarfs, Bootes II and Coma (for Segue 1 recent work does not support the same association; see Geha et al. [111]). It is then natural to postulate that many if not all of these ultrafaint dwarfs are indeed satellites of satellites, the luminous counterparts of subhalos of subhalos seen in the latest generation of cosmological simulations resolving scales of tens of parsecs [108]. However, establishing such a link will require further studies since current cosmological simulations capable of resolving satellites of satellites do not include the baryons yet. If they were accreted as members of subgroups, the ultrafaint dwarfs might have undergone tidal stirring, and perhaps even ram pressure stripping, by a larger parent dwarf before falling into the Milky Way or M31 halo [24, 68]. The first cosmological, hydrodynamical simulations of the formation of low mass galaxies (with masses comparable with the likely progenitors of Sagittarius or Fornax) are under way as we write [89]. They will be the first step to study the nature of satellites of dwarf galaxies and assess how plausible the idea that many of the ultrafaint dwarfs are satellites of satellites.

9. Towards a Coherent Picture: Two Populations of dSphs Produced by the Combined Action of Tides, Ram Pressure, and the Cosmic Ionizing Background

According to the scenario that we presented in this paper, a coherent paper is emerging on the role of environment in

shaping the nature of dwarf spheroidal galaxies. In particular, we posited two main formation paths for dwarf spheroidals: one for the classic dSphs and one for the ultrafaint dwarfs. Classic dwarf spheroidals live in tidally truncated halos with present-day masses of 10^7-$10^8 M_\odot$, which were typically a factor of 10, more massive, 10^8-$10^9 M_\odot$, before infall into the halos of the Milky Way and M31. They were thus born in halo potential wells too deep for suppression of gas accretion and/or photoevaporation to play a major role in determining their final properties. Instead, we argue that their current properties, including their baryonic content and mass-to-light ratio, were determined mostly by the effect of ram pressure and tides after infall into the potential of the primary galaxies, with the cosmic UV background still playing some role in the thermodynamics of the gas and in regulating star-formation both before and after infall. For classic dSphs two main outcomes are then possible depending on when they were accreted by the primary halo. At $z > 1$, when the cosmic ionizing UV background is more than an order of magnitude higher than today, infalling dwarfs underwent complete stripping of their gas after one or two orbits and rapid truncation of star formation. This early infall mode explains an object like Draco, with a star formation history truncated about 10 billion years ago and a very high mass-to-light ratio. At $z < 1$, the weaker UV background implies colder and more tightly bound gas in the infalling dwarfs; stripping is thus less efficient and does not lead to complete gas removal. Instead, the remaining gas is consumed in bursts of star-formation at pericenter passages due to bar-driven inflows and tidal compression. This late infall mode explains dSphs like Fornax, with an extended star formation history and moderate mass-to-light ratio. For both early and late "infallers", we argue that they had a disky, rotating stellar component before infall, as in most present-day dIrrs, that was later turned into a pressure-supported spheroidal by tidally induced instabilities and tidal heating, a transformation mechanism that we dubbed tidal stirring. On the other hand, for ultrafaint dwarfs the formation path is governed by the effect of reionization, as expected based on their much lower mass scale, which would place them in halos with masses $<10^7 M_\odot$ even prior to prolonged tidal mass loss within the primary halo. They were likely born as spheroidal, pressure-supported objects before reionization, and lost most of their baryons due to photoevaporation thereafter ("reionization fossils"). In light of this scenario it is then clear how to interpret the the anticorrelation between luminosity and M/L [52], which extends all the way from Fornax to Segue 1, one of the faintest newly discovered dwarfs. This is the result of ram pressure and tidal stripping combined with the UV background at the bright/high mass end ($\sigma > 6$ km/s, corresponding to an initial $V_{\rm peak} > 20$ km/s before infall), and the product of photoevaporation by the UV background at the faint/low mass end ($\sigma < 6$ km/s, corresponding to an initial $V_{\rm peak} < 15$–20 km/s before infall). It remains to demonstrate quantitatively that the efficiency of these various mechanisms for the removal of the baryons in dwarfs increases with decreasing mass in the way implied by the observed correlation.

Finally, Kravtsov et al. [24] have noted how the radial distribution of present-day dSph satellites of the MW and M31 can be used to constrain different scenarios for their origin. Dwarf spheroidals appear to be more clustered towards the center of the primary compared to the average subhalos, hence they have a steeper than average radial distribution profile. By comparing the distribution of various subsets of the substructure population of MW-sized halos in cosmological simulations with the one observed for dSphs, they were able to exclude, for example, models in which dSphs are hosted by the most massive substructures [36], while they found acceptable models in which dSphs are some of the most massive substructures prior to infall (this being consistent with the assumption behind all our works, namely, that they lost a significant fraction of their mass since they were accreted). Strigari et al. [44] reached analogous conclusions based on the analysis of the mass function of the most massive substructures. The question is as follows would tidal stirring be consistent with the observed radial distribution of dSphs? This will have to be investigated dirctly in cosmological simulations with hydrodynamics and star formation and with enough resolution to study the satellites' population. New simulations obtain a radial distribution profile of luminous subhalos that is comparable to that of observed dSphs [112] but they do not have enough resolution to explore the morphologies of luminous satellites yet, nor can they reliably model hydrodynamical mechanisms such as ram-pressure stripping. However, for the time being, there is no expected inconsistency. Indeed the assumption that the dark-matter-dominated dSphs had to be accreted at $z > 1$, for the morphological transformation to be effective [41] naturally implies that they were accreted on fairly tight orbits (high orbital energy, short orbital times); this automatically implies a radial distribution profile steeper than that of the overall satellites' population.

10. Caveats, Alternatives, and Future Prospects: Thick Disks, Infalling Subgroups, and Dark Matter Cores

The tidal stirring simulations carried out so far have always assumed an initial configuration in which the disky progenitor is constructed using an equilibrium model with a relatively thin disk of gas and stars. In reality the stellar disks of dwarfs with $V_c < 40$ km/s are expected to be rather thick as the gas that formed the disk in low mass halos reached centrifugal equilibrium with a fairly high scale height at the mean temperature of 1.5–3×10^4 K expected in the presence of the cosmic ionizing background at $z > 1$ [77]. Thermal pressure, as opposed to rotation, would be crucial to explain the initial equilibrium structure of dwarfs embedded halos with $V_c < 20$ km/s that likely hosted the progenitors of ultrafaint dwarfs. At some level it may also have affected the initial conditions of massive systems that produced the classic dSphs, and thus should be investigated further with models capable of capturing the multiphase structure of the ISM. A more diffuse, hotter stellar component argues in favor of a stronger effect of tides, but dynamical instabilities

such as the bar and buckling instabilities invoked in tidal stirring are physically associated to an initially cold, rotating stellar configuration. Gas stripping by ram pressure should instead be enhanced in an initially hotter, more diffuse stellar system because of the reduced gravitational restoring force of the gas. We are currently investigating the tidal stirring and ram pressure of a realistic gas-rich dwarf with a turbulent, multiphase interstellar medium formed self-consistently in a cosmological simulation (Callegari, Mayer et al., in preparation).

Recently, an alternative model has been proposed according to which some of the classic dSphs did not fall into the Milky Way halo as individual satellites but rather joined the system as part of a subgroup centered around the Large Magellanic Cloud [68]. That some satellites are brought inside of the primary halo as part of subgroups is indeed found in cosmological simulations [24, 113]. The model is not necessarily in contrast with the general tidal stirring scenario since the dwarf might have been tidally perturbed significantly by the LMC, which is 1-2 orders of magnitude more massive than even the brightest among dSphs (Fornax), and then stirred even more by the Milky Way as the subgroup was broken up by the tides of the latter soon after infall. This model would explain the possible alignment of some of the dSphs with the orbits of the Magellanic Clouds. It would also imply that a large fraction, if not half of the luminous dSphs, came in as satellites of the LMC. This would be naturally explained by how the cooling time scales with halo mass. Gas removed by the cosmic ionizing background or by tidal/ram pressure stripping as the dwarfs were part of the LMC system would have been reaccreted much more easily by the subhalos relative to the case in which they would be part of a larger halo such as that of the Milky Way. In fact, assuming that such gas would quickly thermalize with the ambient gas temperature, reaching thus the virial temperature of the primary halo, the cooling time would be much shorter ($t_{\rm cool} \ll T_{\rm hubble}$) at the virial temperature of the LMC halo, $\sim 10^5$ K. However, in this model it is still unclear why dSphs have two main modes of star formation history (truncated or bursty and extended) that do not appear to be linked with their being part of the putative LMC subgroup. That being said, the potential wells of the dSphs halos might be sufficiently deep to reaccrete gas while they are still embedded in groups with the virial masses as those of the LMC halo, possibly undergoing an extended star formation history. It will be interesting to assess if other intermediate mass galaxies in the Local Group, such as M33, massive enough to be a primary of a subgroup, have dSphs, surviving or already disrupted into streams, associated to them. Future surveys of the M31 system will shed light on this possibility.

Previous work has shown that a cuspy dark matter halo fitted by an NFW or Moore profile might develop a core as a result of a strong mass outflow such as that caused by supernovae winds during a burst of star formation [100]. More recently, the first high-resolution cosmological simulations of dwarf galaxy formation have shown that this mechanism may indeed be efficient at high redshift in the low mass progenitors of present-day gas-rich dwarfs, producing a galaxy with a kiloparsec-scale core at $z = 0$ whose slowly rising rotation curve matches those of typical late-type dwarfs (Governato, Brook, Mayer et al., in prep.) . A clumpy, turbulent interstellar medium may also contribute to core formation via exchange of energy and angular momentum with the surrounding dark matter halo [114]. It is thus possible that the progenitors of Local Group dSphs had a cored halo when they accreted onto the Milky Way and M31. The scenario for baryonic stripping presented in this review is mostly based on dwarf galaxy models with cuspy (NFW) dark matter halos. Our conclusions regarding the crucial effect of the environment for dSphs would be even stronger if their progenitors had cores. Indeed, the various modes of ram-pressure stripping discussed earlier are all enhanced if the gravitational restoring force is lower in the inner region of the dwarf, as expected in a constant density core. Tidal shocks will also be enhanced because the response of the system will be more impulsive with a central core, rendering the instabilities and the resulting morphological transformation more efficient. Indeed this was observed in Mayer et al. [18], where NFW halos were first introduced in dwarf galaxy models, as opposed to Mayer et al. [13, 14], where truncated isothermal halos with a small core of a few hundred parsecs were used. Other mechanisms that can enhance considerably the intensity of tidal shocks are disk shocking (see pages 21-22 and [73]) and resonances. D'Onghia et al. (2009b) have recently shown that disky satellites that plunge close to the disk of a more massive companion can undergo a resonant interaction between their rotational motion and their orbital motion which can heat the stars into a spheroid, along with stripping a large fraction of them, after only one close pericentric passage. This happens when the spin angular frequency of the disk of the dwarf and the angular frequency of its orbit are commensurate, and the spin angular momentum and orbital angular momentum are nearly aligned (that is, in a nearly prograde encounter). This mechanism could be an important extension of tidal stirring, perhaps crucial to explain dSphs orbiting far from the primary, such as Tucana and Cetus in the LG. Ongoing studies aimed at characterizing in detail the stellar component of these isolated dSphs, including their star formation history, will soon provide useful constraints on these new ideas (e.g., [115]; see also http://www.iac.es/project/LCID). Such individual, close encounters may have been more common when the primary halo was still in the process of assembling from subgroups and their subhalos were interacting with much larger companions, the size of the LMC or so. Some of such encounters may have also resulted into mergers between dwarfs since the typical velocity dispersions in subgroups should have been quite low. Whether this could be another channel of early dSphs formation is currently under investigation (Klimentowski et al., in preparation). While all these different tidal mechanisms relying on the idea of preprocessing, the morphology of the dwarf satellite population before they are accreted by the primary may play a role at some level; they need to be consistent with the morphology-density relation, a crucial constraint that tidal stirring can naturally satisfy.

As our understanding of dwarf galaxy formation from cosmological initial conditions improves, interaction simulations will have to be revisited to better calibrate the quantitative effects of the various mechanisms discussed in this review. While tidal stirring may be only one part of the overall picture of dSphs formation and evolution, the new studies just recalled to reinforce the idea that tides, in various forms and at different stages of the evolution of satellites, played a key role in shaping dSphs as they are today. "Nurture" rather than "nature" is thus the most likely explanation of the origin of the classic dSphs.

Acknowledgments

The author thanks all his main collaborators through the years that made possible to carry out all the work presented in this review: Stelios Kazantzidis, Chiara Mastropietro, Fabio Governato, Ben Moore, Thomas Quinn, James Wadsley, Monica Colpi, Ewa Lokas, Jaroslaw Klimentowski, Gary Mamon, Tobias Kaufmann, Beth Willman, and Joachim Stadel as well as also Ph.D. students Simone Callegari and Robert Feldmann for continuing the study of the environmental effects described in this review within the new generation of cosmological hydrodynamical simulations. The author also thanks Cristiano Porciani for his help on issues regarding the effects of the local ionizing ultraviolet radiation and George Lake, Justin Read, Nick Gnedin, Oleg Gnedin, Andrey Kravtsov, James Bullock, Piero Madau, Avishai Dekel, Elena D'Onghia, Carme Gallart, Evan Skillman, Pierre-Alain Duc, Julio Navarro, Arif Babul, Martin Weinberg, Neal Katz, Andrea Ferrara, Wyn Evans, Gerry Gilmore, Vassily Belokurov, Michael Hilker, Pavel Kroupa, Thorsten Lisker, and Jorge Pennarrubia for interesting and helpful discussions on dwarf galaxies and galaxy interactions over the years.

References

[1] M. Mateo, "Dwarf galaxies of the local group," *Annual Review of Astronomy & Astrophysics*, vol. 36, no. 1, pp. 435–506, 1998.

[2] X. Hernandez, G. Gilmore, and D. Valls-Gabaud, "Non-parametric star formation histories for four dwarf spheroidal galaxies of the local group," *Monthly Notices of the Royal Astronomical Society*, vol. 317, no. 4, pp. 831–842, 2000.

[3] M. G. Coleman and J. T. A. de Jong, "A deep survey of the Fornax dSph. I. Star formation history," *The Astrophysical Journal*, vol. 685, no. 2, pp. 933–946, 2008.

[4] C. Orban, O. Y. Gnedin, D. R. Weisz, E. D. Skillman, A. E. Dolphin, and J. A. Holtzman, "Delving deeper into the tumultuous lives of galactic dwarfs: modeling star formation histories," *The Astrophysical Journal*, vol. 686, no. 2, pp. 1030–1044, 2008.

[5] K. Chiboucas, I. D. Karachentsev, and R. B. Tully, "Discovery of new dwarf galaxies in the M81 group," *The Astronomical Journal*, vol. 137, no. 2, pp. 3009–3037, 2009.

[6] I. Misgeld, M. Hilker, and S. Mieske, "The early-type dwarf galaxy population of the Centaurus cluster," *Astronomy & Astrophysics*, vol. 496, no. 3, pp. 683–693, 2009.

[7] S. J. Penny, C. J. Conselice, S. De Rijcke, and E. V. Held, "*Hubble Space Telescope* survey of the Perseus Cluster. I. The structure and dark matter content of cluster dwarf spheroidals," *Monthly Notices of the Royal Astronomical Society*, vol. 393, no. 3, pp. 1054–1062, 2009.

[8] A. Dekel and J. Silk, "The origin of dwarf galaxies, cold dark matter, and biased galaxy formation," *The Astrophysical Journal*, vol. 303, no. 1, pp. 39–55, 1986.

[9] J. Einasto, E. Saar, A. Kaasik, and A. D. Chernin, "Missing mass around galaxies: morphological evidence," *Nature*, vol. 252, no. 5479, pp. 111–113, 1974.

[10] D. N. C. Lin and S. Faber, "Some implications of nonluminous matter in dwarf spheroidal galaxies," *The Astrophysical Journal*, vol. 266, no. 1, pp. L21–L25, 1983.

[11] J. S. Bullock, A. V. Kravtsov, and D. H. Weinberg, "Reionization and the abundance of galactic satellites," *The Astrophysical Journal*, vol. 539, no. 2, pp. 517–521, 2000.

[12] H. Susa and M. Umemura, "Formation of dwarf galaxies during the cosmic reionization," *The Astrophysical Journal*, vol. 600, no. 1, pp. 1–16, 2004.

[13] L. Mayer, F. Governato, M. Colpi, et al., "Tidal stirring and the origin of dwarf spheroidals in the local group," *The Astrophysical Journal*, vol. 547, no. 2, pp. L123–L127, 2001.

[14] L. Mayer, F. Governato, M. Colpi, et al., "The metamorphosis of tidally stirred dwarf galaxies," *The Astrophysical Journal*, vol. 559, no. 2, pp. 754–784, 2001.

[15] E. K. Grebel, "The stellar content of local group galaxies," in *Proceedings of the 192nd Symposium of the International Astronomical Union (IAU '99)*, P. Whitelock and R. Cannon, Eds., p. 17, ASP, Cape Town, South Africa, 1999.

[16] J. Diemand, M. Kuhlen, and P. Madau, "Formation and evolution of galaxy dark matter halos and their substructure," *The Astrophysical Journal*, vol. 667, no. 2, pp. 859–877, 2007.

[17] S. E. Koposov, J. T. A. de Jong, V. Belokurov, et al., "The discovery of two extremely low luminosity Milky Way globular clusters," *The Astrophysical Journal*, vol. 669, pp. 337–342, 2007.

[18] L. Mayer, B. Moore, T. Quinn, F. Governato, and J. Stadel, "Tidal debris of dwarf spheroidals as a probe of structure formation models," *Monthly Notices of the Royal Astronomical Society*, vol. 336, no. 1, pp. 119–130, 2002.

[19] L. Mayer, "The environment of dwarf spheroidal satellites; ram pressure, tides and external radiation fields," in *Near-Field Cosmology with Dwarf Elliptical Galaxies*, H. Jerjen and B. Binggeli, Eds., vol. 220 of *Proceedings of the International Astronomical Union Symposia and Colloquia, no. 198*, Cambridge University Press, Cambridge, UK, 2005.

[20] L. Mayer, C. Mastropietro, J. Wadsley, J. Stadel, and B. Moore, "Simultaneous ram pressure and tidal stripping; how dwarf spheroidals lost their gas," *Monthly Notices of the Royal Astronomical Society*, vol. 369, no. 3, pp. 1021–1038, 2006.

[21] A. Klypin, A. V. Kravtsov, O. Valenzuela, and F. Prada, "Where are the missing galactic satellites?" *The Astrophysical Journal*, vol. 522, no. 1, part 1, pp. 82–92, 1999.

[22] B. Moore, S. Ghigna, F. Governato, et al., "Dark matter substructure within galactic halos," *The Astrophysical Journal*, vol. 524, no. 1, pp. L19–L22, 1999.

[23] S. Ghigna, B. Moore, F. Governato, G. Lake, T. Quinn, and J. Stadel, "Dark matter haloes within clusters," *Monthly Notices of the Royal Astronomical Society*, vol. 300, no. 1, pp. 146–162, 1998.

[24] A. V. Kravtsov, O. Y. Gnedin, and A. A. Klypin, "The tumultuous lives of galactic dwarfs and the missing satellites problem," *The Astrophysical Journal*, vol. 609, no. 2, pp. 482–497, 2004.

[25] S. P. D. Gill, A. Knebe, B. K. Gibson, and M. A. Dopita, "The evolution of substructure. II. Linking dynamics to environment," *Monthly Notices of the Royal Astronomical Society*, vol. 351, no. 2, pp. 410–422, 2004.

[26] O. Y. Gnedin, L. Hernquist, and J. P. Ostriker, "Tidal shocking by extended mass distributions," *The Astrophysical Journal*, vol. 514, no. 1, part 1, pp. 109–118, 1999.

[27] G. Taffoni, L. Mayer, M. Colpi, and F. Governato, "On the life and death of satellite haloes," *Monthly Notices of the Royal Astronomical Society*, vol. 341, no. 2, pp. 434–448, 2003.

[28] L. A. Aguilar and S. D. M. White, "The density profiles of tidally stripped galaxies," *The Astrophysical Journal*, vol. 307, no. 1, pp. 97–109, 1986.

[29] J. E. Taylor and A. Babul, "The dynamics of sinking satellites around disk galaxies: a poor man's alternative to high-resolution numerical simulations," *The Astrophysical Journal*, vol. 559, no. 2, pp. 716–735, 2001.

[30] J. I. Read, M. I. Wilkinson, N. W. Evans, G. Gilmore, and J. T. Kleyna, "The tidal stripping of satellites," *Monthly Notices of the Royal Astronomical Society*, vol. 366, no. 2, pp. 429–437, 2006.

[31] J. I. Read, M. I. Wilkinson, N. W. Evans, G. Gilmore, and J. T. Kleyna, "The importance of tides for the local group dwarf spheroidals," *Monthly Notices of the Royal Astronomical Society*, vol. 367, no. 1, pp. 387–399, 2006.

[32] M. Colpi, L. Mayer, and F. Governato, "Dynamical friction and the evolution of satellites in virialized halos: the theory of linear response," *The Astrophysical Journal*, vol. 525, no. 2, pp. 720–733, 1999.

[33] J. Peñarrubia, A. J. Benson, D. Martínez-Delgado, and H. W. Rix, "Modeling tidal streams in evolving dark matter halos," *The Astrophysical Journal*, vol. 645, no. 1, pp. 240–255, 2006.

[34] S. Kazantzidis, L. Mayer, C. Mastropietro, J. Diemand, J. Stadel, and B. Moore, "Density profiles of cold dark matter substructure: implications for the missing-satellites problem," *The Astrophysical Journal*, vol. 608, no. 2, pp. 663–679, 2004.

[35] J. Peñarrubia, A. W. McConnachie, and J. F. Navarro, "The cold dark matter halos of local group dwarf spheroidals," *The Astrophysical Journal*, vol. 672, no. 2, pp. 904–913, 2008.

[36] F. Stoehr, S. D. M. White, G. Tormen, and V. Springel, "The satellite population of the Milky Way in a ΛCDM universe," *Monthly Notices of the Royal Astronomical Society*, vol. 335, no. 4, pp. L84–L88, 2002.

[37] J. Peñarrubia, J. F. Navarro, and A. W. McConnachie, "The tidal evolution of local group dwarf spheroidals," *The Astrophysical Journal*, vol. 673, no. 1, pp. 226–240, 2008.

[38] P. Madau, J. Diemand, and M. Kuhlen, "Dark matter subhalos and the dwarf satellites of the Milky Way," *The Astrophysical Journal*, vol. 679, no. 2, pp. 1260–1271, 2008.

[39] J. Klimentowski, E. L. Lokas, S. Kazantzidis, L. Mayer, and G. Mamon, "Tidal evolution of discy dwarf galaxies in the Milky Way potential: the formation of dwarf spheroidals," *Monthly Notices of the Royal Astronomical Society*, vol. 397, no. 4, pp. 2015–2029, 2009.

[40] J. Klimentowski, E. L. Łokas, S. Kazantzidis, L. Mayer, G. A. Mamon, and F. Prada, "The orientation and kinematics of inner tidal tails around dwarf galaxies orbiting the Milky Way," *Monthly Notices of the Royal Astronomical Society*, vol. 400, no. 4, pp. 2162–2168, 2009.

[41] L. Mayer, S. Kazantzidis, C. Mastropietro, and J. Wadsley, "Early gas stripping as the origin of the darkest galaxies in the universe," *Nature*, vol. 445, no. 7129, pp. 738–740, 2007.

[42] E. L. Lokas, "Dark matter distribution in dwarf spheroidal galaxies," *Monthly Notices of the Royal Astronomical Society*, vol. 333, no. 3, pp. 697–708, 2002.

[43] A. R. Zentner and J. S. Bullock, "Halo substructure and the power spectrum," *The Astrophysical Journal*, vol. 598, no. 1, pp. 49–72, 2003.

[44] L. E. Strigari, J. S. Bullock, M. Kaplinghat, J. Diemand, M. Kuhlen, and P. Madau, "Redefining the missing satellites problem," *The Astrophysical Journal*, vol. 669, no. 2, pp. 676–683, 2007.

[45] E. K. Grebel and J. S. Gallagher III, "The impact of reionization on the stellar populations of nearby dwarf galaxies," *The Astrophysical Journal*, vol. 610, no. 2, pp. L89–L92, 2004.

[46] J. E. Gunn and J. R. I. Gott, "On the infall of matter into clusters of galaxies and some effects on their evolution," *The Astrophysical Journal*, vol. 176, p. 1, 1972.

[47] M.-M. Mac Low and A. Ferrara, "Starburst-driven mass loss from dwarf galaxies: efficiency and metal ejection," *The Astrophysical Journal*, vol. 513, no. 1, pp. 142–155, 1999.

[48] J. I. Read, A. P. Pontzen, and M. Viel, "On the formation of dwarf galaxies and stellar haloes," *Monthly Notices of the Royal Astronomical Society*, vol. 371, no. 2, pp. 885–897, 2006.

[49] F. Haardt and P. Madau, "Radiative transfer in a clumpy universe. II. The ultraviolet extragalactic background," *The Astrophysical Journal*, vol. 461, no. 1, part 1, pp. 20–37, 1996.

[50] A. A. Cole, E. D. Skillman, E. Tolstoy, et al., "Leo A: a late-blooming survivor of the epoch of reionization in the local group," *The Astrophysical Journal*, vol. 659, no. 1, pp. L17–L20, 2007.

[51] B. Willman, J. J. Dalcanton, D. Martínez-Delgado, et al., "A new Milky Way dwarf galaxy in URSA major," *The Astrophysical Journal*, vol. 626, no. 2, pp. L85–L88, 2005.

[52] J. D. Simon and M. Geha, "The kinematics of the ultra-faint Milky Way satellites: solving the missing satellite problem," *The Astrophysical Journal*, vol. 670, no. 1, pp. 313–331, 2007.

[53] I. D. Karachentsev, "The local group and other neighboring galaxy groups," *The Astronomical Journal*, vol. 129, no. 1, pp. 178–188, 2005.

[54] A. Bouchard, G. S. da Costa, and H. Jerjen, "The environmental influence on the evolution of local galaxies," *The Astronomical Journal*, vol. 137, no. 2, pp. 3038–3052, 2009.

[55] F. Fraternali, E. Tolstoy, M. J. Irwin, and A. A. Cole, "Life at the periphery of the local group: the kinematics of the Tucana dwarf galaxy," *Astronomy & Astrophysics*, vol. 499, no. 1, pp. 121–128, 2009.

[56] F. Governato, L. Mayer, J. Wadsley, et al., "The formation of a realistic disk galaxy in Λ-dominated cosmologies," *The Astrophysical Journal*, vol. 607, no. 2, pp. 688–696, 2004.

[57] J. Klimentowski, E. L. Lokas, S. Kazantzidis, F. Prada, L. Mayer, and G. A. Mamon, "Mass modelling of dwarf spheroidal galaxies: the effect of unbound stars from tidal tails and the Milky Way," *Monthly Notices of the Royal Astronomical Society*, vol. 378, no. 1, pp. 353–368, 2007.

[58] N. Raha, J. A. Sellwood, R. A. James, and F. D. Kahn, "A dynamical instability of bars in disk galaxies," *Nature*, vol. 352, no. 6334, pp. 411–412, 1991.

[59] V. P. Debattista, L. Mayer, C. M. Carollo, B. Moore, J. Wadsley, and T. Quinn, "The secular evolution of disk structural parameters," *The Astrophysical Journal*, vol. 645, no. 1, pp. 209–227, 2006.

[60] J. Kormendy, "Kinematics of extragalactic bulges: evidence that some bulges are really disks," in *Galactic Bulges*, H.

DeJonghe and H. J. Habing, Eds., p. 209, Kluwer Academic Publishers, Dodrecht, The Netherlands, 1993.

[61] C. Mastropietro, B. Moore, L. Mayer, V. P. Debattista, R. Piffaretti, and J. Stadel, "Morphological evolution of discs in clusters," *Monthly Notices of the Royal Astronomical Society*, vol. 364, no. 2, pp. 607–619, 2005.

[62] V. Belokurov, D. B. Zucker, N. W. Evans, et al., "A faint new Milky Way satellite in bootes," *The Astrophysical Journal*, vol. 647, no. 2, pp. L111–L114, 2006.

[63] M. G. Walker, V. Belokurov, N. W. Evans, et al., "LEO V: spectroscopy of a distant and disturbed satellite," *The Astrophysical Journal*, vol. 694, no. 2, pp. L144–L147, 2009.

[64] T. Lisker, E. K. Grebel, and B. Binggeli, "Virgo cluster early-type dwarf galaxies with the sloan digital sky survey. I. On the possible disk nature of bright early-type dwarfs," *The Astronomical Journal*, vol. 132, no. 2, pp. 497–513, 2006.

[65] E. L. Lokas, J. Klimentowski, S. Kazantzidis, and L. Mayer, "The anatomy of Leo I: how tidal tails affect the kinematics," *Monthly Notices of the Royal Astronomical Society*, vol. 390, no. 2, pp. 625–634, 2008.

[66] J. I. Read, L. Mayer, A. M. Brooks, F. Governato, and G. Lake, "A dark matter disc in three cosmological simulations of Milky Way mass galaxies," *Monthly Notices of the Royal Astronomical Society*, vol. 397, no. 1, pp. 44–51, 2009.

[67] E. L. Łokas, S. Kazantzidis, J. Klimentowski, L. Mayer, and S. Callegari, "The stellar structure and kinematics of dwarf spheroidal galaxies formed by tidal stirring," *Astrophysical Journal*, vol. 708, no. 2, pp. 1032–1047, 2010.

[68] E. D'Onghia and G. Lake, "Small dwarf galaxies within larger dwarfs: why some are luminous while most go dark," *The Astrophysical Journal*, vol. 686, no. 2, part 2, pp. L61–L65, 2008.

[69] S. Kazantzidis, A. V. Kravtsov, A. R. Zentner, B. Allgood, D. Nagai, and B. Moore, "The effect of gas cooling on the shapes of dark matter halos," *The Astrophysical Journal*, vol. 611, no. 2, pp. L73–L76, 2004.

[70] S. E. Koposov, H. W. Rix, and D. W. Hogg, "Constraining the Milky Way potential with a 6-D phase-space map of the GD-1 stellar stream," submitted to *The Astrophysical Journal*.

[71] L. V. Sales, J. F. Navarro, D. G. Lambas, S. D. M. White, and D. J. Croton, "Satellite galaxies and fossil groups in the Millennium Simulation," *Monthly Notices of the Royal Astronomical Society*, vol. 382, no. 4, pp. 1901–1916, 2007.

[72] P. J. Quinn and J. Goodman, "Sinking satellites of spiral systems," *The Astrophysical Journal*, vol. 309, pp. 472–495, 1986.

[73] E. D'Onghia, V. Springel, L. Hernquist, and D. Keres, "Substructure depletion in the Milky Way halo by the disk," *The Astrophysical Journal*, vol. 709, no. 2, pp. 1138–1147, 2010.

[74] L. Mayer, F. Governato, and T. Kaufmann, "The formation of disk galaxies in computer simulations," *Advanced Science Letters*, vol. 1, no. 1, pp. 7–27, 2008.

[75] F. Governato, B. Willman, L. Mayer, et al., "Forming disc galaxies in ACDM simulations," *Monthly Notices of the Royal Astronomical Society*, vol. 374, no. 4, pp. 1479–1494, 2007.

[76] L. Mayer, "Baryons in SPH simulation of structure formation and evolution; approaching the end of the dark era," in *Proceedings of "Baryons in Dark Matter Halos"*, R. Dettmar, U. Klein, and P. Salucci, Eds., Proceedings of Science, p. 37.1, SISSA, Novigrad, Croatia, October 2004.

[77] T. Kaufmann, L. Mayer, J. Wadsley, J. Stadel, and B. Moore, "Angular momentum transport and disc morphology in smoothed particle hydrodynamics simulations of galaxy formation," *Monthly Notices of the Royal Astronomical Society*, vol. 375, no. 1, pp. 53–67, 2007.

[78] S. E. Koposov, J. Yoo, H. W. Rix, D. H. Weinberg, A. V. Macci, and J. M. Escud, "A quantitative explanation of the observed population of Milky Way satellite galaxies," *The Astrophysical Journal*, vol. 696, no. 2, pp. 2179–2194, 2009.

[79] R. R. Muñoz, S. R. Majewski, S. Zaggia, et al., "Exploring halo substructure with giant stars. XI. The tidal tails of the Carina dwarf spheroidal galaxy and the discovery of magellanic cloud stars in the Carina foreground," *The Astrophysical Journal*, vol. 649, no. 1, pp. 201–223, 2006.

[80] D. Martínez-Delgado, A. Aparicio, M. A. Gómez-Flechoso, and R. Carrera, "Tidal streams in the galactic halo: evidence for the sagittarius northern stream or traces of a new nearby dwarf galaxy," *The Astrophysical Journal*, vol. 549, no. 2, pp. L199–L202, 2001.

[81] R. R. Muñoz, S. R. Majewski, and K. V. Johnston, "Modeling the structure and dynamics of dwarf spheroidal galaxies with dark matter and tides," *The Astrophysical Journal*, vol. 679, no. 1, pp. 346–372, 2008.

[82] K. R. Sembach, B. P. Wakker, B. D. Savage, et al., "Highly ionized high-velocity gas in the vicinity of the galaxy," *The Astrophysical Journal, Supplement Series*, vol. 146, no. 1, pp. 165–208, 2003.

[83] S. D. Murray, S. D. M. White, J. M. Blondin, and D. N. C. Lin, "Dynamical instabilities in two-phase media and the minimum masses of stellar systems," *The Astrophysical Journal*, vol. 407, no. 2, pp. 588–596, 1993.

[84] O. Agertz, B. Moore, J. Stadel, et al., "Fundamental differences between SPH and grid methods," *Monthly Notices of the Royal Astronomical Society*, vol. 380, no. 3, pp. 963–978, 2007.

[85] J. I. Read, T. Hayfield, and O. Agertz, "Resolving mixing in smoothed particle hydrodynamics," submitted to *Monthly Notices of the Royal Astronomical Society*.

[86] P. E. J. Nulsen, "Transport processes and the stripping of cluster galaxies," *Monthly Notices of the Royal Astronomical Society*, vol. 198, pp. 1007–1016, 1982.

[87] S. Mashchenko, C. Carignan, and A. Bouchard, "Impact of ultraviolet radiation from giant spirals on the evolution of dwarf galaxies," *Monthly Notices of the Royal Astronomical Society*, vol. 352, no. 1, pp. 168–180, 2004.

[88] C. Leitherer, L. I-Hui, D. Calzetti, and T. M. Heckman, "Global far-ultraviolet (912–1800 Å) properties of star-forming galaxies," *The Astrophysical Journal* , vol. 140, no. 2, pp. 303–329, 2002.

[89] F. Governato, C. B. Brook, A. M. Brooks, et al., "Forming a large disc galaxy from a $z < 1$ major merger," *Monthly Notices of the Royal Astronomical Society*, vol. 398, no. 1, pp. 312–320, 2009.

[90] A. Fernandez-Soto, K. M. Lanzetta, and H. W. Chen, "The UV escape fraction of high-redshift galaxies," in *Galaxy Evolution: Theory & Observations*, vol. 17 of *Revista Mexicana de Astronomía y Astrofísica*, pp. 218–219, 2003.

[91] A. E. Shapley, C. C. Steidel, M. Pettini, K. L. Adelberger, and D. K. Erb, "The direct detection of lyman continuum emission from star-forming galaxies at $z \sim 3$," *The Astrophysical Journal*, vol. 651, no. 2, pp. 688–703, 2006.

[92] M. Geha, M. R. Blanton, M. Masjedi, and A. A. West, "The baryon content of extremely low mass dwarf galaxies," *The Astrophysical Journal*, vol. 653, no. 1, pp. 240–254, 2006.

[93] A. K. Leroy, F. Walter, E. Brinks, et al., "The star formation efficiency in nearby galaxies: measuring where gas forms stars

effectively," *The Astronomical Journal*, vol. 136, no. 6, pp. 2782–2845, 2008.

[94] J. Schaye, "Star formation thresholds and galaxy edges: why and where," *The Astrophysical Journal*, vol. 609, no. 2, pp. 667–682, 2004.

[95] E. Gardan, J. Braine, K. F. Schuster, N. Brouillet, and A. Sievers, "Particularly efficient star formation in M 33," *Astronomy & Astrophysics*, vol. 473, no. 1, pp. 91–104, 2007.

[96] N. Y. Gnedin, K. Tassis, and A. V. Kravtsov, "Modeling molecular hydrogen and star formation in cosmological simulations," *The Astrophysical Journal*, vol. 697, no. 1, pp. 55–67, 2009.

[97] B. E. Robertson and A. V. Kravtsov, "Molecular hydrogen and global star formation relations in galaxies," *The Astrophysical Journal*, vol. 680, no. 2, pp. 1083–1111, 2008.

[98] J. F. Navarro, V. R. Eke, and C. S. Frenk, "The cores of dwarf galaxy haloes," *Monthly Notices of the Royal Astronomical Society*, vol. 283, no. 3, pp. L72–L78, 1996.

[99] O. Y. Gnedin and H. Zhao, "Maximum feedback and dark matter profiles of dwarf galaxies," *Monthly Notices of the Royal Astronomical Society*, vol. 333, no. 2, pp. 299–306, 2002.

[100] J. I. Read and G. Gilmore, "Mass loss from dwarf spheroidal galaxies: the origins of shallow dark matter cores and exponential surface brightness profiles," *Monthly Notices of the Royal Astronomical Society*, vol. 356, no. 1, pp. 107–124, 2005.

[101] J. Dubinski and R. G. Carlberg, "The structure of cold dark matter halos," *The Astrophysical Journal*, vol. 378, no. 2, pp. 496–503, 1991.

[102] P. James, "An infrared study of dwarf galaxies in the Virgo cluster," *Monthly Notices of the Royal Astronomical Society*, vol. 250, no. 1, pp. 544–554, 1991.

[103] V. Belokurov, D. B. Zucker, N. W. Evans, et al., "Cats and dogs, hair and a hero: a quintet of new Milky Way companions," *The Astrophysical Journal*, vol. 654, no. 2, pp. 897–906, 2007.

[104] R. Barkana and A. Loeb, "The photoevaporation of dwarf galaxies during reionization," *The Astrophysical Journal*, vol. 523, no. 1, pp. 54–65, 1999.

[105] R. S. Somerville, "Can photoionization squelching resolve the substructure crisis?" *The Astrophysical Journal*, vol. 572, no. 1, pp. L23–L26, 2002.

[106] M. Ricotti and N. Y. Gnedin, "Formation histories of dwarf galaxies in the local group," *The Astrophysical Journal*, vol. 629, no. 1, pp. 259–267, 2005.

[107] N. Y. Gnedin and A. V. Kravtsov, "Fossils of reionization in the local group," *The Astrophysical Journal*, vol. 645, no. 2, pp. 1054–1061, 2006.

[108] P. Madau, M. Kuhlen, J. Diemand, et al., "Fossil remnants of reionization in the halo of the Milky Way," *The Astrophysical Journal*, vol. 689, no. 1, pp. L41–L44, 2008.

[109] S. Kazantzidis, L. Mayer, and B. Moore, "Galaxies and overmerging: what does it take to destroy a satellite galaxy?" *Astronomical Society of the Pacific*, vol. 327, p. 155, 2004.

[110] V. Belokurov, et al., "The discovery of Segue 2: a prototype of the population of satellites of satellites," *Monthly Notices of the Royal Astronomical Society*, vol. 397, no. 4, pp. 1748–1755, 2009.

[111] M. Geha, B. Willman, J. D. Simon, et al., "The least-luminous galaxy: spectroscopy of the Milky Way satellite segue 1," *The Astrophysical Journal*, vol. 692, no. 2, pp. 1464–1475, 2009.

[112] A. V. Maccio, X. Kang, F. Fontanot, R. S. Somerville, S. E. Koposov, and P. Monaco, "Luminosity function and radial distribution of Milky Way satellites in a ΛCDM Universe," submitted to *Monthly Notices of the Royal Astronomical Society*.

[113] Y.-S. Li and A. Helmi, "Infall of substructures on to a Milky Way-like dark halo," *Monthly Notices of the Royal Astronomical Society*, vol. 385, no. 3, pp. 1365–1373, 2008.

[114] S. Mashchenko, J. Wadsley, and H. M. P. Couchman, "Stellar feedback in dwarf galaxy formation," *Science*, vol. 319, no. 5860, pp. 174–177, 2008.

[115] E. J. Bernard, M. Monelli, C. Gallart, et al., "The ACS LCID project. I. Short-period variables in the isolated dwarf spheroidal galaxies cetus and tucana," *The Astrophysical Journal*, vol. 699, no. 2, pp. 1742–1764, 2009.

Hindawi Publishing Corporation
Advances in Astronomy
Volume 2010, Article ID 194345, 14 pages
doi:10.1155/2010/194345

Research Article

The Effect of Tidal Stripping on Composite Stellar Populations in Dwarf Spheroidal Galaxies

Laura V. Sales,[1] Amina Helmi,[1] and Giuseppina Battaglia[2]

[1] *Kapteyn Astronomical Institute, P.O. Box 800, 9747 AD Groningen, The Netherlands*
[2] *European Organisation for Astronomical Research in the Southern Hemisphere, Karl-Schwarzschild-Straße 2, 85740 Garching bei Muenchen, Germany*

Correspondence should be addressed to Laura V. Sales, lsales@astro.rug.nl

Received 30 April 2009; Revised 30 August 2009; Accepted 1 October 2009

Academic Editor: Andrey V. Kravtsov

We use N-body simulations to study the effects of tides on the kinematical structure of satellite galaxies orbiting a Milky Way-like potential. Here we focus on the evolution of a spherical, dark matter dominated satellite, which is modelled with two stellar components set ab initio to be spatially and kinematically segregated, in a way that resembles the configuration of the metal poor and metal rich stellar populations in several dwarf spheroidals of the Local Group. We find that an important attenuation of the initial differences in the distribution of the two stellar components occurs for orbits with small pericentric radii. This is mainly due to (i) the loss of the gravitational support provided by the dark matter component after tidal stripping takes place and (ii) tides preferentially affect the more extended stellar component, leading to a net decrease in its velocity dispersion as a response for the mass loss, which thus shrinks the kinematical gap. We apply these ideas to the Sculptor and Carina dwarf spheroidals. Differences in their orbits might help to explain why in the former a clear kinematical separation between metal poor and metal rich stars is apparent, while in Carina this segregation is significantly more subtle.

1. Introduction

Dwarf galaxies are by number the most common kind of galaxies in the Local Group. Among all types of dwarf galaxies, such as dwarf irregulars, dwarf ellipticals, transition types, and dwarf spheroidal (dSphs), the latter dominate the satellite population of the large spirals.

Dwarf spheroidal galaxies are faint (with luminosities between 10^3–$10^7 L_\odot$), metal poor and tend not to be rotationally supported. The dark matter mass enclosed within the optical extent of these small objects ranges between 10^5–$10^8 M_\odot$ [1], which extrapolated at large radii would give virial masses of the order of 10^8–$10^9 M_\odot$ and higher [2]. The star formation histories of these small objects are known to be complex and vary from object to object, but all dSphs contain ancient stellar populations, with ages >10 Gyr old. In most dSphs the ancient stellar component is the dominant one or even the only one present (e.g., Sculptor, Draco, Ursa Minor); there are however a few cases where intermediate age stars (3–6 Gyr old) are also present (such as Carina) or dominate the overall stellar population (e.g., Fornax, Leo I) [3–5].

An intriguing observational feature of dSphs is that, notwithstanding their small sizes, the star formation and chemical enrichment histories are not uniform inside these objects, but varied as exemplified by the presence of spatial gradients in the average metallicity and sometimes age properties of their stellar populations. Harbeck et al. [6] used wide-field imaging to study a set of 9 Local Group dwarfs and examined the spatial distribution of stars in different evolutionary phases as selected from the colour-magnitude diagram (CMD). In particular, the authors used horizontal branch (HB) stars, known to be ancient (>10 Gyr old), and determined the relative spatial distribution of the blue and red (horizontal branch) populations (BHB and RHB, resp.) in order to identify the existence of metallicity/age variations. Harbeck et al. found that segregation of populations may not be uncommon in dSphs although it is not *necessarily* present in all of them.

Further new evidence on the presence of multiple populations came a couple of years later, when Tolstoy et al. [7] added to wide-field imaging also the information from wide-field spectroscopy, which yielded metallicities and line-of-sight velocities for hundreds individual stars in the Sculptor dSph. These authors found that metal rich stars in Sculptor are more centrally concentrated and have on average lower velocity dispersions than those of the metal poor component, which on the contrary show hotter kinematics and are more extended. Clear stellar population gradients have been confirmed for Tucana, Sextans, Sculptor and And VI [6], and more recently in Draco and And II [8, 9]. On the other hand, weak or no gradients have been found in other satellite galaxies of the Local Group as well, such is the case for Carina, Leo I [10], And III and And V-VI [6]. Carina, for example, shows a mild segregation between HB and red clump stars, comparable in amplitude to the metallicity gradient found for spectroscopically confirmed Carina red giant stars [11]. When kinematical information is also available it is found that these stellar populations differences sometimes clearly show up as multiple kinematical components as in the case of Sculptor and Fornax [12]. In other cases such as in Carina the kinematical distinction of stars with different metallicities is more subtle.

The eventual occurrence and evolution of this spatial and kinematical segregation of stars in dwarf galaxies constitutes an interesting problem for models of galaxy formation. Tolstoy et al. [7] put forward several hypotheses in order to explain their findings in Sculptor: two episodes of star formation with an inactive period between them, the accretion of gas from the dwarf surroundings able to cool and condensate in the core of them or the photoevaporation of the outer gas layers due to a UV background [7]. In the recent work, Kawata et al. [13] followed the formation of a dwarf galaxy in a self-consistent cosmological numerical simulation up to redshift ∼6. These authors found that the complex interplay between star formation and feedback, coupled to chemical evolution, resulted in a system with a marked metallicity gradient. Kawata et al. thus proposed that a sufficiently steep continuous gradient of a *single* stellar population may appear to observations as two kinematically different metal-poor and metal-rich populations. Even though this constitutes an interesting possibility, the metallicity distribution and velocity dispersion profiles in this model are only marginally consistent with observations, and the system may evolve further (e.g., in mass) from redshift 6 to the present-day.

Tides might also play an important role on the evolution of multiple stellar components in dSphs. Given the proximity to the primary galaxy, tidal effects are likely to be relevant on satellite galaxies such as the MW dSph. In some models, the strong tidal field induced by the proximity to the primary may lead to fundamental changes in the dwarfs internal configuration. These include the development of bars and bending instabilities that strongly affect the internal kinematics of the satellite, transforming rotationally supported systems into hot spheroidals [14, 15]. Such processes are triggered especially for eccentric orbits, implying that the properties of the dwarfs we observe today around bright galaxies could possibly give us indirect clues about their primordial (original) state, that is, before interactions with the primary shaped them differently.

In this paper we explore how gravitational effects may induce a mixing of two initially distinct stellar components in dwarf spheroidal galaxies orbiting an MW-like host potential. Our aim is to gauge the evolution of multiple component dwarfs as they move through the host potential and how this depends on their specific orbital path. In particular, we focus on the differences shown when the same fiducial satellite is placed and evolved on four orbits around the host with different periods and pericenter distances. We therefore do not attempt to explain the origin of such metallicity/kinematical segregation in the dwarfs in the present paper.

We describe the numerical experiments in Section 2, present and discuss our results in Section 3, and summarise our findings in Section 5.

2. Numerical Experiments

Observations of the radial velocities of stars in dSph suggest that these are in general dark matter dominated systems, with only a very small (≤5%) fraction of their baryonic mass in gaseous form [3–5]. This allows a reasonable modeling of their present-day properties and recent evolution by means of collisionless N-body simulations. Here we use GADGET-2 [16] to simulate satellite galaxies orbiting in a (static) Milky Way-like halo. Specifically, we focus on the evolution of satellites with two spherical stellar components embedded in an extended dark matter halo.

2.1. The Model for the Host Potential. We model the (Milky Way) host potential as a (fixed) three-component system with the following:

(i) a Navarro et al. [17] dark matter halo:

$$\rho(r) \propto \frac{1}{x(1+cx)^2} \tag{1}$$

with mass $M_{\rm dm} = 1 \times 10^{12} M_\odot$ and concentration $c = 12$ (Klypin et al. [18]),

(ii) a Hernquist [19] bulge:

$$\rho(r) = \frac{M_{\rm blg} d}{2\pi r} \frac{1}{(r+d)^3} \tag{2}$$

with mass and scale length: $M_{\rm blg} = 3.4 \times 10^{10} M_\odot$ and $d = 0.7$ kpc,

(iii) a Miyamoto and Nagai [20] disk:

$$\rho(R,z) = \frac{b^2 M_{\rm dsk}}{2\pi} \frac{aR^2 + \left(a + 3\sqrt{z^2+b^2}\right)\left(a+\sqrt{z^2+b^2}\right)^2}{\left[R^2 + \left(a+\sqrt{z^2+b^2}\right)^2\right]^{5/2} (z^2+b^2)^{3/2}} \tag{3}$$

with parameters: $M_{\rm dsk} = 1 \times 10^{11} M_\odot$, $a = 6.5$ kpc and $b = 0.26$ kpc (Johnston et al. [21]).

2.2. The Model for the Satellite. The satellite model consists of two baryonic components following Plummer density profiles:

$$\rho_i = \frac{3M_i b_i^2}{4\pi} \frac{1}{\left(r^2 + b_i^2\right)^{5/2}} \tag{4}$$

of different masses M_i and scale lengths b_i that mimic a concentrated metal rich and more extended metal poor stellar components (C_1 and C_2, resp.). Both spheres are embedded within a Hernquist-profile dark matter halo. The masses of each of these components are set to $1.5, 3.5 \times 10^6$ and $2 \times 10^9 M_\odot$ for C_1, C_2, and dark halo. The Plummer spheres scale lengths for C_1 and C_2 are $b_1 = 0.11$ kpc and $b_2 = 0.35$ kpc, respectively. For the dark matter, the scale radius is $a = 2.7$ kpc, which gives a half mass radius ~6.5 kpc.

The satellite galaxy is modelled using ~310 000 particles distributed in a dark matter halo (200 000) and two luminous components (110 000) set by construction to have an initial spatial and kinematic segregation. The procedure to generate the initial condition for simulations of compound galaxies was developed by Hernquist [22] and invokes the moments of the Collisional Boltzman Equations (CBEs) to self-consistently approximate the (unknown) distribution functions of particles in all galaxy components. We briefly describe this procedure in what follows and refer the reader to the original paper [22] for further details.

For an isotropic, spherically symmetric system, the second moment of the CBE can be written as

$$\langle v_r^2 \rangle = \frac{1}{\rho} \int_r^\infty \rho(r) \frac{d\Phi}{dr} dr, \tag{5}$$

where $\langle v_r^2 \rangle$ is the velocity dispersion in the radial direction, ρ is the mass density distribution, and Φ the total gravitational potential of the system. This formula can be extended to the case where several subcomponents coexist in mutual equilibrium. For such configurations, the second velocity moment of the component C_j would be given by

$$\left\langle v_{r,j}^2 \right\rangle = \frac{1}{\rho_j} \int_r^\infty \sum_{i=1}^{n_c} \rho_j \frac{d\Phi_i}{dr} dr, \tag{6}$$

(where j and i vary over the n_c different components of the system). Once the density profiles ρ_j for each of the components have been fixed, the solution to this equation may be found, either analytic or numerically. To set up the particles velocities we assume isotropic Gaussian distribution functions. This procedure then allows us to assign a velocity v to a particle located at a distance r in component C_j, where v is taken randomly from the distribution:

$$F_j(r, v) = 4\pi \left(\frac{1}{2\pi\sigma_j^2} \right)^{3/2} v^2 \exp\left(-\frac{v^2}{2\sigma_j^2} \right) \tag{7}$$

with dispersion $\sigma_j = \langle v_{r,j}^2 \rangle$.

The softening lengths in multiple component systems must be chosen carefully. We follow the prescriptions described in [23], which give in each case is: $\epsilon_{C1} \sim 7$ pc, $\epsilon_{C2} \sim 21$ pc, and $\epsilon_{\rm DM} \sim 60$ pc. Figure 1 shows the resulting (projected) density and velocity profiles for this model (hereafter, R and r refer to projected and three-dimensional distances, resp.). As a consequence of this set-up, the initial configuration of the simulated dwarf has a slightly rising $\sigma_{\rm los}$ profile in the inner regions, that can be explained as the transition from the more concentrated to the more extended stellar components; [24].

The baryonic components of the simulated dwarf are deeply embedded within the potential well of the dark matter halo. The core radius is ~7.3% $r_{\rm max}$, where $r_{\rm max}$ is the radius at which the circular velocity of the dark matter halo peaks; in good agreement with suggestions from numerous theoretical models [25–27]. Such segregation with respect to the dark matter halo turns the stellar components of the satellite galaxies more resilient to tidal stripping, increasing the probability of survival for many orbital times without appreciable changes in their observable properties. Notice that stars account only for less than 0.25% of the total mass, the bulk of the dwarf mass is largely dominated by the dark matter component, with an M/L ~ 35 within the tidal radius (we have assumed here a conversion factor $\gamma = 2.9$ to compute the luminosity out of the mass in the baryonic components, this is roughly consistent with a ~10 Gyr old stellar population of mean metallicity [Fe/H] = −2 (as derived from the BASTI model isochrones) (http://www.te.astro.it/BASTI/index.php.).

The stellar and dark matter masses have been chosen to approximately match the typical line-of-sight velocities dispersions ($\sigma_{\rm los} \sim 10$ km/s), luminosities and structural parameters (such as core R_c and tidal R_t radius) that are observed in Local Group satellites. Throughout this paper we define the characteristic radii R_c and R_t by finding the best-fitting King profiles to the projected density of particles in the luminous components. Notice that with this definition, the tidal radius is not necessarily related to the physical radius that divides the bound from the unbound population of stars in cases where tidal stripping takes place.

The simulated satellite constructed in this way is first relaxed (evolved in isolation) during 1 Gyr before being placed on orbit around the host potential for a longer timescale of $t \sim 6$ Gyr.

The stability of our initial conditions against numerical and relaxation effects can be appreciated in Figure 1. Overplayed using thin lines we show the final configuration (projected density and velocity dispersion profiles) for the same satellite model but evolved in *isolation* during $t \sim 6$ Gyr. The close match between the initial conditions (thick lines) and this control model (thin lines) indicates that any departure from the initial set up will be driven by the evolution of the satellite into the host potential and is not a consequence of an out-of-equilibrium initial configuration.

2.3. Satellite Orbits. The gravitational forces that a satellite galaxy experiences are strongly dependent on its orbit, in particular on the pericenter distances and the orbital radial period (that determine the number of pericenter passages that occur in a given time span), both of which are related

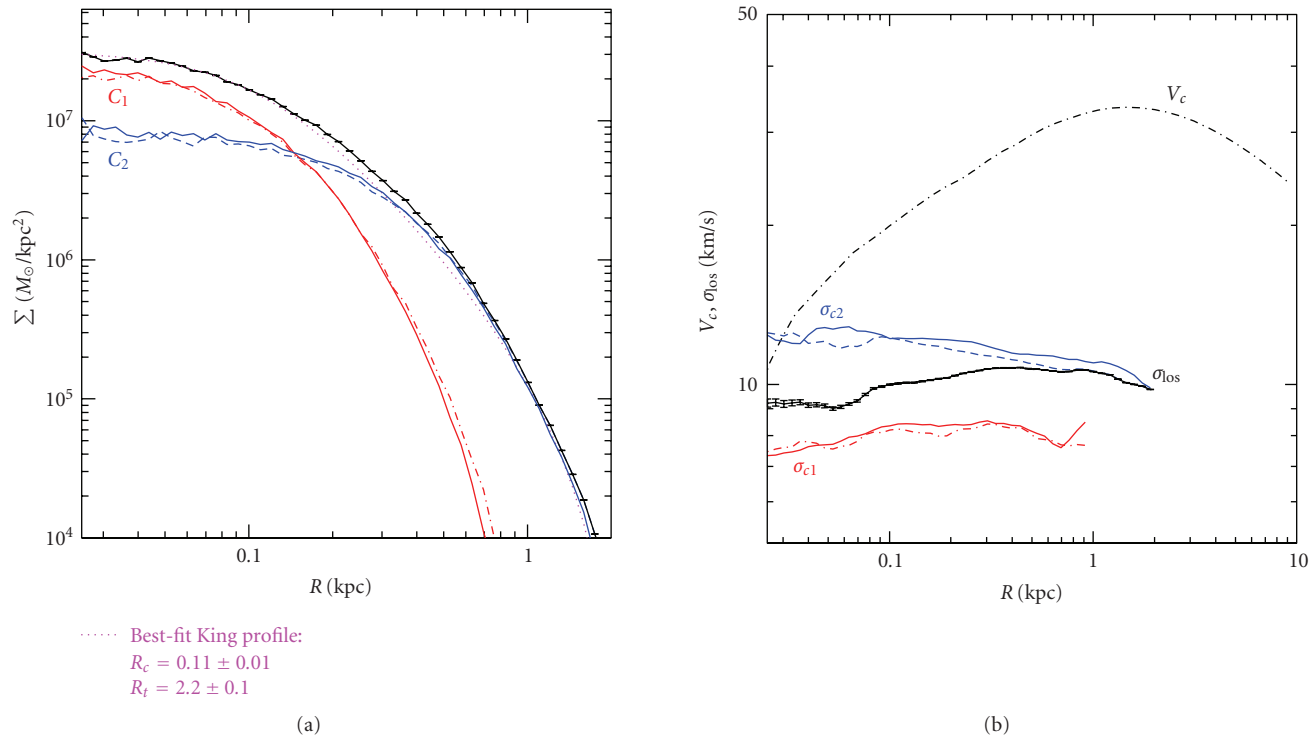

Figure 1: Surface mass density (a) and velocity (b) profiles for the simulated satellite as a function of the (projected) distance from the centre, R. (a), (b), red dot-dashed and blue-dashed curves distinguish the contributions from the more concentrated (C_1) and more extended (C_2) components, respectively, while the thick solid black shows the total values obtained for all the stars (i.e., no distinction between populations). In the left panel, the magenta dotted line shows the best-fit King profile obtained for the total distribution of stellar mass, and the numbers quoted correspond to the derived core and tidal radii, respectively. The right panel shows the circular velocity (black dashed) plus the line-of-sight velocity dispersion profiles associated to each luminous component. Poisson uncertainties are shown for the total density and velocity dispersion profiles in our model, although they are generally smaller than the thickness of the curves. Thin lines in (a), (b) correspond to a control model, which is evolved from this initial configuration in isolation during $t \sim 6$ Gyr.

to the eccentricity of the orbit. While the dark matter halo associated to a satellite provides some sort of "shielding" for the baryons, the removal of the luminous component may start after the dark mass has been reduced to less than 10% its original value. However, the changes in the equilibrium state produced by a significant depletion of the dark matter halo could in principle affect the properties of the baryonic component even before begin to be stripped.

We explore this by placing our fiducial satellite in four different orbits within the host potential (see Figure 2), and integrating its evolution in time for $t \sim 6$ Gyr (this may vary ± 0.3 Gyr depending on the timing of their orbit apocenter passage). This integration timescale is chosen to be consistent with the average time of accretion of the surviving population of satellites found in semianalytical models and numerical simulations of galaxy formation [30–33]. In order to facilitate the interpretation of the results in terms of Local Group galaxies, we have generated two orbits from the present day positions, radial velocities and proper motions of Sculptor and Carina, as reported by Piatek et al. [28, 29]. These correspond to Orb1 and Orb2 in Figure 2, for Sculptor and Carina respectively. Even though the errors in the velocity determinations are appreciable (~50%), which leads to a wide range of possible orbits, the more likely values give rise to interesting differences in their orbits (Orb1 and Orb2). Orbits 3 and 4 correspond to two random orbits generated under the condition of comparable present-day galactocentric distances ($r \sim 90$–100 kpc) to orbits 1 and 2.

Figure 2 shows that despite their similar present-day distance from the host, an orbit such as that suggested by Sculptor's proper motions (Orb1) is significantly more external than Carina's (Orb2), with apocenters exceeding 150 kpc and pericenter distances of ~75 kpc. Orb2 is much more constrained to the inner parts of the Milky Way potential, with pericenters smaller than 30 kpc and orbital periods ~1.6 Gyr, almost 2.4 times shorter than estimated for Scl. Orb3 has comparable pericenters to Orb2, but its apocenters are 50% larger, which translates into a longer orbital radial period. Finally Orb4 is similar to Orb2, and is also consistent with Car proper motions, but has much smaller pericenter values ($r_{\mathrm{per}} \sim 9$ kpc).

A given satellite placed on these four orbits will thus be subject to different tidal field strengths, and consequently, will present structural and dynamical properties that may differ substantially after $t \sim 6$ Gyr of evolution in the host potential. We focus on these aspects in the next section, with special attention to the effects imprinted in the internal kinematics of the stellar components. At this

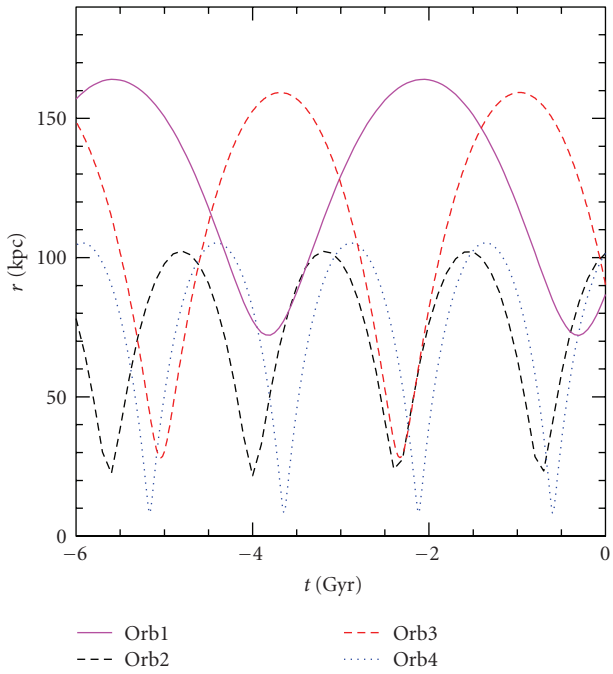

FIGURE 2: Galactocentric distance r as function of time for the four different orbits explored in this paper. Orbits 1 and 2 have been generated from the present-day positions and proper motions of the Sculptor and Carina dwarfs, as reported by Piatek et al. [28, 29] respectively.

point in time, the satellite is located near the apocenter for Orb2 and Orb4, where it will spend most of its time. The system will then reconfigure to its new equilibrium state and the configuration during apocenter passages is the most representative of their final state. On the other hand, at the final snapshot, satellites in Orb1 and Orb3 are at arbitrary points on their orbits. However, given their more external orbital configuration, the final properties for these systems do not strongly depend on the location along their orbits.

3. Results

After ∼6 Gyr of evolution of the model satellite in the host potential, we are able to identify a self-bound satellite remnant for all four explored orbits. However, in spite of the originally identical settings, the structural properties of the surviving dwarf vary appreciably depending on the different orbits. A brief summary of the retained mass fractions and the structural parameter for each model can be found in Table 1.

3.1. Final Distribution of Satellite's Stars. Figure 3 shows a snapshot view of the final system evolved in each of the orbits. Black, blue and red correspond to the dark matter, metal poor and metal rich stellar components, respectively. Visual inspection of this figure suggests that the shapes of the remnants at the final time keep some imprints about the history of each dwarf. For example, for external orbits such as Orb1 and Orb3, the stars in both components are distributed in a spherical fashion, reminiscent of (and determined by) the initial setting of the progenitor. On the other hand, satellites on Orb2 and Orb4 have developed tails of unbound material as a result of a stronger tides suffered during their small pericenter passages. It is interesting to note that since tidal disruption affects earlier and more appreciably the extended C_2 component than C_1, the shape of the metal poor stellar distribution may be more elongated than the metal rich when mass depletion has not yet proceeded into the inner regions of the dwarf. Such is the case of the model in Orb2, which has retained 100% and 88% of the initial mass in components C_1 and C_2, respectively (see Table 1). However, once tidal stripping affects also the more concentrated population, the distribution of metal rich and metal poor stars will both turn elliptical in shape as seen for Orb4.

The final projected mass density profiles for each simulation are shown in Figure 4, together with their best-fitting King profiles. The corresponding core and tidal radii (R_c and R_t resp.) are listed in Table 1, together with the fractions of mass in each component that has remained bound. We have tested the effect of the particular alignment of the tidal tails with the line-of-sight to the observer by computing the density profiles obtained from 10 different random projections of each satellite. These are depicted by thin lines in Figure 4, which show that orientation is not particularly important for the fairly undisturbed systems, and its impact is minor in the case of Orb4.

As quoted in Table 1, the tidal forces have affected significantly less the stellar components than the associated dark matter halo of the dwarf. For example, the satellite on orbits 2 and 3 has retained only 5% and 20% of its dark matter mass, respectively, but more than 90% of the initial stellar mass. Notice that the structural parameters of the baryons (quantified by the projected King profile best fit parameters) are robust to the ongoing pruning of the satellite's outskirts, in particular, the core radii show no variations in any of the experiments (see discussion in [34]). On the other hand, the external parts, and consequently the tidal radius do show more significant changes. In the case of the orbit with the smallest pericenters (Orb4) the tidal radius has shrunk by a factor ∼2 from its original value. Also projection effects are in this case more important, due to different contributions of unbound stars according to the alignment of the tails with the line-of-sight [35]. For the other three orbits, the tidal radius and density profiles have been only barely affected by the stripping.

We observe that the segregation in the spatial distribution between components C_1 and C_2 is also modified, although remains present in all of our experiments (however, this clearly depends on the length of the integration, see Section 3.3). For example, the mass ratio between C_1 and C_2 within the core radius tends to increase in cases where tidal stripping is significant. This is naturally expected as tides will lead to a larger (and earlier) stripping of the most extended (C_2) component compared to C_1. For orbits 2 and 4, m_{C_1}/m_{C_2} increases from ∼2 in the initial model, to 2.6 and

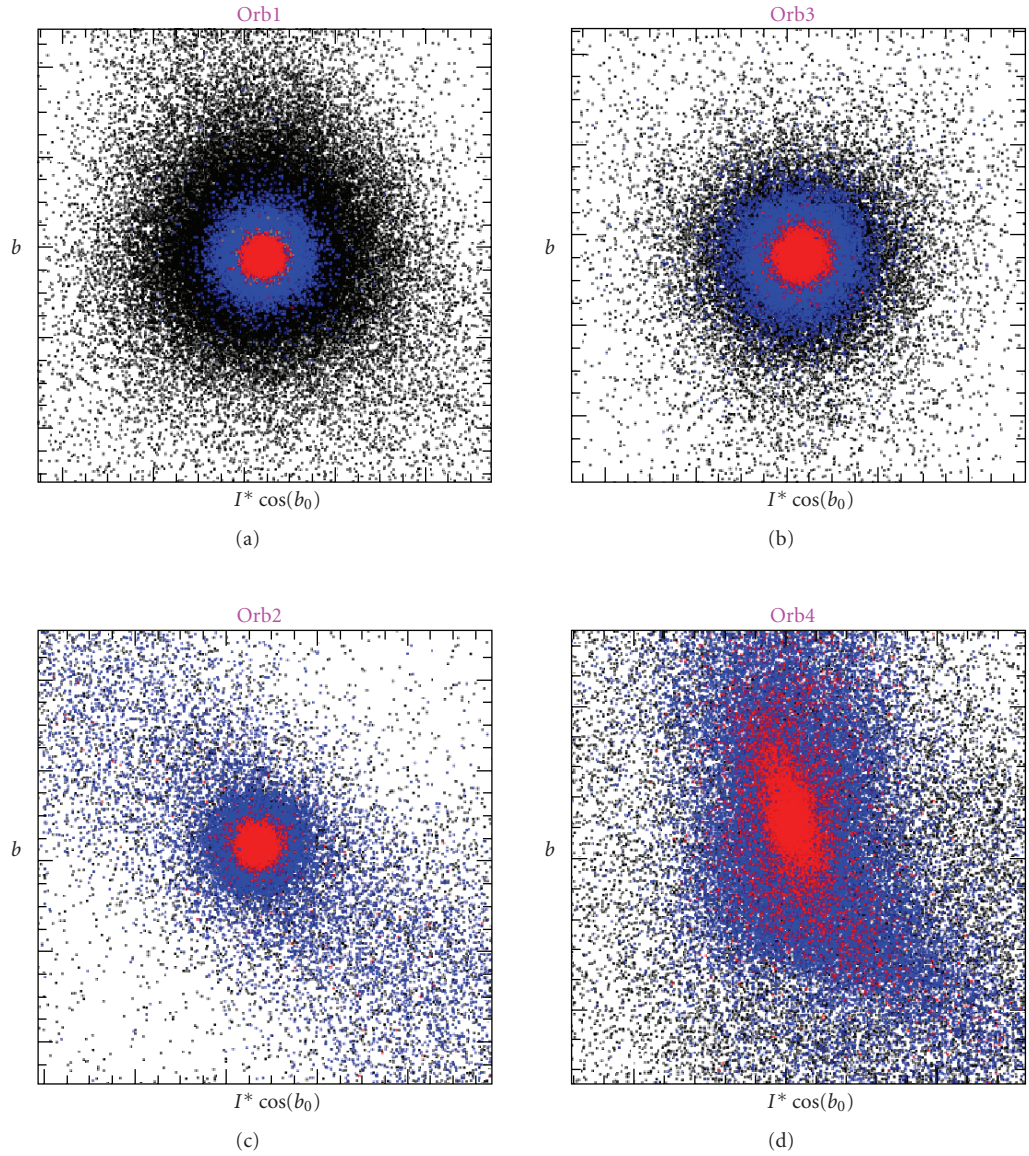

Figure 3: Final projected view (arbitrary units) of the dark matter (black), metal poor (blue) and metal rich (red) stellar components for the models evolved in orbits 1–4 during $t \sim 6$ Gyr. Due to the different degree of tidal disruption experienced in each case, some satellites have turned more elliptical in shape in either one (Orb2) or both (Orb4) their stellar components. Satellites in orbits 1 and 4 remain still quite spherical as the progenitor model.

Table 1: Structural properties of the satellite models after its evolution for $t = 6$ (± 0.3) Gyr within the fixed Galactic potential. The first row in the table shows the initial values and subsequent rows show the present-day values for the experiments on Orb1–Orb4. R_c and R_t refer to the best-fitting King profile values to the surface density profile of the luminous components. The last 3 columns indicate the fraction of mass in each component that remains bound to the dwarf in the final configuration.

Orbit	R_c (kpc)	R_t (kpc)	f_{C1} (%)	f_{C2} (%)	f_{DM} (%)
Initial	0.11 ± 0.01	2.2 ± 0.1	100	100	100
Orb1	0.11 ± 0.01	2.0 ± 0.1	100	99	44
Orb2	0.11 ± 0.01	1.9 ± 0.1	100	88	5
Orb3	0.11 ± 0.01	2.2 ± 0.1	100	98	20
Orb4	0.11 ± 0.01	1.0 ± 0.1	87	20	3

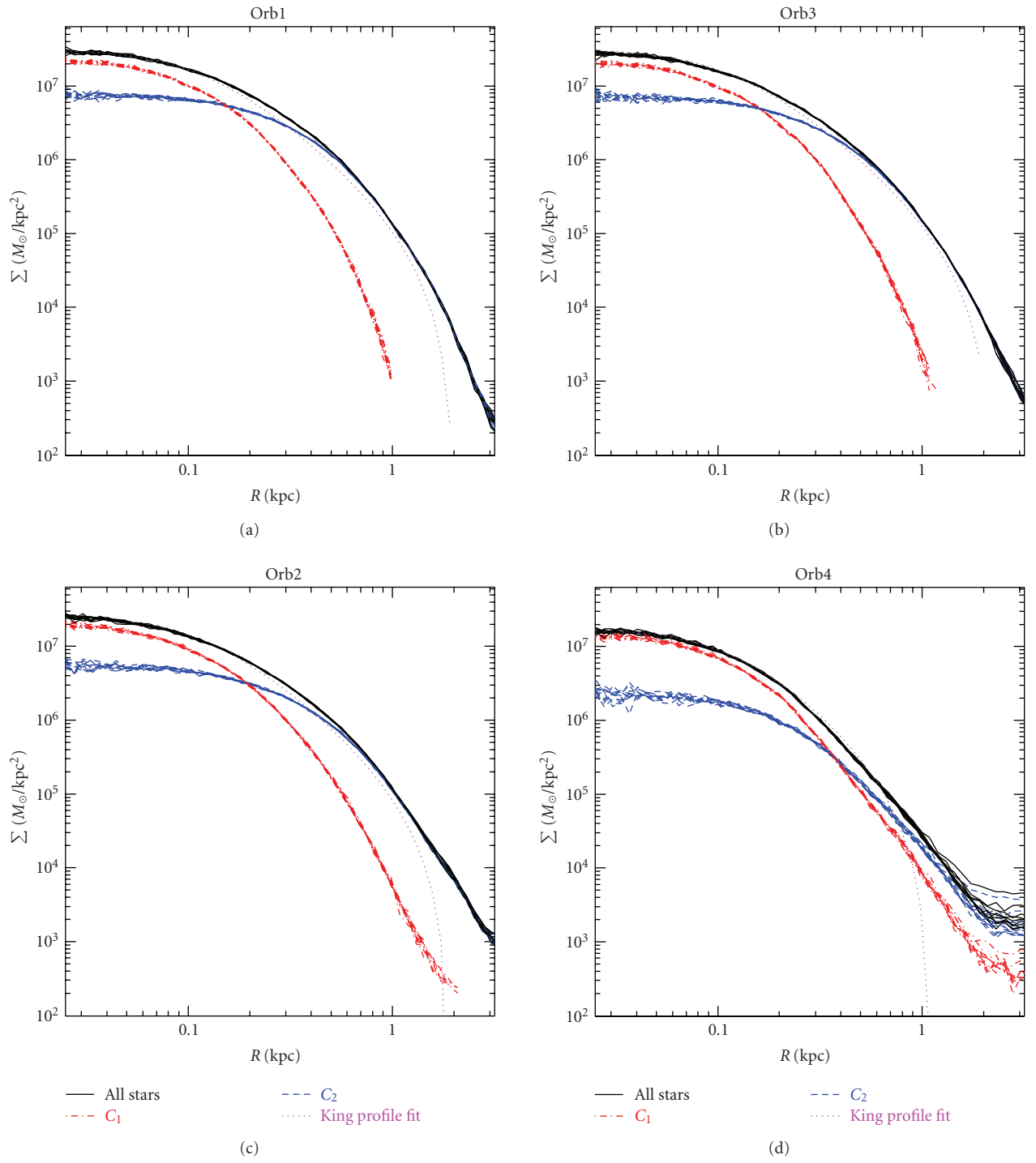

Figure 4: Surface mass density profiles of all our models after ~6 Gyr of integration in the host potential. The color codding is the same as that used in Figure 1.

4.9, respectively (orbits 1 and 3 show no variation). For the same orbits (2 and 4) this ratio for the more external region $0.5 < R < 1$ kpc changes from an initial value $m_{C_1}/m_{C_2} \sim 0.02$, to ~0.12 and ~0.62, respectively.

This gradient of m_{C_1}/m_{C_2} with radius implies that the spatial distinction between both luminous components is still present in the dwarf galaxy. Notice however that some redistribution of the stars in the components has taken place. For example, in the external regions ($0.5 < R < 1$ kpc) of the dwarfs in orbits 2 and 4, the contribution of particles from component C_1 changes from negligible (less than ~2%) to significant (~10–60%) as a result of the ongoing tidal perturbations that require the dwarf to find new equilibrium configurations (see also Figure 3).

3.2. Dynamics of Satellite's Stars. Also worth highlighting is the dynamical response of the system to such structural changes. The velocity dispersion in spherically symmetric systems is determined by the amount of mass contained within a given radius (i.e., the density profile) and by the velocity anisotropy associated to the particles orbits [38]. We naively expect from the results discussed above that not only the structural parameters but also the kinematical properties (such as the line-of-sight velocity dispersion, $\sigma_{\rm los}$) will be affected by the mass removal experienced by the satellite. This is shown in Figure 5, where we plot the (1D, line-of-sight) velocity dispersion profiles as a function of the projected radius from the center of the satellite. To avoid contamination by unbound particles, and following the method applied to observations [36], we have removed all particles whose line-of-sight velocity exceeds by $\pm 3\sigma_{\rm los}$ the mean velocity of the system ($|\overline{V}(R) - V_{\rm los}| > 3\sigma_{\rm los}$).

The panels in Figure 5 correspond to each one of the orbits explored, with thin lines showing the velocity dispersion in each radial bin for each population. The long dashed blue and the solid red curves refer to the more extended (C_2) and concentrated (C_1) luminous components, respectively. In order to illustrate the effects introduced by the geometry of the problem and the different alignments between possible streams and the line-of-sight direction we show curves corresponding to 10 different random projections for each satellite. The error bars in this figure are estimated as follows. We randomly extract a (sub)set of 500 particles from the luminous components of the simulated satellite, maintaining the mass ratio between population C_1 and C_2 and their spatial distribution. The size of each subsample (500 points) is comparable to the size of current observational samples of line-of-sight velocities in dSphs [1, 36]. For each subsample we derive $\sigma_{\rm los}$-R curves, similar to those shown in Figure 5, albeit with larger noise due to the poorer number statistics. The average scatter between these $\sigma_{\rm los}$-R relations obtained from the 100 realizations is then shown as error bars in Figure 5. In order to guide the eye, we have included as well in this figure the initial conditions for the satellite (dotted lines).

Figure 5 shows that when a strong segregation exists between the luminous and dark components, the velocity dispersions of the stars are only weakly affected by the removal of the extended dark halo. For example, experiments Orb1 and Orb3 show that the dark matter halo has been reduced to only ∼45% and 20%, respectively, of the initial mass, yet the kinematics of the luminous components remained essentially intact. *Tidal effects proceed outside-in, preserving the central regions of the satellites (where baryons are located) roughly unchanged*.

However, the situation is different when trimming sets in the stellar components, as is the case for the satellite on orbits 2 and 4 (Figure 5(e), 5(f)). The tidal stripping tends to shrink the initial gap between the velocity dispersion of the luminous components. Furthermore, the limited sizes of available observational samples (∼500 member stars) will lead to additional uncertainties preventing a clear distinction between the kinematics of the two populations, (see [39]). Even though components C_1 and C_2 experience a decrease in their $\sigma_{\rm los}$, they are not affected in the same degree, mainly due to their relative spatial segregation that determines an earlier and stronger removal of stars from component C_2 compared to C_1. In such cases, the preferential stripping of the more extended component (mimicking the metal-poor component of satellites) should lead to the presence of metallicity gradients along the stellar streams of the remnant. Evidence for such trends has recently been found in the streams of the Sagittarius dwarf, where BHB are significantly (at $\sim 4.8\,\sigma$ level) more abundant than red clump stars in comparison to the core of this galaxy [40]. This is interpreted as the preferential removal of the old metal poor (BHB) stars from the outskirts of Sagittarius, compared to the intermediate-age red clump population that has remained in the core of the dwarf less affected by external tides, in strong analogy with our simulations.

The velocity dispersion profiles for each of the luminous components decline with radius (instead of being roughly flat as in the initial model) as stripping proceeds on the simulated galaxies. Beyond the tidal radius (recall this is defined purely by the best-fitting King profile to the projected mass distribution of the stars), the velocity dispersion increases reaching $\sigma \geq 15$ km/s, as a result of the larger contribution from gravitationally unbound stars (that the $\pm 3\sigma$ cut described above is unable to remove). This effect is particularly important for Orb2 and Orb4, where the tidal stripping of stars proceeded. Note that this upturn in $\sigma_{\rm los}$ disappears once the analysis is restricted to particles that remain gravitationally bound to the satellite. In agreement with Klimentowski et al. [35], we find that depending on the orientation of such tails with respect to the line-of-sight, different $\sigma_{\rm los}$ profiles are obtained. When the radial vector to the satellite is well aligned with the direction of these tails, the contamination by unbound material is maximized, producing a raising velocity dispersion profile towards the dwarf's outskirts.

Taken at face value, these velocity dispersion profiles may seem at odds with the typical flatness of the $\sigma_{\rm los}$ profiles observed for Local Group dwarfs. As an example, observed data corresponding to the line-of-sight velocity dispersion inferred for Sculptor and Carina are shown in Figures 5(e), 5(f). Data for these two dwarfs was taken from [11, 36, 37], respectively. However, unless the stripping is considerably large, our simulations do still reproduce reasonably flat (or even rising) *total* velocity dispersion profiles, when no distinction between stars from population C_1 and C_2 is made, (see also [24]). This is shown by the magenta, black, red and blue lines in Figures 5(e), 5(f), corresponding to the total velocity dispersion profiles predicted for Orb1–Orb4 (notice color-codding follows Figure 2). Our models in Orb1 and Orb2 reasonably fit the observed velocity dispersion data for Sculptor and Carina, respectively.

We find that while projections have profound effects on $\sigma_{\rm los}$, it only causes mild variations on the projected density profiles around the formal tidal radius (see Figure 1). A closer look at this indicates that while only ∼5–10% contamination from unbound stars is enough to increase the velocity dispersion profiles by few km/s, at least twice this fraction is needed to drive significant changes on the surface

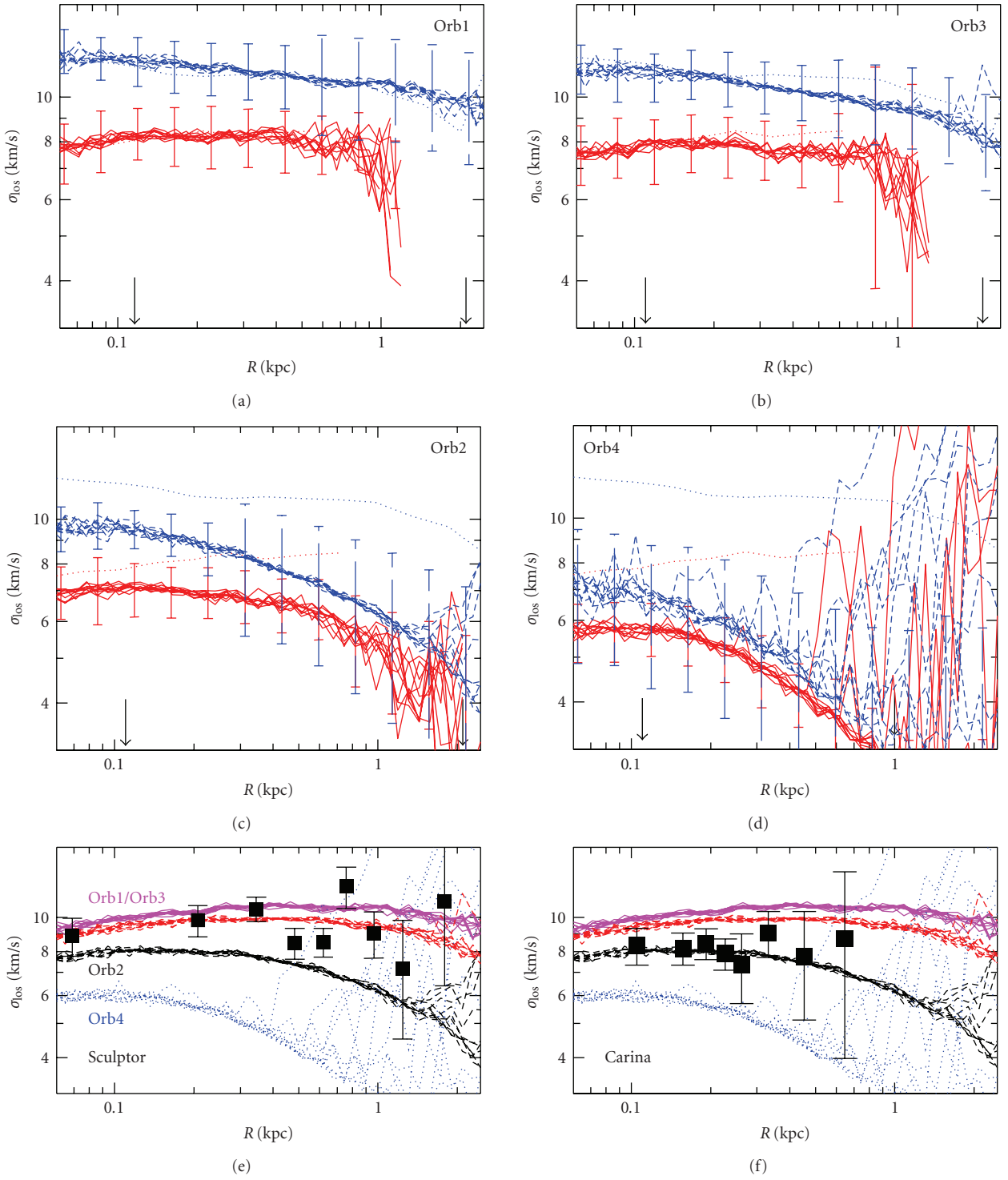

FIGURE 5: (a)–(d) Line-of-sight velocity dispersions for both luminous components as a function of the (projected) distance from the center of the satellite. Solid red and dashed blue curves correspond to the concentrated (C_1) and the more extended (C_2) components, respectively. The error bars indicate the rms dispersion on the σ_{los} profiles of 100 random samples containing 500 particles each (see text for details). For reference, the dotted lines show the initial configuration of the model satellite. Black arrows indicate the positions of the core and tidal radii in each experiment. (e), (f) Velocity dispersion profiles for Sculptor and Carina dwarfs (squares with error bars). Data was taken from Battaglia et al., koch et al., and Helmi et al. [11, 36, 37]. The *total* (no distinction between components) σ_{los} profiles for our models in the 10 different projections are also shown in magenta, black, red and blue lines for Orb1–Orb4, respectively.

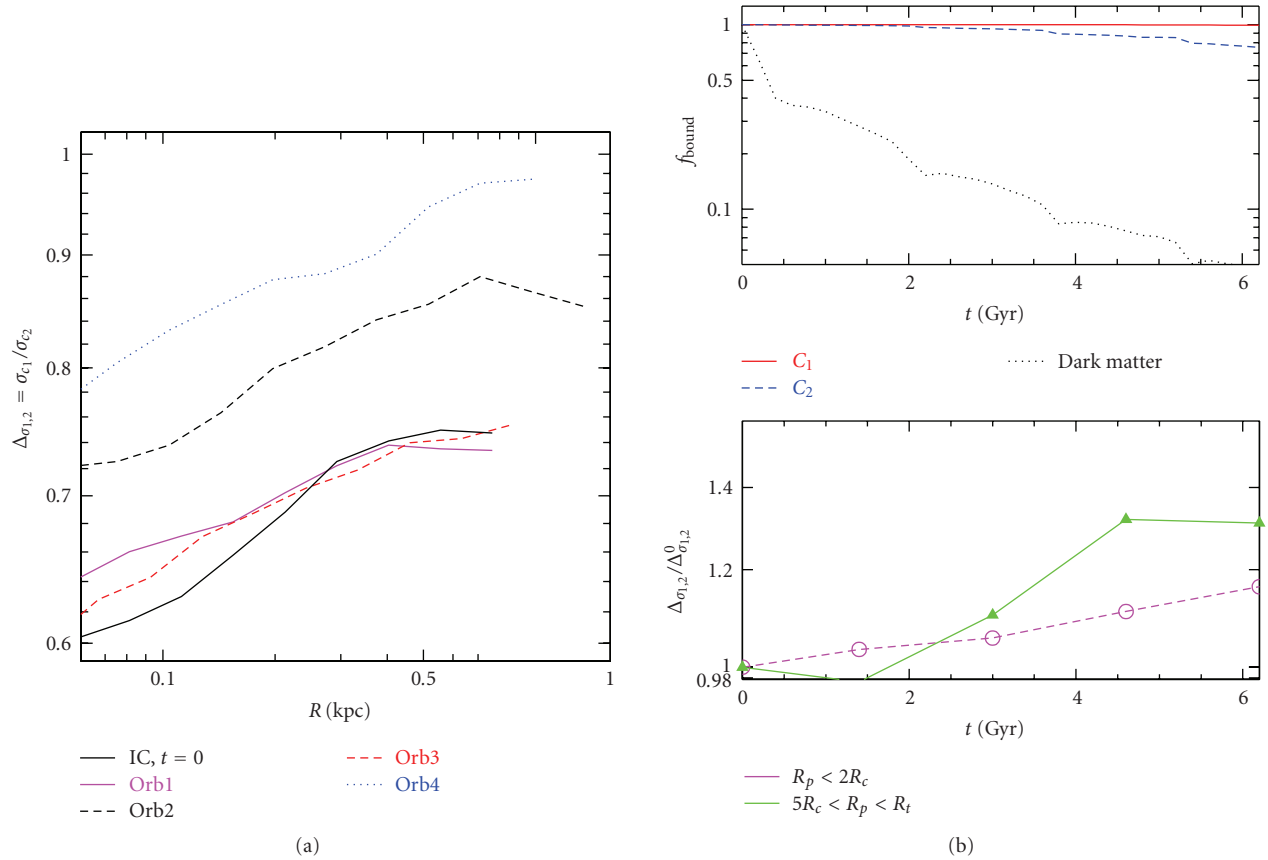

FIGURE 6: (a) Ratio between the line-of-sight velocity dispersions for component C_1 and C_2 ($\Delta_{\sigma_{1,2}} = \sigma_{c1}/\sigma_{c2}$) as a function of the projected distance from the center of the dwarf. The mos distant bin considered has at least 20 particles from each component (and more for for bins closer in). (b) The upper panel shows the fraction of mass (compared to the initial value) that remains bound to the satellite as a function of time for orbit 2. Dotted, red solid and blue-dashed curves are used to indicate the dark matter, and stellar components C_1 and C_2 respectively. In the bottom the evolution with time of the ratio between the velocity dispersions of C_1 and C_2 is shown for two regions within the dwarf: stars within two core radii (magenta dashed) and stars approximately lying closer to the tidal radius (green solid). These ratios have been normalized to the original values ($\Delta^0_{\sigma_{1,2}}$, thin black line in the right panel).

density profiles. For example, the model in orbit 4 shows an increase in σ_{los} at $R \sim 600$ pc, where the fraction of unbound stars accounts for ~8–10% of the mass at that radius. However, bottom right panel of Figure 4 shows that an excess of stars appears in the surface density only for $R > 1500$ pc, when the unbound contribution is ≥20%.

We finally point out that the shape of the line-of-sight velocity profiles may depend on the level of rotational support of the initial progenitor, which we have neglected in this study. A comparison between properties of the remnant of a disky versus a spheroidal progenitor is undoubtedly interesting and deferred to future work.

The preferential pruning by tides of the more extended component is the main responsible for the attenuation of the kinematical distinction between both stellar populations. This can be seen on the Figure 6(a), which shows the final velocity gap between components C_1 and C_2 as a function of distance from the center of the satellite. The vertical axis corresponds to the ratio between the velocity dispersion in these components, $\Delta_{\sigma_{1,2}} = \sigma_{C_1}/\sigma_{C_2}$, for each of the orbits we have explored. For an easier comparison, the black dotted curve shows the initial configuration. When the model satellite is evolved on orbits such as 1 or 3 (solid magenta, long-dashed red) the distinction set by construction between both luminous populations remains essentially unchanged at any radius within the dwarf. In spite of the pruning of 60–80% of the dark matter content on these satellites, these two experiments showed negligible stripping of their stellar components, signaling that a certain degree of stellar mass removal must take place before the relative kinematics of the two populations is noticeably altered.

On the other hand, the simulated satellites on orbits 2 and 4 experienced significant stellar stripping and show kinematical gaps between the luminous components that have been reduced by ~20–30%. Such "mixing" proceeds typically outside-in, starting soon after the tides begin to strip stars from the dwarf. Figure 6(b) shows the evolution of the bound mass with time (upper panel) together with the kinematical gap (bottom panel) for the simulated satellite on orbit 2. Notice that mass removal is not a continuous process but rather presents a stepwise behaviour closely related to the orbital pericenter crossings. After the first

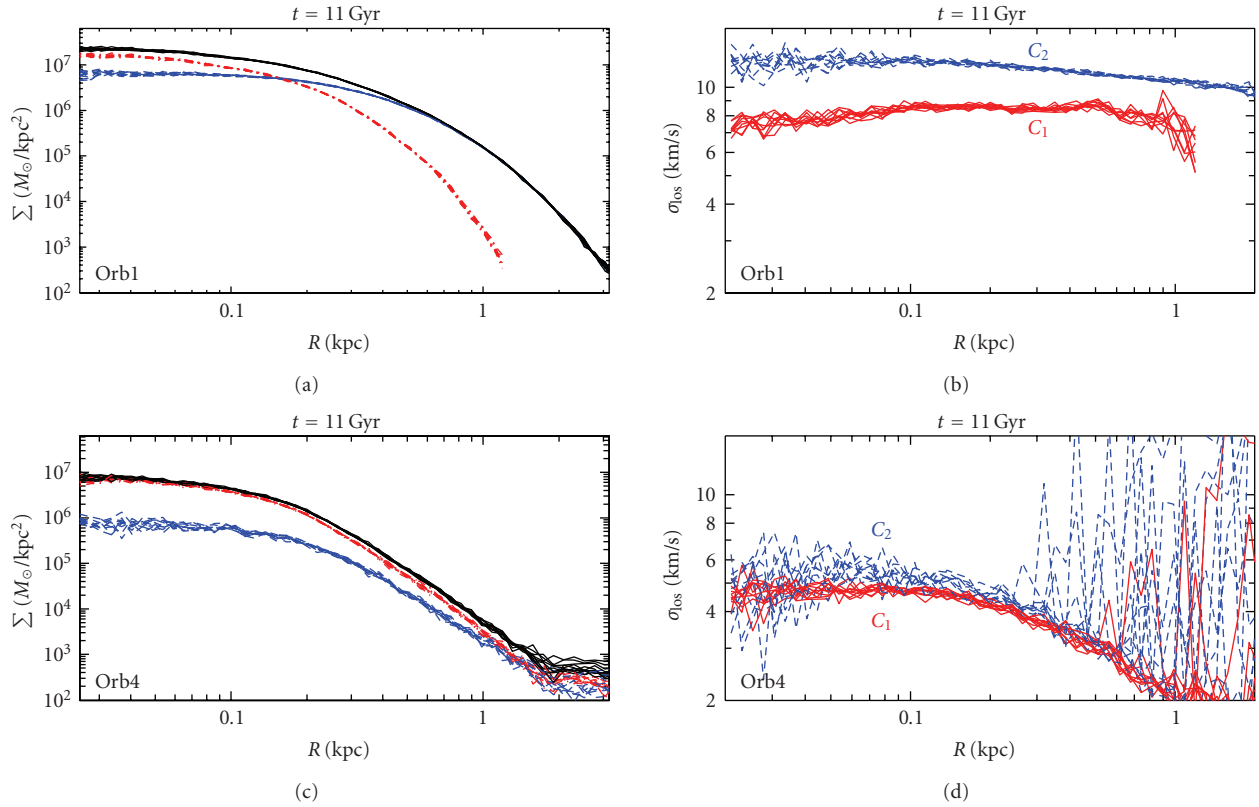

Figure 7: Projected density (a) and velocity dispersion (b) profiles for satellites evolved in Orb1 and Orb4 for a longer time interval: $t \sim 11$ Gyr, instead of the fiducial $t \sim 6$ Gyr. Notice for Orb4 that, as mass depletion proceeds further, the spatial and kinematical segregation between C_1 and C_2 is increasingly erased.

pericenter passage, the dark matter content of the satellite has dropped by almost a factor of 2. However, the stellar mass is more resilient and shows signs of ongoing stripping only after the third pericentric passage, when the dark matter mass has shrunk to only ∼10% of the original value. It is thus when the stripping of the stellar mass begins that the relative kinematical differences between the two luminous components show a significant departure from the original configuration (see bottom right panel of Figure 6). This figure also shows that only the more extended (C_2) stellar component is affected, with C_1 conserving 100% of its initial mass during the whole time integration. This helps to explain why the kinematical gap changes more appreciably in the outskirts than in the core of the satellite galaxy, which will tend to remain less affected by tidal forces.

3.3. Effect of a Different Time Integration. Models that attempt to reproduce the present-day properties of dwarf galaxies are usually degenerate with respect to the unknown initial structure of the objects (density profile, mass, characteristic scales) and their orbital paths. Even though current data allow to reasonably characterize the present-day structural properties of the nearby dwarf galaxies, these are a combined result of (i) their initial configuration, (ii) their orbital motion within the Local Group, and (iii) evolution of the host gravitational potential field, all three factors with hardly any strong observational constraints. Proper motions help us to partially reconstruct the orbits, but unfortunately, errors are still prohibitive, with uncertainties of the order ∼20–100% [28, 29, 41].

As a rule of thumb, for a fixed final configuration, more massive, concentrated objects are needed if we desire to increase the time integration in the host potential keeping the orbit of the object fixed (see, e.g., [42, Section 3.3]). For the analysis presented above, we have chosen a fiducial value for the time integration of $t \sim 6$ Gyr; which is, at some extent, arbitrary. We explore in Figure 7 the effects induced by a longer time integration ($t \sim 11$ Gyr) on the density profile (a) and velocity dispersion (b) for two of our models (Orb1 and Orb4).

For external orbits such as Orb1, with long orbital period and large pericenter distances, the effect of (almost) doubling the time integration is negligible. Objects on such orbits can preserve most of their luminous component bound, showing very little evolution in their spatial and kinematical properties with respect to the initial configuration.

On the other hand, if tides are as strong as on Orb4, the increase in the integration translates into lower densities in the core of the dwarf, and to a further mixing of the spatial and kinematical profiles of both stellar populations. For example, for the satellite evolved in Orb4 during $t \sim 11$ Gyr, the bound mass fraction of components C_1 and C_2 drop to about 38% and 4% of their initial configuration,

respectively. This seems to be enough to completely erase the kinematical gap between both components (see Figure 7(d)) as well as their initial spatial segregation (Figure 7(c)).

We note that this object shows, at the end of the experiment, an overall velocity dispersion $\sigma \sim 5$ km/s, that is about half the initial value, quite low compared to the typical value of the classical satellites in the Local Group. However, given the degeneracies in this type of modelling mentioned above, a larger velocity dispersion $\sigma_{\rm los} \sim$8-9 km/s may be reconciled with a time integration as long as $t \sim 11$ Gyr provided we increase accordingly the initial $\sigma_{\rm los}$ of the progenitor system [42].

The behaviour shown in Figure 7 confirms the conclusions from Section 3; namely, that tides affecting the luminous components are needed in order to effectively erase the structural and kinematical biases between two initially segregated stellar populations.

4. Application to the Local Group: Sculptor and Carina Dwarfs

The results reported in Section 3 can be extrapolated to particular examples within the Local Group. Among the dwarf spheroidals orbiting around our Galaxy, Carina and Sculptor are perhaps the most instructive cases to interpret in light of our results given their proximity and good quality data currently available. Sculptor shows clear spatial variations in the properties of its stellar populations, such as spatial variations in the relative distribution of RHB and BHB stars, a clear metallicity variation with radius as derived from spectroscopic data and also kinematical differences associated to each metallicity population. Carina instead shows no gradient in the distribution of horizontal branch stars themselves, but a distinction is possible between HB stars and red clump stars. Signs of a weak metallicity gradient were found by Koch et al. [11] using ∼500 giant branch stars. However this gradient is only mild and, unlike Sculptor, no kinematical distinction has been identified so far.

The Sculptor and Carina dSphs are found today at comparable distances from the Milky Way (∼100 kpc), although numerical integration of their proper motions suggests that their orbital paths could have been quite different in the past (see Orb1 and Orb2 in Figure 2). The most likely orbit of Carina seems to be confined much more to the inner regions of the Milky Way halo, with smaller pericenter passages and shorter periods than that of Sculptor. Our numerical experiments suggest that a satellite galaxy orbiting in a Carina-like orbit (Orb2) is likely to be exposed to tidal forces that drive significant mass removal. This in turn triggers a mixing and weakening of the kinematical gap that may have existed between its luminous components, which may be challenging to detect with the current spectroscopic samples.

On the other hand, the same model evolved in a more external orbit like Sculptor's maintains the kinematical and spatial properties of the luminous components almost unchanged after ∼6 Gyr of evolution in the host potential.

A simple extrapolation of these results suggests that the lack of a stronger and clear metallicity gradient in Carina, or equivalently, the nondetection of distinct kinematics associated to different stellar populations might be partly due to the effect of strong tidal forces inherent to Carina's orbit. It is possible that in the past, Carina could have had a double component configuration, where the metallicity gradient and kinematical gaps were larger than today's measurements suggest. Notice that according to our simulations, this can only happen if tidal stripping has already taken place on the luminous components of Carina. Interestingly, observational evidence points toward the presence of unbound stars beyond the formal tidal radius of this dwarf [43, 44], (however see discussion in [45]).

These conclusions are subject to an important caveat. Our models do not take into account the gas content of the satellite, and therefore, all star formation activity that might occur after the infall time (our fiducial $t \sim 6$ Gyr) has been neglected. This could be of particular relevance for Carina, given the more extended star formation activity suggested by observations (e.g., Rizzi et al. [46]). Simulations have shown that during pericenter passages episodes of star formation may be triggered for gas rich systems (Mayer et al. [14, 47]). Such events would reestablish a spatial (and presumably kinematical) bias between the old and newly formed stars. This could certainly lower the efficiency of tides to spatially and kinematically mix the dwarf's stellar populations discussed in our models. This is, however, unlikely to render invalid the results explored in Section 3, and their applicability to Carina. Notice that according to the recent models of Carina's star formation history, the bulk of stars is older than ∼5 Gyr [46, 48], which means that subsequent star formation episodes are unlikely to contribute to a large fraction of the total mass. Moreover, after the satellite has lost most of its dark matter mass, the mixing proceeds fast as the luminous components start to become stripped. Therefore, depending on the orbit it is still possible that mixing could have worked, at least partially, in Carina even if modest integration times, comparable or lower than the age of the dominant population, are invoked.

All these arguments are based on a model of a dwarf galaxy with two initially segregated stellar components. However, neither the origin nor how often galaxies are expected to show such configurations has yet been properly understood. Further constraints on the validity (or not) of the extrapolations of our results to cases such as that of Carina's will come from a better understanding of the mechanisms able to generate metallicity gradients and spatial plus kinematical segregation of stellar populations in the dwarf spheroidal galaxies.

5. Discussion and Conclusions

We have studied, by means of N-body numerical simulations, the effects of the tidal forces induced by a host galactic potential on a multicomponent satellite galaxy. The model satellite is set up *adhoc* to initially have two spherical different stellar populations, that are kinematically and spatially segregated. A more centrally concentrated and with lower velocity dispersion C_1 (reminiscent of a "metal rich"

population) and a more extended, higher velocity ("metal poor") C_2 population. These two components are deeply embedded within a dark matter halo that largely dominates the total mass of the system. This satellite model roughly matches the structural properties of classical Local Group dwarfs. We have followed the evolution of such object in time for $t \sim 6$ Gyr on four different orbits around a Milky Way-like host.

We find that the ability to distinguish kinematically the two stellar components (set initially in our model to differ by $\sigma_2 - \sigma_1 \sim 4$ km/s) is strongly dependent on the amplitude of the tides experienced by the satellite during its orbit. In cases where a significant amount of mass has been removed, the velocity gap between the more concentrated (colder) stellar population and the more extended (hotter) component can decrease between ∼30–70% of its initial value, thus partly erasing the initial kinematical segregation between the stellar populations. The magnitude of this effect is tightly related to the tidal stripping experienced by the satellite, and in particular, the removal of luminous mass is necessary for this effect to be significant. Such conditions are more easily obtained for orbits restricted to the inner regions of the host potential, whose close pericenter passages and short orbital periods promote the tidal stripping of the satellite's particles.

We apply these ideas to Sculptor and Carina, two of the classical dwarf galaxies of the Milky Way. Sculptor shows a stronger metallicity gradient, together with a lower velocity dispersion for the more centrally concentrated, metal rich stars compared to the metal poor population. On the other hand, in Carina trends are considerably more subtle, with no kinematical distinction between populations detected to date. We argue that differences in the orbital paths of these two dwarfs can be partially responsible for the weakening of the velocity gap in Carina, while leaving Sculptor unaffected due to its more external and longer period orbit.

Further validation of the tidal "mixing" scenario that has been proposed in this *Paper* depends upon efforts from theoretical as well as observational studies. Comprehensive models to understand the formation of the metallicity gradients as well as their likelihood in dwarf galaxies are of fundamental relevance. The structure of the dark matter halos of dwarf spheroidals (core vs cusped) might also play an important role. Cored profiles could provide less gravitational support to oppose the tidal stripping forces compared to our cusped models, perhaps changing (albeit we expect only quantitatively) the timescales and relevance of the effects studied here. Larger samples of line-of-sight velocities for stars associated to dwarfs spheroidals of the Local Group may improve the detectability of double stellar components kinematically segregated in cases where such feature has not yet been identified. Finally, our models predict that some degree of mass depletion on the stellar components must take place in order to considerably affect the kinematical segregation of dwarfs with composite stellar populations. Deep photometric surveys mapping the outskirts of these satellites, specially beyond their tidal radii, should be able to provide definite clues on the existence (or not) of tidally unbound stars associated to each of these objects, a necessary (although not sufficient) condition for our models to apply.

Acknowledgments

The first author would like to thank Eline Tolstoy for enlightening discussions. The first author and The second author gratefully acknowledge NWO and NOVA and the Coimbra Group for financial support. They also thank both anonymous referees for useful suggestions and comments.

References

[1] M. G. Walker, M. Mateo, E. W. Olszewski, et al., "Velocity dispersion profiles of seven dwarf spheroidal galaxies," *The Astrophysical Journal*, vol. 667, no. 1, pp. L53–L56, 2007.

[2] L. E. Strigari, J. S. Bullock, M. Kaplinghat, et al., "A common mass scale for satellite galaxies of the Milky Way," *Nature*, vol. 454, no. 7208, pp. 1096–1097, 2008.

[3] J. S. Gallagher III and R. F. G. Wyse, "Dwarf spheroidal galaxies: keystones of galaxy evolution," *Astronomical Society of the Pacific*, vol. 106, pp. 1225–1238, 1994.

[4] M. Mateo, "Dwarf galaxies of the Local Group," *Annual Review of Astronomy & Astrophysics*, vol. 36, no. 1, pp. 435–506, 1998.

[5] E. K. Grebel, J. S. Gallagher III, and D. Harbeck, "The progenitors of dwarf spheroidal galaxies," *The Astronomical Journal*, vol. 125, no. 4, pp. 1926–1939, 2003.

[6] D. Harbeck, E. K. Grebel, J. Holtzman, et al., "Population gradients in local group dwarf spheroidal galaxies," *The Astronomical Journal*, vol. 122, no. 6, pp. 3092–3105, 2001.

[7] E. Tolstoy, M. J. Irwin, A. Helmi, et al., "Two distinct ancient components in the sculptor dwarf spheroidal galaxy: first results from the dwarf abundances and radial velocities team," *The Astrophysical Journal*, vol. 617, no. 2, pp. L119–L122, 2004.

[8] D. Faria, S. Feltzing, I. Lundström, et al., "The usage of Strömgren photometry in studies of local group dwarf spheroidal galaxies: application to Draco: a new catalogue of Draco members and a study of the metallicity distribution function and radial gradients," *Astronomy & Astrophysics*, vol. 465, no. 2, pp. 357–373, 2007.

[9] A. W. McConnachie, N. Arimoto, and M. Irwin, "Deconstructing dwarf galaxies: a suprime-cam survey of Andromeda II," *Monthly Notices of the Royal Astronomical Society*, vol. 379, no. 1, pp. 379–392, 2007.

[10] A. Koch, M. I. Wilkinson, J. T. Kleyna, et al., "Stellar kinematics and metallicities in the Leo I dwarf spheroidal galaxy—wide-field implications for galactic evolution," *The Astrophysical Journal*, vol. 657, no. 1, article 1, pp. 241–261, 2007.

[11] A. Koch, E. K. Grebel, R. F. G. Wyse, et al., "Complexity on small scales: the metallicity distribution of the Carina dwarf spheroidal galaxy," *The Astronomical Journal*, vol. 131, no. 2, pp. 895–911, 2006.

[12] G. Battaglia, E. Tolstoy, A. Helmi, et al., "The DART imaging and CaT survey of the Fornax dwarf spheroidal galaxy," *Astronomy & Astrophysics*, vol. 459, no. 2, pp. 423–440, 2006.

[13] D. Kawata, N. Arimoto, R. Cen, and B. K. Gibson, "Origin of two distinct populations in dwarf spheroidal galaxies," *The Astrophysical Journal*, vol. 641, no. 2, pp. 785–794, 2006.

[14] L. Mayer, F. Governato, M. Colpi, et al., "Tidal stirring and the origin of dwarf spheroidals in the local group," *The Astrophysical Journal*, vol. 547, no. 2, pp. L123–L127, 2001.

[15] L. Mayer, F. Governato, M. Colpi, et al., "The metamorphosis of tidally stirred dwarf galaxies," *The Astrophysical Journal*, vol. 559, no. 2, pp. 754–784, 2001.

[16] V. Springel, S. D. M. White, A. Jenkins, et al., "Simulations of the formation, evolution and clustering of galaxies and quasars," *Nature*, vol. 435, no. 7042, pp. 629–636, 2005.

[17] J. F. Navarro, C. S. Frenk, and S. D. M. White, "A universal density profile from hierarchical clustering," *The Astrophysical Journal*, vol. 490, no. 2, pp. 493–508, 1997.

[18] A. Klypin, H. Zhao, and R. S. Somerville, "ΛCDM-based models for the Milky Way and M31. I. Dynamical models," *The Astrophysical Journal*, vol. 573, no. 2, pp. 597–613, 2002.

[19] L. Hernquist, "An analytical model for spherical galaxies and bulges," *The Astrophysical Journal*, vol. 356, no. 2, pp. 359–364, 1990.

[20] M. Miyamoto and R. Nagai, "Three-dimensional models for the distribution of mass in galaxies," *Publications of the Astronomical Society of Japan*, vol. 27, pp. 533–543, 1975.

[21] K. V. Johnston, S. Sigurdsson, and L. Hernquist, "Measuring mass-loss rates from galactic satellites," *Monthly Notices of the Royal Astronomical Society*, vol. 302, no. 4, pp. 771–789, 1999.

[22] L. Hernquist, "N-body realizations of compound galaxies," *The Astrophysical Journal*, vol. 86, no. 2, pp. 389–400, 1993.

[23] E. Athanassoula, E. Fady, J. C. Lambert, and A. Bosma, "Optimal softening for force calculations in collisionless N-body simulations," *Monthly Notices of the Royal Astronomical Society*, vol. 314, no. 3, pp. 475–488, 2000.

[24] A. W. McConnachie, J. Peñarrubia, and J. F. Navarro, "Multiple dynamical components in local group dwarf spheroidals," *Monthly Notices of the Royal Astronomical Society*, vol. 380, no. 1, pp. L75–L79, 2007.

[25] E. L. Łokas, "Velocity dispersions of dwarf spheroidal galaxies: dark matter versus MOND," *Monthly Notices of the Royal Astronomical Society*, vol. 327, no. 2, pp. L21–L26, 2001.

[26] E. Hayashi, J. F. Navarro, J. E. Taylor, J. Stadel, and T. Quinn, "The structural evolution of substructure," *The Astrophysical Journal*, vol. 584, no. 2, pp. 541–558, 2003.

[27] J. Peñarrubia, A. W. McConnachie, and J. F. Navarro, "The cold dark matter halos of local group dwarf spheroidals," *The Astrophysical Journal*, vol. 672, no. 2, pp. 904–913, 2008.

[28] S. Piatek, C. Pryor, E. W. Olszewski, et al., "Proper motions of dwarf spheroidal galaxies from Hubble space telescope imaging. II. Measurement for Carina," *The Astronomical Journal*, vol. 126, no. 5, pp. 2346–2361, 2003.

[29] S. Piatek, C. Pryor, P. Bristow, et al., "Proper motions of dwarf spheroidal galaxies from Hubble Space Telescope imaging. IV. Measurement for sculptor," *The Astronomical Journal*, vol. 131, no. 3, pp. 1445–1460, 2006.

[30] J. S. Bullock and K. V. Johnston, "Tracing galaxy formation with stellar halos. I. Methods," *The Astrophysical Journal*, vol. 635, no. 2, pp. 931–949, 2005.

[31] A. S. Font, K. V. Johnston, J. S. Bullock, and B. E. Robertson, "Chemical abundance distributions of galactic halos and their satellite systems in a ΛCDM universe," *The Astrophysical Journal*, vol. 638, no. 2, pp. 585–595, 2006.

[32] A. S. Font, K. V. Johnston, J. S. Bullock, and B. E. Robertson, "Phase-space distributions of chemical abundances in Milky Way-type galaxy halos," *Astrophysical Journal*, vol. 646, no. 2, pp. 886–898, 2006.

[33] L. V. Sales, J. F. Navarro, M. G. Abadi, and M. Steinmetz, "Satellites of simulated galaxies: survival, merging and their relationto the dark and stellar haloes," *Monthly Notices of the Royal Astronomical Society*, vol. 379, no. 4, pp. 1464–1474, 2007.

[34] J. Peñarrubia, J. F. Navarro, and A. W. McConnachie, "The tidal evolution of local group dwarf spheroidals," *The Astrophysical Journal*, vol. 673, no. 1, pp. 226–240, 2008.

[35] J. Klimentowski, E. L. Łokas, S. Kazantzidis, F. Prada, L. Mayer, and G. A. Mamon, "Mass modelling of dwarf spheroidal galaxies: the effect of unbound stars from tidal tails and the Milky Way," *Monthly Notices of the Royal Astronomical Society*, vol. 378, no. 1, pp. 353–368, 2007.

[36] G. Battaglia, A. Helmi, E. Tolstoy, M. Irwin, V. Hill, and P. Jablonka, "The kinematic status and mass content of the sculptor dwarf spheroidal galaxy," *The Astrophysical Journal*, vol. 681, no. 1, pp. L13–L16, 2008.

[37] A. Helmi, J. F. Navarro, B. Nordström, J. Holmberg, M. G. Abadi, and M. Steinmetz, "Pieces of the puzzle: ancient substructure in the Galactic disc," *Monthly Notices of the Royal Astronomical Society*, vol. 365, no. 4, pp. 1309–1323, 2006.

[38] J. Binney and S. Tremaine, *Galactic Dynamics*, Princeton University Press, Princeton, NJ, USA, 2nd edition, 2008.

[39] U. Ural and M. Wilkinson, "Multiple stellar populations in dwarf spheroidal galaxies," *Astronomische Nachrichten*, vol. 329, no. 9-10, pp. 1040–1041, 2008.

[40] M. Bellazzini, H. J. Newberg, M. Correnti, F. R. Ferraro, and L. Monaco, "Detection of a population gradient in the Sagittarius stream," *Astronomy & Astrophysics*, vol. 457, no. 2, pp. L21–L24, 2006.

[41] M. G. Walker, M. Mateo, and E. W. Olszewski, "Systemic proper motions of milky way satellites from stellar redshifts: the Carina, Fornax, Sculptor, and Sextans dwarf spheroidals," *The Astrophysical Journal*, vol. 687, no. 2, part 2, pp. L75–L78, 2008.

[42] L. V. Sales, A. Helmi, E. Starkenburg, et al., "On the genealogy of the Orphan Stream," *Monthly Notices of the Royal Astronomical Society*, vol. 389, no. 3, pp. 1391–1398, 2008.

[43] S. R. Majewski, P. M. Frinchaboy, W. E. Kunkel, et al., "Exploring halo substructure with giant stars. VI. Extended distributions of giant stars around the Carina dwarf spheroidal galaxy: how reliable are they?" *The Astronomical Journal*, vol. 130, no. 6, pp. 2677–2700, 2005.

[44] R. R. Muñoz, S. R. Majewski, S. Zaggia, et al., "Exploring halo substructure with giant stars. XI. The tidal tails of the Carina dwarf spheroidal galaxy and the discovery of magellanic cloud stars in the Carina foreground," *The Astrophysical Journal*, vol. 649, no. 1, pp. 201–223, 2006.

[45] J. Peñarrubia, J. F. Navarro, A. W. McConnachie, and N. F. Martin, "The signature of galactic tides in local group dwarf spheroidals," *The Astrophysical Journal*, vol. 698, no. 1, pp. 222–232, 2009.

[46] L. Rizzi, E. V. Held, G. Bertelli, and I. Saviane, "Clues to the evolution of the Carina dwarf spheroidal galaxy from the color distribution of its red giant stars," *The Astrophysical Journal*, vol. 589, no. 2, pp. L85–L88, 2003.

[47] L. Mayer, C. Mastropietro, J. Wadsley, J. Stadel, and B. Moore, "Simultaneous ram pressure and tidal stripping; how dwarf spheroidals lost their gas," *Monthly Notices of the Royal Astronomical Society*, vol. 369, no. 3, pp. 1021–1038, 2006.

[48] D. Hurley-Keller, M. Mateo, and J. Nemec, "The star formation history of the Carina dwarf galaxy," *The Astronomical Journal*, vol. 115, no. 5, pp. 1840–1855, 1998.

Hindawi Publishing Corporation
Advances in Astronomy
Volume 2010, Article ID 735284, 7 pages
doi:10.1155/2010/735284

Review Article

Tidal Dwarf Galaxies and Missing Baryons

Frederic Bournaud

CEA Saclay, DSM/IRFU/SAP, F 91191 Gif-Sur-Yvette Cedex, France

Correspondence should be addressed to Frederic Bournaud, frederic.bournaud@cea.fr

Received 23 June 2009; Accepted 4 August 2009

Academic Editor: Elias Brinks

Tidal dwarf galaxies form during the interaction, collision, or merger of massive spiral galaxies. They can resemble "normal" dwarf galaxies in terms of mass, size, and become dwarf satellites orbiting around their massive progenitor. They nevertheless keep some signatures from their origin, making them interesting targets for cosmological studies. In particular, they should be free from dark matter from a spheroidal halo. Flat rotation curves and high dynamical masses may then indicate the presence of an unseen component, and constrain the properties of the "missing baryons," known to exist but not directly observed. The number of dwarf galaxies in the Universe is another cosmological problem for which it is important to ascertain if tidal dwarf galaxies formed frequently at high redshift, when the merger rate was high, and many of them survived until today. In this paper, "dark matter" is used to refer to the nonbaryonic matter, mostly located in large dark halos, that is, CDM in the standard paradigm, and "missing baryons" or "dark baryons" is used to refer to the baryons known to exist but hardly observed at redshift zero, and are a baryonic dark component that is additional to "dark matter".

1. Introduction: The Formation of Tidal Dwarf Galaxies

Tidal dwarf galaxy (TDG) is, per definition, a massive, gravitationally bound object of gas and stars, formed during a merger or distant tidal interaction between massive spiral galaxies, and is as massive as a dwarf galaxy [1] (Figure 1). It should also be relatively long-lived, so that it survives after the interaction, either orbiting around its massive progenitor or expelled to large distances. This requires a lifetime of at least 1 gigayear, and a transient structure during a galaxy interaction would not deserve to be considered as a real TDG. The formation of TDGs in mergers has been postulated for decades [2], including potential candidates in the Antennae galaxies (NGC4038/39) [3], and became an increasingly active research topic after the study of these tidal dwarf candidates by Mirabel et al. [4].

Tidal tails are a common feature in galaxy interactions. There are also some tidal bridges and collisional rings that come about from the same processes and have similar properties, even though some details differ. The tidal tails are those long filaments seen around many interacting galaxies. They are made up of material expelled from the disk of a parent spiral galaxy [6]. This material is expelled partly under the effect of tidal forces exerted by the other interacting galaxy, as the name suggests, but in fact for a large part by gravitational torques as the name does not suggest. The perturbing galaxy exerts nonradial forces in the disturbed disk, so that some gas loses angular momentum, flows toward the center where it can fuel a starburst [7], and some other gas gains angular momentum and flies away in long tidal tails.

At least two mechanisms can lead to the formation of massive substructures in tidal tails (Figures 1 and 2). First, gravitational instabilities can develop, as in any gas-rich medium. Having the material expelled from the disk eases gravitational collapse, as the stabilizing effect of rotation in the parent disk disappears, or weakens. The process is then a standard Jeans instability: when a region collects enough gas to overcome internal pressure support, it collapses into a self-bound object. The same process is believed to drive the formation of molecular clouds in spiral galaxy. The difference is that the interaction stirs and heats the gas, and increases its velocity dispersion [8]. As a result, the typical Jeans mass is high, enabling relatively massive objects to form. These star-forming gas clumps form at the Jeans mass, with a regular spacing, the Jeans wavelength, all along the long tidal tails. They resemble "beads on a string" [9]. Numerical

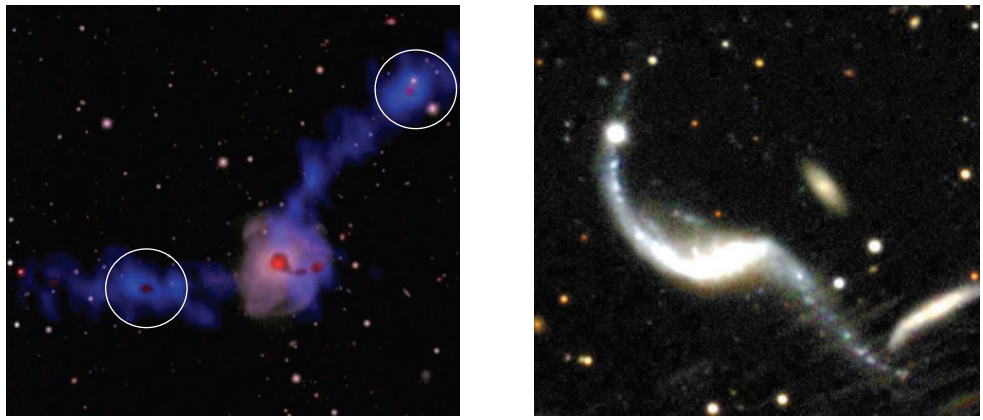

(a) (b)

Figure 1: NGC7252 (a) is a recent merger of two spiral galaxies into a partially-relaxed central spheroidal galaxy. Two massive TDGs are found near the tip of the two long tidal tails (blue = HI, pink = Hα – image courtesy of Pierre-Alain Duc). AM 1353-272 (b) does not have prominent, massive TDGs at the tip of tidal tails, but has instead may lower-mass objects all along its tail [5]. The bright spot on the northern tail is a foreground star.

simulations model their formation accurately, provided that the resolution is high (to revolve the instability length) and gas content is accounted for with some hydrodynamic model [10]. This mechanism can result in relatively numerous TDGs, maybe ten per major merger, but these are not very massive, at most a few 10^7 M_O. The same process can form a large number of less massive structures, which are super star clusters rather than dwarf galaxies, potentially evolving into globular clusters.

Some tidal dwarfs are much more massive, a few 10^8 or 10^9 solar masses, and typically form as single objects at the tip of tidal tails [12]. They cannot form just by local instabilities in a tidal tail. These massive TDGs result from the displacement of a large region of the outer disk of the progenitor spiral galaxy into the outer regions of the tidal tail, where material piles up and remains or becomes self-bound [13, 14]. As the interaction stirs the gas, the increased turbulence will provide the required pressure support to avoid fragmentation into many lower-mass objects. The shape of cold dark matter haloes, which are much more extended than the visible part of galaxies, making this process more efficient [15]. The pile-up of material in massive TDGs often occurs at the tip of tidal tails, and can also occur in different situations like gas captured and swung around the companion [9, 16] or gas bridges linking two interacting galaxies [17, 18].

A few tidal dwarfs of moderate mass, from the first mechanism, are found frequently in observed interacting galaxies. Massive TDGs in the very outer regions are more rare, at most 2–3 per merger, but some mergers do not have any at all. Observations suggest that the presence of one type of TDG reduces the number of TDGs of the other type [19]. This is likely because the formation of a massive, tip-of-tail TDG collects a large fraction of the gas, and less remains available for the formation of numerous low-mass TDGs along the tail, by the first mechanism [19].

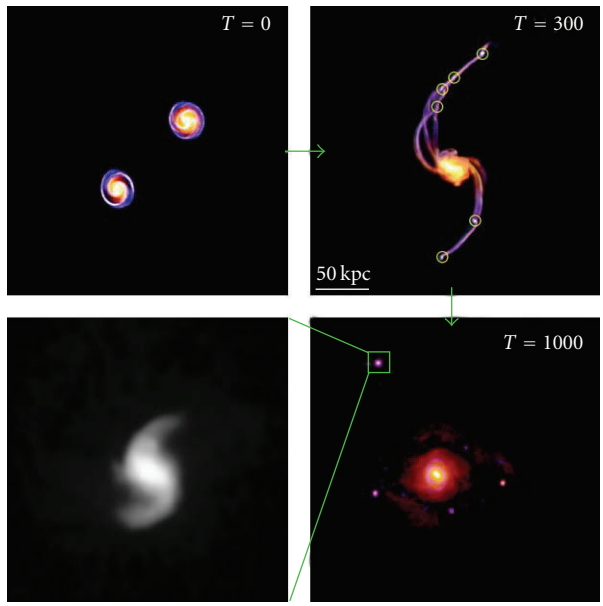

Figure 2: Simulation of the formation of long-lived TDGs, from the Bournaud & Duc sample [11]. The two colliding spiral galaxies are initially seen face-on. Yellow-red to blue colors code old stars versus young stars; time is in megayear. Massive TDGs form at the tip of the tails, and some lower-mass ones also form in particular in the Northern tail. A multi-grid technique increases the resolution on the most massive TDG to 10 parsec. It is resolved with a small internal spiral structure, and survives several gigayears around a massive red elliptical galaxy.

Sections 2 and 3 will review the internal mass content of TDGs and how this can constrain the nature of missing baryons. Different constraints, arising from statistics on TDG formation and survival, will be discussed in Section 4.

(a)

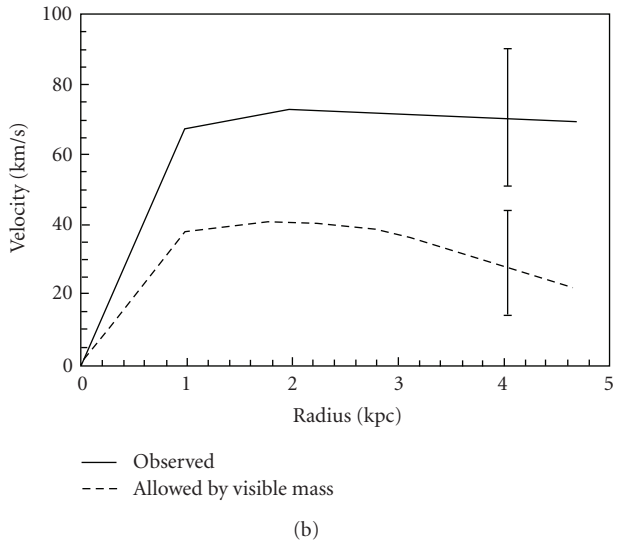

(b)

Figure 3: The collisional ring of NGC5291 and its tidal dwarfs (same as Figure 1) and the rotation curve of one of the TDGs [22]. The observed rotation velocity is too high, and the rotation curve too flat at large radius, to be accounted for by the visible mass distribution alone. Typical 1-sigma error bars are indicated. The rotation curve was measured from HI data and the visible mass estimated from stellar SEDs, HI, and CO data.

2. Why Should Tidal Dwarf Galaxies Be Free of Dark Matter?

A common property of all TDGs is that they are formed by a local instability, or by the gathering of a large portion of the progenitor spiral galaxy at the tip of a tidal tail, is that they are made-up only from material that comes from the *disk* of the parent spiral galaxy. Indeed, only the material initially in rotating disks, with velocity dispersions much lower than the rotation velocity, is strongly affected by tidal forces and gravity torques and forms tidal tails—and subsequently tidal dwarfs. Spheroids dominated by random velocity dispersions instead of rotation will barely develop a weak egg-shaped distortion during the interaction, but no long and dense tidal tail; this applies to the bulge of a spiral galaxy, a whole elliptical galaxy, and also to the dark matter halo of any galaxy.

Dark matter forms a spheroidal halo around galaxies, in both the standard Cold Dark Matter theories [20] and in other models (e.g., Warm Dark Matter [21]). All simulations show that this dark matter cannot participate in the formation of TDGs [10, 11, 14]. Once a TDG has formed, its escape velocity is low, at most a few tens of km s^{-1} for the biggest ones. The TDG will be embedded in the large halo of the parent spiral galaxy (since halos are much more extended than stellar and gaseous disks), so some dark matter particles will cross the TDG, but without being held by the gravitational well of the TDG. Indeed, the randomly-oriented velocities of dark matter particles in the halo of a spiral galaxy like the Milky Way are around 200 km s^{-1}, so the vast majority of these particles escape the tidal dwarf. At any instant, some dark matter particles from the halo will incidentally be at the position of the TDG, but this makes up only a negligible fraction of the mass of any TDG, at most a few percent.

TDGs should then be free of dark matter. This means that the dynamical mass measured from their rotation velocity and size, should not exceed their visible mass in stars and gas—in contrast with "normal" dwarf galaxies and spiral galaxies. Finding a dynamical mass in significant excess would mean that TDGs contain an unseen component. This could be dark matter only if (part of the) dark matter is in a rotating disk component in their progenitor spiral galaxies, just like stars and gas. Otherwise, this would require an unseen baryonic component in spiral galaxies, not just in the form of a hot gas halo—this one does not participate in the formation of TDGs—but in the form of very cold gas in the rotating disk. If not caused by some sort of matter, the dynamical mass excess could be attributed to Modified Gravity, which is a theoretical alternative to dark matter in all types of galaxies. These various possibilities will be discussed in the following section, in the context of observations of NGC5291.

3. The Dynamical Mass of Tidal Dwarf Galaxies

3.1. The Collisional Ring NGC5291. The collisional ring in NGC5291 was formed by a particular head-on collision, which formed a ring instead of the usual tails. Nevertheless, it formed Tidal Dwarfs just like more typical mergers with tails. The high metallicity of the dwarfs in this ring, and the young age of their stars, confirmed that they are formed recently from tidal material. They are also too numerous to simply be "normal" dwarf galaxies that randomly happen to lie in the collisional ring (Figure 3).

The three largest TDGs in this system are spatially resolved in spectroscopic observations of their ionized Hα gas [12] and their neutral atomic (HI) gas [22]. The molecular gas observations by Braine et al. [23] did not require a dynamical mass larger than the visible mass. However new observations of the atomic gas [22] resolve internal velocity gradients in the TDGs, tracing their rotation up to their outermost regions. This confirms they are rotating, self-gravitating, decoupled from the large and diffuse HI ring in which they formed, and enables the dynamical mass to be

measured from the rotation velocity and radius. This is what Bournaud et al. [22] did, and they found that the mass of these TDGs is in significant excess compared to their visible mass in stars, molecular gas, and atomic gas. The excess is just a factor of 2 or 3, not a factor 10 like in classical dwarf galaxies (Figure 3). This confirms the expected lack of dark matter in TDGs. Still, there should be an unseen component there, amounting to the mass of the visible one or even a bit more. Furthermore, rotation curves are surprisingly flat: the rotation velocity remains high far from the center of these three TDGs, while equilibrium with the visible mass can be achieved only if the velocity decreases in the outskirts. This adds evidence for the presence of some sort of unseen mass, mostly in the outer regions of these tidal dwarfs.

This observation remains compatible with most dark matter being in a large halo around spiral galaxies, but means that there was another dark component in the spiral galaxies from which the material now belonging to NGC5291's dwarfs was expelled.

Unseen Molecular Gas. The "visible" mass of the TDGs in NGC5291 is for a large part atomic gas (HI), and also molecular gas. Most of the molecular gas mass is made-up of H_2, which cannot be directly observed. The molecular mass is traced by the emission of the CO molecule, using a standard "CO-to-H_2" conversion factor, which is somewhat uncertain. If the unseen mass in these TDGs is molecular gas, this would imply that the conversion factor changes much more than expected—by a factor 10, while the TDGs have a nearly-solar metallicity so no change by more than a factor of 2 or 3 was anticipated. A classical phase of molecular gas not well traced by CO would have other effects, like destabilizing the disk and triggering very active star formation, which is not observed [24]. More likely, the unseen component would be a nonstandard phase of molecular gas, very cold, and gathered in low-mass, dense, but nonstar-forming H_2 blobs ([25, 26], and Review by Pfenniger et al. [27]). Finding it in TDGs would imply it was also present in the disk of the progenitor spiral galaxy, at least in its outer regions. This can be compatible with observations of the Milky Way [25, 26, 28] and the general dynamics of spiral galaxies [29], at least if one assumes this "dark molecular gas" comes in addition to a nonbaryonic dark matter halo, not instead of it.

Modified Gravity. Another possible explanation to the large rotation velocities in NGC5291's TDGs is Modified Gravity (MOND). As it should affect any galaxy regardless of its origin (tidal or else), a high dynamical-to-visible mass ratio is naturally expected for TDGs in this context. While TDGs do not seem to have a dynamical-to-visible mass ratio as high as classical dwarfs, Gentile et al. [30] and Milgrom [31] have shown that the MOND theory can successfully account for their rotation curves.

A Disk of Cold Dark Matter. There could finally be another explanation that does not require a modification of the gravity, and not even any additional mass component. While dark matter is mostly in a spheroidal halo around spiral galaxies, there would be a part that is actually in a thick dark disk around the stellar disk. This could be brought in by small satellites that merge with the disk, and simulations by Read et al. [32] suggest such "dark disks" can be relatively massive (see also Purcell et al. [33]). In the CDM theory, this dark disk may naturally come in addition to the more massive spheroidal halo. Then, if the velocity dispersion of dark matter particles in this component is not too high, it could participate to the formation of TDGs just like the rest of the disk material (B. G. Elmegreen, priv. comm.). This hypothesis remains to be directly tested in simulations. It is in particular unclear how much of this disk dark matter will be dispersed during the merger, and how much will end-up in TDGs, potentially giving them a dark matter component massive enough to explain their observed rotation curves.

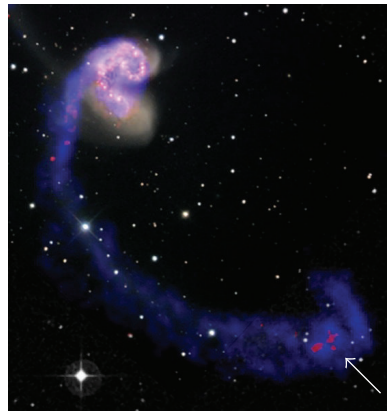

Figure 4: The Southern tail of the Antennae contains several star-forming clumps in a larger HI condensation. This, together with the almost face-on orientation of the system, makes it difficult to estimate a dynamical mass from the HI velocity curve. A recently revised distance estimate [34] may nevertheless indicate a dynamical mass higher than previously believed in the HI cloud. (Figure courtesy of Pierre-Alain Duc.)

3.2. Other Potential Cases. Error bars on NGC5291's data are such that the result is significant at ~2.5 sigma when one takes into account that 3 TDGs have been observed there. There are nevertheless errors that would affect the three observed TDGs in the same way, like the distance of the system, or its inclination. So the three "detections" are largely independent, but not completely. Can the result be confirmed in other systems?

The most famous pair of colliding galaxies, the Antennae (NGC4038/39, Figure 4), has some tidal dwarf galaxies. It has long been thought that their dynamical and visible masses were similar. The original distance estimate to these galaxies could however be overestimated [34], which would make the dynamical mass two or three times higher than the visible mass, just as in NGC5291. The revision of the distance to the Antennae however remains largely uncertain [35]. There are other sources of uncertainty: first, TDGs in the Antennae are very young, still forming, maybe not at equilibrium. Rotation velocities may not trace the mass accurately—TDGs

in NGC5291 were older, making the analysis more robust. Also, there is one blob of HI gas comprising three star forming regions. It is thus quite unclear if the HI velocities trace the total mass of these three objects, or the individual mass of each one—another problem that did not affect NGC5291, where each TDG corresponds to a single, resolved HI cloud. Another attempt in an old TDG in the Virgo Cluster [36] resulted again in a likely excess of dynamical mass, compared to the visible mass, but with large error bars.

Robust confirmations of an "unseen mass" in TDGs remain needed. They can be obtained, if relatively old TDGs are observed at high resolution and with a high signal-to-noise ratio, for instance, with modern interferometers. This would definitely tell whether or not TDGs contain an unseen component, which has important implications, whatever the outcome, for the mass content of typical spiral galaxies.

4. Could (Some) Dwarf Satellite Galaxies Be of Tidal Origin?

We show in the above section that the internal properties of TDGs (their visible mass compared to their rotation speed) may be related to the nature of some "missing" baryonic component. Tidal Dwarf Galaxies have another, completely different implication for the baryonic content of the universe, which does not relate to their own internal properties, but to the number of dwarf galaxies formed by a tidal mechanism, compared to the total number of dwarf galaxies of any origin in the Universe.

TDGs may indeed contribute to the total population of dwarf galaxies, in particular, dwarf satellites around massive galaxies—for instance, some of the dwarf satellites of the Milky Way might, in principle, be tidal debris from collisions that occurred long ago. This would of course change the expected number of dwarf galaxies and the low-mass end of the mass function of galaxies—maybe not in the right direction if the predicted number of dwarf galaxies is already too high.

The key point is the survival of tidal dwarf galaxies. They must survive around, typically, one billion year for the merger in which they formed to be relaxed, so that they can appear as "normal" dwarf satellite galaxies around a "normal" galaxy (not an ongoing merger). They must survive 5 or 10 gigayears for mergers at high redshift to produce dwarf satellites at redshift zero. Is it frequently the case? Several factors can destroy TDGs: "internal" processes like the initial starbursts when gas-dominated TDGs begin to form stars and supernovae potentially eject their gas, and "external" processes, like a disruptive tidal field exerted by the very same galaxy that had formed the TDGs during an interaction.

Large samples with tens of simulations [11] are useful to tackle this question. The most massive tidal dwarf galaxies, that are large, massive ($10^{8\text{-}9}$) solar masses), rotating, formed preferentially at the tip of tidal tails do not come in large numbers. Rarely more than 2 or 3 form in a major merger, sometimes none at all. Roughly half of them are destroyed within a couple of billions years, falling back onto their progenitor galaxy or being disrupted by its tidal field. For most of today's dwarf satellites to be TDGs from past mergers, one would need to form ~10 TDGs per major merger, each surviving a Hubble Time [37]. Hence, simulations suggest that only a modest fraction of modern dwarf satellite galaxies are of tidal origin—but not a completely negligible fraction: overall several percent. This fraction could be higher around red early-type galaxies that experienced more mergers than spiral galaxies: this is because TDGs are expected to form mostly in mergers of spiral galaxies, and after the merger these progenitor galaxies generally become red early-type galaxies [38].

Lower mass TDGs that form with $\sim 10^6$ solar masses of baryons can be more numerous in each galaxy merger. They are more difficult to study in numerical simulations, as they require high spatial and mass resolution. Nevertheless, they can survive their initial starburst—but lose a large fraction of their mass [39]. They can also survive against the tidal field during more than a gigayear after their formation [40]. Simulations have never followed these low-mass objects for a long time; it seems plausible that some could form at high redshift and survive down to redshift zero, but probably as low mass remnants, potentially hard to detect at all, or evolving into compact, globular star clusters rather than dwarf galaxies [40].

While it then seems unlikely that the majority of today's dwarf galaxies are of tidal origin, they can have a significant contribution. There are known examples of TDGs forming at high redshift [41] and maybe some have survived down to redshift zero. Known examples of dwarf galaxies with unusual colors or metallicity could be long-lived tidal dwarfs [36, 42]. The quest for robust and numerous cases of old tidal dwarfs remains open, however.

5. Summary

The formation of tidal dwarf galaxies (TDGs) is frequently observed in galaxy mergers, and has been extensively studied with the help of numerical simulations. While the long-term evolution and potential survival of these objects remains largely debated, their formation mechanisms are now well understood.

A clear prediction from all models is that TDGs cannot contain a significant mass fraction from the dark matter halo of their progenitor spiral galaxy. Observations suggest in several cases that the total, dynamical mass of TDGs exceeds their visible mass in gas and stars, which would indicate that they do contain some unseen component. This result, well established only for NGC5291, still needs a robust confirmation in other cases. An unseen component in TDGs could potentially constrain the presence of "missing baryons" in a cold gas phase.

Another cosmological implication of TDGs relates to their long-term survival, and how they can affect the mass function of dwarf galaxies. This question is still largely unsolved, but there is significant hope that modern numerical models that can resolve the internal physics of TDGs in simulations of major mergers could lead to significant progress in the following years.

Acknowledgments

The author acknowledges the editors of the "Dwarf Galaxies and Cosmology" special volume for inviting him to write this tutorial review. Useful comments on an earlier version by Elias Brinks, Pierre-Alain Duc, Jonathan Braine, and two referees are appreciated, as well as discussions with Bruce Elmegreen, Moti Milgrom, and Daniel Pfenniger on the origin of the mass discrepancy in tidal dwarf galaxies.

References

[1] P.-A. Duc, E. Brinks, V. Springel, B. Pichardo, P. Weilbacher, and I. F. Mirabel, "Formation of a tidal dwarf galaxy in the interacting system ARP 245 (NGC 2992/93)," *The Astronomical Journal*, vol. 120, no. 3, pp. 1238–1264, 2000.

[2] F. Zwicky, "Multiple galaxies," in *Ergebnisse der Exakten Naturwissenschaften*, vol. 29, pp. 344–385, 1956.

[3] F. Schweizer, "Galaxies with long tails," in *Structure and Properties of Nearby Galaxies*, E. M. Berkhuijsen and R. Wielebinski, Eds., vol. 77 of *IAU Symposium Series*, pp. 279–284, 1978.

[4] I. F. Mirabel, H. Dottori, and D. Lutz, "Genesis of a dwarf galaxy from the debris of the antennae," *Astronomy & Astrophysics*, vol. 256, pp. L19–L22, 1992.

[5] P. M. Weilbacher, U. Fritze-v. Alvensleben, P.-A. Duc, and K. J. Fricke, "Large velocity gradients in the tidal tails of the interacting galaxy AM 1353-272 ("the dentist's chair")," *The Astrophysical Journal*, vol. 579, pp. L79–L82, 2002.

[6] A. Toomre, "Mergers and some consequences," in *Evolution of Galaxies and Stellar Populations*, B. M. Tinsley and R. B. Larson, Eds., vol. 197, p. 401, Yale University Observatory, New Haven, Conn, USA, 1977.

[7] P. di Matteo, F. Bournaud, M. Martig, F. Combes, A.-L. Melchior, and B. Semelin, "On the frequency, intensity, and duration of starburst episodes triggered by galaxy interactions and mergers," *Astronomy & Astrophysics*, vol. 492, no. 1, pp. 31–49, 2008.

[8] C. Struck, M. Kaufman, E. Brinks, M. Thomasson, B. G. Elmegreen, and D. M. Elmegreen, "The grazing encounter between IC 2163 and NGC 2207: pushing the limits of observational modelling," *Monthly Notices of the Royal Astronomical Society*, vol. 364, no. 1, pp. 69–90, 2005.

[9] B. J. Smith, C. Struck, M. Hancock, et al., "Stochastic "beads on a string" in the accretion tail of ARP 285," *The Astronomical Journal*, vol. 135, no. 6, pp. 2406–2423, 2008.

[10] M. Wetzstein, T. Naab, and A. Burkert, "Do dwarf galaxies form in tidal tails?" *Monthly Notices of the Royal Astronomical Society*, vol. 375, no. 3, pp. 805–820, 2007.

[11] F. Bournaud and P.-A. Duc, "From tidal dwarf galaxies to satellite galaxies," *Astronomy & Astrophysics*, vol. 456, no. 2, pp. 481–492, 2006.

[12] F. Bournaud, P.-A. Duc, P. Amram, F. Combes, and J.-L. Gach, "Kinematics of tidal tails in interacting galaxies: tidal dwarf galaxies and projection effects," *Astronomy & Astrophysics*, vol. 425, no. 3, pp. 813–823, 2004.

[13] B. G. Elmegreen, M. Kaufman, and M. Thomasson, "An interaction model for the formation of dwarf galaxies and 10 exp 8 solar mass clouds in spiral disks," *The Astrophysical Journal*, vol. 412, no. 1, pp. 90–98, 1993.

[14] P.-A. Duc, F. Bournaud, and F. Masset, "A top-down scenario for the formation of massive tidal dwarf galaxies," *Astronomy & Astrophysics*, vol. 427, no. 3, pp. 803–814, 2004.

[15] F. Bournaud, P.-A. Duc, and F. Masset, "The large extent of dark matter haloes probed by the formation of tidal dwarf galaxies," *Astronomy & Astrophysics*, vol. 411, no. 2, pp. L469–L472, 2003.

[16] F. Bournaud and F. Combes, "Formation of polar ring galaxies," *Astronomy & Astrophysics*, vol. 401, no. 3, pp. 817–833, 2003.

[17] B. Koribalski and J. M. Dickey, "Neutral hydrogen gas in interacting galaxies: the NGC 6221/6215 galaxy group," *Monthly Notices of the Royal Astronomical Society*, vol. 348, no. 4, pp. 1255–1274, 2004.

[18] M. Hancock, B. J. Smith, C. Struck, M. L. Giroux, and S. Hurlock, "Candidate tidal dwarf galaxies in arp 305: lessons on dwarf detachment and globular cluster formation," *The Astrophysical Journal*, vol. 137, pp. 4643–4654, 2009.

[19] K. A. Knierman, S. C. Gallagher, J. C. Charlton, et al., "From globular clusters to tidal dwarfs: structure formation in the tidal tails of merging galaxies," *The Astronomical Journal*, vol. 126, pp. 1227–1244, 2003.

[20] J. F. Navarro, C. S. Frenk, and S. D. M. White, "The structure of cold dark matter halos," *The Astrophysical Journal*, vol. 462, no. 2, pp. 563–575, 1996.

[21] J. S. Bullock, A. V. Kravtsov, and P. Colín, "Angular momentum profiles of warm dark matter halos," *The Astrophysical Journal*, vol. 564, pp. L1–L4, 2002.

[22] F. Bournaud, P.-A. Duc, E. Brinks, et al., "Missing mass in collisional debris from galaxies," *Science*, vol. 316, no. 5828, pp. 1166–1169, 2007.

[23] J. Braine, P.-A. Duc, U. Lisenfeld, et al., "Abundant molecular gas in tidal dwarf galaxies: on-going galaxy formation," *Astronomy & Astrophysics*, vol. 378, no. 1, pp. 51–69, 2001.

[24] M. Boquien, P.-A. Duc, J. Braine, E. Brinks, U. Lisenfeld, and V. Charmandaris, "Polychromatic view of intergalactic star formation in NGC 5291," *Astronomy & Astrophysics*, vol. 467, no. 1, pp. 93–106, 2007.

[25] D. Pfenniger, F. Combes, and L. Martinet, "Is dark matter in spiral galaxies cold gas? I. Observational constraints and dynamical clues about galaxy evolution," *Astronomy & Astrophysics*, vol. 285, pp. 79–93, 1994.

[26] D. Pfenniger and F. Combes, "Is dark matter in spiral galaxies cold gas? II. Fractal models and star non-formation," *Astronomy & Astrophysics*, vol. 285, pp. 94–118, 1994.

[27] D. Pfenniger, S. D. Ryder, D. J. Pisano, M. A. Walker, and K. C. Freeman, Eds., vol. 220 of *IAU Symposium Series*, p. 241, 2004.

[28] P. M. W. Kalberla, L. Dedes, J. Kerp, and U. Haud, "Dark matter in the Milky Way II. The HI gas distribution as a tracer of the gravitational potential," *Astronomy and Astrophysics*, vol. 469, no. 2, pp. 511–527, 2007.

[29] Y. Revaz, D. Pfenniger, F. Combes, and F. Bournaud, "Simulations of galactic disks including a dark baryonic component," *Astronomy & Astrophysics*, vol. 501, no. 1, pp. 171–187, 2009.

[30] G. Gentile, B. Famaey, F. Combes, P. Kroupa, H. S. Zhao, and O. Tiret, "Tidal dwarf galaxies as a test of fundamental physics," *Astronomy & Astrophysics*, vol. 472, no. 2, pp. L25–L28, 2007.

[31] M. Milgrom, "MOND and the mass discrepancies in tidal dwarf galaxies," *The Astrophysical Journal*, vol. 667, p. L45, 2007.

[32] J. I. Read, G. Lake, O. Agertz, and V. P. Debattista, "Thin, thick and dark discs in ΛcDM," *Monthly Notices of the Royal Astronomical Society*, vol. 389, no. 3, pp. 1041–1057, 2008.

[33] C. W. Purcell, J. S. Bullock, and M. Kaplinghat, "The dark disk of the milky way," submitted to *The Astrophysical Journal*.

[34] I. Saviane, Y. Momany, G. S. da Costa, R. M. Rich, and J. E. Hibbard, "A new red giant-based distance modulus of 13.3 Mpc to the antennae galaxies and its consequences," *The Astrophysical Journal*, vol. 678, no. 1, pp. 179–186, 2008.

[35] F. Schweizer, C. R. Burns, B. F. Madore, et al., "A new distance to the antennae galaxies (NGC 4038/39) based on the type ia supernova 2007," *The Astronomical Journal*, vol. 136, no. 4, pp. 1482–1489, 2008.

[36] P.-A. Duc, J. Braine, T. J. Lisenfeld, E. Brinks, and M. Boquien, "VCC 2062: an old tidal dwarf galaxy in the Virgo cluster?" *Astronomy & Astrophysics*, vol. 475, no. 1, pp. 187–197, 2007.

[37] T. Okazaki and Y. Taniguchi, "Dwarf galaxy formation induced by galaxy interactions," *The Astrophysical Journal*, vol. 543, no. 1, pp. 149–152, 2000.

[38] M. Martig, F. Bournaud, R. Teyssier, and A. Dekel, "Morphological quenching of star formation: making early-type galaxies red," submitted to *The Astrophysical Journal*.

[39] S. Recchi, C. Theis, P. Kroupa, and G. Hensler, "The early evolution of tidal dwarf galaxies," *Astronomy & Astrophysics*, vol. 470, no. 1, pp. L5–L8, 2007.

[40] F. Bournaud, P.-A. Duc, and E. Emsellem, "High-resolution simulations of galaxy mergers: resolving globular cluster formation," *Monthly Notices of the Royal Astronomical Society*, vol. 389, no. 1, pp. L8–L12, 2008.

[41] D. M. Elmegreen, B. G. Elmegreen, T. Ferguson, and B. Mullan, "Smooth and starburst tidal tails in the GEMS and GOODS fields," *The Astrophysical Journal*, vol. 663, pp. 734–751, 2007.

[42] L. Michel-Dansac, D. G. Lambas, M. S. Alonso, and P. Tissera, "The mass—metallicity relation of interacting galaxies," *Monthly Notices of the Royal Astronomical Society*, vol. 386, no. 1, pp. L82–L86, 2008.

Hindawi Publishing Corporation
Advances in Astronomy
Volume 2010, Article ID 407394, 11 pages
doi:10.1155/2010/407394

Review Article

Kinematics of Milky Way Satellites: Mass Estimates, Rotation Limits, and Proper Motions

Louis E. Strigari

Kavli Institute for Particle Astrophysics and Cosmology, Stanford University, Stanford, CA 94305, USA

Correspondence should be addressed to Louis E. Strigari, strigari@stanford.edu

Received 8 May 2009; Revised 6 August 2009; Accepted 29 September 2009

Academic Editor: Andrey V. Kravtsov

In the past several years kinematic data sets from Milky Way satellite galaxies have greatly improved, furthering the evidence that these systems are the most dark matter dominated objects known. This paper discusses a maximum likelihood formalism that extracts important quantities from these kinematic data sets, including the amplitude of a rotational signal, proper motions, and the mass distributions. Using a simple model for galaxy rotation it is shown that the expected error on the amplitude of a rotational signal is ~ 0.5 km s^{-1} with $\sim 10^3$ stars from either classical or ultra-faint satellites. As an example Sculptor is analyzed for the presence of a rotational signal; no significant detection of rotation is found, with a 90% c.l. upper limit of ~ 2 km s^{-1}. A criterion for model selection is presented that determines the parameters required to describe the dark matter halo density profiles and the stellar velocity anisotropy. Applied to four data sets with a wide range of velocities, models with variable velocity anisotropy are preferred relative to those with constant velocity anisotropy, and that central dark matter profiles both less cuspy and more cuspy than Lambda-Cold Dark Matter-based fits are equally acceptable.

1. Introduction

Since their initial discovery [1], dwarf spheroidals (dSphs) have offered a unique insight into the formation of galaxies and structure on the smallest scales. Initially characterized as unusual and ghostly stellar systems, photometric studies tended to find that these systems contained old stellar populations with no recent signature of star formation activity [2]. Though photometrically well studied since their discovery over seventy years ago, as late as nearly 30 years ago minimal was known on the internal kinematic properties of their stellar populations or on the kinematic properties of these objects in the Milky Way (MW) halo.

Aaronson [3] provided the first measurement of the line of sight velocities of stars in Milky Way dSphs. From the spectra of merely three carbon stars, Aaronson suggested a mass-to-light ratio for the Draco dSph nearly an order of magnitude greater than that of Galactic globular clusters. Follow-up studies of several dSphs, including Sextans, Fornax, Ursa Minor, Sculptor, increased the velocity samples by an order of magnitude, and in the process established these systems to be dark matter dominated [4–6]. It was further suggested that all of these systems share a similar dark matter halo mass of $\sim [1\text{–}5] \times 10^7 M_\odot$ [6]. Even at the time of these early measurements, it was understood that the mass distributions of these systems provide strong constraints on the properties of the particle nature of dark matter, including its mass and primordial phase-space density [7–9].

With the advent of high resolution, multiobject spectroscopy, the velocity samples from the brightest dSphs initially studied in [4–6] have now increased by up to three orders of magnitude [10–12]. These new data sets have revealed that the velocity dispersions of the systems are all ~ 10 km s^{-1}, and in all cases the dispersions remain constant even out to the projected radius of the outermost velocity measurements [11]. Though the data sets have increased by more than tenfold, the more modern analysis of these systems still confirms the global conclusion established from the initial observations that dSphs are strongly dark matter dominated [10, 11, 13, 14].

Not only has the past several years seen an increase in the kinematic data sets for the brightest dSphs, the number of known Milky Way satellites has more than doubled due to the Sloan Digital Sky Survey (SDSS). As of the writing of

this paper, the SDSS has discovered 14 new Galactic satellites [15–17]. The new SDSS systems have lower luminosities and surface brightnesses than the 11 classical Milky Way satellites that were known prior to SDSS. The half-light radius for several of these new objects is less than ∼100 pc; this radius is smaller than the typical half-light radius of the classical satellites but still somewhat larger than the typical globular cluster half-light radius of ∼1–10 pc.

Several kinematics studies on the ultra-faint population of SDSS satellites have been undertaken in the past several years [18–21]. Using spectra from eight of the SDSS satellites, Simon and Geha [20] concluded that these objects are strongly dark matter dominated. Several of the ultra-faint satellites have velocity dispersions as low as $\sim 5\,\mathrm{km\ s^{-1}}$, making them the most-promising systems to study the phase space limits of the dark matter. It has additionally been observed that the ultra-faint satellites are the most metal-poor systems known, and that they form a continuation of the luminosity metallicity trend set by the brightest dSphs [21, 22].

With the above data sets now available, it is becoming increasingly necessary to develop better theoretical tools to interpret them. An important aspect of the theoretical modeling will necessarily require an interpretation of the kinematic data sets for the population of MW satellites; a detailed understanding of these kinematic data sets will be important not only for determining the mass distributions of each individual system, but for a global comparison to theories of Cold Dark Matter (CDM) [13, 23]. Understanding the mass distributions will also be important for interpretation of limits on particle dark matter masses and annihilation cross sections in high-energy gamma-ray experiments [24–26]. Further, understanding the kinematics of these systems may eventually reveal whether they have dark matter cusps or cores, which would in itself provide a stringent test of the CDM paradigm [27].

The primary aim of this paper is to discuss a maximum likelihood formalism that is used for extracting important physical quantities from dSph kinematic data sets. Section 2 begins by reviewing the properties of the kinematic data sets and defining the likelihood. Section 3 then uses the likelihood to extract rotational and proper motion signals. Section 4 discusses mass modeling and a new calculation for model selection. Section 5 presents the conclusions.

2. Likelihood Function and Error Modeling

Information on the kinematic properties of dSphs is extracted from the line of sight velocities of their individual stars. This section introduces the likelihood used in the data analysis and projections for the errors attainable on several parameters using the likelihood.

2.1. Likelihood Function. The probability for a velocity data set, $\vec{v}$, is assumed to be of the form

$$p(\vec{v} \mid u, \sigma_{\mathrm{los}}) = \prod_{i=1}^{n} \frac{1}{\sqrt{2\pi\left(\sigma_{m,i}^2 + \sigma_{\mathrm{los}}^2\right)}} \exp\left[-\frac{(v_i - u)^2}{2\left(\sigma_{m,i}^2 + \sigma_{\mathrm{los}}^2\right)}\right]. \tag{1}$$

In (1) the dispersion of the distribution is given by the sum of the measurement uncertainty on a star, σ_m, and the intrinsic dispersion of the system at the projected radius of the star. The latter quantity is symbolized by σ_{los} and is determined by the model; Section 4 provides more details on this quantity and specifically how it relates to the mass of the systems. The systemic line of sight velocity in the direction of the ith star is given by u. Written in the above form, (1) may be read as the probability for the data set, given the parameters u and σ_{los}. Appealing to Bayes' theorem and defining the likelihood function as

$$\mathcal{L}(u, \sigma_{\mathrm{los}}) = p(u, \sigma_{\mathrm{los}} \mid \vec{v}), \tag{2}$$

the parameters u and σ_{los} may be determined directly from the data by the maximization of (2). Equation (2) assumes uniform priors on the model parameters.

The form of (1) results from the convolution of Gaussian distribution which represents the measurement error on the velocity of a given star with a separate sampling distribution that is assumed to be Gaussian. It is the sampling distribution of velocities that is connected to physical quantities such as the velocity anisotropy of the stars, and the potential of the stellar and dark matter components. For a given model of the galaxy, the true line of sight velocity distribution function may indeed be non-Gaussian; certain limiting cases of the velocity distribution for analytic potentials have been considered in [28]. This paper shows that when attempting to reconstruct the line of sight velocity distribution for a given model, degeneracies exist between the stellar velocity anisotropy and the stellar and dark matter potentials. Though more information may be gained on model parameters if the true velocity distribution was known, and thus utilized in the parameter estimation, the Gaussian approximation provides the most conservative sampling distribution in reconstructing model parameters in variance estimation problems (for a specific discussion of this point, see the discussion in Chapter 8 of [29]). Further, the mass estimations presented here using the likelihood in (2) agree with mass estimates that use a Gaussian likelihood in the binned velocity dispersion [30]; in this latter case the velocity dispersion does not necessarily correspond to the variance of a Gaussian line of sight velocity distribution, making it self-consistent to determine parameters such as the velocity anisotropy.

The distribution function in (1) provides the simplest description of a data set. Including higher-order effects naturally introduces a larger set of model parameters. The first modification to (1) from higher order corrections comes from noting that the mean velocity, u, varies as a function of the position of the star in the galaxy. This variation in the mean velocity results from the fact that, for lines of sight with larger angles from the line of sight directly to the center of the galaxy, the proper motion of the object contributes an increasingly larger component to the line of sight velocity. To describe how the line of sight velocity varies as a function of position, consider a cartesian coordinate system in which the z-axis points in the direction of the observer from the center of the galaxy, the x-axis points in

the direction of decreasing right ascension, and the y-axis points in the direction of increasing declination. The angle ϕ is measured counter-clockwise from the positive x-axis, and ρ is the angular separation from the center of the galaxy. The mean line of sight velocity is then

$$u = v_x \sin\rho\cos\phi + v_y \sin\rho\sin\phi - v_z\cos\rho. \quad (3)$$

In the small angle approximation, $\sin\rho \simeq R/D$, where $R = \sqrt{x^2+y^2}$, and D is the distance from the observer to the center of the dSph. Then $\sin\phi = y/R$, so that (3) can be written as $u = v_x x/D + v_y y/D - v_z$. In the limit that the vector pointing from the observer to the center of the galaxy is exactly parallel to the lines-of-sight to each star, $u \simeq -v_z$.

Equation (3) show that the line of sight velocity of a system increases roughly linearly with the increase of the projected distance from the center of the dSph. This effect is purely geometric and may be used to recover the proper motion of a dSph with similar accuracy to the proper motions attained in ground and space-based measurements [12, 31]; an application to a specific data set of Sculptor is given. The extraction of dSph proper motions in this manner is analogous to the determination of the proper motions for the Large Magellanic Clould [32] and for M31 [33] from their stellar and satellite distributions, respectively.

There may also be rotational motion, in addition to the dominant contribution from random motions, present in the galaxy. Though rotation is intrinsic to the dynamics of the system and is not purely geometric as that described by (3), a simple parameterization is possible if the rotation amplitude is described by a term $A\sin(\phi-\phi_0)$, where ϕ_0 defines the projected axis of rotation. Adding all of the terms together gives the following expression for the line of sight velocity of a star:

$$u = v_x \sin\rho\cos\phi + v_y \sin\rho\sin\phi - v_z\cos\rho + A\sin(\phi-\phi_0). \quad (4)$$

With the addition of each of the terms in (4), our likelihood function now reads

$$\mathcal{L}\left(v_x, v_y, v_z, A, \phi_0, \sigma_{\rm los}\right) = p\left(v_x, v_y, v_z, A, \phi_0, \sigma_{\rm los} \mid \vec{v}\right), \quad (5)$$

and the vector set of 6 parameters $(v_x, v_y, v_z, A, \phi_0, \sigma_{\rm los})$ may be directly determined from the data. In the sections below these parameters is determined from an example data set; before jumping into this data analysis the following subsection provides a discussion of the theoretical predictions for the errors attainable on these quantities.

2.2. Error Modeling. From the likelihood function defined in (1) and (5), the Fisher matrix formalism may be used to derive projected errors on the model parameters. For m model parameters that are varied, the Fisher matrix is defined as an m by m matrix so that the entry for the ath and bth parameters is given by

$$F_{ab} = -\left\langle \frac{\partial^2 \ln\mathcal{L}}{\partial\theta_a \partial\theta_b} \right\rangle. \quad (6)$$

Here $\vec{\theta}$ is a vector defining the set of parameters. In the simple case studied in this section, the parameters are given by $\vec{\theta} = \{v_x, v_y, v_z, A, \phi_0, \sigma_{\rm los}\}$. According to the Rao-Cramer inequality, the minimum possible variance attainable on a parameter using maximum likelihood statistics is given by the inverse of the Fisher information matrix, $\sqrt{\mathbf{F}^{-1}_{aa}}$. The average in (6) is taken over the data, and the derivatives are evaluated at the true model of parameter space. The inverse of the Fisher matrix thus provides an approximation for the true covariance of the parameters, and using $\mathbf{F}^{-1}$ provides a good approximation to the errors on parameters that are well-constrained by the data.

The Fisher matrix is constructed by differentiating the log of the likelihood function in (5). It will be understood that the total dispersion $\sigma_i^2 = {\sigma_{\rm los}}^2 + {\sigma_m}^2$ is evaluated at the projected radius of the ith star. Averaging over the likelihood function, and using the above definition of u, the final expression for the Fisher matrix is

$$F_{ab} = \sum_{i=1}^{N}\left(\frac{1}{\sigma_i^2}\frac{\partial u_i}{\partial\theta_a}\frac{\partial u_i}{\partial\theta_b} + \frac{1}{2}\frac{1}{\sigma_i^4}\frac{\partial\sigma_{\rm los}^2}{\partial\theta_a}\frac{\partial\sigma_{\rm los}^2}{\partial\theta_b}\right). \quad (7)$$

The sum is over the N number of observed stars in the galaxy. The analysis in this section considers the simplified case that $\sigma_{\rm los}^2$ does not in itself depend on any model parameters. A more detailed model would consider this quantity as a function of the parameters that describe the mass modeling of the system; this is discussed in more detail in Section 4.

In the second term in (7), the derivatives are with respect to the theory dispersion alone, whereas both of the contributions to the variance sum in the denominator. For the well-studied satellites, with intrinsic velocity dispersions of 10 km s^{-1}, the dispersion from the distribution function dominates the dispersion from the measurement uncertainty, while for many of the newly-discovered satellites, both contributions to the dispersions are similar. Equation (7) shows that, to determine the error on any of the $\vec{\theta}$ parameters, one must determine (1) the distribution of stars within the dSph that have measured velocities, and (2) the error on the velocity of each star. This implies that the projected errors are independent of the mean velocity of the stars. Additionally, under the approximation that $\sin\rho \ll 1$ and no rotation, the first term in (7) vanishes, and the errors are independent of the parameters describing the mean motion of the system.

The projected errors obtained using (7) provide an excellent estimate of the measured errors on both v_x and v_y [12, 31]. Though there has been no conclusive detection of a parameter similar to A in published kinematic data samples, it is interesting to determine the expected error on this quantity given expected future data samples. Figure 1 shows example error projections for A, for two different model galaxies. The upper solid curve assumes structural parameters similar to that of Segue 1, with a Plummer radius of 0.03 kpc and a stellar limiting radius of 0.1 kpc [34]. The lower dashed curve assumes structural parameters similar to that of Draco, with a King core radius of 0.18 kpc and a King limiting radius of 0.93 kpc [35]. Each curve assumes that the measurement uncertainty on each star is 2 km s^{-1}. In both

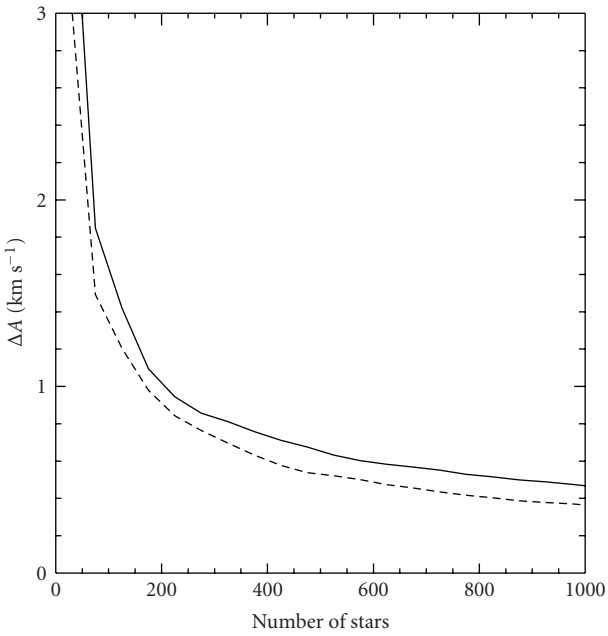

FIGURE 1: The projected one-sigma error on the amplitude of the rotation parameter, A, as defined in 4. The upper solid curve assumes structural parameters similar to that of Segue 1, while the lower dashed curve assumes structural parameters similar to that of Draco. Each curve assumes that the measurement uncertainty on each star is 2 km s^{-1}.

cases, the stars have been uniformly distributed at projected positions in the galaxies; this provides a good representation of the present observational configurations.

In addition to their interesting applications for understanding the rotation and proper motion of the dSphs, the calculations presented in this section are crucial for uncovering properties of underlying dark matter distributions. For example a strong gradient may reflect ongoing tidal disruption, which would clearly affect dark matter mass modeling, as is discussed in more detail in Section 4.

3. Proper Motions and Rotation

This section discusses an application of the maximum likelihood formalism introduced in Section 2, with a specific focus on the methodology for extracting an intrinsic rotational signal and proper motions using an example data set. Extracting rotation from a data set is important for reasons discussed above, and, in addition to its phenomenological interests, extracting the proper motions of MW satellites may have important implications for understanding the origin of the accretion history of MW [36–38]. Specifically determining the latter would present a unique observational test of MW halo formation within the CDM paradigm.

Several dSphs have kinematics data sets large enough that statistically significant constraints may be placed on the parameters v_x, v_y, and A. For illustrative purposes this section considers just one example, the Sculptor dSph. Sculptor is located at a distance of 80 kpc and has a measured King limiting radius for its stellar distribution of ∼1.6 kpc [39]. Given these parameters it is one of the more spatially extended dSphs. The mass content of Sculptor has been estimated in several recent papers [13, 14, 40], and it has been shown that Sculptor may contain some degree of rotational support [40]. Further, the previous determinations of the proper motion of Sculptor from its line of sight velocities may indicate a discrepancy between the proper motion as determined from this method and from ground- and space-based measurements [12]. This latter fact may in itself be indicative of the presence of an intrinsic rotational component, provided that the systematics on the ground- and space-based determinations of the Sculptor proper motions are well-understood [41].

To extract the rotation and proper motion signal, a simplified model is considered by assuming that the likelihood function is characterized by the six parameters introduced in Section 2. It is assumed that the intrinsic dispersion $\sigma_{\rm los}$ is uniform throughout the galaxy and does not depend on any of the parameters of the mass modeling introduced in Section 4. Introducing the set of parameters discussed in Section 4 does not affect the reconstruction of the parameters discussed in this section since the intrinsic dispersion is uncorrelated with the parameters of the function u [31].

In order to determine the probability distributions of the parameters $\vec{\theta} = (v_x, v_y, v_z, A, \phi_0, \sigma_{\rm los})$, a standard metropolis-hastings algorithm [29] is used to sample the likelihood function as written in (5). For all runs described here 10^4 accepted points were obtained in each chain, with the first 10% excluded to account for a conservative burn-in phase. For simplicity, a uniform proposal distribution is assumed for each of the parameters over a wide range chosen to encompass physically-acceptable values for each of these parameters. The line of sight velocity data used is taken from the Walker et al. [42] sample, and only those stars with > 90% c.l. probably for membership are used in the analysis.

Figure 2 shows the posterior probability distributions for the proper motion components corresponding to v_x and v_y, $v_x[\text{km s}^{-1}] = 4.74[D/\text{pc}, \mu_\alpha/\mu\,\text{as yr}]$ and $v_y[\text{km s}^{-1}] = 4.74[D/\text{pc}, \mu_\delta/\mu\,\text{as yr}]$, respectively. The remaining parameters $(v_x, A, \phi_0, \sigma_{\rm los})$ are marginalized over. Though the distributions in Figure 2 were obtained by allowing the A parameter to float freely, the distributions are found to be relatively unaffected if A is instead fixed so that $A = 0$. This reflects the fact that the radial gradient in the velocity of the stars is distinct from the intrinsic rotational component, which has a sinusoidal behavior as a functional of the position angle. The results presented in Figure 2 are in agreement with the measurements of Walker et al. [12], though here a larger set of parameters is marginalized over in this analysis.

Figure 3 shows the corresponding probability distribution for the rotational parameter A. Again the remaining five parameters $(v_x, v_y, v_z, \phi_0, \sigma_{\rm los})$ are marginalized over. The result is that, given the rotational parameterization and the using entire distribution of 1352 Sculptor stars, there is no statistically significant detection of rotation. From Figure 3 the 90% c.l. upper limit on the rotation is found to be

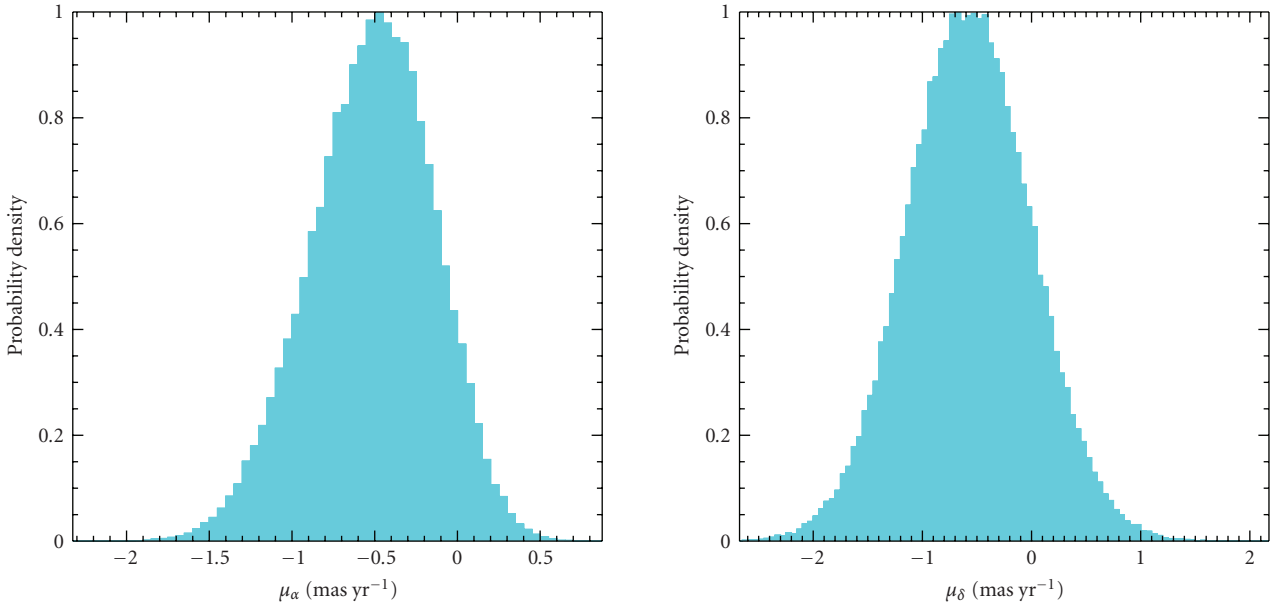

FIGURE 2: Probability densities for the velocity components of Sculptor transverse to the line of sight. The components μ_α and μ_δ give the proper motions in the directions of increasing right ascension and declination, respectively.

$\sim 2\,\mathrm{km\,s^{-1}}$. The result presented in Figure 3 is somewhat degenerate with the parameters describing u; for example if v_x and v_y were (unphysically) set to zero, the implied upper limit on A reduces by about 50%.

Figure 3 represents the averaged value of A throughout the entire galaxy. It may be possible that the rotation amplitude in the outer region differs from the rotation rate in the inner region; if this were the case then it is plausible that this effect is washed out in the averaging process. To provide a simple test for a possible differential rotation rate, an additional likelihood analysis was considered with just the outer sample of Sculptor stars. Here the outer stars are defined as only those with projected radius beyond 0.5 kpc. Even in this case, there is no statistically significant detection of A, though in this case the 90% c.l. upper limit increases to $10\,\mathrm{km\,s^{-1}}$.

4. Mass Distributions and Model Selection Criteria

This section discusses the extension of the maximum likelihood analysis developed in Section 2, with a goal of using the kinematic data to determine dark matter mass distributions. A calculation of the gravitating mass of a stellar system is one of the more fundamental tasks in astronomy, and simple scaling arguments provide some guidance to anticipate the results. It is worthwhile to first review these arguments as applied to the dSphs before undertaking a more detailed and model dependent treatment.

4.1. Spherical Mass Modeling

4.1.1. Initial Estimates. Under the assumption that a star cluster is spherically symmetric, the orbital distribution of the tracer particles is isotropic, that mass follows light, and the cluster is isolated from any external gravitational potential, the virial theorem provides a mass estimate of $M_{\mathrm{vir}} \simeq r_e\sigma_\star^2/G$, where r_e is the observed extent of the cluster and $\sigma_\star$ is the velocity dispersion of the stars. Although this is probably the simplest estimate one can make for the mass of a star cluster, it does provide a useful extremum bound. For example Merritt [43] has show that the virial theorem may be used to derive a lower bound on the mass of a star cluster, which is obtained from the assumption that all of the mass is concentrated as a point in the center. This minimum mass is given by $M_{\mathrm{min}} = 3\sigma_\star^2/\langle r^{-1}\rangle G$, where $1/\langle r^{-1}\rangle$ is the harmonic mean stellar radius in the cluster.

Of course for dSphs it is not consistent to assume that these systems are isolated, since they are orbiting within the extended dark matter halo of the MW. For dSphs orbiting with the MW halo, the minimum mass estimate above is particularly useful, as it in turn provides a conservative estimate of the radius at which particles would be stripped due to the MW potential. As an example consider the case of Segue 1, which is an MW satellite with a stellar luminosity $\sim 340\,\mathrm{L}_\odot$ at a Galactocentric distance of 28 kpc. From the de-projected light distribution, the harmonic mean stellar radius is ~ 10 pc, and given the velocity dispersion of $4.3\,\mathrm{km\,s^{-1}}$ [21], the implied minimum mass of Segue 1 is $\sim 4\times 10^5\,\mathrm{M}_\odot$. Assuming that Segue 1 is a point mass orbiting in the potential of the MW, the radius at which particles would be presently getting stripped is the Jacobi radius, $r_t = [M/3M_{\mathrm{MW}}]^{1/3}D$, where $D = 28$ kpc. Assuming the minimum mass of $M = M_{\mathrm{min}}$, $r_t \simeq 300$ pc. It is important to note that this provides only an estimate of the instantaneous tidal radius; if Segue 1 came significantly closer to the MW in the past then this estimate would differ. The above estimate

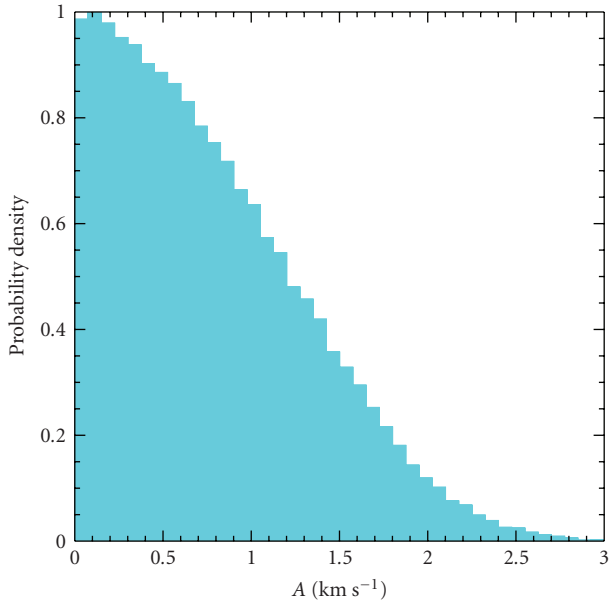

FIGURE 3: The probability density for the amplitude of the rotational signal in Sculptor, using the model discussed in the text.

provides a lower bound on the radius at which particles would be getting stripped, under the assumption of a circular orbit. A similar argument for the tidal radius of Segue 1 was considered in Geha et al. [21] using the Illingworth approximation for the mass as $M_{\rm min}$ (for an alternative interpretation for the origin of Segue 1, see [44].)

4.1.2. Jeans Equation. At the next level of detail from the dynamical perspective, an estimate for the mass of the dSphs may be obtained by appealing to the spherically symmetric jeans equation, assuming that the gravitating mass of the system consists of both stars and dark matter. The analysis here closely follows the treatment given in the appendix of Strigari et al. [13] and refers to this paper for further details. A standard discussion of the spherical jeans equations comes from [45].

The spherical jeans equation is

$$r\frac{d(\rho_\star\sigma_r^2)}{dr} = -\rho_\star(r)V_c^2(r) - 2\beta(r)\rho_\star\sigma_r^2. \tag{8}$$

Here $\rho_\star$ is the deprojected stellar density profile, the circular velocity is $V_c(r) = GM/r$, and the parameter $\beta(r) = 1-\sigma_r^2/\sigma_t^2$ characterizes the difference between the radial and tangential velocity dispersions of the stars. Integrating σ_r^2 along the line of sight gives the velocity dispersion as a function of projected radius, R,

$$\sigma_{\rm los}^2(R) = \frac{2}{I(R)}\int_R^\infty\left(1-\beta\frac{R^2}{r^2}\right)\frac{\rho_\star\sigma_r^2 r}{\sqrt{r^2-R^2}}dr. \tag{9}$$

Here, $I(R)$ is the projected surface density of the stellar distribution, and $\rho_\star$ is the three-dimensional stellar distribution. In (9), σ_r depends on the parameterization of the mass distribution of the dark matter component. The stellar density profile is taken to be fixed; for example the measurements of the projected density profiles for many of the classical satellites come from [46], and more updated profiles from, for example, [35, 47–49], while measurements of the density profiles for the ultra-faint satellite come from [34]. It is important to note that fixing the stellar density profile may introduce a degeneracy in determining the projected velocity dispersion profile, particularly in the central regions [50]. However the effect on the integrated mass distributions as considered here is less severe, motivating the assumption of fixing $\rho_\star$, rather than marginalizing over it, in the analysis.

Given the above assumption for the velocity anisotropy of the stars and for the shape of the dark matter profile for the galaxy, the likelihood function can now schematically be written as

$$\mathcal{L}\left[\vec{y},\sigma_{\rm los}\left(\vec{\beta},\vec{\Phi}\right)\right] = p\left[\vec{y},\sigma_{\rm los}\left(\vec{\beta},\vec{\Phi}\right)\mid\vec{v}\right]. \tag{10}$$

For compactness, the vector $\vec{y} = (v_x, v_y, v_z, A, \phi_0)$ has been defined, and $\vec{\beta}$ and $\vec{\Phi}$ are vectors that describe the stellar velocity anisotropy and the gravitational potential of the system, respectively. The line of sight velocity dispersion is dependent on $\vec{\beta}$ and $\vec{\Phi}$ through the spherical jeans equation. The mass of the system, as well as quantities related to the mass distribution, are determined via $\vec{\Phi}$, and thus by integrating out the model parameters one may determine the probability density for the mass of the system contained within a fixed physical radius.

4.1.3. Error Projections on Mass Distribution. Before performing an example calculation using (10), it is interesting to get an idea as to how the errors on the mass distribution depend on the physical radius within which the mass is determined. To perform these estimates, we again appeal to the Fisher matrix formalism outlined above. However the analysis here is different from above in that now the likelihood depends on the vector set of parameters $\vec{\beta}$ and $\vec{\Phi}$ in addition to $\vec{y}$.

The example considered here uses the velocity data sample from Fornax of Walker et al. [42], specifically the stars with $> 90\%$ c.l. for membership. This gives a total of 2409 Fornax members. The three-dimensional surface density profile for Fornax is assumed to take the form

$$\rho_\star(r) \propto \frac{1}{x^a(1+x^b)^{(c-a)/b}}\,e^{-r^2/2r_{\rm cut}^2}, \tag{11}$$

with the parameters $\{a, b, c, [r_0/\text{kpc}], [r_{\rm cut}/\text{kpc}]\} = \{0.3, 1.2, 3.0, 0.8, 1.1\}$. A profile of this form with these parameters is consistent with the recent measurements of Fornax star counts [49], though generally the results presented are independent of the normalization of the surface density profile. The stellar mass-to-light ratio is assumed to be unity, consistent with the results presented in [49]. The dark matter density profile is assumed to be the einasto profile

$$\ln\left[\frac{\rho(r)}{\rho_{-2}}\right] = \left(-\frac{2}{\alpha}\right)\left[\left(\frac{r}{r_{-2}}\right)^\alpha - 1\right], \tag{12}$$

and following CDM simulations, $\alpha = 0.17$ [51]. The velocity anisotropy is assumed to be of the following form

$$\beta(r) = (\beta_\infty - \beta_0) r^2 / \left(r_\beta^2 + r^2\right) + \beta_0. \quad (13)$$

Thus in the Fisher matrix calculation the base set of parameters are now given by $\vec{\theta} = \{\rho_{-2}, r_{-2}, \beta_0, \beta_1, r_\beta\}$ (the rotational and geometric parameters, $\vec{\gamma}$ are ignored here: this is justified given that the Fornax data is consistent with $A = 0$ and that the $\vec{\gamma}$ parameters do not correlate with the parameters that determine the mass).

Given the base set of parameters in $\vec{\theta}$ used to calculate **F**, the error on a derived parameter, g, is given by

$$\sigma_g^2 = \sum_{i,j} \left(\frac{\partial g}{\partial \theta_i}\right) \left(\mathbf{F}^{-1}\right)_{ij} \left(\frac{\partial g}{\partial \theta_j}\right). \quad (14)$$

The derived parameter specifically considered here is the log of the mass within a given fixed physical radius (see [52] for another example where the derived parameter considered is the log slope of the dark matter density profile). Where desired Gaussian priors may be taken by simply adding $1/\sigma_{aa}^2$ to the *aa* component of the Fisher matrix.

Figure 4 shows the error on the log of mass as a function of the physical radius within which the mass is measured. Here the fiducial baseline parameters for the velocity anisotropy have been taken as $\{\beta_0, \beta_1, r_\beta/\text{kpc}\} = \{-0.5, 0, 0.2\}$, implying slightly tangential orbits in the central region of the halo and isotropic orbits at outer radii. Different combinations of $\{\rho_{-2}, r_{-2}\}$ have been taken as indicated to represent the degeneracy between these two parameters when fitting the data. Each of these parameters sets, combined with an anisotropy model, produces a velocity dispersion profile that roughly fits the profile of Fornax. While the goal here is to not undertake a direct fit to the data and to explore the exact degeneracy space of these parameters, examining these three sets of fiducial parameters gives a feel for how the constraints on the mass depend on the fiducial parameter set. Priors on each of r_{-2} and r_β are taken as $1/(5\ \text{kpc})^2$, while priors on β_0 and β_1 are taken as $1/1^2$. Each of these priors are motivated by the range of these parameters scanned in the algorithm described in following the subsection below. As is seen, for the stellar profile considered above and the fiducial set of parameters taken, the best-constrained mass is at a radius ~0.6–1.0 kpc. This best constrained radius is found to be relatively weakly dependent on the sets of fiducial parameters, particularly near the best constrained mass, provided that they give a good fit to both the star count and velocity dispersion data of Fornax. This notion that the mass is a strongly constrained at the half-light radius is found to be a general property of dispersion supported systems, as discussed in [53, 54].

4.1.4. Fornax Mass Distribution. The posterior probability density for the mass distribution of Fornax is now determined directly from the kinematic data, and compared to the projected error on the mass distribution as determined from Figure 4. As above, a metropolis hastings algorithm is used to determine the respective posteriors, and the same data for both the star counts and the line of sight velocity distribution have been used. In the parameter scan, uniform priors have been taken on each of the parameters over the following ranges as follows: $\{\log_{10}[\rho_{-2}/(M_\odot\ \text{kpc}^{-3})], r_{-2}/\text{kpc}, \beta_0, \beta_0, r_\beta\} = \{[6:10], [0:10], [-5:1], [-5:1], [0:10]\}$.

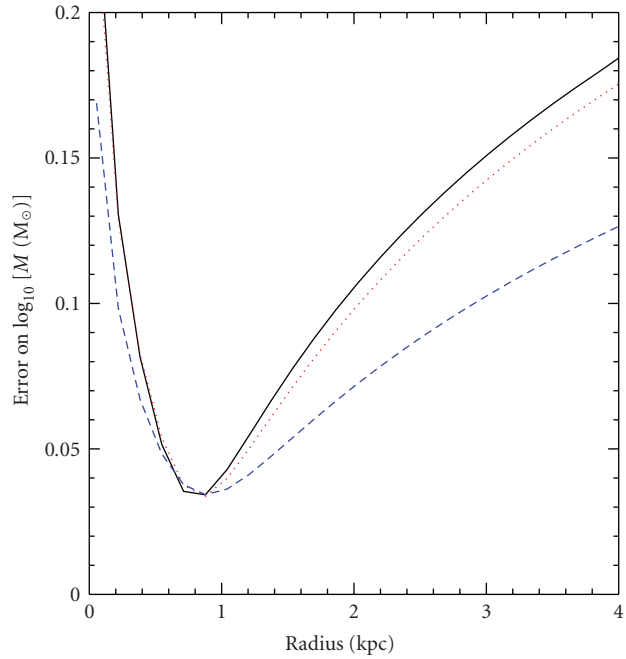

FIGURE 4: Projections for the error on the log of the mass within a given physical radius for Fornax. The position and the errors on the stars from the Walker et al. [42] data sample have been used. Each curve assumes a different fiducial model for the einasto parameters of the dark matter halo: $\rho_{-2} = 2 \times 10^7\ \text{M}_\odot\text{kpc}^{-3}$ and $r_{-2} = 1$ kpc (solid black), $\rho_{-2} = 1 \times 10^7 \text{M}_\odot\text{kpc}^{-3}$ and $r_{-2} = 2$ kpc (dotted red), and $\rho_{-2} = 0.5 \times 10^7\ \text{M}_\odot\text{kpc}^{-3}$ and $r_{-2} = 5$ kpc (dashed blue).

Figure 5 shows two example probability distributions for the Fornax mass, within 0.6 kpc (*left*) and within the approximate Fornax stellar tidal radius of 3 kpc (*right*). The probability distributions are seen to be slightly non-Gaussian, particularly the M(3 kpc) distribution. Comparing the approximate width of each of these distributions with the errors projected in Figure 4 provides generally good agreement, in spite of the intrinsic assumption in the Fisher matrix formalism that the errors on the parameters are Gaussian. Specifically for the left panel, a Gaussian fit gives $\log_{10}[\text{M}\ (0.6\,\text{kpc})/\ \text{M}_\odot] = 7.47 \pm 0.04$. These results confirm the general trend seen in Figure 4 that the error on the integrated mass within a fixed physical radius increases at larger radii towards outer regions of the halo.

Results of the calculations for the mass distributions of the entire population of dSphs are presented in [13, 23, 53, 54]. These results, as well as more recent determinations, show that the central mass distributions for the dSphs are very similar, despite an over four order of magnitude variation in their luminosities. The average density within a spherical radius of ~0.3 kpc is $\sim 0.1\,\text{M}_\odot\text{pc}^{-3}$;

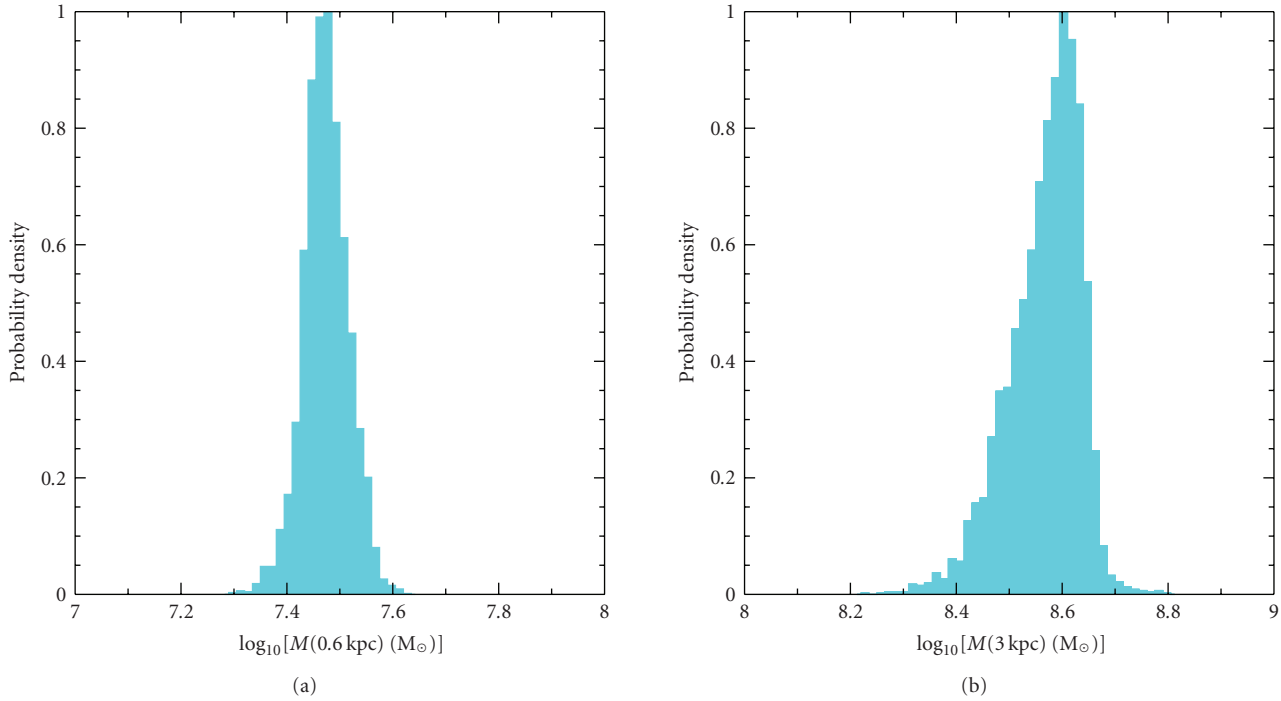

Figure 5: The probability density for the mass of Fornax within 0.6 kpc (a) and the mass within its stellar tidal radius (b), defined here to be 3 kpc.

for the brightest satellites baryons can contribute to the potential in this central region, while for the least luminous satellites the potential is dominated by dark matter within this region. Within the context of spherical models, these constant central density results are robust to the specific parameterization of the mass distribution, primarily due to the fact that the integrated mass is directly constrained via the jeans equation and the approximately similar scale for the velocity dispersion profiles [13].

4.1.5. Model Selection. The likelihood formalism introduced above does not give any information regarding the optimal parameterization of the dark matter mass profile. For example referring to the calculation above, is the einasto profile with just two free parameters an acceptable description of the data? Given the parameterization of the dynamics via the spherical jeans equation, we can answer this question and determine how many parameters are required to describe the mass profile given the maximum likelihood formalism. Moreover, we can determine how the parameterization of the density profile depends on the given data sets. For example Segue 1, with only 24 measured line of sight velocities, may require a smaller set of parameters than does Fornax, which has ∼2400 measured line of sight velocities.

To specifically answer the question of how to determine the appropriate set of parameters in maximum likelihood theory one may appeal to the bayes evidence. For the purposes here the evidence, E, is defined as the integral of the likelihood in (10) over all of the model parameters. When comparing models, the ratio of their respective evidences gives an idea of how much more probable one model is over another. For example if $1 < \Delta \ln E < 2.5$, the difference between the two models is substantial; for $2.5 < \Delta \ln E < 5$, the difference between the two models is strong, and for $\Delta \ln E > 5$ the difference between the two models is decisive [55].

As an illustration, four different dSphs that span a wide range in their respective number of velocities are considered: Segue 1, Sextans, Sculptor, and Fornax. These dSphs have 24, 424, 1352, and 2409 stars, respectively; for the latter three galaxies we consider only those stars that have a probability of >90% membership from the Walker et al. [42] sample. For each dSph we determine how many model parameters are necessary to describe the data, and we consider several different models.

For the "Baseline" 3 parameter model, the following range of parameter space is integrated over for Fornax, Sculptor, and Sextans: $\log_{10}[\rho_0/\mathrm{M}_\odot \mathrm{kpc}^{-3}] = [6 : 10]$, $\log_{10}[r_0/\mathrm{kpc}] = [-1 : 1]$. The velocity anisotropy is assumed to be a constant, β, with a range given by $\beta \equiv \beta_0 = \beta_1 = [-2 : 0.5]$. For Segue 1 the ranges are the same except for the scale radius, which is taken to vary over the range $\log_{10}[r_0/\mathrm{kpc}] = [-2 : 0]$; this range is motivated by the likely upper limit to the dark matter tidal radius for Segue 1 [21]. All of the ranges above are chosen as plausible values to describe the halos of dSphs. A flat prior is chosen over these regions; as a further detail one may chose a prior that weights each of these parameters differently, for by example considering the scatter in the $\rho_s - r_s$ relation as seen in CDM simulations [56]. The bayes evidence for the Baseline model will be denoted as E_0.

Table 1: Parameter ranges and evidences for various models. The columns are for different dSphs, and the rows are for different models as described in the text. Each entry in the table gives the ratio of the evidence for the given model, $E_{\rm model}$, with respect to the Baseline 3 parameter model, E_0, defined in the text, $\ln(E_{\rm model}/E_0)$.

dSph	Segue 1	Sextans	Sculptor	Fornax
No. of stars	24	424	1352	2409
Exp	3.4	3.3	3.3	3.6
$\vec{\beta}$	1.6	0.9	0.8	1.3
$\vec{\beta}$ + Exp	5.0	4.3	4.1	4.9

Three different models are compared to this Baseline 3 parameter model: (i) a model in which the parameter space for α is enlarged in the range $[0.14 : 0.3]$ (corresponding to $1/\alpha \simeq [3\text{–}7]$), so that central slopes that are both more flat and more steep than the CDM value are allowed (ii) a model with the Baseline 3-parameter $\rho(r)$ profile, but with a three-parameter velocity anisotropy profile which depends on the three-dimensional physical radius as in (13), and (iii) a model in which $\alpha = [0.14 : 0.3]$ and the $\beta(r)$ profile in (13) is assumed.

Model (i) is thus described by four parameters, while model (ii) is described by five free parameters, and model (iii) is described by six free parameters. In Table 1, we define model (i) as the "Exp" model, model (ii) is denoted as the "$\vec{\beta}$" model, and model (iii) is denoted as "$\vec{\beta}$ + EXP." These models provide useful illustrations of the calculation of the evidence as applied to dSphs; alternative models may of course be defined and even larger parameter spaces may be explored. The utility of the above models as defined allows us to explore to what extent CDM-like inner slopes are more favored, and to what extent an alternative parameterization of the velocity anisotropy provides a better fit to the data as compared to simply changing the value of the inner slope.

The results for the ratio of the bayes evidence for the various models, relative to E_0, are shown in Table 1. For each of the galaxies, we see roughly the same pattern; as more parameters are added, the better the model fits the data. This result implies that models with larger sets of parameters are favored even after penalization for the larger volume of parameter space that is integrated over. Allowing for a larger volume of parameter space for the dark matter density profile affects the evidence more than simply varying the shape of the anisotropy profile. In total, the best fitting models are those that allow both the velocity anisotropy and the central slope to vary freely, that is, the $\vec{\beta}$ + EXP models.

The results in Table 1 indicate that for all four galaxies variable velocity anisotropies are slightly preferred relative to those with constant velocity anisotropy, and that central dark matter profiles both less cuspy and more cuspy than ΛCDM-based fits are equally acceptable. Future data sets, both line of sight velocities and potential proper motion measurements for stars in dSphs [52, 57, 58], will be important in narrowing the acceptable ranges for both the velocity anisotropy and the central slope.

5. Conclusion

This paper has discussed the analysis of kinematic data from Milky Way dwarf spheroidals, with a primary motivation of (1) understanding physical quantities that are well-constrained by the data and (2) understanding the systematics that underly the determination of the dark matter masses of these systems, given the simplest assumption that the dSphs are purely pressure supported systems. Of the possible systematics perhaps the most significant and observationally-accessible is the determination of a velocity gradient in the data sample, which may be indicative of tidal disruption from the potential well of the Milky Way. The results in the literature indicate that, based on the kinematic data alone, velocity gradients due to tidal disruption or rotation are not conclusively present in any of the dSphs. This paper has provided an example, using a simple parameterization, of how to search for rotation in the kinematic data sets using a maximum likelihood analysis. The kinematic sample of Sculptor was analyzed, and it was found that the maximum likelihood rotational amplitude is zero, with an upper limit of $\sim 2\,\mathrm{km\ s^{-1}}$ at 90% c.l. The magnitude of these errors is consistent with the projected magnitude of the errors from theoretical modeling.

When modeling the mass distribution of the dark matter halos of the dSphs, degeneracies between model parameters affect the determination of the total mass profiles, even in the context of the simplest spherical models. To shed light on these degeneracies, this paper has discussed a new criteria for model selection applied to the dSph kinematic data sets, taking a step towards determining how many parameters are needed to describe the mass distribution of spherical halos. For the four dSphs studied here, chosen because they have a wide range of available line of sight velocities, it is shown that, assuming CDM-motivated Einasto profiles for the dark matter halos, models with variable velocity anisotropy are slightly preferred relative to those with constant velocity anisotropy. Further, central slopes for the dark matter profile that are found in CDM simulations are not a unique description of the data sets; both more cuspy and less cuspy models are allowed for the central slope. This is primarily due to the degeneracy between the central dark matter slope with the central stellar profile and the velocity anisotropy distribution [52].

Future photometric and kinematic data sets promise to further pin down the mass distributions of the dSph dark matter halos. Upcoming data for the ultra-faint satellites will be particularly important and may be able to show whether any tidal effects are present in these galaxies. Further more, development of nonspherical distributions for both the light and dark matters should be considered given these data sets (for initial results along these lines see [59]). Controlling systematics in these data sets will prove to be important step towards further testing the currently favored ΛCDM theory of structure formation.

Acknowledgments

The author is grateful to Andrey Kravtsov, Matt Walker, and Beth Willman for discussion and comments on this

paper. I additionally acknowledge the anonymous referee for constructive comments and critique that improved the content and presentation. The support for this work was provided by NASA through Hubble Fellowship Grant HF-01225.01 awarded by the Space Telescope Science Institute, which is operated by the Association of Universities for Research in Astronomy, Inc., for NASA, under Contract NAS 5-26555.

References

[1] H. Shapley, "A stellar system of a new type," *Harvard College Observatory Bulletin*, no. 908, pp. 1–11, 1938.

[2] M. Mateo, "Dwarf galaxies of the local group," *Annual Review of Astronomy and Astrophysics*, vol. 36, no. 1, pp. 435–506, 1998.

[3] M. Aaronson, "Accurate radial velocities for carbon stars in Draco and Ursa Minor—the first hint of a dwarf spheroidal mass-to-light ratio," *The Astrophysical Journal*, vol. 266, pp. L11–L15, 1983.

[4] N. B. Suntzeff, M. Mateo, D. M. Terndrup, E. W. Olszewski, D. Geisler, and W. Weller, "Spectroscopy of giants in the Sextans dwarf spheroidal galaxy," *The Astrophysical Journal*, vol. 418, no. 1, pp. 208–228, 1993.

[5] M. Mateo, E. Olszewski, D. L. Welch, P. Fischer, and W. Kunkel, "A kinematic study of the fornax dwarf spheroidal galaxy," *The Astronomical Journal*, vol. 102, no. 3, pp. 914–926, 1991.

[6] M. Mateo, E. W. Olszewski, C. Pryor, D. L. Welch, and P. Fischer, "The Carina dwarf spheroidal galaxy: how dark is it?" *The Astronomical Journal*, vol. 105, no. 2, pp. 510–526, 1993.

[7] G. Lake, "The distribution of dark matter in Draco and Ursa Minor," *Monthly Notices of the Royal Astronomical Society*, vol. 244, pp. 701–705, 1990.

[8] O. E. Gerhard and D. N. Spergel, "Dwarf spheroidal galaxies and the mass of the neutrino," *The Astrophysical Journal*, vol. 389, no. 1, pp. L9–L11, 1992.

[9] S. M. Faber and D. N. C. Lin, "Is there nonluminous matter in dwarf spheroidal galaxies," *The Astrophysical Journal*, vol. 266, pp. L17–L20, 1983.

[10] G. Gilmore, M. I. Wilkinson, R. F. G. Wyse, et al., "The observed properties of dark matter on small spatial scales," *The Astrophysical Journal*, vol. 663, no. 2, pp. 948–959, 2007.

[11] M. G. Walker, M. Mateo, E. W. Olszewski, et al., "Velocity dispersion profiles of seven dwarf spheroidal galaxies," *The Astrophysical Journal*, vol. 667, pp. L53–L56, 2007.

[12] M. G. Walker, M. Mateo, and E. W. Olszewski, "Systemic proper motions of Milky Way satellites from stellar redshifts: the Carina, Fornax, Sculptor, and Sextans dwarf spheroidals," *The Astrophysical Journal*, vol. 687, no. 2, pp. L75–L78, 2008.

[13] L. E. Strigari, J. S. Bullock, M. Kaplinghat, et al., "A common mass scale for satellite galaxies of the Milky Way," *Nature*, vol. 454, no. 7208, pp. 1096–1097, 2008.

[14] E. L. Lokas, "The mass and velocity anisotropy of the Carina, Fornax, Sculptor and Sextans dwarf spheroidal galaxies," *Monthly Notices of the Royal Astronomical Society*, vol. 394, pp. L102–L106, 2009.

[15] B. Willman, M. R. Blanton, A. A. West, et al., "A new Milky Way companion: unusual globular cluster or extreme dwarf satellite?" *The Astronomical Journal*, vol. 129, no. 6, pp. 2692–2700, 2005.

[16] B. Willman, J. J. Dalcanton, D. Martinez-Delgado, et al., "A new Milky Way dwarf galaxy in Ursa major," *The Astrophysical Journal*, vol. 626, no. 2, pp. L85–L88, 2005.

[17] V. Belokurov, D. B. Zucker, N. W. Evans, et al., "Cats and dogs, hair and a hero: a quintet of new Milky Way companions," *The Astrophysical Journal*, vol. 654, no. 2, pp. 897–906, 2007.

[18] R. R. Munoz, J. L. Carlin, P. M. Frinchaboy, D. L. Nidever, S. R. Majewski, and R. J. Patterson, "Exploring halo substructure with giant stars: the dynamics and metallicity of the dwarf spheroidal in bootes," *The Astrophysical Journal*, vol. 650, no. 1, pp. L51–L54, 2006.

[19] N. F. Martin, R. A. Ibata, S. C. Chapman, M. Irwin, and G. F. Lewis, "A Keck/DEIMOS spectroscopic survey of faint galactic satellites: searching for the least massive dwarf galaxies," *Monthly Notices of the Royal Astronomical Society*, vol. 380, no. 1, pp. 281–300, 2007.

[20] J. D. Simon and M. Geha, "The kinematics of the ultra-faint Milky Way satellites: solving the missing satellite problem," *The Astrophysical Journal*, vol. 670, no. 1, pp. 313–331, 2007.

[21] M. Geha, B. Willman, J. D. Simon, et al., "The least luminous galaxy: spectroscopy of the Milky Way satellite segue 1," *The Astrophysical Journal*, vol. 692, pp. 1464–1475, 2009.

[22] E. N. Kirby, J. D. Simon, M. Geha, P. Guhathakurta, and A. Frebel, "Uncovering extremely metal-poor stars in the Milky Way's ultrafaint dwarf spheroidal satellite galaxies," *The Astrophysical Journal*, vol. 685, no. 1, pp. L43–L46, 2008.

[23] L. E. Strigari, J. S. Bullock, M. Kaplinghat, J. Diemand, M. Kuhlen, and P. Madau, "Redefining the missing satellites problem," *The Astrophysical Journal*, vol. 669, no. 2, pp. 676–683, 2007.

[24] L. E. Strigari, S. M. Koushiappas, J. S. Bullock, and M. Kaplinghat, "Precise constraints on the dark matter content of Milky Way dwarf galaxies for gamma-ray experiments," *Physical Review D*, vol. 75, no. 8, Article ID 083526, 2007.

[25] R. Essig, N. Sehgal, and L. E. Strigari, "Bounds on cross sections and lifetimes for dark matter annihilation and decay into charged leptons from gamma-ray observations of dwarf galaxies," *Physical Review D*, vol. 80, no. 2, Article ID 023506, 2009.

[26] G. D. Martinez, J. S. Bullock, M. Kaplinghat, L. E. Strigari, and R. Trotta, "Indirect dark matter detection from dwarf satellites: joint expectations from astrophysics and supersymmetry," *Journal of Cosmology and Astroparticle Physics*, vol. 2009, no. 6, article 014, 2009.

[27] C. J. Hogan and J. J. Dalcanton, "New dark matter physics: clues from halo structure," *Physical Review D*, vol. 62, Article ID 063511, 2000.

[28] O. E. Gerhard, "A new family of distribution functions for spherical galaxies," *Monthly Notices of the Royal Astronomical Society*, vol. 250, pp. 812–830, 1991.

[29] P. C. Gregory, *Bayesian Logical Data Analysis for the Physical Sciences: A Comparative Approach with 'Mathematica' Support*, Cambridge University Press, Cambridge, UK, 2005.

[30] L. E. Strigari, S. M. Koushiappas, J. S. Bullock, et al., "The most dark-matter-dominated galaxies: predicted gamma-ray signals from the faintest Milky Way dwarfs," *The Astrophysical Journal*, vol. 678, no. 2, pp. 614–620, 2008.

[31] M. Kaplinghat and L. E. Strigari, "Proper motion of Milky Way dwarf spheroidals from line-of-sight velocities," *The Astrophysical Journal*, vol. 682, no. 2, pp. L93–L96, 2008.

[32] R. P. van der Marel, D. R. Alves, E. Hardy, and N. B. Suntzeff, "New understanding of large magellanic cloud structure, dynamics, and orbit from carbon star kinematics," *The Astronomical Journal*, vol. 124, pp. 2639–2663, 2002.

[33] R. P. van der Marel and P. Guhathakurta, "M31 transverse velocity and local group mass from satellite kinematics," *Astrophysical Journal*, vol. 678, no. 1, pp. 187–199, 2008.

[34] N. F. Martin, J. T. A. de Jong, and H.-W. Rix, "A comprehensive maximum likelihood analysis of the structural properties of faint Milky Way satellites," *The Astrophysical Journal*, vol. 684, no. 2, pp. 1075–1092, 2008.

[35] M. Odenkirchen, E. K. Grebel, D. Harbeck, et al., "New insights on the Draco dwarf spheroidal galaxy from the Sloan Digital Sky Survey: a larger radius and no tidal tails," *The Astronomical Journal*, vol. 122, no. 5, pp. 2538–2553, 2001.

[36] D. Lynden-Bell, "Dwarf galaxies and globular clusters in high velocity hydrogen streams," *Monthly Notices of the Royal Astronomical Society*, vol. 174, pp. 695–710, 1976.

[37] E. D'Onghia and G. Lake, "Small dwarf galaxies within larger dwarfs: why some are luminous while most go dark," *The Astrophysical Journal*, vol. 686, no. 2, pp. L61–L65, 2008.

[38] M. Metz, P. Kroupa, C. Theis, G. Hensler, and H. Jerjen, "Did the Milky Way dwarf satellites enter the halo as a group?" *The Astrophysical Journal*, vol. 697, no. 1, pp. 269–274, 2009.

[39] K. B. Westfall, S. R. Majewski, J. C. Ostheimer, et al., "Exploring halo substructure with giant stars. VIII. The extended structure of the Sculptor dwarf spheroidal galaxy," *The Astronomical Journal*, vol. 131, no. 1, pp. 375–406, 2006.

[40] G. Battaglia, A. Helmi, E. Tolstoy, M. Irwin, V. Hill, and P. Jablonka, "The kinematic status and mass content of the Sculptor dwarf spheroidal galaxy," *The Astrophysical Journal*, vol. 681, no. 1, pp. L13–L16, 2008.

[41] S. Piatek, C. Pryor, P. Bristow, et al., "Proper motions of dwarf spheroidal galaxies from Hubble Space Telescope imaging. IV. Measurement for Sculptor," *The Astronomical Journal*, vol. 131, no. 3, pp. 1445–1460, 2006.

[42] M. G. Walker, M. Mateo, and E. W. Olszewski, "Stellar velocities in the Carina, Fornax, Sculptor, and Sextans dsph galaxies: data from the magellan/MMFS survey," *The Astronomical Journal*, vol. 137, no. 2, pp. 3100–3108, 2009.

[43] D. Merritt, "The distribution of dark matter in the coma cluster," *The Astrophysical Journal*, vol. 313, pp. 121–135, 1987.

[44] M. Niederste-Ostholt, V. Belokurov, N. W. Evans, G. Gilmore, R. F. G. Wyse, and J. E. Norris, "The origin of Segue 1," *Monthly Notices of the Royal Astronomical Society*, vol. 398, no. 4, pp. 1771–1781, 2009.

[45] J. Binney and S. Tremaine, *Galactic Dynamics*, Princeton University Press, Princeton, NJ, USA, 2nd edition, 2008.

[46] M. Irwin and D. Hatzidimitriou, "Structural parameters for the galactic dwarf spheroidals," *Monthly Notices of the Royal Astronomical Society*, vol. 277, pp. 1354–1378, 1995.

[47] R. R. Munoz, S. R. Majewski, S. Zaggia, et al., "Exploring halo substructure with giant stars. XI. The tidal tails of the Carina dwarf spheroidal galaxy and the discovery of magellanic cloud stars in the Carina foreground," *The Astrophysical Journal*, vol. 649, no. 1, pp. 201–223, 2006.

[48] V. Smolcic, D. B. Zucker, E. F. Bell, et al., "Improved photometry of sloan digital sky survey crowded-field images: structure and dark matter content in the dwarf spheroidal galaxy Leo I," *The Astronomical Journal*, vol. 134, no. 5, pp. 1901–1915, 2007.

[49] M. G. Coleman and J. T. A. de Jong, "A deep survey of the Fornax dSph. I. Star formation history," *The Astrophysical Journal*, vol. 685, no. 2, pp. 933–946, 2008.

[50] H.-S. Zhao, "Analytical dynamical models for double power-law galactic nuclei," *Monthly Notices of the Royal Astronomical Society*, vol. 287, no. 3, pp. 525–537, 1997.

[51] J. F. Navarro, A. Ludlow, V. Springel, et al., "The diversity and similarity of cold dark matter halos," http://arxiv.org/abs/0810.1522.

[52] L. E. Strigari, J. S. Bullock, and M. Kaplinghat, "Determining the nature of dark matter with astrometry," *The Astrophysical Journal*, vol. 657, no. 1, part 2, pp. L1–L4, 2007.

[53] M. G. Walker, M. Mateo, E. W. Olszewski, J. Peñarrubia, N. Wyn Evans, and G. Gilmore, "A universal mass profile for dwarf spheroidal galaxies?" *The Astrophysical Journal*, vol. 704, pp. 1274–1287, 2009.

[54] J. Wolf, G. D. Martinez, J. S. Bullock, et al., "Accurate masses for dispersion-supported galaxies," http://arxiv.org/abs/0908.2995.

[55] H. Jeffreys, *Theory of Probability*, Oxford University Press, Oxford, UK, 1961.

[56] V. Springel, J. Wang, M. Vogelsberger, et al., "The Aquarius Project: the subhaloes of galactic haloes," *Monthly Notices of the Royal Astronomical Society*, vol. 391, no. 4, pp. 1685–1711, 2008.

[57] M. I. Wilkinson, J. Kleyna, N. W. Evans, and G. Gilmore, "Dark matter in dwarf spheroidals - I. Models," *Monthly Notices of the Royal Astronomical Society*, vol. 330, no. 4, pp. 778–791, 2002.

[58] S. R. Majewski, J. Bullock, A. Burkert, et al., "Galactic dynamics and local dark matter," in *SIM Lite Astrometric Observatory*, American Astronomical Society, Washington, DC, USA, 2009.

[59] E. L. Lokas, S. Kazantzidis, J. Klimentowski, L. Mayer, and S. Callegari, "The stellar structure and kinematics of dwarf spheroidal galaxies formed by tidal stirring," http://arxiv.org/abs/0906.5084.

Hindawi Publishing Corporation
Advances in Astronomy
Volume 2010, Article ID 162083, 15 pages
doi:10.1155/2010/162083

Review Article

The Dark Matter Annihilation Signal from Dwarf Galaxies and Subhalos

Michael Kuhlen

School of Natural Science, Institute for Advanced Study, Einstein Lane, Princeton, NJ 08540, USA

Correspondence should be addressed to Michael Kuhlen, mqk@astro.berkeley.edu

Received 8 June 2009; Accepted 13 August 2009

Academic Editor: Andrey V. Kravtsov

Dark Matter annihilation holds great potential for directly probing the clumpiness of the Galactic halo that is one of the key predictions of the Cold Dark Matter paradigm of hierarchical structure formation. Here we review the γ-ray signal arising from dark matter annihilation in the centers of Galactic subhalos. We consider both known Galactic dwarf satellite galaxies and dark clumps without a stellar component as potential sources. Utilizing the *Via Lactea II* numerical simulation, we estimate fluxes for 18 Galactic dwarf spheroidals with published central densities. The most promising source is Segue 1, followed by Ursa Major II, Ursa Minor, Draco, and Carina. We show that if any of the known Galactic satellites can be detected, then at least ten times more subhalos should be visible, with a significant fraction of them being dark clumps.

1. Introduction

A decade has gone by since the emergence of the "Missing Satellite Problem" [1, 2], which refers to the apparent discrepancy between the observed number of Milky Way satellite galaxies, 23 by latest count [3–12], and the predicted number of dark matter (DM) subhalos that should be orbiting in the Milky Way's halo. The latest cosmological numerical simulations [13–15] resolve close to 100,000 individual self-bound clumps of DM within the Galactic virial volume—remnants of the hierarchical build-up of the Milky Way's DM halo. Several hundred of these may be large enough to host a dwarf galaxy. A consensus seems to be emerging that this discrepancy is not a short-coming of the otherwise tremendously successful Cold Dark Matter (CDM) hypothesis [16, 17], but instead reflects the complicated baryonic physics that determines which subhalos are able to host a luminous stellar component and which are not [18–24]. If this explanation is correct, then an immediate consequence is that the Milky Way dark halo should be filled with clumps on all scales down to the CDM free-streaming scale at 10^{-12} to $10^{-4}\,M_\odot$ for cold thermal relics (e.g., supersymmetric CDM) [25–28] or as low as $\sim 10^{-20}\,M_\odot$ in the case of non-thermal cold axions [29–31]. At the moment there is little empirical evidence for or against this prediction, and this has motivated searches for new signals that could provide tests of this hypothesis, and ultimately help to constrain the nature of the DM particle.

One of the most promising such signals is DM annihilation [32]. In regions of sufficiently high density, for example in the centers of Galactic subhalos, the DM pair annihilation rate might become large enough to allow for a detection of neutrinos, energetic electrons and positrons, or γ-ray photons, which are the by-products of the annihilation process. This is one of the few ways in which the dark sector can be coupled to ordinary matter and radiation amenable to astronomical observation. Belying its commonly used name of "indirect detection", DM annihilation is really the only way we can hope to directly probe the clumpiness of the Galactic DM distribution. One could argue that it is a more "direct" method than trying to constrain DM clumpiness from its effects on strong gravitational lensing (see Zackrisson & Riehm's contribution in this special edition), or from the kinematics of stars orbiting in DM-dominated potentials [33], or from perturbations of cold stellar structures like globular cluster tidal streams [34–37] or the heating of the Milky Way's stellar disk [38–40], although all of these are also worthwhile approaches to take.

The only trouble with the DM annihilation signal is that so far there have been no undisputed claims of its detection.

Recently there have been several reports of "anomalous" features in the local cosmic ray flux: the PAMELA satellite reported an increasing positron fraction at energies between 10 and 100 GeV [41], where standard models of cosmic ray propagation predict a decreasing fraction; the ATIC [42] and PPB-BETS [43] balloon-borne experiments reported a surprisingly large total electron and positron flux at ~500 GeV, although recent *Fermi* [44] and H.E.S.S. data [45] appear to be inconsistent with it. Either of these cosmic ray anomalies might be the long sought after signature of local DM annihilation. However, since the currently available data can equally well be explained by conventional astrophysical sources (e.g., nearby pulsars or supernova remnants), they hardly provide incontrovertible evidence for DM annihilation. The next few years hold great potential for progress, since the recently launched *Fermi Gamma-ray Space Telescope* will conduct a blind survey of the γ-ray sky at unprecedented sensitivity, energy extent, and angular resolution. At the same time, Atmospheric Cerenkov Telescopes, such as H.E.S.S., VERITAS, MAGIC, and STACEE, are greatly increasing their sensitivity, and have only recently begun to search for a DM annihilation signal from the centers of nearby dwarf satellite galaxies [46–50].

The purpose of this paper is to provide an overview of the potential DM annihilation signal from individual Galactic DM subhalos, either as dwarf satellite galaxies or as dark clumps. It does not cover a number of very interesting and closely related topics, which are actively being researched and deserve to be examined in equal detail. These include the diffuse flux from Galactic substructure and its anisotropies (e.g., [51–53]), the relative strength of the signal from individual subhalos compared with that from the Galactic Center or an annulus around it [54, 55], the effect of a nearby DM subhalo on the amplitude and spectrum of the local high energy electron and positron flux [56, 57], and the role of the Sommerfeld enhancement [58] on the DM annihilation rate and its implications for substructure signals [59–61].

This paper is organized as follows: we first review the basic physics of DM annihilation, briefly touching on the relic density calculation, the "WIMP miracle", DM particle candidates, and, in more detail, the sources of γ-rays from DM annihilation. In the following section we review what numerical simulations have revealed about the basic properties of DM subhalos that are relevant for the annihilation signal. We go on to consider known Milky Way dwarf spheroidal galaxies as sources, using the *Via Lactea II* simulation to infer the most likely annihilation fluxes from published values of the dwarfs' central masses. Next we discuss the possibility of a DM annihilation signal from dark clumps, halos that have too low a mass to host a luminous stellar component. Lastly, we briefly discuss the role of the substructure boost factor for the detectability of individual DM subhalos.

2. Dark Matter Annihilation

If DM is made up of a so-called "thermal relic" particle, (An alternative DM candidate is the axion, a non-thermal relic particle motivated as a solution to the strong CP problem [62]. Since it does not produce an annihilation signal today, we do not further consider it here.) its abundance today is set by its annihilation cross section in the early universe. The thermal relic abundance calculation relating today's abundance of DM to the properties of the DM particle (its mass and annihilation cross section) is straightforward and elegant, and has been described in pedagogical detail previously [63–65]. We briefly summarize the story here.

At sufficiently early times, the DM particles are in thermal equilibrium with the rest of the universe. As long as they remain relativistic ($T \gg m_\chi$), their creation and destruction rates are balanced, and hence their comoving abundance remains constant. Once the universe cools below the DM particle's rest-mass ($T < m_\chi$), its equilibrium abundance is suppressed by a Boltzmann factor $\exp(-m_\chi/T)$. If equilibrium had been maintained until today, the DM particles would have completely annihilated away. Instead the expansion of the universe comes to the rescue and causes the DM particles to fall out of equilibrium once the expansion rate (given by $H(a)$, the Hubble constant at cosmological scale factor a) exceeds the annihilation rate $\Gamma(a) = n\langle\sigma v\rangle$, that is, when DM particles can no longer find each other to annihilate. The comoving number density of DM particles is then fixed at a "freeze-out" temperature that turns out to be approximately $T_f \simeq m_\chi/20$, with only a weak additional logarithmic dependence on the mass and cross section of the DM particle. A back of the envelope calculation results in the following relation between Ω_χ, the relic mass density in units of the critical density of the universe $\rho_{\rm crit} = 3H_0^2/8\pi G$, and $\langle\sigma v\rangle$, the thermally averaged velocity-weighted annihilation cross section:

$$\omega_\chi = \Omega_\chi h^2 = \frac{3\times 10^{-27}\,\mathrm{cm^3\,s^{-1}}}{\langle\sigma v\rangle}. \quad (1)$$

Note that this relation is independent of m_χ. The WMAP satellite's measurement of the DM density is $\omega_\chi = 0.1131 \pm 0.0034$ [66], implying a value of

$$\langle\sigma v\rangle \approx 3\times 10^{-26}\,\mathrm{cm^3\,s^{-1}}. \quad (2)$$

A more accurate determination of $\langle\sigma v\rangle$ must rely on a numerical solution of the Boltzmann equation in an expanding universe, taking into account the full temperature dependence of the annihilation rate, including the possibilities of resonances and coannihilations into other, nearly degenerate dark sector particles (e.g., [67, 68]). It is a remarkable coincidence that this value of $\langle\sigma v\rangle$ is close to what one expects for a cross section set by the weak interaction. This is the so-called "WIMP miracle", and it is the main motivation for considering weakly interacting massive particles (WIMPs) as prime DM candidates.

The Standard Model of particle physics actually provides one class of WIMPs, massive neutrinos. Although neutrinos thus constitute a form of DM, they cannot make up the bulk of it, since their small mass, $\sum m_\nu < 0.63\,\mathrm{eV}$ [66], implies a cosmological mass density of only $\omega_\nu = 7.1\times 10^{-3}$. Since the standard neutrino is a hot dark matter particle, increasing its contribution to the total matter density would

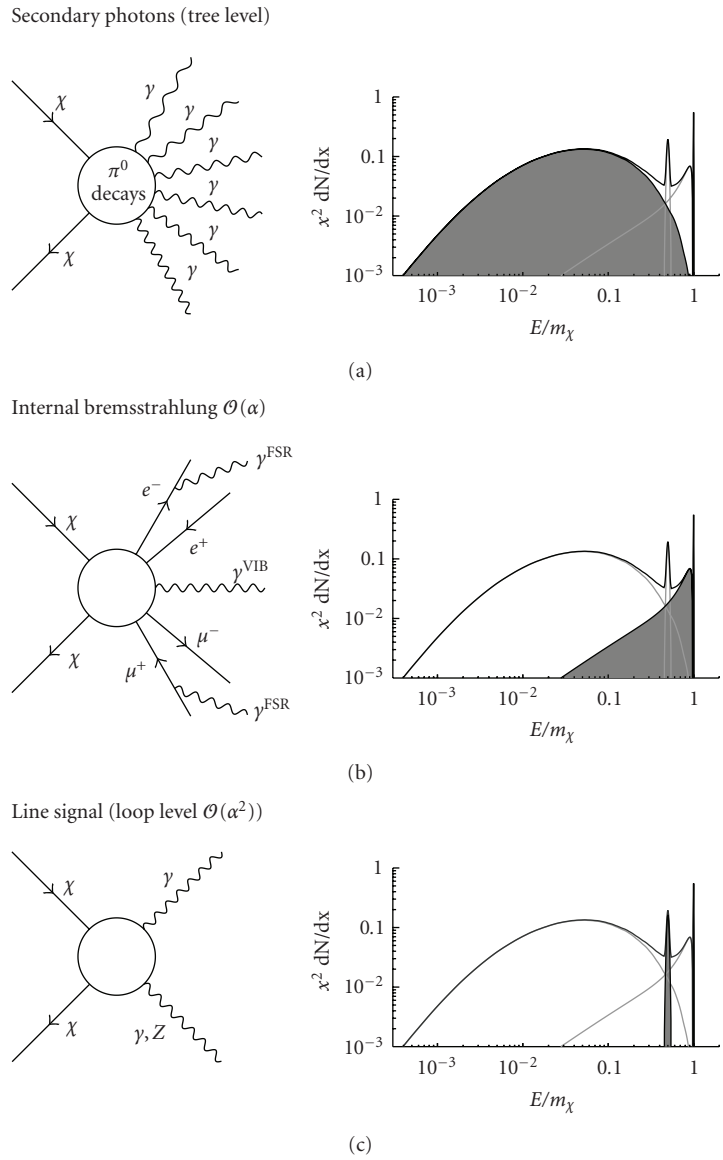

Figure 1: A schematic of the different sources and energy distributions of γ-rays from WIMP annihilation. (a) Secondary photons arising from the decay of neutral pions produced in the hadronization of primary annihilation products. (b) Internal bremsstrahlung photons associated with charged annihilation products, either in the form of final state radiation (FSR) from external legs or as virtual internal bremsstrahlung (VIB) from the exchange of virtual charged particles. (c) Monochromatic line signals from the prompt annihilation into two photons or a photon and Z boson. This process occurs only at loop level, and hence is typically strongly suppressed.

destroy small scale structure and violate constraints from galaxy clustering and the Lyman alpha forest. The attention thus turns to extensions of the Standard Model, which themselves are theoretically motivated by the hierarchy problem (the enormous disparity between the weak and Planck scales) and the quest for a unification of gravity and quantum mechanics. The most widely studied class of such models consists of supersymmetric extensions of the Standard Model. Additionally models with extra dimensions have received a lot of attention in recent years. Both of these approaches offer good DM particle candidates: the lightest supersymmetric particle (LSP), typically a *neutralino* in R-parity conserving supersymmetry, and the lightest Kaluza-Klein particle (LKP), typically the $B^{(1)}$ particle, the first Kaluza-Klein excitation of the hypercharge gauge boson, in Universal Extra Dimension models. For much more information, we recommend the comprehensive recent review of particle DM candidates by Bertone et al. [65].

The direct products of the annihilation of two DM particles are strongly model dependent. Typical channels include annihilations into charged leptons ($e^+e^-, \mu^+\mu^-$, $\tau^+\tau^-$), quark-antiquark pairs, and gauge and Higgs bosons (W^+W^-, ZZ, Zh, hh). In the end, however, the decay and hadronization of these annihilation products results in only three types of emissions: (i) high energy neutrinos and antineutrinos, (ii) relativistic electrons and protons and their antiparticles, and (iii) γ-ray photons. Additional lower energy photons can result from the interaction of

the relativistic electrons with magnetic fields (synchrotron radiation), with interstellar material (bremsstrahlung), and with the CMB and stellar radiation fields (inverse Compton scattering). In the following we will focus on the γ-rays, since they are likely the strongest signal from Galactic DM substructure. γ-rays are produced in DM annihilations in three ways (see accompanying Figure 1).

(i) Since the DM particle is neutral, there is no direct coupling to photons. Nevertheless, copious amounts of secondary γ-ray photons can be produced through the decay of neutral pions, $\pi^0 \rightarrow \gamma\gamma$, arising in the hadronization of the primary annihilation products. Since the DM particles are non-relativistic, their annihilation results in a pair of monoenergetic particles with energy equal to m_χ, which fragment and decay into π-meson dominated "jets". In this way a single DM annihilation event can produce several tens of γ-ray photons. The result is a broad spectrum with a cutoff around m_χ.

(ii) An important additional contribution at high energies ($E \lesssim m_\chi$) arises from the internal bremsstrahlung process [69], which may occur with any charged annihilation product. One can distinguish between final state radiation, in which the photon is radiated from an external leg, and virtual internal bremsstrahlung, arising from the exchange of a charged virtual particle. Note that neither of these processes requires an external electromagnetic field (hence the name *internal* bremsstrahlung). The resulting γ-ray spectrum is peaked towards $E \sim m_\chi$ and exhibits a sharp cutoff. Although it is suppressed by one factor of the coupling α compared to pion decays, it can produce a distinctive spectral feature at high energies. This could aide the confirmation of a DM annihilation nature of any source and might allow a direct determination of m_χ.

(iii) Lastly, it is possible for DM particles to directly produce γ-ray photons, but one has to go to loop-level to find contributing Feynman diagrams, and hence this flux is typically strongly suppressed by two factors of α (although exceptions exist [70]). On the other hand, the resulting photons would be monochromatic, and a detection of such a line signal would provide strong evidence of a DM annihilation origin of any signal. While annihilations directly into two photons, $\chi\chi \rightarrow \gamma\gamma$, would produce a narrow line at $E = m_\chi$, in some models it is also possible to annihilate into a photon and a Z boson, $\chi\chi \rightarrow \gamma Z$, and this process would result in a somewhat broadened (due to the mass of the Z) line at $E \sim m_\chi(1 - m_Z^2/4m_\chi^2)$.

The relative importance of these three γ-ray production channels and the resulting spectrum dN_γ/dE depend on the details of the DM particle model under consideration. For any given model, realistic γ-ray spectra can be calculated using sophisticated and publicly available computer programs, such as the PYTHIA Monte-Carlo event generator [71], which is also contained in the popular DarkSUSY package [72].

3. Dark Matter Substructure as Discrete γ-Ray Sources

DM subhalos as individual discrete γ-ray sources hold great potential for providing a "smoking gun" signature of DM annihilation [32, 54, 54, 73–83]. Compared to diffuse γ-ray annihilation signals, these discrete sources should be easier to distinguish from astrophysical backgrounds and foregrounds [84], since (a) typical astrophysical sources of high energy γ-rays, such as pulsars and supernova remnants, are very rare in dwarf galaxies, owing to their predominantly old stellar populations, (b) the DM annihilation flux should be time-independent, (c) angularly extended, and (d) not exhibit any (or only very weak) low energy emission due to the absence of strong magnetic fields or stellar radiation fields. (Inverse Compton radiation from scattering off the CMB, however, may be present.)

We can distinguish between DM subhalos hosting a Milky Way dwarf satellite galaxy and dark clumps that, for whatever reason, do not host a luminous stellar population, or one that is too faint to have been detected up to now. Before we go on to discuss the prospects of detecting a DM annihilation signal from these two classes of sources, we review the basic properties of DM subhalos common to both.

Numerical simulations have shown that pure DM (sub)halos have density profiles that are well described by a Navarro, Frenk & White (NFW) [85] profile over a wide range of masses [86, 87],

$$\rho_{\rm NFW}(r) = \frac{4\rho_s}{(r/r_s)(1 + r/r_s)^2}. \quad (3)$$

The parameter r_s indicates the radius at which the logarithmic slope $\gamma(r) \equiv d\ln\rho/d\ln r = -2$, and $\rho(r_s) = \rho_s$. The very highest resolution simulations have recently provided some indications of a flattening of the density profile in the innermost regions [15, 88]. In this case a so-called Einasto profile may provide a better overall fit,

$$\rho_{\rm Einasto}(r) = \rho_s \exp\left[-\frac{2}{\alpha}\left(\left(\frac{r}{r_s}\right)^\alpha - 1\right)\right]. \quad (4)$$

Here the additional parameter α governs how fast the profile rolls over, and has been found to have a value of $\alpha \approx 0.17 \pm 0.03$ in numerical simulations [88]. Note that the two density profiles actually do not differ very much until $r \ll r_s$ (cf. Figure 2(a)). Simulated DM halos are of course not perfectly spherically symmetric, and instead typically exhibit prolate or triaxial isodensity contours that become more elongated towards the center [89]. The degree of prolateness decreases with mass, and galactic subhalos have axis ratios of $\gtrsim 0.7$ [90].

The "virial" radius $R_{\rm vir}$ of a halo is defined as the radius enclosing a mean density equal to $\Delta_{\rm vir}\rho_0$, where $\Delta_{\rm vir} \approx 389$ (from a spherical collapse calculation [91]) and ρ_0 is the mean density of the universe. The corresponding virial mass $M_{\rm vir}$ is the mass within $R_{\rm vir}$, and a halo's concentration

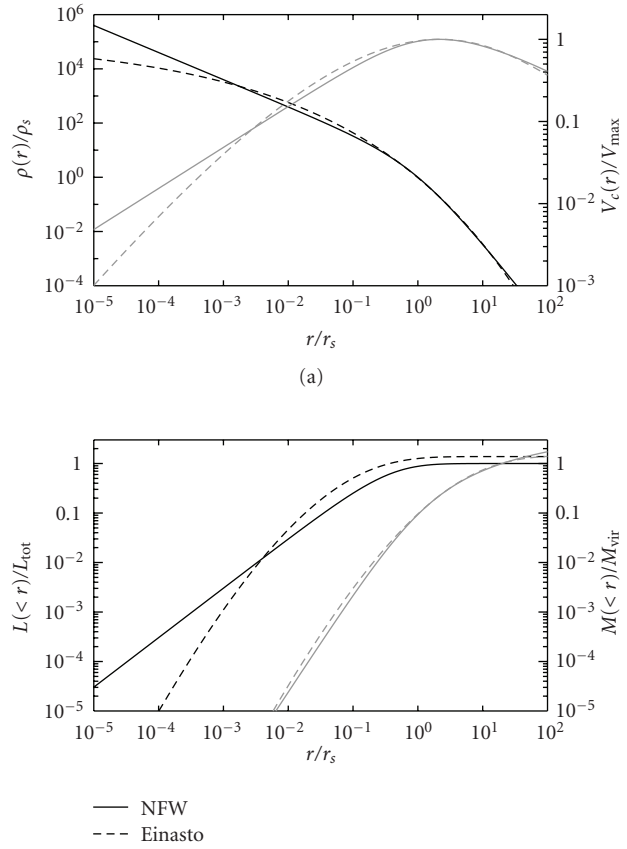

FIGURE 2: A comparison of NFW and Einasto ($\alpha = 0.17$) radial profiles of density (top, dark lines, left axis), circular velocity (top, light lines, right axis), enclosed annihilation luminosity (bottom, dark lines, left axis), enclosed mass (bottom, light lines, right axis). The density profiles have been normalized to have the same $V_{\max}$ and $r_{\rm Vmax}$.

can then be defined as $c = R_{\rm vir}/r_s$. While these quantities are well defined for isolated halos and commonly used in analytic models, they are somewhat less applicable to galactic subhalos, since the outer radius of a subhalo is set by tidal truncation, which depends on the subhalo's location within its host halo. Furthermore, in numerical simulations it is difficult to resolve r_s in low mass subhalos. For this reason we prefer to work with $V_{\max}$, the maximum of the circular velocity curve $V_c(r)^2 = GM(<r)/r$ and a proxy for a subhalo's mass, and $r_{\rm Vmax}$, the radius at which $V_{\max}$ occurs. These quantities are much more robustly determined for subhalos in numerical simulations than (M, c). Note that even $(V_{\max}, r_{\rm Vmax})$ can be affected by tidal interactions with the host halo, especially for subhalos close to the host halo center. For this reason we also sometimes consider $V_{\rm peak}$, the largest value of $V_{\max}$ that a subhalo ever acquired during its lifetime (i.e., before tidal stripping began to lower its $V_{\max}$) and $r_{\rm Vpeak}$, the corresponding radius.

Since DM annihilation is a two body process, its rate is proportional to the square of the local density, and the annihilation "luminosity" is given by the volume integral of $\rho(r)^2$,

$$\mathcal{L}(<r) \equiv \int_0^r \rho^2 dV. \tag{5}$$

$\mathcal{L}$ has dimensions of (mass)^2 (length)$^{-3}$, and we express it in units of $\mathrm{M}_\odot^2\ \mathrm{pc}^{-3}$. In order to convert to a conventional luminosity, one must multiply by a particle physics term,

$$L = c^2 \frac{\langle \sigma v \rangle}{m_\chi} \mathcal{L}, \tag{6}$$

where c is the speed of light, m_χ the mass of the DM particle and $\langle \sigma v \rangle$ the thermally averaged velocity-weighted annihilation cross section discussed in the previous section. This is the *total* luminosity, but we are interested here only in the fraction emitted as γ-rays. Furthermore, a given detector is only sensitive to γ-rays above a threshold energy of $E_{\rm th}$ and below a maximum energy of $E_{\max}$. In that case the effective γ-ray luminosity is

$$L_\gamma^{\rm eff} = \left[\frac{\langle \sigma v \rangle}{2 m_\chi^2} \int_{E_{\rm th}}^{E_{\max}} E \frac{dN_\gamma}{dE} dE \right] \mathcal{L}, \tag{7}$$

where dN_γ/dE is the spectrum of γ-ray photons produced in a single annihilation event.

A comparison of the enclosed luminosity and mass profiles is shown in the bottom panel of Figure 2. Clearly, $\mathcal{L}$ is much more centrally concentrated than M: ~90% of the total luminosity is produced within r_s, compared with only 10% of the total mass. In terms of $(V_{\max}, r_{\rm Vmax})$, the total luminosity of a halo is given by

$$\mathcal{L} = f \frac{V_{\max}^4}{G^2 r_{\rm Vmax}}, \tag{8}$$

where f is an $\mathcal{O}(1)$ numerical factor that depends on the shape of the density profile; for an NFW profile $f = 1.227$, and for an $\alpha = 0.17$ Einasto profile $f = 1.735$. In physical units, the total annihilation luminosity is

$$\mathcal{L} = \begin{matrix} 1.1 \\ 1.5 \end{matrix} \times 10^7\ \mathrm{M}_\odot^2\ \mathrm{pc}^{-3} \left(\frac{V_{\max}}{20\ \mathrm{km\ s}^{-1}} \right)^4 \left(\frac{r_{\rm Vmax}}{1\ \mathrm{kpc}} \right)^{-1}, \tag{9}$$

for NFW (top) and $\alpha = 0.17$ Einasto (bottom). Note that even though the slope of the Einasto profile is shallower than NFW in the very center, the total luminosity exceeds that of an NFW halo with the same $(V_{\max}, r_{\rm Vmax})$. This is due to the fact that the Einasto profile rolls over less rapidly than the NFW profile, and actually has slightly higher density than NFW between r_s and a cross-over point at $\sim 10^{-3} r_s$.

4. Milky Way Dwarf Spheroidal Galaxies

There are several advantages of known dwarf satellite galaxies as DM annihilation sources: firstly, the kinematics of individual stars imply mass-to-light ratios of up to several hundred [92–95], and hence there is an a priori expectation of high DM densities; secondly, since we know their location

in the sky, it is possible to directly target them with sensitive atmospheric Cerenkov telescopes (ACT) such as H.E.S.S., VERITAS, MAGIC, and STACEE, whose small field of view makes blind searches impractical; lastly, our approximate knowledge of the distances to many dwarf satellites would allow a determination of the absolute annihilation rate, which may lead to a direct constraint on the annihilation cross section, if the DM particle mass can be independently measured (from the shape of the spectrum, e.g.).

Recent observational progress utilizing the Sloan Digital Sky Survey (SDSS) has more than doubled the number of known dwarf spheroidal (dSph) satellite galaxies orbiting the Milky Way [4–12], raising the total from the 9 "classical" ones to 23. Many of the newly discovered satellites are so-called "ultra-faint" dSph's, with luminosities as low as $1,000 L_\odot$ and only tens to hundreds of spectroscopically confirmed member stars. Simply accounting for the SDSS sky coverage (about 20%), the total number of luminous Milky Way satellites can be estimated to be at least 70. Taking into account the SDSS detection limits [96] and a radial distribution of DM subhalos motivated by numerical simulations, this estimate can grow to several hundreds of satellite galaxies in total [97, 98].

In order to assess the strength of the DM annihilation signal from these dSph's, it is necessary to have an estimate of the total dynamical mass, or at least $V_{\rm max}$, of the DM halo hosting the galaxies. Owing to the extreme faintness of these objects and their lack of a detectable gaseous component [99], it has been very difficult to obtain kinematic information that allows for such measurements. Progress has been made through spectroscopic observations of individual member stars, whose line-of-sight velocity dispersions have confirmed that these objects are in fact strongly DM dominated [92–95]. Such data best constrain the enclosed dynamical mass within the stellar extent, which on average is about 0.3 kpc for current data sets. A recent analysis has determined $M_{0.3} \equiv M(< 0.3\,\text{kpc})$ for 18 of the Milky Way dSph's, and found that, surprisingly, they all have $M_{0.3} \approx 10^7\,\text{M}_\odot$ to within a factor of two [33]. At present the physical meaning of this mass scale is unclear, but it may provide a clue to the nature of the baryonic processes that govern dwarf galaxy formation.

State-of-the-art cosmological numerical simulations of the formation of the DM halo of a Milky Way scale galaxy, such as those of the Via Lactea Project [13, 80] and the Aquarius Project [14], have now reached an adequate mass and force resolution to directly determine $M_{0.3}$ in their simulated subhalos. This makes it possible to infer the most likely values of $(V_{\rm max}, r_{\rm Vmax})$ for a Milky Way dSph of a given $M_{0.3}$ and Galacto-centric distance D, by identifying all simulated subhalos with comparable $M_{0.3}$ and D and averaging over their $(V_{\rm max}, r_{\rm Vmax})$. This analysis was performed for the 9 "classical" dwarfs using the *Via Lactea I* simulation [22], and we extend it here to all 18 dwarfs published in [33] and with the more recent and higher resolution *Via Lactea II* (VL2) simulation.

For each of the Milky Way dSph's studied in [33] we created a list of all VL2 subhalos with numerically determined $M_{0.3}$ within the published $1-\sigma$ error bars and distances within 40% of the measured distance of the given dSph. The distances were calculated for 100 random observer locations 8kpc from the host halo center. We then determined the median value and the 16th and 84th percentiles of $(V_{\rm max}, r_{\rm Vmax})$ and $(V_{\rm peak}, r_{\rm Vpeak})$ of the subhalos associated with each dSph. These values are given in Table 1. The median values of $V_{\rm max}$ range from $5.0\,\text{km s}^{-1}$ (Leo IV) to $19\,\text{km s}^{-1}$ (Draco, Leo I), and of $V_{\rm peak}$ from $6.7\,\text{km s}^{-1}$ (Leo IV) to $30\,\text{km s}^{-1}$ (Ursa Minor, Carina). Note that, as expected, dSph's closer to the Galactic Center typically show a larger reduction from $V_{\rm peak}$ to $V_{\rm max}$, sometimes by more than a factor of 2.

In the same fashion, we then determine the most likely annihilation luminosities for the 18 dSph's by using (9) for an NFW profile to calculate the total luminosity $\mathcal{L}_{\rm tot}$ for every simulated subhalo. Additionally, we also determine $\mathcal{L}_{0.3}$, the luminosity within 0.3 kpc from the center, motivated by the fact that we only have dynamical evidence for a DM dominated potential out to this radius. Lastly we also consider two measures of the brightness of each halo: $\mathcal{F}_{\rm tot} = \mathcal{L}_{\rm tot}/4\pi D^2$, the total expected flux from the dSph, and $\mathcal{F}_c$, the flux from a central region subtending 0.15°, which is comparable to the angular resolution of *Fermi* above 3 GeV. $\mathcal{F}_c$ thus corresponds to the brightest "pixel" in a *Fermi* γ-ray image of a subhalo. These numbers are given in Table 2.

4.1. Current Observational Constraints. Several ACT have performed observations of a handful of dSph's.

(i) The H.E.S.S. array (consisting of four $107\,\text{m}^2$ telescopes with a 5° field of view and an energy threshold of 160 GeV [100]) has obtained an 11 hour exposure of the Sagittarius dwarf galaxy. No γ-ray signal was detected, resulting in a flux limit of $3.6 \times 10^{-12}\,\text{cm}^{-2}\,\text{s}^{-1}$ (95% confidence) at $E > 250\,\text{GeV}$, and a corresponding limit on the cross section of $\langle\sigma v\rangle \lesssim 10^{-23}\,\text{cm}^3\,\text{s}^{-1}$ for an NFW profile and $\langle\sigma v\rangle \lesssim 2 \times 10^{-25}\,\text{cm}^3\,\text{s}^{-1}$ for a cored profile (for a $m_\chi = 100\,\text{GeV} - 1\,\text{TeV}$ higgsino-type neutralino) [46]. Note that the Sagittarius dwarf is undergoing a strong tidal interaction with the Milky Way galaxy [101], and no confident determination of $M_{0.3}$ has been possible.

(ii) The VERITAS array (consisting of four $144\,\text{m}^2$ telescopes with a 3.5° field of view and an energy threshold of 100 GeV [102]) has conducted a 15 hours observation of Willman 1 and 20 hour observations each of Draco and Ursa Minor [47]. No γ-ray signal was detected at a flux limit of ~1% of the flux from the Crab Nebula, corresponding to a limit of $2.4 \times 10^{-12}\,\text{cm}^{-2}\,\text{s}^{-1}$ (95% confidence) at $E > 200\,\text{GeV}$ [103].

(iii) Additionally the MAGIC [48, 49] and STACEE [50] telescopes have reported observations of Willman 1 and Draco, resulting in comparable or slightly higher flux limits.

To convert the values of $\mathcal{F}_c$ in Table 2 into physical fluxes that can directly be compared to these observational limits, it would be necessary to obtain values of the particle

Table 1: The properties of likely DM subhalos of the 18 Milky Way dSph galaxies for which $M_{0.3}$ values (column 3) have been published [33]. $V_{\rm max}$ and $r_{\rm Vmax}$ are the maximum circular velocity and its radius, $V_{\rm peak}$ and $r_{\rm Vpeak}$ the largest $V_{\rm max}$ a subhalo ever acquired and its corresponding radius. The first number is the median over all *Via Lactea II* subhalos matching the dSph's distance and $M_{0.3}$, the numbers in parentheses the 16th and 84th percentiles (see text for details).

Name	D [kpc]	$M_{0.3}$ [$10^7\,M_\odot$]	$V_{\rm max}$ [km s^{-1}]	$r_{\rm Vmax}$ [kpc]	$V_{\rm peak}$ [km s^{-1}]	$r_{\rm Vpeak}$ [kpc]
Segue 1	23	$1.58^{+3.30}_{-1.11}$	$10\,\left(^{17}_{8.4}\right)$	$0.43\,\left(^{0.89}_{0.29}\right)$	$26\,\left(^{55}_{13}\right)$	$2.4\,\left(^{33}_{1.4}\right)$
Ursa Major II	32	$1.09^{+0.89}_{-0.44}$	$13\,\left(^{17}_{11}\right)$	$0.59\,\left(^{0.89}_{0.31}\right)$	$27\,\left(^{33}_{17}\right)$	$3.3\,\left(^{14}_{2.4}\right)$
Wilman 1	38	$0.77^{+0.89}_{-0.42}$	$8.3\,\left(^{11}_{7.5}\right)$	$0.38\,\left(^{0.62}_{0.29}\right)$	$15\,\left(^{27}_{10}\right)$	$2.0\,\left(^{3.9}_{0.90}\right)$
Coma Berenices	44	$0.72^{+0.36}_{-0.28}$	$9.1\,\left(^{12}_{8.2}\right)$	$0.42\,\left(^{0.62}_{0.31}\right)$	$15\,\left(^{25}_{11}\right)$	$1.9\,\left(^{3.4}_{0.97}\right)$
Ursa Minor	66	$1.79^{+0.37}_{-0.59}$	$18\,\left(^{21}_{15}\right)$	$0.81\,\left(^{1.8}_{0.61}\right)$	$30\,\left(^{56}_{21}\right)$	$3.8\,\left(^{9.7}_{2.8}\right)$
Draco	80	$1.87^{+0.20}_{-0.29}$	$19\,\left(^{22}_{17}\right)$	$0.86\,\left(^{2.4}_{0.81}\right)$	$28\,\left(^{37}_{26}\right)$	$3.8\,\left(^{32}_{2.4}\right)$
Sculptor	80	$1.20^{+0.11}_{-0.37}$	$13\,\left(^{15}_{12}\right)$	$0.64\,\left(^{1.0}_{0.54}\right)$	$20\,\left(^{25}_{16}\right)$	$2.9\,\left(^{5.6}_{1.6}\right)$
Sextans	86	$0.57^{+0.45}_{-0.14}$	$9.7\,\left(^{12}_{8.5}\right)$	$0.52\,\left(^{0.89}_{0.37}\right)$	$14\,\left(^{19}_{11}\right)$	$1.6\,\left(^{3.0}_{0.97}\right)$
Carina	101	$1.57^{+0.19}_{-0.10}$	$17\,\left(^{22}_{16}\right)$	$1.00\,\left(^{2.3}_{0.69}\right)$	$30\,\left(^{42}_{24}\right)$	$3.8\,\left(^{32}_{3.3}\right)$
Ursa Major I	106	$1.10^{+0.70}_{-0.29}$	$14\,\left(^{17}_{13}\right)$	$0.84\,\left(^{1.3}_{0.61}\right)$	$20\,\left(^{30}_{16}\right)$	$3.2\,\left(^{6.8}_{1.6}\right)$
Fornax	138	$1.14^{+0.09}_{-0.12}$	$15\,\left(^{16}_{14}\right)$	$1.1\,\left(^{1.3}_{0.64}\right)$	$20\,\left(^{24}_{18}\right)$	$3.0\,\left(^{6.1}_{1.9}\right)$
Hercules	138	$0.72^{+0.51}_{-0.21}$	$11\,\left(^{14}_{9.4}\right)$	$0.69\,\left(^{1.1}_{0.45}\right)$	$14\,\left(^{20}_{12}\right)$	$1.9\,\left(^{3.8}_{1.2}\right)$
Canes Venatici II	151	$0.70^{+0.53}_{-0.25}$	$11\,\left(^{13}_{8.9}\right)$	$0.67\,\left(^{1.1}_{0.44}\right)$	$14\,\left(^{19}_{11}\right)$	$1.8\,\left(^{3.7}_{1.1}\right)$
Leo IV	158	$0.39^{+0.50}_{-0.29}$	$5.0\,\left(^{7.2}_{4.2}\right)$	$0.35\,\left(^{0.57}_{0.22}\right)$	$6.7\,\left(^{10}_{5.0}\right)$	$0.84\,\left(^{1.7}_{0.48}\right)$
Leo II	205	$1.43^{+0.23}_{-0.15}$	$18\,\left(^{21}_{16}\right)$	$1.5\,\left(^{2.1}_{0.93}\right)$	$24\,\left(^{28}_{19}\right)$	$4.1\,\left(^{8.2}_{2.4}\right)$
Canes Venatici I	224	$1.40^{+0.18}_{-0.19}$	$18\,\left(^{20}_{16}\right)$	$1.5\,\left(^{2.1}_{1.0}\right)$	$22\,\left(^{29}_{18}\right)$	$2.9\,\left(^{6.1}_{2.1}\right)$
Leo I	250	$1.45^{+0.27}_{-0.20}$	$19\,\left(^{21}_{17}\right)$	$1.7\,\left(^{3.1}_{1.1}\right)$	$25\,\left(^{27}_{19}\right)$	$2.9\,\left(^{6.3}_{2.1}\right)$
Leo T	417	$1.30^{+0.88}_{-0.42}$	$16\,\left(^{21}_{13}\right)$	$1.2\,\left(^{2.4}_{0.85}\right)$	$19\,\left(^{26}_{17}\right)$	$2.4\,\left(^{6.1}_{1.6}\right)$

physics term of (7) by performing a scan of the DM model parameter space. This is beyond the scope of this work, but a similar analysis has been performed by others [83, 103–106]. Current ACT observations of dSph's are beginning to directly constrain DM models, and future longer exposure time observations of additional dSph's (in particular Segue 1 and Ursa Major II) with a lower threshold energy hold great potential. We also eagerly await the first *Fermi* data on fluxes from the known dSph galaxies.

5. Dark Clumps

An annihilation signal from dark clumps not associated with any known luminous stellar counterpart would provide evidence for one of the fundamental implications of the CDM paradigm of structure formation: abundant Galactic substructure. Barring a serendipitous discovery with an ACT, the discovery of such a source will have to rely on all-sky surveys, such as provided by *Fermi*. Of course even a weak and tentative identification of a dark clump with *Fermi* could be followed up with an ACT.

Unlike for known dSph galaxies, for which we at least have some astronomical observations to guide us, we must rely entirely upon numerical simulations to quantify the prospects of detecting the annihilation signal from dark clumps. Recent significant progress [107] notwithstanding, it is at present not yet possible to perform realistic cosmological hydrodynamic galaxy-formation simulations, which include, in addition to the DM dynamics, all the relevant baryonic physics of gas cooling, star formation, supernova and AGN feedback, and so forth. that may have a significant impact on the DM distribution at the centers of massive halos. Instead we make use of the extremely high resolution, purely collisionless DM-only *Via Lactea II* (VL2) simulation [13], which provides an exquisite view of the clumpiness

Table 2: Estimated luminosities and fluxes for the 18 dSph from Table 1. $\mathcal{L}_{\rm tot}$ is the total luminosity and $\mathcal{L}_{0.3}$ the luminosity from within the central 0.3 kpc. $\mathcal{F}_{\rm tot} = \mathcal{L}_{\rm tot}/4\pi D^2$ is the total flux and $\mathcal{F}_c$ the flux from a central region subtending 0.15° (about the angular resolution of *Fermi* above 3 GeV). The first number is the median over all subhalos matching the dSph distance and $M_{0.3}$, the numbers in parentheses are the 16th and 84th percentiles. The table is ordered by decreasing $\mathcal{F}_{\rm tot}$.

Name	D [kpc]	$\mathcal{L}_{\rm tot}$ [$10^6\,M_\odot^2\,pc^{-3}$]	$\mathcal{L}_{0.3}$ [$10^6\,M_\odot^2\,pc^{-3}$]	$\mathcal{F}_{\rm tot}$ [$10^{-5}\,M_\odot^2\,pc^{-5}$]	$\mathcal{F}_c$ [$10^{-5}\,M_\odot^2\,pc^{-5}$]
Segue 1	23	$2.8\,\binom{7.2}{0.93}$	$2.5\,\binom{6.1}{0.89}$	$41\,\binom{110}{14}$	$12\,\binom{34}{5.6}$
Ursa Major II	32	$3.5\,\binom{7.2}{2.8}$	$3.1\,\binom{6.1}{2.5}$	$28\,\binom{56}{21}$	$9.5\,\binom{18}{7.7}$
Ursa Minor	66	$6.2\,\binom{9.4}{5.1}$	$4.7\,\binom{7.3}{3.1}$	$11\,\binom{17}{9.3}$	$5.2\,\binom{8.4}{2.5}$
Draco	80	$7.0\,\binom{9.9}{6.0}$	$5.6\,\binom{8.2}{3.1}$	$8.8\,\binom{12}{7.4}$	$4.3\,\binom{6.4}{1.7}$
Carina	101	$7.0\,\binom{9.4}{4.8}$	$5.6\,\binom{7.3}{3.5}$	$5.5\,\binom{7.3}{3.7}$	$3.1\,\binom{3.8}{1.6}$
Wilman 1	38	$0.88\,\binom{2.9}{0.55}$	$0.85\,\binom{2.7}{0.53}$	$4.9\,\binom{16}{3.0}$	$2.6\,\binom{6.4}{1.5}$
Coma Berenices	44	$1.2\,\binom{2.8}{0.78}$	$1.1\,\binom{2.5}{0.70}$	$4.8\,\binom{11}{3.2}$	$2.5\,\binom{5.1}{1.6}$
Sculptor	80	$2.9\,\binom{3.7}{2.3}$	$2.5\,\binom{3.3}{2.0}$	$3.7\,\binom{4.6}{2.8}$	$2.0\,\binom{2.8}{1.6}$
Ursa Major I	106	$3.3\,\binom{5.4}{2.3}$	$2.5\,\binom{4.5}{1.9}$	$2.3\,\binom{3.8}{1.6}$	$1.3\,\binom{2.4}{0.91}$
Fornax	138	$3.5\,\binom{4.4}{3.0}$	$2.9\,\binom{3.3}{2.3}$	$1.4\,\binom{1.8}{1.3}$	$1.00\,\binom{1.2}{0.74}$
Sextans	86	$1.2\,\binom{2.0}{0.77}$	$1.1\,\binom{1.8}{0.69}$	$1.3\,\binom{2.1}{0.83}$	$0.86\,\binom{1.4}{0.55}$
Leo II	205	$4.6\,\binom{6.5}{3.8}$	$3.1\,\binom{4.7}{2.1}$	$0.88\,\binom{1.2}{0.73}$	$0.55\,\binom{0.85}{0.37}$
Canes Venatici I	224	$4.6\,\binom{7.9}{3.8}$	$3.1\,\binom{5.0}{2.3}$	$0.73\,\binom{1.3}{0.60}$	$0.48\,\binom{0.79}{0.35}$
Leo I	250	$5.2\,\binom{7.9}{3.9}$	$3.2\,\binom{5.4}{2.3}$	$0.66\,\binom{1.0}{0.50}$	$0.41\,\binom{0.73}{0.31}$
Hercules	138	$1.4\,\binom{2.6}{0.94}$	$1.2\,\binom{2.2}{0.80}$	$0.57\,\binom{1.1}{0.39}$	$0.42\,\binom{0.74}{0.28}$
Canes Venatici II	151	$1.2\,\binom{2.5}{0.79}$	$1.1\,\binom{2.0}{0.68}$	$0.44\,\binom{0.88}{0.27}$	$0.33\,\binom{0.59}{0.21}$
Leo T	417	$3.5\,\binom{8.2}{2.4}$	$2.2\,\binom{4.1}{1.7}$	$0.16\,\binom{0.38}{0.11}$	$0.12\,\binom{0.24}{0.093}$
Leo IV	158	$0.14\,\binom{0.43}{0.063}$	$0.13\,\binom{0.39}{0.060}$	$0.043\,\binom{0.14}{0.020}$	$0.039\,\binom{0.12}{0.018}$

of the Galactic DM distribution, but at the expense of not capturing all the relevant physics at the baryon-dominated Galactic center. For the abundance, distribution, and internal properties of the DM subhalos that are the focus of this work, the neglect of baryonic physics is less of a problem, since they are too small to allow for much gas cooling and significant baryonic effects (this is supported by the high mass-to-light ratios observed in the Milky Way dSph's), although tidal interactions with the Galactic stellar and gaseous disk might significantly affect the population of nearby subhalos.

With a particle mass of $4,100\,M_\odot$ and a force softening of 40 pc, the VL2 simulation resolves over 50,000 subhalos today within the host's $r_{200} = 402$ kpc (the radius enclosing an average density 200 times the mean matter value). Above ~200 particles per halo, the differential subhalo mass function is well-fit by a single power law, $dN/dM \sim M^{-1.9}$, and the cumulative $V_{\rm max}$ function is $N(>V_{\rm max}) \sim V_{\rm max}^{-3}$ [13]. The radial distribution of subhalos is "antibiased" with respect to the host halo's density profile, meaning that the mass distribution becomes less clumpy as one approaches the host's center [13, 90]. Similar results have been obtained by the Aquarius group [14, 88]. Typical subhalo concentrations, defined as $\Delta_V = \langle\rho(<r_{\rm Vmax})\rangle/\rho_{\rm crit}$, grow towards the center, owing to a combination of earlier formation times [108, 109] and stronger tidal stripping of central subhalos: VL2 subhalos on average have a 60 times higher Δ_V at 8 kpc than at 400 kpc [13]. Note that this also implies ~7 times higher annihilation luminosities for central subhalos, since $\mathcal{L} \sim V_{\rm max}^4/r_{\rm Vmax} \sim V_{\rm max}^3\sqrt{\Delta_V}$. The counter-acting trends of decreasing relative abundance of subhalos and increasing annihilation luminosity towards the center makes it more difficult for (semi-)analytical methods to accurately assess the role of subhalos in the Galactic annihilation signal, and motivate future, even higher resolution, numerical

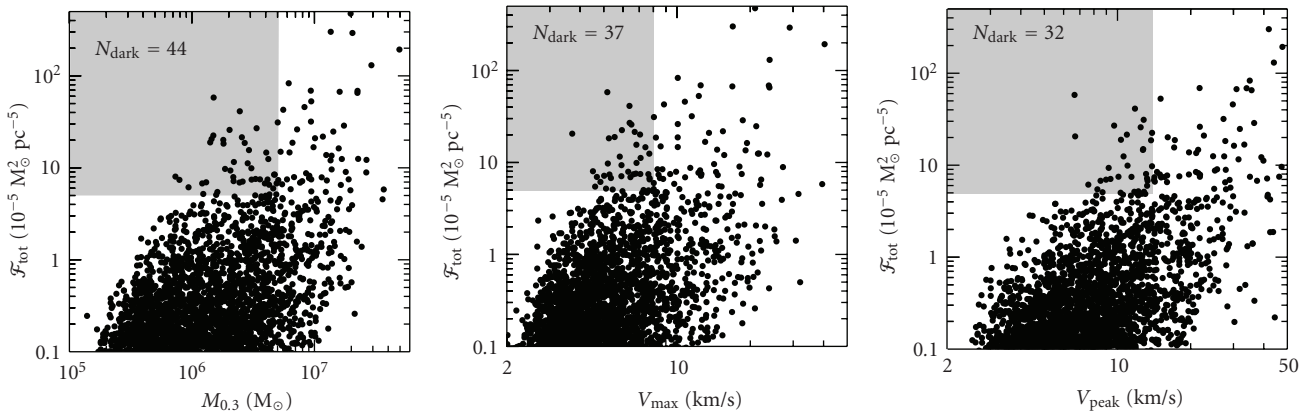

FIGURE 3: The annihilation flux $\mathcal{F}_{\rm tot}$ from subhalos in the *Via Lactea II* simulation versus their $M_{0.3}$, $V_{\rm max}$, and $V_{\rm peak}$. The gray shaded areas indicate regions containing subhalos with $\mathcal{F}_{\rm tot}$ as least as high as the fifth-brightest Milky Way dSph galaxy (Carina), but with $M_{0.3} < 5 \times 10^6\,M_\odot$, $V_{\rm max} < 8\,{\rm km\,s^{-1}}$, and $V_{\rm peak} < 14\,{\rm km\,s^{-1}}$, that is, probable dark clumps. Only one of the 100 random observer locations used in the analysis is shown here. The number $N_{\rm dark}$ in the top left refers to the number of "dark clumps" for this particular observer location.

simulations of the formation and evolution of Galactic DM (sub-)structure. A direct analysis of the VL2 simulations in terms of the detectability with *Fermi* of individual subhalos was performed by [82]. They found that for reasonable particle physics parameters a handful of subhalos should be able to outshine the astrophysical backgrounds and would be detected at more than 5σ significance over the lifetime of the *Fermi* mission.

As discussed in the previous section, we have directly calculated the annihilation luminosities for all VL2 subhalos using (9) and assuming an NFW density profile. The luminosities would be ∼40% *higher* if an Einasto ($\alpha = 0.17$) profile had been adopted instead. We then converted these luminosities to fluxes by dividing by $4\pi D^2$, where the distances D were determined for 100 randomly chosen observer locations 8 kpc from the host halo center. The resulting values of $\mathcal{F}_{\rm tot}$ are plotted in Figure 3, for just one of the 100 observer positions, as a function of the subhalos' $M_{0.3}$, $V_{\rm max}$, and $V_{\rm peak}$. Although the distributions show quite a bit of scatter, in all three cases a clear trend is apparent of more massive subhalos having higher fluxes. This trend could simply be the result of the higher luminosities of more massive halos, but one might have expected smaller mass subhalos to be brighter, since their greater abundance should result in lower typical distances and hence higher fluxes. This latter effect could be artificially suppressed in the numerical simulations, if smaller mass subhalos, whose dense centers are not as well resolved, were more easily tidally disrupted closer to the Galactic Center, or if the subhalo finding algorithm had trouble identifying low mass halos in the high background density central region. In Figure 4 we plot the subhalos' $V_{\rm max}$ against their distance to the host halo center $\hat{D}$. There appears to be a dearth of the lowest $V_{\rm max}$ subhalos ($V_{\rm max} \lesssim 2\,{\rm km\,s^{-1}}$) at small distances, but at the moment it is not clear whether this suppression is a real effect or a numerical artifact. It is also worth noting that such small subhalos might be more susceptible to disruption by

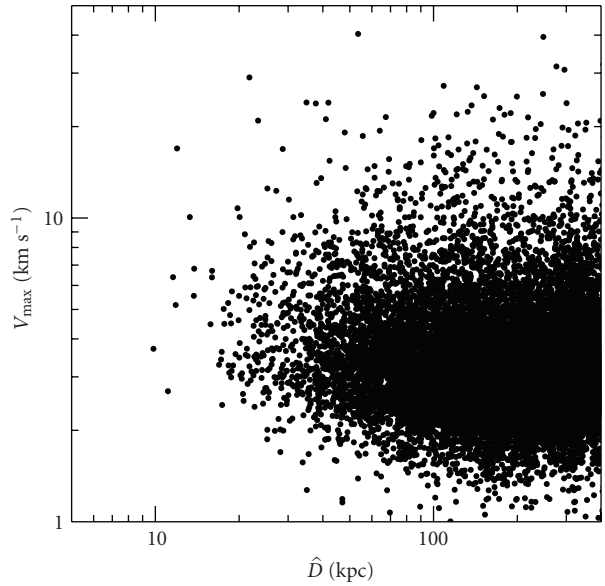

FIGURE 4: VL2 subhalo $V_{\rm max}$ versus distance to host halo $\hat{D}$.

interactions with the Milky Way's stellar and gaseous disk. At any rate, we can obtain an analytic estimate of the scaling of the typical subhalo flux with $V_{\rm max}$ by noting that the luminosity scales as $\mathcal{L} \sim V_{\rm max}^3\sqrt{\Delta_V}$ and the typical distance as $D \sim n^{-1/3} \sim V_{\rm max}^{4/3}$ (since $dn/dV_{\rm max} \sim V_{\rm max}^{-4}$). The typical flux should thus scale as $\mathcal{F} \sim \mathcal{L}/D^2 \sim V_{\rm max}^{1/3}\sqrt{\Delta_V}$, and would be higher for more massive subhalos at a fixed Δ_V. Actually lower $V_{\rm max}$ subhalos might be expected to have higher Δ_V due to their earlier formation times, but it remains to be seen to what degree this expectation is borne out in numerical simulations.

The points in Figure 3 can be directly compared with the values for the known Milky Way dSph's in Tables 1 and 2:

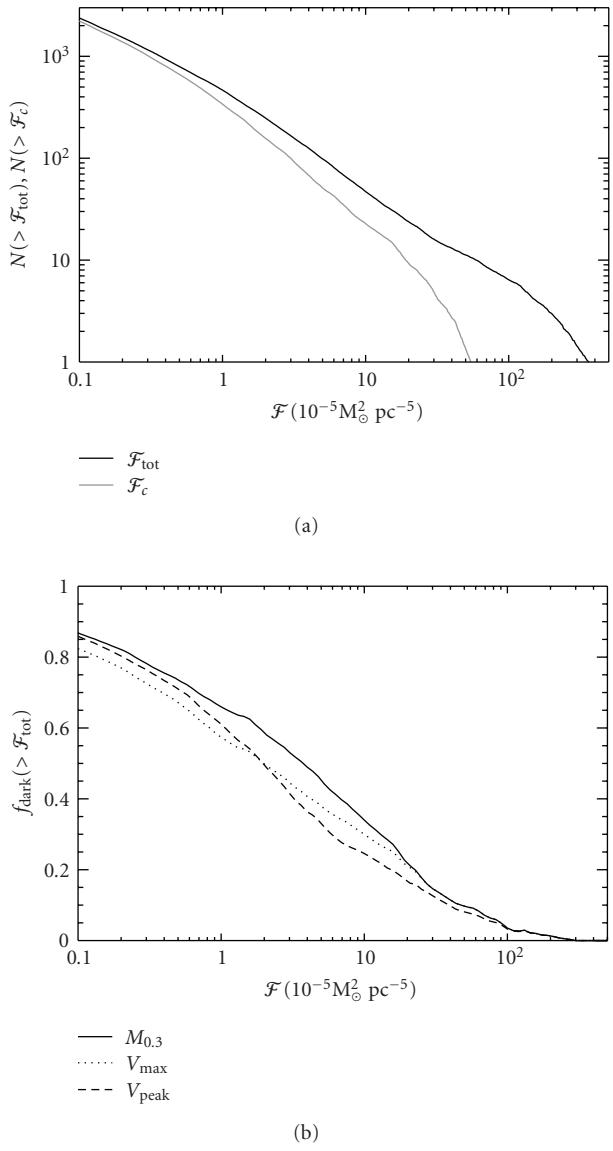

FIGURE 5: (a) The cumulative number of subhalos with flux exceeding $\mathcal{F}_{\rm tot}$, $\mathcal{F}_c$. (b) The fraction of dark clumps, that is, subhalos likely not hosting any stars and defined by $M_{0.3} < 5 \times 10^6\,\mathrm{M}_\odot$, $V_{\rm max} < 8\,\mathrm{km\,s^{-1}}$, or $V_{\rm peak} < 14\,\mathrm{km\,s^{-1}}$, as a function of limiting flux $\mathcal{F}_{\rm tot}$. These distributions are averages over 100 randomly chosen observer locations 8 kpc from the host halo center.

it appears that there are many DM subhalos at least as bright as the known Milky Way dSph's. This impression is confirmed by the top panel of Figure 5, in which we show the cumulative number of subhalos with fluxes greater than $\mathcal{F}_{\rm tot}$ and $\mathcal{F}_c$. These distributions were obtained by averaging over 100 randomly chosen observer locations 8 kpc from the host halo center. The mean number of DM subhalos with $\mathcal{F}_{\rm tot}$ greater than that of (Carina, Draco, Ursa Minor, Ursa Major, Segue 1) is $(90^{+4}_{-5}, 54^{+3}_{-3}, 43^{+3}_{-3}, 17^{+1}_{-1}, 13^{+1}_{-1})$ where the sub- and superscripts refer to the 16th and 84th percentile. The corresponding numbers for $\mathcal{F}_c$ are $(96^{+4}_{-6}, 62^{+5}_{-4}, 49^{+3}_{-2}, 24^{+2}_{-3}, 19^{+3}_{-3})$. This demonstrates that if a DM annihilation signal from any of the known Milky Way dSph's is detected, then many more DM subhalos should be visible. The plot also implies that Segue 1, the dSph with the highest $\mathcal{F}_{\rm tot}$ and $\mathcal{F}_c$ of the currently known sample, is unlikely to be the brightest DM subhalo in the sky. Of course some of these additional bright sources could very well have stellar counterparts that have simply been missed so far, due to the limited sky coverage of current surveys or insufficiently deep exposures. To assess what fraction of high flux sources are likely to be genuinely dark clumps without any stars, we split the sample by a limiting value of $M_{0.3} = 5 \times 10^6\,\mathrm{M}_\odot$, $V_{\rm max} = 8\,\mathrm{km\,s^{-1}}$, and $V_{\rm peak} = 14\,\mathrm{km\,s^{-1}}$. We assume that DM subhalos below these limits are too small to have been able to form any stars, and hence are truly dark clumps. Of the known dSph's listed in Table 1 only Leo IV falls below these limits. In the bottom panel of Figure 5 we plot $f_{\rm dark}(>\mathcal{F}_{\rm tot})$, the fraction of subhalos without stars, as a function of the limiting annihilation flux $\mathcal{F}_{\rm tot}$. $f_{\rm dark}$ falls monotonically with $\mathcal{F}_{\rm tot}$, which makes sense given that higher flux sources are typically more massive and hence more likely to host stars. Between 30% and 40% of all DM subhalos brighter than Carina are expected to be dark clumps. This fraction drops to 10% for subhalos brighter than Segue 1.

5.1. Boost Factor? The analysis presented here so far has been limited to known dSph galaxies and clumps resolved in the VL2 simulation, whose resolution limit is set by the available computational resources, and has nothing to do with fundamental physics. Indeed, the CDM expectation is that the clumpiness should continue all the way down to the cutoff in the matter power spectrum, set by collisional damping and free streaming in the early universe Green2005, Loeb2005. For typical WIMP DM, this cutoff occurs at masses of $m_0 = 10^{-12}$ to $10^{-4}\,\mathrm{M}_\odot$ [27, 28], some 10 to 20 orders of magnitude below VL2's mass resolution. Since the annihilation rate goes as ρ^2 and $\langle\rho^2\rangle > \langle\rho\rangle^2$, this sub-resolution clumpiness will lead to an enhancement of the total luminosity compared to the smooth mass distribution in the simulation.

The magnitude of this so-called substructure boost factor depends sensitively on the properties of subhalos below the simulation's resolution limit, in particular on the behavior of the concentration-mass relation. A simple power law extrapolation of the contribution of simulated subhalos to the total luminosity of the host halo leads to boosts on order of a a few hundred [55]. More sophisticated (semi-)analytical models, accounting for different possible continuations of the concentration-mass relation to lower masses, typically find smaller boosts of around a few tens [81, 82, 105, 110].

More importantly, this boost refers to the enhancement of the *total* annihilation luminosity of a subhalo, but this is not likely the quantity most relevant for detection. At the distances where subhalos might be detectable as individual sources, their projected size exceeds the angular resolution of today's detectors. The surface brightness profile from annihilations in the smooth DM component would be strongly peaked towards the center (yet probably still resolved by *Fermi* [82]), owing to the $\rho(r)^2$ dependence

of the annihilation rate. The luminosity contribution from a subhalo's sub-substructure population (i.e., its boost), however, is much less centrally concentrated: at best it follows the subhalo mass density profile $\rho(r)$, although it might very well even be antibiased. This implies that substructure would preferentially boost the outer regions of a subhalo, where the surface brightness typically remains below the level of astrophysical backgrounds and hence does not contribute much to the detection significance. In other words, the boost factor might apply to $\mathcal{F}_{\rm tot}$, but much less (or not at all) to $\mathcal{F}_c$; yet it is $\mathcal{F}_c$ that is likely to determine whether a given subhalo can be detected with *Fermi* or an ACT. It thus seems unlikely that the detectability of Galactic subhalos would be significantly enhanced by their own substructure. (This is in contrast to many previous claims in the literature, including some by the present author (e.g., [82]). A re-analysis of that work (in progress) with an improved treatment of the angular dependence of the substructure boost, indeed finds that the boost only weakly increases the number of detectable subhalos.) On the other hand, a substructure boost could be very important for diffuse DM annihilation signals, either from extragalactic sources, where the boost would simply increase the overall amplitude [111], or from Galactic DM, where the boost could affect the amplitude and angular profile of the signal, as well as the power spectrum of its anisotropies [51–53, 55, 81, 82].

Note also that local substructure boost factors of up to several hundreds, which have been invoked to explain the PAMELA satellite's measurement of an anomalously rising positron fraction at energies above 10 GeV as a DM annihilation signal, appear to be inconsistent with the results from high resolution numerical simulations like VL2 and Aquarius.

6. Summary and Conclusions

In this work we have reviewed the DM annihilation signal from Galactic subhalos. After going over the basics of the annihilation process with a focus on the resulting γ-ray output, we summarized the properties of DM subhalos relevant for estimating their annihilation luminosity. In the remainder of the paper we used the *Via Lactea II* simulation to assess the strength of the annihilation flux from both known Galactic dSph galaxies as well as from dark clumps not hosting any stars. By matching the distances D and central masses $M_{0.3}$ of simulated subhalos to the corresponding published values of 18 known dSph's, we were able to infer most probable values, and the 1-σ scatter around them, for $V_{\rm max}$ and $r_{\rm Vmax}$, and hence for the annihilation luminosity $\mathcal{L}$ and flux $\mathcal{F}$ of all dwarfs. According to this analysis, the recently discovered dSph Segue 1 should be the brightest of the known dSph's, followed by Ursa Major II, Ursa Minor, Draco, and Carina. Further, we showed that if any of the known Galactic dSph's are bright enough to be detected, then at least 10 times more subhalos should appear as visible sources. Some of these would be as-of-yet undiscovered luminous dwarf galaxies, but a significant fraction should correspond to dark clumps not hosting any stars. The fraction of dark clump sources is 10% for subhalos at least as bright as Segue 1 and grows to 40% for subhalos brighter than Carina. Lastly, we briefly considered the role that a substructure boost factor should play in the detectability of individual Galactic dSph's and other DM subhalos. We argued that any boost is unlikely to strongly increase their prospects for detection, since its shallower angular dependence would preferentially boost the outer regions of subhalos, which typically do not contribute much to the detection significance.

Several caveats to these findings are in order. Probably the most important of these is that our simulation completely neglects the effects of baryons. Gas cooling, star formation, and the associated feedback processes are unlikely to strongly affect most subhalos, owing to their low masses. However, tidal interactions with the baryonic components of the Milky Way galaxy might do so. The Sagittarius dSph, for example, is thought to be in the process of complete disruption from tidal interactions with the Milky Way. A second caveat is that our analysis is based on only one, albeit very high resolution, numerical simulation, and so we cannot assess the importance of cosmic variance, or the dependence on cosmological parameters such as σ_8 and n_s. Other work has found considerable halo-to-halo scatter [14, 112, 113], with a factor of $\sim$2 variance in the total subhalo abundance, for example.

These caveats motivate further study and future, higher resolution numerical simulations, including the effects of baryonic physics. The characterization of the Galactic DM annihilation signal is of crucial importance in guiding observational efforts to shed light on the nature of DM. We are hopeful that in the next few years the promise of a DM annihilation signal will come to fruition, and will help us to unravel this puzzle.

Acknowledgments

Support for this work was provided by the William L. Loughlin membership at the Institute for Advanced Study. The author would like to thank his collaborators from the Via Lactea Project for their expertise and invaluable contributions.

References

[1] A. Klypin, A. V. Kravtsov, O. Valenzuela, and F. Prada, "Where are the missing galactic satellites?" *Astrophysical Journal*, vol. 522, no. 1, part 1, pp. 82–92, 1999.

[2] B. Moore, S. Ghigna, F. Governato, et al., "Dark matter substructure within galactic halos," *Astrophysical Journal*, vol. 524, no. 1, part 2, pp. L19–L22, 1999.

[3] M. Mateo, "Dwarf galaxies of the local group," *Annual Review of Astronomy and Astrophysics*, vol. 36, pp. 435–506, 1998.

[4] B. Willman, M. R. Blanton, A. A. West, et al., "A new Milky Way companion: unusual globular cluster or extreme dwarf satellite?" *Astronomical Journal*, vol. 129, no. 6, pp. 2692–2700, 2005.

[5] B. Willman, J. J. Dalcanton, D. Martinez-Delgado, et al., "A new Milky Way dwarf galaxy in URSA Major," *Astrophysical Journal*, vol. 626, no. 2, part 2, pp. L85–L88, 2005.

[6] V. Belokurov, D. B. Zucker, N. W. Evans, et al., "The field of streams: sagittarius and its siblings," *Astrophysical Journal*, vol. 642, no. 2, part 2, pp. L137–L140, 2006.

[7] D. B. Zucker, V. Belokurov, N. W. Evans, et al., "A new Milky Way dwarf satellite in canes venatici," *Astrophysical Journal*, vol. 643, no. 2, part 2, pp. L103–L106, 2006.

[8] D. B. Zucker, V. Belokurov, N. W. Evans, et al., "A curious Milky Way satellite in Ursa Major," *Astrophysical Journal*, vol. 650, no. 1, part 2, pp. L41–L44, 2006.

[9] T. Sakamoto and T. Hasegawa, "Discovery of a faint old stellar system at 150 kpc," *Astrophysical Journal*, vol. 653, no. 1, part 2, pp. L29–L32, 2006.

[10] V. Belokurov, D. B. Zucker, N. W. Evans, et al., "Cats and dogs, hair and a hero: a quintet of new Milky Way companions," *Astrophysical Journal*, vol. 654, no. 2, part 1, pp. 897–906, 2007.

[11] M. J. Irwin, V. Belokurov, N. W. Evans, et al., "Discovery of an unusual dwarf galaxy in the outskirts of the Milky Way," *Astrophysical Journal*, vol. 656, no. 1, part 2, pp. L13–L16, 2007.

[12] S. M. Walsh, H. Jerjen, and B. Willman, "A pair of boötes: a new Milky Way satellite," *Astrophysical Journal*, vol. 662, no. 2, part 2, pp. L83–L86, 2007.

[13] J. Diemand, M. Kuhlen, P. Madau, et al., "Clumps and streams in the local dark matter distribution," *Nature*, vol. 454, no. 7205, pp. 735–738, 2008.

[14] V. Springel, J. Wang, M. Vogelsberger, et al., "The Aquarius Project: the subhaloes of galactic haloes," *Monthly Notices of the Royal Astronomical Society*, vol. 391, no. 4, pp. 1685–1711, 2008.

[15] J. Stadel, D. Potter, B. Moore, et al., "Quantifying the heart of darkness with GHALO—a multibillion particle simulation of a galactic halo," *Monthly Notices of the Royal Astronomical Society*, vol. 398, no. 1, pp. L21–L25, 2009.

[16] S. D. M. White and M. J. Rees, "Core condensation in heavy halos—a two-stage theory for galaxy formation and clustering," *Monthly Notices of the Royal Astronomical Society*, vol. 183, pp. 341–358, 1978.

[17] G. R. Blumenthal, S. M. Faber, J. R. Primack, and M. J. Rees, "Formation of galaxies and large-scale structure with cold dark matter," *Nature*, vol. 311, no. 5986, pp. 517–525, 1984.

[18] A. Dekel and J. Silk, "The origin of dwarf galaxies, cold dark matter, and biased galaxy formation," *Astrophysical Journal*, vol. 303, pp. 39–55, 1986.

[19] J. S. Bullock, A. V. Kravtsov, and D. H. Weinberg, "Reionization and the abundance of galactic satellites," *Astrophysical Journal*, vol. 539, no. 2, part 1, pp. 517–521, 2000.

[20] A. V. Kravtsov, O. Y. Gnedin, and A. A. Klypin, "The tumultuous lives of galactic dwarfs and the missing satellites problem," *Astrophysical Journal*, vol. 609, no. 2, part 1, pp. 482–497, 2004.

[21] L. Mayer, C. Mastropietro, J. Wadsley, J. Stadel, and B. Moore, "Simultaneous ram pressure and tidal stripping; how dwarf spheroidals lost their gas," *Monthly Notices of the Royal Astronomical Society*, vol. 369, no. 3, pp. 1021–1038, 2006.

[22] P. Madau, J. Diemand, and M. Kuhlen, "Dark matter subhalos and the dwarf satellites of the Milky Way," *Astrophysical Journal*, vol. 679, no. 2, pp. 1260–1271, 2008.

[23] S. E. Koposov, J. Yoo, H.-W. Rix, D. H. Weinberg, A. V. Macciò, and J. M. Escudé, "A quantitative explanation of the observed population of Milky Way satellite galaxies," *Astrophysical Journal*, vol. 696, pp. 2179–2194, 2009.

[24] A. V. Maccio', X. Kang, F. Fontanot, R. S. Somerville, S. E. Koposov, and P. Monaco, "On the origin and properties of Ultrafaint Milky Way Satellites in a LCDM Universe," submitted, http://arxiv.org/abs/0903.4681.

[25] A. M. Green, S. Hofmann, and D. J. Schwarz, "The first WIMPy halos," *Journal of Cosmology and Astroparticle Physics*, vol. 2005, no. 8, article 3, pp. 41–71, 2005.

[26] A. Loeb and M. Zaldarriaga, "Small-scale power spectrum of cold dark matter," *Physical Review D*, vol. 71, no. 10, Article ID 103520, 7 pages, 2005.

[27] S. Profumo, K. Sigurdson, and M. Kamionkowski, "What mass are the smallest protohalos?" *Physical Review Letters*, vol. 97, no. 3, Article ID 031301, 4 pages, 2006.

[28] T. Bringmann, "Particle models and the small-scale structure of dark matter," *New Journal of Physics*, vol. 11, no. 10, Article ID 105027, 105027 pages, 2009.

[29] E. W. Kolb and I. I. Tkachev, "Femtolensing and picolensing by axion miniclusters," *Astrophysical Journal*, vol. 460, no. 1, part 2, pp. L25–L28, 1996.

[30] C. Schmid, D. J. Schwarz, and P. Widerin, "Amplification of cosmological inhomogeneities by the QCD transition," *Physical Review D*, vol. 59, no. 4, Article ID 043517, 20 pages, 1999.

[31] P. Sikivie, "Axion cosmology," in *Axions: Theory, Cosmology, and Experimental Searches*, M. Kuster, G. Raffelt, and B. Beltrán, Eds., vol. 741 of *Lecture Notes in Physics*, p. 19, Springer, Berlin, Germany, 2008.

[32] L. Bergström, J. Edsjö, P. Gondolo, and P. Ullio, "Clumpy neutralino dark matter," *Physical Review D*, vol. 59, no. 4, Article ID 043506, 11 pages, 1999.

[33] L. E. Strigari, J. S. Bullock, M. Kaplinghat, et al., "A common mass scale for satellite galaxies of the Milky Way," *Nature*, vol. 454, no. 7208, pp. 1096–1097, 2008.

[34] R. A. Ibata, G. F. Lewis, M. J. Irwin, and T. Quinn, "Uncovering cold dark matter halo substructure with tidal streams," *Monthly Notices of the Royal Astronomical Society*, vol. 332, no. 4, pp. 915–920, 2002.

[35] K. V. Johnston, D. N. Spergel, and C. Haydn, "How lumpy is the Milky Way's dark matter halo?" *Astrophysical Journal*, vol. 570, no. 2, part 1, pp. 656–664, 2002.

[36] J. Peñarrubia, A. J. Benson, D. Martínez-Delgado, and H. W. Rix, "Modeling tidal streams in evolving dark matter halos," *Astrophysical Journal*, vol. 645, no. 1, part 1, pp. 240–255, 2006.

[37] J. M. Siegal-Gaskins and M. Valluri, "Signatures of ΛCDM substructure in tidal debris," *Astrophysical Journal*, vol. 681, no. 1, pp. 40–52, 2008.

[38] G. Toth and J. P. Ostriker, "Galactic disks, infall, and the global value of Ω," *Astrophysical Journal*, vol. 389, no. 1, pp. 5–26, 1992.

[39] J. I. Read, G. Lake, O. Agertz, and V. P. Debattista, "Thin, thick and dark discs in ΛCDM," *Monthly Notices of the Royal Astronomical Society*, vol. 389, no. 3, pp. 1041–1057, 2008.

[40] S. Kazantzidis, A. R. Zentner, A. V. Kravtsov, J. S. Bullock, and V. P. Debattista, "Cold dark matter substructure and galactic disks. II. Dynamical effects of hierarchical satellite accretion," *Astrophysical Journal*, vol. 700, no. 2, pp. 1896–1920, 2009.

[41] O. Adriani, G. C. Barbarino, G. A. Bazilevskaya, et al., "An anomalous positron abundance in cosmic rays with energies 1.5–100 GeV," *Nature*, vol. 458, no. 7238, pp. 607–609, 2009.

[42] J. Chang, J. H. Adams Jr., H. S. Ahn, et al., "An excess of cosmic ray electrons at energies of 300–800 GeV," *Nature*, vol. 456, no. 7220, pp. 362–365, 2008.

[43] S. Torii, T. Yamagami, T. Tamura, et al., "High-energy electron observations by PPB-BETS flight in Antarctica," submitted, http://arxiv.org/abs/0809.0760.

[44] A. A. Abdo, M. Ackermann, M. Ajello, et al., "Measurement of the cosmic ray $e^+ + e^-$ spectrum from 20 GeV to 1 TeV with the fermi large area telescope," *Physical Review Letters*, vol. 102, no. 18, Article ID 181101, 2009.

[45] F. Aharonian, A. G. Akhperjanian, G. Anton, et al., "Probing the ATIC peak in the cosmic-ray electron spectrum with H.E.S.S," submitted, http://arxiv.org/abs/0905.0105.

[46] F. Aharonian, A. G. Akhperjanian, A. R. Bazer-Bachi, et al., "Observations of the Sagittarius dwarf galaxy by the HESS experiment and search for a dark matter signal," *Astroparticle Physics*, vol. 29, no. 1, pp. 55–62, 2008.

[47] C. M. Hui, "VERITAS Observations of Extragalactic Non-Blazars," in *High Energy Gamma-Ray Astronomy: Proceedings of the 4th International Meeting on High Energy Gamma-Ray Astronomy*, F. A. Aharonian, W. Hofmann, and F. Rieger, Eds., vol. 1085 of *American Institute of Physics Conference Series*, pp. 407–410, 2008.

[48] J. Albert, E. Aliu, H. Anderhub, et al., "Upper limit for γ-ray emission above 140 GeV from the dwarf spheroidal galaxy draco," *Astrophysical Journal*, vol. 679, no. 1, pp. 428–431, 2008.

[49] E. Aliu, H. Anderhub, L. A. Antonelli, et al., "Upper limits on the vhe gamma-ray emission from the willman 1 satellite galaxy with the magic telescope," *Astrophysical Journal*, vol. 697, no. 2, pp. 1299–1304, 2009.

[50] D. D. Driscoll, C. E. Covault, J. Ball, et al., "Search for dark matter annihilation in Draco with the Solar Tower Atmospheric Cherenkov Effect Experiment," *Physical Review D*, vol. 78, no. 8, Article ID 087101, 4 pages, 2008.

[51] J. M. Siegal-Gaskins, "Revealing dark matter substructure with anisotropies in the diffuse gamma-ray background," *Journal of Cosmology and Astroparticle Physics*, vol. 2008, no. 10, article 40, 2008.

[52] S. Ando, "Gamma-ray background anisotropy from Galactic dark matter substructure," *Physical Review D*, vol. 80, no. 2, Article ID 023520, 16 pages, 2009.

[53] M. Fornasa, L. Pieri, G. Bertone, and E. Branchini, "Anisotropy probe of galactic and extra-galactic dark matter annihilations," *Physical Review D*, vol. 80, no. 2, Article ID 023518, 2009.

[54] F. Stoehr, S. D. M. White, V. Springel, G. Tormen, and N. Yoshida, "Dark matter annihilation in the halo of the Milky Way," *Monthly Notices of the Royal Astronomical Society*, vol. 345, no. 4, pp. 1313–1322, 2003.

[55] V. Springel, S. D. M. White, C. S. Frenk, et al., "Prospects for detecting supersymmetric dark matter in the Galactic halo," *Nature*, vol. 456, no. 7218, pp. 73–76, 2008.

[56] P. Brun, T. Delahaye, J. Diemand, S. Profumo, and P. Salati, "Cosmic ray lepton puzzle in the light of cosmological N-body simulations," *Physical Review D*, vol. 80, no. 3, Article ID 035023, 5 pages, 2009.

[57] M. Kuhlen and D. Malyshev, "ATIC, PAMELA, HESS, and Fermi data and nearby dark matter subhalos," *Physical Review D*, vol. 79, no. 12, Article ID 123517, 12 pages, 2009.

[58] N. Arkani-Hamed, D. P. Finkbeiner, T. R. Slatyer, and N. Weiner, "A theory of dark matter," *Physical Review D*, vol. 79, no. 1, Article ID 015014, 16 pages, 2009.

[59] M. Lattanzi and J. Silk, "Can the WIMP annihilation boost factor be boosted by the Sommerfeld enhancement?" *Physical Review D*, vol. 79, no. 8, Article ID 083523, 8 pages, 2009.

[60] L. Pieri, M. Lattanzi, and J. Silk, "Constraining the dark matter annihilation cross-section with Cherenkov telescope observations of dwarf galaxies," *Monthly Notices of the Royal Astronomical Society*, vol. 399, no. 4, pp. 2033–2040, 2009.

[61] M. Kuhlen, P. Madau, and J. Silk, "Exploring dark matter with milky way substructure," *Science*, vol. 325, no. 5943, pp. 970–973, 2009.

[62] M. S. Turner, "Windows on the axion," *Physics Report*, vol. 197, no. 2, pp. 67–97, 1990.

[63] E. W. Kolb and M. S. Turner, "The early universe," in *Frontiers in Physics*, Addison-Wesley, Reading, Mass, USA, 1990.

[64] G. Jungman, M. Kamionkowski, and K. Griest, "Supersymmetric dark matter," *Physics Report*, vol. 267, no. 5-6, pp. 195–373, 1996.

[65] G. Bertone, D. Hooper, and J. Silk, "Particle dark matter: evidence, candidates and constraints," *Physics Reports*, vol. 405, no. 5-6, pp. 279–390, 2005.

[66] G. Hinshaw, J. L. Weiland, R. S. Hill, et al., "Five-year wilkinson microwave anisotropy probe observations: data processing, sky maps and basic results," *Astrophysical Journal*, vol. 180, no. 2, pp. 225–245, 2009.

[67] K. Griest and D. Seckel, "Three exceptions in the calculation of relic abundances," *Physical Review D*, vol. 43, no. 10, pp. 3191–3203, 1991.

[68] P. Gondolo and G. Gelmini, "Cosmic abundances of stable particles: improved analysis," *Nuclear Physics B*, vol. 360, no. 1, pp. 145–179, 1991.

[69] T. Bringmann, L. Bergström, and J. Edsjö, "New gamma-ray contributions to supersymmetric dark matter annihilation," *Journal of High Energy Physics*, vol. 2008, no. 1, p. 49, 2008.

[70] M. Gustafsson, E. Lundström, L. Bergström, and J. Edsjö, "Significant gamma lines from inert higgs dark matter," *Physical Review Letters*, vol. 99, no. 4, Article ID 041301, 4 pages, 2007.

[71] T. Sjöstrand, "High-energy-physics event generation with PYTHIA 5.7 and JETSET 7.4," *Computer Physics Communications*, vol. 82, no. 1, pp. 74–89, 1994.

[72] P. Gondolo, J. Edsjö, P. Ullio, L. Bergström, M. Schelke, and E. A. Baltz, "DarkSUSY: computing supersymmetric dark matter properties numerically," *Journal of Cosmology and Astroparticle Physics*, vol. 2004, no. 7, article 8, pp. 145–179, 2004.

[73] C. Calcáneo-Roldán and B. Moore, "Surface brightness of dark matter: unique signatures of neutralino annihilation in the galactic halo," *Physical Review D*, vol. 62, no. 12, Article ID 123005, 10 pages, 2000.

[74] E. A. Baltz, C. Briot, P. Salati, R. Taillet, and J. Silk, "Detection of neutralino annihilation photons from external galaxies," *Physical Review D*, vol. 61, no. 2, Article ID 023514, 10 pages, 2000.

[75] A. Tasitsiomi and A. V. Olinto, "Detectability of neutralino clumps via atmospheric Cherenkov telescopes," *Physical Review D*, vol. 66, no. 8, Article ID 083006, 16 pages, 2002.

[76] R. Aloisio, P. Blasi, and A. V. Olinto, "Gamma-ray constraints on neutralino dark matter clumps in the galactic halo," *Astrophysical Journal*, vol. 601, no. 1, part 1, pp. 47–53, 2004.

[77] N. W. Evans, F. Ferrer, and S. Sarkar, "A travel guide to the dark matter annihilation signal," *Physical Review D*, vol. 69, no. 12, Article ID 123501, 10 pages, 2004.

[78] S. M. Koushiappas, A. R. Zentner, and T. P. Walker, "Observability of gamma rays from neutralino annihilations in the Milky Way substructure," *Physical Review D*, vol. 69, no. 4, Article ID 043501, 11 pages, 2004.

[79] S. M. Koushiappas, "Proper motion of gamma rays from microhalo sources," *Physical Review Letters*, vol. 97, no. 19, Article ID 191301, 4 pages, 2006.

[80] J. Diemand, M. Kuhlen, and P. Madau, "Dark matter substructure and gamma-ray annihilation in the Milky Way halo," *Astrophysical Journal*, vol. 657, no. 1, part 1, pp. 262–270, 2007.

[81] L. Pieri, G. Bertone, and E. Branchini, "Dark matter annihilation in substructures revised," *Monthly Notices of the Royal Astronomical Society*, vol. 384, no. 4, pp. 1627–1637, 2008.

[82] M. Kuhlen, J. Diemand, and P. Madau, "The dark matter annihilation signal from galactic substructure: predictions for glast," *Astrophysical Journal*, vol. 686, no. 1, pp. 262–278, 2008.

[83] L. E. Strigari, S. M. Koushiappas, J. S. Bullock, et al., "The most dark-matter-dominated galaxies: predicted gamma-ray signals from the faintest Milky Way dwarfs," *Astrophysical Journal*, vol. 678, no. 2, pp. 614–620, 2008.

[84] E. A. Baltz, J. E. Taylor, and L. L. Wai, "Can astrophysical gamma-ray sources mimic dark matter annihilation in galactic satellites?" *Astrophysical Journal*, vol. 659, no. 2, part 2, pp. L125–L128, 2007.

[85] J. F. Navarro, C. S. Frenk, and S. D. M. White, "A universal density profile from hierarchical clustering," *Astrophysical Journal*, vol. 490, no. 2, part 1, pp. 493–508, 1997.

[86] A. V. Macciò, A. A. Dutton, F. C. van den Bosch, B. Moore, D. Potter, and J. Stadel, "Concentration, spin and shape of dark matter haloes: scatter and the dependence on mass and environment," *Monthly Notices of the Royal Astronomical Society*, vol. 378, no. 1, pp. 55–71, 2007.

[87] J. Diemand, B. Moore, and J. Stadel, "Convergence and scatter of cluster density profiles," *Monthly Notices of the Royal Astronomical Society*, vol. 353, no. 2, pp. 624–632, 2004.

[88] J. F. Navarro, A. Ludlow, V. Springel, et al., "The diversity and similarity of simulated cold dark matter halos," submitted, http://arxiv.org/abs/0810.1522.

[89] B. Allgood, R. A. Flores, J. R. Primack, et al., "The shape of dark matter haloes: dependence on mass, redshift, radius and formation," *Monthly Notices of the Royal Astronomical Society*, vol. 367, no. 4, pp. 1781–1796, 2006.

[90] M. Kuhlen, J. Diemand, and P. Madau, "The shapes, orientation, and alignment of galactic dark matter subhalos," *Astrophysical Journal*, vol. 671, no. 2, pp. 1135–1146, 2007.

[91] G. L. Bryan and M. L. Norman, "Statistical properties of X-ray clusters: analytic and numerical comparisons," *Astrophysical Journal*, vol. 495, no. 1, part 1, pp. 80–99, 1998.

[92] J. T. Kleyna, M. I. Wilkinson, N. Evans, and G. Gilmore, "Ursa Major: a missing low-mass CDM halo?" *Astrophysical Journal*, vol. 630, no. 2, part 2, pp. L141–L144, 2005.

[93] R. R. Muñoz, J. L. Carlin, P. M. Frinchaboy, D. L. Nidever, S. R. Majewski, and R. J. Patterson, "Exploring halo substructure with giant stars: the dynamics and metallicity of the dwarf spheroidal in Boötes," *Astrophysical Journal*, vol. 650, no. 1, part 2, pp. L51–L54, 2006.

[94] N. F. Martin, R. A. Ibata, S. C. Chapman, M. Irwin, and G. F. Lewis, "A Keck/DEIMOS spectroscopic survey of faint Galactic satellites: searching for the least massive dwarf galaxies," *Monthly Notices of the Royal Astronomical Society*, vol. 380, no. 1, pp. 281–300, 2007.

[95] J. D. Simon and M. Geha, "The kinematics of the ultra-faint Milky Way satellites: solving the missing satellite problem," *Astrophysical Journal*, vol. 670, no. 1, pp. 313–331, 2007.

[96] S. Koposov, V. Belokurov, N. W. Evans, et al., "The luminosity function of the Milky Way satellites," *Astrophysical Journal*, vol. 686, no. 1, pp. 279–291, 2008.

[97] E. J. Tollerud, J. S. Bullock, L. E. Strigari, and B. Willman, "Hundreds of Milky Way satellites? Luminosity bias in the satellite luminosity function," *Astrophysical Journal*, vol. 688, no. 1, pp. 277–289, 2008.

[98] S. M. Walsh, B. Willman, and H. Jerjen, "The invisibles: a detection algorithm to trace the faintest Milky Way satellites," *Astronomical Journal*, vol. 137, no. 1, pp. 450–469, 2009.

[99] J. Grcevich and M. E. Putman, "H_I in local group dwarf galaxies and stripping by the galactic halo," *Astronomical Journal*, vol. 696, pp. 385–395, 2009.

[100] K. Bernlöhr, O. Carrol, R. Cornils, et al., "The optical system of the H.E.S.S. imaging atmospheric Cherenkov telescopes—part I: layout and components of the system," *Astroparticle Physics*, vol. 20, no. 2, pp. 111–128, 2003.

[101] D. Martínez-Delgado, M. Á. Gómez-Flechoso, A. Aparicio, and R. Carrera, "Tracing out the northern tidal stream of the Sagittarius dwarf spheroidal galaxy," *Astrophysical Journal*, vol. 601, no. 1, part 1, pp. 242–259, 2004.

[102] J. Holder, V. A. Acciari, E. Aliu, et al., "Status of the VERITAS observatory," in *High Energy Gamma-Ray Astronomy: Proceedings of the 4th International Meeting on High Energy Gamma-Ray Astronomy* , F. A. Aharonian, W. Hofmann, and F. Rieger, Eds., vol. 1085 of *American Institute of Physics Conference Series*, pp. 657–660, 2008.

[103] R. Essig, N. Sehgal, and L. E. Strigari, "Bounds on cross sections and lifetimes for dark matter annihilation and decay into charged leptons from gamma-ray observations of dwarf galaxies," *Physical Review D*, vol. 80, no. 2, Article ID 023506, 2009.

[104] J. Bovy, "Substructure boosts to dark matter annihilation from Sommerfeld enhancement," *Physical Review D*, vol. 79, no. 8, Article ID 083539, 2009.

[105] G. D. Martinez, J. S. Bullock, M. Kaplinghat, L. E. Strigari, and R. Trotta, "Indirect dark matter detection from dwarf satellites: joint expectations from astrophysics and supersymmetry," *Journal of Cosmology and Astroparticle Physics*, vol. 6, p. 14, 2009.

[106] L. Pieri, A. Pizzella, E. M. Corsini, E. Dalla Bontà, and F. Bertola, "Could the Fermi Large Area Telescope detect γ-rays from dark matter annihilation in the dwarf galaxies of the local group?" *Astronomy and Astrophysics*, vol. 496, no. 2, pp. 351–360, 2009.

[107] F. Governato, B. Willman, L. Mayer, et al., "Forming disc galaxies in ΛCDM simulations," *Monthly Notices of the Royal Astronomical Society*, vol. 374, no. 4, pp. 1479–1494, 2007.

[108] J. Diemand, P. Madau, and B. Moore, "The distribution and kinematics of early high-σ peaks in present-day haloes: implications for rare objects and old stellar populations," *Monthly Notices of the Royal Astronomical Society*, vol. 364, no. 2, pp. 367–383, 2005.

[109] B. Moore, J. Diemand, P. Madau, M. Zemp, and J. Stadel, "Globular clusters, satellite galaxies and stellar haloes from early dark matter peaks," *Monthly Notices of the Royal Astronomical Society*, vol. 368, no. 2, pp. 563–570, 2006.

[110] L. E. Strigari, S. M. Koushiappas, J. S. Bullock, and M. Kaplinghat, "Precise constraints on the dark matter content of Milky Way dwarf galaxies for gamma-ray experiments," *Physical Review D*, vol. 75, no. 8, Article ID 083526, 2007.

[111] P. Ullio, L. Bergström, J. Edsjö, and C. Lacey, "Cosmological dark matter annihilations into γ rays: a closer look," *Physical Review D*, vol. 66, no. 12, Article ID 123502, 2002.

[112] D. Reed, F. Governato, T. Quinn, J. Gardner, J. Stadel, and G. Lake, "Dark matter subhaloes in numerical simulations," *Monthly Notices of the Royal Astronomical Society*, vol. 359, no. 4, pp. 1537–1548, 2005.

[113] T. Ishiyama, T. Fukushige, and J. Makino, "Variation of the subhalo abundance in dark matter halos," *The Astrophysical Journal*, vol. 696, pp. 2115–2125, 2009.

Hindawi Publishing Corporation
Advances in Astronomy
Volume 2010, Article ID 357342, 9 pages
doi:10.1155/2010/357342

Review Article

Dwarf Galaxies, MOND, and Relativistic Gravitation

Arthur Kosowsky

Department of Physics and Astronomy, University of Pittsburgh, 3941 O'Hara Street, Pittsburgh, PA 15260, USA

Correspondence should be addressed to Arthur Kosowsky, kosowsky@pitt.edu

Received 5 June 2009; Revised 12 August 2009; Accepted 2 October 2009

Academic Editor: Elias Brinks

MOND is a phenomenological modification of Newton's law of gravitation which reproduces the dynamics of galaxies, without the need for additional dark matter. This paper reviews the basics of MOND and its application to dwarf galaxies. MOND is generally successful at reproducing stellar velocity dispersions in the Milky Way's classical dwarf ellipticals, for reasonable values of the stellar mass-to-light ratio of the galaxies; two discrepantly high mass-to-light ratios may be explained by tidal effects. Recent observations also show MOND describes tidal dwarf galaxies, which form in complex dynamical environments. The application of MOND to galaxy clusters, where it fails to reproduce observed gas temperatures, is also reviewed. Relativistic theories containing MOND in the non-relativistic limit have now been formulated; they all contain new dynamical fields, which may serve as additional sources of gravitation that could reconcile cluster observations with MOND. Certain limits of these theories can also give the accelerating expansion of the Universe. The standard dark matter cosmology boasts numerous manifest triumphs; however, alternatives should also be pursued as long as outstanding observational issues remain unresolved, including the empirical successes of MOND on galaxy scales and the phenomenology of dark energy.

1. Why MOND?

In 1983, Mordehai Milgrom published a set of three papers in the Astrophysical Journal postulating a fundamental modification of either Newton's Law of Gravitation or Newton's Second Law [1–3]. This modification was designed to explain the Tully-Fisher relation for spiral galaxies, which relates luminosity to rotational velocity, without using dark matter. Unlike many other proposed modifications of gravity, Milgrom's is not at a particular length or energy scale, but rather at an *acceleration* scale $a_0 = 1.2 \times 10^{-10}\ \mathrm{m/s^2}$. This is a very small acceleration, which makes any laboratory-based probes nearly impossible; the consequences of Milgrom's modification manifest themselves only on astronomical scales. In particular, Milgrom aimed to address the phenomenology of dark matter: are the departures from Newtonian gravitation we see in galaxies actually due to some breakdown of Newton's Law of Gravitation, rather than due to the action of otherwise undetected dark matter obeying the standard gravitational law?

For spiral galaxies, redshift measurements reveal how rapidly stars and neutral hydrogen gas in the disk are rotating around the center of the galaxy. It has been known since the early 1970's that the overwhelming majority of spiral galaxies have flat rotation curves: the rotational velocity $v(R)$ at a radius R from the center of the galaxy becomes independent of R past a certain radius. (A small fraction of galaxies have rotation curves which are still increasing with R at the largest-radius data point. Only a few exhibit any significant decrease; see, [4] for an example.) This behavior is impossible to reconcile with the Newtonian gravitational field produced by the visible matter in the galaxy. At large distances, beyond the majority of the galaxy's visible mass, the Newtonian gravitational field from the visible matter begins to approximate the field from a point mass, so that rotational velocities due to the visible matter alone would drop like $v(R) \propto R^{-1/2}$, as with planetary orbital velocities in the solar system. No known spiral galaxy exhibits this behavior in its rotation curve, even though many have rotation curves probed well beyond the bulk of the visible matter via neutral hydrogen clouds. We have only two possible logical explanations: either a large amount of unseen dark matter is present to increase the gravitational field over the Newtonian value, or Newton's Law of Gravitation does not hold on the scales of spiral galaxies.

From the beginning, dark matter was considered as almost certainly the explanation for galaxy observations, buttressed by candidate dark matter particles which arise naturally in many extensions of the standard model of particle physics, particularly in supersymmetry. The dark matter hypothesis has been extremely successful at explaining a wide range of cosmological observations, including the growth of large-scale structure and gravitational lensing. Many experimental groups are in hot pursuit of the direct detection of dark matter particles, under the assumption that they interact via the weak nuclear force. Large cosmological N-body simulations have converged on detailed predictions for the distribution of dark matter on scales ranging from superclusters down to dwarf galaxies, and a large subfield of cosmology is devoted to figuring out the relationship between the theoretical dark matter distribution and the observed visible matter distribution, using a range of observations, simulations, and models. Certainly dark matter cosmology has been highly successful in explaining a wide range of observations and in providing a compelling theoretical framework for the standard cosmological model.

Is there a viable alternative? Milgrom considered the following ad hoc modification to the Newtonian law for gravitational force on a mass m due to another mass M at a distance r:

$$F = \begin{cases} ma_N, & a_N \gg a_0, \\ m(a_N a_0)^{1/2}, & a_N \ll a_0, \end{cases} \tag{1}$$

where $a_N = GM/r^2$ is the usual Newtonian acceleration due to gravity, and some smooth interpolating function between the two limits is assumed. If the Newtonian gravitational force on an object results in an acceleration greater than a_0, the Milgrom gravitational force is proportional to r^{-2}, the same as the Newtonian force, but if the Newtonian force gives an acceleration smaller than a_0, then the Milgrom gravitational force is larger than the corresponding Newtonian force, dropping off like r^{-1}. Remarkably, this simple modification is highly successful at reproducing the rotation curves of spiral galaxies from the visible matter distribution alone, that is, without dark matter, under the assumption that stars in disk galaxies follow circular orbits around the center of the galaxy. Many rotation curves have been fit this way; see, for example, [5–9]. Some galaxy rotation curves are not fit by this formula, but these are generally galaxies which visually appear to be out of dynamical equilibrium or which possess strong bars or other features departing from circular symmetry, and thus likely violate the assumption that stars follow circular orbits. Milgrom dubbed this force law modification MOND, for MOdified Newtonian Dynamics. A large literature has developed about MOND. This paper aims to give a brief introduction to the current state of the topic with useful points of entry to the literature, but is not a complete review of the literature or the science.

A cursory analysis of the force law in (1) reveals a fundamental shortcoming: it does not conserve momentum [10]. It is simple to construct a situation with two different masses where the force of the small mass on the large mass is not the same as the force of the large mass on the small mass. Shortly after Milgrom's original papers, Bekenstein and Milgrom proposed a generalization of the Poisson equation, instead of the Newtonian force law, which overcomes this difficulty [11]:

$$\nabla \cdot \left[\mu(|\nabla\Phi|/a_0)\nabla\Phi\right] = 4\pi G\rho, \tag{2}$$

where Φ is the physical gravitational potential, ρ is the baryonic mass density, and $\mu(x)$ is some smooth function with the asymptotic forms $\mu \sim x$, $x \ll 1$ and $\mu \sim 1$, $x \gg 1$. (The precise form of $\mu(x)$ makes little difference in the resulting phenomenology; commonly $\mu(x) = x/(1 + x^2)^{1/2}$ is used. But see also [5], which claims that $\mu(x) = x/(1 + x)$ gives a more realistic estimate for the visible disk mass in high surface-brightness spirals.) Note that in the regime where $|\nabla\Phi| \gg a_0$ this equation becomes the usual Poisson equation. One particular feature of this equation which differs from the usual Newtonian equation is that it is not linear: the gravitational force on an object cannot be obtained simply by adding the gravitational forces of all objects acting on it. One implication is the external field effect: a galaxy will behave according to the MOND force law with the mass of the galaxy providing the source term only as long as the internal accelerations in the galaxy are larger than the local acceleration coming from the gravitational field of external objects. This behavior was postulated in the original Milgrom papers to explain why open star clusters within our galaxy do not display MOND-like behavior, and to give a consistent explanation of how to reconcile the MOND-like behavior of different objects. The modified Poisson Equation in (2) automatically incorporates this behavior, given an arbitrary mass distribution.

Milgrom's modified force law not only explains spiral galaxy rotation curves, but also can explain a number of other phenomenological successes. It predicts that the amount of inferred dark matter in a bound system is not a function of the size of the system, but rather of the characteristic acceleration. This matches what we observe: the solar system, globular clusters, and some elliptical galaxies appear to have little or no dark matter, while dwarf galaxies and large spirals have large amounts of dark matter. But the characteristic acceleration scale of these systems successfully sorts them by dark matter content. The Milgrom force law also contains the observed Tully-Fisher Relation (luminosity scaling like the fourth power of the asymptotic rotation velocity) in spiral galaxies as a special case, implies Freeman's Law for spirals (upper limit on surface brightness), and implies the Fish Law (constant surface brightness) and the Faber-Jackson relation (luminosity scaling with the fourth power of the velocity dispersion) in elliptical galaxies. Milgrom also predicted that low surface brightness galaxies should be dark matter dominated at all radii, which was later confirmed. See [12] for an excellent review discussing the range of MOND phenomenology.

What is the effectiveness of the Milgrom force law telling us? In his original papers, Milgrom advocated that the force law is the actual fundamental force law of nature, suggesting that it either shows a modification of the law of gravity in the weak gravity regime, or a modification

of Newton's second law connecting force and acceleration. Despite observational successes, most physicists dismiss this possibility. But regardless of its fundamental status, the Milgrom force law can be viewed as an effective force law for gravitation in galaxies: if dark matter is causing the excess forces we observe, it must arrange itself in a way so that (1) represents the total gravitational force due to the combined visible and dark matter. It is not at all clear in the standard cosmological model why this should be. (Unfortunately, the immediate assertion in the original Milgrom papers that (1) represents a fundamental modification of physics caused many cosmologists to ignore the whole business. All cold dark matter advocates should still have the Milgrom Relation as part of their suite of known facts about galaxies, like the Tully-Fisher Relation; requiring dark matter models to reproduce this phenomenology might give interesting clues about the nature of the dark matter or galaxy dynamics.)

2. MOND and Dwarf Galaxies

As dwarf galaxies (particularly dwarf spheroidals) exhibit the largest discrepancies between visible matter and gravitational field of any known bound systems, they are important laboratories for testing both the dark matter and the modified gravity hypotheses. On the other hand, local dwarfs are usually irregular or spheroidal, and thus do not present an easily-measured rotation curve. Generally, redshift measurements of individual stars in dwarf spheroidals give an estimate of velocity dispersion as a function of the angular distance from the dwarf center, along with the dwarf's overall line-of-sight velocity. These measurements provide two possible probes of MOND: are internal dynamics of dwarf galaxies consistent with the MOND force law, and are the motions of dwarf galaxies around their parent galaxies consistent with the MOND force law? We briefly consider both questions here.

2.1. Internal Dynamics of Dwarfs. MOND was originally formulated to fit measured rotation curves of spiral galaxies. Extrapolating from the force law in (1) led to the prediction that low surface-brightness galaxies should have rotation curves which implied dark matter domination at all radii from the center; this prediction was eventually born out by later observations. Extending this analysis to dwarf spheroidal galaxies, which also have low surface brightness, Milgrom also predicted "... when velocity-dispersion data is available for the (spheroidal) dwarfs, a large mass discrepancy will result when the conventional dynamics is used to determine the masses." The dynamically determined mass is predicted to be larger by a factor of order 10 or more than that which is accounted for by stars [2]. This prediction was of course ultimately born out, with dwarf galaxies having the largest mass-light ratios of any known systems.

The lack of linearity in (1) implies that the gravitational force on an object is not determined solely by the mass that it orbits, but also depends on the external gravitational field. As Milgrom explained in detail [2, 11], for an object like a dwarf galaxy orbiting the Milky Way, orbits of stars within the dwarf are governed by (1), with the mass M equal to the dwarf baryonic mass within the star's orbital radius, as long as the internal gravitational acceleration $a_{\rm in}$ of the star due to the dwarf mass is larger than the external gravitational acceleration $a_{\rm ex}$ of the dwarf as it orbits the Milky Way. Otherwise, the dwarf is in the so-called "quasi-Newtonian regime," in which case the dwarf dynamics are nearly Newtonian with an effective gravitational constant. If the internal accelerations in the dwarf are small compared to a_0, then $G \rightarrow G/\mu(a_{\rm ex}/a_0)$, and the MOND value for the baryonic M/L ratio is simply the Newtonian value time $\mu(a_{\rm ex}/a_0)$. When analyzing dwarf galaxy dynamics in the context of MOND, care must be taken to determine whether the gravitational acceleration is dominated by the internal or external field.

For the quasi-Newtonian regime, estimators for the dwarf mass based on the stellar velocity dispersion are textbook formulas. In the opposite limit, where the external gravitational field is negligible (the "isolated" regime), (2) leads to the relation $M = 9\sigma_3^4/(4Ga_0)$ for the mass M of a stationary, isolated system with $a_{\rm in} \ll a_0$ [13], where σ_3 is the three-dimensional velocity dispersion of the system. We cannot directly measure σ_3, but if the system is statistically isotropic (having the same line-of-sight velocity dispersion σ in all directions), then $\sigma_3 = \sqrt{3}\sigma$. Effects which can give significant departures from this simple mass estimator include anisotropy in the velocity dispersion for systems which are not spherically symmetric and coherent velocities due to tidal effects. These are potentially visible with sufficiently sensitive photometry and spectroscopy. Brada and Milgrom (2000) analyzed these effects in more detail in the context of MOND, showing, for example, that dwarfs are more susceptible to tidal disruption than for Newtonian gravity with dark matter haloes [14] (see also [15] for a more detailed analysis).

Stellar population studies strongly suggest that the baryonic mass-light ratio Υ for dwarf satellites of the Milky Way should be in the range $1 < \Upsilon < 3$ (see, e.g., [16, 17]); these satellites generally have negligible gas contribution to their baryonic mass. A total dwarf mass derived from MOND should give a value of Υ in this range, by comparing with the measured luminosity. Gerhard and Spergel [18] and Gerhard [19] analyzed seven dwarf spheroidals using MOND and claimed values for Υ ranging from around 0.2 for Fornax to around 10 for Ursa Minor and Leo II. However, in a paper whimsically entitled "MOND and the Seven Dwarfs" [20], Milgrom persuasively argued that published uncertainties in the measurements of velocity dispersion used by Gerhard and Spergel were sufficient to explain the anomalous baryonic M/L ratios. He also noted how difficult it is to determine the photometric structural parameters of dwarfs, including central surface brightness, core radius, tidal radius, and total luminosity. Using measurements of dwarf parameters from Mateo (1994) [21] plus several subsequent measurements, Milgrom found that MOND was completely consistent with reasonable values for Υ between 1 and 3 for all seven dwarf spheroidals considered (Sculptor, Sextans, Carina, Draco, Leo II, Ursa Minor, and Fornax). This analysis estimates the mass using only the central

velocity dispersion σ for each dwarf, and computes M in either the quasi-Newtonian or the isolated limit.

The most detailed analysis of the classical dwarf galaxies has been done by Angus (2008), incorporating many improvements in observed dwarf properties over the previous decade, and also using measured variations of the velocity dispersion with radius in each dwarf for which it is measured [22]. This analysis thus provides a substantially more stringent test of MOND compared to the Seven Dwarfs paper. Angus finds best-fit values and errors for Υ, plus two parameters describing possible velocity dispersion anisotropy, Of the eight dwarfs considered, six (Sculptor, Carina, Leo I, Leo II, Ursa Minor, and Fornax) are consistent with a reasonable value of Υ. for the stellar content. Sextans and Draco both give discrepantly high values for Υ, but within 2σ of the accepted range. Draco has been previously known to present a problem for MOND [23, 24], and the problem is worse for different measurements of velocity dispersions [25] than Angus uses. Angus notes that distance and velocity dispersion uncertainties for these two dwarfs may have a significant impact, and that possible tidal effects introduce uncertainties which are large enough to explain Angus' marginally high values of Υ for these two dwarfs. However, Draco in particular shows no morphological evidence of tidal disruption. Angus speculates that it could be in the early stages of tidal heating peculiar to MOND [14] as it approaches the Milky Way. Numerical simulations would be required to decide whether this explanation is plausible. An alternate explanation is that the stellar samples are contaminated with unbound stars which are not part of the dwarf galaxy. These can inflate the inferred line-of-sight velocities in the stellar sample, leading to systematically high values for Υ. (An anonymous referee for this paper claims that this is a particular issue for Sextans and Carina, while data for Draco and Ursa Minor are not yet public.)

A provocative comparison between dark matter and MOND has recently been performed using tidal dwarfs. Bournaud and collaborators [26] have measured rotational velocities for three gas-rich dwarfs forming from collisional debris debris orbiting NGC5291. Using the VLA, they obtained rotation curves from the 21 cm gas emission. The stellar mass in these systems is a small fraction of the gas mass, so the total mass can be determined with little uncertainty. The rotation curves are symmetric, implying that the systems are rotationally supported and in equilibrium. It is straightforward to derive mass estimates based on Newtonian gravity: the total mass in the systems is about three times the observed baryonic mass. The authors claim that this is a problem based on numerical dark matter simulations showing that gaseous dwarfs condensing out of tidal debris should contain very little dark matter [27, 28]. Tidal dwarfs have complex dynamical histories and a range of baryonic effects are important, so it is hard to know whether the comparison with simulations really is a problem. On the other hand, Milgrom [29] and Gentile et al. [30] have both shown that the tidal dwarfs are well accounted for with MOND, with *no free parameters*. This consistency is very difficult to explain in dark matter models, as tidal dwarfs form from tumultuous dynamical processes with strong dependence on initial conditions while being affected by numerous baryonic processes. Why should their dark matter content be precisely that needed to make them land right on the MOND force law? Clearly a larger sample of these very interesting dynamical systems is an observational priority.

A recent interesting set of observations has been performed on the distant and diffuse globular cluster Palomar 14 [31], among other applications of MOND to distant globular clusters (e.g., [32–34]). The radial velocities of 17 red giant stars in the cluster have been measured with the VLT and Keck telescopes, giving an estimate of the line-of-sight velocity dispersion. This dispersion is consistent with Newtonian gravity, even though the globular cluster should be well within the MOND regime, and the authors claim the observations taken at face value rule out MOND. However, the paper also constructs a scenario where the stellar velocities could still be consistent with MOND if it were on a highly elliptical orbit in the Milky Way potential, passing in and out of the MOND regime as the external gravitational field changes. This picture is related to tidal shocking [35, 36] which can decrease the stellar velocity dispersion for dwarfs with Newtonian gravity. The cluster is very distant and faint, so prospects for obtaining a proper velocity on the sky, and thus a clearer characterization of the cluster's recent orbital history around the Milky Way, is likely remote. Mass segregation of the red giants in the cluster may also be an issue. But these systems put some significant pressure on MOND.

The other smaller Milky Way dwarfs which have recently been discovered in Sloan Digital Sky Survey data (see, e.g., [37, 38]) have even higher ratios of visible mass to inferred dark matter mass than the classical dwarf spheroidals, presenting another stringent test of MOND in galactic systems down to still smaller scales than have been so far analyzed. Sanchez-Salcedo and Hernandez [15] performed a preliminary analysis concluding that the required MOND value for Υ increases at low luminosities and is too high to be realistic. This is a consequence of these dwarf spheroidals being consistent with a universal central velocity dispersion. This provocative conclusion clearly warrants further study. Systematic effects related to a host of assumptions about the Milky Way gravitational potential, tidal effects in the dwarfs, stellar interlopers in the data, and other considerations can dominate the uncertainties in these calculations.

2.2. Can a Dwarf Galaxy Rule Out MOND? The results described in the previous section raise a tricky question for MOND. On one hand, the theory is in principle more predictive than dark matter: the gravitational field of a distribution of visible matter is completely determined given the baryonic mass-light ratio Υ and the distance, which sets the length scale in (1). Both of these numbers can be determined or constrained by other observations. (In practice, Υ is usually left as a free parameter, and then its MOND-derived value is compared to the stellar

population to determine whether it is reasonable.) On the other hand, the gravitational field is probed via the dynamics of test objects, generally the motions of stars in the galaxy. We generally do not have available the full velocity vector or velocity dispersion, but only the line-of-sight components. The transverse components contain crucial information about the full dynamical state of the dwarf: did its past trajectory create tidal heating or disruption? To what extent is its internal velocity dispersion anisotropic? How rapidly is the external gravitational field varying? Without this information, a range of gravitational potentials are consistent with the current dynamical state of any galaxy. In the absence of other difficult observations (like proper motions, which allow reconstructing the actual galaxy trajectory), we must settle for determining whether the observed galaxy dynamics requires only believable additional assumptions about unobservable effects.

This is the same issue facing MOND fits of large galaxies as well. Large galaxies tend to have much less significant external gravitational field effects than dwarfs, leaving less freedom to explaining marginal MOND fits. The remarkable point about MOND is that, despite the limited freedom the model provides in fitting galaxy dynamics, very few galaxies, ranging over several orders of magnitude in mass and more than an order of magnitude in size, provide a true challenge for MOND.

In contrast, the dark matter situation is more forgiving. The standard cosmology in principle is completely deterministic, once the properties of dark matter are specified. Small initial density perturbations, specified by measurements of the cosmic microwave background temperature anisotropies, evolve according to completely specified equations of cosmological evolution. However, we are not yet able to make detailed *ab initio* predictions for the dark matter halo associated with a particular class of galaxies. Since the baryonic mass is coupled gravitationally to the dark matter, a complete understanding of the dark matter distribution today requires detailed knowledge of the history of the baryon distribution, and this in turn is shaped by complex baryonic physics, including heating, cooling, star formation and evolution, and energy feedback from stars and quasars. This is not simply an academic point: most of the outstanding issues with dark matter involve small scales, where the baryon densities can be comparable to the dark matter densities. Eventually, our modeling and computations may reach the point where we can simulate the evolution of realistic galaxies starting only from cosmological initial conditions, but this prospect is many years away. Until then, visible galaxies' rotation curves or velocity dispersions are generally fit using a parameterized model for the dark matter halo, and we have few constraints on the halo parameters for an individual galaxy. So for an individual galaxy, fitting a dark matter halo provides more freedom than fitting a MOND value for Υ.

2.3. Dwarfs as Dynamical Tracers. The motions of dwarf galaxies themselves as they orbit around their parent galaxy can also be used as a test of MOND. Typically, for large elliptical galaxies, satellite galaxies are observable to much larger radii than the stars in the central galaxy, so the satellites probe the gravitational field over a larger region. However, any individual galaxy has a relatively small number of observable satellites, making gravitational potential constraints inconclusive. To get around this, Klypin and Prada [39] have used a sample of 215,000 red galaxies with redshifts between $z = 0.010$ and $z = 0.083$ from the Sloan Digital Sky Survey Data Release 4. From this catalog, they select a set of satellites according to the criteria that the satellite is at least a factor of four fainter than its host, has a projected distance from its host of less than 1 Mpc, and has a velocity difference from its host of less than 1500 km/s. This results in about 9500 satellites around 6000 host galaxies. They then form a composite satellite velocity dispersion as a function of radius for a number of bins in host galaxy luminosity by stacking all of the satellites and using a maximum-likelihood estimator. A homogeneous background level, reflecting random alignments of unrelated galaxies, is subtracted to give a final velocity dispersion for each luminosity bin.

Klypin and Prada compare this velocity dispersion with circular dark matter velocities around large isolated haloes drawn from N-body simulations, and find very good agreement. They make the assumption that the density of dwarf galaxies traces the dark matter density, which holds in dark matter simulations [40]. They further claim that velocity dispersions derived by solving the Jeans equation with the MOND gravitational potential in (2) can only fit the data using highly contrived forms for the velocity dispersion anisotropy, corresponding to highly elliptical stellar orbits. This conclusion has been disputed by Angus and McGaugh [41], who claim that the same anisotropy is actually very reasonable, based on numerical simulations of elliptical galaxy formation in MOND [42]. The two papers also disagree on a number of other points, including whether gravitational fields external to the SDSS galaxies should be relevant and what constitutes reasonable mass-light ratios for the host galaxies. Further independent analysis of this interesting data set is clearly warranted.

3. Galaxy Clusters and MOND

While the Milgrom force law, (1), and its generalization to the modified Poisson equation in (2), is a highly successful phenomenological description of galaxies ranging from the smallest dwarfs to the largest spirals, and over the full range of observed surface brightness, its efficacy does not extend to the larger scales of galaxy clusters. A typical galaxy cluster must contain a total mass several times its visible gas and stellar mass for its gas temperatures and galaxy velocities to be explained by the Milgrom force law [43]. Simply postulating an increased cluster value for the baryonic mass-light ratio Υ is not realistic, since the baryonic mass is dominated by gas and does not have the intrinsic uncertainty in Υ that stellar populations do. In the absence of large systematic errors in the cluster data, we have several choices for explaining galaxy clusters.

(1) MOND is simply not a fundamental theory, but only a phenomenological relationship for the distribution of dark matter in galaxies, inapplicable to larger bound systems.

(2) MOND does represent a fundamental force law, but clusters contain additional dark matter while galaxies do not.

(3) MOND represents a fundamental force law for galaxies, but this force law gets modified on larger scales.

The first possibility is widely accepted: galaxy clusters simply rule out MOND as a modification of gravity. The second possibility is not as outlandish as it appears at first glance. If dark matter were in the form of light neutrinos with a mass of around 2 eV, for example, which had relativistic velocities at the time of their decoupling, they would not be gravitationally bound in galaxies, but could be bound in the much larger and more massive clusters [44, 45]. Current best limits on neutrino masses come from cosmology, but these assume the standard cosmological model, which may be modified if MOND actually represents a fundamental force law. Angus [46] postulates a slightly heavier (11 eV) sterile neutrino, which a numerical calculation shows can reproduce the acoustic peaks in the microwave background assuming that early-universe physics is not affected by MOND effects. Producing the forced acoustic oscillations revealed by precision measurements of the microwave background power spectrum is an important challenge for any cosmology with different dark matter or gravitation from the standard cosmology. Dynamical analysis shows that such a neutrino can reproduce observed galaxy cluster phenomenology while not affecting galaxy rotation curves [47]. Pressure is put on these models from analyses of gravitational lensing [48–50], although these all make specific assumptions about lensing in MOND, which is not uniquely determined without the context of a relativistic theory.

The most relevant observations for MOND are the gravitational lensing observations of the famous "bullet" cluster 1E 0657-558 [51] and the cluster MACS J0025.4-1222 [52]. In these systems of two merging galaxy clusters, the peak of the gravitational potential, revealed by weak lensing, is offset from the peak of the mass distribution, visible in hot gas. This offset is consistent with the clusters containing substantial dark matter; when the clusters merge, the dark matter, which is assumed to be collisionless, continues to move unimpeded, while the gas composing the bulk of the visible matter is slowed via shock heating. The offset is NOT consistent with MOND, or with *any* modified gravity theory where the gravitational field is generated solely by the visible matter: the geometry of the gravitational field is different from the geometry of the visible matter [53]. The merging-cluster observations decisively demonstrate that (2) cannot by itself describe gravitation. This is consistent with the earlier observations showing the inferred cluster dark matter content is discrepant with the MOND force law prediction, but further rules out the discrepancy being due to additional modifications of the gravitational force law on cluster scales (case 3 above). Unlike individual galaxies, galaxy clusters *must* possess some source of gravitation in addition to that provided by the visible matter (i.e., dark matter!).

4. Relativistic MOND and Dark Matter

Many people felt relieved that the cluster lensing results meant they could finally stop hearing about all of this pesky MOND business. However, option 2 above is still viable, although most cosmologist view it as an unnaturally complicated theoretical possibility. As mentioned above, clusters could contain hot dark matter, like light neutrinos, which would be sufficient to explain the observed gravitational and gas morphology of the merging clusters. While this solution invokes two separate pieces of new physics (sufficiently massive neutrinos and a MOND force law), it is not immediately obvious how much more speculative this should be considered than standard dark matter models, given that neutrinos are already known to have non-zero masses from neutrino oscillation observations. But the most interesting option for MOND may come from a different direction.

Two years before the bullet cluster observations showed that the gravitational field must be generated by more than just the visible matter, Jacob Bekenstein published a relativistic gravitation theory which reduced to MOND in the point-source limit [54]. For many years, the fact that MOND had no relativistic basis was often cited as a compelling argument against the idea. (I sometimes joked that people claimed a relativistic MOND extension was ruled out by the Bekenstein Theorem. This theorem stated that Bekenstein had tried to do it and failed, so therefore it was not possible. Later, Bekenstein told me that he had actually never put much effort into the problem.) With a full relativistic theory of gravitation, diverse observations ranging from solar system constraints on post-Newtonian parameters to gravitational lensing, cosmological structure formation, and the expansion history of the universe, can be addressed. All of these areas were speculated about using the MOND force law or modified Poisson equation, and reasoning by analogy with general relativity. But this is clearly an unsatisfactory approach: any results contradicting observations can simply be explained away as the result of an insufficiently sophisticated theory.

Several variations on the Bekenstein proposal are now on the table [55, 56]. These theories all share the common element of additional dynamical fields which act as gravitational sources. The most elegant scheme so far has been dubbed Einstein Aether gravity [57]. A dynamical time-like vector field A_μ with $A_\mu A^\mu = -1$ is incorporated into gravity by adding a term $\mathcal{F}(\mathcal{K})$ to the Einstein-Hilbert gravitational action, where $\mathcal{F}$ is a function to be determined and

$$\mathcal{K} \propto c_1 \nabla_\mu A_\nu \nabla^\mu A^\nu + c_2 (\nabla_\mu A^\mu)^2 + c_3 \nabla_\mu A^\nu \nabla_\nu A^\mu \quad (3)$$

with c_1, c_2, and c_3 undetermined constants. This is an unusual theory because the time-like vector field picks out a preferred frame at each point in spacetime (in which the time coordinate direction aligns with A) and thus violates local

Lorentz invariance. But if this symmetry breaking is small enough it would be below the level of current experimental bounds. This class of theories has a line of theoretical precedents (see, e.g., [58–60]).

Remarkably, the constants in $\mathcal{K}$ and the function $\mathcal{F}$ can be chosen so that the nonrelativistic limit of the theory reduces to a modified Poisson equation of the form (2): the MOND limit can be reproduced in this class of relativistic models. Much analysis has yet to be performed, but it is at least plausible that the excess gravitational forces induced by the vector field A^μ could match the departures from MOND seen in galaxy clusters. Relativistic MOND theories involving extra dynamical fields are, in some sense, an abdication of the original MOND philosophy that the visible matter creates all of the observed gravitational force in the universe; but we are forced into this by observations. The physical content of these theories is quite different from traditional models; the "dark sector" is governed by physics different from particle dark matter.

5. Challenges

Relativistic extensions of MOND have not been widely explored, in contrast to the overwhelming amount of work on the standard cosmological model. So it is simply not yet known whether particular relativistic MOND theories can reproduce all known gravitational phenomena, including gravitational lensing, post-Newtonian constraints from the solar system and binary pulsars, tidal streams, galaxy cluster gravitational potentials, and the observed dynamics of merging galaxy clusters. All of these phenomena are successfully explained by the standard dark matter cosmology, and represent a tall order for any new gravitational theory. Relativistic MOND theories also must be nonlinear, since MOND itself is, making these analyses challenging. However, relativistic MOND theories hold the promise of explaining two observations that the standard cosmology cannot: (1) the effectiveness of the Milgrom force law, equation (1), and related phenomenology of galaxy dynamics, and remarkably, (2) the accelerating expansion of the Universe.

Milgrom immediately realized that the MOND acceleration scale a_0 is the same order as cH_0 and thus also the same order as $c\Lambda^{1/2}$, where H_0 is the Hubble parameter and Λ is the cosmological constant which would explain the accelerating expansion of the universe. It is difficult to see how a_0, which manifests itself on scales of dwarf galaxies, can be related to either H_0 or Λ in the standard cosmological model, but a relativistic basis for MOND may provide insight. Reference [57] discusses conditions under which the additional vector field in Einstein Aether gravity will influence the expansion rate of the Universe. In fact, they display a choice of $\mathcal{F}$ which gives a late-time expansion history identical to that of general relativity with a cosmological constant. This is highly provocative: could a conceptually simple modification of relativistic gravitation explain the phenomenology of both dark matter and dark energy? The particular theory considered in [57] has substantial freedom in it, and is also challenging to analyze because it is nonlinear. But substantial effort in this direction is clearly warranted, as the theory easily reproduces MOND-like behavior and accelerating cosmological expansion with different choices of the free parameters and the free function.

Most cosmologists pay little attention to the highly successful galaxy phenomenology of MOND, even though they should, because they do not believe in MOND as a fundamental theory. The merging galaxy cluster observations have now ruled out the possibility that (2) applied to visible matter represents the entire fundamental theory of gravitation, while dark matter cosmology has had remarkable success in explaining the growth of structure in the Universe and providing a simple standard cosmological model which explains most observations. On the other hand, dark matter cosmology still faces some serious issues, mostly related to reproducing this MOND phenomenology (with the obvious exception of dark energy). The recent observation implying tidal dwarfs obey MOND [30] is one intriguing example. We should not allow the successes of our leading theories to blind us to other possibilities.

The discovery of the accelerating expansion of the Universe changed the playing field for cosmology. Prior to the late 1990's, many established cosmologists would greet any suggestion of a modification of gravity as the explanation for observed gravitational force excesses with contempt. Today, some of these same scientists author papers advocating a modification of gravity as a possible explanation for the observed accelerating expansion. Until the predominant picture of dark matter cosmology can explain all of the observations, other competing ideas should be pursued, either as a way of sharpening the case for dark matter cosmology, or, perhaps, uncovering an eventual replacement.

Acknowledgments

The author thank Andrew Zentner for insightful discussions about galaxy formation. Two anonymous referees helpfully pointed out recent relevant literature, and one emphasized how unbound stellar interlopers can increase inferred mass-light ratios in dwarf spheroidals. This work was partially supported by NSF Grant AST-0807790.

References

[1] M. Milgrom, "A modification of the Newtonian dynamics as a possible alternative to the hidden mass hypothesis," *The Astrophysical Journal*, vol. 270, pp. 365–370, 1983.

[2] M. Milgrom, "A modification of the Newtonian dynamics—implications for galaxies," *The Astrophysical Journal*, vol. 270, pp. 371–389, 1983.

[3] M. Milgrom, "A modification of the newtonian dynamics—implications for galaxy systems," *The Astrophysical Journal*, vol. 270, p. 384, 1983.

[4] M. S. del Ríío, E. Brinks, and J. Cepa, "HIgh-resolution H i observations of the galaxy NGC 404: a dwarf S0 with abundant interstellar gas," *The Astronomical Journal*, vol. 128, pp. 89–102, 2004.

[5] R. H. Sanders and E. Noordermeer, "Confrontation of modified newtonian dynamics with the rotation curves of early-type disc galaxies," *Monthly Notices of the Royal Astronomical Society*, vol. 379, no. 2, pp. 702–710, 2007.

[6] M. Milgrom and R. H. Sanders, "Modified newtonian dynamics rotation curves of very low mass spiral galaxies," *The Astrophysical Journal*, vol. 658, p. 17, 2007.

[7] E. I. Barnes, A. Kosowsky, and J. A. Sellwood, "Milgrom relation models for spiral galaxies from two dimensional velocity maps," *The Astronomical Journal*, vol. 133, no. 4, pp. 1698–1709, 2007.

[8] R. H. Sanders and M. A. W. Verheijen, "Rotation curves of Ursa major galaxies in the context of modified newtonian dynamics," *The Astrophysical Journal*, vol. 503, no. 1, pp. 97–108, 1998.

[9] W. J. G. de Blok and S. S. McGaugh, "Testing modified newtonian dynamics with low surface brightness galaxies: rotation curve fits," *The Astrophysical Journal*, vol. 508, no. 1, pp. 132–140, 1998.

[10] J. E. Felten, "Milgrom's revision of Newton's laws—dynamical and cosmological consequences," *The Astrophysical Journal*, vol. 286, p. 3, 1984.

[11] J. D. Bekenstein and M. Milgrom, "Does the missing mass problem signal the breakdown of Newtonian gravity?" *The Astrophysical Journal*, vol. 286, p. 7, 1984.

[12] R. H. Sanders and S. S. McGaugh, "Modified Newtonian dynamics as an alternative to dark matter," *Annual Review of Astronomy and Astrophysics*, vol. 40, pp. 263–317, 2002.

[13] M. Milgrom, "Modified dynamics predictions agree with observations of the H I kinematics in faint dwarf galaxies contrary to the conclusions of Lo, Sargent, and Young," *The Astrophysical Journal*, vol. 429, no. 2, pp. 540–544, 1994.

[14] R. Brada and M. Milgrom, "Dwarf satellite galaxies in the modified dynamics," *The Astrophysical Journal*, vol. 541, no. 2, pp. 556–564, 2000.

[15] F. J. Sanchez-Salcedo and X. Hernandez, "Masses, tidal radii, and escape speeds in dwarf spheroidal galaxies under mond and dark halos compared," *The Astrophysical Journal*, vol. 667, no. 2, pp. 878–890, 2007.

[16] E. F. Bell and R. S. de Jong, "Stellar mass-to-light ratios and the Tully-Fisher relation," *The Astrophysical Journal*, vol. 550, no. 1, pp. 212–229, 2001.

[17] R. S. de Jong and E. F. Bell, "Dynamical and stellar population mass-to-light ratio estimates," in *Island Universes: Structure and Evolution of Disk Galaxies*, p. 107, Springer, Berlin, Germany, 2007.

[18] O. E. Gerhard and D. N. Spergel, "Dwarf spheroidal galaxies and non-Newtonian gravity," *The Astrophysical Journal*, vol. 397, no. 1, pp. 38–43, 1992.

[19] O. E. Gerhard, in *Proceedings of the ESO/OHP Workshop "Dwarf Galaxies"*, G. Meylan and P. Prugniel, Eds., 1994.

[20] M. Milgrom, "Mond and the seven dwarfs," *The Astrophysical Journal*, vol. 455, no. 2, pp. 439–442, 1995.

[21] M. Mateo, in *Proceedings of the ESO/OHP Workshop "Dwarf Galaxies"*, G. Meylan and P. Prugniel, Eds., 1994.

[22] G. W. Angus, "Dwarf spheroidals in MOND," *Monthly Notices of the Royal Astronomical Society*, vol. 387, p. 1481, 2008.

[23] E. L. Łokas, "Dark matter distribution in dwarf spheroidal galaxies," *Monthly Notices of the Royal Astronomical Society*, vol. 333, no. 3, pp. 697–708, 2002.

[24] E. Lokas, G. Mamon, and F. Prada, "The Draco dwarf in CDM and MOND," in *Mass Profiles and Shapes of Cosmological Structures*, G. Mamon, F. Combes, C. Deffayet, and B. Fort, Eds., vol. 20 of *EAS Publications Series*, pp. 113–118, 2006.

[25] M. I. Wilkinson, et al., "Kinematically cold populations at large radii in the draco and ursa minor dwarf spheroidal galaxies," *The Astrophysical Journal*, vol. 611, p. 21, 2004.

[26] F. Bournaud, P.-A. Duc, E. Brinks, et al., "Missing mass in collisional debris from galaxies," *Science*, vol. 316, no. 5828, pp. 1166–1169, 2007.

[27] J. E. Barnes and L. Hernquist, "Formation of dwarf galaxies in tidal tails," *Nature*, vol. 360, no. 6406, pp. 715–717, 1992.

[28] F. Bournaud and P.-A. Duc, "From tidal dwarf galaxies to satellite galaxies," *Astronomy & Astrophysics*, vol. 456, no. 2, pp. 481–492, 2006.

[29] M. Milgrom, "MOND and the mass discrepancies in tidal dwarf galaxies," *The Astrophysical Journal Letters*, vol. 667, pp. L45–L48, 2007.

[30] G. Gentile, B. Famaey, F. Combes, et al., "Tidal dwarf galaxies as a test of fundamental physics," *Astronomy & Astrophysics*, vol. 472, no. 2, pp. L25–L28, 2007.

[31] K. Jordi, et al., "Testing fundamental physics with distant star clusters: analysis of observational data on Palomar 14," *The Astronomical Journal*, vol. 137, p. 4586, 2009.

[32] H. Baumgardt, E. K. Grebel, and P. Kroupa, "Using distant globular clusters as a test for gravitational theories," *Monthly Notices of the Royal Astronomical Society*, vol. 359, pp. L1–L4, 2005.

[33] H. Haghi, H. Baumgardt, P. Kroupa, et al., "Testing fundamental physics with distant star clusters: theoretical models for pressure-supported stellar systems," *Monthly Notices of the Royal Astronomical Society*, vol. 395, no. 3, pp. 1549–1557, 2009.

[34] A. Sollima and C. Nipoti, "Globular clusters in modified Newtonian dynamics: velocity-dispersion profiles from self-consistent models," *Monthly Notices of the Royal Astronomical Society*. In press.

[35] O. Y. Gnedin and J. P. Ostriker, "Destruction of the galactic globular cluster system," *The Astrophysical Journal*, vol. 474, no. 1, pp. 223–255, 1997.

[36] J. I. Read, M. I. Wilkinson, N. W. Evans, et al., "The importance of tides for the local group dwarf spheroidals," *Monthly Notices of the Royal Astronomical Society*, vol. 367, no. 1, pp. 387–399, 2006.

[37] J. D. Simon and M. Geha, "The kinematics of the ultra-faint milky way satellites: solving the missing satellite problem," *The Astrophysical Journal*, vol. 670, no. 1, pp. 313–331, 2007.

[38] L. E. Strigari, J. S. Bullock, M. Kaplinghat, et al., "A common mass scale for satellite galaxies of the milky way," *Nature*, vol. 454, no. 7208, pp. 1096–1097, 2008.

[39] A. Klypin and F. Prada, "Testing gravity with motion of satellites around galaxies: newtonian gravity against modified Newtonian dynamics," *The Astrophysical Journal*, vol. 690, no. 2, pp. 1488–1496, 2009.

[40] L. V. Sales, J. F. Navarro, D. G. Lambas, S. D. M. White, and D. J. Croton, "Satellite galaxies and fossil groups in the millennium simulation," *Monthly Notices of the Royal Astronomical Society*, vol. 382, no. 4, pp. 1901–1916, 2007.

[41] G. W. Angus and S. S. McGaugh, "The collision velocity of the bullet cluster in conventional and modified dynamics," *Monthly Notices of the Royal Astronomical Society*, vol. 383, no. 2, pp. 417–423, 2008.

[42] C. Nipoti, P. Londrillo, and L. Ciotti, "Dissipationless collapses in modified newtonian dynamics," *The Astrophysical Journal*, vol. 660, no. 1, pp. 256–266, 2007.

[43] A. Aguirre, J. Schaye, and E. Quataert, "Problems for modified Newtonian dynamics in clusters and the Lyα forest?" *The Astrophysical Journal*, vol. 561, no. 2, pp. 550–558, 2001.

[44] R. H. Sanders, "Clusters of galaxies with modified Newtonian dynamics," *Monthly Notices of the Royal Astronomical Society*, vol. 342, no. 3, pp. 901–908, 2003.
[45] G. W. Angus, et al., "On the proof of dark matter, the law of gravity, and the mass of neutrinos," *The Astrophysical Journal*, vol. 654, p. 13, 2007.
[46] G. W. Angus, "Is an 11 eV sterile neutrino consistent with clusters, the cosmic microwave background and modified Newtonian dynamics?" *Monthly Notices of the Royal Astronomical Society*, vol. 394, no. 1, pp. 527–532, 2009.
[47] G. W. Angus, B. Famaey, and A. Diaferio, "Equilibrium configurations of 11eV sterile neutrinos in MONDian galaxy clusters," http://arxiv.org/abs/0906.3322.
[48] P. Natarajan and H. Zhao, "MOND plus classical neutrinos are not enough for cluster lensing," *Monthly Notices of the Royal Astronomical Society*, vol. 389, no. 1, pp. 250–256, 2008.
[49] I. Ferreras, M. Sakellariadou, and M. F. Yusaf, "Necessity of dark matter in modified newtonian dynamics within galactic scales," *Physical Review Letters*, vol. 100, Article ID 031302, 4 pages, 2008.
[50] L. Tian, H. Hoekstra, and H. Zhao, "The relation between stellar mass and weak lensing signal around galaxies: implications for modified Newtonian dynamics," *Monthly Notices of the Royal Astronomical Society*, vol. 393, no. 3, pp. 885–893, 2009.
[51] D. Clowe, et al., "A direct empirical proof of the existence of dark matter," *The Astrophysical Journal*, vol. 648, pp. 109–L113, 2006.
[52] M. Bradač, S. W. Allen, T. Treu, et al., "Revealing the properties of dark matter in the merging cluster MACS J0025.4-1222," *The Astrophysical Journal*, vol. 687, no. 2, pp. 959–967, 2008.
[53] J. A. Sellwood and A. Kosowsky, "Distinguishing dark matter from modified gravity," in *The Dynamics, History, and Structure of Galaxies*, G. S. Da Costa and E. M. Sadler, Eds., 2002.
[54] J. D. Bekenstein, "Relativistic gravitation theory for the modified Newtonian dynamics paradigm," *Physical Review D*, vol. 70, no. 8, Article ID 083509, 28 pages, 2004.
[55] R. H. Sanders, "A tensor-vector-scalar framework for modified dynamics and cosmic dark matter," *Monthly Notices of the Royal Astronomical Society*, vol. 363, no. 2, pp. 459–468, 2005.
[56] I. Navarro and K. Van Acoleyen, "Modified gravity, dark energy and modified Newtonian dynamics," *Journal Cosmology Astroicle Physics*, vol. 2006, no. 9, p. 006, 2006.
[57] T. G. Zlosnik, P. G. Ferreira, and G. D. Starkman, "Modifying gravity with the aether: an alternative to dark matter," *Physical Review D*, vol. 75, no. 4, Article ID 044017, 2007.
[58] C. M. Will and K. Nordvedt, "Conservation laws and preferred frames in relativistic gravity I," *The Astrophysical Journal*, vol. 177, p. 757, 1973.
[59] T. Jacobson and D. Mattingly, "Gravity with a dynamical preferred frame," *Physical Review D*, vol. 64, no. 2, Article ID 024028, 9 pages, 2001.
[60] S. M. Carroll and E. A. Lim, "Lorentz-violating vector fields slow the universe down," *Physical Review D*, vol. 70, no. 12, Article ID 123525, 6 pages, 2004.